Université de Montréal

Contrôle de l'organisation moléculaire en 2D et 3D par l'utilisation de liaisons hydrogène, de coordination métallique et d'autres interactions

Par

Adam Duong

Département de chimie

Faculté des arts et des sciences

Thèse présentée à la Faculté des arts et des sciences

en vue de l'obtention du grade de

Philosophiae Doctor (Ph.D.)

en chimie

02 Avril 2011

Université de Montréal

Faculté des arts et des sciences

Cette thèse intitulée :

Contrôle de l'organisation moléculaire en 2D et 3D par l'utilisation de liaisons hydrogène, de coordination métallique et d'autres interactions

Présentée par :

Adam Duong

a été évaluée par un jury composé des personnes suivantes

Professeur Andreea Schmitzer	président-rapporteur
Professeur James D. Wuest	directeur de recherche
Professeur Garry Hanan	membre du jury
Professeur Louis Cuccia	examinateur externe
Professeur Richard Leonelli	représentant du doyen de la FES

Sommaire

La stratégie de la tectonique moléculaire a montré durant ces dernières années son utilité dans la construction de nouveaux matériaux. Elle repose sur l'auto-assemblage spontané de molécule dite intelligente appelée *tecton*. Ces molécules possèdent l'habilité de se reconnaitre entre elles en utilisant diverses interactions intermoléculaires. L'assemblage résultant peut donner lieu à des matériaux moléculaires avec une organisation prévisible. Cette stratégie exige la création de nouveaux tectons, qui sont parfois difficiles à synthétiser et nécessitent dans la plupart des cas de nombreuses étapes de synthèse, ce qui empêche ou limite leur mise en application pratique. De plus, une fois formées, les liaisons unissant le corps central du tecton avec ces groupements de reconnaissance moléculaire ne peuvent plus être rompues, ce qui ne permet pas de remodeler le tecton par une procédure synthétique simple.

Afin de contourner ces obstacles, nous proposons d'utiliser une stratégie hybride qui se sert de la coordination métallique pour construire le corps central du tecton, combinée avec l'utilisation des interactions plus faibles pour contrôler l'association. Nous appelons une telle entité *métallotecton* du fait de la présence du métal. Pour explorer cette stratégie, nous avons construit une série de ligands ditopiques comportant soit une pyridine, une bipyridine ou une phénantroline pour favoriser la coordination métallique, substitués avec des groupements diaminotriazinyles (DAT) pour permettre aux complexes de s'associer par la formation de ponts hydrogène.

En plus de la possibilité de créer des métallotectons par coordination, ces ligands ditopiques ont un intérêt intrinsèque en chimie supramoléculaire en tant qu'entités pouvant s'associer en 3D et en 2D. En parallèle à notre étude de la chimie de coordination, nous avons

examiné l'association des ligands, ainsi que celle des analogues, par la diffraction des rayons-X (XRD) et par la microscopie de balayage à effet tunnel (STM). L'adsorption de ces molécules sur la surface de graphite à l'interface liquide-solide donne lieu à la formation de différents réseaux 2D par un phénomène de nanopatterning. Pour comprendre les détails de l'adsorption moléculaire, nous avons systématiquement comparé l'organisation observée en 2D par STM avec celle favorisée dans les structures 3D déterminées par XRD. Nous avons également simulé l'adsorption par des calculs théoriques. Cette approche intégrée est indispensable pour bien caractériser l'organisation moléculaire en 2D et pour bien comprendre l'origine des préférences observées. Ces études des ligands eux-mêmes pourront donc servir de référence lorsque nous étudierons l'association des métallotectons dérivés des ligands par coordination.

Notre travail a démontré que la stratégie combinant la chimie de coordination et la reconnaissance moléculaire est une méthode de construction rapide et efficace pour créer des réseaux supramoléculaires. Nous avons vérifié que la stratégie de la tectonique moléculaire est également efficace pour diriger l'organisation en 3D et en 2D, qui montre souvent une homologie importante. Nous avons trouvé que nos ligands hétérocycliques ont une aptitude inattendue à s'adsorber fortement sur la surface de graphite, créant ainsi des réseaux organisés à l'échelle du nanomètre. L'ensemble de ces résultats promet d'offrir des applications dans plusieurs domaines, dont la catalyse hétérogène et la nanotechnologie.

Mots clés : tectonique moléculaire, interactions intermoléculaires, stratégie hybride, coordination métallique, diffraction des rayons-X, microscopie de balayage à effet tunnel, graphite, phénomène de nanopatterning, calculs théoriques, ponts hydrogène, chimie supramoléculaire, ligands hétérocycliques, groupements DAT, catalyse hétérogène, nanotechnologie.

Summary

In recent years, molecular tectonics has been a useful strategy in the construction of new materials. It relies on the spontaneous self-assembly of molecules called *tectons*. These molecules have the ability to recognize themselves using various intermolecular interactions. The resulting assembly can produce molecular materials with predictable organization. This strategy requires the creation of new tectons, which are sometimes difficult to synthesize and require in most cases many synthetic steps, which prevents or limits their practical application. Moreover, once formed, the bonds joining the central core of the tecton with the groups used for molecular recognition cannot be broken, which means that it is not possible to recycle or reform the tecton by simple synthetic procedures.

To avoid these obstacles, we propose to use a hybrid strategy that uses metal coordination to build the central core of the tecton, combined with the use of weaker interactions to control the association. We call such entities *metallotectons* due to the presence of metal. To explore this strategy, we constructed a series of ditopic ligands containing either pyridine, bipyridine or phenanthroline to promote metal coordination, substituted with diaminotriazinyl groups (DAT) to allow inter-complex association by the formation of hydrogen bonds.

In addition to the possibility of creating metallotectons by coordination, these ditopic ligands have an intrinsic interest in supramolecular chemistry as entities that can associate in 3D and 2D. In parallel to our study of coordination chemistry, we examined the association of ligands by X-ray diffraction (XRD) and scanning tunneling microscopy (STM). The adsorption of these molecules on the graphite surface at the liquid-solid interface results in the formation of different networks through a process of 2D nanopatterning. To understand the details of

molecular adsorption, we systematically compared the 2D organization observed STM with the 3D structures determined by XRD. We also simulated the adsorption by theoretical calculations. This integrated approach is essential to characterize the molecular organization in 2D and to understand the origin of the observed preferences. These studies of the ligands themselves may therefore serve as a reference when we study the association of metallotectons derived by ligands coordination.

Our work demonstrates that the strategy combining coordination chemistry and molecular recognition is a rapid and an efficient method to create supramolecular networks. We verified that the strategy of molecular tectonics is also effective in leading the organization in 3D and 2D, which often shows a significant homology. We found that our heterocyclic ligands have unexpected ability to adsorb strongly on the graphite surface, creating networks organize in nanoscale. Together, these results provide promising applications in several fields, including heterogeneous catalysis and nanotechnology.

Keywords : molecular tectonics, intermolecular interactions, hybrid strategy, metal coordination, X-ray diffraction, scanning tunneling microscopy, graphite, nanopatterning phenomenon, theoretical calculations, hydrogen bonds, supramolecular chemistry, ligands, DAT groups, heterogeneous catalysis, nanotechnology.

Table des matières

Chapitre 1 : Introduction

Chapitre 4 : Homologie en 2D et en 3D

Chapitre 5 : Similarité structurelle des réseaux retenus par ponts hydrogène

Chapitre 6 : Synthèses et structures des 2,2'-bipyridines et 1,10-phénantrolines substituées avec des groupements diaminotriazinyles

Chapitre 9 : Conclusions et perspectives

Annexes

Liste des tableaux

Liste des schémas

Liste des figures

Fin de l'article 3

Fin de l'article 5

Fin de l'article 7

Liste des abréviations

A	: accepteur (de pont hydrogène)
Å	: Ångström
ADN	: acide désoxyribonucléique
Anal.	: analyse
br	: broad (signal large, en RMN)
°C	: degré Celsius
cm	: centimètre
calcd	: calculated
δ	: déplacement chimique (en RMN)
°	: degré
Δ	: chaleur ou variation
D	: donneur (de pont hydrogène)
d	: doublet (en RMN)
D	: densité
DAT	: 2,4-diamino-1,3,5-triazine
dec.	: décomposition
DFT	: density functional theory
DMSO	: diméthyl sulfoxyde
eq	: équivalent
ESI	: electro-spray ionisation
Fw	: formula weight
g	: gramme
GoF	: goodness-of-fit
h	: heure
HOPG	: highly-oriented pyrolytic graphite
HRMS	: high-resolution mass spectrometry
Hz	: hertz
I	: intensité (rayons-X)
IR	: infrarouge
J	: constante de couplage
K	: kelvin
kcal	: kilocalorie
kJ	: kilojoule
M	: molaire
μ	: coefficient d'absorption
μm	: micromètre
m	: multiplet (en RMN)
m/e	: rapport masse/charge
mg	: milligramme
MHz	: mégahertz

mL	: millilitre
mm	: millimètre
mM	: millimolaire
mmol	: millimole
mol	: mole
mp	: melting point
MS	: mass spectrometry
nA	: nanoampere
NMR	: nuclear magnetic resonance
ORTEP	: Oak Ridge Thermal Ellipsoid Program
q	: quadruplet (en RMN)
R1	: facteur d'accord sur les réflexions observées
RMN	: résonance magnétique nucléaire
RT	: room temperature
σ	: écart-type
s	: singulet (en RMN)
SEM	: scanning electronic microscopy
STM	: scanning tunneling microscopy
t	: triplet (en RMN)
T	: température
TMA	: acide benzène-1,3,5-tricarboxylique
TMEDA	: tétraméthyléthylènediamine
TMS	: triméthylsilyle
UHV	: ultra-high vacuum
V	: volt
ωR2	: facteur d'accord pondéré
w/v	: weight per volume
ν	: fréquence (de vibration en infrarouge)
Z	: nombre d'unités formulaires par maille

Remerciements

C’est avec beaucoup d’émotion que je complète la rédaction de cette thèse en remercient les personnes qui ont contribué de près ou de loin à la réalisation de ce magnifique travail. Je désire exprimer ma profonde gratitude :

À mon directeur de thèse pour avoir accepté de me diriger, pour son soutien durant cette thèse, mais aussi pour m’avoir donné une totale liberté dans ma créativité. Je tiens à le remercier de l’encouragement, de la confiance et des conseils qu’il m’a apportés au cours de ces années. Son professionnalisme ainsi que sa culture générale sont un modèle à imiter. Grâce à lui, je suis devenu plus solide intellectuellement que je ne l’étais avant. On peut dire qu’il m’a fait subir une métamorphose comme lorsqu’un forgeron transforme son métal en une joaillerie précieuse.

Au Dr. Thierry Maris qui m’a formé en cristallographie. Je dirai tout simplement qu’il est l’un des éléments majeurs durant cette thèse. Pour reprendre les paroles des anciens membres du groupe : « Son professionnalisme et sa bonne humeur me marqueront toujours ». Encore un grand merci pour tous.

J’aimerais également remercier Dr. Alain Rochefort et Marc-André Dubois pour leurs contributions dans les calculs théoriques.

Mes remerciements vont aussi au Dr. Valérie Métivaud pour les études de diffraction de poudre.

Je tiens à remercier tous les membres du groupe STM, notamment Dr. Antonio Nanci et Ji-Hyun Yi de la faculté de médecine dentaire, pour m'avoir donné accès à leur instrument et pour leur soutien technique.

Je tiens à remercier tous les membres du groupe Wuest et en particulier Olivier Lebel pour m'avoir préparé pour le prédoc, Hui Zhou, Fatima Helzy, François Raymond, Huy Che Quang et Éric Gagnon pour la bonne ambiance passée dans les laboratoires. Bien entendu, je n'oublie pas tous les autres membres du groupe Wuest. Merci à tous.

Un remerciement tout particulier au Dr. Hung Dang pour avoir été le pionnier en chimie de surface dans le groupe Wuest.

Mes pensées vont également à toute l'équipe du département qui a joué un rôle important dans la progression de ce travail, à savoir les professeurs, les employés des laboratoires de la spectrométrie de masse, des laboratoires de la résonance magnétique nucléaire et du secrétariat, sans oublier les techniciennes des laboratoires d'enseignement. Mesdames, je n'oublierai jamais les bons moments que nous avons passé ensemble à transmettre nos savoirs aux étudiants.

Pour finir, j'aimerais affectueusement remercier ma famille, ma femme Hang et ma fille Léa, mes proches et tous particulièrement les foqaras qui m'ont soutenu durant ces longues années. Je remercie mon Shaykh Sidi Hamza Boutchichiya d'avoir éveillé mon cœur. Maître, tu es l'alchimiste de mon cœur.

Notes et contributions personnelles

Les notes suivantes apportent une vue globale sur les contributions personnelles d'Adam Duong aux travaux rapportés dans cette thèse ainsi que les contributions de chacun des co-auteurs.

1. La numérotation des figures, schémas, tableaux, molécules et références de chaque article est indépendante de celle du reste de la thèse afin de rester consistant avec les documents publiés en ligne.
2. Tous les exemples de structures cristallographiques et les schémas présentés dans le chapitre d'introduction ont été redessinés pour harmoniser l'ensemble du memoire de thèse.
3. Les parties supplémentaires de l'article 5 et les fichiers CIF de l'article 6, jugés non nécessaires à la compréhension immédiate du texte, sont disponibles sur internet sur les sites de l'*American Chemical Society*.
4. Les études présentées dans cette thèse s'appuient principalement sur les données cristallographiques. Pour confirmer qu'une structure cristalline est bien représentative de l'ensemble de l'échantillon, des spectres de diffraction de poudre ont été réalisés et sont rapportés dans les annexes.
5. Tous les articles ont été écrits par Adam Duong et corrigés par le professeur James D. Wuest avec la participation du Dr. Thierry Maris.

Contributions détaillées d'Adam Duong aux articles

Premier article

- Le travail expérimental a été fait par Adam Duong.
- Les études cristallographiques ont été effectuées par Adam Duong et Thierry Maris.

Deuxième article

- Le travail expérimental a été fait par Adam Duong.
- Les calculs théoriques ont été effectués par Marc-André Dubois avec la participation d'Adam Duong.

Troisième article

- Le travail expérimental a été fait par Adam Duong.
- Les calculs théoriques ont été effectués par Marc-André Dubois et Pr. Alain Rochefort avec la participation d'Adam Duong.
- Les études cristallographiques ont été effectuées par Adam Duong et Thierry Maris.
- Valérie Métivaud a mesuré les diagrammes de poudre.

Quatrième article

- Le travail expérimental a été fait par Adam Duong.
- Les études cristallographiques ont été effectuées par Adam Duong et Thierry Maris.
- Valérie Métivaud a mesuré les diagrammes de poudre.

Cinquième article

- Le travail expérimental a été fait par Adam Duong.
- Les études cristallographiques ont été effectuées par Adam Duong et Thierry Maris.

Sixième article

- Le travail expérimental a été fait par Adam Duong.
- Les études cristallographiques ont été effectuées par Adam Duong et Thierry Maris.

Septième article

- Le travail expérimental a été fait par Adam Duong.
- Les études cristallographiques ont été effectuées par Adam Duong et Thierry Maris.
- Valérie Métivaud a mesuré les diagrammes de poudre.

Chapitre 1

Introduction

1.1 La chimie supramoléculaire

Depuis la nuit des temps, l'homme de part sa curiosité et sa volonté d'apprendre n'a sans cesse cherché à mimer tout ce qui l'entoure. Il suffit de penser au nombre d'inventions qu'il a réalisé sous l'inspiration de son entourage. Les mythologies grecques rappellent encore aujourd'hui l'ingéniosité des hommes. Le mythe de Dédale est un exemple de la faculté des hommes à mimer la nature. Le mythe raconte que pour fuir du labyrinthe dans lequel Dédale était prisonnier celui-ci avait fabriqué des ailes de plumes et de cires pour s'envoler comme les oiseaux (Figure 1.1).[1] De là, Dédale a démontré l'habilité des humains à imiter la nature.

Figure 1.1. Le mythe de Dédale, la fuite par les aires.

[1] Frontisi-Ducroux, F. *Dédale : Mythologie de l'artisan en Grèce ancienne*. Editions la Découverte/Poche, 2000.

De nos jours, les hommes n'ont pas changé et leurs inventions sont de plus en plus nombreuses et surtout de plus en plus spectaculaires. On peut citer, par exemple, la création de l'avion. D'autres découvertes, sur une échelle plus petite, s'inspirent également de la nature et sont plus étroitement liées à la chimie. Par exemple, Geim et collaborateurs se sont inspirés des motifs intérieurs des pattes d'un lézard de la famille du gecko pour concevoir un ruban adhésif à l'aide de polyimide s'adhérant à toutes les surfaces et de façon réversible.[3] La Figure 1.2 présente une patte de gecko et une image obtenue par microscopie électronique à balayage (SEM) montrant l'architecture du ruban adhésif.

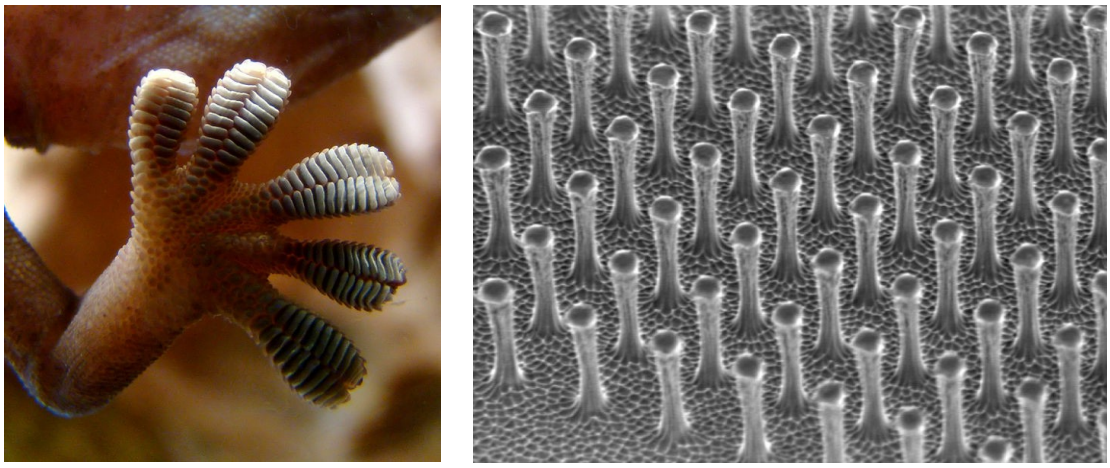

a **b**

Figure 1.2. (a) Les pattes de gecko présentant des lamelles adhésives.[2] (b) Une image SEM d'une surface d'un ruban adhésif comportant des poils de polyimide.[3]

[2] http://en.wikipedia.org/wiki/File:Gecko_foot_on_glass.JPG (20/06/2011)
[3] Geim, A. K.; Dubonos, S. V.; Grigorieva, I. V.; Novoselov, K. S.; Zhukov, A. A.; Shapoval, S. Y. *Nature Mater.* **2003**, *2*, 461.

Avec la technologie moderne, l'homme ne se limite plus aux exemples du monde visible. En effet, il est capable d'observer des objets invisibles à l'œil grâce à la microscopie électronique et d'autres méthodes analytiques. Ainsi, il étudie l'organisation de la matière afin de comprendre les interactions à l'échelle moléculaire et atomique. Cette compréhension lui permet de reproduire, de modifier ou de créer d'autres matières et de former des objets selon son inspiration.

La chimie est à la base de ces manipulations. La chimie s'intéresse classiquement à la formation et à la rupture des liaisons entre les atomes de façon précise et contrôlée. Plus particulièrement, la chimie a élaboré des méthodes puissantes pour créer des molécules de manière prédictible. En 1828, le chimiste allemand Friedrich Wöhler a marqué l'histoire de la chimie dite organique en synthétisant pour la toute première fois l'urée, sans avoir recourt à l'utilisation d'un rein ou d'un animal dans sa synthèse.[4] La chimie de synthèse basée sur les interactions covalentes a progressivement évolué plus récemment pour intégrer la chimie supramoléculaire, dont l'objectif est de parvenir à acquérir la maîtrise des liaisons intermoléculaires. En 1987, Jean-Marie Lehn donna une définition concrète de la chimie supramoléculaire :

> *"Supramolecular chemistry is the chemistry of the intermolecular bond, covering the structures and functions of the entities formed by association of two or more chemical species."*[5]

[4] Wöhler, F. *Ann. Physik Chem.* **1828**, *88*, 253.
[5] Lehn, J.-M. *Angew. Chem., Int. Ed.* **1988**, *27*, 89.

En d'autres termes, la chimie supramoléculaire est la chimie des assemblages ou encore la chimie au-delà de la molécule. La chimie supramoléculaire repose sur les interactions non-covalentes telles que les ponts hydrogène, les liaisons de coordination, les liens électrostatiques, les interactions π-π, les interactions dipôle-dipôle, les interactions de van der Waals et les interactions hydrophobes.[6] En comparaison avec les interactions covalentes, les liaisons non-covalentes sont relativement faibles et par ce fait sont formées réversiblement. Dans la nature, on retrouve plusieurs exemples de phénomènes utilisant des interactions faibles : (1) La reconnaissance des substrats lors des réactions enzymatiques, qui font souvent intervenir des interactions van der Waals et des ponts hydrogène,[7] (2) le transport de l'oxygène par l'hémoglobine dans lequel les molécules d'O_2 interagissent avec le fer par liaison de coordination[8] et (3) l'enroulement du brin d'ADN en double hélice, ce qui est obtenu par ponts hydrogène.[9] Parallèlement, de nouveaux champs de recherche ont émergé à l'issu de cette chimie dans le domaine des substances d'origine non-naturelle, donc les matériaux moléculaires synthétiques. Certains chimistes se sont progressivement spécialisés dans le design de ces matériaux, tel qu'illustré dans les paragraphes suivants.

1.2 L'ingénierie cristalline

Le terme *crystal engineering* a été énoncé par Schmidt en 1971 lors de ses travaux décrivant des réactions topochimiques de l'acide cinnamique à l'état cristallin.[10] L'ingénierie

[6] Desiraju, G. R. *Acc. Chem. Res.* **2002**, *35*, 565.
[7] Vasella, A.; Davies, G. J.; Bohm, M. *Curr Opin Chem Biol.* **2002**, *6(5)*, 619. Koshland, D. E. *Proc. Natl. Acad. Sci.* **1958**, *44 (2)*, 98.
[8] Paoli, M.; Liddington, R.; Tame, J.; Wilkinson, A.; Dodson, G. *J. Mol. Biol.* **1996**, *256*, 775.
[9] Crouse, D. T. *J. Chem. Educ.* **2007**, *84 (5)*, 803
[10] Schmidt, G. M. J. *Pure Appl. Chem.* **1971**, *27*, 647.

cristalline est une science qui s'intéresse à la construction de cristaux avec des propriétés voulues. L'outil principal de construction découle de la chimie supramoléculaire, ce qui dirige l'organisation des molécules à l'état cristallin. En effet, lors de la cristallisation, les molécules se reconnaissent selon une combinaison complexe de facteurs géométriques et chimiques, dans une relation de complémentarité bien précise entre les molécules sélectionnées pour former le cristal. L'ingénierie cristalline consiste à édifier le réseau supramoléculaire par assemblage régi par des interactions faibles intermoléculaires qui se répètent dans les trois dimensions de l'espace. Dans ce processus, la prédiction de l'organisation du cristal est parfois difficile, voire impossible, contrairement à la synthèse organique où toutes les liaisons entre les atomes sont covalentes et la construction de la molécule est donc plus facile à diriger de manière confiante. De nombreux groupes de recherche s'attardent à déterminer les facteurs permettant de contrôler l'arrangement cristallin des molécules d'une manière plutôt qu'une autre.[11] Ces travaux sont essentiels, car les propriétés physico-chimiques d'un matériau dépendent de sa composition, mais aussi de l'arrangement des molécules entre elles. Un solide peut donc avoir des propriétés différentes dépendamment de la forme polymorphique dans laquelle il cristallise.[12] Plusieurs approches ont été proposées pour contrôler l'organisation des molécules. À l'heure actuelle, les chimistes ont catalogué les interactions faibles suivantes utiles en ingénierie cristalline, qui sont présentées et discutées ci-dessous.

[11] Chong, J. H.; MacLachlan, M. J. *Chem. Soc. Rev.* **2009**, *38*, 3301. Desiraju, G. R. *Angew. Chem., Int. Ed*. **2007**, *46(44)*, 8342. Zaworotko, M. J. *Angew. Chem., Int. Ed***. 1998**, *37*, 1211. Pitt, M. A.; Johnson, D. W. *Chem. Soc. Rev***. 2007**, *36*, 1441. Burrows, A. D.; Chan, C.-W.; Chowdhry, M. M.; McGrady, J. E.; Mingos, D. M. P. *Chem. Soc. Rev*. **1995**, *24*, 329. Zaworotko, M. J. *Chem. Soc. Rev.* **1994**, *23*, 283.

[12] Bond, A. D.; Boese, R.; Desiraju, G. R. *Am. Pharm. Rev*. **2007**, *10*, 24.

1.2.1 Le pont hydrogène : Définition et concept

Le pont hydrogène est une interaction faible entre un atome portant un hydrogène acide et un autre atome ou groupement possédant un ou plusieurs doublets d'électrons libres ou des électrons π polarisables. L'atome portant l'hydrogène est appelé donneur de pont hydrogène (D) tandis que celui possédant le ou les doublets électroniques disponibles est désigné accepteur de pont hydrogène (A). Différentes catégories de liaison hydrogène sont connues, dont les interactions simples (si la liaison implique un centre donneur, un seul accepteur et un total de quatre électrons) et les liaisons multiples nommées bifurquée ou trifurquée (Schéma 1.1).[13]

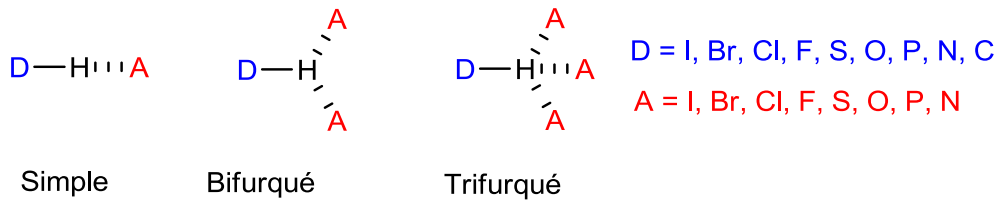

Schéma 1.1. Représentation des différents modes d'interactions par liaison hydrogène (simple, bifurquée et trifurquée).

Plusieurs groupements de reconnaissance moléculaire régie par ponts hydrogène ont été proposés parmi lesquels sont les acides carboxyliques, les acides boroniques, les phénols, les pyridones et les diaminotriazines. Quelques exemples de molécules incorporant les groupements de reconnaissance moléculaire cités ci-dessus sont montrés au Schéma 1.2.

[13] Jeffrey, G. A. *An Introduction to Hydrogen Bonding*, Oxford University Press, Oxford, 1997.

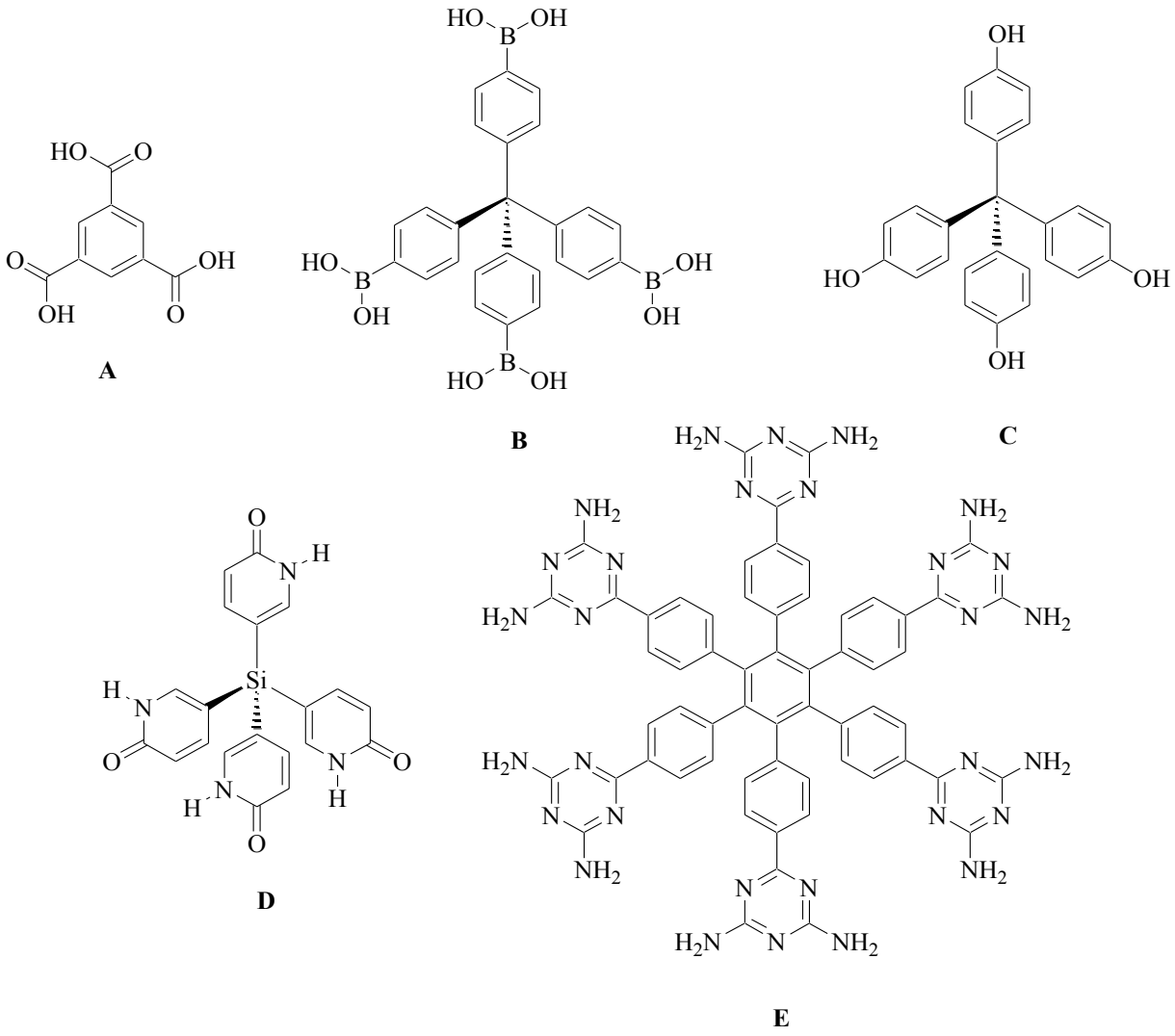

Schéma 1.2. Représentation schématique de quelques composés étudiés en ingénierie cristalline : l'acide trimésique **A**,[14] l'acide tétraboronique **B**,[15] le tétraphénol **C**,[16] le tétrapyridone **D**[17] et l'hexakis(diaminotriazine) **E**.[18]

[14] Griessl, S.; Lackinger, M.; Edelwirth, M.; Hietschold, M.; Heckl, W. M. *Single Mol***. 2002***, 3,* 25.
[15] Fournier, J.-H; Maris, T.; Wuest, J. D.; Guo, W.; Galoppini, E. *J. Am. Chem. Soc***. 2003**, *125*, 1002.
[16] Fournier, J.-H.; Maris, T.; Simard, M.; Wuest, J. D. *Cryst. Growth Des*. **2003**, *3*, 535.
[17] Wang, X.; Simard, M.; Wuest, J. D. *J. Am. Chem. Soc.* **1994**, *116*, 12119.
[18] Maly, K. E.; Gagnon, E.; Maris, T.; Wuest. J. D. *J. Am. Chem. Soc.* **2007**, *129*, 4306.

Parmi les groupements de reconnaissance impliquant des ponts hydrogène qui nous intéressent, le groupement 4,6-diamino-1,3,5-triazinyle (DAT) s'est avéré particulièrement utile. En effet, l'unité DAT peut être utilisée pour générer une grande variété de motifs par la formation de ponts hydrogène, car il comporte de nombreux sites pouvant jouer le rôle de donneur et d'accepteur de liaison hydrogène. Le Schéma 1.3 montre les principaux modes de reconnaissance par la formation de ponts hydrogène dans lesquels participent les groupements DAT. Un des avantages de ce groupe de reconnaissance est la facilité de l'introduire à différents corps moléculaires. De plus, ce groupement conduit à l'obtention de composés stables à l'air et parfois à des conditions très extrêmes. Bien que possédant des atomes d'azote, l'unité DAT est inefficace à la coordination métallique en comparaison avec d'autres groupements de reconnaissance par liaison hydrogène, ce qui permet d'éviter les réactions de compétition lors de la coordination métallique. Nous avons également choisi le groupement DAT pour sa forme planaire, car nous souhaitons élaborer des molécules pouvant être déposées sur une surface.

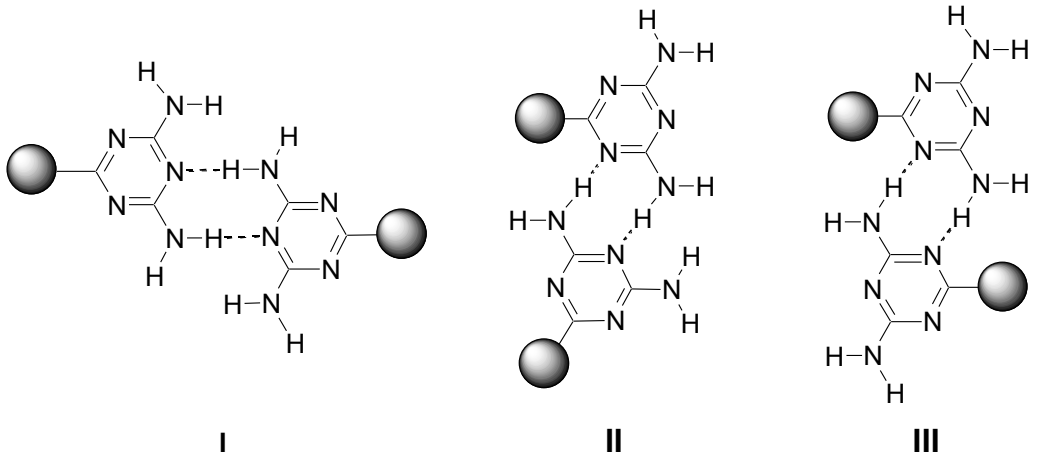

Schéma 1.3. Modes de reconnaissance principales par ponts hydrogène des groupements DAT. **I**. Face-à-face. **II**. Face-à-côté. **III**. Côté-à-côté.[19]

1.2.2 Liaison de coordination : Définition et concept

Bien que les liaisons hydrogène aient largement été employées pour la construction des édifices supramoléculaires, les liaisons de coordination sont devenues à l'heure actuelle une autre stratégie incontournable. Le concept de base a été élaboré il y a plus d'un siècle par Alfred Werner, le pionnier en chimie de coordination.[20] L'utilisation de ce concept a permis d'obtenir toute une variété de complexes par coordination de ligands organiques aux métaux avec une géométrie prévisible. L'ingénierie cristalline a exploité cette stratégie pour construire des architectures supramoléculaires comportant de nouvelles propriétés indisponibles par d'autres voies de synthèse. Les réseaux de coordination sont des architectures métallo-organiques obtenues à partir de l'assemblage d'un ligand et d'un corps métallique. L'énergie de ces liaisons

[19] Sauriat-Dorizon, H.; Maris, T.; Wuest, J. D. *J. Org. Chem*. **2003**, *68*, 240.
[20] Bowman-James, K. *Acc. Chem. Res.* **2005**, *38*, 671.

de coordination peut atteindre le 350 kJ/mol[21] et provient de l'interaction entre l'ion métallique et un hétéroatome ayant un ou plusieurs doublets libres tels que O, N, S ou P. Deux modèles ont été proposés depuis que Werner a développé le concept : (1) le modèle covalent, basé sur la théorie des orbitales moléculaires,[22] qui considère la liaison de coordination comme une liaison covalente au sens de Lewis, c'est-à-dire une mise en commun d'électrons avec l'établissement d'orbitales moléculaires liantes et anti-liantes; (2) le modèle ionique, basé sur la théorie du champ cristallin (ou encore appelé champs des ligands), qui repose sur l'existence d'interactions électrostatiques entre des doublets libres d'un hétéroatome et d'un cation métallique. Le champ cristallin généré par les ligands sur l'élément métallique provoque une dégénérescence des orbitales d du métal.[23] Cet éclatement orbitalaire varie selon la nature de l'hétéroatome donneur ainsi que selon la géométrie de coordination qu'adopte le cation métallique. La réalité est située plutôt à mi-chemin entre ces deux modèles, donc on parlera plus de pourcentage de caractères ioniques ou covalents. Dans la littérature, on retrouve de nombreux exemples d'architecture supramoléculaire obtenue à partir de la chimie de coordination telle que les métallomacrocycles,[24] les cages métalliques,[25] les hélicates,[26] les grilles,[27] les cylindres,[28] les caténanes[29] et les rotaxanes.[30] Ces complexes métallo-organiques sont présentés successivement dans les paragraphes qui suivent.

---

[21] Biradha, K. *CrystEngComm* **2003**, 5, 374.
[22] Jean, Y : *Les orbitales moléculaires dans les complexes*. Editions de l'école polytechnique, 2006.
[23] Van Vleck, J. H. *Phys. Rev*. **1932**, *41(2)*, 208.
[24] Su, C.; Goforth, A. M.; Smith, M. D.; Zur Loye, H. D. *Inorg. Chem.* **2003**, *42*, 5685. Fujita, M.; Sasaki, O.; Mitsuhashi, T.; Fujita, T.; Yasaki, J.; Yamagushi, K.; Ogura, K. *J. Chem. Soc., Chem. Commun.* **1996**, 1535. Stang, P. J.; Chen, K.; Arif, A.M. *J. Am. Chem. Soc.* **1995**, *117*, 8793.
[25] Sun, X.; Johnson, D. W.; Caulder, D. L.; Raymond, K. N.; Wong, E. H. *J. Am. Chem. Soc.* **2001**, *12*, 2752. Cross, W. I.; Godfrey, S. M.; McAuliffe, C. A.; Pritchard, R. G. *Chem. Commun.* **2001**, 1764. Park, S. J.; Hong, J. I. *Chem. Commun.* **2001**, 1554. Ikeda, A.; Udzu, H.; Zhong, Z.; Shinkai, S.; Sakamoto, S.; Yamaguchi, K. *J. Am. Chem. Soc.* **2001**, *123*, 3872. Fochi, F.; Jacopozzi, P.; Wegelius, E.; Rissanen, K.; Cozzini, P.; Marastoni, E.; Fisicaro, E.; Manini, P.; Fokkens, R.; Dalcanale, E. *J. Am. Chem. Soc.* **2001**, *123,* 7539. U. Ikeda, A.; Yoshimura, M.; Udzu, H.; Fukuhara, C.; Shinkai, S. *J. Am. Chem. Soc.* **1999**, *121*, 4296. Fox, O. D.; Dalley, N. K.; Harrison, R. G. *J. Am. Chem. Soc.* **1998**, *120*, 7111.
[26] Senegas, J.-M.; Koeller, S.; Bernardinelli, G.; Piguet, C. *Chem. Commun.* **2005**, 2235.
Ronson, T. K.; Adams, H.; Ward, M. D. *Inorg. Chim. Acta* **2005**, *358*, 1943.
[27] Fischer, J.; Youinou, M. T. *Angew. Chem., Int. Ed. Engl.* **1994**, *33*, 2284.

1.2.2.1 Les assemblages moléculaires finis

Les assemblages moléculaires finis sont des entités métallo-organiques discrètes obtenues par coordination de ligands à des métaux.[31] Les métallomacrocycles, les cages, les caténanes, les rotaxanes, les hélicates, les grilles et les cylindres peuvent faire partie de cette catégorie d'entités moléculaires finies. Des exemples d'architectures de ces entités sont présentés ci-dessous. Pour plus de clarté, les structures cristallographiques seront parfois simplifiées, marquées par des couleurs différentes, et les hydrogènes ainsi que les contre-ions seront parfois volontairement omis. Les métallomacrocycles sont des entités finies comportant une partie organique et un centre métallique où sont impliqués des ligands multidentates rigides permettant de relier de façon cyclique les métaux par des liens de coordination. Un des exemples les plus majestueux a été réalisé par le groupe de Fujita. Dans leur travail, une architecture finie de type carré a été élaborée à partir d'un ligand linéaire ditopique (une bipyridine) lié à un métal de géométrie carrée dont deux positions de la sphère de coordination sont occupées par un ligand chélatant, laissant deux autres à 90^{o} pour la coordination des bipyridines (Figure 1.3). D'autres topologies de métallomacrocycle peuvent être encore construites par cette méthode, à savoir la topologie pentagonale, hexagonale et encore bien d'autres (Figure 1.4).

---

[28] Baxter, P. N. W.; Lehn, J.-M.; De Cian, A.; Fischer, J. *Angew. Chem., Int. Ed. Engl.* **1993**, *32*, 69. Baxter, P. N. W.; Lehn, J.-M.; Kneisel, B. O.; Baum, G.; Fenske, D. *Chem. Eur. J.* **1999**, *5*, 113.

[29] Wong, W. W. H.; Cookson, J.; Evans, E. A. L.; McInnes, E. J. L.; Wolowska, J.; Maher, J. P.; Bishop, P.; Beer, P. D. *Chem. Commun.* **2005**, 2214. Dietrich-Buchecker, C.; Geum, N.; Hori, A. Fujita, M.; Sakamoto, S.; Yamaguchi, K.; Sauvage, J.-P. *Chem. Commun.* **2001**, 1182.

[30] Sauvage, J.-P. *Chem. Commun.* **2005**, 1507.

[31] Blight, B. A.; Wisner, J. A.; Jennings, M. C. *Inorg. Chem*. **2009**, *48*, 1920. Ozaki, Y.; Kawano, M.; Fujita, M. *Chem. Commun*. **2009**, 4245. Blight, B. A.; Wisner, J. A.; Jennings, M. C. *Angew. Chem., Int. Ed*. **2007**, *46*, 2835. Hoffart, D. J.; Loeb, S. J. *Angew. Chem., Int. Ed.* **2005**, *44*, 901. Leigh, D. A.; Lusby, P. J.; Slawin, A. M. Z.; Walker, D. B. *Angew. Chem., Int. Ed.* **2005**, *44*, 4557. Kumazawa, K.; Biradha, K.; Kusukawa, T.; Okano, T.; Fujita, M. *Angew. Chem., Int. Ed.* **2003**, *42*, 3909. Ovitt, T. M.; Coates, G. W.; *J. Am. Chem. Soc.* **2002**, *124,* 1316.

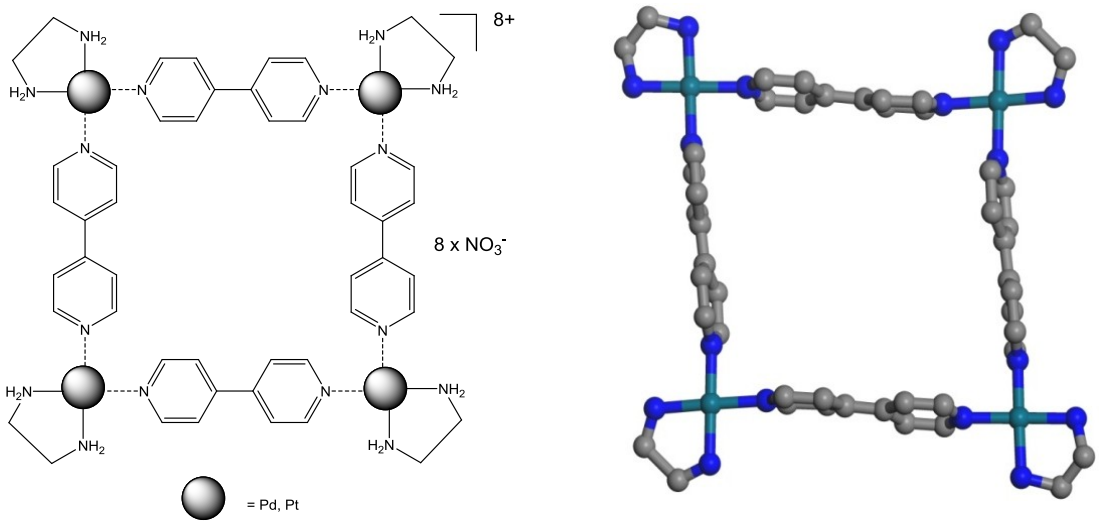

Figure 1.3. Conception d'un métallomacrocycle. (a) Schéma montrant un métallomacrocycle de forme carré. (b) Représentation de la structure cristallographique du métallomacrocycle en boules et bâtonnets.[32] Les atomes d'hydrogène ainsi que les contres-ions ont été enlevés pour plus de clarté. Les atomes de carbone sont représentés en gris, l'azote en bleu et le palladium en vert.

[32] Fujita, M.; Sasaki, O.; Mitsuhashi, T.; Fujita, T.; Yazaki, J.; Yamaguchi, K.; Ogura, K. *Chem. Commun*. **1996**, 1535. Fujita, M.; Yazaki, J.; Ogura, K. *J. Am. Chem. Soc*. **1990**, *112(14)*, 5645.

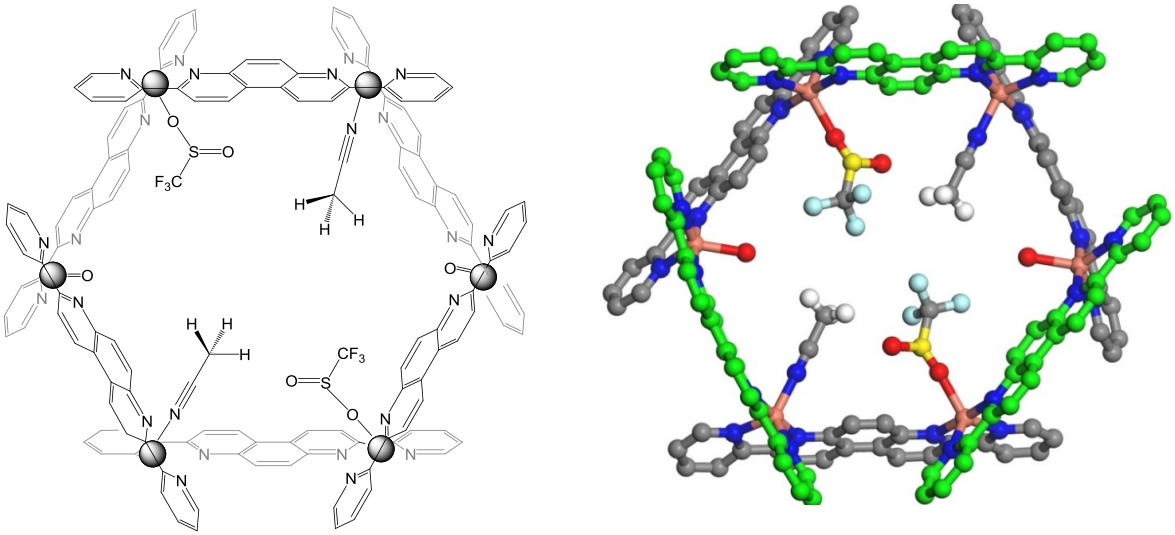

a **b**

Figure 1.4. (a) (a) Schéma montrant un métalloamacrocycle de forme hexagonale. (b) Représentation de la structure cristallographique d'un métallomacrocycle de topologie hexagonale comportant six atomes de cuivre en boules et bâtonnets.[33] Pour plus de clarté, certains ligands ont été coloriés en vert et certains hydrogènes ainsi que les contres-ions ont été enlevés. Les atomes de carbone sont représentés en gris, l'hydrogène en blanc, l'azote en bleu, l'oxygène en rouge, le soufre en jaune, le fluor en bleu pâle et le cuivre en rose excepté dans les ligands marqués.

La stratégie pour la construction des metallacages est similaire que celle pour les métallomacrocycles, sauf que la géométrie des constituants doit permettre l'obtention d'une structure tridimensionnelle. La Figure 1.5 illustre un exemple de métallocage dont la structure a été déterminée par le groupe de Fujita.[34]

[33] Baxter, P. N. W.; Khoury, R. G.; Lehn, J.-M; Baum, G.; Fenske, D. *Chem. Eur. J.* **2000**, *6,* 4140.
[34] Kusukawa, T.; Fujita, M. *J. Am. Chem. Soc*. **2002**, *124*, 13576.

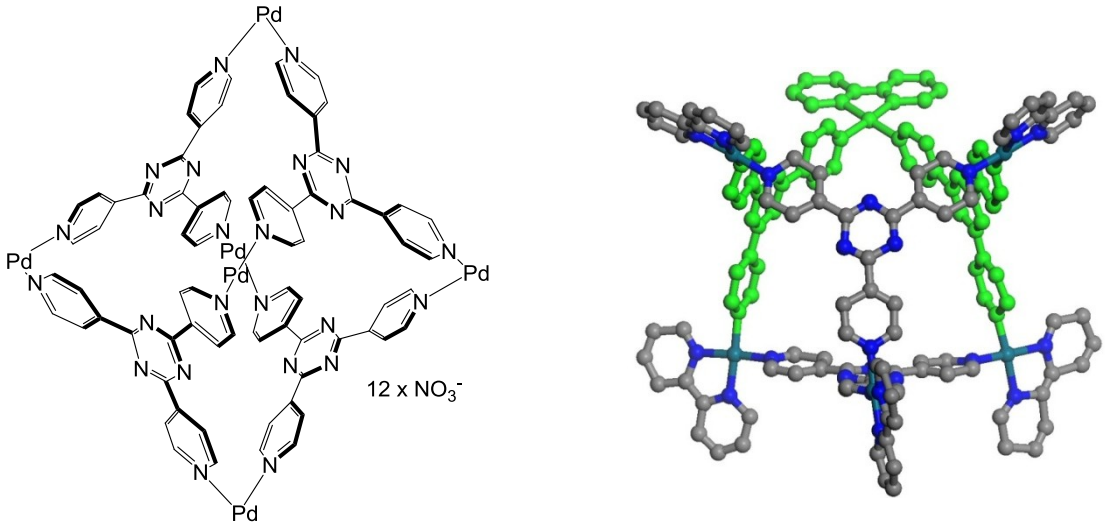

a **b**

Figure 1.5. Conception d'une métallocage. (a) Schéma montrant une métallocage. (b) Représentation de la structure cristallographique de la métallocage comportant six atomes de Pd(II) en boules et bâtonnets. Pour plus de clarté, certains ligands ont été coloriés en vert et certains hydrogènes ainsi que les contres-ions ont été enlevés. Les atomes de carbone sont représentés en gris, l'azote en bleu et le palladium en vert foncé excepté dans les molécules marquées.

Les hélicates sont des complexes hélicoïdaux discrets dont la construction est typiquement basée sur l'emploi de ligands pouvant s'enrouler autour du métal. De nombreuses structures en double hélice di- et trinucléaires ont été formées à partir de ligands de type oligopyridine. Lehn et collaborateurs ont rapporté la synthèse d'hélicate circulaire pentanucléaire (Figure 1.6) obtenu par enroulement d'oligobipyridine autour des atomes de Fe(II).[35]

[35] Hasenknopf, B.; Lehn, J.–M.; Kneisel, B. O.; Baum, G.; Fenske, D. *Angew. Chem., Int. Ed*. **1996**, *35*, 1838.

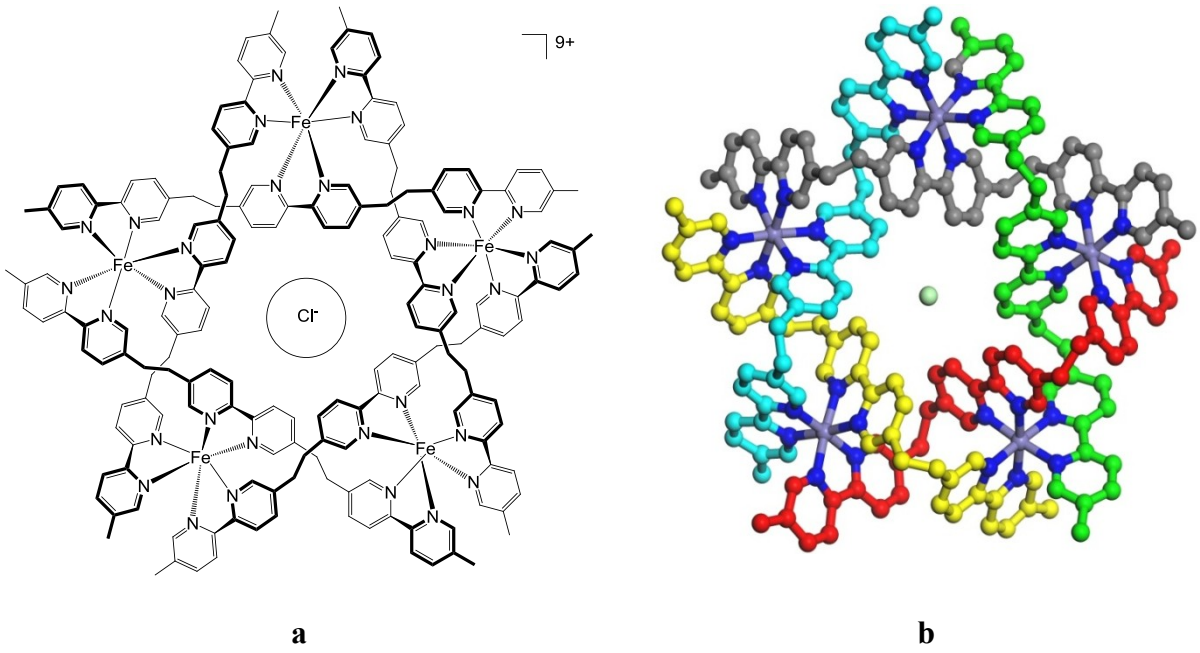

a **b**

Figure 1.6. Auto-assemblage circulaire de double hélice. (a) Représentation de la structure assemblée. (b) Sa structure cristallographique représentée en boules et bâtonnets. Pour plus de clarté, certains ligands ont été coloriés en vert, jaune et bleu clair et les hydrogènes ainsi que les contres-ions ont été enlevés. Les atomes de carbone sont représentés en gris, l'azote en bleu, le chlore en vert pâle et le fer en mauve, sauf dans les molécules marquées.

Les grilles[36] et les cylindres[37] moléculaires caractérisés jusqu'à présent sont typiquement construits à partir de polypyridines. Ces entités sont édifiées à partir de ligands rigides connectés entre eux par des métaux. Le design du ligand ainsi que la géométrie de coordination autour du

[36] Ruben, M.; Breuning, E.; Lehn, J.–M.; Ksenofontov, V.; Renz, F.; Guetlich, P.; Vaughan, G. B. M. *Chem. Eur. J.* **2003,** *9*, 4422. Breuning, E.; Ruben, M.; Lehn, J.–M.; Renz, F.; Garcia, Y.; Ksenofontov, V.; Gutlich, P.; Wegelius, E.; Rissanen, K. *Angew. Chem., Int. Ed.* **2000**, *39*, 2504. Rojo, J.; Romero-Salguero, F. J.; Lehn, J.–M.; Baum, G.; Fenske, D. *Eur. J. Inorg. Chem*. **1999**, *9*, 1421. Garcia, A. M.; Romero-Salguero, F. J.; Bassani, D. M.; Lehn, J.–M.; Baum, G.; Fenske, D. *Chem. Eur. J*. **1999**, *5*, 1803. Hanan, G. S.; Volkmer, D.; Schubert, V. S.; Lehn, J.-M.; Baum, G.; Fenske, D. *Angew. Chem., Int. Ed.* **1997**, *36*, 1842.

[37] Baxter, P.; Lehn, J.-M.; DeCian, A.; Fischer, J. *Angew. Chem., Int. Ed. Engl*. **1993**, *32*, 89. Baxter, P. N. W.; Lehn, J.–M.; Kneisel, B. O.; Baum, G.; Fenske, D. *Chem. Eur. J*. **1999**, *5*, 113. Marquis-Rigault, A.; Dupont-Gervais, A.; Baxter, P. N. W.; Van Dorsselaer, A.; Lehn, J.-M. *Inorg. Chem*. **1996**, *35*, 2307.

métal déterminent la topologie de l'édifice. La coordination d'une polypyridine en zig-zag à un métal de géométrie octaédrique a permis de construire des grilles moléculaires (Figure 1.7). Les cylindres moléculaires sont quant à eux obtenus à partir de deux types de ligands. Des chaines de bipyridine servent de poutre et des plateaux sont constitués de ligands tritopiques tels qu'est illustré à la Figure 1.8.

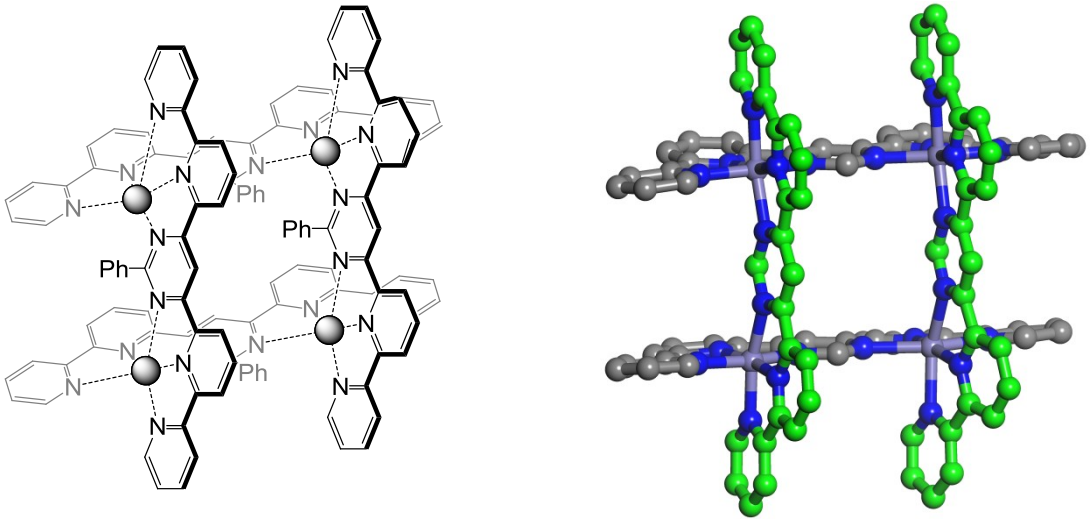

a **b**

Figure 1.7. Schéma d'une grille. (b) Sa structure cristallographique représentée en boules et bâtonnets. Pour plus de clarté, certains ligands ont été partiellement coloriés en vert et les groupements phenyles ont été omit. Les atomes de carbone sont représentés en gris, l'azote en bleu et le fer en mauve sauf dans les molécules marquées.

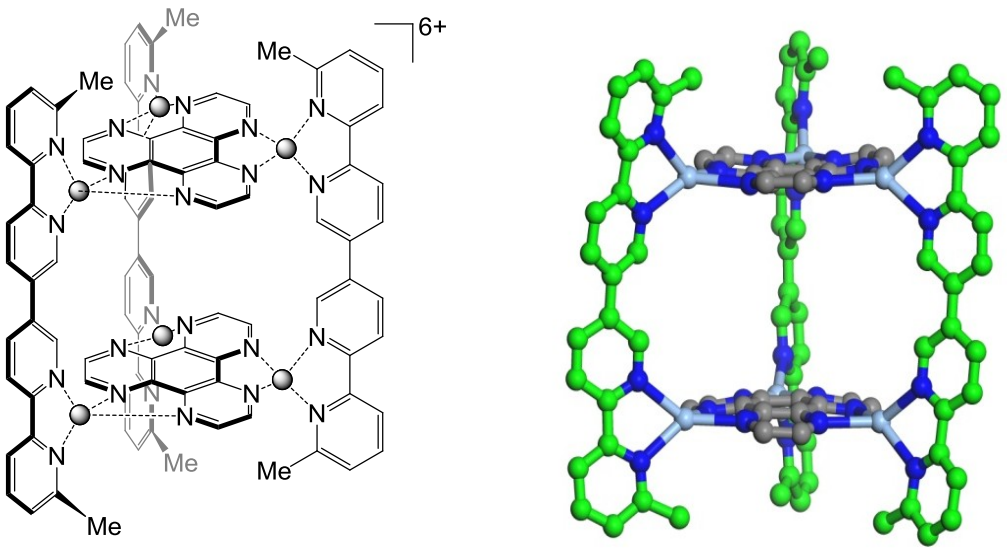

Figure 1.8. (a) Schéma d'un cylindre. (b) Structure cristallographique représentée en boules et bâtonnets. Pour plus de clarté, certains ligands ont été coloriés en vert et les contres-ions ont été omis. Les atomes de carbone sont représentés en gris, l'azote en bleu et l'argent en mauve pâle sauf dans les molécules marquées.

Pour finir cette présentation sur les différentes architectures discrètes, nous terminons par les anneaux moléculaires, dont les rotaxanes et les caténanes. Dans ce domaine d'anneau moléculaire, on peut citer les travaux des groupes de Sauvage et Stoddart. Les rotaxanes sont formés à partir de chaînes moléculaires qui passent irréversiblement à travers un ou plusieurs macrocycles. Les scientifiques s'intéressent à leur obtention, car ils peuvent servir de modèles de moteurs moléculaires. Le groupe de Sauvage a proposé la synthèse d'un rotaxane comportant quatre macrocycles maintenus ensembles par deux ligands linéaires.[38] La structure

[38] Frey, J.; Tock, C.; Collin, J. P; Heitz, V.; Sauvage, J.-P.; Rissanen, K. *J. Am. Chem. Soc*. **2008**, *130*, 11013.

cristallographique, représentée à la Figure 1.9, montre que l'enfilement des ligands linéaires à travers les macrocycles est assuré par des liens de coordination.

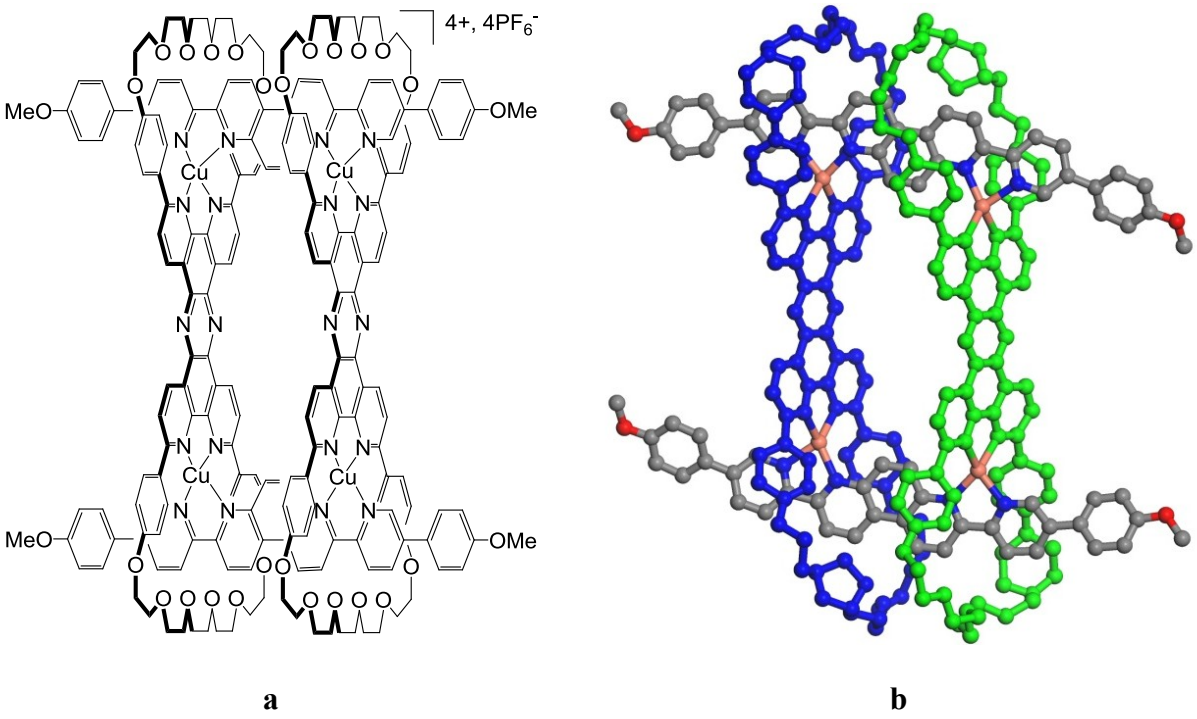

a **b**

Figure 1.9. Rotaxane formé par liaisons de coordination aux atomes de cuivre. (a) Schéma d'un double rotaxane. (b) Sa structure cristallographique représentée en boules et bâtonnets. Pour plus de clarté, les macrocycles ont été coloriés en vert et bleu et les hydrogènes et les contres-ions ont été omis. Les atomes de carbone sont représentés en gris, l'azote en bleu, l'oxygène en rouge et le cuivre en rose pâle, sauf dans les molécules marquées.

Les caténanes sont formés de deux ou plusieurs macrocycles interconnectés. Par coordination, en utilisant deux centres métalliques différents, il est possible d'avoir des anneaux interconnectés. Un exemple d'architecture interconnectée impliquant trois macrocycles a été

rapporté par le groupe de Stoddart. Un caténane appelé Borroméen est obtenu par coordination avec le Zn(II).[39] Il s'agit de trois macrocycles obtenus par coordination de ligands cycliques. La structure cristallographique du caténane Borroméen est montrée à la Figure 1.10.

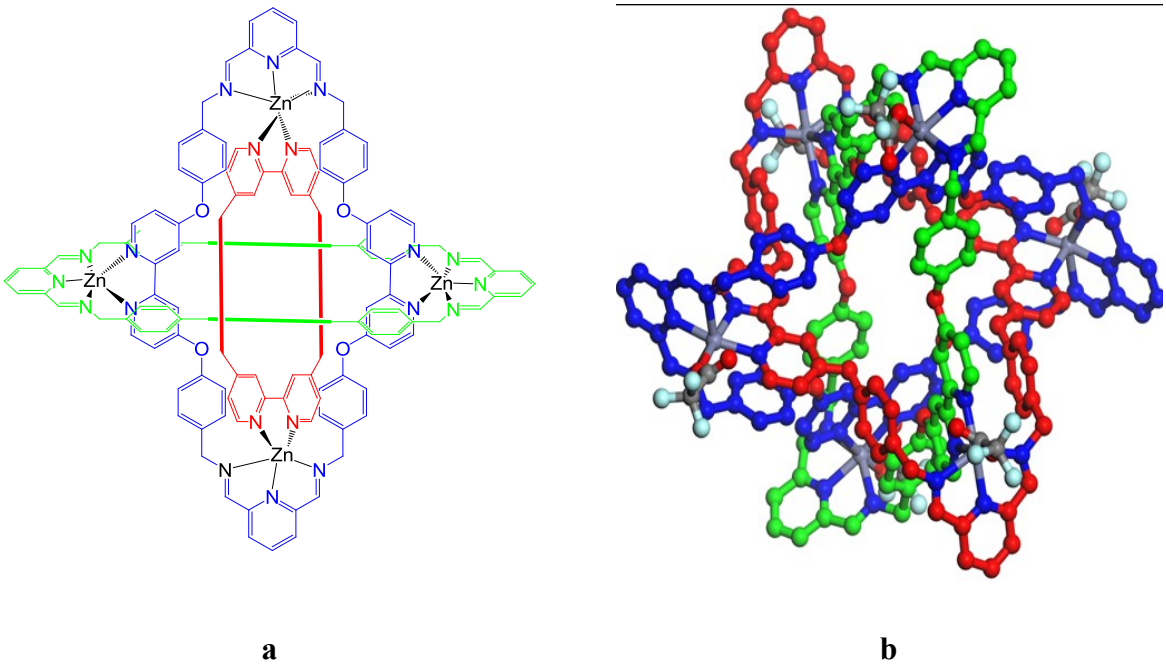

a **b**

Figure 1.10. (a) Schéma d'un caténane Borroméen à trois cycles. (b) Sa structure moléculaire montrant comment les trois macrocycles sont interconnectés par les liaisons de coordination avec le Zn(II). Pour plus de clarté, certains ligands ont été coloriés en vert, bleu foncé et rouge et certains hydrogènes ainsi que les contres-ions ont été enlevés. Les atomes d'azote sont représentés en bleu, l'oxygène en rouge, le fluor en bleu pâle et le zinc en violet.

[39] Meyer, C. D.; Joiner, C. S.; Stoddart, J. F. *Chem. Soc. Rev*. **2007**, *36,* 1705. Chichak, K. S.; Peters, A. J.; Cantrill, S. J.; Stoddart, J. F. *J. Org. Chem*. **2005**, *70*, 7956. Peters, A. J.; Chichak, K. S.; Cantrill, S. J.; Stoddart, J. F. *Chem. Commun.* **2005**, 3394. Chichak, K. S.; Cantrill, S. J.; Stoddart, J. F. *Chem. Commun.* **2005**, 3391.Chichak, K. S.; Cantrill, S. J.; Pease, A. R.; Chiu, S.-H.; Cave, G. W. V.; Atwood, J. L.; Stoddart, J. F. *Science* **2004**, *304*, 1308.

1.2.2.2 Les assemblages moléculaires infinis[40]

L'obtention d'un réseau moléculaire métallo-organique infini de coordination par auto-assemblage nécessite un processus répétitif de coordination ayant pour constituant un ligand et un métal. Ces réseaux peuvent donc être vus comme une association de ligands reliés entre eux par des métaux. La topologie des réseaux est définie par la géométrie du ligand et celle du métal. Les propriétés diverses de ces réseaux justifient l'effort énorme consacré à leur élaboration. Cependant, le contrôle de la topologie et la dimension de ces structures reste un défi difficile à maîtriser.

a) Les réseaux moléculaires 1D :

Deux catégories peuvent être distinguées : (1) les fils simples, se présentant sous la forme de topologie soit linéaire, ondulée, en zig-zag, en créneau ou en hélice et (2) les fils multiples comportant comme le nom l'indique au moins deux brins souvent entrelacés ou sous forme d'hélices multiples.

Les fils simples sont généralement construits par des ligands bidentates, le métal servant de pontage entre les ligands disposés en file indienne. Un exemple de fil simple est montré à la

[40] Deiters, E.; Bulach, V.; Wais Hosseini, M. *New J. Chem*. **2008**, *32(1),* 99. Chae, H.; Siberio-Perez, D. Y.; Kim, J.; Go, J.; Eddaoudi, M.; Matzger, A.; O'Keeffe, M.; Yaghi, O. M. *Nature* **2004**, *427*, 523. Ohmori, O.; Kawano, M.; Fujita, M. *Angew. Chem., Int. Ed*. **2005**, *44*, 1962. Ohmori, O.; Kawano, M.; Fujita, M. *J. Am. Chem. Soc*. **2004**, *126*, 16292. Eddaoudi, M.; Kim, J.; Rosi, N.; Vodak, D.; O'Keeffe, M.; Yaghi, O. M. *Science* **2002**, *295*, 469. Klein, C.; Graf, E.; Wais Hosseini, M. *New J. Chem*. **2001**, *25(2),* 207. Biradha, K.; Hongo, Y.; Fujita, M. *Angew. Chem., Int. Ed.* **2000**, *39*, 3843.

Figure 1.11. Les atomes d'Ag(I) sont connectés entre eux par la 4,4'-bipyridine pour donner une topologie linéaire.[41]

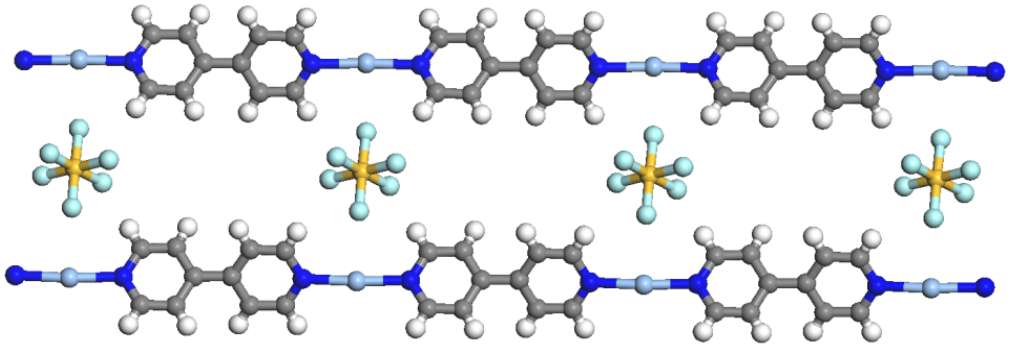

Figure 1.11. Représentation de la structure cristallographique en boules et bâtonnets d'un réseau moléculaire 1D de topologie linéaire. Les atomes de carbone sont représentés en gris, l'azote en bleu, le fluor en bleu pâle, le phosphore en jaune et l'argent en mauve pâle.

b) Les réseaux moléculaires 2D :

Dans la catégorie des réseaux moléculaires 2D, on peut citer les grilles dont les formes sont variables telles que les carrés, les rectangles, les losanges et les hexagones. Un réseau de coordination 2D en forme de grille a été décrit par Fujita et collaborateurs,[42] qui ont utilisé un ligand ditopique coordonné avec du Ni(II) (Figure 1.12).

[41] Mantero, D. G.; Neels, A.; Stoeckli-Evans, H. *Acta Crystallogr*. **2006**, *E62*, 1381.
[42] Biradha, K.; Fujita, M. *Dalton Trans.* **2000**, *21*, 3805.

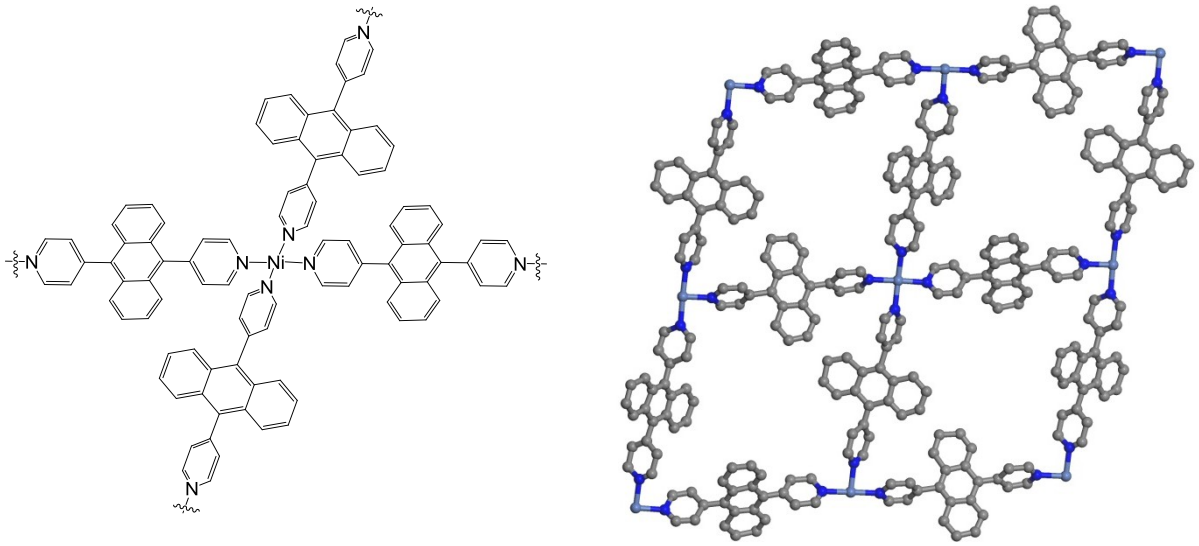

a **b**

Figure 1.12. Réseau moléculaire 2D infini. (a) Schéma montrant la coordination autour du Ni(II). (b) Représentation en boules et bâtonnets de sa structure 2D en forme de grille. Pour plus de clarté, les hydrogènes ainsi que les contres-ions ont été enlevés. Les atomes de carbone sont représentés en gris, l'azote en bleu et le nickel en bleu pâle.

c) Les réseaux moléculaires 3D :

Les réseaux moléculaires 3D sont des architectures présentant le plus grand degré de dimensionnalité et de complexité. De ce fait, la construction de ces réseaux est souvent difficile à réaliser, à prévoir et à analyser, surtout à cause de la possibilité que les réseaux s'interpénètrent. La Figure 1.13 montre une structure cristallographique en forme de prisme dont la base est

construite de l'acide benzène-1,3,5-tricarboxylique et les côtés sont formés des ligands bidentates de type bipyridine.[43]

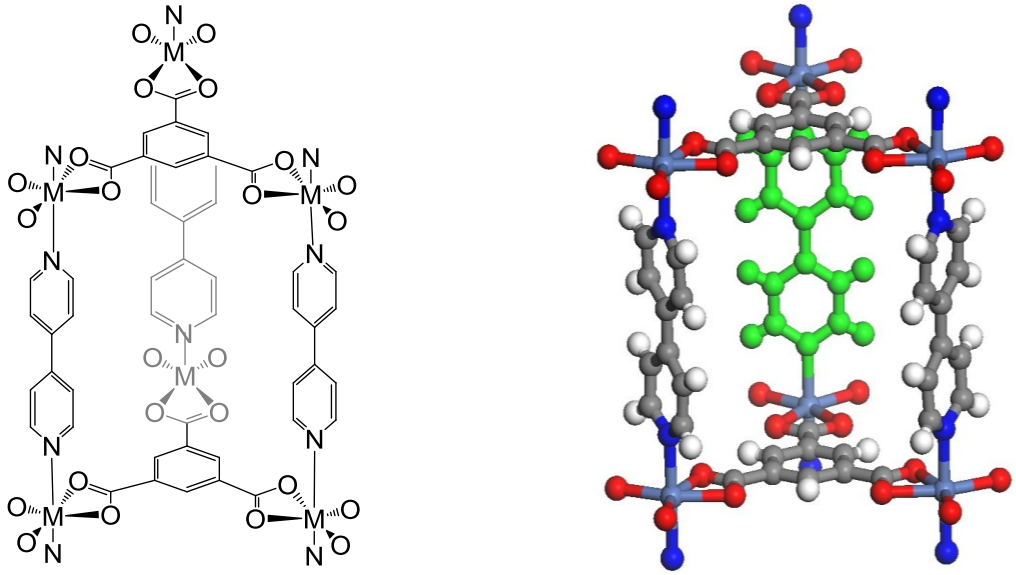

a **b**

Figure 1.13. Réseau moléculaire 3D infini. (a) Représentation schématique de l'unité de base en forme de prisme triangulaire. (b) Sa structure cristallographique représentée en boules et bâtonnets. Pour plus de clarté, un ligand a été marqué en vert. Les atomes de carbone sont représentés en gris, l'azote en bleu, l'oxygène en rouge et le nickel en violet pâle, sauf que dans les ligands 4,4-bipyridine qui sont coloriés en vert.

[43] Gao, C.; Liu, S.; Xie, L.; Ren, Y.; Cao, J.; Sun, C. *CrystEngComm* **2007**, *9*, 545.

1.3 La tectonique moléculaire

Inspirés par les observations de la tectonique des plaques et par les concepts de la tectonique en architecture, Wuest et collaborateurs ont introduit pour la première fois en 1991 la stratégie de la tectonique moléculaire.[44] Ce concept repose sur l'auto-assemblage spontané de molécule dite intelligente qu'ils ont appelé *tecton*. Ces molécules intègrent des sites de reconnaissance directionnelle ayant pour capacité de s'auto-assembler de manière prédictible.[45] Le processus d'association de ces tectons met souvent en opposition deux forces importantes : (1) celle impliquant des interactions van der Waals et favorisant un empilement moléculaire compact et (2) celle dirigée par des interactions intermoléculaires directionnelles, favorisant ainsi une structure qui n'est pas nécessairement conforme à la tendance naturelle des molécules à former un empilement compact dans des phases condensées. Ces interactions spécifiques et directionnelles sont souvent dominantes, donc le processus d'auto-assemblage régi par les sites de reconnaissance moléculaire des tectons mène typiquement à la formation de réseaux supramoléculaires ouverts (Figure 1.14).

[44] Simard, M.; Su, D.; Wuest, J. D. *J. Am. Chem. Soc*. **1991**, *113*, 4696.
[45] Wang, X.; Simard, M.; Wuest, J. D. *J. Am. Chem. Soc.* **1994**, *116*, 12119. Ermer, O. *J . Am. Chem. Soc.* **1989,** *110*, 3747. Brunet, P.; Demers, E.; Maris, T.; Enright, G. D.; Wuest, J. D. *Angew. Chem. Int. Ed.* **2003**, *42*, 5303.

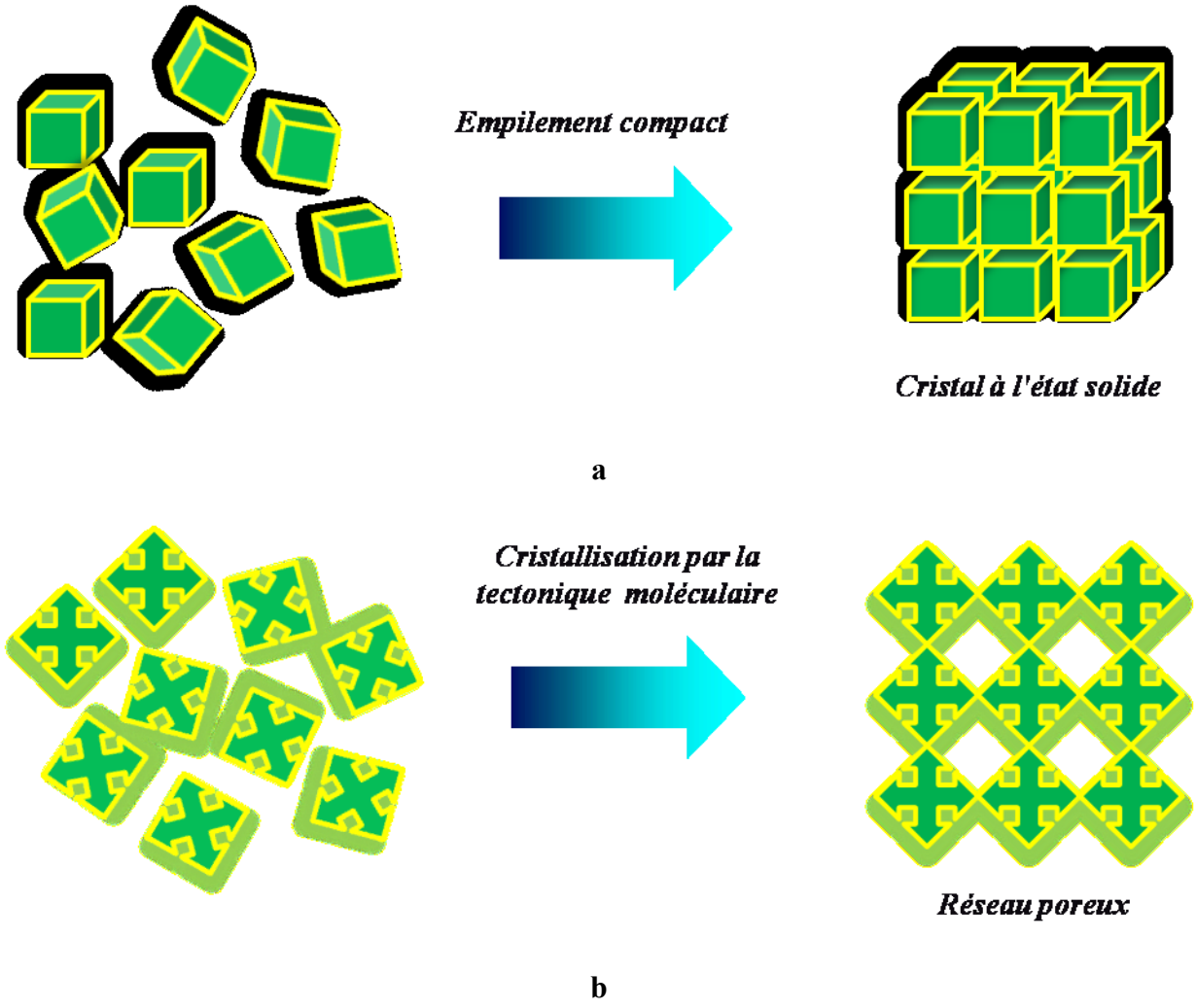

Figure 1.14. (a) Représentation schématique de la tendance naturelle des molécules normales à former un empilement compact. Les molécules, symbolisées par des cubes, formeront préférentiellement un arrangement compact qui maximise les interactions de van der Waals et minimise la présence d'espace vide, défavorisé énergétiquement. (b) Formation d'un réseau supramoléculaire par la stratégie de la tectonique moléculaire. Les molécules, symbolisées par les croix, représentent les tectons, dont les interactions sont dominées par des forces spécifiques et directionnelles.

En utilisant la stratégie de la tectonique moléculaire, il est possible de former des réseaux de topologies variées telles que hexagonale,[46] diamantoïde[36] et beaucoup d'autres. Quelle que soit l'architecture adoptée par le cristal, le processus d'assemblage spontané laisse généralement de l'espace libre pour l'inclusion de molécules invitées. Ces cavités ne sont pas normalement vides et sont le plus souvent occupées par des molécules de solvants utilisés lors de la cristallisation. Un exemple de 1997 démontre bien l'utilité de la tectonique moléculaire dans la formation de réseaux poreux, illustré par la cristallisation de la tétrakis(diaminotriazine) **F** comme unité tectonique (Figure 1.15).[47] Sa structure cristallographique a été résolue par diffraction des rayons-X de monocristaux obtenus dans un mélange d'acide formique et de dioxane. Le réseau poreux obtenu à l'issu de cet auto-assemblage présente 63% du volume occupé par des molécules invitées. Cette structure démontre que l'utilisation de la tectonique moléculaire permet d'avoir des architectures robustes bien que sa formation ne repose pas sur une cristallisation compacte (voir Figure 1.14) et sur des interactions covalentes.

[46] Melendez, R. E.; Sharma, C. V. K.; Zaworotko, M. J.; Bauer, C.; Rogers, R. D. *Angew. Chem., Int. Ed. Engl*. **1996**, *35*, 2213.
[47] Brunet, P.; Simard, M.; Wuest, J. D. *J. Am. Chem. Soc.* **1997**, *119*, 2737.

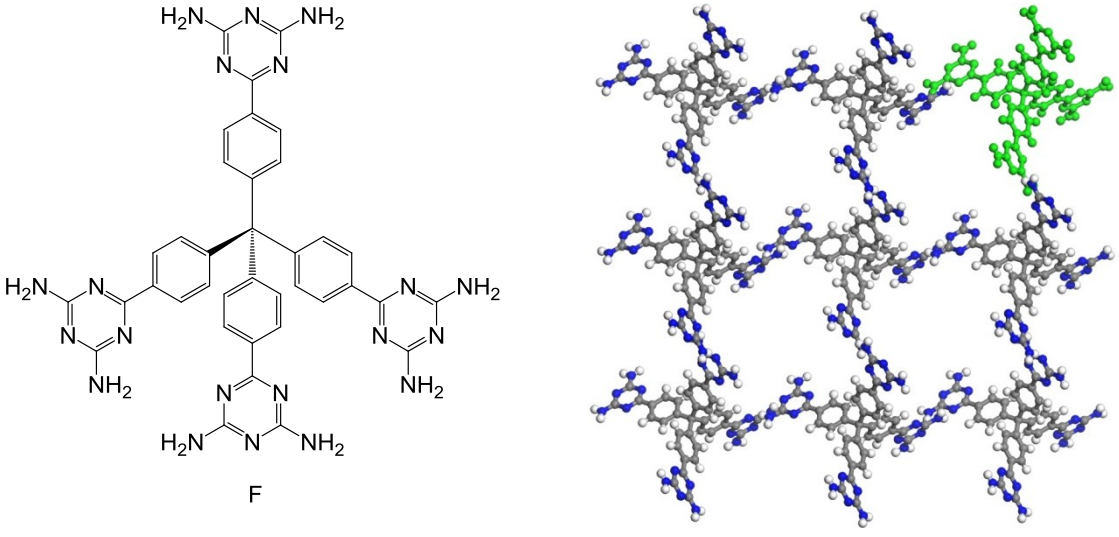

Figure 1.15. Réseau 3D. **(**a) Tecton **F**. (b) Structure cristallographique du réseau obtenu par la cristallisation du tecton **F**. Pour plus de clarté, un tecton a été colorié en vert et les molécules invitées de solvants ont été omises. Les atomes de carbones sont représentés en gris et l'azote en bleu sauf pour le tecton colorié en vert.

La tectonique moléculaire est devenue aujourd'hui une stratégie incontournable pour la conception de nouveaux matériaux. Différents types d'interactions faibles peuvent être employés pour diriger l'auto-assemblage. En particulier, on peut citer le potentiel des ponts hydrogène qui a largement été utilisé dans ce domaine, car les interactions sont directionnelles et robustes. En plus des groupements de reconnaissance moléculaire, les chercheurs se sont également attardés à étudier les unités centrales des tectons car elles déterminent l'orientation des sites de reconnaissance. Par exemple, Wuest et collaborateurs ont étudié une panoplie d'unités centrales dont la géométrie et la rigidité ont été variées de manière systématique. Des tectons basés sur des

cœurs de carbone sp^3,[48] de silicium,[49] de bore,[50] de carbone sp^2,[51] et bien d'autres ont fait l'objet de plusieurs études.

Cette approche a montré son utilité, mais un problème se pose : les tectons sont parfois difficiles à préparer et nécessitent dans la plupart des cas de nombreuses étapes de synthèse, ce qui empêche ou limite leur mise en application pratique. De plus, une fois formées, les liaisons unissant le corps central et les groupements de reconnaissance moléculaire ne peuvent plus être rompues, ce qui ne permet pas de remodeler le tecton par une procédure synthétique simple. Récemment, une stratégie combinant la chimie de coordination et d'autres interactions intermoléculaires a été proposée pour la synthèse des tectons. Cette méthode consiste à synthétiser des ligands possédant à la fois des sites de coordination et de reconnaissance moléculaire qui agissent sélectivement de manière orthogonale. Une fois que les sites de coordination sont liés au métal, les sites de reconnaissance inter-complexe (par exemple, des sites offrant la possibilité de former des ponts hydrogène) interagissent de façon normale, dirigée par la géométrie de coordination autour du métal prédite par la chimie théorique et observée dans des complexes plus simples déjà caractérisés. L'entité obtenue par cette stratégie est appelée *métallotecton*, qui est en fait un tecton mais dont le cœur est un complexe métallique. Cette stratégie est avantageuse, car elle donne accès à une panoplie de métallotectons, simplement en mélangeant un même ligand avec différents métaux, ce qui diminue considérablement le nombre d'étapes de synthèse et augmente la diversité moléculaire par une approche potentiellement combinatoire. De plus, la présence des métaux peut apporter de nouvelles propriétés aux

[48] Demers, E.; Maris, T.; Wuest, J. D. *Cryst. Growth Des*. **2005**, *5*, 1227.
[49] Saied, O.; Maris, T.; Simard, M.; Wuest, J. D. *Acta Crystallogr*. **2005**, *E61*, 4136.
[50] Malek, N.; Maris, T.; Simard, M.; Wuest, J. D. *J. Am. Chem. Soc.* **2005**, *129*, 5910.
[51] Maly, K. E; Gagnon, E.; Maris T.; Wuest, J. D. *J. Am. Chem. Soc*. **2007**, *129*, 4306.

matériaux comme, par exemple, l'activité catalytique, la fluorescence ou le magnétisme. Plusieurs exemples de cette stratégie ont été réalisés dans différents groupes de recherche. Un exemple de métallotectons tiré des travaux du groupe Wuest est montré à la Figure 1.16. Un ligand bidentate de la famille des pyrroles comportant des groupements DAT a été coordonné à un centre de Co(II) de géométrie octaédrique pour donner un métallotecton chiral. L'association inter-complexe des groupements DAT a fourni une structure en hexagone.[52]

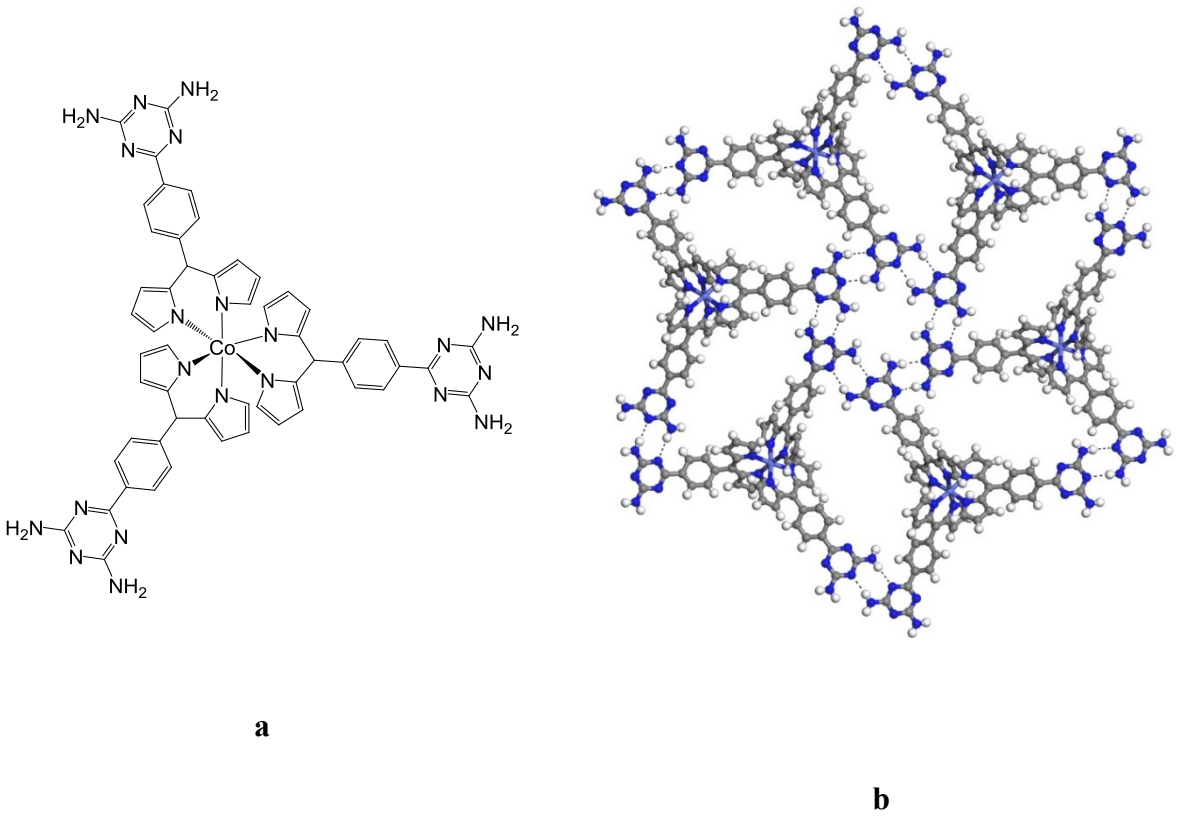

Figure 1.16. **(**a) Schéma du métallotecton au Co(II). (b) Sa structure cristallographique représentée en boules et bâtonnets. Les atomes de carbone sont représentés en gris, l'azote en bleu, l'hydrogène en blanc et le cobalt en bleu pâle.

[52]Telfer, S. G.; Wuest, J. D. *Chem. Commun*. **2007**, 3166.

La stratégie de la tectonique moléculaire, développée initialement pour contrôler l'organisation à l'intérieur des solides cristallins, s'applique également à diriger l'organisation 3D en phases moins bien organisées, ainsi qu'à contrôler la structure 2D des molécules adsorbées sur des surfaces.[53] L'organisation contrôlée en 2D promet d'avoir des applications dans plusieurs domaines, dont la catalyse hétérogène et la nanotechnologie. Avec les avancées technologiques, la cristallisation des molécules en 2D peut être observée directement par microscopie à balayage à effet tunnel (STM). Pour contrôler la topologie de la surface, la tectonique moléculaire peut être mise en œuvre.

Dans cette thèse, nous décrivons notre recherche sur des ligands pouvant être utilisés pour la synthèse de métallotectons et sur l'utilisation de ces structures pour générer des architectures en 3D et en 2D. Le contrôle de la cristallisation en 3D dirigée par l'approche d'auto-assemblage par des interactions faibles a largement été étudié et caractérisé à l'aide de la diffraction des rayons-X. Ce n'est que depuis les trente dernières années que l'organisation 2D des molécules a pu être observée, grâce à l'invention de la STM sous haute vide (UHV)[54] ou à l'interface solide-liquide.[55] Étant donné que la STM sera utilisée intensivement dans notre étude, nous proposons dans cette thèse une brève présentation de ses principes de base.

---

[53] Zhou, H.; Dang, H.; Yi, J. -H.; Nanci, A.; Rochefort, A.; Wuest, J. D. *J. Am. Chem. Soc*. **2007**, *129*, 13774. Dang, H.; Maris, T.; Yi, J.-H.; Rosei, F.; Nanci, A.; Wuest, J. D. *Langmuir* **2007**, *23*, 11980. Nath, K. G.; Ivasenko, O.; Miwa, J. A.; Dang, H.; Wuest, J. D.; Nanci, A.; Perepichka, D. F.; Rosei, F. *J. Am. Chem. Soc*. **2006**, *128*, 4212.

[54] Classen, T.; Lingenfelder, M.; Wang, Y.-L.; Chopra, R.; Virojanadara, C.; Starke, U.; Costantini, G.; Fratesi, G.; Fabris, S.; Baroni, S.; Haq, S.; Raval, R.; Kern, K. *J. Phys. Chem*. *A* **2007**, *111*, 12589. Barth, J. V.; Weckesser, J.; Lin, N.; Dmitriev, A.; Kern, K. *Appl. Phys*. *A* **2003**, *76*, 645. Messina, P.; Dmitriev, A.; Lin, N.; Spillmann, H.; Abel, M.; Barth, J. V.; Kern, K. *J. Am. Chem. Soc*. **2002**, *124*, 14000. Li, Z.; Han, B.; Wan, L.; Wandlowski, T. *Langmuir* **2005**, *21*, 6915. Su, G.-J.; Zhang, H.-M.; Wan, L.-J.; Bai, C.-L.; Wandlowski, T. *J. Phys. Chem*. *B* **2004**, *108*, 1931.

[55] Lackinger, M.; Griessl, S.; Heckl, W. M.; Hietschold, M.; Flynn, G. W. *Langmuir* **2005**, *21*, 4984. Lackinger, M.; Griessl, S.; Kampschulte, L.; Jamitzky, F; Heckl, W. M. *Small* **2005**, *5*, 532.

1.4 Microscopie à effet tunnel

La STM a été développée en 1982 par le groupe de recherche du laboratoire IBM de Zurich.[56] La technique permet de voir individuellement les atomes. L'invention a été récompensée par le prix Nobel de physique en 1986, partagé par Binnig, Rohrer et Herber. La STM est devenue une méthode puissante pour étudier la topologie des surfaces au niveau atomique. Elle a joué un rôle majeur dans le développement récent de la biochimie, de la nanotechnologie, des sciences de surfaces et de la chimie supramoléculaire. Les premières applications ont été réalisées sur des composés inorganiques sous haute vide (UHV). Depuis, la STM est utilisée pour étudier la physisorption des molécules organiques à l'interface solide-liquide dans des conditions de température et de pression ambiantes. La STM a été largement utilisée pour explorer la topologie, la chiralité, la réactivité et la dynamique au niveau moléculaire.

1.4.1 Principe du fonctionnement de la STM

Pour simplifier, il s'agit d'approcher une pointe à la surface d'un objet conducteur, couplé avec l'ajustement du potentiel entre la pointe et la surface. La pointe balaie la surface pour en déterminer la topologie. Durant le mouvement de la pointe, un ordinateur ajuste en temps réel la hauteur de la pointe pour maintenir un courant constant (courant tunnel) et enregistre cette hauteur qui permet de reconstituer la topologie de la surface. À l'aide d'un système piézoélectrique, la pointe est positionnée avec une grande précision par rapport à la surface à

[56] Binning, G.; Rohrer, H.; Gerber, C.; Weibel, E. *Phys. Rev. Lett*. **1982**, *49*, 57.

étudier. On mesure durant l'expérience le courant résultant du passage d'électrons entre la pointe et la surface, ce qui est proportionnel à la distance de séparation. On balaie ainsi la pointe au dessus de l'échantillon et on ajuste la hauteur de la pointe de manière à conserver une intensité du courant tunnel constante, au moyen d'une boucle de rétroaction. On peut alors déterminer la topologie de la surface avec une précision similaire aux distances interatomiques.

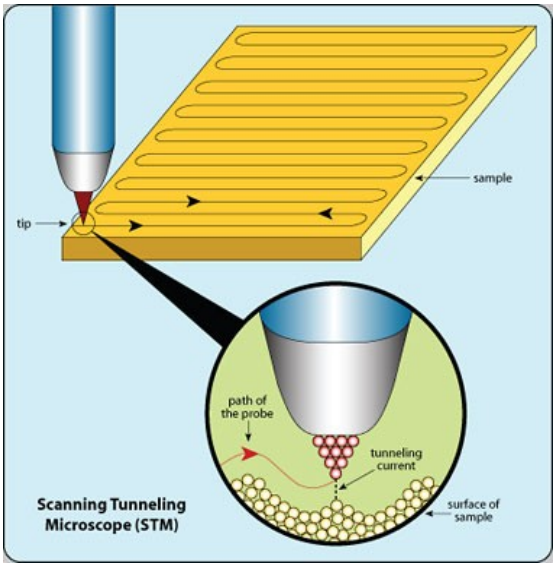

Figure 1.17. Schéma montrant la détermination de la topologie d'une surface conductrice par la technique STM.[57]

1.4.2 L'effet tunnel

Pour comprendre la théorie de la microscopie à effet tunnel (STM) sans entrer dans les grands détails de la physique et de la mathématique, voici une analyse simplifiée de l'effet tunnel,

[57]http ://www.nisenet.org/publicbeta/articles/seeing_atoms/index.html (20/11/2010)

le phénomène à la base de ce que nous observons expérimentalement. L'effet tunnel est un mécanisme important qui permet d'expliquer comment un électron parvient à traverser une barrière d'énergie dite interdite en physique classique mais permise avec la théorie quantique. La Figure 1.18 ci-dessous montre la différence entre la physique classique et la théorie quantique en illustrant l'effet tunnel à travers une barrière d'énergie.

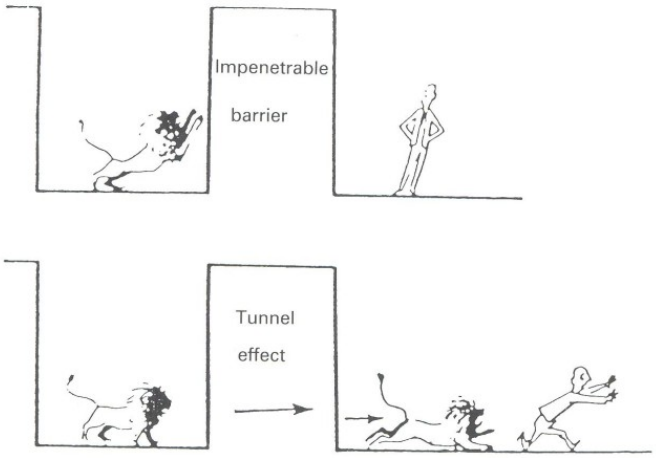

Figure 1.18. Illustration de la différence entre la physique classique (en haut) et la théorie quantique (en bas) montrant l'effet tunnel à travers une barrière d'énergie.[58]

En STM, l'effet tunnel correspond à passage d'électron de la pointe vers l'échantillon ou vice versa (voir Figure 1.19). Ce mécanisme de transfert d'électron n'existe que lorsqu'une tension polarisée est imposée entre la pointe et l'échantillon. Quand un électron est incident sur une barrière à vide avec une énergie potentielle plus grande que l'énergie cinétique de l'électron,

[58] Wiesendanger, R. *Scanning Probe Microscopy and Spectroscopy*, Cambridge University Press, Cambridge, 1994.

il existe une probabilité non nulle qu'il peut traverser la zone interdite et réapparaître de l'autre côté de la barrière.

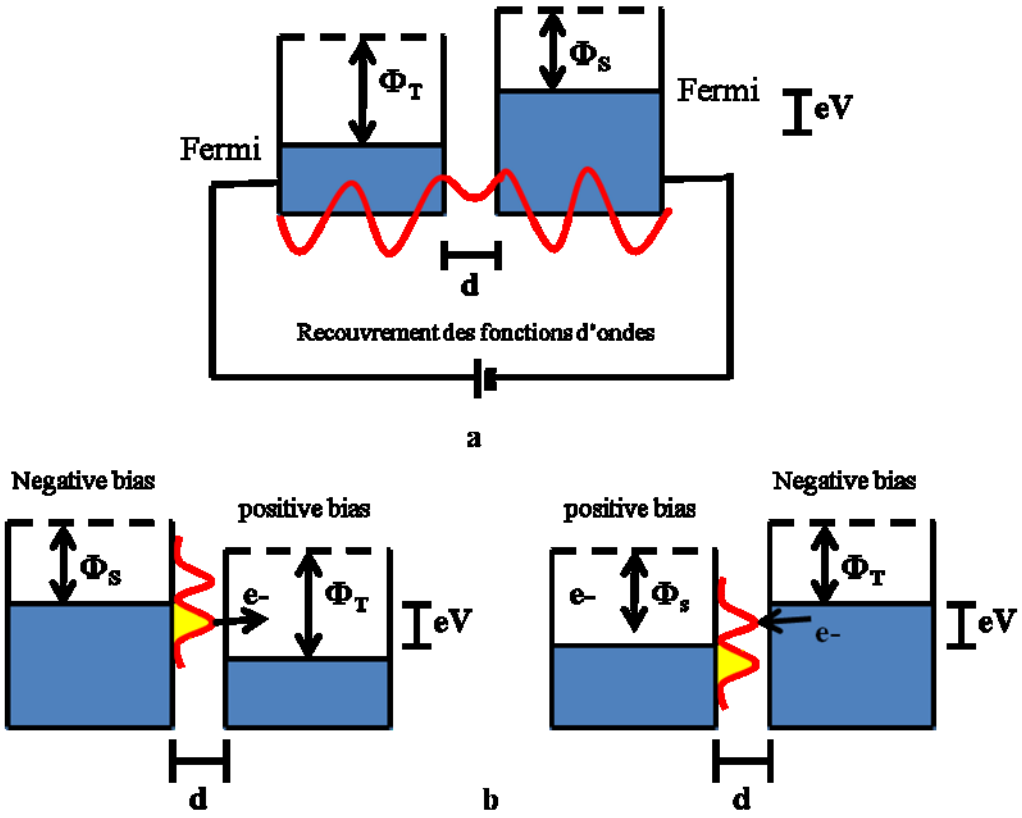

Figure 1.19. (a) Une application d'une polarisation négative sur l'échantillon produit un courant tunnel de l'échantillon vers la pointe. (b) L'application d'une polarisation positive sur l'échantillon produit un courant tunnel de la pointe vers l'échantillon. Les symboles Φ_S et Φ_T ($\Phi \propto (\partial \ln I/\partial d)^2$) représentent l'écart entre le niveau de Fermi et la hauteur de la barrière d'énergie, respectivement, de l'échantillon et de la pointe.[59]

[59] http://www.chembio.uoguelph.ca/educmat/chm729/STMpage/stmdet.htm

En d'autres termes, lorsque la pointe est amenée très proche de l'échantillon de l'ordre de 10 Å, les fonctions d'onde électroniques de chacun des deux se chevauchent, ce qui permet le passage du courant. L'équation donnant la relation entre la distance et le courant est :

$$I \propto \exp(-2Kd)$$

où $K = (2m\Phi)^{1/2}/h$, m est la masse de l'électron, Φ est la hauteur de la barrière d'énergie, h est la constante de Planck et d la distance qui sépare la pointe et l'échantillon.

En STM, ce que nous observons représente les densités d'états électroniques (DOS). Pour les interpréter, il est possible de les prédire à l'avance en utilisant des méthodes de calculs. La DOS correspond au nombre d'états électroniques possédant une énergie donnée dans le matériau considéré. La conductance du tunnel est proportionnelle à la densité d'états électroniques locale (LDOS) :

$$\sigma \propto \rho(r_o, E)$$

où $\rho(r_o, E)$ est la densité d'états électroniques de l'échantillon étudié. Ainsi, en gardant une séparation constante entre la pointe et l'échantillon durant une mesure du courant, on peut sonder la densité d'états électroniques locale de l'échantillon étudié.

1.4.3 Instrumentation de la STM

Tel qu'est illustre à la Figure 1.20, les éléments indispensables pour constituer un instrument de STM sont : 1) une pointe placée très proche de l'échantillon, 2) un système pour contrôler la position de la pointe suivant les axes x et y parallèle à la surface de l'échantillon et 3)

un ordinateur pour contrôler en temps réel le courant constant. L'instrument de STM peut travailler en deux modes, en courant constant et en hauteur constante. L'instrument que nous utilisons pour les travaux de cette thèse est un JEOL JSPM-5200 haute résolution scanning-probe microscope (SPM) avec une possibilité de travailler soit en pression et température ambiante, soit à des températures qui peuvent varier de -143 ^{o}C à 500 ^{o}C.

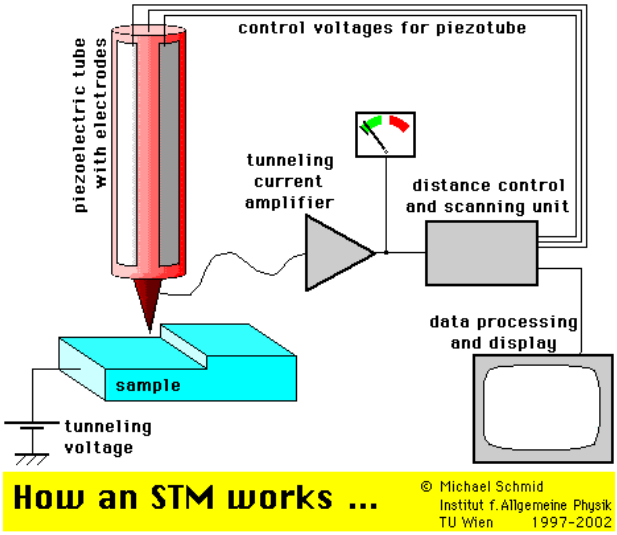

Figure 1.20. Schéma représentant les différentes composantes d'un appareil STM.[60]

1.4.4 Investigations

L'organisation des molécules en 2D par leur adsorption sur des surfaces est déterminée par la structure des molécules, par leurs interactions intermoléculaires et par leurs interactions avec la surface. L'adsorption des tectons est particulièrement intéressante parce que le positionnement relatif de ces composés peut être dirigé par leur géométrie, combinée à l'effet des

[60]http ://www.answers.com/topic/scanning-tunneling-microscope (10/11/2010)

interactions spécifiques et directionnelles. Plusieurs composés simples pouvant s'organiser en réseaux régis par la formation de ponts hydrogène prévisibles, tels que l'acide trimésique (TMA) ou encore la mélamine, ont été déjà étudiés en STM. Ces tectons servent aujourd'hui de modèles pour des études de molécules plus complexes. Deux polymorphes 2D principaux, en ruche d'abeille et en fleur, ont été observés par STM pour l'adsorption du TMA sur graphite (Figure 1.21). La mélamine a également été extensivement étudiée avec différents substrats tels que l'or, l'argent et le graphite. Une structure commune en hexagone est souvent retrouvée et son image STM est montrée à la Figure 1.22. De nombreux groupes travaillent encore aujourd'hui sur des études de co-déposition utilisant la TMA ou la mélamine. Prises comme jonction trigonale, ces molécules peuvent diriger l'organisation lors d'une co-cristallisation.

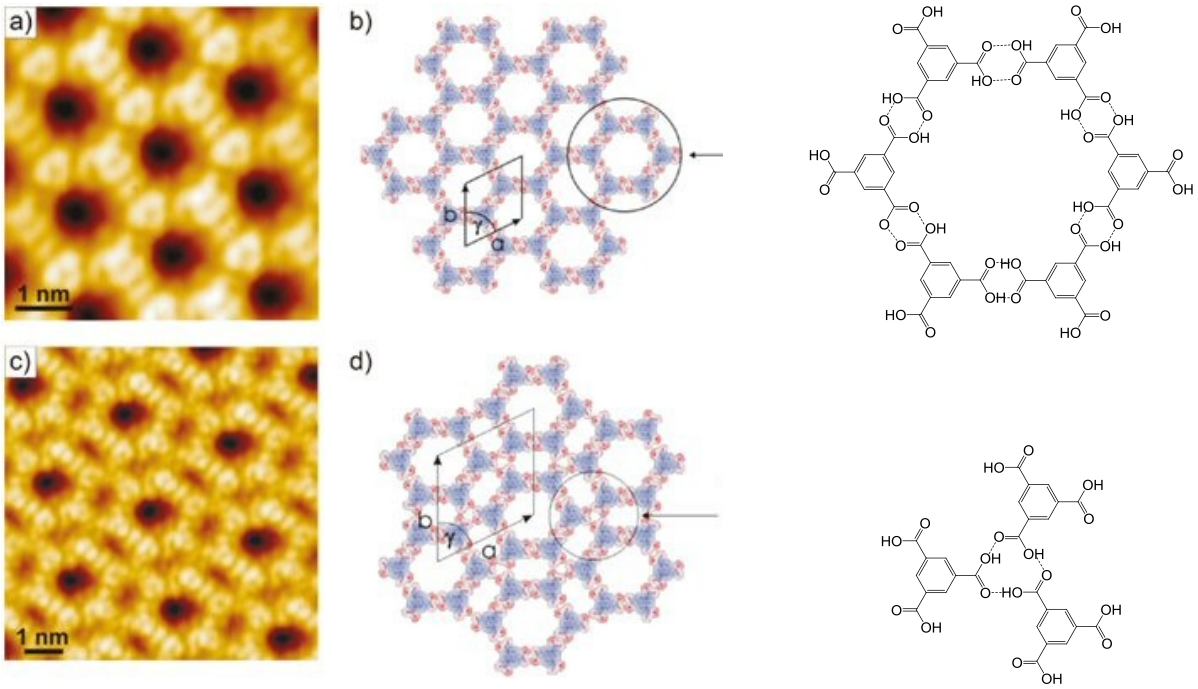

Figure 1.21. Images STM (a et c) et modèles moléculaires (b et d) de deux polymorphes de la l'acide trimésique (TMA) adsorbé sur la surface de graphite.[10]

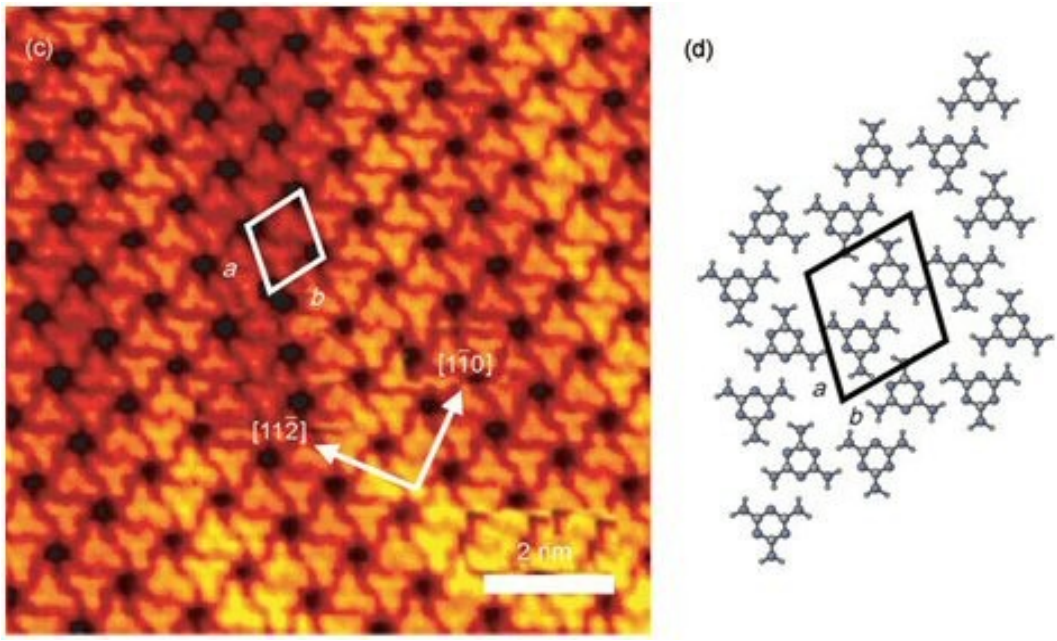

Figure 1.22. Image STM et modèle moléculaire de la mélamine adsorbée sur Au(111).[61]

Plus récemment, une stratégie utilisant la chimie de coordination a été mise en place pour obtenir des réseaux supramoléculaires métallo-organiques 2D. Deux méthodes sont communément employées pour ce type de construction : (1) un ligand et un métal sont déposés en même temps sur une surface, puis par coordination durant la cristallisation 2D le réseau métallo-organique est formé (Figure 1.23 a) et (2) la déposition d'un ligand sur une surface métallique peut mener à une organisation 2D régulière par un processus dans lequel les atomes de métal nécessaires pour la coordination proviennent de la surface elle-même (Figure 1.23 b).

[61] Xu, W.; Dong, M.; Gersen, H.; Rauls, E.; Vazquez-Campos, S.; Crego-Calama, M.; Reinhoudt, D. N.; Stensgaard, I.; Laegsgaard, E.; Linderoth, T. R.; Besenbacher, F. *Small* **2007**, *3*, 854.

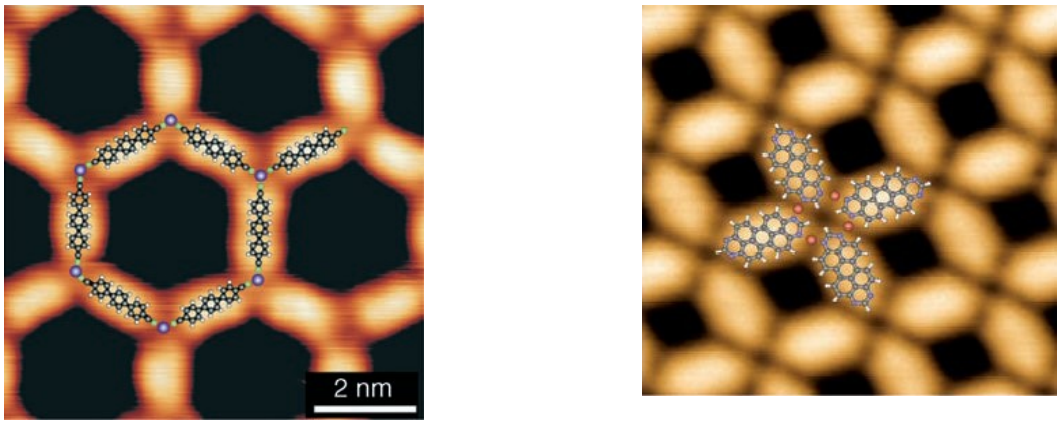

a **b**

Figure 1.23. (a) Une image STM à haute résolution d'un assemblage infini obtenu par coordination de Co(II) avec un ligand linéaire sur Ag(111) (I = 0.3 nA et V = 1.9 V).[62] (b) Une image STM 5.3 × 5.3 nm^2 d'un auto-assemblage par coordination du 1,3,8,10-tétraazapéropyrène sur une surface de Cu(111) (I = 20 pA et V = 0.4 V).[63]

1.5 Objectif de la thèse

La tectonique moléculaire peut être vue comme un jeu de Lego dans lequel le constructeur assemble de petits objets plastiques les uns dans les autres pour former diverses architectures tridimensionnelles. Une publicité pour Lego présentant des enfants qui jouent au Lego donne une aperçue simplifiée de la tâche de travail de l'ingénieur cristallin (Figure 1.24). Les voies classiques de construction de réseaux supramoléculaires consistaient jusqu'à présent à utiliser des molécules composées d'atomes reliés par des liaisons covalentes et à assembler ces molécules en se servant des interactions intermoléculaires directionnelles.

[62] Stepanow, S.; Lin, N.; Payer, D.; Schlickum, U.; Kappenberger, F.; Zoppellaro, G.; Ruben, M.; Brune, H.; Barth, J. V.; Kern, K. *Angew. Chem., Int. Ed*. **2007**, *46*, 710.
[63] Matena, M.; Riehm, T.; Stohr, M.; Jung, T. A.; Gade, L. H. *Angew. Chem., Int. Ed*. **2008**, *47*, 2414.

Figure 1.24. Publicité pour Lego.[64]

L'un des problèmes majeurs de cette approche tectonique réside dans la synthèse des molécules employées. En effet, leur préparation nécessite souvent de nombreuses étapes de synthèse. Avec les méthodes traditionnelles, les atomes constituant le tecton sont maintenus entre eux par des liaisons covalentes, ce qui ne permet pas de les défaire. Par conséquent, une fois les liens formés il est très difficile de modifier l'architecture du tecton. Ainsi, pour chaque modification réalisée sur le tecton les étapes de synthèse doivent être réitérées. Afin de contourner ces problèmes, qui rendent les synthèses des tectons parfois laborieuses et compliquées, une combinaison de la chimie de coordination et des liaisons hydrogène a été proposée afin d'obtenir plus rapidement des tectons utiles. Des molécules sophistiquées peuvent être facilement synthétisées par cette méthode avec en plus une grande élégance.

Cette thèse a pour but d'étudier l'efficacité de la stratégie combinant la chimie de coordination et les ponts hydrogène pour diriger l'assemblage supramoléculaire. Cette approche consiste à assembler de petites molécules à un métal pour créer un ensemble, qui agit comme métallotecton. La construction de métallotectons nécessite donc la recherche de ligand ayant une

[64] http ://creative.lego.com/en-us/FamilyTime/default.aspx (14/11/2010)

double aptitude, c'est-à-dire un caractère coordonnant et une structure permettant la formation de ponts hydrogène selon des motifs caractéristiques. Ces ligands seront appelés plus particulièrement *tectoligands* du fait de leur double aptitude. Le Schéma 1.4 résume le concept de la stratégie utilisée dans cette thèse pour construire les métallotectons.

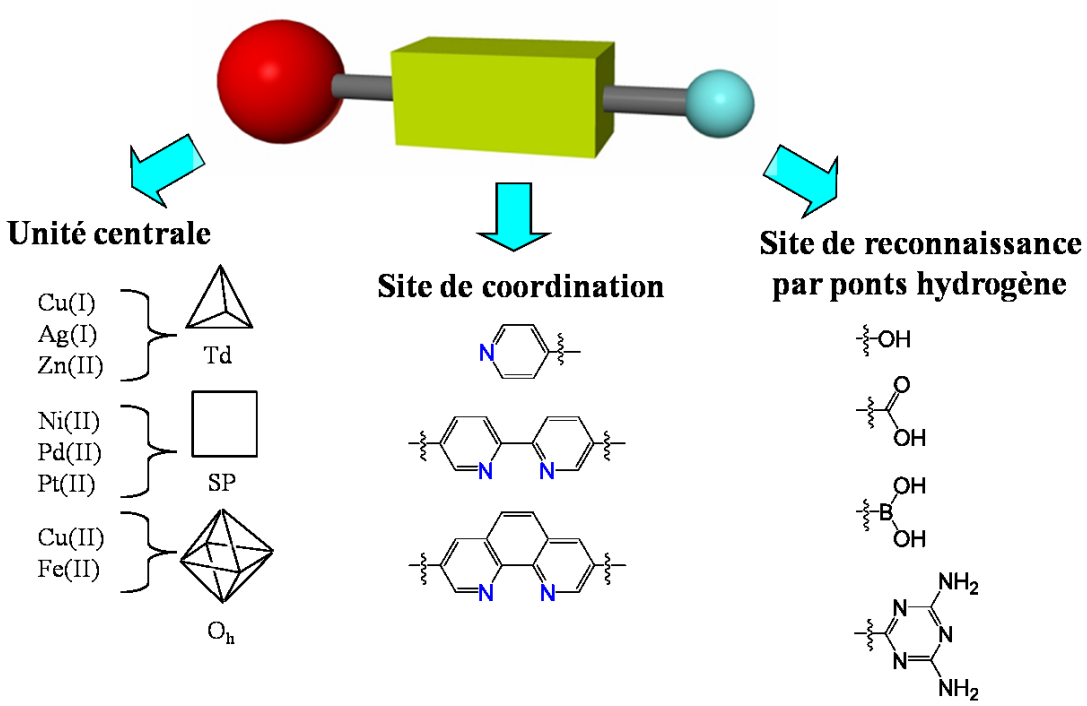

Schéma 1.4. Représentation schématique de la stratégie combinant la chimie de coordination et les ponts hydrogène pour diriger l'assemblage supramoléculaire. Dans cette stratégie, le métal peut être choisi pour adopter une géométrie tétraédrique (Td), plane carrée (SP) ou octaédrique (O_h). Différents sites de coordination peuvent être exploités, dont les pyridines, bipyridines et phénantrolines illustrées dans le schéma. Finalement, divers sites de reconnaissance peuvent être liés au site de coordination pour compléter la construction du métallotecton.

L'objectif ultime de la thèse est de présenter des études de structure 3D des métallotectons, qui présentent un intérêt majeur en ingénierie cristalline. Cependant, pour mieux

comprendre l'origine des préférences structurales observées, nous avons entrepris une étude de l'organisation de certains tectoligands eux-mêmes, non complexés aux métaux. L'étude de ces composés, construits à partir d'une pyridine, bipyridine ou phénantroline substituée avec des groupements DAT, servira de référence pour analyser des molécules plus complexes.

Pour simplifier davantage, nous avons également examiné le comportement d'une série de tectons simples dérivés de la triazine-1,3,5. Ces composés, commercialement disponibles, nous ont donné un bon point de départ pour interpréter, voire même prédire, l'organisation des molécules plus élaborées incorporant des unités DAT. Pour élargir et approfondir notre compréhension de base, nous avons fait une étude parallèle d'association des tectons comportant une unité pyridine substituée avec des groupements carboxyliques. Cette seconde étude devrait permettre d'identifier le rôle de l'azote de la pyridine et ainsi de comprendre les structures 2D observées par STM lorsqu'on dépose nos tectoligands sur des surfaces. L'accumulation d'information obtenue par ces multiples études permettra de mieux interpréter et de bien comprendre comment nos tectoligands s'organisent. Cette thèse se propose de fonder un début d'approche méthodologique pour interpréter des images STM de molécules dérivant de la pyridine substituée à des groupements triazinyles.

Après avoir déterminé et étudié les tectoligands, nous avons préparé deux séries de métallotectons par coordination des tectoligands aux métaux de transition. Selon le sel métallique utilisé, il est possible de choisir le nombre de liens de coordination ainsi que la topologie du métallotecton. Des métallotectons de géométrie carrée et tétraédrique déformée seront discutés au cours de ces travaux.

Chapitre 2

Co-cristallisation en 2D et 3D des aminoazines avec les acides alcanecarboxyliques

2.1 Introduction

Malgré les progrès de la science, l'organisation moléculaire reste un phénomène difficile à comprendre. Pour apprendre à maîtriser cette organisation, une approche particulièrement efficace est explorée dans cette thèse. Elle consiste à compiler des composants bien définis qui permettent de placer avec confiance des molécules par interactions intermoléculaires directionnelles telles que les ponts hydrogène. En principe, l'organisation moléculaire pourrait générer des objets finis ou périodiques, avec des dimensions variant de zéro à trois. D'une importance capitale pour les applications technologiques est le contrôle de l'organisation des molécules sur les surfaces (2D) ou en matériaux 3D. Nous avons donc mis un accent double sur ces deux aspects de l'organisation moléculaire.

2.2 Nos objectifs

Depuis les années 90, la tectonique moléculaire a été utilisée comme une stratégie efficace dans la construction d'édifices supramoléculaires en 3D. Une nouvelle opportunité existe présentement d'adopter cette stratégie pour construire des réseaux moléculaires bien définis en 2D à la surface de divers substrats. Dans ce chapitre, une série de molécules de la famille des aminoazines a été choisie pour tester l'efficacité de la tectonique moléculaire dans le but de contrôler l'organisation des molécules sur la surface de graphite. Ces composés ont été utilisés pour la simplicité de leurs structures, leurs topologies planaires et leurs aptitudes à s'auto-assembler de manière prévisible par ponts hydrogène. Les objectifs principaux de cette étude sont 1) de mettre la stratégie de la tectonique moléculaire à l'épreuve pour diriger l'organisation des

molécules de manière prévisible en 2D, 2) d'interpréter de manière confiante les images STM en comparent les structures 2D et 3D caractérisées respectivement par STM et par diffraction des rayons-X et 3) de créer une base de données qui servira de support pour interpréter les images STM de molécules plus complexes.

Un objectif secondaire est de pouvoir identifier les facteurs favorisant une organisation similaire en 2D et en 3D, ce qui pourrait par exemple faciliter la préparation de couches minces ayant des structures homogènes indépendamment de l'épaisseur. Pour tester notre approche, nous avons visé une série de molécules de type aminoazine pouvant s'organiser de façon analogue en 2D et en 3D. Dans notre travail, nous avons entrepris une étude comparative 2D et 3D pour mieux comprendre les organisations moléculaires. Ce que nous avons fait illustre une approche plutôt rare en science des matériaux. Notre travail a offert un éclairage sur l'organisation moléculaire en 2D, observée par la technique de la microscopie de balayage à l'effet tunnel (STM), et en 3D, déterminée par diffraction des rayons-X (XRD). Cette approche hybride permet de démontrer que les structures 3D déterminées par XRD peuvent être utiles pour fournir une base solide pour l'interprétation des images 2D obtenues par STM. En même temps, les études STM en 2D peuvent identifier la position des molécules individuelles, offrant ainsi des détails qui ne sont pas révélés par une étude XRD.

2.3 Article 1

Engineering Homologous Molecular Organization in 2D and 3D. Cocrystallization of Aminoazines and Alkanecarboxylic Acids

Adam Duong, Thierry Maris, and James D. Wuest*

Crystal Engineering Communications **2011**, in press

Abstract

Amino-substituted azines such as aminotriazines have simple planar structures with an affinity for adsorption on graphite. In addition, aminoazines associate predictably with carboxylic acids according to a reliable hydrogen-bonded motif. Together, these properties help predispose aminoazines and alkanecarboxylic acids to cocrystallize and to coadsorb on graphite to give related 3D and 2D structures built from essentially planar tapes. These results illustrate how molecular materials that reliably adopt similar ordered structures in both adlayers and bulk samples can be devised by choosing components that combine an affinity for surfaces with a tendency to form sheets held together by strong coplanar intermolecular interactions.

Introduction

Molecular organization in materials is a highly complex phenomenon that depends on the structure of the individual components and on diverse interactions that control how the components are positioned with respect to their neighbors. Learning how to control this organization is a prerequisite for advances in technology based on new molecular materials made by design. Unfortunately, science has developed only a limited understanding of how the structure and properties of molecular materials emerge collectively from the identity and interactions of the individual components.[1]

In a particularly effective approach, predictably ordered molecular materials can be built from structurally well-defined components that are positioned by strong directional intermolecular interactions such as hydrogen bonds.[2] This strategy can be used to help control molecular organization, both in bulk materials and in thin films.[3] The scope and reliability of the strategy can be explored advantageously by comparing the 3D crystallization of selected families of molecules, as revealed by structural studies using X-ray diffraction (XRD), with 2D crystallization induced by adsorption on surfaces, as determined by scanning probe microscopy (SPM).[4,5] Such integrated analyses of 3D and 2D crystallization are still uncommon, but they offer insights about molecular organization that are unlikely to result from narrower studies using XRD or SPM alone. In particular, (1) 3D structures rigorously determined by XRD can help provide a sound basis for interpreting images of 2D crystallization obtained by SPM; (2) studies of 2D crystallization by SPM can reveal defects and dynamic phenomena that are essentially invisible in 3D structures resolved by XRD; and (3) comparison of 3D and 2D structures can

probe the importance of forces that act at interfaces relative to those that control molecular organization in bulk materials.

Molecular materials that exhibit similar organization in 3D and 2D are of special interest, especially for uses requiring behavior that depends predictably on dimensions, such as in thin-film devices. It is well understood from decades of previous research that adsorption on properly ordered surfaces can induce epitaxial 2D molecular organization, leading in favorable cases to the layer-by-layer growth of thin films or bulk crystalline phases with similar 3D structures.[6] Unfortunately, however, no general prescription exists for designing molecules that will reliably yield homologous 3D and 2D structures, particularly when the lattice parameters of the underlying surface and the ultimate 3D crystal are unlikely to be well matched.

Improved tools for favoring homologous 3D and 2D molecular crystallization are needed. We are exploring an approach that builds directly on the imposing foundation of earlier studies of epitaxy and related phenomena of surface-induced crystallization, but offers additional elements. In particular, it features molecular components that are designed to engage in mutual interactions that are particularly strong and specific. The goal is to use these interactions to direct crystallization predictably in 3D and 2D, rather than to allow more diffuse interactions with an underlying surface to play a dominant role. This approach to engineering homologous 3D and 2D crystallization may be more effective than alternatives involving compounds that participate in relatively weak intermolecular interactions with low directionality.[7]

Using strong directional interadsorbate interactions is potentially advantageous for many reasons. For example, it may allow similar 3D and 2D crystallization to occur even when true epitaxy is impossible, such as when the underlying surface is not commensurate, flat, or ordered. In addition, structurally well-defined molecules that engage in multiple strong directional interactions do not tend to crystallize in 3D in widely different polymorphic forms, and extensive polymorphism may also be disfavored in 2D.[8] For such reasons, an approach based on the use of strong directional interadsorbate interactions promises to yield families of compounds that crystallize in 3D and 2D with predictable homology.

Clearly, such compounds should be designed to have an affinity for underlying surfaces, combined with a strong propensity to engage in specific directional intermolecular interactions, particularly within a parallel plane.[4,5] To further test this strategy, we have chosen to study 2-aminoazines, which engage in reliable hydrogen-bonded supramolecular heterosynthon **I** with carboxylic acids.[9,10] The atoms involved in synthon **I** are expected to be nearly coplanar.

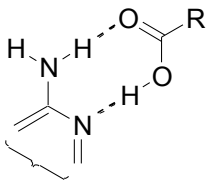

I

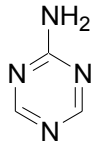

1

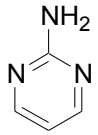

2

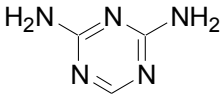

3

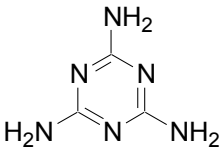

4

Moreover, recent experimental studies and DFT calculations have shown that aminoazines have a marked affinity for graphite, possibly resulting in part from specific interactions of NH_2 groups with the underlying surface.[5,11-12] By combining aminoazines with alkanecarboxylic acids, we hoped to create an effective alignment of three tendencies : (1) the inherently strong adsorption of

aminotriazines on graphite; (2) the favorable creation of planar hydrogen-bonded motif **I**; and (3) the well-established adsorption of alkyl chains on graphite.[13] We have found that diverse aminoazines, including 2-amino-1,3,5-triazine (**1**), 2-aminopyrimidine (**2**), 2,4-diamino-1,3,5-triazine (**3**), and melamine (**4**), cocrystallize with alkanecarboxylic acids to produce 3D and 2D structures with similar molecular composition and organization.[14] An attractive feature of these coassemblies is the ability to alter the structural parameters in a methodical way by changing the alkanecarboxylic acid component.

Results and Discussion

3D Cocrystallization of 2-Aminotriazine 1 with Nonanoic Acid. Slow evaporation of a solution of 2-aminotriazine **1** in nonanoic acid at 25 °C yielded cocrystals of composition **1** • 2 nonanoic acid. The cocrystals proved to belong to the triclinic space group *P*-1, and other crystallographic data are summarized in Table 1. Views of the structure are provided in Figure 1. Each molecule of aminotriazine **1** forms hydrogen bonds with two molecules of nonanoic acid, confirming the importance of motif **I** as a key determinant of molecular organization. The crystallographic data confirm that full proton transfer does not occur to give the corresponding aminotriazinium carboxylate salt.[15-17] The observed O-H···N and N-H···O distances have normal average values (2.73 and 2.98 Å, respectively),[10] and nonanoic acid adopts a fully extended conformation. The resulting ternary aggregates, which are essentially planar, then associate to form tapes aligned with the *b* axis (Figure 1a), which are held together by bifurcated N-H···N hydrogen bonds (average H···N distance = 2.68 Å),[18] augmented by C-H···O interactions (average H···O distance = 2.36 Å, average C-H···O angle = 140.1°).[19-20] In this way, every atom of N and

H in aminotriazine **1** engages in intermolecular interactions involving a total of six neighboring molecules, all located approximately in the same plane. Antiparallel hydrogen-bonded tapes then pack to form sheets (Figure 1b), which stack with a slight offset to give the full 3D structure (Figure 1c).

Table 1. Crystallographic Data for Cocrystals of 2-Aminotriazine **1**, 2-Aminopyrimidine (**2**), and 2,4-Diaminotriazine **3.**

cocrystal	**1** • 2 nonanoic acid	**2** • 2 nonanoic acid	**3** • 2 heptanoic acid
formula	$C_{21}H_{40}N_4O_4$	$C_{22}H_{41}N_3O_4$	$C_{17}H_{33}N_5O_4$
crystal system	triclinic	monoclinic	orthorhombic
space group	$P\bar{1}$	Pc	$Pmn2_1$
a (Å)	5.2387(8)	5.4326(2)	51.630(4)
b (Å)	7.0211(11)	5.4441(2)	4.7775(3)
c (Å)	33.169(6)	40.3743(17)	4.1290(3)
α (°)	90.775(17)	90	90
β (°)	92.741(12)	96.146(2)	90
γ (°)	101.073(8)	90	90
V (Å^3)	1195.6(3)	1187.2(1)	1018.47(12)
Z	2	2	2
ρ_{calcd} (g cm^{-3})	1.146	1.151	1.211
T (K)	150	150	150
μ (mm^{-1})	0.639	0.630	0.713
R_1, $I > 2\sigma$ (%)	8.17	8.19	7.93
R_1, all data (%)	12.29	8.91	8.31
ωR_2, $I > 2\sigma$ (%)	20.76	25.49	23.98
ωR_2, all data(%)	24.17	26.17	24.24
measured reflections	14716	16255	13035
independent reflections	4206	4042	1060
observed reflections, $I > 2\sigma(I)$	2529	3487	962

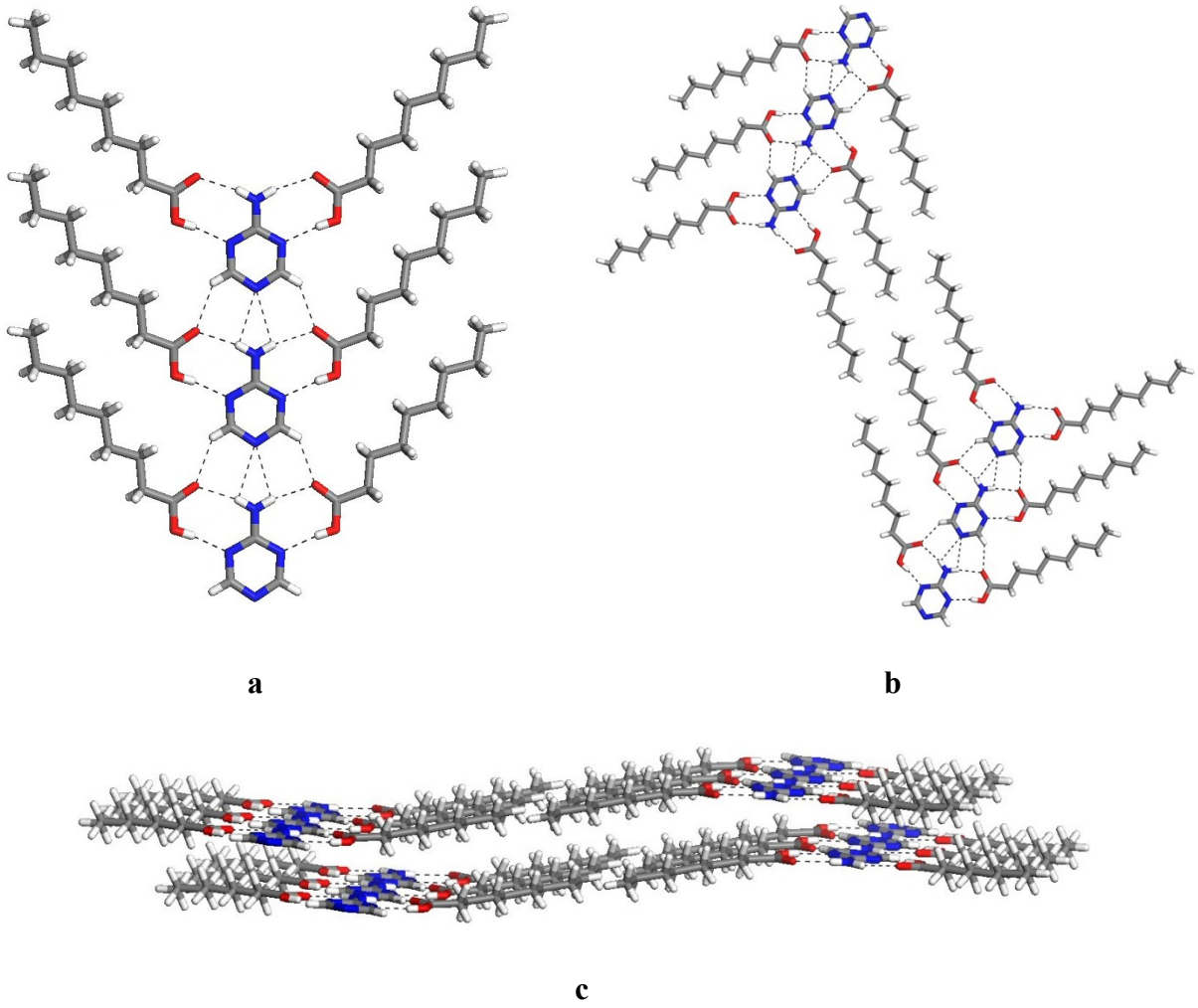

Figure 1. Views of the structure of 1:2 cocrystals of 2-aminotriazine **1** with nonanoic acid. (a) View of part of a single tape, with key interactions represented by broken lines. Carbon atoms are shown in gray, hydrogen atoms in white, nitrogen atoms in blue, and oxygen atoms in red. (b) View of the formation of sheets by the contact of adjacent coplanar antiparallel tapes. (c) View of two stacked sheets.

2D Cocrystallization of 2-Aminotriazine 1 with Alkanecarboxylic Acids. The presence of extensively hydrogen-bonded sheets in the 3D structure suggested that aminotriazine **1** might coadsorb with alkanecarboxylic acids on graphite to give an analogous 2D assembly. To test this possibility, we added a saturated solution of 2-aminotriazine **1** in nonanoic acid to the freshly exposed surface of highly oriented pyrolytic graphite (HOPG), and we analyzed the liquid-solid interface by scanning tunneling microscopy (STM), which revealed an ordered adlayer. A representative image is shown in Figure 2, along with a superimposed molecular model. Examination of the periodic patterns of contrast, combined with analysis of the unit cell parameters (a = 8.3 Å, b = 33 Å, γ = 43°), established that adsorption produces alternating regions of aminotriazine **1** (brighter) and nonanoic acid (darker), which are organized in antiparallel tapes fully analogous to those observed by XRD (Figure 1a). These observations suggest that aminotriazine **1** and nonanoic acid cocrystallize in 3D and 2D in essentially the same way. Given the impossibility of confidently predicting the structure of molecular crystals consisting of a single component, it is remarkable that both composition and organization are maintained in both 3D and 2D in the complex coassembly of aminotriazine **1** and nonanoic acid.

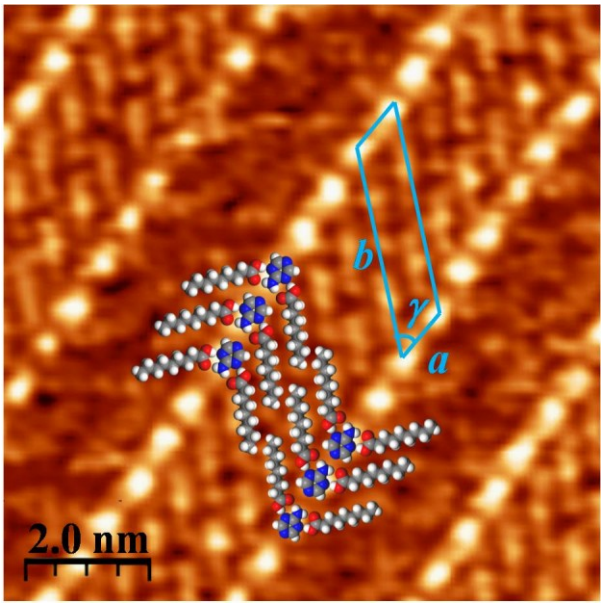

Figure 2. STM image of the 2D cocrystallization of 2-aminotriazine **1** and nonanoic acid on HOPG (deposition from nonanoic acid, with V_{bias} = -1.39 V and I_{set} = 0.22 nA). Superimposed on the image are a scale bar, the measured unit cell, and a model of the proposed assembly.

Similar STM images were obtained when solutions of aminotriazine **1** in other alkanecarboxylic acids were deposited on HOPG. These observations suggest that the formation of antiparallel tapes built from hydrogen-bonded 1:2 aggregates of aminotriazine **1** and alkanecarboxylic acids may reflect a general structural preference, both in 3D and 2D. Maintenance of a consistent pattern of molecular organization, despite the altered length of the alkanecarboxylic acid, creates an opportunity to control structural parameters in a rational way, and it shows that commensurate adsorption is not needed to ensure homologous crystallization in 3D and 2D.

Quantitative comparison of structural parameters in 3D and 2D confirmed that molecular organization within the sheets is nearly identical. In the 3D structure of 1:2 cocrystals of 2-aminotriazine **1** and nonanoic acid, molecular separation along the tapes (*b* axis) is 7.021(1) Å, adjacent tapes are separated by approximately 34 Å (as measured along the line defined by the extended alkyl chains of nonanoic acid), and the angle defined by the *b* axis and the alkyl chains is approximately 45°. These values resemble the unit cell parameters observed in 2D (a = 8.3 Å, b = 33 Å, γ = 43°). The slight differences may in part reflect efforts to achieve a commensurate or coincident orientation with respect to the substrate. Indeed, large-area STM images show that tapes in adjacent domains intersect at an angle of 120°, suggesting preferential orientation of alkyl chains along the symmetry axes of graphite.[21] In addition, hydrogen bonding of the associated aminoazine and alkanecarboxylic acid may be weakened slightly by adsorption, thereby leading to altered molecular separation in certain cases.[5,11,22]

Homologous 3D and 2D crystallization may be particularly likely when interadsorbate interactions are strong relative to the energy of adsorption. Previously published experimental and computational studies suggest that this condition is met by adducts of aminoazines with alkanecarboxylic acids.[5,11,22] However, the observation of epitaxial alignment of alkyl chains shows that the tendency of the molecular components to associate according to favored patterns of hydrogen bonding does not completely mask the organizing effect of the surface, at least in the present system.

The observed structural parameters for the 2D cocrystallization of aminotriazine **1** with alkanecarboxylic acids on graphite do not rigorously exclude the possibility that full proton

transfer occurs in the process of adsorption, producing hydrogen-bonded adlayers consisting of 2-aminotriazinium carboxylate salts. However, computational studies of closely related systems suggest that salts of this type do not correspond to energy minima, either in the gas phase or the adsorbed state.[5,11,22]

3D Cocrystallization of 2-Aminopyrimidine (2) with Nonanoic Acid. Although the primary focus of our study of aminoazines was on derivatives of 1,3,5-triazine, we briefly examined the behavior of 2-aminopyrimidine (**2**), which differs from 2-aminotriazine **1** only by the replacement of N at one position by CH. Slow evaporation of a solution of compound **2** in nonanoic acid at 25 °C yielded cocrystals of composition **2** • 2 nonanoic acid. The crystals were found to belong to the monoclinic space group *Pc*, and other crystallographic data are summarized in Table 1. As shown in Figure 3a, the structure is similar to the one formed by cocrystallization of 2-aminotriazine **1** and nonanoic acid. Again, the aminoazine and nonanoic acid form hydrogen-bonded ternary 1:2 aggregates according to motif **I**, with normal average O-H···N and N-H···O distances (2.72 and 2.86 Å, respectively).[10] The ternary aggregates are then joined into tapes along the *ab* diagonal by C-H···N interactions (H···N distance = 2.72 Å, C-H···N angle = 178.2°) and C-H···O interactions (average H···O distance = 2.72 Å, average C-H···O angle = 131.2°).[19-20] In the resulting structure, each atom of N and H in aminopyrimidine **2** is involved in coplanar intermolecular interactions with a total of six neighboring molecules. Molecular separation along the tapes is 7.649(1) Å, which is slightly longer than the corresponding distance in the tapes of the corresponding aminotriazine **1** (7.021(1) Å), where the intermolecular interactions are stronger. Moreover, adjacent tapes in the 1:2 cocrystals of aminopyrimidine **2**

with nonanoic acid do not lie in essentially the same plane to form sheets, as they do in the related cocrystal of aminotriazine **1**.

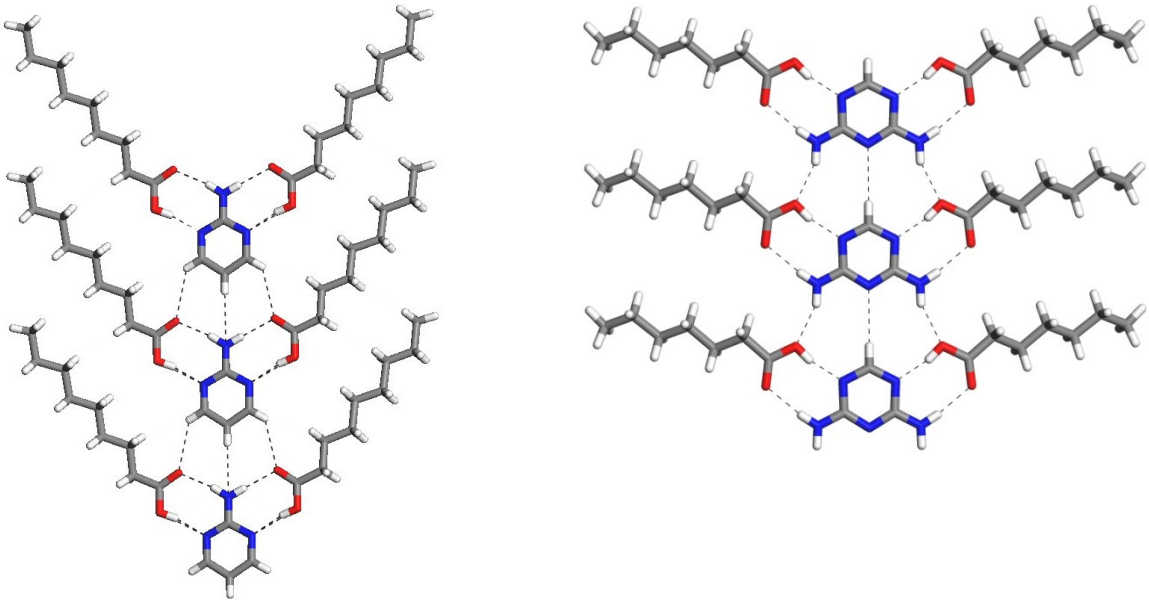

a **b**

Figure 3. (a) Representation of hydrogen-bonded tapes present in the structure of 1:2 cocrystals of 2-aminopyrimidine (**2**) with nonanoic acid. (b) Representation of hydrogen-bonded tapes present in the structure of 1:2 cocrystals of 2,4-diaminotriazine **3** with heptanoic acid. Key interactions are represented by broken lines, and carbon atoms are shown in gray, hydrogen atoms in white, nitrogen atoms in blue, and oxygen atoms in red.

3D Cocrystallization of 2,4-Diaminotriazine 3 with Heptanoic Acid. Slow evaporation of a solution of 2,4-diaminotriazine **3** in heptanoic acid at 25 °C yielded cocrystals of composition **3** • 2 heptanoic acid. The crystals proved to belong to the orthorhombic space group $Pmn2_1$, and other crystallographic data are summarized in Table 1. A view of the structure is

provided in Figure 3b. Like related aminoazines **1**-**2**, compound **3** forms hydrogen-bonded ternary 1:2 aggregates according to heterosynthon **I**, with normal O-H···N and N-H···O distances (2.62 and 2.92 Å, respectively).[10] The ternary aggregates are linked into tapes along the *bc* diagonal by N-H···O hydrogen bonds (2.94 Å) and C-H···N interactions (H···N distance = 2.70 Å, C-H···N angle = 174.2°).[19-20] Each atom of N and H in diaminotriazine **3** is thereby involved in coplanar intermolecular interactions with a total of six neighboring molecules, but adjacent tapes do not lie in essentially the same plane. In this respect, the structure resembles that of the cocrystal of 2-aminopyrimidine (**2**) and differs from that of the cocrystal of 2-aminotriazine **1**, where adjacent tapes are nearly coplanar. Despite this difference, the structures of 3D cocrystals of aminoazines **1**-**3** with alkanecarboxylic acids show significant overall similarity, and all are built from essentially planar tapes composed of hydrogen-bonded 1:2 aggregates (Figures 1a, 3a, and 3b).

2D Cocrystallization of Melamine (4) with Alkanecarboxylic Acids. Earlier STM studies carried out by Walch, Lackinger, and collaborators revealed that melamine (**4**) can be coadsorbed with alkanecarboxylic acids on HOPG.[23-25] With acids ranging from pentanoic to tridecanoic, they consistently observed well-ordered hexagonal arrays, which were considered to result from the close packing of aggregates composed of a chiral cyclic hexameric core of melamine (rosette **5** or its enantiomorph) surrounded by a total of twelve hydrogen-bonded molecules of alkanecarboxylic acid. This model is consistent with the observation that the lattice parameters increase linearly as a function of the length of the alkanecarboxylic acid.

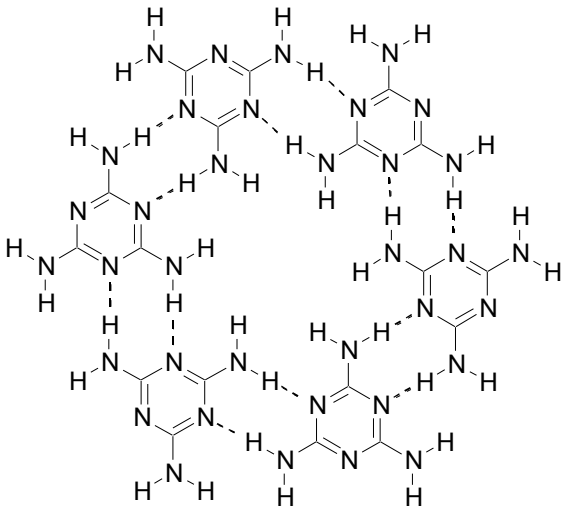

5

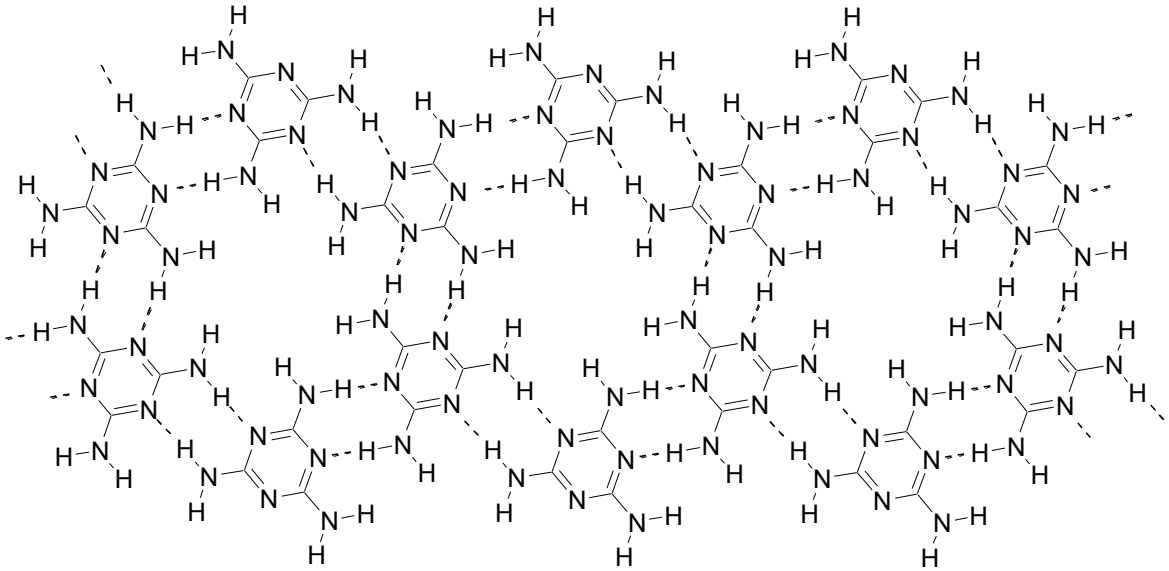

6

When melamine (**4**) and alkanecarboxylic acids are coadsorbed under conditions that reduce the relative amount of acid available, we observe a different periodic pattern, as shown in Figure 4 for the case of heptanoic acid. Bands of alternating contrast suggest that the pattern is again constructed from tapes, with regions consisting of melamine (brighter) and heptanoic acid (darker). The observed unit cell parameters (a = 9.7 Å, b = 23 Å, γ = 93°) are consistent with the hypothesis that chiral rosettes **5** are linked by hydrogen bonds to form chains **6**, and that the

edges of the chains interact with carboxylic acids according to established heterosynthon **I** to complete the formation of planar tapes. As shown by other work, full proton transfer from the carboxylic acid to melamine (**4**) is unlikely.[5,11,22] As expected, enantiomorphic domains can be observed, and replacement of heptanoic acid with other alkanecarboxylic acids leads to analogous structures in which the separation of chains **6** changes accordingly.[21] These results show that melamine (**4**) can be induced to cocrystallize in 2D with alkanecarboxylic acids to form hydrogen-bonded tapes related to those formed by analogous aminoazines **1**-**3**. However, the tapes formed by melamine (**4**) incorporate chains of cyclic hexamers rather than chains of simple monomeric aminoazines.

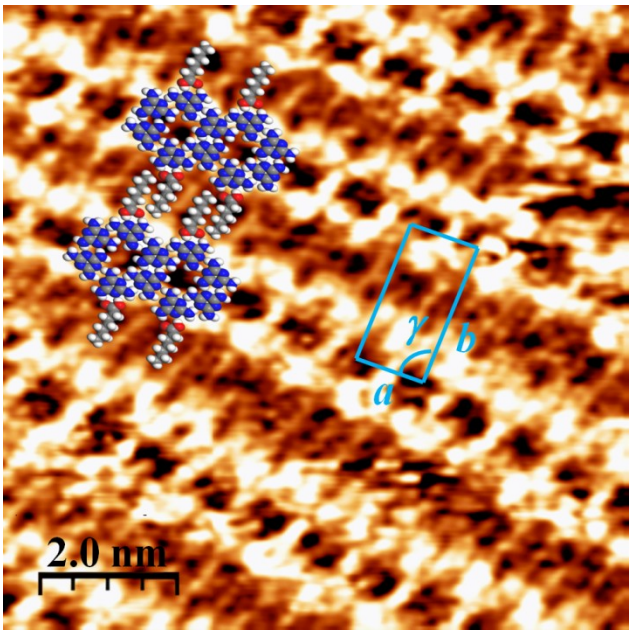

Figure 4. STM image of the 2D cocrystallization of melamine (**4**) and heptanoic acid on HOPG (deposition from heptanoic acid, with V_{bias} = -1.39 V and I_{set} = 0.10 nA). Superimposed on the image are a scale bar, the measured unit cell, and a model of the proposed assembly.

Conclusions

To help reveal how analogous 3D and 2D structures can be built by design, we have used XRD and STM in combination to analyze and compare the cocrystallization of aminoazines **1**-**4** with alkanecarboxylic acids. These components are attractive candidates for a comparative study for three primary reasons: (1) Aminoazines and alkanecarboxylic acids have strong individual affinities for the surface of graphite; (2) together, they tend to form predictable coplanar hydrogen-bonded aggregates that are also strongly adsorbed on graphite; and (3) the alkanecarboxylic acids can in principle be varied to change the metrics of 3D and 2D assemblies in a rational way.

In ideal comparisons of molecular organization in 3D and 2D, each compound studied should yield 3D crystals suitable for analysis by XRD and well-ordered 2D assemblies for characterization by STM, all under essentially the same conditions. These highly demanding criteria could not be met for the entire series of aminoazines **1**-**4**. However, when both 3D and 2D crystallization could be achieved, as in the case of 2-aminotriazine **1**/nonanoic acid, the resulting assemblies proved to be identical in composition and remarkably similar in structure. In the cases of aminoazines **2**-**4**, it was not possible to find conditions allowing 3D and 2D crystallization of the same components to be compared directly; collectively, however, the observed 3D and 2D structures show a consistent preference for molecular association by coplanar hydrogen bonding, leading to the formation of flat tapes. We suggest that preferred formation of these tapes helps account for similarities in molecular organization observed in 3D and 2D.

Our work focuses on the behavior of a particular family of compounds and their adsorption on a single surface. However, the results reflect a potentially general pattern of homologous 3D and 2D organization that has also been observed in studies of other compounds.[4,5] Together, these observations help confirm the key elements of a logical strategy for devising molecular materials that predictably adopt similar ordered structures in both thin layers and bulk samples. This strategy is based on choosing components that combine an affinity for surfaces with a tendency to form sheets held together by strong coplanar intermolecular interactions such as hydrogen bonds. Combined, these interactions should be similar in strength to the overall energy of molecular adsorption, so that the resulting organization is not dictated primarily by the nature of the surface.

Our experimental observations support computational evidence that aminoazines and related compounds are bound by graphite with a strength similar to that of interadsorbate hydrogen bonding.[5,11] Moreover, the existence of specific stabilizing interactions with graphite does not appear to prevent the NH_2 groups of aminoazines from simultaneously engaging in intermolecular hydrogen bonds that help direct predictable 2D crystallization. Our results may therefore help identify other families of compounds that dependably favor analogous crystallization in 3D and 2D, possibly even when multiple surfaces are used and when significant epitaxy is not present.

Experimental Section

General Notes. All compounds were purchased from commercial sources and used without further purification.

Studies of 2D Crystallization by STM. All STM experiments were performed at room temperature (20-25 °C) using a JEOL-5200 SPM instrument equipped with a narrow scanner. Platinum/iridium STM tips were mechanically cut from wire (Pt/Ir, 80%/20%, diameter = 0.25 mm). In typical experiments, the freshly cleaved basal surface of HOPG (Structure Probe, Inc., SPI-1 grade) was first imaged to determine the quality of the Pt/Ir tip and the smoothness of the graphite surface. Once this was determined, a droplet (~ 1 μL) of a saturated solution of aminoazines **1**-**4** in alkanecarboxylic acids was applied. STM investigations were then carried out at the liquid-solid interface in the constant-current mode. STM imaging was performed by changing the tunneling parameters (voltage applied to the tip and the average tunneling current). Raw STM images were processed using a JEOL software package (WinSPM Data Processing System, Version 2.15, R. B. Leane, JEOL Ltd.) and a freeware (WSxM 5.0 Develop 1.2, Nanotec Electrónica S. L.).[26] A smooth 3 × 3 matrix convolution filter was used to produce the final images.

Studies of 3D Crystallization by XRD. Cocrystals were obtained by slow evaporation of solutions of aminoazines **1**-**3** in alkanecarboxylic acids. Crystallographic data were collected at 150 K using a Bruker Microstar diffractometer with Cu Kα radiation. The structures were solved by direct methods using SHELXS-97 and refined with SHELXL-97.[27] Non-hydrogen atoms were

refined anisotropically, whereas hydrogen atoms were placed in ideal positions and refined as riding atoms. In all structural studies, calculated powder X-ray diffraction patterns closely matched those obtained experimentally by analysis of bulk crystalline samples.[21]

Acknowledgments

We are grateful to the Natural Sciences and Engineering Research Council of Canada, the Ministère de l'Éducation du Québec, the Canada Foundation for Innovation, the Canada Research Chairs Program, and Université de Montréal for financial support. In addition, we thank Dr. Valérie Métivaud (Département de Chimie, Université de Montréal) for analyzing bulk crystalline samples by powder X-ray diffraction, and we are grateful to Ji-Hyun Yi and Prof. Antonio Nanci for helping us obtain STM images.

Supporting Information Available. Additional crystallographic details (including thermal atomic displacement ellipsoid plots, powder X-ray diffraction patterns, and tables of structural data in CIF format), supplementary STM images, and analyses of 2D unit cell parameters. This material is available free of charge via the Internet at http://pubs.rsc.org.

Notes and References

1. For illustrative summaries of the challenges encountered in predicting the structures and properties of molecular crystals, see: J. D. Dunitz, *Chem. Commun.*, 2003, 545-548. G. R. Desiraju, *Nature Materials*, 2002, **1**, 77-79. A. Gavezzotti, *Acc. Chem. Res.*, 1994, **27**, 309-314. J. Maddox, *Nature*, 1988, **335**, 201.

2. For recent overviews of the strategy, see: M. D. Ward, *Struct. Bond.*, 2009, **132**, 1-23. J. D. Wuest, *Chem. Commun.*, 2005, 5830-5837. M. W. Hosseini, *Acc. Chem. Res.*, 2005, **38**, 313-323.
3. For recent examples of the 2D crystallization of structurally well-defined compounds able to engage in multiple intermolecular interactions, see: A. G. Phillips, L. M. A. Perdigão, P. H. Beton and N. R. Champness, *Chem. Commun.*, 2010, 2775-2777. N. T. N. Ha, T. G. Gopakumar, R. Gutzler, M. Lackinger, H. Tang and M. Hietschold, *J. Phys. Chem. C*, 2010, **114**, 3531-3636. A. Ciesielski, L. Piot, P. Samorì, A. Jouaiti and M. W. Hosseini, *Adv. Mater.*, 2009, **21**, 1131-1136. W. Mamdouh, R. E. A. Kelly, M. Dong, L. N. Kantorovich and F. Besenbacher, *J. Am. Chem. Soc.*, 2008, **130**, 695-702. H. Zhou, H. Dang, J.-H. Yi, A. Nanci, A. Rochefort and J. D. Wuest, *J. Am. Chem. Soc.*, 2007, **129**, 13774-13775. M. Ruben, D. Payer, A. Landa, A. Comisso, C. Gattinoni, N. Lin, J.-P. Collin, J.-P. Sauvage, A. De Vita and K. Kern, *J. Am. Chem. Soc.*, 2006, **128**, 15644-15651. T. Yokoyama, S. Yokoyama, T. Kamikado, Y. Okuno and S. Mashiko, *Nature*, 2001, **413**, 619-621.
4. For examples of this approach, see: K. G. Nath, O. Ivasenko, J. M. MacLeod, J. A. Miwa, J. D. Wuest, A. Nanci, D. F. Perepichka and F. Rosei, *J. Phys. Chem. C*, 2007, **111**, 16996-17007. H. Dang, T. Maris, J.-H. Yi, F. Rosei, A. Nanci and J. D. Wuest, *Langmuir*, 2007, **23**, 11980-11985.
5. A. Duong, M.-A. Dubois, T. Maris, V. Métivaud, J.-H. Yi, A. Nanci, A. Rochefort and J. D. Wuest, *J. Phys. Chem. C*, 2011, **115**, in press.
6. For reviews of the subject of molecular epitaxy on solid surfaces, see: G. Witte and C. Wöll, *J. Mater. Res.*, 2004, **19**, 1889-1916. D. E. Hooks, T. Fritz and M. D. Ward, *Adv. Mater.*, 2001, **13**, 227-241. S. R. Forrest, *Chem. Rev.*, 1997, **97**, 1793-1896.

7. For representative recent examples, see: C. Meier, K. Landfester and U. Ziener, *J. Phys. Chem. C*, 2009, **113**, 1507-1514. X. Zeng, L. Wang, L. Duan and Y. Qiu, *Cryst. Growth Des.* 2008, **8**, 1617-1622. M. Campione, S. Caprioli, M. Moret and A. Sassella, *J. Phys. Chem. C*, 2007, **111**, 12741-12746.
8. K. E. Maly, E. Gagnon, T. Maris and J. D. Wuest, *J. Am. Chem. Soc.*, 2007, **129**, 4306-4322.
9. A. Nangia and G. R. Desiraju, *Top. Curr. Chem.*, 1998, **198**, 57-95. G. R. Desiraju, *Angew. Chem., Int. Ed.*, 1995, **34**, 2311-2327.
10. For examples, see: V. R. Pedireddi, S. Chatterjee, A. Ranganathan and C. N. R. Rao, *Tetrahedron*, 1998, **54**, 9457-9474. M. C. Etter and D. A. Adsmond, *Chem. Commun.*, 1990, 589-591. F. Garcia-Tellado, S. Goswami, S.-K. Chang, S. J. Geib and A. D. Hamilton, *J. Am. Chem. Soc.*, 1990, **112**, 7393-7394.
11. A. Rochefort and J. D. Wuest, *Chem. Commun.*, 2010, 2923-2925.
12. For a related computational study, see: M. Mura, N. Martsinovich and L. Kantorovich, *Nanotechnology*, 2008, **19**, 465704.
13. For recent examples and further discussion, see: T. K. Phillips, T. Bhinde, S. M. Clarke, S. Y. Lee, K. S. Mali and S. De Feyter, *J. Phys. Chem. C*, 2010, **114**, 6027-6034. N. T. M. Hai, M. Van der Auweraer, K. Müllen and S. De Feyter, *J. Phys. Chem. C*, 2009, **113**, 11567-11574. K. E. Plass, K. Kim and A. J. Matzger, *J. Am. Chem. Soc.*, 2004, **126**, 9042-9053.
14. For an overview of the use of carboxylic acids to help direct 2D self-assembly, see: M. Lackinger and W. M. Heckl, *Langmuir*, 2009, **25**, 11307-11321.
15. The small difference between the pK_a values of alkanecarboxylic acids and those of the conjugate acids of aminoazines such as melamine (pK_a ~5)[16] provides little driving force for proton transfer.[17]

16. Y. H. Jang, S. Hwang, S. B. Chang, J. Ku and D. S. Chung, *J. Phys. Chem. A*, 2009, **113**, 13036-13040. T. Tashiro, *J. Heterocyclic Chem.*, 2002, **39**, 615-622. R. C. Hirt, R. G. Schmitt, H. L. Strauss and J. G. Koren, *J. Chem. Eng. Data*, 1961, **6**, 610-612. J. R. Dudley, *J. Am. Chem. Soc.*, 1951, **73**, 3007-3008. J. K. Dixon, N. T. Woodberry and G. W. Costa, *J. Am. Chem. Soc.*, 1947, **69**, 599-603.
17. For discussion, see: G. He, P. S. Chow and R. B. H. Tan, *Cryst. Growth. Des.*, 2009, **9**, 4529-4532. S. Mohamed, D. A. Tocher, M. Vickers, P. G. Karamertzanis and S. L. Price, *Cryst. Growth. Des.* 2009, **9**, 2881-2889. S. L. Childs, G. P. Stahly and A. Park, *Mol. Pharmaceutics*, 2007, **4**, 323-338. B. R. Bhogala, S. Basavoju and A. Nangia, *CrystEngComm*, 2005, **7**, 551-562.
18. For examples of related bifurcated hydrogen bonds, see: H. Aghabozorg, J. A. Gharamaleki, M. M. Olmstead, Z. Derikvand and S. Hooshmand, *Acta Crystallogr.*, 2009, **E65**, m186-m187. T. Šmejkal and B. Breit, *Angew. Chem., Int. Ed.*, 2008, **47**, 311-315. A. J. Preston, J. C. Gallucci and J. R. Parquette, *Chem. Commun.*, 2005, 3280-3282. T. W. Bell, A. B. Khasanov and M. G. B. Drew, *J. Am. Chem. Soc.*, 2002, **124**, 14092-14103. T. W. Bell, A. B. Khasanov, M. G. B. Drew, A. Filikov and T. L. James, *Angew. Chem., Int. Ed.*, 1999, **38**, 2543-2547.
19. G. R. Desiraju and T. Steiner, *The Weak Hydrogen Bond in Structural Chemistry and Biology*; Oxford University Press: Oxford, U. K., 1999.
20. For a review of C-H···O interactions, see: G. R. Desiraju, *Chem. Commun.*, 2005, 2995-3001.
21. See the Supporting Information for details.
22. A. Rochefort and J. D. Wuest, *Langmuir*, 2009, **25**, 210-215.

23. H. Walch, A.-K. Maier, W. M. Heckl and M. Lackinger, *J. Phys. Chem. C*, 2009, **113**, 1014-1019.

24. For a related study of the adsorption and coadsorption of melamine (**4**) on HOPG, see: X. Zhang, T. Chen, Q. Chen, L. Wang and L.-J. Wan, *Phys. Chem. Chem. Phys.*, 2009, **11**, 7708-7712.

25. For related studies of the adsorption or coadsorption of melamine (**4**) on other surfaces, see: C.-A. Palma, J. Bjork, M. Bonini, M. S. Dyer, A. Llanes-Pallas, D. Bonifazi, M. Persson and P. Samorì, *J. Am. Chem. Soc.*, 2009, **131**, 13062-13071. H.-M. Zhang, Z.-K. Pei, Z.-X. Xie, L.-S. Long, B.-W. Mao, X. Xu and L.-S. Zheng, *J. Phys. Chem. C*, 2009, **113**, 13940-13946. R. Madueno, M. T. Räisänen, C. Silien and M. Buck, *Nature*, 2008, **454,** 618-621. F. Silly, A. Q. Shaw, M. R. Castell, G. A. D. Briggs, M. Mura, N. Martsinovich and L. Kantorovich, *J. Phys. Chem. C*, 2008, **112**, 11476-11480. L. M. A. Perdigão, A. Saywell, G. N. Fontes, P. A. Staniec, G. Goretzki, A. G. Phillips, N. R. Champness and P. H. Beton, *Chem. Eur. J.*, 2008, **14**, 7600-7607. P. A. Staniec, L. M. A. Perdigão, B. L. Rogers, N. R. Champness and P. H. Beton, *J. Phys. Chem. C*, 2007, **111**, 886-893. W. Xu, M. Dong, H. Gersen, E. Rauls, S. Vázquez-Campos, M. Crego-Calama, D. N. Reinhoudt, I. Stensgaard, E. Laegsgaard, T. R. Linderoth and F. Besenbacher, *Small*, 2007, **3**, 854-858. L. M. A. Perdigão, N. R. Champness and P. H. Beton, *Chem. Commun.*, 2006, 538-540. J. A. Theobald, N. S. Oxtoby, M. A. Phillips, N. R. Champness and P. H. Beton, *Nature*, 2003, **424**, 1029-1031.

26. I. Horcas, R. Fernández, J. M. Gómez-Rodríguez, J. Colchero, J. Gómez-Herrero and A. M. Baro, *Rev. Sci. Instrum.*, 2007, **78**, 01375.

27. G. M. Sheldrick, *Acta Crystallogr*., 2008, **A64**, 112-122.

2.4 Conclusions

Nos études sur les composés aminoazine ont confirmé la tendance de ces molécules à co-cristalliser avec les acides alcanecarboxyliques par la formation de ponts hydrogène. Ces agrégations favorisent la création de rubans sensiblement planaires qui s'organisent en couche à la fois en 2D et en 3D. La stratégie que nous avons suivie ici est basée sur le choix des composantes moléculaires qui ont une affinité pour s'adsorber sur les surfaces, ainsi qu'une tendance à former des feuillets maintenus ensemble par de fortes interactions intermoléculaires coplanaires telles que les liaisons hydrogène. Nos observations expérimentales ont été soutenues par des calculs théoriques qui suggèrent que les aminoazines ainsi que des composés apparentés ont une affinité particulière pour le graphite. En outre, bien que les calculs aient montré l'existence d'interactions spécifiques stabilisantes entre les groupements NH_2 et le graphite, cela n'empêche pas d'avoir des interactions intermoléculaires si fortes que la surface ne joue qu'un rôle mineur dans l'organisation 2D. L'ensemble de ces résultats suggèrent qu'il est possible de concevoir d'autres familles de composés qui favorisent une cristallisation analogue en 3D et en 2D tel que sera presenté dans les chapitres 3 et 4 qui suivent.

Chapitre 3

Organisation 2D des acides pyridinecarboxyliques adsorbés sur le graphite

3.1 Introduction

Attirés à la fois par le potentiel des applications que pourraient engendrer les études d'organisation 2D et par le désir d'acquérir une meilleure compréhension générale des associations moléculaires, nous avons entrepris une étude des acides pyridinecarboxyliques, une deuxième famille de molécules identifiée pour sa capacité de favoriser une organisation prévisible, régie par les ponts hydrogène, à la surface du graphite. Ce choix a été basé sur des calculs théoriques de la théorie de la fonctionnelle de densité (DFT) et des structures cristallographiques en 3D, qui suggèrent que les acides pyridinecarboxyliques présentent une forte affinité pour le graphite et une capacité à s'organiser en 2D par liaisons hydrogène.

3.2 Objectif

Le chapitre précédent a démontré l'efficacité de la tectonique moléculaire pour diriger l'assemblage des molécules en 2D. Nous avons vu que les aminoazines s'organisent avec des acides carboxyliques de manière prévisible, avec une forte analogie en 2D et en 3D. L'étude que nous décrivons dans le chapitre 3 a été motivée par le succès du travail précédent avec les aminoazines. Notre objectif est d'explorer davantage l'organisation 2D sur le graphite et de mieux comprendre comment cette organisation dépend de la nature des molécules adsorbées. Nous avons sélectionné une série de composés de type pyridyle substitué avec des groupements acides carboxyliques pour augmenter l'affinité pour la surface et introduire en même temps la possibilité de former des ponts hydrogène avec l'atome d'azote de la partie pyridyle. Les résultats de ce chapitre et le précédent serviront de base de données pour des études de composés analogues qui combinent les groupements aminoazinyle et pyridyle.

3.3 Article 2

2D Molecular Organization of Pyridinecarboxylic Acids Adsorbed on Graphite

Adam Duong, Marc-André Dubois, and James D. Wuest*

Langmuir **2010**, *26(23)*, 18089-18096

Abstract

Pyridinecarboxylic acids **3-9** are adsorbed from solution onto graphite to produce well-ordered adlayers that can be imaged by STM. Hydrogen bonds involving the carboxyl groups and the nitrogen atom of the pyridyl ring play key roles in controlling the observed 2D organization. Pyridinecarboxylic acids have a strong tendency to associate to form hydrogen-bonded chains and cyclic oligomers, which then pack to produce sheets. The preference for sheets ensures that molecular organization in 2D and 3D typically shows a significant degree of homology. Together, our observations highlight the potential of engineering similarly ordered 2D and 3D structures built from simple compounds that combine an inherent affinity for surfaces with an ability to engage in strong coplanar intermolecular interactions.

Introduction

Molecules can be physisorbed on suitable surfaces to produce ordered adlayers.[1] Adsorption thereby allows the creation of thin molecular layers with defined structures and properties, and these layers can alter the behavior of the underlying material. As a result, the creation of molecules designed to be adsorbed on surfaces as organized arrays is a subject of very active research, driven both by the potential for applications and by the desire to acquire a deeper understanding of molecular association.[1-6] Molecules designed to produce particular patterns of adsorption need an inherently strong affinity for the underlying surface, combined with an ability to engage in specific coplanar intermolecular interactions that help direct organization. The resulting organization can be analyzed in molecular detail on atomically flat surfaces by using scanning probe microscopy.[7]

The basal plane of graphite provides a flat ordered surface suitable for adsorbing various molecular compounds from solution. Most previous studies of adsorption on graphite from solution have involved compounds with long alkyl chains, which have a well-established affinity for graphite and align preferentially with specific directions on the surface.[8] However, recent studies using scanning tunneling microscopy (STM) have revealed that well-ordered adlayers can also be created on graphite by simple functionalized aromatic compounds without alkyl chains, when properly designed to engage in strong adsorbate-adsorbate and surface-adsorbate interactions.[4-6,9-10] Such studies have significantly expanded the scope of engineering 2D molecular structures. For example, trimesic acid (**1**) is adsorbed from solution onto the surface of graphite as ordered 2D networks held together by hydrogen bonding of carboxyl groups (COOH)

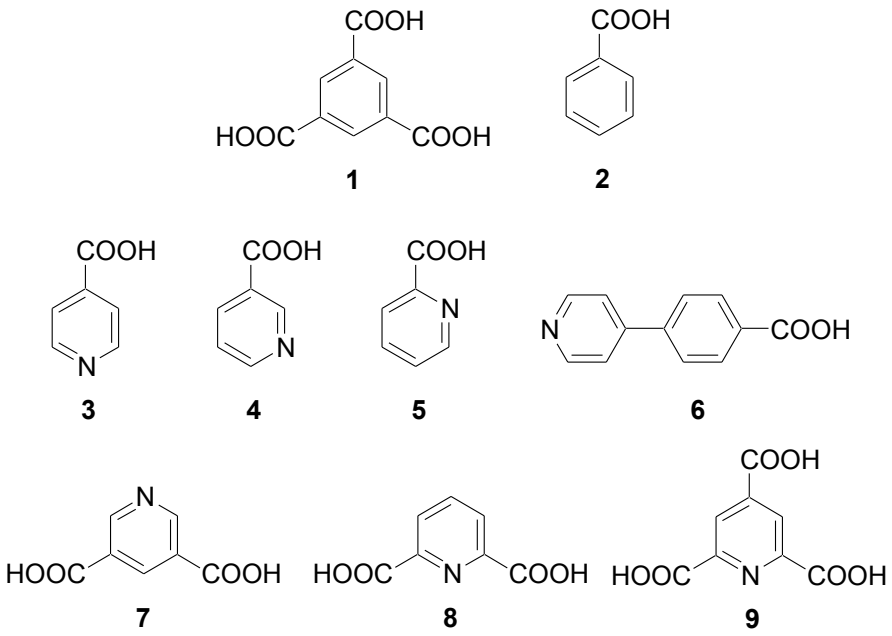

according to characteristic motifs.[6,11] The three carboxyl groups in trimesic acid (**1**) act in synergy to introduce electronic effects that increase the affinity for graphite,[10] and the groups also ensure that all molecules are linked to multiple neighbors by strong coplanar interadsorbate interactions, thereby giving the resulting 2D networks special kinetic and thermodynamic stability. When a lower degree of functionalization is present, as in benzoic acid (**2**), synergy is reduced, and well-ordered adsorption on graphite is expected to be less favorable. Indeed, characterization by STM of adlayers on graphite composed solely of benzoic acid (**2**) has not been reported.[12-14]

We reasoned that analogous pyridinecarboxylic acids **3-9** might generate characterizable 2D networks on graphite, both because the pyridyl core is more strongly adsorbed than benzene[9] and because compounds **3-9** can engage in strong intermolecular hydrogen bonding involving carboxyl groups and the nitrogen atom of pyridyl rings.[15-23] Surprisingly, no detailed studies of the adsorption of any of these compounds on graphite have been published previously,and there

are few reports of their interaction with other surfaces.[24-25] We have found that compounds **3-9** are all adsorbed on graphite to yield well-ordered arrays with predictable features directed in part by hydrogen bonding.

Results and Discussion

Compounds **3-9** were obtained from commercial sources and used without further purification. In typical experiments, droplets of saturated solutions of the compounds in heptanoic acid were placed on the surface of highly-oriented pyrolytic graphite (HOPG), and the resulting adsorption was imaged by STM at the liquid-solid interface.

Adsorption of 4-Pyridinecarboxylic Acid (3). A representative STM image of the adsorption of 4-pyridinecarboxylic acid (**3**) on HOPG appears in Figure 1, along with a superimposed unit cell and a model of the proposed molecular organization. The unit cell parameters are a = 9.6 Å, b = 10.3 Å, and γ = 40°. As expected, the molecules bind to HOPG to form well-ordered arrays, which can be interpreted as consisting of head-to-tail chains linked primarily by O-H···N hydrogen bonds augmented by secondary C-H···O interactions,[26-27] as found in other periodic structures in which pyridines interact with carboxylic acids.[15-23] Full proton transfer from O to N, which would lead to an alternative zwitterionic pyridiniumcarboxylate structure joined by $COO^-\cdots H\text{-}N^+$ hydrogen bonds, cannot be rigorously excluded by analysis of the STM images alone.[28] Packing of the chains is presumably controlled in part by the formation of interchain C-H···O interactions. Together, these interactions give rise to the proposed chiral 2D structure shown in Figure 1b, in which all chains run in the same direction.

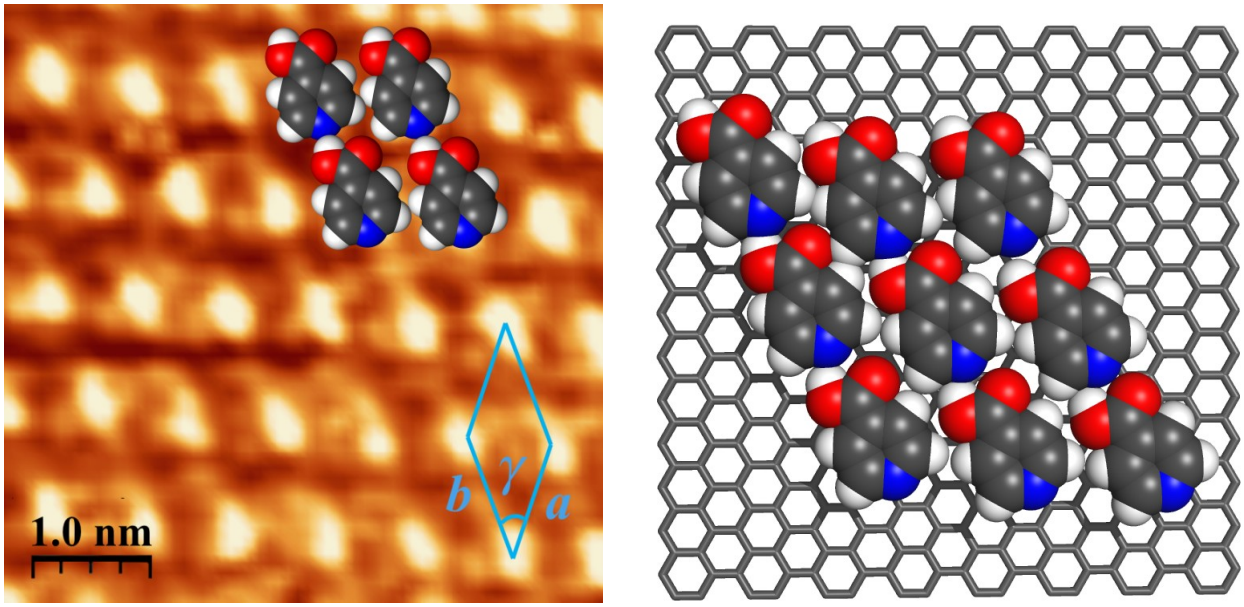

a **b**

Figure 1. (a) STM image of the adsorption of 4-pyridinecarboxylic acid (**3**) on HOPG (deposition from heptanoic acid, with V_{bias} = -1.39 V and I_{set} = 0.13 nA). Superimposed on the image are a scale bar, the measured unit cell, and approximate molecular models added as visual aids to facilitate interpretation of the pattern of contrasts. (b) Detailed semiempirical model of a possible 2D assembly.

Support for the structural hypothesis shown in Figure 1 is provided by a related study of the adsorption of 4-pyridinecarboxylic acid (**3**) on Ag(111) under high vacuum, which is believed to occur in essentially the same way.[24] Our interpretation of the STM data is further reinforced by the observation that compound **3** crystallizes from water to give a nonionic 3D structure built from hydrogen-bonded chains fully analogous to those postulated in Figure 1.[16] In the 3D crystals, adjacent chains are not strictly coplanar but can be considered to define corrugated sheets parallel to (100), in which all chains run along the *b* axis and are oriented head-to-tail in

the same direction. All chains in adjacent sheets also run head-to-tail along the *b* axis but in the opposite direction.

In the 3D structure, molecular separation along the chains (*b* axis) is 7.469(1) Å, which is similar to the corresponding parameter estimated by STM in 2D (a = 9.6 Å). The difference may in part reflect efforts to achieve registration with the substrate. In addition, hydrogen bonding may be somewhat weakened by adsorption,[9-10] leading to the possibility of increased molecular separation within the chains. In 3D, the centroids of neighboring pyridyl rings in adjacent chains in the same sheet are separated by 6.392(1) Å, whereas the corresponding 2D value is 10.3 Å. These distances cannot be compared directly because molecules in the 3D structure are not confined to a common plane. However, the larger interchain distance in 2D may also result in part from potential dipolar repulsion of parallel head-to-tail hydrogen-bonded chains within the adlayer. This effect is counterbalanced in 3D by the opposed orientation of adjacent sheets, but no obvious compensation is provided in 2D. As a result, it is possible that the true 2D structure of 4-pyridinecarboxylic acid (**3**) is not that proposed in Figure 1 but rather a related alternative in which adjacent hydrogen-bonded chains are antiparallel.

Indeed, the observed 3D crystal structure of compound **3** can also be interpreted as consisting of hydrogen-bonded head-to-tail chains that define corrugated sheets parallel to (101), in which adjacent chains adopt an antiparallel orientation. It is unclear why this plausible alternative was not considered in the previous study of the adsorption of compound **3** on Ag(111).[24] Whether the hydrogen-bonded chains are parallel or antiparallel, the increased

intrachain distance observed in 2D makes it unlikely that compound **3** is adsorbed in zwitterionic form, which would presumably lead to the formation of shortened ionic hydrogen bonds.[29]

The behavior of 4-pyridinecarboxylic acid (**3**) offers a compelling illustration of the following principles, which are emerging as key guidelines for controlling molecular organization in 2D and 3D : 1) Predictably ordered adlayers can be produced from a diversity of small molecules that combine an affinity for surfaces with an ability to engage in multiple coplanar interadsorbate interactions;[4-6] 2) by designing such molecules so that they associate to form sheets, it is possible to engineer 2D and 3D structures with a high degree of homology;[5] and 3) when interadsorbate interactions are sufficiently strong, they can play a dominant role in organizing adlayers and can help direct the formation of a single 2D structure, regardless of the method of deposition, the identity of the substrate, or the relative orientation of the underlying surface.

Compound **3** adheres to these principles and displays a preference for a single 2D polymorph, as shown by the similar modes of adsorption that are observed on graphite and Ag, using deposition either under vacuum or from solution. It would be possible to test this preference more thoroughly by examining adsorption under a wider range of conditions, in which the substrate, solvent, concentration, temperature, and other parameters are changed. However, instead of focusing narrowly on the single pyridinecarboxylic acid **3**, we elected to compare its behavior with that of a series of related compounds under similar conditions.

Adsorption of 3-Pyridinecarboxylic Acid (4). A typical STM image of the adsorption of isomeric 3-pyridinecarboxylic acid (**4**) on HOPG is shown in Figure 2, together with a superimposed unit cell and a model of the postulated molecular organization. The unit cell parameters are a = 7.2 Å, b = 15.1 Å, and γ = 88°. These data suggest that compound **4** is adsorbed as distinct tight pairs, presumably head-to-tail dimers held together by two hydrogen bonds. The dimers may consist of compound **4** in either nonionic or zwitterionic form. The overall 2D assembly results from packing of the dimers, possibly controlled in part by the formation of C-H···O interactions.

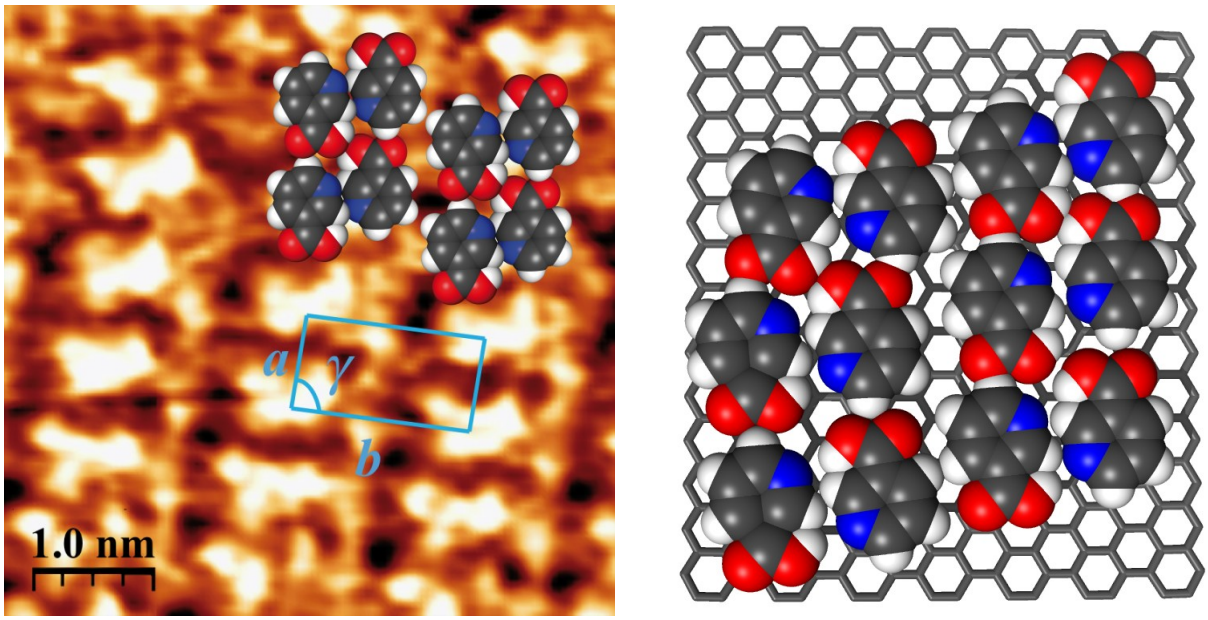

a **b**

Figure 2. (a) STM image of the adsorption of 3-pyridinecarboxylic acid (**4**) on HOPG (deposition from heptanoic acid, with V_{bias} = -1.50 V and I_{set} = 0.08 nA). Superimposed on the image are a scale bar, the measured unit cell, and approximate molecular models added as visual aids to facilitate interpretation of the pattern of contrasts. (b) Detailed semiempirical model of a possible 2D assembly.

In contrast, 3-pyridinecarboxylic acid (**4**) is known to crystallize from water or aqueous ethanol to give a 3D structure built from zig-zag chains in which individual nonionic molecules are linked head-to-tail along the *b* axis by primary O-H···N hydrogen bonds and secondary C-H···O interactions.[17-18] These chains then form stacks held together along the *c* axis by aromatic interactions of pyridyl rings. It is not clear why similar hydrogen-bonded chains are disfavored in 2D under the conditions we have examined. Compound **4** has a simple, nearly planar, and relatively rigid structure, and it is readily adsorbed on HOPG to form an adlayer ordered in part by hydrogen bonding, as planned. However, these predicted features do not guarantee that the 2D and 3D structures will automatically show a high degree of homology. It is possible, of course, that the observed 2D organization will prove to be more fully homologous with the 3D structure of an undiscovered polymorph of compound **4**.

Adsorption of 2-Pyridinecarboxylic Acid (5). Figure 3 shows a representative STM image of the adsorption of 2-pyridinecarboxylic acid (**5**) on HOPG, along with a superimposed unit cell and a model of the proposed molecular organization. The unit cell parameters are a = 7.2 Å, b = 9.8 Å, and γ = 87°. Like isomer **4**, compound **5** appears to be adsorbed as tight pairs, presumably either nonionic or zwitterionic head-to-tail dimers linked by two hydrogen bonds. The ultimate 2D organization results from packing of these dimers, possibly directed in part by C-H···O interactions.

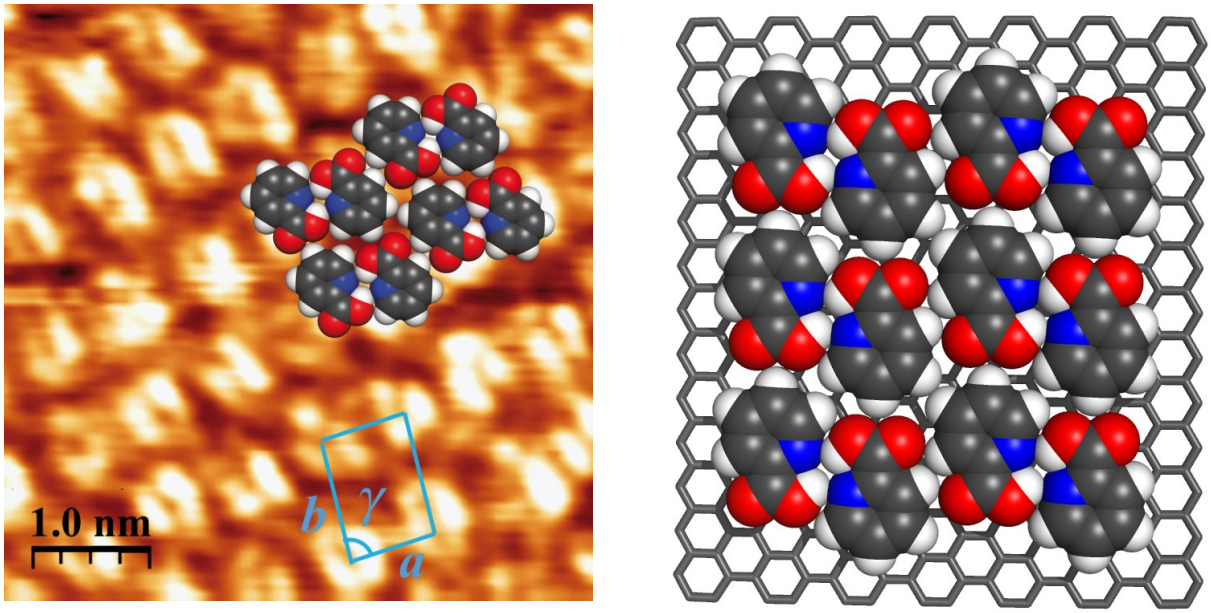

a **b**

Figure 3. (a) STM image of the adsorption of 2-pyridinecarboxylic acid (**5**) on HOPG (deposition from heptanoic acid, with V_{bias} = -1.50 V and I_{set} = 0.09 nA). Superimposed on the image are a scale bar, the measured unit cell, and approximate molecular models added as visual aids to facilitate interpretation of the pattern of contrasts. (b) Detailed semiempirical model of a possible 2D assembly.

In contrast, crystallization of 2-pyridinecarboxylic acid (**5**) from benzene was found to produce a 3D structure that can be considered to be a 1:1 cocrystal of the nonionic and zwitterionic forms.[19-20] The structure is composed of zig-zag chains in which alternating nonionic and zwitterionic molecules are linked head-to-head and tail-to-tail along the *c* axis by N-H^{+}···N and COO-H···$^{-}$OOC hydrogen bonds. These chains then pack to form sheets parallel to (101). As in the case of isomer **4**, compound **5** is properly designed to be adsorbed on HOPG to give an ordered adlayer with a structure directed in part by hydrogen bonding. The molecular

arrangements in 2D and 3D show a shared preference for the formation of hydrogen-bonded sheets, as expected, but the structures are not fully homologous.

Adsorption of 4-(4-Carboxyphenyl)pyridine (6). 4-(4-Carboxyphenyl)pyridine (**6**) is an elongated version of 4-pyridinecarboxylic acid (**3**) and might therefore be expected to be adsorbed on HOPG to give an analogous structure built from linear hydrogen-bonded head-to-tail chains. A typical STM image of the adsorption of compound **6** is shown in Figure 4, along with a superimposed unit cell and a model of the postulated molecular organization. The unit cell parameters are a = 9.1 Å, b = 12.9 Å, and γ = 50°. Comparison of Figures 1 and 4 reveals a closely similar pattern of contrasts, which can be interpreted to mean that compound **3** and its extended analogue **6** both form chiral 2D structures built from parallel head-to-tail chains consisting of molecules linked by predictable O-H···N hydrogen bonds.

No 3D structure of compound **6** has been reported, but related substances have been observed to be adsorbed on Ag(111) as similar hydrogen-bonded chains.[30] As in the case of compound **3**, we cannot rigorously exclude the possibility that compound **6** is adsorbed as a zwitterion or that the hydrogen-bonded chains have an antiparallel orientation. Indeed, the upper left part of the STM image shown in Figure 4a appears to show antiparallel chains that define the boundary between two enantiomorphous domains.

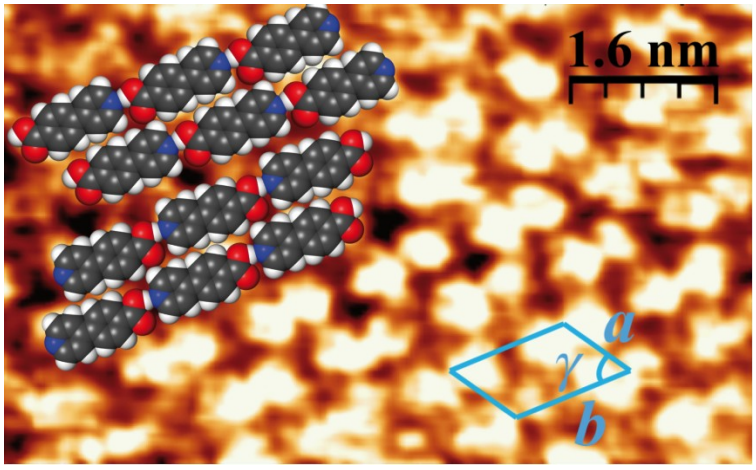

a

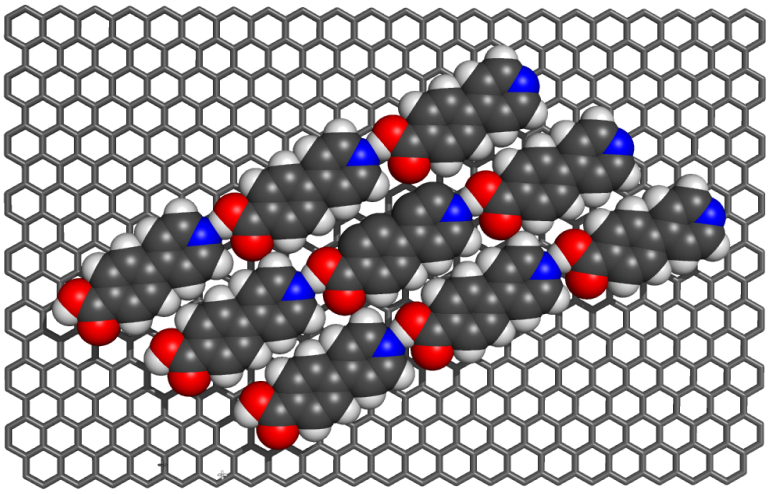

b

Figure 4. (a) STM image of the adsorption of 4-(4-carboxyphenyl)pyridine (**6**) on HOPG (deposition from heptanoic acid, with V_{bias} = -1.50 V and I_{set} = 0.27 nA). Superimposed on the image are a scale bar, the measured unit cell, and approximate molecular models added as visual aids to facilitate interpretation of the pattern of contrasts. (b) Detailed semiempirical model of a possible 2D assembly.

Coulombic interactions in the zwitterionic forms of 4-pyridinecarboxylic acid (**3**) and its elongated analogue **6** are presumably less stabilizing than those in the corresponding forms of 3-pyridinecarboxylic acid (**4**) and 2-pyridinecarboxylic acid (**5**), where the charges are closer together. Moreover, compounds **3** and **6** cannot yield tightly hydrogen-bonded pairs like those postulated for compounds **4** and **5**. For these reasons, compounds **3** and **6** have fewer attractive options for forming different structures, possibly leading to the higher degree of homology that we observe in their 2D and 3D structures.

Adsorption of 3,5-Pyridinedicarboxylic Acid (7). The adsorption of 3,5-pyridinedicarboxylic acid (**7**) on HOPG produces at least two types of periodic adlayers, as illustrated in Figures 5 and 6, which show representative STM images along with superimposed unit cells and models of the proposed molecular organization. The unit cell parameters for the mode of assembly shown in Figure 5 are a = 8.6 Å, b = 10.1 Å, and γ = 70°. The STM image of Figure 5 is consistent with the formation of zig-zag head-to-tail chains consisting of nonionic molecules linked by primary O-H···N hydrogen bonds involving the pyridyl nitrogen atom and one of the two carboxyl groups. Alternatively, the adsorbed molecules may be zwitterionic. In either case, further packing to give a sheet is directed in part by the formation of O-H···O hydrogen bonds involving carboxyl groups not used in forming the primary chains.

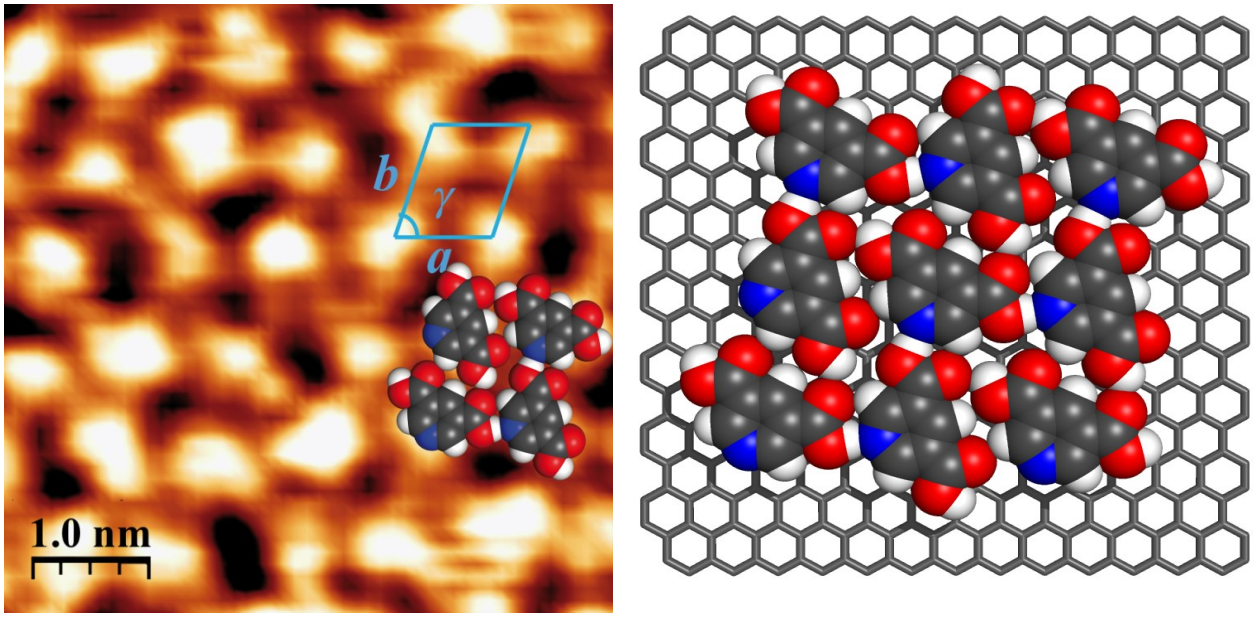

a **b**

Figure 5. (a) STM image showing one mode of adsorption of 3,5-pyridinedicarboxylic acid (**7**) on HOPG (deposition from heptanoic acid, with V_{bias} = -1.49 V and I_{set} = 0.10 nA). Superimposed on the image are a scale bar, the measured unit cell, and approximate molecular models added as visual aids to facilitate interpretation of the pattern of contrasts. (b) Detailed semiempirical model of a possible 2D assembly.

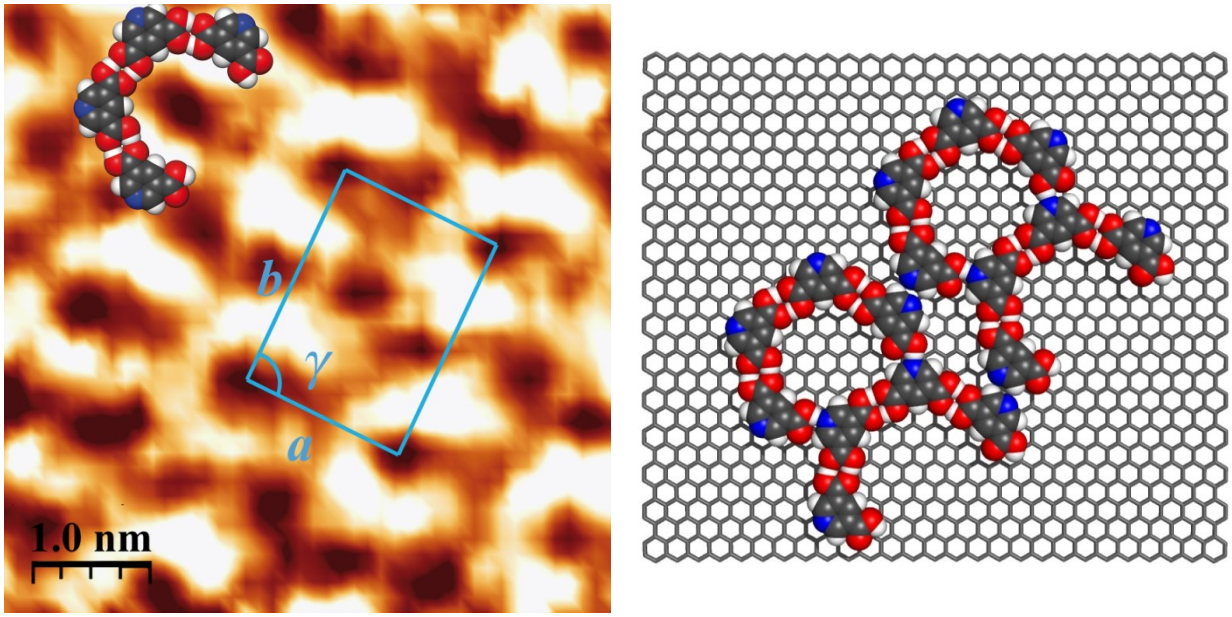

a **b**

Figure 6. (a) STM image showing a second mode of adsorption of 3,5-pyridinedicarboxylic acid (**7**) on HOPG (deposition from heptanoic acid, with V_{bias} = -1.49 V and I_{set} = 0.10 nA). Superimposed on the image are a scale bar, the measured unit cell, and approximate molecular models added as visual aids to facilitate interpretation of the pattern of contrasts. (b) Detailed semiempirical model of a possible 2D assembly.

Support for this interpretation of the STM image of Figure 5 is provided by detailed analysis of crystals of compound **7** grown from water, which have a closely related structure.[21-22] In this structure, the geometry of the molecular components suggests that they are zwitterionic, with the nitrogen atom protonated and one carboxyl group deprotonated. The molecules are linked along the *a* axis by ionic $COO^{-}\cdots H\text{-}N^{+}$ hydrogen bonds and associated C-H···O interactions to form zig-zag chains, which pack to produce sheets similar to those postulated in Figure 5.

In the 3D structure of 3,5-pyridinedicarboxylic acid (**7**), molecular separation along the chains is 7.330(1) Å, and the centroids of neighboring pyridyl rings in adjacent chains are separated by 9.699(1) Å. As noted in our quantitative comparison of the 2D and 3D structures of 4-pyridinecarboxylic acid (**3**), both of the 3D parameters for compound **7** are similar to the corresponding 2D distances estimated by STM (a = 8.6 Å, b = 10.1 Å). Again, differences may reflect adjustments to attain registration with the substrate, intrinsically weaker hydrogen bonding between adsorbed molecules,[9-10] and potentially repulsive dipolar interactions of the hydrogen-bonded chains in 2D that are counterbalanced in 3D by the orientation of adjacent sheets. The slightly larger intrachain distance measured in 2D can be interpreted to mean that compound **7** is adsorbed in its nonionic form, which would presumably lead to longer hydrogen bonds than those observed in the zwitterionic 3D structure.[29]

For the second mode of assembly of 3,5-pyridinedicarboxylic acid (**7**), illustrated in Figure 6, the unit cell parameters are a = 14.9 Å, b = 19.1 Å, and γ = 90°. The distinctive pattern of contrasts, which can be described as rows of horseshoes, is neatly consistent with the model proposed in Figure 6b. In this model, four nonionic molecules associate by double O-H···O hydrogen bonding typical of carboxyl groups to form each horseshoe, which is then connected by O-H···N hydrogen bonds and C-H···O interactions to the next horseshoes in the same row. Adjacent rows of horseshoes appear to be linked by pairs of C-H···N interactions involving pyridyl rings in contact.

A noteworthy feature of the STM image of Figure 6a is the discontinuity of contrast within the rows, which allows individual horseshoes to be distinguished clearly. This

discontinuity presumably reflects subtle differences that distinguish hydrogen bonding within horseshoes (O-H···O) from hydrogen bonding between horseshoes (O-H···N), which in turn alters intermolecular distances, the electronic properties of the pyridyl rings, and tunneling between the STM tip and the underlying surface of HOPG. The proposed 2D organization is uniquely consistent with the observed discontinuity. In addition, the postulated structure has features found in established supramolecular assemblies. For example, it is similar to cyclic hexamers of trimesic acid (**1**), which are formed in both 2D and 3D by hydrogen-bonded pairing of carboxyl groups,[6,11] and it also contains features found in the 3D structure of 3-pyridinecarboxylic acid (**4**),[17-18] which incorporates zig-zag chains held together by O-H···N hydrogen bonds. When combined, these known structures create a plausible hybrid that is equivalent to the organization proposed in Figure 6b. However, this organization offers a lower density of coverage than the more compact 2D polymorph shown in Figure 5, so it is presumably metastable or favored only when low concentrations are adsorbed.[3]

Adsorption of 2,6-Pyridinedicarboxylic Acid (8). Figure 7 shows a typical STM image of the adsorption of 2,6-pyridinedicarboxylic acid (**8**) on HOPG, along with a superimposed unit cell and a model of the postulated molecular organization. The unit cell parameters are $a = b =$ 19.3 Å and $\gamma = 60°$. The image unmistakeably shows a periodic array of cyclic structures. These structures appear to be largely hexameric and presumably result from association of compound **8** in nonionic form directed by hydrogen-bonded pairing of carboxyl groups, as observed in the 2D and 3D organization of trimesic acid (**1**).[6,11] In the pattern of contrasts shown in the STM image (Figure 7a), the bright rings are not perfectly coincident with the postulated cyclic hexamers but instead appear to follow their inner circumference. Detailed theoretical analysis of the image is

beyond the scope of the present work, but we attribute the observed pattern to effects on tunnelling caused by molecular tilting relative to the surface or by asymmetry in the π molecular orbitals of pyridinedicarboxylic acid **8**, induced by electron-withdrawing N atoms and COOH groups located along the inner circumference of the cyclic hexamers.[9-10,31]

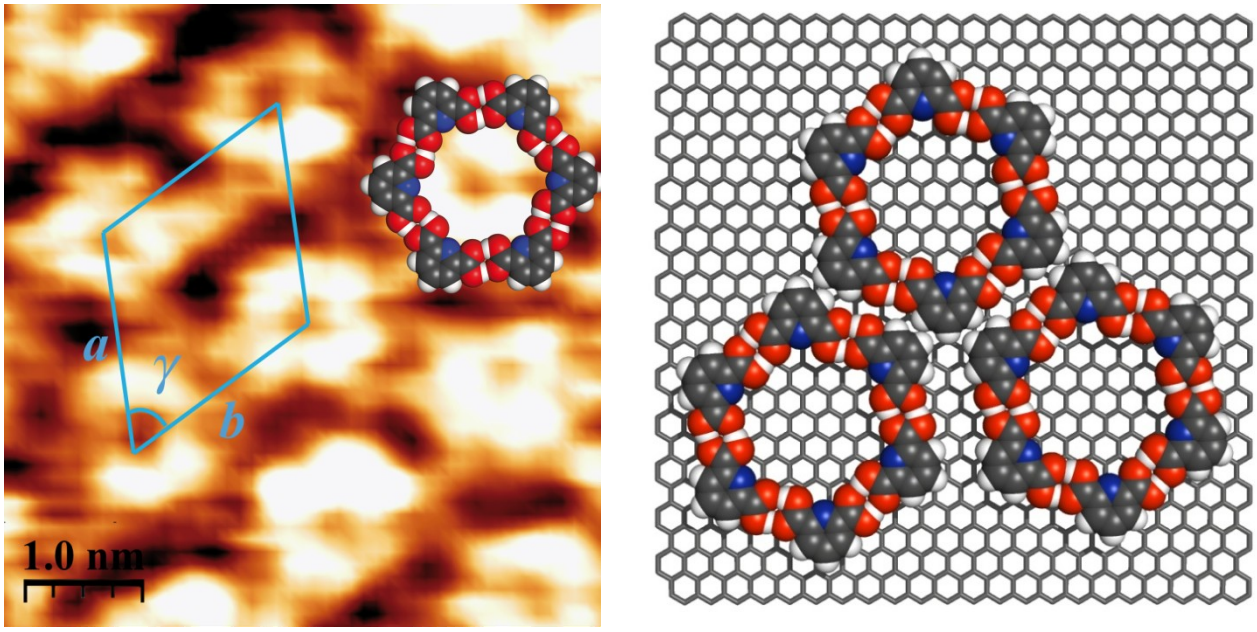

a **B**

Figure 7. (a) STM image showing the adsorption of 2,6-pyridinedicarboxylic acid (**8**) on HOPG (deposition from heptanoic acid, with V_{bias} = -0.70 V and I_{set} = 0.23 nA). Superimposed on the image are a scale bar and the measured unit cell. (b) Detailed model of a possible 2D assembly.

2,6-Pyridinedicarboxylic acid (**8**) is known to crystallize from water to produce a structure with features similar to those observed in adlayers.[23] In particular, the 3D crystals also contain sheets formed by molecules in the nonionic form, which again associate by hydrogen-bonded

pairing of carboxyl groups. However, the molecules are linked not into rings but rather into zig-zag chains, which run along the *b* axis and pack to form sheets parallel to (101). In 2D, such an organization would presumably offer a higher density of surface coverage than the observed periodic array of cyclic hexamers, which may be metastable or favored only when the concentration of compound **8** is low.[3]

Adsorption of 2,4,6-Pyridinetricarboxylic Acid (9). A representative STM image of the adsorption of 2,4,6-pyridinetricarboxylic acid (**9**) on HOPG appears in Figure 8, along with a superimposed unit cell and a model of the proposed molecular organization. The unit cell parameters are $a = b = 23.5$ Å and $\gamma = 60°$. As in the case of 2,6-pyridinedicarboxylic acid (**8**), adsorption of compound **9** produces a periodic array that incorporates cyclic structures. The organization appears to be analogous to the characteristic flower pattern adopted in 2D by trimesic acid (**1**).[6] In the structural model shown in Figure 8b, cyclic hexamers result from association of compound **9** in nonionic form, directed by hydrogen-bonded pairing of two of the three carboxyl groups. The third carboxyl group participates in the formation of a cyclic trimer that unites three adjacent hexamers. This results in a higher density of surface coverage than that produced by the alternative 2D honeycomb motif, in which all three carboxyl groups of compound **9** form doubly hydrogen-bonded pairs. Bright rings in the STM image (Figure 8a) are not fully coincident with the cyclic hexamers but are instead aligned with their inner circumference, as seen in the case of related pyridinedicarboxylic acid **8** (Figure 7a), presumably because of effects on tunneling due to molecular tilting or asymmetry in the π molecular orbitals.[9-10,31]

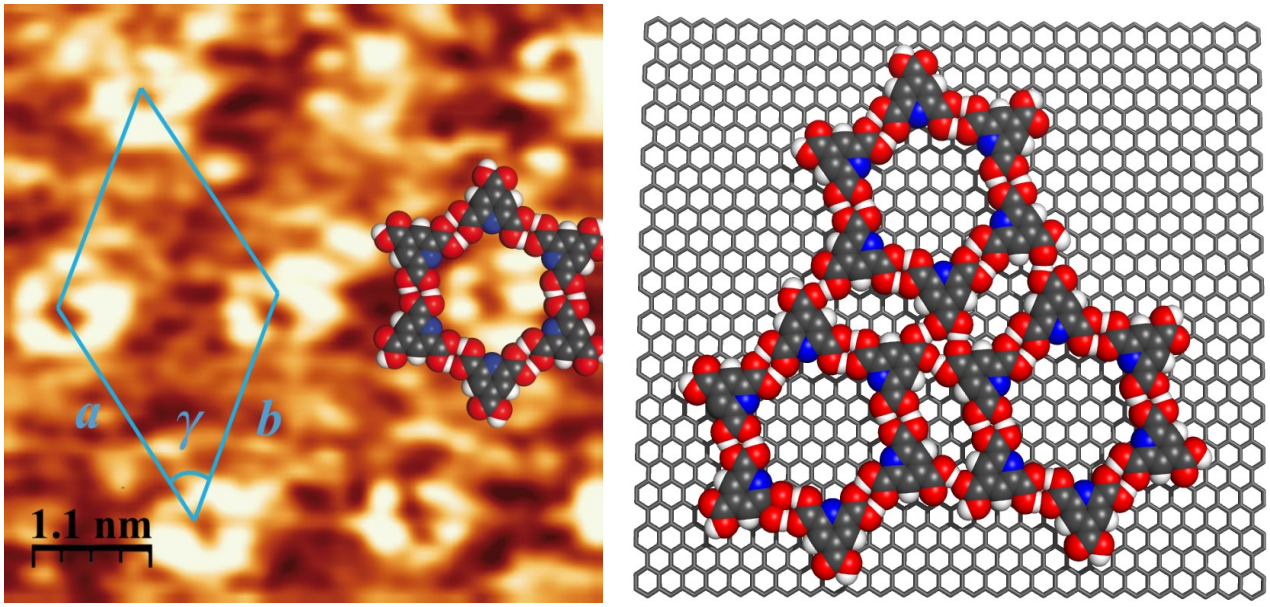

a **b**

Figure 8. (a) STM image showing the adsorption of 2,4,6-pyridinetricarboxylic acid (**9**) on HOPG (deposition from heptanoic acid, with V_{bias} = -1.50 V and I_{set} = 0.01 nA). Superimposed on the image are a scale bar and the measured unit cell. (b) Detailed model of a possible 2D assembly.

Figure 8b shows all nitrogen atoms of pyridyl rings directed toward the interior of the cyclic hexamers, but there is no reason to assume that the observed adlayer is fully ordered in this way. Indeed, the STM image of Figure 8a suggests the presence of numerous defects that may reflect orientational disorder of individual molecular components, cyclic structures that are not hexameric, or horseshoes resulting from incomplete cyclization. The structure of crystals composed uniquely of 2,4,6-pyridinetricarboxylic acid (**9**) has not been reported, so it is impossible to compare the organization of the compound in 2D and 3D.

Conclusions

In every case examined, pyridinecarboxylic acids can be adsorbed from solution onto graphite to produce ordered adlayers that can be imaged by STM. As expected, hydrogen bonds involving the carboxyl groups and the nitrogen atom of the pyridyl ring play key roles in controlling the observed 2D organization. Our results confirm that pyridinecarboxylic acids are particularly well designed to associate to form hydrogen-bonded chains and cyclic oligomers, which then pack to produce sheets. The preference for sheets ensures that molecular organization in 2D and 3D typically shows a significant degree of homology. Together, our observations highlight the potential of engineering predictably ordered 2D and 3D structures built from simple compounds that combine an inherent affinity for surfaces with an ability to engage in strong coplanar intermolecular interactions.

Experimental Section

General Notes. All compounds were purchased from commercial sources and used without further purification.

Studies of 2D Molecular Organization by STM. All STM experiments were performed at room temperature (20-25 °C) using a JEOL-5200 SPM instrument equipped with a narrow scanner. Platinum/iridium STM tips were mechanically cut from wire (Pt/Ir, 80%/20%, diameter = 0.25 mm). In typical experiments, the freshly cleaved basal surface of HOPG (Structure Probe, Inc., SPI-1 grade) was first imaged to determine the quality of the Pt/Ir tip and the smoothness of

the graphite surface. Once this was determined, a droplet (~ 1 μL) of a saturated solution of compounds **3**-**9** in heptanoic acid was applied. STM investigations were then carried out at the liquid-solid interface in the constant-height mode. STM imaging was performed by changing the tunneling parameters (voltage applied to the tip and the average tunneling current). Raw STM images were processed using a JEOL software package (WinSPM Data Processing System, Version 2.15, R. B. Leane, JEOL Ltd.) and a freeware (WSxM 5.0 Develop 1.2, Nanotec Electrónica S. L.).[32] A smooth 3 × 3 matrix convolution filter was used to produce the final images.

Modeling 2D Molecular Organization in Adlayers on Graphite. Profiles of patterns of contrast in STM images were analyzed to estimate unit cell parameters and to allow initial structural hypotheses to be formulated. Detailed molecular models based on these hypotheses were then calculated, using the semiempirical method RM1.[33] This method is expected to yield models of 2D organization that are qualitatively reliable. However, the method requires only modest computational resources, unlike high-level density-functional approaches in which long-range dispersive interactions are taken into account, such as those we have reported earlier.[9-10, 34]

Working with either HyperChem Pro 8.0 (PC-based) or HyperChem 4.0 (Intel Mac-based), we first used the Amber force field to minimize the energy of an isolated molecule of the adsorbate and a model graphene sheet large enough to accommodate multiple adsorbates. We then allowed the molecule to approach the graphene sheet, which was kept fixed to simplify computation. Once the molecule had adjusted in response to the underlying surface, as computed using Amber, copies were placed in neighboring positions on the surface according to the initial

structural hypothesis. In the simplest approach, only a circle of neighbors in direct contact with the central molecule was added. A more sophisticated version introduced a second set of copies in contact with the outer perimeter of the circle of primary neighbors. The energy of the adsorbed aggregate was then reminimized using Amber to provide a starting geometry for semiempirical RM1 calculations. These calculations yielded the reported models, in which the assembled molecules have adjusted in response to the presence of their neighbors and an underlying fixed graphene sheet.

This approach to modeling 2D molecular organization on surfaces is attractive for three reasons : 1) It specifically assesses the effect of the underlying surface; 2) it takes neighboring molecules into account; and 3) it can be undertaken with modest computational resources but follows a strategy of analysis related to those used in higher-level DFT approaches.[9-10] Minor shortcomings include the slight aperiodicity seen in many of the Figures 1-8, which results from the small finite number of absorbed molecules used in the calculations and the slightly different environments of the central molecule and its incompletely surrounded neighbors.

Acknowledgments

We are grateful to the Natural Sciences and Engineering Research Council of Canada, the Ministère de l'Éducation du Québec, the Canada Foundation for Innovation, the Canada Research Chairs Program, and Université de Montréal for financial support. In addition, we thank Prof. Alain Rochefort and Dr. Thierry Maris for helpful discussions, and we are grateful to Ji-Hyun Yi and Prof. Antonio Nanci for helping us obtain STM images.

Supporting Information Available. Supplementary STM images and analyses of unit cell parameters. This material is available free of charge via the Internet at http://pubs.acs.org.

Notes and References

1. For recent reviews, see: Elemans, J. A. A. W.; De Feyter, S. *Soft Matter* **2009**, *5*, 721-735. Elemans, J. A. A. W.; Lei, S.; De Feyter, S. *Angew. Chem., Int. Ed.* **2009**, *48*, 7298-7332. Furukawa, S.; De Feyter, S. *Top. Curr. Chem.* **2009**, *287*, 87-133. Kühnle, A. *Curr. Opin. Colloid Interface Sci.* **2009**, *14*, 157-168. Yang, Y.; Wang, C. *Curr. Opin. Colloid Interface Sci.* **2009**, *14*, 135-147. Stepanow, S.; Lin, N.; Barth, J. V. *J. Phys.: Condens. Matter* **2008**, *20*, 184002. Plass, K. E.; Grzesiak, A. L.; Matzger, A. J. *Acc. Chem. Res.* **2007**, *40*, 287-293. Barth, J. V. *Annu. Rev. Phys. Chem.* **2007**, *58*, 375-407. Wan, L.-J. *Acc. Chem. Res.* **2006**, *39*, 334-342. Barth, J. V.; Costantini, G.; Kern, K. *Nature* **2005**, *437*, 671-679. De Feyter, S.; De Schryver, F. *J. Phys. Chem. B* **2005**, *109*, 4290-4302. Smith, R. K.; Lewis, P. A.; Weiss, P. S. *Prog. Surf. Sci.* **2004**, *75*, 1-68. De Feyter, S.; De Schryver, F. *Chem. Soc. Rev.* **2003**, *32*, 139-150. Hecht, S. *Angew. Chem., Int. Ed.* **2003**, *42*, 24-26. Giancarlo, L. C.; Flynn, G. W. *Acc. Chem. Res.* **2000**, *33*, 491-501.
2. Gutzler, R.; Sirtl, T.; Dienstmaier, J. F.; Mahata, K.; Heckl, W. M.; Schmittel, M.; Lackinger, M. *J. Am. Chem. Soc.* **2010**, *132*, 5084-5090. Marie, C.; Silly, F.; Tortech, L.; Müllen, K.; Fichou, D. *ACS Nano* **2010**, *4*, 1288-1292. Phillips, A. G.; Perdigão, L. M. A.; Beton, P. H.; Champness, N. R. *Chem. Commun.* **2010**, 2775-2777. Palma, C.-A.; Bjork, J.; Bonini, M.; Dyer, M. S.; Llanes-Pallas, A.; Bonifazi, D.; Persson, M.; Samorì, P. *J. Am. Chem. Soc.* **2009**, *131*, 13062-13071. Li, Y.; Ma, Z.; Qi, G.; Yang, Y.; Zeng, Q.; Fan, X.; Wang, C.; Huang, W. *J. Phys. Chem. C* **2008**, *112*, 8649-8653. Madueno, R.; Räisänen, M.

T.; Silien, C.; Buck, M. *Nature* **2008**, *454*, 618-621. Ruben, M.; Payer, D.; Landa, A.; Comisso, A.; Gattinoni, C.; Lin, N.; Collin, J.-P.; Sauvage, J.-P.; De Vita, A.; Kern, K. *J. Am. Chem. Soc.* **2006**, *128*, 15644-15651. Yokoyama, T.; Yokoyama, S.; Kamikado, T.; Okuno, Y.; Mashiko, S. *Nature* **2001**, *413*, 619-621.

3. Lei, S.; Tahara, K.; De Schryver, F. C.; Van der Auweraer, M.; Tobe, Y.; De Feyter, S. *Angew. Chem., Int. Ed.* **2008**, *47*, 2964-2968. Kampschulte, L.; Werblowsky, T. L.; Kishore, R. S. K.; Schmittel, M.; Heckl, W. M.; Lackinger, M. *J. Am. Chem. Soc.* **2008**, *130*, 8502-8507. Palma, C.-A.; Bonini, M.; Llanes-Pallas, A.; Breiner, T.; Prato, M.; Bonifazi, D.; Samorì, P. *Chem. Commun.* **2008**, 5289-5291.
4. Ciesielski, A.; Piot, L.; Samorì, P.; Jouaiti, A.; Hosseini, M. W. *Adv. Mater.* **2009**, *21*, 1131-1136. Mamdouh, W.; Kelly, R. E. A.; Dong, M.; Kantorovich, L. N.; Besenbacher, F. *J. Am. Chem. Soc.* **2008**, *130*, 695-702. Zhou, H.; Dang, H.; Yi, J.-H.; Nanci, A.; Rochefort, A.; Wuest, J. D. *J. Am. Chem. Soc.* **2007**, *129*, 13774-13775.
5. Dang, H.; Maris, T.; Yi, J.-H.; Rosei, F.; Nanci, A.; Wuest, J. D. *Langmuir* **2007**, *23*, 11980-11985.
6. Ha, N. T. N.; Gopakumar, T. G.; Gutzler, R.; Lackinger, M.; Tang, H.; Hietschold, M. *J. Phys. Chem. C* **2010**, *114*, 3531-3636. Lackinger, M.; Heckl, W. M. *Langmuir* **2009**, *25*, 11307-11321. Lackinger, M.; Griessl, S.; Heckl, W. M.; Hietschold, M.; Flynn, G. W. *Langmuir* **2005**, *21*, 4984-4988. Griessl, S.; Lackinger, M.; Edelwirth, M.; Hietschold, M.; Heckl, W. M. *Single Mol.* **2002**, *3*, 25-31.
7. Binning, G.; Rohrer, H.; Gerber, C.; Weibel, E. *Phys. Rev. Lett.* **1982**, *49*, 57-61.
8. For examples and further discussion, see: Phillips, T. K.; Bhinde, T.; Clarke, S. M.; Lee, S. Y.; Mali, K. S.; De Feyter, S. *J. Phys. Chem. C* **2010**, *114*, 6027-6034. Hai, N. T. M.; Van der Auweraer, M.; Müllen, K.; De Feyter, S. *J. Phys. Chem. C* **2009**, *113*, 11567-11574. Plass, K. E.; Kim, K.; Matzger, A. J. *J. Am. Chem. Soc.* **2004**, *126*, 9042-9053.

9. Rochefort, A.; Wuest, J. D. *Chem. Commun.* **2010**, 2923-2925.
10. Rochefort, A.; Wuest, J. D. *Langmuir* **2009**, *25*, 210-215.
11. For studies of the adsorption of trimesic acid (**1**) under other conditions, see: Nath, K. G.; Ivasenko, O.; MacLeod, J. M.; Miwa, J. A.; Wuest, J. D.; Nanci, A.; Perepichka, D. F.; Rosei, F. *J. Phys. Chem. C* **2007**, *111*, 16996-17007. Payer, D.; Comisso, A.; Dmitriev, A.; Strunskus, T.; Lin, N.; Wöll, C.; DeVita, A.; Barth, J. V.; Kern, K. *Chem. Eur. J.* **2007**, *13*, 3900-3906. Ye, Y.; Sun, W.; Wang, Y.; Shao, X.; Xu, X.; Cheng, F.; Li, J.; Wu, K. *J. Phys. Chem. C* **2007**, *111*, 10138-10141. Classen, T.; Lingenfelder, M.; Wang, Y.; Chopra, R.; Virojanadara, C.; Fratesi, G.; Fabris, S.; de Gironcoli, S.; Baroni, S.; Haq, S.; Raval, R.; Kern, K. *J. Phys. Chem. A* **2007**, *111*, 12589-12603. Li, M.; Deng, K.; Yang, Y.-L.; Zeng, Q.-D.; He, M.; Wang, C. *Phys. Rev. B* **2007**, *76*, 155438. Han, B.; Li, Z.; Pronkin, S.; Wandlowski, T. *Anal. Bioanal. Chem.* **2007**, *388*, 121-129. MacLeod, J. M.; Ivasenko, O.; Perepichka, D. F.; Rosei, F. *Nanotechnology* **2007**, *18*, 424031. Sheerin, G.; Cafolla, A. A. *Surf. Sci.* **2005**, *577*, 211-219. Ishikawa, Y.; Ohira, A.; Sakata, M.; Hirayama, C.; Kunitake, M. *Chem. Commun.* **2002**, 2652-2653. Dmitriev, A.; Lin, N.; Weckesser, J.; Barth, J. V.; Kern, K. *J. Phys. Chem. B* **2002**, *106*, 6907-6912.
12. For a related study of the adsorption of benzoic acid (**2**) on graphite using atomic force microscopy, see: Martin, D. S. *Surf. Sci.* **2003**, *536*, 15-23.
13. For a report of the coadsorption of benzoic acid (**2**) and a trialkylamine on graphite, see: Lei, S.-B.; Wang, C.; Fan, X.-L.; Wan, L.-J.; Bai, C.-L. *Langmuir* **2003**, *19*, 9759-9763.
14. For a related study of the adsorption of phthalic acids on graphite, see : Lackinger, M.; Griessl, S.; Markert, T.; Jamitzky, F.; Heckl, W. M. *J. Phys. Chem. B* **2004**, *108*, 13652-13655.
15. For recent references, see: Singh, D.; Bhattacharyya, P. K.; Baruah, J. B. *Cryst. Growth Des.* **2010**, *10*, 348-356. Shattock, T. R.; Arora, K. K.; Vishweshwar, P.; Zaworotko, M. J. *Cryst.*

Growth Des. **2008**, *8*, 4533-4545. Babu, N. J.; Nangia, A. *Cryst. Growth Des.* **2006**, *6*, 1995-1999. Aakeröy, C. B.; Desper, J.; Urbina, J. F. *CrystEngComm* **2005**, 7, 193-201. Dale, S. H.; Elsegood, M. R. J.; Hemmings, M.; Wilkinson, A. L. *CrystEngComm* **2004**, 6, 207-214.

16. Takusagawa, F.; Shimada, A. *Acta Crystallogr.* **1976**, *B32*, 1925-1927.
17. Gupta, M. P.; Kumar, P. *Cryst. Struct. Commun.* **1975**, *4*, 365-368.
18. Wright, W. B.; King, G. S. D. *Acta Crystallogr.* **1953**, *6*, 305-317.
19. Takusagawa, F.; Shimada, A. *Chem. Lett.* **1973**, 1089-1090.
20. Tamura, C.; Kuwano, H.; Sasada, Y. *Acta Crystallogr.* **1961**, *14*, 693.
21. Cowan, J. A.; Howard, J. A. K.; McIntyre, G. J.; Lo, S. M.-F.; Williams, I. D. *Acta Crystallogr.* **2005**, *B61*, 724-730.
22. Takusagawa, F.; Hirotsu, K.; Shimada, A. *Bull. Chem. Soc. Jpn.* **1973**, *46*, 2292-2299.
23. Carranza Téllez, V.; Sánchez Gaytán, B.; Bernès, S.; González Vergara, E. *Acta Crystallogr.* **2002**, *C58*, o228-o230.
24. Li, H.; Xu, B.; Evans, D.; Reutt-Robey, J. E. *J. Phys. Chem. C* **2007**, *111*, 2102-2106.
25. Ikezawa, Y.; Sawamura, S. *Electrochim. Acta* **2009**, *54*, 2360-2366. Pinheiro, L. S.; Temperini, M. L. A. *Surf. Sci.* **2007**, *601*, 1836-1843. Wen, R.; Fang, Y. *Vibrational Spectrosc.* **2005**, *39*, 106-113. Schnadt, J.; O'Shea, J. N.; Patthey, L.; Schiessling, J.; Krempaský, J.; Shi, M.; Mårtensson, N.; Brühwiler, P. A. *Surf. Sci.* **2003**, *544*, 74-86.
26. Desiraju, G. R.; Steiner, T., *The Weak Hydrogen Bond in Structural Chemistry and Biology*; Oxford University Press : Oxford, U. K., 1999.
27. For a review of C-H···O interactions, see: Desiraju, G. R. *Chem. Commun.* **2005**, 2995-3001.
28. For further discussion of the relation between N···H-O and N^{+}-H···O^{-} hydrogen bonding in similar systems, see : Mohamed, S.; Tocher, D. A.; Vickers, M.; Karamertzanis, P. G.; Price, S. L. *Cryst. Growth. Des.* **2009**, *9*, 2881-2889. Childs, S. L.; Stahly, G. P.; Park, A. *Mol.*

Pharmaceutics **2007**, *4*, 323-338. Bhogala, B. R.; Basavoju, S.; Nangia, A. *CrystEngComm* **2005**, 7, 551-562.

29. Meot-Ner (Mautner), M. *Chem. Rev.* **2005**, *105*, 213-284.
30. Barth, J. V.; Weckesser, J.; Trimarchi, G.; Vladimirova, M.; De Vita, A.; Cai, C.; Brune, H.; Günter, P.; Kern, K. *J. Am. Chem. Soc.* **2002**, *124*, 7991-8000.
31. For recent references, see: Villagomez, C. J.; Zambelli, T.; Gauthier, S.; Gourdon, A.; Stojkovic, S.; Joachim, C. *Surf. Sci.* **2009**, *603*, 1526-1532. Künzel, D.; Markert, T.; Groß, A.; Benoit, D. M. *Phys. Chem. Chem. Phys.* **2009**, *11*, 8867-8878. Miwa, J. A.; Cicoira, F.; Bedwani, S.; Lipton-Duffin, J.; Perepichka, D. F.; Rochefort, A.; Rosei, F. *J. Phys. Chem. C* **2008**, *112*, 10214-10221. Böhme, T.; Simpson, C. D.; Müllen, K.; Rabe, J. P. *Chem. Eur. J.* **2007**, *13*, 7349-7357. Gawronski, H.; Henzl, J.; Simic-Milosevic, V.; Morgenstern, K. *Appl. Surf. Sci.* **2007**, *253*, 9047-9053.
32. Horcas, I.; Fernández, R.; Gómez-Rodríguez, J. M.; Colchero, J.; Gómez-Herrero, J.; Baro, A. M. *Rev. Sci. Instrum.* **2007**, *78*, 01375.
33. Rocha, G. B.; Freire, R. O.; Simas, A. M.; Stewart, J. J. P. *J. Comput. Chem.* **2006**, *27*, 1101-1111.
34. For recent related calculations of physisorption on graphene, see: Henwood, D.; Carey, J. D. *Mol. Simul.***2008**, *34*, 1019-1023. Zhechkov, L.; Heine, T.; Seifert, G. *Int. J. Quantum Chem.* **2006**, *106*, 1375-1382.

3.4 Conclusions

Dans l'étude résumée dans ce chapitre, nous avons examiné l'adsorption des composés de type acide pyridinecarboxylique sur le graphite. Comme prévu, les liaisons hydrogène impliquant les groupements acides carboxyliques et l'atome d'azote du cycle pyridyle jouent un rôle clé dans le contrôle de l'organisation observée en 2D. Nos résultats confirment que les acides pyridinecarboxyliques sont particulièrement bien conçus pour s'associer par ponts hydrogène et que ces composés favorisent la formation des chaînes et des oligomères cycliques qui s'arrangent en feuillet. La préférence de ces molécules à former des feuillets en 2D et en 3D montre généralement un degré important d'homologie. L'ensemble de nos observations met en évidence le potentiel de l'ingénierie cristalline pour construire des structures prévisibles en 2D et en 3D obtenues à partir de composés simples qui combinent une affinité intrinsèque pour les surfaces et une capacité à s'engager dans de fortes interactions intermoléculaires coplanaires.

Chapitre 4

Homologie en 2D et en 3D

4.1 Introduction

Dans les chapitres 2 et 3, nous avons successivement décrit l'organisation 2D et 3D d'une famille d'aminoazines ainsi que d'acides pyridinecarboxyliques. Ces études ont permis de comprendre l'origine des préférences associatives de ces composés. En particulier, ils ont montré une forte tendance à s'adsorber sur le graphite et à former des réseaux supramoléculaires dirigés par ponts hydrogène de manière prévisible. De plus, nous avons relevé une forte prédisposition de ces composés à s'organiser de manière analogue en 2D et en 3D. Les informations généralisées sur le comportement de ces composés ont permis d'identifier une nouvelle série de molécules plus complexes possédant en même temps des groupements azinyle et pyridyle.

4.2 Nos objectifs

Dans ce chapitre, nous allons montrer qu'il est possible de choisir avec confiance des molécules aptes à s'organiser de manière prévisible et analogue en 2D et en 3D en se servant des résultats des chapitres précédents. En créant une famille de composés combinant un cycle pyridyle substitué avec un group diaminotriazinyle (DAT), nous obtenons des structures moléculaires avec une forte capacité de s'associer avec des acides carboxyliques par ponts hydrogène, générant ainsi des agrégats disposés à s'organiser en couches. Les molécules présentées dans ce chapitre peuvent donc cocristalliser avec les acides alcanecarboxyliques de manière analogue en 2D et 3D.

4.3 Article 3

Engineering Homologous Molecular Organization in 2D and 3D. Cocrystallization of Pyridyl-Substituted Diaminotriazines with Alkanecarboxylic Acids

Adam Duong,[†] Marc-André Dubois,[†] Thierry Maris,[†] Valérie Métivaud,[†] Ji-Hyun Yi,[‡] Antonio Nanci,[‡] Alain Rochefort,[§] and James D. Wuest*[,†]

Journal of Physical Chemistry C, **2011**, in press

Abstract

Isomeric pyridyl-substituted diaminotriazines **2a-c** and elongated analogue **3** are designed to adopt flattened structures with features that favor adsorption on surfaces and participation in multiple intermolecular interactions. In particular, pyridyl and diaminotriazinyl groups have strong affinities for graphite, and both form coplanar hydrogen-bonded adducts with alkanecarboxylic acids according to reliable motifs. Together, these properties predispose compounds **2a-c** and **3** to be coadsorbed with alkanecarboxylic acids on graphite and to cocrystallize as structures built from hydrogen-bonded sheets. Comparison of the 2D structures of the ordered adlayers (as determined by scanning tunneling microscopy) with the 3D structures of the cocrystals (as determined by X-ray diffraction) showed striking homology, typically with quantitatively similar structural parameters. Together, these results illustrate how series of related compounds can be engineered to form ordered adlayers and crystalline solids with closely analogous 2D and 3D structures. Specifically, the molecular components should have an affinity for the underlying surface and should engage in coplanar interactions that are strong relative to the energy of adsorption, thereby ensuring that the components are positioned reliably in sheets despite the effect of the surface. In general, compounds with these features should favor similar organization in different states, including monolayers, thin films, and bulk materials, and they promise to be useful in applications requiring behavior that depends predictably on dimensions, such as in thin-film molecular devices.

Introduction

The scope of molecular crystal engineering has broadened dramatically in recent years, and its early emphasis on understanding and controlling order in three dimensions (3D)[1] has expanded to encompass a growing interest in the organization of molecules adsorbed on surfaces in two dimensions (2D).[2-3] As a result, the insights of crystal engineers are contributing to advances in all areas of science and technology where molecular organization must be controlled, both in bulk materials and in thin films. Despite the growing utility of crystal engineering, it is still a young field with major unsolved problems. In particular, accurate predictions of the 3D structure of molecular crystals remain notoriously difficult,[4] and the problems are compounded in 2D by the subtle effects of the underlying surface on molecular arrangement. Stiff challenges must therefore be met before molecular organization can be truly mastered in either 2D or 3D.

The challenges of crystal engineering in 2D and 3D are intimately linked. This calls out for an integrated approach in which molecular organization in 3D, determined by X-ray diffraction (XRD) or other methods, is compared systematically with 2D organization on surfaces, as revealed by scanning probe microscopy (SPM). This integrated approach promises to yield insights unlikely to emerge from studies focused more narrowly on 2D or 3D organization alone. In particular, (1) 3D structures resolved unambiguously by XRD can provide sound models for interpreting images of 2D organization obtained by SPM; (2) SPM can probe fine details of crystallization that cannot readily be examined by XRD, including dynamic phenomena involving individual molecules, structural features at the boundaries of domains, and the nature of defects within domains; and (3) systematic comparison of 2D and 3D structures can clarify the role and relative importance of diverse forces that control molecular organization. Surprisingly,

however, there are few reports of integrated analyses of 2D and 3D structures in extended series of related compounds.[5]

Devising compounds that predictably favor similar structures in 2D and 3D is a particularly severe test of our current ability to understand and control molecular organization. When intermolecular forces are weak and diffuse, the structuring effect of underlying surfaces may be dominant, and organization in 2D and 3D may show little similarity. However, when intermolecular interactions are strong and directional, they may balance or even outweigh the effect of surfaces and thereby favor closely analogous organization in different states, including monolayers, thin films, and bulk materials. Deeper understanding of this phenomenon is likely to have valuable applications, such as in the design and fabrication of active layers for thin-film molecular devices.

Helpful guidelines have resulted from decades of studying crystallization induced by ordered surfaces, which can lead in favorable cases to epitaxial molecular adsorption in 2D, followed by the layer-by-layer growth of thin films or bulk crystalline phases with similar 3D structures.[6] However, these studies have not provided general prescriptions for devising compounds that crystallize to give predictably homologous 2D and 3D structures, particularly when the underlying surface is not ordered or atomically flat, or when its lattice parameters are not well matched with those of 3D crystals of the adsorbate. New tools for ensuring homologous 2D and 3D molecular crystallization are needed.

We are exploring an approach based on existing knowledge of epitaxy and related phenomena of surface-induced crystallization, modified by incorporating emerging principles of crystal engineering.[7] Specifically, we have chosen to use compounds with two key properties: (1)

The individual compounds have flattened topologies and an inherent affinity for adsorption on surfaces; and (2) the compounds can engage in multiple strong directional interactions in a single plane and can thereby place neighboring molecules in predictable coplanar positions. The goal is to ensure that molecular topology and interactions act in concert to help dictate how crystallization occurs in 2D and 3D, rather than allowing the underlying surface to play a dominant role.

This approach differs from the one followed by many earlier studies of surface-directed crystallization, which have tended to focus on the behavior of relatively simple compounds with weak and nondirectional interactions.[8] In contrast, the use of strong directional coplanar interactions may help make organization more predictably homologous in 2D and 3D, even when true epitaxy is impossible and the underlying surface is not commensurate, atomically flat, or ordered. In addition, previous work has suggested that the ability to engage in well-defined interactions helps prevent molecules from crystallizing in widely different polymorphic forms in 3D,[9] so extensive polymorphism may also be disfavored in 2D. For all these reasons, molecules that engage in strong directional coplanar interactions are potentially valuable components for building predictably homologous 2D and 3D structures.

To facilitate direct structural comparisons, we carried out 2D and 3D crystallizations under conditions as similar as possible. Single crystals were grown from solution without the presence of surfaces except those of the surrounding vessel, and adlayers were deposited from similar or identical solvents, followed by analysis of molecular organization in situ at the liquid-solid interface by scanning tunneling microscopy (STM).[10] As the underlying surface, we selected the basal plane of graphite, which adsorbs a wide range of molecules from solution to produce well-defined adlayers.

Recent experimental[11-12] and theoretical[13-14] studies have revealed that melamine (**1**) and related aminotriazines have a strong affinity for graphite. In addition, such compounds associate by engaging in reliable hydrogen-bonded supramolecular synthons,[15] including homosynthon

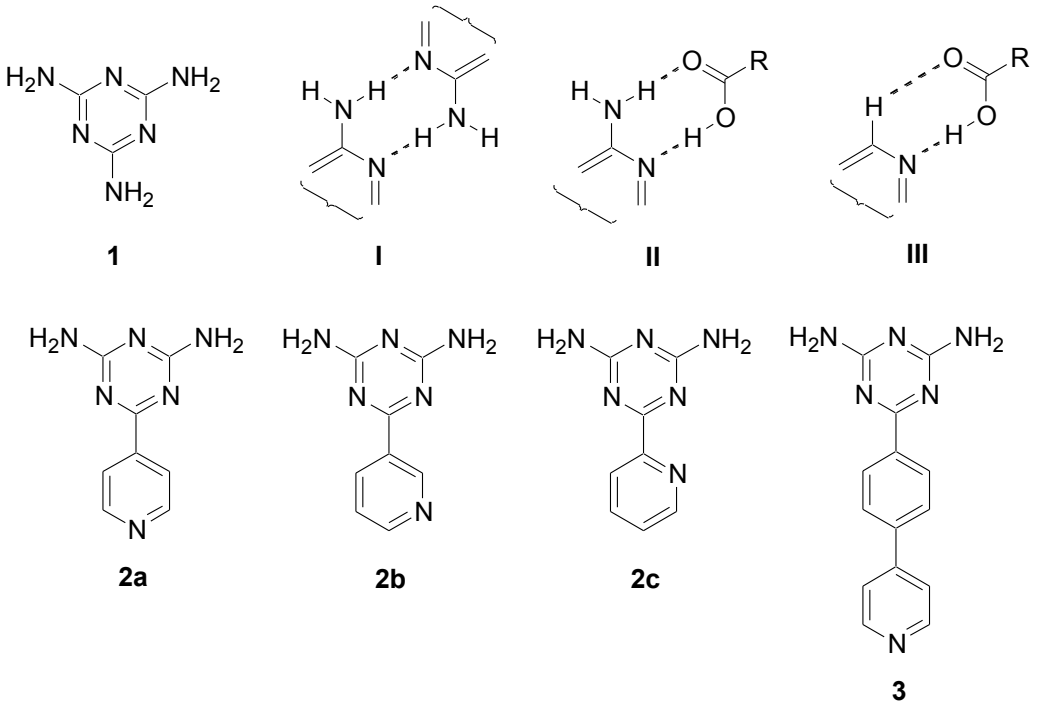

I[9,16-18] and heterosynthon **II** with carboxylic acids.[11,19] The principal atoms involved in both synthons lie in essentially the same plane, ensuring that the planarity of the aminotriazinyl core is extended to a larger assembly. Moreover, pyridyl-substituted aminotriazines **2a-c** are expected to allow further coplanar association with carboxylic acids according to heterosynthon **III**,[20] in which a primary O-H···N hydrogen bond is reinforced by a secondary C-H···O interaction.[21-22] To make the affinity of hydrogen-bonded aggregates of aminotriazines **2a-c** for graphite even greater, we decided to use alkanecarboxylic acids as the hydrogen-bonding partners to take added advantage of the strong adsorption of alkyl chains.[23] In this way, the following factors are expected to act in synergy to favor analogous 2D and 3D assemblies : (1) Aminotriazines **2a-c** and alkanecarboxylic acids can adopt flattened conformations and have an inherently high

affinity for graphite; (2) they can interact by forming multiple coplanar hydrogen bonds according to reliable patterns **I-III**; and (3) the resulting hydrogen-bonded aggregates can adopt flattened topologies suitable for packing in tapes or sheets. Coassembly is a noteworthy feature of the system we have elected to study, because in principle it allows the alkanecarboxylic acid component to be varied without necessarily changing the basic pattern of molecular organization, leading to rational control of metrics in 2D and 3D.

Together, pyridyl-substituted diaminotriazines **2a**-**c** and lengthened analogue **3** form a coherent set of compounds with systematic structural alterations. Earlier work has established that triazinyl rings and aryl substituents are normally nearly coplanar.[9,16-18] As a result, compounds **2a**-**c** and **3** are particularly well designed to form supramolecular aggregates with substantial affinity for graphite, in which a nearly flat aryl-substituted triazinyl core forms hydrogen bonds with multiple coplanar molecules of alkanecarboxylic acid. As described below, we have found that all four compounds **2a**-**c** and **3** behave as planned, by cocrystallizing with alkanecarboxylic acids to form 2D and 3D structures with striking homology.

Results and Discussion

3D Cocrystallization of 2,4-Diamino-6-(4-pyridyl)-1,3,5-triazine (2a) with Alkanecarboxylic Acids. Slow evaporation of a solution of 2,4-diamino-6-(4-pyridyl)-1,3,5-triazine (**2a**) in octanoic acid at 25 °C yielded cocrystals of composition **2a** • 2 octanoic acid. The cocrystals proved to belong to the triclinic space group *P*-1, and other crystallographic data are summarized in Table 1. Views of the structure are provided in Figure 1. Molecules of compound **2a** were found to be statistically disordered (50:50) with respect to a center of inversion.[34] To simplify discussion, structural data for only one orientation are presented.

Table 1. Crystallographic Data for Cocrystals of 2,4-Diamino-6-(4-pyridyl)-1,3,5-triazine (**2a**), 2,4-Diamino-6-(3-pyridyl)-1,3,5-triazine (**2b**), and 2,4-Diamino-6-(2-pyridyl)-1,3,5-triazine (**2c**) with Alkanecarboxylic Acids (**C8** = Octanoic Acid and **C9** = Nonanoic Acid).

cocrystal	**2a** • 2 **C8**	**2a** • 2 **C9**	**2b** • 1 **C9**	**2c** • 1 **C8**	**2c** • 1 **C9**
formula	$C_{24}H_{40}N_6O_4$	$C_{26}H_{44}N_6O_4$	$C_{17}H_{26}N_6O_2$	$C_{16}H_{24}N_6O_2$	$C_{17}H_{26}N_6O_2$
crystal system	triclinic	triclinic	triclinic	triclinic	triclinic
space group	$P\bar{1}$	$P\bar{1}$	$P\bar{1}$	$P\bar{1}$	$P\bar{1}$
a (Å)	4.8615(6)	7.5805(6)	10.3277(19)	8.8653(4)	8.0471(4)
b (Å)	7.4585(9)	11.1838(9)	13.405(2)	9.4282(4)	10.3951(5)
c (Å)	19.034(3)	25.627(2)	13.648(2)	10.7014(5)	11.6890(5)
α (°)	83.881(7)	94.378(4)	92.130(11)	104.685(2)	67.342(2)
β (°)	84.671(7)	92.854(4)	106.824(12)	90.861(2)	85.030(2)
γ (°)	79.308(7)	101.374(3)	95.855(12)	98.832(3)	89.545(2)
V (Å^3)	672.44(15)	2119.0(3)	1794.6(5)	853.62(7)	898.59(7)
Z	1	3	4	2	2
ρ_{calcd} (g cm^{-3})	1.177	1.186	1.282	1.293	1.280
T (K)	150	150	150	150	150
μ (mm^{-1})	0.660	0.654	0.711	0.726	0.710
R_1, $I>2\sigma$ (%)	6.32	6.58	8.70	7.01	4.22
R_1, all data (%)	13.55	14.19	15.84	7.44	4.33
ωR_2, $I>2\sigma$ (%)	15.87	16.51	20.91	18.49	11.64
ωR_2, all data(%)	19.75	21.41	25.63	19.55	11.77
measured reflections	9662	29039	20766	14242	13101
independent reflections	2369	5617	6368	3105	3214
Observed reflections, $I>2\sigma(I)$	1208	2775	3085	2749	3069

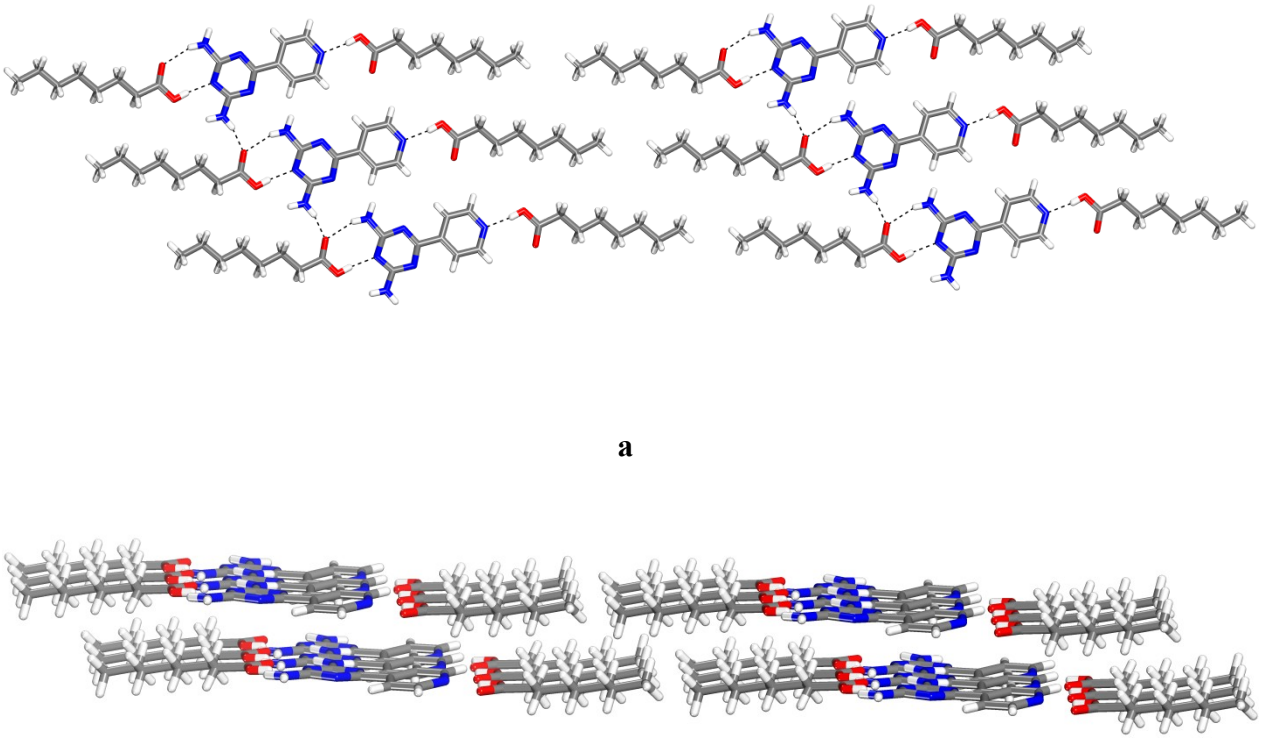

a

b

Figure 1. Views of the structure of 1:2 cocrystals of 2,4-diamino-6-(4-pyridyl)-1,3,5-triazine (**2a**) with octanoic acid. (a) View of part of a sheet constructed from hydrogen-bonded tapes. Hydrogen bonds are represented by broken lines, and carbon atoms are shown in gray, hydrogen atoms in white, nitrogen atoms in blue, and oxygen atoms in red. (b) View of two stacked sheets.

Each molecule of pyridyl-substituted diaminotriazine **2a** forms hydrogen bonds with two molecules of octanoic acid according to well-established supramolecular synthons **II** and **III**. The crystallographic data show that full proton transfer does not occur to give the corresponding aminotriazinium or pyridinium carboxylate salts.[37-39] The observed O-H···N(triazine), O···H-N(triazine), and O-H···N(pyridine) distances in synthons **II** and **III** have normal values (2.661 Å, 2.938 Å, and 2.611 Å, respectively).[19,20] The secondary C-H···O interaction that normally uses an α C-H bond of pyridines to help stabilize synthon **III** has an H···O distance (3.057 Å) longer than

the sum of the van der Waals radii. Nevertheless, the carboxyl group is maintained in the plane of the pyridyl ring, and the alkyl chain adopts a fully extended conformation. As expected, the angle formed by the average planes of the triazinyl and pyridyl rings is small (11.1°), resulting in ternary aggregates that are essentially planar. The aggregates then pack to form tapes aligned with the *b* axis (Figure 1a), which are held together by an additional N-H···O hydrogen bond (2.636 Å), augmented by a C-H···O interaction involving an α-pyridyl C-H bond (H···O distance = 2.874 Å). The hydrogen-bonded tapes then pack to form sheets (Figure 1a), which stack with a slight offset to give the full 3D structure (Figure 1b).

Under similar conditions, cocrystallization of pyridyl-substituted diaminotriazine **2a** with nonanoic acid in place of octanoic acid proved to yield a fully analogous structure. The cocrystals were found to belong to the triclinic space group *P*-1, and other crystallographic data are presented in Table 1. Views of the structure are shown in Figure 2. Molecules of compound **2a** proved to be statistically disordered (50:50) with respect to a center of inversion.[34] For simplification, structural data for only one orientation and one molecule in the asymmetric unit are presented. Again, the observed O-H···N(triazine), O···H-N(triazine), and O-H···N(pyridine) distances are normal (2.805 Å, 2.936 Å, and 2.481 Å, respectively),[19,20] and synthon **III** is reinforced as usual by a secondary C-H···O interaction (H···O distance = 2.822 Å). The average angle defined by the planes of the triazinyl and pyridyl rings is characteristically small (9.0°), leading again to nearly planar ternary aggregates that associate to form tapes aligned with the *a* axis (Figure 2a). Cohesion of the tapes is ensured in part by an additional N-H···O hydrogen bond (2.710 Å), along with a C-H···O interaction involving an α-pyridyl C-H bond (H···O distance = 2.776 Å). Packing of the hydrogen-bonded tapes then gives sheets (Figure 2a), which stack to produce the 3D structure (Figure 2b).

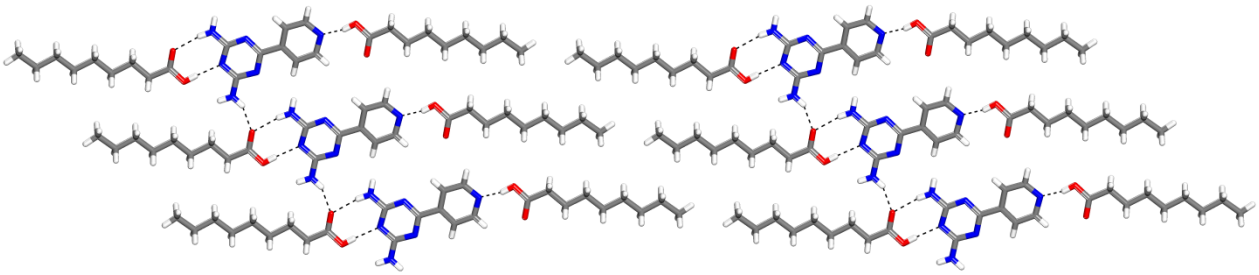

a

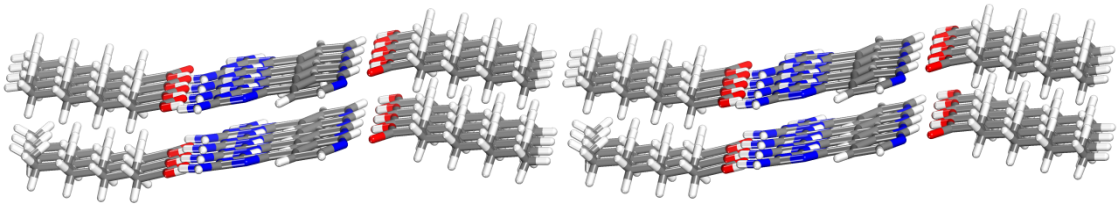

b

Figure 2. Views of the structure of 1:2 cocrystals of 2,4-diamino-6-(4-pyridyl)-1,3,5-triazine (**2a**) with nonanoic acid. (a) View of part of a sheet constructed from hydrogen-bonded tapes. Hydrogen bonds are represented by broken lines, and carbon atoms are shown in gray, hydrogen atoms in white, nitrogen atoms in blue, and oxygen atoms in red. (b) View of two stacked sheets.

2D Cocrystallization of 2,4-Diamino-6-(4-pyridyl)-1,3,5-triazine (2a) with Alkanecarboxylic Acids. The observation that both 3D structures consist of hydrogen-bonded sheets with identical 1:2 compositions and closely analogous molecular organization suggests that pyridyl-substituted diaminotriazine **2a** is inherently disposed to coadsorb with alkanecarboxylic acids on graphite to give analogous 2D assemblies. To test this hypothesis, we added a saturated solution of compound **2a** in heptanoic acid to the freshly exposed surface of highly oriented pyrolytic graphite (HOPG), and we analyzed the liquid-solid interface by scanning tunneling microscopy (STM), which revealed an ordered adlayer. A representative image is shown in Figure 3, along with a superimposed unit cell and a model of the proposed molecular organization, calculated by the semiempirical method described in the Experimental Section. Examination of the periodic patterns of contrast, combined with analysis of the unit cell parameters (a = 7.4 Å, b = 35.1 Å, γ = 60°), established that adsorption produces alternating regions of compound **2a** (brighter) and heptanoic acid (darker), which appear to be organized in chiral tapes fully analogous to those observed by XRD (Figures 1a and 2a). These observations suggest that compound **2a** and alkanecarboxylic acids cocrystallize in 2D and 3D in an essentially identical way. This homology is striking because it shows that the components have chosen to form aggregates with the same composition and organization despite potentially disruptive influences such as the effect of the underlying surface.

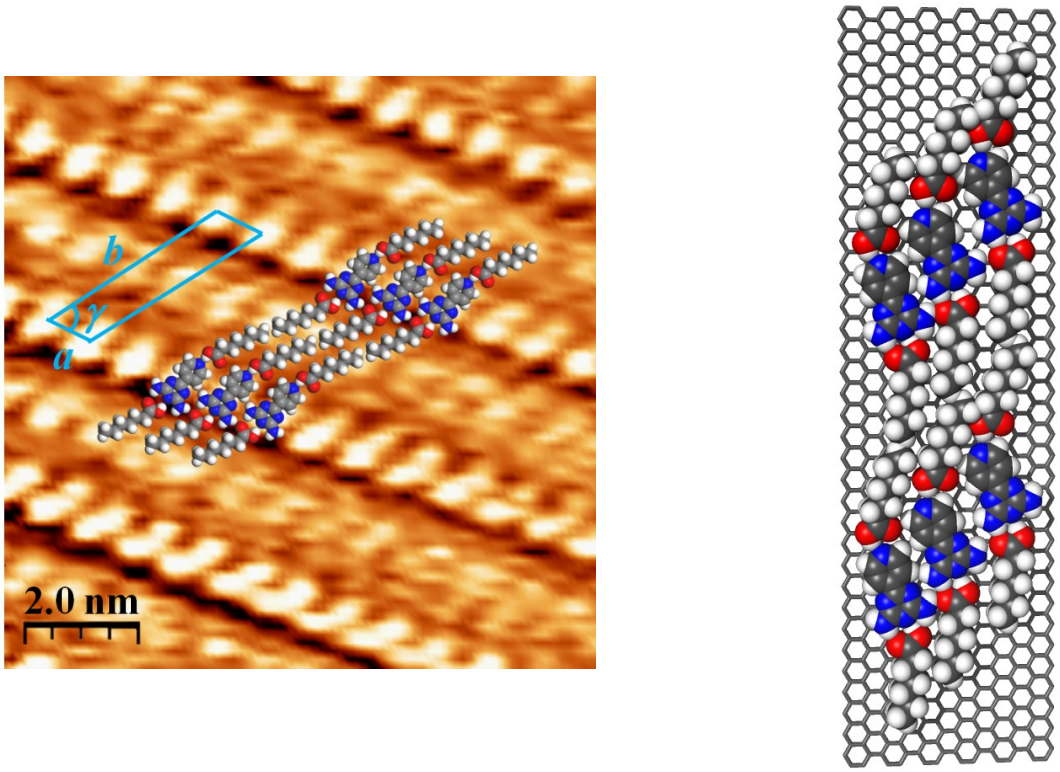

a **b**

Figure 3. (a) STM image of the adsorption of 2,4-diamino-6-(4-pyridyl)-1,3,5-triazine (**2a**) on HOPG (deposition from heptanoic acid, with V_{bias} = -1.51 V and I_{set} = 0.09 nA). Superimposed on the image are a scale bar, the measured unit cell, and approximate molecular models added as visual aids to facilitate interpretation of the pattern of contrasts. (b) Detailed semiempirical model of the postulated 2D structure.

Detailed quantitative analysis of structural parameters in 2D and 3D supports the conclusion that molecular organization is nearly identical. Molecular separation along the tapes in 3D, which is 7.459 Å in cocrystals with octanoic acid and 7.581 Å in cocrystals with nonanoic acid, is virtually the same as that observed in 2D (a = 7.4 Å). In addition, adjacent tapes in 3D cocrystals with octanoic acid are separated by approximately 35.3 Å, as measured along the line defined by the extended alkyl chains, and the value is 37.6 Å in 3D cocrystals with nonanoic acid. Both parameters are consistent with the corresponding distance in 2D cocrystals with

heptanoic acid (b = 35.1 Å). Moreover, angles defined by the tapes and alkyl chains in 3D (approximately 47° and 46° in cocrystals with octanoic acid and nonanoic acid, respectively) are similar to the angle observed in 2D (γ = 60°). We attribute the small differences to slight nonplanarity of the sheets observed in 3D and to efforts of the adsorbates to achieve registration with graphite in 2D.

Although the close quantitative similarity of structural parameters in 2D and 3D suggests that the assembled species and their organization are virtually identical, it is difficult to exclude a plausible alternative in which full proton transfer is facilitated by adsorption, leading to the formation of hydrogen-bonded adlayers consisting of carboxylate salts of protonated aminotriazine **2a**. To assess this possibility, which has not been noted previously, we calculated the ability of acetic acid to interact with a simplified model, 2-amino-1,3,5-triazine (**4**), to give

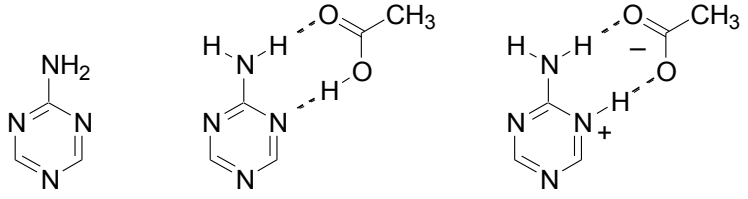

4 **5** **6**

neutral hydrogen-bonded complex **5** or the salt (**6**) formed by full proton transfer, both in the gas phase and in the adsorbed state on a graphene model. As described in detail in earlier work,[13] our calculations were based initially on the local density approximation (LDA) of density functional theory (DFT), and they employed a fixed graphene sheet of defined size and geometry. The basis set chosen for atoms of carbon was STO-3G, and 6-31G* was used for all other atoms. The

structures were optimized, and bond dissociation energies of complexes were calculated with respect to the appropriate ground-state species asymptote. In a subsequent step in the calculations, we evaluated the contribution of dispersive interactions, which are not formally taken into account within LDA limits. This was achieved by using the PBE functional to perform single-point calculations on LDA-optimized geometries,[38] in conjunction with semiempirical dispersion corrections (D).[39]

The calculated energies of adsorption, described as being at the PBE+D level, appear in Table 2. In addition, we found that the association of acetic acid with aminotriazine **4** to give hydrogen-bonded complex **5** is exothermic by 23.8 kcal/mol in the gas phase, and salt **6** does not correspond to an energy minimum, either in the gas phase or the adsorbed state. Together, the calculations suggest that the energy of intermolecular association of the adsorbates is similar to their combined energy of adsorption. This confirms that interadsorbate interactions can indeed play a key role in directing molecular organization in 2D, and it provides a theoretical basis for the hypothesis that related 2D and 3D structures can be generated rationally by using flat molecular components that engage in strong directional interactions.

Table 2. Energies of Adsorption of Acetic Acid, 2-Amino-1,3,5-triazine (**4**), and Hydrogen-Bonded Complex **5** on Graphene, as Calculated at the PBE+D Level.

adsorbate	energy of adsorption (kcal/mol)
acetic acid	13.8
2-amino-1,3,5-triazine (**4**)	23.1
complex **5**	28.2

Detailed examination of Table 2 reveals that complex **5** is strongly adsorbed (28.2 kcal/mol), but more weakly (by 8.7 kcal/mol) than the sum of its individual components (36.9 kcal/mol). Hydrogen bonding therefore appears to be weakened slightly by adsorption, as observed in related systems,[13,30] presumably because when NH_2 and COOH groups engage in normal hydrogen bonding, they can no longer maintain an optimal orientation with respect to the underlying surface. Nevertheless, our calculations show that the geometries and atomic charges of hydrogen-bonded complex **5** remain essentially the same in the gas phase and in the adsorbed state on graphene. Together, these results indicate that adsorption does not facilitate full proton transfer, and we conclude that the adsorbed species are the same as those established to be present in 3D structures by XRD.

3D Cocrystallization of 2,4-Diamino-6-(3-pyridyl)-1,3,5-triazine (2b) with Alkanecarboxylic Acids. To confirm that the strikingly similar 2D and 3D structures of pyridyl-substituted diaminotriazine **2a** are the result of proper design and not accident, we examined the behavior of isomeric 2,4-diamino-6-(3-pyridyl)-1,3,5-triazine (**2b**). By slow evaporation of a solution of compound **2b** in nonanoic acid at 25 °C, cocrystals of composition **2b** • 1 nonanoic acid were obtained. The cocrystals proved to belong to the triclinic space group *P*-1, and other crystallographic data are provided in Table 1. Views of the structure are provided in Figure 4. The particular geometry of compound **2b** allows head-to-tail dimerization by hydrogen bonding of NH_2 groups and the pyridyl nitrogen atom (Figure 4a), and the resulting pairs are linked into chains along the *b* axis by additional hydrogen bonding according to standard synthon **I**. Further association with nonanoic acid according to synthon **II** then yields flat tapes analogous to those formed in 2D and 3D by isomeric pyridyl-substituted diaminotriazine **2a**. Packing of the tapes produces sheets with interdigitated alkyl chains (Figure 4a), which stack to generate the 3D structure (Figure 4b).

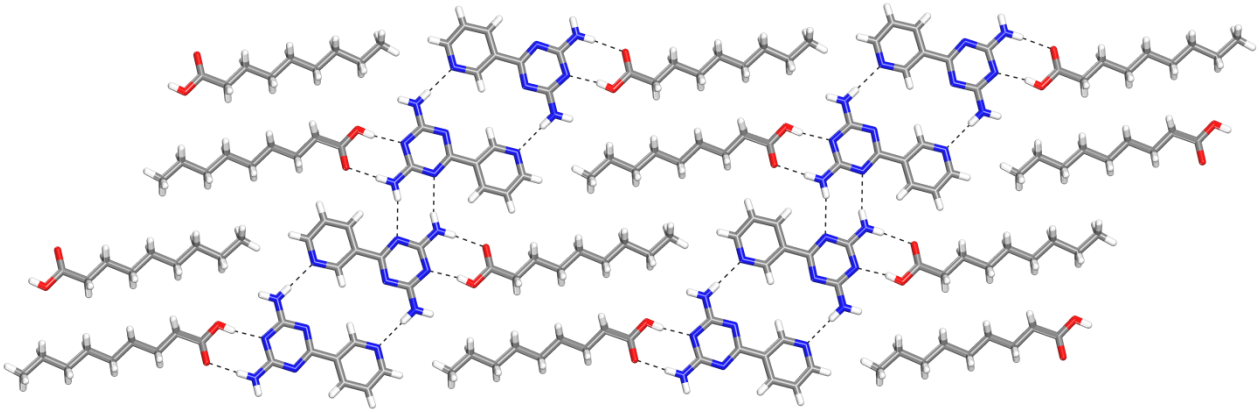

a

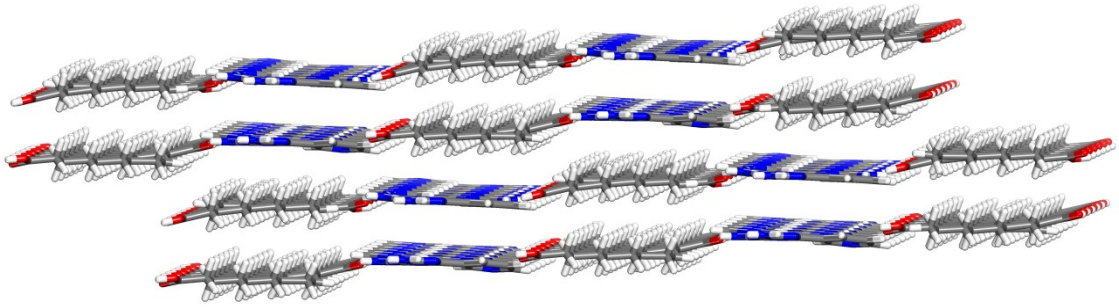

b

Figure 4. Views of the structure of 1:1 cocrystals of 2,4-diamino-6-(3-pyridyl)-1,3,5-triazine (**2b**) with nonanoic acid. (a) View of part of a sheet constructed from hydrogen-bonded tapes. Hydrogen bonds are represented by broken lines, and carbon atoms are shown in gray, hydrogen atoms in white, nitrogen atoms in blue, and oxygen atoms in red. (b) View of four stacked sheets.

The crystallographic data show that full proton transfer does not occur to give the corresponding aminotriazinium carboxylate salts.[37-39] The average N-H···N distances within the hydrogen-bonded pairs (2.958 Å) and synthon **I** (3.157 Å) have the expected values, and O-H···N and O···H-N distances in synthon **II** are also normal (2.721 and 2.833 Å, respectively).[19,20] As expected, the average angle formed by the planes of the triazinyl and pyridyl rings is small (3.8°).

2D Cocrystallization of 2,4-Diamino-6-(3-pyridyl)-1,3,5-triazine (2b) with Alkanecarboxylic Acids. The preference for hydrogen-bonded sheets in 3D suggests that pyridyl-substituted diaminotriazine **2b** is predisposed to favor a similar molecular organization when coadsorbed with alkanecarboxylic acids on graphite. Addition of a saturated solution of compound **2b** in heptanoic acid to the surface of HOPG yielded an ordered adlayer. Figure 5 shows a representative image, along with a superimposed unit cell and a model of the postulated structure, based on a semiempirical calculation. The patterns of contrast show clear pairing of molecules of compound **2b**, as observed in 3D. Moreover, the unit cell parameters (a = 15.4 Å, b = 23.2 Å, γ = 60°) provide strong evidence for the formation of chiral tapes that are essentially the same as those observed in 3D (Figure 4a). In 3D, hydrogen-bonded pairs are positioned in the tapes with a periodicity of 13.405(2) Å in 3D, and a similar distance is found in 2D (a = 15.4 Å). In addition, adjacent tapes in 3D cocrystals with nonanoic acid are separated by approximately 23.9 Å (as measured along the line defined by the extended alkyl chains), which is consistent with the corresponding distance in 2D cocrystals with heptanoic acid (b = 23.2 Å). Furthermore, the angle defined by the tapes and alkyl chains in 3D (approximately 54°) is similar to that found in 2D (γ = 60°). The small differences between 2D and 3D structural parameters may result in part from efforts to attain optimal registration with the underlying substrate.

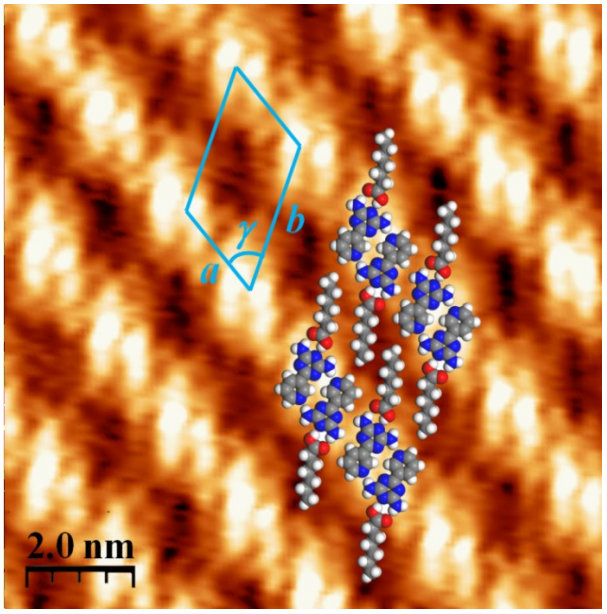

a

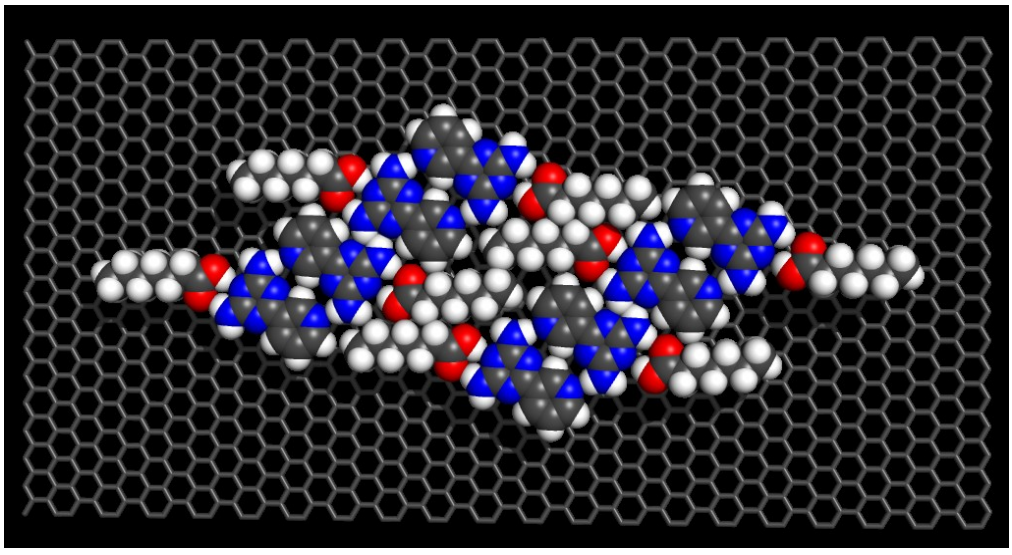

b

Figure 5. (a) STM image of the adsorption of 2,4-diamino-6-(3-pyridyl)-1,3,5-triazine (**2b**) on HOPG (deposition from heptanoic acid, with V_{bias} = -1.50 V and I_{set} = 0.09 nA). Superimposed on the image are a scale bar, the measured unit cell, and approximate molecular models added as visual aids to facilitate interpretation of the pattern of contrasts. (b) Detailed semiempirical model of the proposed 2D structure.

Analogous STM images were obtained when pyridyl-substituted diaminotriazine **2b** was coabsorbed on HOPG with nonanoic acid.[34] As a result, compound **2b** resembles isomer **2a** in its behavior, by cocrystallizing with various alkanecarboxylic acids in 2D and 3D in virtually the same way, as planned. Under all conditions, adjacent domains of adsorbed compound**s** tended to intersect at angles defined by multiples of 60°, revealing the importance of a particular registration with the underlying surface. This presumably reflects the preference of alkyl chains to align with the symmetry axes of graphite.[34] The strategy of using highly associated adsorbates increases the importance of interadsorbate interactions relative to adsorbate-surface forces, but it does not completely mask the organizing effect of the surface, at least in the present system.

3D Cocrystallization of 2,4-Diamino-6-(2-pyridyl)-1,3,5-triazine (2c) with Alkanecarboxylic Acids. The notion that certain classes of compounds can be designed to favor similar molecular organization in 2D and 3D was further tested by studying the cocrystallization of isomeric 2,4-diamino-6-(2-pyridyl)-1,3,5-triazine (**2c**) with alkanecarboxylic acids. Slow evaporation of a solution of compound **2c** in octanoic acid at 25 °C yielded cocrystals of composition **2c** • 1 octanoic acid. They were found to belong to the triclinic space group *P*-1, and other crystallographic data are summarized in Table 1. A view of the structure is shown in Figure 6. The particular geometry of compound **2c** inhibits the pyridyl nitrogen atom from freely engaging in intermolecular interactions, and individual molecules are linked into chains primarily by normal N-H···N hydrogen bonding (2.917 Å) of the aminotriazinyl groups according to synthon **I**. The angle formed by the average planes of the triazinyl and pyridyl rings (15.9°) is larger than those observed in isomeric pyridyl-substituted diaminotriazines **2a**-**b**, presumably because an attractive interaryl N···H contact has been replaced by a repulsive N···N contact.

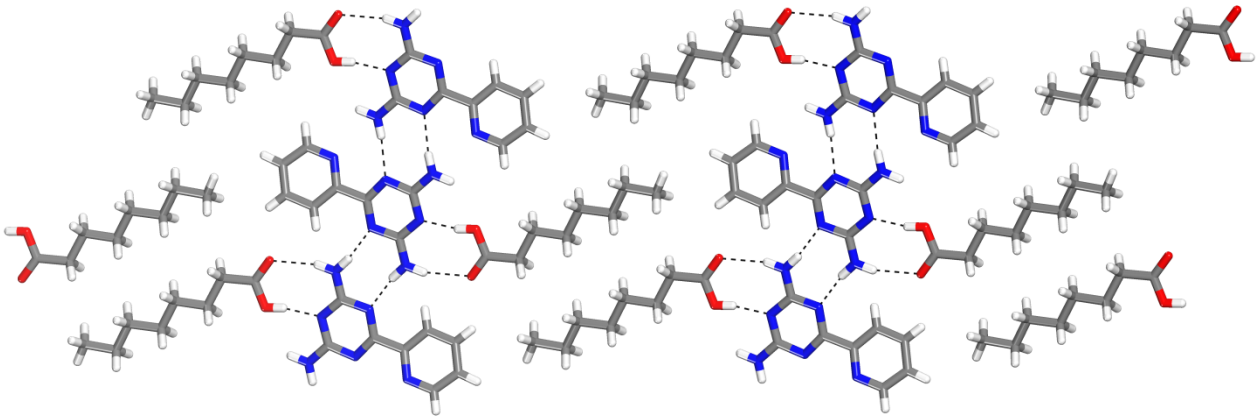

Figure 6. View of the structure of 1:1 cocrystals of 6-(2-pyridyl)-2,4-diamino-1,3,5-triazine (**2c**) with octanoic acid, showing part of a sheet constructed from hydrogen-bonded tapes. Principal hydrogen bonds are represented by broken lines, and carbon atoms are shown in gray, hydrogen atoms in white, nitrogen atoms in blue, and oxygen atoms in red.

Additional interactions within the chains of compound **2c** include bifurcated N-H···N hydrogen bonds involving the pyridyl nitrogen atom and an NH_2 group (2.998 Å),[40] augmented by a C-H···N interaction (H···N distance = 2.573 Å, C-H···N angle = 141.8°).[21] Further association of the chains with octanoic acid according to synthon **II** yields flat tapes closely analogous to those formed in 2D and 3D by isomeric pyridyl-substituted diaminotriazine **2b**. O-H···N and O···H-N distances in the tapes are normal (2.622 and 3.080 Å, respectively).[19,20] Packing of the tapes forms sheets with interdigitated alkyl groups (Figure 6), which stack to produce the 3D structure.[34]

As expected, evaporation of solutions of compound **2c** in nonanoic acid yielded 1:1 cocrystals with a closely analogous structure (Table 1).[34] The similarity is clearly revealed by

comparing key structural parameters, including intermolecular separation within the tapes, the separation between adjacent tapes (as measured along the line defined by the extended alkyl chains), and the angle defined by the tapes and alkyl chains. These parameters are 6.2 Å, 21.3 Å, and 59.6°, respectively, in cocrystals with octanoic acid, and they are 6.1 Å, 22.2 Å, and 61.6° in cocrystals with nonanoic acid.

2D Cocrystallization of 2,4-Diamino-6-(2-pyridyl)-1,3,5-triazine (2c) with Alkanecarboxylic Acids. The strong tendency of pyridyl-substituted diaminotriazine **2c** to cocrystallize with alkanecarboxylic acids to form hydrogen-bonded sheets in 3D suggests that a similar molecular organization will be favored when the components are coadsorbed on graphite. An ordered adlayer was formed on the surface of HOPG when a saturated solution of compound **2c** in heptanoic acid was added. A representative image appears in Figure 7, along with a superimposed unit cell and a model of the proposed structure, calculated by semiempirical methods. The patterns of contrast indicate that compound **2c** forms chiral hydrogen-bonded tapes like those observed in 3D. Moreover, the unit cell parameters (a = 7.7 Å, b = 18.2 Å, γ = 60°) are consistent with the intra-tape separations (6.2 Å and 6.1 Å), inter-tape distances (21.3 Å and 22.2 Å), and angles (59.6° and 61.6°) found in 3D cocrystals with octanoic acid and nonanoic acid. Again, pyridyl-substituted diaminotriazine **2c** resembles isomers **2a**-**b** by cocrystallizing with alkanecarboxylic acids in 2D and 3D in virtually the same way, according to design.

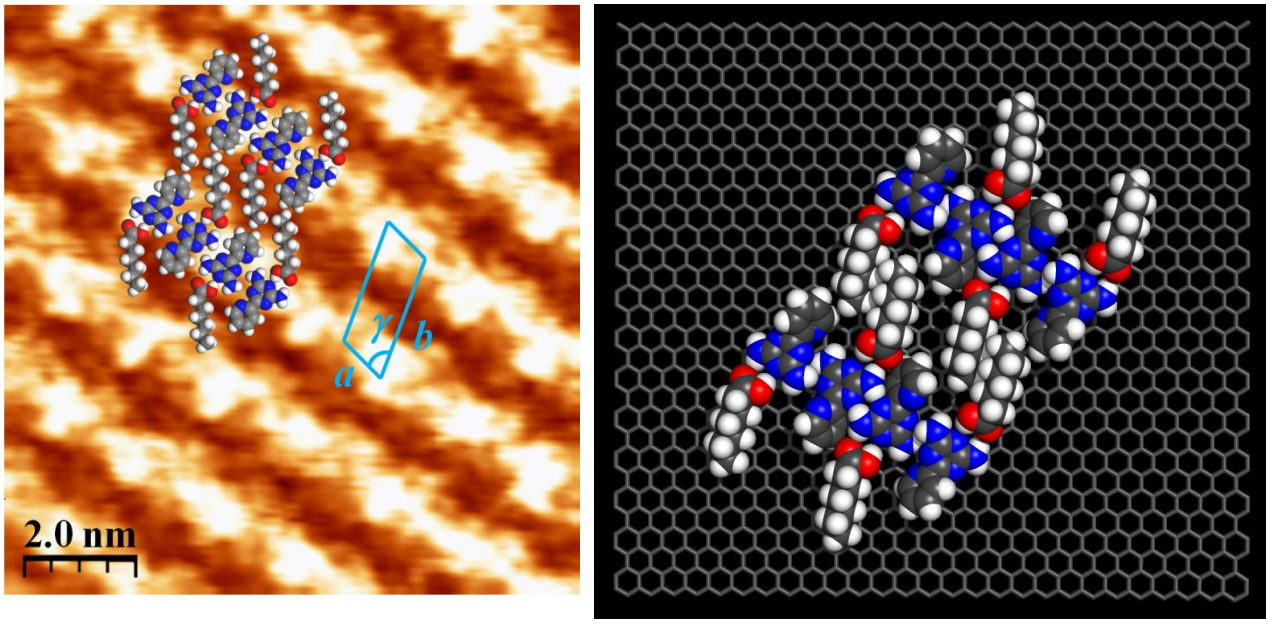

a **b**

Figure 7. (a) STM image of the adsorption of 2,4-diamino-6-(2-pyridyl)-1,3,5-triazine (**2c**) on HOPG (deposition from heptanoic acid, with V_{bias} = -1.50 V and I_{set} = 0.06 nA). Superimposed on the image are a scale bar, the measured unit cell, and approximate molecular models added as visual aids to facilitate interpretation of the pattern of contrasts. (b) Detailed semiempirical model of the proposed 2D structure.

3D Cocrystallization of 2,4-Diamino-6-[4-(4-pyridyl)phenyl]-1,3,5-triazine (3) with Alkanecarboxylic Acids. To further probe the predisposition of pyridyl-substituted diaminotriazines to crystallize similarly in 2D and 3D, we examined the behavior of an extended analog, 2,4-diamino-6-[4-(4-pyridyl)phenyl]-1,3,5-triazine (**3**). By slowly evaporating a solution of compound **3** in heptanoic acid at 25 °C, we obtained cocrystals of composition **3** • 2 heptanoic acid. They proved to belong to the monoclinic space group *C*2/c, and other crystallographic data are summarized in Table 3. Views of the structure appear in Figure 8. Like simpler pyridyl-substituted diaminotriazine **2a**, each molecule of elongated analog **3** forms hydrogen bonds with two molecules of heptanoic acid according to synthons **II** and **III** to produce ternary aggregates.

The observed O-H···N(triazine), O···H-N(triazine), and O-H···N(pyridine) distances in synthons **II** and **III** have normal values (2.608, 3.081, and 2.637 Å, respectively),[19,20] as does the H···O distance (2.705 Å) in the secondary C-H···O interaction of synthon **III**. The carboxyl group is thereby held close to the plane of the pyridyl ring, the alkyl chains adopt an extended conformation, and compound **3** favors a flattened conformation with small interaryl dihedral angles, giving ternary aggregates similar to those observed in 3D structures of cocrystals of analog **2a** with alkanecarboxylic acids.

Table 3. Crystallographic Data for Cocrystals of 2,4-Diamino-6-[4-(4-pyridyl)phenyl]-1,3,5-triazine (**3**) with Alkanecarboxylic Acids (**C7** = Heptanoic Acid and **C9** = Nonanoic Acid).

cocrystal	**3** • 2 **C7**	**3** • 2 **C9**
formula	$C_{28}H_{40}N_6O_4$	$C_{32}H_{48}N_6O_4$
crystal system	monoclinic	monoclinic
space group	*C*2/c	*C*2/c
a (Å)	50.606(4)	58.554(7)
b (Å)	7.9595(7)	7.9545(10)
c (Å)	14.0826(12)	14.0407(15)
α (°)	90	90
β (°)	95.126(4)	102.299(5)
γ (°)	90	90
V (Å^3)	5649.8(8)	6389.6(13)
Z	8	8
ρ_{calcd} (g cm^{-3})	1.234	1.208
T (K)	150	150
μ (mm^{-1})	0.679	0.646
R_1, $I > 2\sigma$ (%)	5.97	9.81
R_1, all data (%)	13.32	15.53
ωR_2, $I > 2\sigma$ (%)	13.67	25.34
ωR_2, all data(%)	17.03	29.54
measured reflections	37062	48619
independent reflections	5020	4231
Observed reflections, $I > 2\sigma(I)$	2591	2484

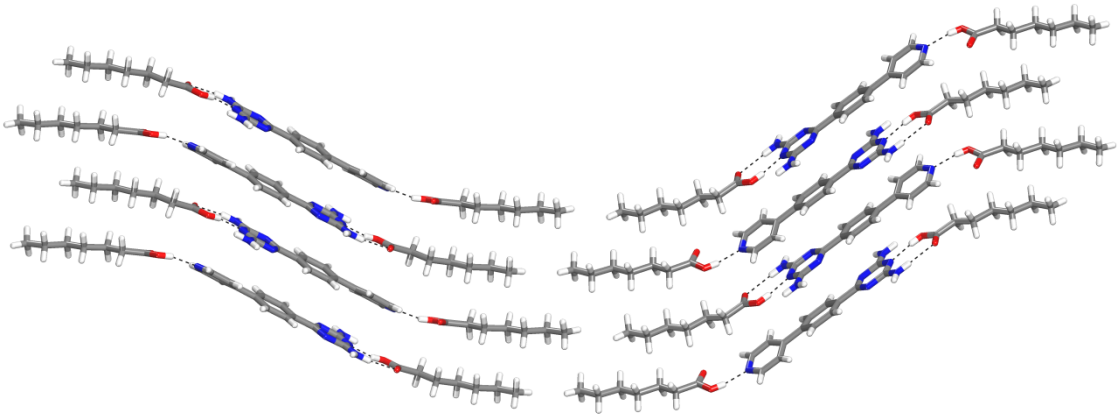

a

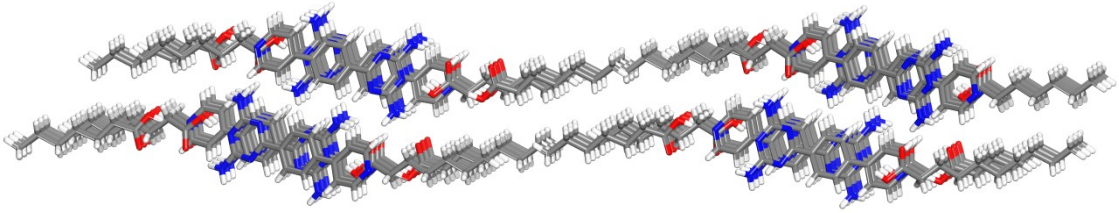

b

Figure 8. Views of the structure of 1:2 cocrystals of 2,4-diamino-6-[4-(4-pyridyl)phenyl]-1,3,5-triazine (**3**) with heptanoic acid. (a) View of part of a sheet constructed from hydrogen-bonded tapes. Hydrogen bonds are represented by broken lines, and carbon atoms are shown in gray, hydrogen atoms in white, nitrogen atoms in blue, and oxygen atoms in red. (b) View of two stacked sheets, showing the nearly perpendicular orientation of molecules of compound **3**.

In the case of pyridyl-substituted diaminotriazine **2a**, the ternary aggregates are linked into flat tapes by the formation of in-plane hydrogen bonds and secondary C-H···O interactions. In contrast, the formation of tapes from elongated analog **3** is dominated by extensive face-to-face aromatic interactions (Figure 8a). Again, packing of the tapes produces sheets; however, molecules of compound **3** are nearly perpendicular to the planes of the sheets (Figure 8b),

whereas molecules of simpler analog **2a** lie within the planes. We attribute this difference to the larger aromatic surface of compound **3**.

Slow evaporation of a solution of compound **3** in nonanoic acid produced cocrystals of composition **3** • 2 nonanoic acid. These cocrystals were found to have a molecular organization essentially identical to that of cocrystals grown from heptanoic acid (Figure 8), as suggested by comparison of the structural parameters in Table 3.[34] Together, these observations confirm that pyridyl-substituted diaminotriazines **2a-c** and **3** all behave similarly and are properly designed to form closely analogous 3D structures built from sheets incorporating alkanecarboxylic acids. As a result, we were optimistic that compound **3** would resemble relatives **2a-c** by producing analogous 2D cocrystals as well, although we recognized that the perpendicular molecular orientation found in 3D (Figure 8b) would presumably require a degree of alteration to optimize adsorption on graphite.

2D Cocrystallization of 2,4-Diamino-6-[4-(4-pyridyl)phenyl]-1,3,5-triazine (3) with Alkanecarboxylic Acids. Addition of a saturated solution of compound **3** in heptanoic acid to the surface of HOPG generated an ordered adlayer. Figure 9 shows a representative image, along with a superimposed unit cell and a model of the suggested structure, based on semiempirical calculations. As expected, the patterns of contrast and unit cell parameters (a = 16.6 Å, b = 41.2 Å, γ = 30°) are consistent with the formation of chiral hydrogen-bonded tapes directly related to those observed in 3D, except that molecules of compound **3** are turned to that they lie in the plane of the adsorbed sheet, parallel to the underlying surface. Again, pyridyl-substituted diaminotriazine **3** resembles analogs **2a-c** by cocrystallizing with alkanecarboxylic acids in 2D and 3D in nearly the same way, as planned.

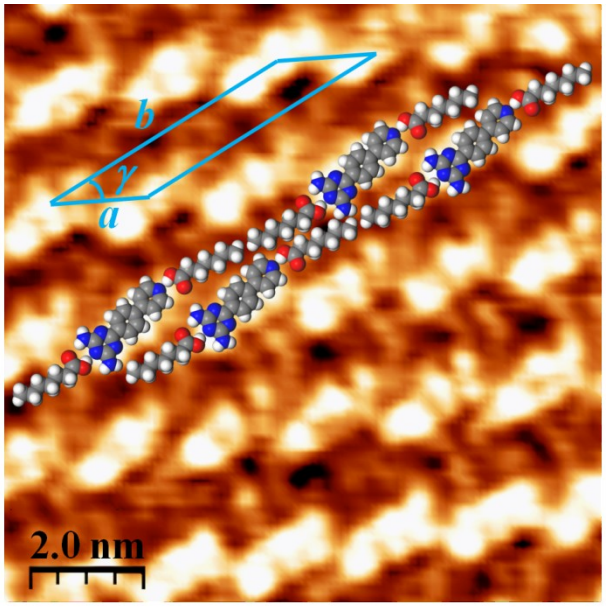

a

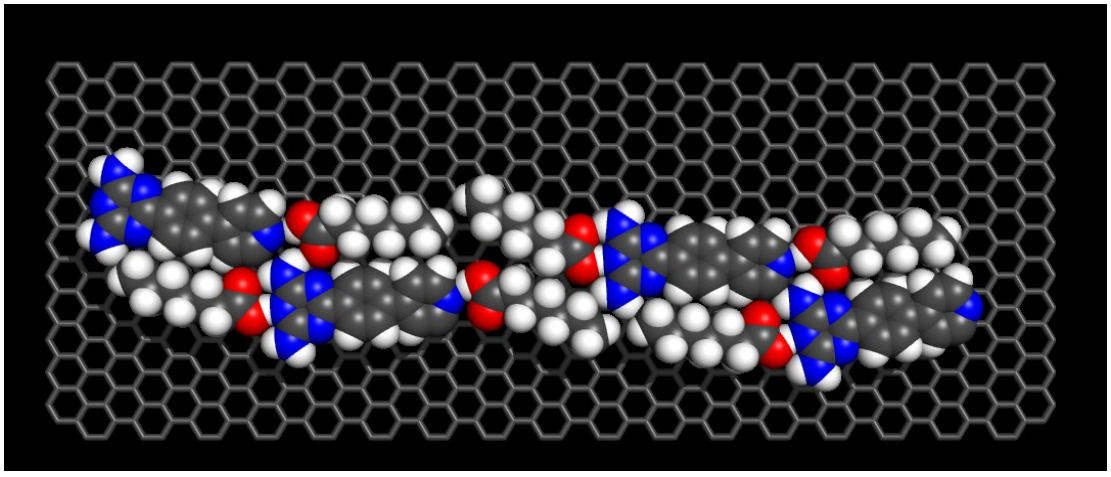

b

Figure 9. (a) STM image of the adsorption of 2,4-diamino-6-[4-(4-pyridyl)phenyl]-1,3,5-triazine (**3**) on HOPG (deposition from heptanoic acid, with V_{bias} = -1.16 V and I_{set} = 0.09 nA). Superimposed on the image are a scale bar, the measured unit cell, and approximate molecular models added as visual aids to facilitate interpretation of the pattern of contrasts. (b) Detailed semiempirical model of the postulated 2D structure.

Conclusions

Our results establish that extended series of compounds can be designed to form ordered adlayers and crystalline solids with closely analogous 2D and 3D structures. The observed analogies suggest that the following principles are critical elements of successful design: (1) The molecular components should have a pronounced affinity for the underlying surface; (2) the components should ensure consistent and predictable molecular organization by engaging in strong self-association, directed by reliable interactions; (3) the cumulative strength of interadsorbate interactions should approach or exceed the energy of adsorption; and (4) interadsorbate interactions should be directed primarily within a single plane so that association favors the formation of robust sheets.

The behavior of compounds **2a-c** and **3** persuasively illustrates the potential of this approach. In particular, the pyridyl and diaminotriazinyl groups ensure strong adsorption, and the compounds are designed to form hydrogen bonds with alkanecarboxylic acids according to reliable coplanar motifs, thereby ensuring the formation of closely analogous sheets in 2D and 3D. The success of this strategy underscores the rapidly expanding scope of molecular crystal engineering and its potential as a fundamental tool in materials science. We expect our approach to have general value as a source of new molecular materials that favor similar organization in different states, including monolayers, thin films, and bulk solids, allowing their use in applications requiring behavior that depends predictably on dimensions, such as in thin-film devices.

Experimental Section

Syntheses of Pyridyl-Substituted Diaminotriazines 2a-c and 3. Compounds **2a**,[18] **2b**,[24] and **2c**[25] were prepared by methods reported previously. Extended analogue **3** was synthesized in 80% overall yield by the route summarized below, which used Suzuki-Miyaura coupling of 4-bromobenzonitrile with 4-pyridineboronic acid to make 4-(4-cyanophenyl)pyridine,[26] followed by heating with dicyandiamide according to standard methods.[27] Reagents needed for these syntheses were purchased from commercial sources and used without further purification.

4-(4-Cyanophenyl)pyridine.[26] A dried pressure tube was charged with $Pd(OAc)_2$ (0.030 g, 0.13 mmol), 4-bromobenzonitrile (0.50 g, 2.7 mmol), 4-pyridineboronic acid (0.37 g, 3.0 mmol), and SPhos (0.11 g, 0.27 mmol). Toluene (15 mL), water (5 mL), and methanol (5 mL) were added, and the tube was capped with a septum. The mixture was stirred under N_2 for 10 min at 25 ^oC, and then K_3PO_4 (5.8 g, 27 mmol) was added. The septum was replaced with a screw cap, and the mixture was heated at 110 ^oC until 4-bromobenzonitrile was consumed, as judged by thin-layer chromatography. The mixture was cooled to 25 ^oC and extracted with dichloromethane. Solvent was removed from the extracts by evaporation under reduced pressure, and the residue was purified by flash chromatography (silica gel, ethyl acetate/hexane 1:4) to give 4-(4-cyanophenyl)pyridine (0.41 g, 2.3 mmol, 85%) as a colorless solid: mp 75-76 ^oC; IR (ATR) 2917, 2227 cm^{-1}; ^1H NMR (400 MHz, $CDCl_3$) δ 8.72 (2H, d, ^3J = 5.9 Hz), 7.78 (2H, d, ^3J = 8.2 Hz), 7.73 (2H, d, ^3J = 8.2 Hz), 7.50 (2H, d, ^3J = 5.9 Hz); ^{13}C NMR (100 MHz, $CDCl_3$) δ 151.03, 146.70, 143.00, 133.31, 128.17, 122.01, 118.81, 113.19; HRMS (ESI) calcd for $C_{12}H_8N_2$ + H *m/e* 181.0760, found 181.0764.

2,4-Diamino-6-[4-(pyridinyl)phenyl]-1,3,5-triazine (3). A mixture of 4-(4-cyanophenyl)pyridine (0.59 g, 3.3 mmol),[26] dicyandiamide (0.55 g, 6.5 mmol), and KOH (0.20 g, 3.6 mmol) in 2-methoxyethanol (30 mL) was heated at reflux for 12 h. The resulting mixture was cooled to 25 ^{o}C, the precipitated solid was separated by filtration, and the solid was washed with hot water to give pure 2,4-diamino-6-[4-(pyridinyl)phenyl]-1,3,5-triazine (**3**; 0.82 g, 3.1 mmol, 94%) as a nearly colorless solid: mp 317 ^{o}C; IR (ATR) 3481, 3435, 3399, 3306, 3100, 1647, 1614, 1521, 1436, 1396, 808 cm^{-1}; ^{1}H NMR (400 MHz, DMSO-d_6) δ 8.67 (2H, d, ^{3}J = 3.9 Hz), 8.38 (2H, d, ^{3}J = 7.8 Hz), 7.92 (2H, d, ^{3}J = 7.8 Hz), 7.78 (2H, d, ^{3}J = 3.9 Hz), 6.83 (4H, bs); ^{13}C NMR (100 MHz, DMSO-d_6) δ 170.46, 168.30, 151.19, 147.19, 140.32, 138.73, 129.31, 127.54, 122.11; HRMS (ESI) calcd for $C_{14}H_{12}N_6$ + H *m/e* 265.1196, found 265.1206. Anal. Calcd for $C_{14}H_{12}N_6$: C, 63.62; H, 4.58; N, 31.80. Found: C, 63.03; H, 4.31; N, 31.65.

Studies of 2D Crystallization by STM. All STM experiments were performed at room temperature (20-25 °C) using a JEOL-5200 SPM instrument equipped with a narrow scanner. Platinum/iridium STM tips were mechanically cut from wire (Pt/Ir, 80%/20%, diameter = 0.25 mm). In typical experiments, the freshly cleaved basal surface of HOPG (Structure Probe, Inc., SPI-1 grade) was first imaged to determine the quality of the Pt/Ir tip and the smoothness of the graphite surface. Once this was determined, a droplet (~ 1 μL) of a saturated solution of pyridyldiaminotriazines **2a-c** and **3** in alkanecarboxylic acids was applied. STM investigations were then carried out at the liquid-solid interface in the constant-height mode. STM imaging was performed by changing the tunneling parameters (voltage applied to the tip and the average tunneling current). Raw STM images were processed using a JEOL software package (WinSPM Data Processing System, Version 2.15, R. B. Leane, JEOL Ltd.) and a freeware (WSxM 5.0 Develop 1.2, Nanotec Electrónica S. L.).[28] A smooth 3 × 3 matrix convolution filter was used to produce the final images.

Semiempirical Modeling of 2D Molecular Organization in Adlayers on Graphite. Profiles of patterns of contrast in STM images were analyzed to estimate unit cell parameters and to allow initial structural hypotheses to be formulated. Detailed molecular models based on these hypotheses were then calculated, using the semiempirical method RM1.[29] This method is expected to yield models of 2D organization that are qualitatively reliable. However, the method requires only modest computational resources, unlike high-level density-functional approaches in which long-range dispersive interactions are taken into account, such as those we and others have reported earlier.[13,30,31]

Working with either HyperChem Pro 8.0 (PC-based) or HyperChem 4.0 (Intel Mac-based), we first used the Amber force field to minimize the energy of an isolated molecule of the adsorbate and a model graphene sheet large enough to accommodate multiple adsorbates. We then allowed the molecule to approach the graphene sheet, which was kept fixed to simplify computation. Once the molecule had adjusted in response to the underlying surface, as computed using Amber, copies were placed in neighboring positions on the surface according to the initial structural hypothesis. In the simplest approach, only a circle of neighbors in direct contact with the central molecule was added. A more sophisticated version introduced a second set of copies in contact with the outer perimeter of the circle of primary neighbors. The energy of the adsorbed aggregate was then reminimized using Amber to provide a starting geometry for semiempirical RM1 calculations, which were carried out with either HyperChem or MOPAC2009.[32] These calculations yielded the reported models, in which the assembled molecules have adjusted in response to the presence of their neighbors and an underlying fixed graphene sheet.

This approach to modeling 2D molecular organization on surfaces is attractive for three reasons: 1) It specifically assesses the effect of the underlying surface; 2) it takes neighboring

molecules into account; and 3) it can be undertaken with modest computational resources but follows a strategy of analysis related to those used in higher-level DFT approaches.[13,30] Minor shortcomings include the slight aperiodicity seen in many of the Figures 3, 5, 7, and 9, which results from the small finite number of absorbed molecules used in the calculations and the slightly different environments of the central molecule and its incompletely surrounded neighbors.

Studies of 3D Crystallization by XRD. Cocrystals were obtained by slow evaporation of solutions of pyridyldiaminotriazines **2a-c** and **3** in alkanecarboxylic acids. Crystallographic data were collected at 150 K using a Bruker Microstar diffractometer with Cu Kα radiation. The structures were solved by direct methods using SHELXS-97, and non-hydrogen atoms were refined anisotropically with SHELXL-97.[33] Hydrogen atoms were treated by first locating them from difference Fourier maps, recalculating their positions using standard values for distances and angles, and then refining them as riding atoms. In all structural studies, calculated powder X-ray diffraction patterns closely matched those obtained experimentally by analysis of bulk crystalline samples, thereby establishing that the samples consisted primarily of a single phase.[34]

Density-Functional Calculations of Adsorption on Graphene. Selected examples of adsorption and coadsorption were modeled by a high-level density-functional approach in which long-range dispersive interactions are taken into account. To allow direct comparison with related studies, we used the same methodogy reported in detail in earlier work.[13] Briefly, our calculations were based initially on the local-density approximation (LDA) of density-functional theory (DFT), and they employed a fixed graphene sheet of defined size and geometry (204 atoms of carbon and 40 peripheral atoms of hydrogen). The basis set chosen for atoms of carbon was STO-3G, and 6-31G* was used for all other atoms. The structures were optimized, and bond

dissociation energies of complexes were calculated with respect to the appropriate ground-state species asymptote. In a subsequent step in the calculations, we evaluated the contribution of dispersive interactions, which are not formally taken into account within LDA limits. This was achieved by using the PBE functional to perform single-point calculations on LDA-optimized geometries,[35] in conjunction with semiempirical dispersion corrections (D).[36] The results of such calculations can be described as being at the PBE+D level.

Acknowledgments

We are grateful to the Natural Sciences and Engineering Research Council of Canada, the Ministère de l'Éducation du Québec, the Canada Foundation for Innovation, the Canada Research Chairs Program, and Université de Montréal for financial support.

Supporting Information Available. Additional crystallographic details (including thermal atomic displacement ellipsoid plots, powder X-ray diffraction patterns, and tables of structural data in CIF format), supplementary STM images, and analyses of 2D unit cell parameters. This material is available free of charge via the Internet at http://pubs.acs.org.

Notes and References

1. Braga, D. *Chem. Commun.* **2003**, 2751-2754. Biradha, K. *CrystEngComm* **2003**, *5*, 374-384. Hollingsworth, M. D. *Science* **2002**, *295*, 2410-2413. *Crystal Engineering: From Molecules and Crystals to Materials*; Braga, D.; Grepioni, F.; Orpen, A. G., Eds.; Kluwer: Dordrecht,

Netherlands, 1999. Desiraju, G. R. *Crystal Engineering: The Design of Organic Solids*; Elsevier: Amsterdam, 1989.

2. For recent reviews, see: Elemans, J. A. A. W.; De Feyter, S. *Soft Matter* **2009**, *5*, 721-735. Elemans, J. A. A. W.; Lei, S.; De Feyter, S. *Angew. Chem., Int. Ed.* **2009**, *48*, 7298-7332. Furukawa, S.; De Feyter, S. *Top. Curr. Chem.* **2009**, *287*, 87-133. Kühnle, A. *Curr. Opin. Colloid Interface Sci.* **2009**, *14*, 157-168. Yang, Y.; Wang, C. *Chem. Soc. Rev.* **2009**, *38*, 2576-2589. Bonifazi, D.; Mohnani, S.; Llanes-Pallas, A. *Chem. Eur. J.* **2009**, *15*, 7004-7025. Stepanow, S.; Lin, N.; Barth, J. V. *J. Phys.: Condens. Matter* **2008**, *20*, 184002. Plass, K. E.; Grzesiak, A. L.; Matzger, A. J. *Acc. Chem. Res.* **2007**, *40*, 287-293. Barth, J. V. *Annu. Rev. Phys. Chem.* **2007**, *58*, 375-407. Otero, R.; Rosei, F.; Besenbacher, F. *Annu. Rev. Phys. Chem.* **2006**, *57*, 497-525. Wan, L.-J. *Acc. Chem. Res.* **2006**, *39*, 334-342. Barth, J. V.; Costantini, G.; Kern, K. *Nature* **2005**, *437*, 671-679. De Feyter, S.; De Schryver, F. *J. Phys. Chem. B* **2005**, *109*, 4290-4302. Smith, R. K.; Lewis, P. A.; Weiss, P. S. *Prog. Surf. Sci.* **2004**, *75*, 1-68. Moresco, F. *Phys. Rep.* **2004**, *399*, 175-225. De Feyter, S.; De Schryver, F. *Chem. Soc. Rev.* **2003**, *32*, 139-150. Hecht, S. *Angew. Chem., Int. Ed.* **2003**, *42*, 24-26. Giancarlo, L. C.; Flynn, G. W. *Acc. Chem. Res.* **2000**, *33*, 491-501.

3. Gutzler, R.; Sirtl, T.; Dienstmaier, J. F.; Mahata, K.; Heckl, W. M.; Schmittel, M.; Lackinger, M. *J. Am. Chem. Soc.* **2010**, *132*, 5084-5090. Marie, C.; Silly, F.; Tortech, L.; Müllen, K.; Fichou, D. *ACS Nano* **2010**, *4*, 1288-1292. Phillips, A. G.; Perdigão, L. M. A.; Beton, P. H.; Champness, N. R. *Chem. Commun.* **2010**, 2775-2777. Palma, C.-A.; Bjork, J.; Bonini, M.; Dyer, M. S.; Llanes-Pallas, A.; Bonifazi, D.; Persson, M.; Samorì, P. *J. Am. Chem. Soc.* **2009**, *131*, 13062-13071. Ciesielski, A.; Piot, L.; Samorì, P.; Jouaiti, A.; Hosseini, M. W. *Adv. Mater.* **2009**, *21*, 1131-1136. Zhang, X.; Chen, T.; Chen, Q.; Wang, L.; Wan, L.-J. *Phys. Chem. Chem. Phys.* **2009**, *11*, 7708-7712. Li, Y.; Ma, Z.; Qi, G.; Yang, Y.; Zeng, Q.; Fan, X.; Wang, C.; Huang, W. *J. Phys. Chem. C* **2008**, *112*, 8649-8653. Madueno,

R.; Räisänen, M. T.; Silien, C.; Buck, M. *Nature* **2008**, *454*, 618-621. Mamdouh, W.; Kelly, R. E. A.; Dong, M.; Kantorovich, L. N.; Besenbacher, F. *J. Am. Chem. Soc.* **2008**, *130*, 695-702. Zhou, H.; Dang, H.; Yi, J.-H.; Nanci, A.; Rochefort, A.; Wuest, J. D. *J. Am. Chem. Soc.* **2007**, *129*, 13774-13775. Ruben, M.; Payer, D.; Landa, A.; Comisso, A.; Gattinoni, C.; Lin, N.; Collin, J.-P.; Sauvage, J.-P.; De Vita, A.; Kern, K. *J. Am. Chem. Soc.* **2006**, *128*, 15644-15651. Yokoyama, T.; Yokoyama, S.; Kamikado, T.; Okuno, Y.; Mashiko, S. *Nature* **2001**, *413*, 619-621.

4. Dunitz, J. D. *Chem. Commun.* **2003**, 545-548. Desiraju, G. R. *Nature Materials* **2002**, *1*, 77-79. Gavezzotti, A. *Acc. Chem. Res.* **1994**, *27*, 309-314. Maddox, J. *Nature* **1988**, *335*, 201.
5. For initial integrated studies of 2D and 3D crystallization of narrower scope, see: Nath, K. G.; Ivasenko, O.; MacLeod, J. M.; Miwa, J. A.; Wuest, J. D.; Nanci, A.; Perepichka, D. F.; Rosei, F. *J. Phys. Chem. C* **2007**, *111*, 16996-17007. Dang, H.; Maris, T.; Yi, J.-H.; Rosei, F.; Nanci, A.; Wuest, J. D. *Langmuir* **2007**, *23*, 11980-11985.
6. For reviews of the subject of molecular epitaxy on solid surfaces, see: Witte, G.; Wöll, C. *J. Mater. Res.* **2004**, *19*, 1889-1916. Hooks, D. E.; Fritz, T.; Ward, M. D. *Adv. Mater.* **2001**, *13*, 227-241. Forrest, S. R. *Chem. Rev.* **1997**, *97*, 1793-1896.
7. For summaries of these principles, see: Wuest, J. D. *Chem. Commun.* **2005**, 5830-5837. Hosseini, M. W. *Acc. Chem. Res.* **2005**, *38*, 313-323.
8. For representative recent examples, see: Meier, C.; Landfester, K.; Ziener, U. *J. Phys. Chem. C* **2009**, *113*, 1507-1514. Zeng, X.; Wang, L.; Duan, L.; Qiu, Y. *Cryst. Growth Des.* **2008**, *8*, 1617-1622. Campione, M.; Caprioli, S.; Moret, M.; Sassella, A. *J. Phys. Chem. C* **2007**, *111* 12741-12746.
9. For recent references, see: Maly, K. E.; Gagnon, E.; Maris, T.; Wuest, J. D. *J. Am. Chem. Soc.* **2007,** *129*, 4306-4322.
10. Binning, G.; Rohrer, H.; Gerber, C.; Weibel, E. *Phys. Rev. Lett.* **1982**, *49*, 57-61.

11. Walch, H.; Maier, A.-K.; Heckl, W. M.; Lackinger, M. *J. Phys. Chem. C* **2009**, *113*, 1014-1019.
12. Zhang, X.; Chen, T.; Chen, Q.; Wang, L.; Wan, L.-J. *Phys. Chem. Chem. Phys.* **2009**, *11*, 7708-7712.
13. Rochefort, A.; Wuest, J. D. *Chem. Commun.* **2010**, 2923-2925.
14. For a related computational study of the adsorption of melamine (**1**) on Au(111), see : Mura, M.; Martsinovich, N.; Kantorovich, L. *Nanotechnology* **2008**, *19*, 465704.
15. Nangia, A.; Desiraju, G. R. *Top. Curr. Chem.* **1998**, *198*, 57-95. Desiraju, G. R. *Angew. Chem., Int. Ed*. **1995**, *34*, 2311-2327.
16. Díaz-Ortiz, Á.; Elguero, J.; Foces-Foces, C.; de la Hoz, A.; Moreno, A.; del Carmen Mateo, M.; Sánchez-Migallón, A.; Valiente, G. *New J. Chem.* **2004**, *28*, 952-958.
17. Ma, D.-L.; Che, C.-M. *Chem. Eur. J.* **2003**, *9*, 6133-6144.
18. Chan, C.-W.; Mingos, D. M. P.; White, A. J. P.; Williams, D. J. *Polyhedron* **1996**, *15*, 1753-1767.
19. Pedireddi, V. R.; Chatterjee, S.; Ranganathan, A.; Rao, C. N. R. *Tetrahedron* **1998**, *54*, 9457-9474. Etter, M. C.; Adsmond, D. A. *Chem. Commun.* **1990**, 589-591. Garcia-Tellado, F.; Goswami, S.; Chang, S.-K.; Geib, S. J.; Hamilton, A. D. *J. Am. Chem. Soc.* **1990**, *112*, 7393-7394.
20. For recent references, see : Singh, D.; Bhattacharyya, P. K.; Baruah, J. B. *Cryst. Growth Des.* **2010**, *10*, 348-356. Shattock, T. R.; Arora, K. K.; Vishweshwar, P.; Zaworotko, M. J. *Cryst. Growth Des.* **2008**, *8*, 4533-4545. Babu, N. J.; Nangia, A. *Cryst. Growth Des.* **2006**, *6*, 1995-1999. Aakeröy, C. B.; Desper, J.; Urbina, J. F. *CrystEngComm* **2005**, 7, 193-201. Dale, S. H.; Elsegood, M. R. J.; Hemmings, M.; Wilkinson, A. L. *CrystEngComm* **2004**, 6, 207-214.
21. Desiraju, G. R.; Steiner, T. *The Weak Hydrogen Bond in Structural Chemistry and Biology*; Oxford University Press : Oxford, U. K., 1999.

22. For a review of C-H···O interactions, see : Desiraju, G. R. *Chem. Commun.* **2005**, 2995-3001.

23. For recent examples and further discussion, see : Phillips, T. K.; Bhinde, T.; Clarke, S. M.; Lee, S. Y.; Mali, K. S.; De Feyter, S. *J. Phys. Chem. C* **2010**, *114*, 6027-6034. Hai, N. T. M.; Van der Auweraer, M.; Müllen, K.; De Feyter, S. *J. Phys. Chem. C* **2009**, *113*, 11567-11574. Plass, K. E.; Kim, K.; Matzger, A. J. *J. Am. Chem. Soc.* **2004**, *126*, 9042-9053.

24. Baibulova, M. S.; Akkulova, Z. G.; Afanas'eva, T. A. *Izv. Akad. Nauk Kazakh. SSR, Ser. Khim.* **1989**, 40-42.

25. Case, F. H.; Koft, E. *J. Am. Chem. Soc.* **1959**, *81*, 905-906.

26. For previous syntheses, see : Cho, S.-D.; Kim, H.-K.; Yim, H.-s.; Kim, M.-R.; Lee, J.-K.; Kim, J.-J.; Yoon, Y.-J. *Tetrahedron* **2007**, *63*, 1345-1352. Evans, O. R.; Lin, W. *Chem. Mater.* **2001**, *13*, 2705-2712. Le Gall, E.; Gosmini, C.; Nédélec, J.-Y.; Périchon, J. *Tetrahedron* **2001**, *57*, 1923-1927. Lin, S.-T.; Yang, F.-M.; Liang, D.; Shiao, M.-J. *J. Chin. Chem. Soc.* **1997**, *44*, 527-533.

27. Simons, J. K.; Saxton, M. R. *Organic Syntheses*; Wiley : New York, 1963; Collect. Vol. IV, p 78.

28. Horcas, I.; Fernández, R.; Gómez-Rodríguez, J. M.; Colchero, J.; Gómez-Herrero, J.; Baro, A. M. *Rev. Sci. Instrum.* **2007**, *78*, 01375.

29. Rocha, G. B.; Freire, R. O.; Simas, A. M.; Stewart, J. J. P. *J. Comput. Chem.* **2006**, *27*, 1101-1111.

30. Rochefort, A.; Wuest, J. D. *Langmuir* **2009**, *25*, 210-215.

31. For recent related calculations of physisorption on graphene, see : Henwood, D.; Carey, J. D. *Mol. Simul.* **2008**, *34*, 1019-1023. Zhechkov, L.; Heine, T.; Seifert, G. *Int. J. Quantum Chem.* **2006**, *106*, 1375-1382.

32. MOPAC2009 Version 9.351M (James J. P. Stewart, Stewart Computational Chemistry; http://OpenMOPAC.net).

33. Sheldrick, G. M. *Acta Crystallogr*. **2008**, *A64*, 112-122.

34. See the Supporting Information for details.

35. The small difference between the pK_a values of alkanecarboxylic acids and those of the conjugate acids of pyridine or aminotriazines such as melamine (pK_a 5)[36] provides little driving force for proton transfer.[37]

36. Jang, Y. H.; Hwang, S.; Chang, S. B.; Ku, J.; Chung, D. S. *J. Phys. Chem. A***2009**, *113*, 13036-13040.

37. For discussion, see : He, G.; Chow, P. S.; Tan, R. B. H. *Cryst. Growth. Des.* **2009**, *9*, 4529-4532. Mohamed, S.; Tocher, D. A.; Vickers, M.; Karamertzanis, P. G.; Price, S. L. *Cryst. Growth. Des.* **2009**, *9*, 2881-2889. Childs, S. L.; Stahly, G. P.; Park, A. *Mol. Pharmaceutics* **2007**, *4*, 323-338. Bhogala, B. R.; Basavoju, S.; Nangia, A. *CrystEngComm* **2005**, 7, 551-562.

38. Perdew, J. P.; Burke, K.; Ernzerhof, M. *Phys. Rev. Lett.* **1996**, *77*, 3865-3868.

39. Grimme, S. *J. Comput. Chem.* **2006**, *27*, 1787-1799.

40. For examples of related bifurcated hydrogen bonds, see : Aghabozorg, H.; Gharamaleki, J. A.; Olmstead, M. M.; Derikvand, Z.; Hooshmand, S. *Acta Crystallogr.* **2009**, *E65*, m186-m187. Šmejkal, T.; Breit, B. *Angew. Chem., Int. Ed.* **2008**, *47*, 311-315. Preston, A. J.; Gallucci, J. C.; Parquette, J. R. *Chem. Commun.* **2005**, 3280-3282. Bell, T. W.; Khasanov, A. B.; Drew, M. G. B. *J. Am. Chem. Soc.* **2002**, *124*, 14092-14103. Bell, T. W.; Khasanov, A. B.; Drew, M. G. B.; Filikov, A.; James, T. L. *Angew. Chem., Int. Ed.* **1999**, *38*, 2543-2547.

4.4 Conclusions

Inspirés par les travaux des chapitres 2 et 3, nous avons conçu une série d'isomères de type pyridyle substitué avec un groupement DAT pour favoriser la formation des couches d'absorption ordonnée en 2D et en 3D. Nos résultats ont démontré qu'il est possible de programmer une longue série de composés aptes à s'organiser de manière prévisible avec une forte homologie en 2D et en 3D par ponts hydrogène. Ce contrôle est assuré par l'affinité des composants à s'adsorber sur le graphite avec néanmoins la capacité de s'associer fortement par interactions intermoléculaires dirigées et fiables. Les images STM de l'organisation de ces composés démontrent que les forces cumulées par les interactions interadsorbate surpassent les énergies d'adsorption par la surface. Les structures observées par STM et par diffraction des rayons-X révèlent une organisation préférentielle en rubans qui se regroupent pour former des feuillets. L'ensemble des résultats obtenus dans les chapitres 2 à 4 illustre de façon convaincante le potentiel d'une approche qui intègre l'étude de l'organisation moléculaire en 2D et en 3D. En particulier, les groupes pyridyle et diaminotriazinyle assurent une forte adsorption et une association fiable maintenue par liaisons hydrogène coplanaires avec les acides alcanecarboxyliques, menant ainsi à la formation de feuillets très analogues en 2D et en 3D. Le succès de cette stratégie souligne l'ampleur croissante de l'ingénierie cristalline moléculaire et son potentiel comme outil fondamental dans la science des matériaux.

Chapitre 5

Similarité structurelle des réseaux maintenus par ponts hydrogène

5.1 Introduction

En plus d'offrir la possibilité de faire du nanopatterning des surfaces en combinaison avec des acides alcanecarboxyliques, les composés de type pyridyle substitué avec un groupe diaminotriazinyle (DAT) ont un intérêt intrinsèque en chimie supramoléculaire en tant qu'entités pouvant s'associer toutes seules en 3D. Dans le chapitre 4, nous avons décrit comment la cocristallisation des composés portant des groupes pyridyle et diaminotriazinyle avec des acides alcanecarboxyliques favorise une organisation similaire en 2D et en 3D. Pour mieux comprendre la capacité intrinsèque des unités DAT à régir l'association moléculaires, nous avons examiné les structures 3D des cristaux des mêmes composés obtenus dans des conditions normales, c'est-à-dire en présence des solvants qui ne s'associent pas fortement avec les groupements DAT. Les études cristallographiques de ces composés présentent une importance non seulement en chimie supramoléculaire mais aussi pour des études de chimie de coordination que nous allons discuter ultérieurement.

5.2 Nos objectifs

L'objectif principal de ce chapitre est d'explorer l'intérêt des composés de type pyridine substitué avec l'unité DAT dans le contexte de l'ingénierie cristallin. Nous avons donc cristallisé ces composés en absence des acides carboxyliques ou d'autres composés pouvant s'associer fortement avec les groupes pyridyle ou DAT, dans le but de comprendre comment ces molécules s'organisent en 3D. Nous avons constaté qu'il est parfois possible de prédire leur organisation en se basant sur les études antécédentes de la structure des molécules qui incluent les unités DAT. Les résultats de ce chapitre sont indispensables pour étayer les connaissances en chimie supramoléculaire et pour nous donner une banque de données essentielles pour pouvoir interpréter le comportement de cette famille de composés en tant que ligands pour la formation de complexes métalliques.

5.3 Article 4

Structural Similarity of Hydrogen-Bonded Networks in Crystals of Isomeric Pyridyl Substituted Diaminotriazines

Adam Duong, Thierry Maris, and James D. Wuest*

Crystal Growth and Design, **2011**, *11(1)*, 287-294

Abstract

Crystals of isomeric pyridyl-substituted diaminotriazines **1a-c** and elongated analogs **2a-b** were grown under various conditions, and their structures were solved by X-ray crystallography. Analysis of the structures revealed three shared features : 1) The compounds favor flattened conformations; 2) they participate in approximately coplanar hydrogen bonding according to motifs characteristic of diaminotriazines; and 3) these interactions play a key role in directing molecular organization. Together, the consistent molecular topologies and the shared presence of a dominant site of association ensure that the compounds crystallize similarly to give structures that feature chains, tapes, and layers. In certain cases, in fact, the molecular organization adopted by different pyridyl-substituted diaminotriazines is virtually identical, even when the length of the molecule or the orientation of the pyridyl group has been changed. Together, these observations show how functional groups such as diaminotriazinyl, which can control association by forming multiple directional intermolecular interactions according to reliable patterns, can be incorporated within more complex molecular structures to determine how crystallization will occur.

Introduction

Isomeric pyridyl-substituted diaminotriazines **1a-c** and elongated analogs **2a-b** define a coherent series of small molecules with well-defined geometries and a marked ability to associate by forming hydrogen bonds, aromatic interactions, and coordinative bonds to metals.

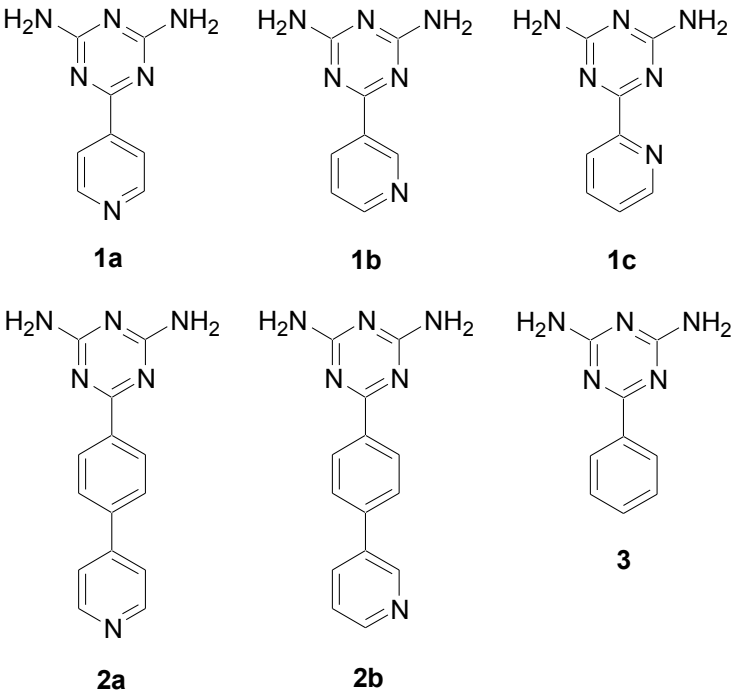

Aryltriazines normally adopt conformations in which the triazinyl ring and aryl substituent are approximately coplanar,[1] and diaminotriazines participate in characteristic patterns of intermolecular hydrogen bonding, as defined by isomeric supramolecular homosynthons **I-III**.[1-5] Together, these properties are expected to play a dominant role in determining how isomeric pyridyl-substituted diaminotriazines **1a-c** and **2a-b** will crystallize, and they should favor a series of related structures in which the compounds adopt flattened conformations and form extensive networks of hydrogen bonds directed primarily within the molecular plane.

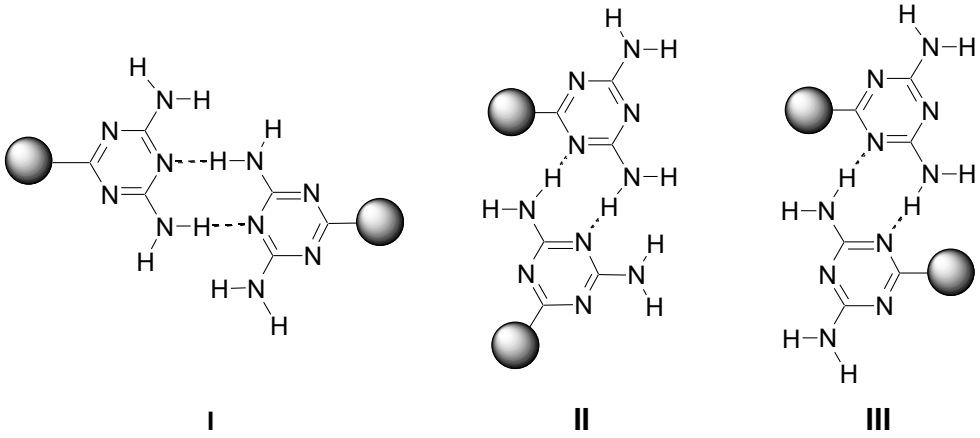

I II III

Results and Discussion

Syntheses of Isomeric Pyridyl-Substituted Diaminotriazines 1a-c and 2a-b. Compounds **1a**,[4] **1b**,[6] **1c**,[7] and **2a**[8] were prepared by methods reported previously. Extended analog **2b** was synthesized in 81% overall yield by Suzuki-Miyaura coupling of 4-bromobenzonitrile with 3-pyridineboronic acid, followed by heating the resulting 3-(4-cyanophenyl)pyridine[9] with dicyandiamide according to standard procedures.[10]

Structure of Crystals of 2,4-Diamino-6-(4-pyridyl)-1,3,5-triazine (1a). Previous work reported the structure of crystals of compound **1a**, which were grown from EtOH and shown to belong to the monoclinic space group *C*2/*c*.[3,4] We have found that crystals grown from DMSO/MeCN have the same structure. To facilitate comparison of this known structure with new ones, it is presented succinctly in Figure 1, and other crystallographic data are summarized in Table 1. Two crystallographically independent molecules are present (**A** and **B**), which are linked along the *ac* diagonal into alternating $(\mathbf{AB})_n$ chains by hydrogen bonding according to a distorted form of motif **III** (Figure 1a). Individual $(\mathbf{AB})_n$ chains are paired to form tapes, primarily by additional hydrogen bonding of molecules **A** according to motif **I** (Figure 1a).

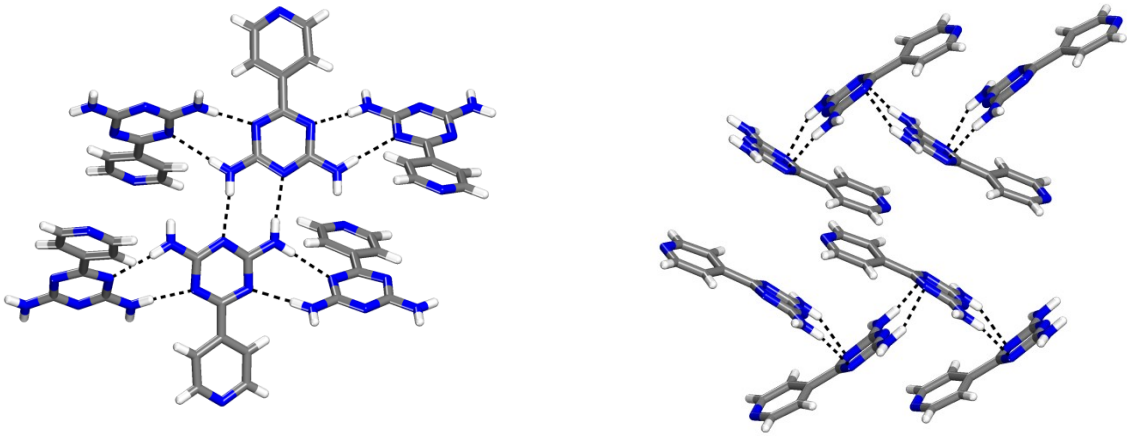

a **b**

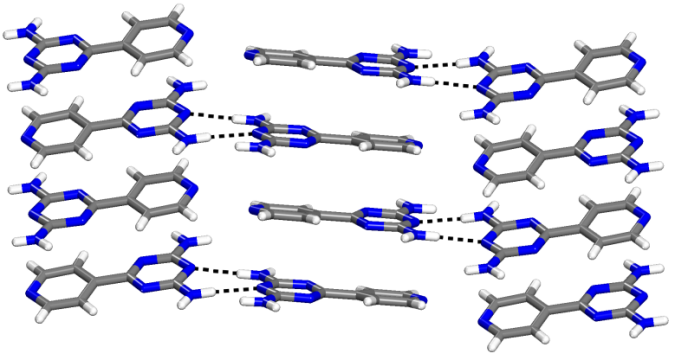

c

Figure 1. Views of the structure of crystals of 2,4-diamino-6-(4-pyridyl)-1,3,5-triazine (**1a**) grown from EtOH[3,4] or DMSO/MeCN. Hydrogen bonds are represented by broken lines, and carbon atoms are shown in gray, hydrogen atoms in white, and nitrogen atoms in blue. (a) View along the *b* axis showing alternating $(\mathbf{AB})_n$ chains of independent molecules **A** and **B**, which are held together by hydrogen bonding according to motif **III**. The chains are paired to form tapes, primarily by hydrogen bonding of molecules **A** according to motif **I**. (b) View showing how the association of tapes is directed in part by π-stacking and by edge-to-face N-H···N interactions within a herringbone arrangement of molecules **B**. (c) View showing further association of tapes controlled by head-to-tail π-stacking of molecules **A** along the *b* axis.

Table 1. Crystallographic Data for Isomeric Pyridyl-Substituted Diaminotriazines **1a-c**.

compound	**1a**	2 **1a** • MeOH	**1b**	**1b**	**1c**	**1c** • DMSO
crystallization medium	DMSO/CH_2Cl_2 DMSO/MeCN	DMSO/MeOH	DMSO	MeCN	MeCN	DMSO
formula	$C_8H_8N_6$	$C_{17}H_{20}N_{12}O$	$C_8H_8N_6$	$C_8H_8N_6$	$C_8H_8N_6$	$C_{10}H_{14}N_6OS$
crystal system	monoclinic	triclinic	monoclinic	orthorhombic	monoclinic	monoclinic
space group	*C*2/*c*	*P*-1	$P2_1/c$	*Pbca*	$P2_1/c$	$P2_1/c$
a (Å)	27.3388(10)	8.4261(6)	12.063(4)	6.8585(2)	11.9471(9)	11.7704(1)
b (Å)	7.1786(3)	10.1297(7)	19.226(5)	13.2958(4)	6.9732(6)	9.0941(1)
c (Å)	19.9614(7)	12.2194(10)	7.016(2)	18.5050(5)	21.0822(18)	11.8294(1)
α (°)	90	75.928(4)	90	90	90	90
β (°)	120.433(1)	87.136(4)	95.029(2)	90	101.590(4)	97.16
γ(°)	90	70.451(4)	90	90	90	90
V (Å^3)	3377.8(2)	952.8(1)	1620.9(8)	1687.46(8)	1720.5(2)	1256.36(2)
Z	16	2	8	8	8	4
ρ_{calc} (g cm^{-3})	1.480	1.424	1.542	1.482	1.453	1.408
T (K)	200	100	100	150	150	100
μ (mm^{-1})	0.835	0.823	0.870	0.836	0.819	2.299
R_1, $I>2\sigma(I)$	0.0408	0.0453	0.0516	0.0307	0.0514	0.0360
R_1, all data	0.0415	0.0523	0.0518	0.0338	0.0538	0.0371
wR_2, $I>2\sigma(I)$	0.0986	0.1339	0.1202	0.0808	0.1569	0.0963
wR_2, all data	0.0990	0.1387	0.1203	0.0835	0.1586	0.0992
independent reflections	3056	3252	2842	1474	2989	2215
observed reflections [$I>2\ \sigma(I)$]	2738	2764	2714	1295	2785	2100

As expected,[1] molecules **A** and **B** both adopt conformations in which the triazinyl ring and pyridyl substituent are nearly coplanar, with torsional angles of approximately 7° and 16°, respectively. In addition, molecules **A**that are paired by hydrogen bonding according to motif **I** lie in essentially the same plane. However, hydrogen bonding of diaminotriazines can accommodate substantial deviations from coplanarity, as illustrated by the distorted geometry of motif **III** in the $(\mathbf{AB})_n$ chains (Figure 1a). These deviations do not appear to weaken the hydrogen bonds substantially, and the average N-H···N distances in the nearly coplanar pair $\mathbf{A}_2$ are similar to those in the deformed pair **AB** (3.033 Å and 3.052 Å, respectively).

Cohesion between the tapes is provided in part by an N-H···N(pyridine) hydrogen bond (3.107 Å) involving the pyridyl nitrogen atom of a molecule **B** andthe single N-H bond of a nearby molecule **A** not used in motifs **I** and **III**. Association of the tapes is also maintained by

unusual N-H···aromatic interactions within a stacked herringbone arrangement of molecules **B** (Figure 1b). In these interactions, the average N-H···N distances (3.177 Å) are significantly longer than those in normal N-H···N hydrogen bonds within tapes (motifs **I** and **III**). The overall network is further stabilized by head-to-tail π-stacking of molecules **A** along the *b* axis (Figure 1c).

In the resulting structure, each molecule **A** participates in a total of seven N-H···N hydrogen bonds with four neighbors, and each molecule **B** engages in nine related interactions (five N-H···N hydrogen bonds and four N-H···aromatic interactions) with five neighbors. Hydrogen bonding of the pyridyl nitrogen atom of compound **1a** plays only a minor role in controlling crystallization, possibly because the diaminotriazinyl groups can compete effectively by forming doubly hydrogen-bonded pairs. This hypothesis is supported by the nearly identical molecular organization found in the structures of compound **1a** and 2,4-diamino-6-phenyl-1,3,5-triazine (**3**), in which the pyridyl group of compound **1a** has been replaced by phenyl.[2]

Key structural features of pyridyl-substituted diaminotriazine **1a** and its phenyl-substituted relative **3**, including their rather rigid flattened shape and ability to form multiple coplanar hydrogen bonds of types **I-III**, help ensure that their options for crystallization are limited to a narrow set of similar possibilities. To test this hypothesis, we grew new crystals of compound **1a** from DMSO/MeOH, which proved to belong to the triclinic space group *P*-1 and to have the composition 2 **1a** • MeOH. Views of the structure appear in Figure 2, and other crystallographic data are summarized in Table 1. The structure consists of two crystallographically independent molecules **A** and **B**, which differ primarily in the torsional angles between the triazinyl and pyridyl rings (approximately 47° and 39°). Both values are atypically high for aryltriazines.[1] Molecules **A** and **B** are linked by N-H···N hydrogen bonds of

type **III** with normal average distances (3.098 Å), thereby producing alternating $(\mathbf{AB})_n$ chains that lie along the *c* axis (Figure 2a). The chains are then connected to form sheets parallel to the *bc* plane by additional N-H···N(pyridine) hydrogen bonds (2.986 Å), and stacking of the sheets is controlled by multiple weak interactions (Figure 2b). As in other structures of pyridyl-substituted diaminotriazine **1a** and its phenyl-substituted relative **3**, crystals grown from DMSO/MeOH show a preference for molecular organization based on the formation of extensively hydrogen-bonded chains.

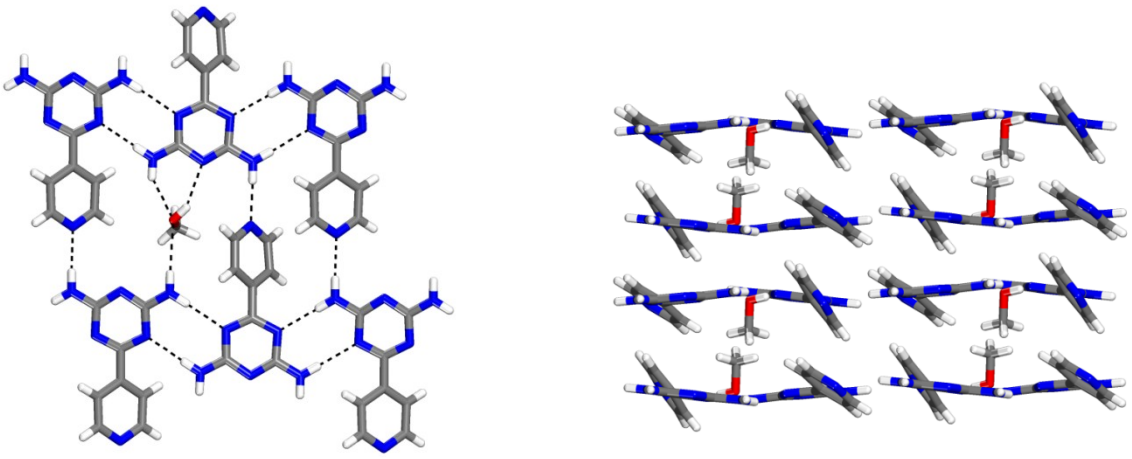

a **b**

Figure 2. Views of the structure of the 2:1 solvate of 2,4-diamino-6-(4-pyridyl)-1,3,5-triazine (**1a**) with MeOH grown from DMSO/MeOH. Hydrogen bonds are represented by broken lines, and carbon atoms are shown in gray, hydrogen atoms in white, nitrogen atoms in blue, and oxygen atoms in red. (a) View showing how N-H···N hydrogen bonds of type **III** link molecules into chains along the *c* axis, and how sheets are formed by additional N-H···N(pyridine) hydrogen bonds. (b) View along the *b* axis showing the packing of four sheets.

Structure of Crystals of 2,4-Diamino-6-(3-pyridyl)-1,3,5-triazine (1b). The similar behavior of pyridyl-substituted diaminotriazine **1a** and phenyl-substituted analog **3** established that the pyridyl nitrogen atom does not necessarily play a decisive role in directing crystallization, thereby suggesting that isomeric pyridyl-substituted diaminotriazine **1b** should also form a closely related structure. Crystals of compound **1b** grown from DMSO were found to belong to the monoclinic space group $P2_1/c$. The molecular organization proved to be essentially identical to that observed in crystals of analogs **1a** and **3** (Figure 1). A view of the structure of compound **1b** is provided in Figure 3, and other crystallographic data are presented in Table 1. The structure incorporates two crystallographically independent molecules **A** and **B** with slightly different torsional angles between the triazinyl and pyridyl rings (approximately 2° and 12°, respectively). As in the structures of analogs **1a** and **3**, molecules **A** and **B** are linked into $(\mathbf{AB})_n$ chains by characteristic hydrogen bonding of type **III**, with an average N-H···N distance of 3.052 Å (Figure 3). The chains are further connected to form tapes aligned with the *a* axis by additional N-H···N hydrogen bonding (3.096 Å) of molecules **A** according to motif **I** (Figure 3). Cohesion of the tapes is ensured by multiple interactions, including 1) N-H···N(pyridine) hydrogen bonds (3.085 Å) involving the pyridyl nitrogen atom of a molecule **B** andthe single N-H bond of a nearby molecule **A** not used in motifs **I** and **III**; 2) π-stacking and edge-to-face N-H···N interactions (3.174 Å) within a herringbone arrangement of molecules **B** (as in Figure 1b); and 3) head-to-tail π-stacking of molecules **A** (as in Figure 1c).

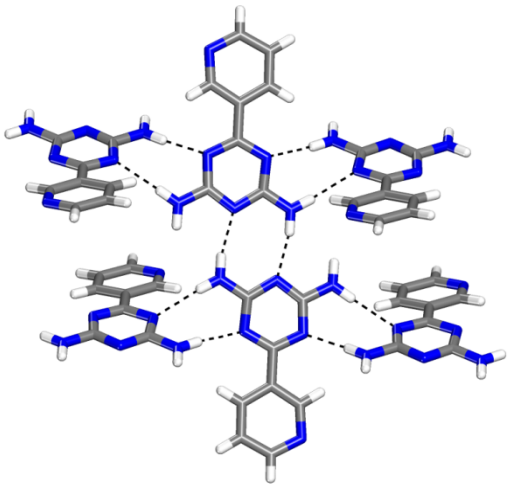

Figure 3. View of the structure of crystals of 2,4-diamino-6-(3-pyridyl)-1,3,5-triazine (**1b**) grown from DMSO. Hydrogen bonds are represented by broken lines, and carbon atoms are shown in gray, hydrogen atoms in white, and nitrogen atoms in blue. Alternating $(\mathbf{AB})_n$ chains of independent molecules **A** and **B** are held together by hydrogen bonding according to motif **III**, and the chains are paired to form tapes, primarily by hydrogen bonding of molecules **A** according to motif **I**.

The closely related behavior of isomeric pyridyl-substituted diaminotriazines **1a-b** and phenyl-substituted analog **3** under various conditions is consistent with the hypothesis that crystallization is controlled primarily by the flattened molecular topology and by the ability of diaminotriazinyl groups to direct the formation of hydrogen-bonded chains. To test this notion further, we grew additional crystals of compound **1b** from MeCN, which proved to belong to the orthorhombic space group *Pbca*. A view of the structure is shown in Figure 4, and other crystallographic data are presented in Table 1. Molecules of compound **1b** adopt a flattened conformation with an inter-aryl angle of approximately 21°, and they associate to form chains along the *a* axis held together by characteristic paired hydrogen bonds of type **II**, with an average N-H···N distance of 3.008 Å (Figure 4). Each molecule in a chain participates in a total of four

additional N-H···N(pyridine) hydrogen bonds (3.020 Å), which connect the chains to form layers parallel to the *ab* plane.[11] The layers are joined by single N-H···N(triazine) hydrogen bonds (3.127 Å) as shown in Figure 4, leading to a three-dimensional network in which each molecule of compound **1b** engages in a total of eight N-H···N hydrogen bonds with six neighbors. These data provide additional evidence that isomeric pyridyl-substituted diaminotriazines **1a-b** and phenyl-substituted analog **3** are predisposed to adopt similar flattened conformations and to engage reliably in approximately coplanar hydrogen bonds of type **I-III**, thereby leading to self-association that predictably favors the formation of related chains, tapes, and layers.

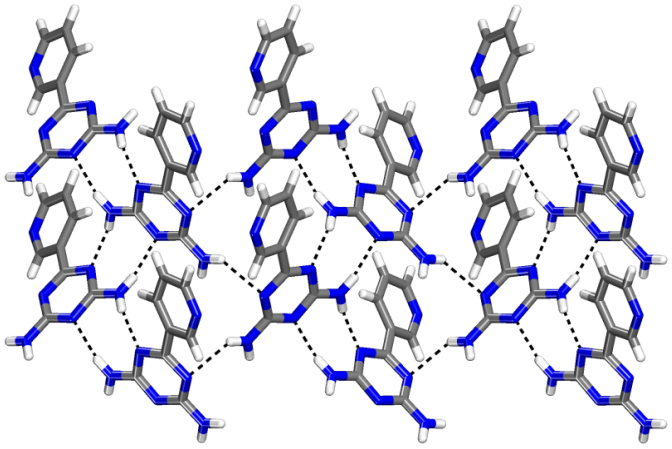

Figure 4. View along the *b* axis of the structure of crystals of 2,4-diamino-6-(3-pyridyl)-1,3,5-triazine (**1b**) grown from MeCN. Hydrogen bonds are represented by broken lines, and carbon atoms are shown in gray, hydrogen atoms in white, and nitrogen atoms in blue. Chains aligned with the *a* axis are held together by paired hydrogen bonds of type **II**. N-H···N(pyridine) hydrogen bonds between the chains (not shown) define layers parallel to the *ab* plane, which are connected by additional single N-H···N(triazine) hydrogen bonds to give a three-dimensional network.

Structure of Crystals of 2,4-Diamino-6-(2-pyridyl)-1,3,5-triazine (1c). The closely related behavior of pyridyl-substituted diaminotriazines **1a-b** and phenyl-substituted analog **3** suggested that isomeric pyridyl-substituted diaminotriazine **1c** would also crystallize in a similar way. Crystals grown from MeCN were found to belong to the monoclinic space group $P2_1/c$, and Table 1 provides additional crystallographic data. As confirmed by Figure 5, the molecular organization is virtually identical to that observed in crystals of isomer **1a** grown from EtOH or DMSO/MeCN (Figure 1), isomer **1b** grown from DMSO (Figure 3), and phenyl-substituted analog **3**.[2] In the structure of compound **1c**, crystallographically independent molecules **A** and **B** have flattened conformations with slightly different torsional angles between the triazinyl and pyridyl rings (approximately 15° and 32°, respectively). $(\mathbf{AB})_n$ chains are linked along the *a* axis by characteristic hydrogen bonding of type **III**, with an average N-H···N distance of 3.068 Å (Figure 5), and the chains are further connected to form tapes by additional N-H···N hydrogen bonding (3.050 Å) of molecules **A** according to motif **I** (Figure 5). Association of the tapes involves multiple interactions, including 1) N-H···N(pyridine) hydrogen bonds of normal average distance (3.115 Å) involving the pyridyl nitrogen atom of a molecule **B** andthe single N-H bond of a nearby molecule **A** not used in motifs **I** and **III**; 2) π-stacking and edge-to-face N-H···N interactions (3.326 Å) within a herringbone arrangement of molecules **B** (as in Figure 1b); and 3) head-to-tail π-stacking of molecules **A** (as in Figure 1c).

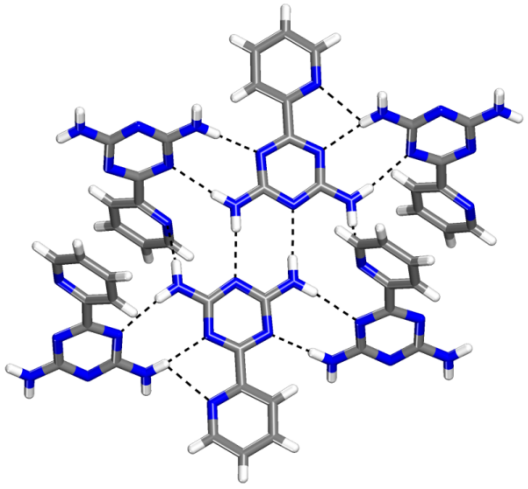

Figure 5. View of the structure of crystals of 2,4-diamino-6-(2-pyridyl)-1,3,5-triazine (**1c**) grown from MeCN. Hydrogen bonds are represented by broken lines, and carbon atoms are shown in gray, hydrogen atoms in white, and nitrogen atoms in blue. Alternating $(\mathbf{AB})_n$ chains of independent molecules **A** and **B** are held together by hydrogen bonding according to motif **III**, and the chains are paired to form tapes, primarily by hydrogen bonding of molecules **A** according to motif **I**.

These observations reinforce the notion that crystallization of isomeric pyridyl-substituted diaminotriazines **1a-c** and phenyl-substituted analog **3** is directed primarily by their similar flattened topologies and their shared ability to form approximately coplanar hydrogen bonds directed by diaminotriazinyl groups. As a further test of structural homology, we grew additional crystals of compound **1c** from DMSO, which proved to belong to the monoclinic space group $P2_1/c$ and to have the composition **1c** • 1 DMSO. Figure 6 shows views of the structure, and Table 1 provides additional crystallographic data. Molecules of compound **1c** have a flattened conformation with an angle of approximately 26° between the average planes of the pyridyl and triazinyl rings. As shown in Figure 6a, chains aligned with the *c* axis result from the formation of typical paired hydrogen bonds of type **III** (average N-H···N distance = 3.086 Å), reinforced by

additional N-H···N(pyridine) hydrogen bonds (3.070 Å). Packing of the chains, controlled in part by π-stacking of pyridyl groups, produces a structure with alternating layers consisting of compound **1c** and hydrogen-bonded molecules of DMSO (Figure 6b).

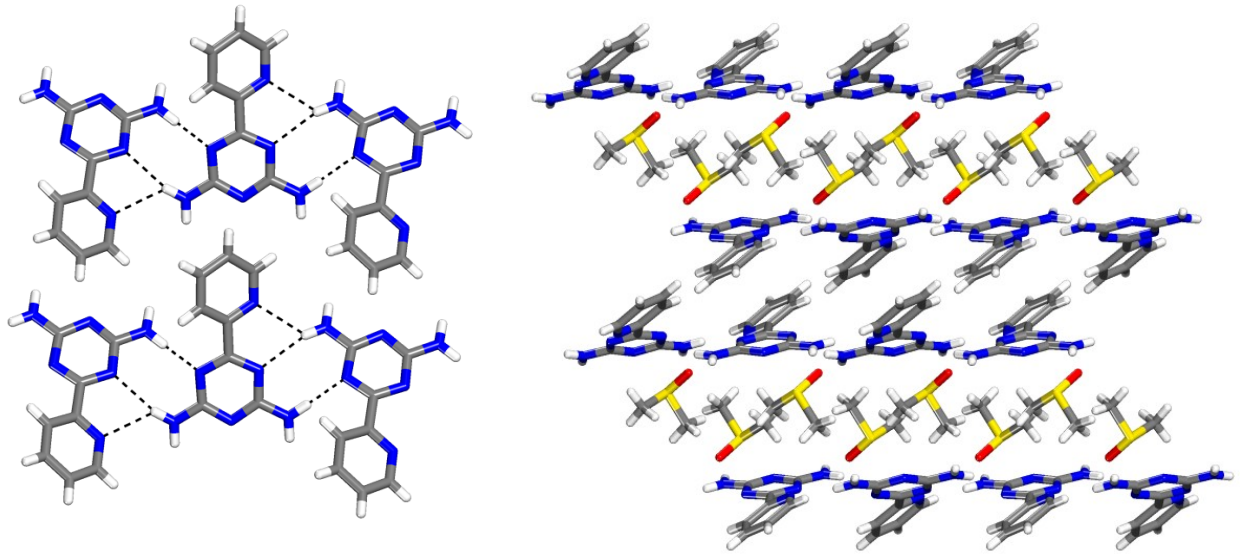

a **b**

Figure 6. Views of the structure of the 1:1 solvate of 2,4-diamino-6-(2-pyridyl)-1,3,5-triazine (**1c**) with DMSO. Hydrogen bonds are represented by broken lines, and carbon atoms are shown in gray, hydrogen atoms in white, nitrogen atoms in blue, oxygen atoms in red, and sulfur atoms in yellow. (a) View showing how N-H···N hydrogen bonds of type **III** and additional N-H···N(pyridine) hydrogen bonds link molecules into chains along the *c* axis. (b) View along the *b* axis showing alternating layers composed of compound **1c** and DMSO.

Structure of Crystals of 2,4-Diamino-6-[4-(4-pyridyl)phenyl]-1,3,5-triazine (2a). Together, our observations confirm that isomeric pyridyl-substituted diaminotriazines **1a-c** and phenyl-substituted analog **3** allinherently favor flattened conformations and participate in approximately coplanar hydrogen bonding according to motifs **I-III**. As a result, the compounds crystallize similarly under various conditions to give structures that feature chains, tapes, and layers. In certain cases, in fact, the overall molecular organization is virtually identical.

To see if these consistent patterns are maintained when molecular topology is altered, we examined the behavior of elongated pyridyl-substituted diaminotriazine **2a**. Crystallization from wet DMSO under various conditions yielded two polymorphs, as well as a monohydrate and a dihydrate. One of the polymorphs proved to belong to the triclinic space group *P*-1. A view of its structure is shown in Figure 7, and other crystallographic data are summarized in Table 2. The molecules have flattened conformations and are linked into chains along the *ab* diagonal by hydrogen bonds of type **II** (average N-H···N distance = 3.151 Å). Adjacent chains are further connected by N-H···N(pyridine) hydrogen bonds (average N-H···N distance = 2.950 Å) to give a three-dimensional network.

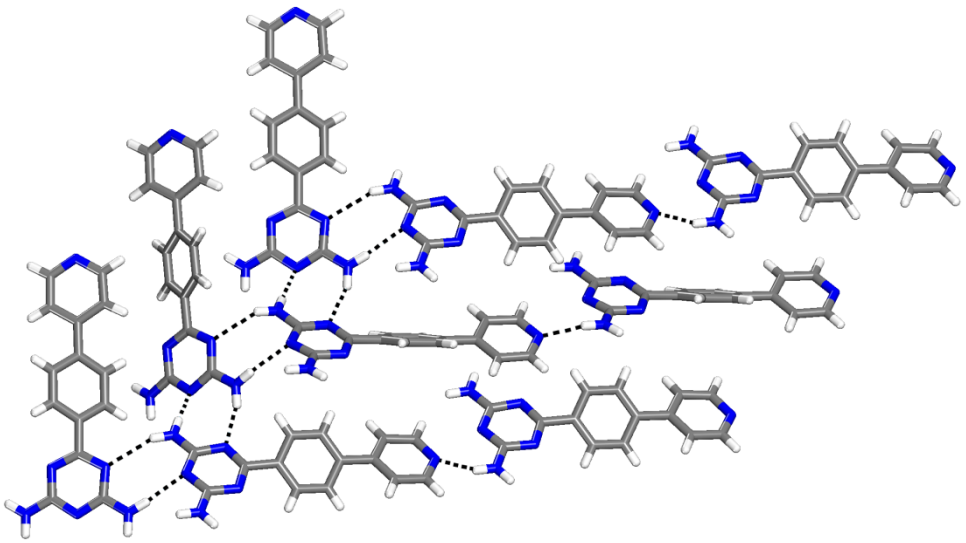

Figure 7. View of the structure of crystals of the triclinic *P*-1 polymorph of 2,4-diamino-6-[4-(4-pyridyl)phenyl-1,3,5-triazine (**2a**) grown from wet DMSO. Hydrogen bonds are represented by broken lines, and carbon atoms are shown in gray, hydrogen atoms in white, and nitrogen atoms in blue. Chains aligned with the *ab* diagonal are formed by hydrogen bonding of type **II** and are further connected to adjacent chains by N-H···N(pyridine) hydrogen bonds to give a three-dimensional network.

Table 2. Crystallographic Data for Elongated Isomeric Pyridyl-Substituted Diaminotriazines **2a-b**.

compound	**2a**	**2a**	**2a** • 1 H_2O	**2a** • 2 H_2O	**2b**
crystallization medium	DMSO/H_2O	DMSO/H_2O	DMSO/H_2O	DMSO/H_2O	DMSO/MeCN
formula	$C_{14}H_{12}N_6$	$C_{14}H_{12}N_6$	$C_{14}H_{14}N_6O$	$C_{14}H_{16}N_6O_2$	$C_{14}H_{12}N_6$
crystal system	triclinic	monoclinic	triclinic	monoclinic	orthorhombic
space group	*P*-1	$P2_1/n$	*P*-1	$P2_1/n$	*Pbca*
a (Å)	9.5053(5)	16.9150(7)	9.310(1)	7.2112(2)	7.0142(2)
b (Å)	14.2146(7)	8.6926(4)	9.719(1)	49.9305(13)	18.5089(4)
c (Å)	19.4909(9)	17.8433(7)	15.859(2)	11.9101(3)	18.5309(4)
α (°)	98.832(2)	90	96.589(2)	90	90
β (°)	94.263(2)	109.956(2)	99.854(2)	103.679(1)	90
γ(°)	104.765(2)	90	111.024(3)	90	90
V (Å^3)	2498.5(2)	2466.06(18)	1295.3(3)	4166.70(19)	2405.78(10)
Z	8	8	4	12	8
ρ_{calc} (g cm^{-3})	1.405	1.424	1.448	1.436	1.459
T (K)	150	150	100	100	100
μ (mm^{-1})	0.738	0.748	0.806	0.840	0.766
R_1, $I>2\sigma(I)$	0.0721	0.0383	0.0371	0.0547	0.0314
R_1, all data	0.1026	0.0391	0.0372	0.0747	0.0322
wR_2, $I>2\sigma(I)$	0.1876	0.1104	0.0880	0.1346	0.0845
wR_2, all data	0.2050	0.1113	0.0881	0.1466	0.0855
independent reflections	42622	4269	4604	7516	2190
observed reflections [$I>2\ \sigma(I)$]	30414	4124	4508	5785	2126

The second polymorph of elongated pyridyl-substituted diaminotriazine **2a** was found to belong to the monoclinic space group $P2_1/n$. Figure 8 provides a view of its structure, and Table 2 summarizes other crystallographic data. The structure consists of crystallographically independent molecules **A** and **B** that adopt flattened conformations and are paired by hydrogen bonding according to motif **I** (average N-H···N distance = 3.056 Å). Pairs are further connected by single N-H···N(pyridine) hydrogen bonds of normal average distance (3.029 Å) to nearly orthogonal adjacent molecules, thereby creating corrugated sheets with extensive edge-to-face aromatic interactions.[11] Packing of the sheets introduces additional aromatic interactions.

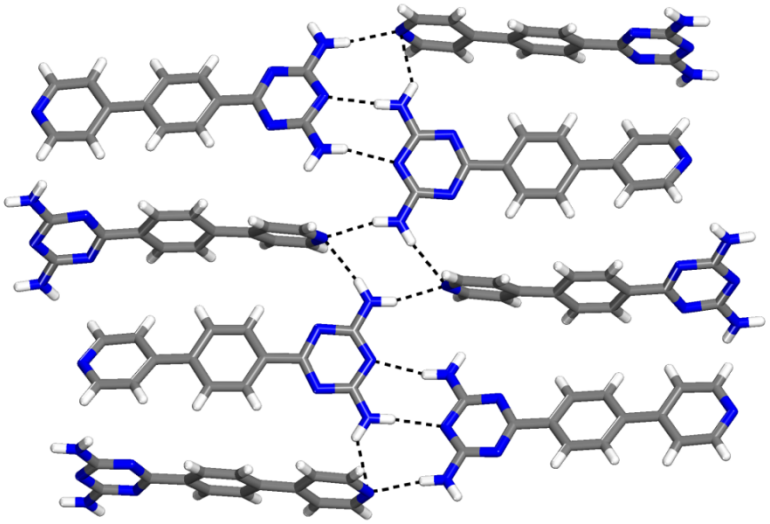

Figure 8. View of the structure of crystals of the monoclinic $P2_1/n$ polymorph of 2,4-diamino-6-[4-(4-pyridyl)phenyl-1,3,5-triazine (**2a**) grown from wet DMSO. Hydrogen bonds are represented by broken lines, and carbon atoms are shown in gray, hydrogen atoms in white, and nitrogen atoms in blue. Pairs of independent molecules **A** and **B** are held together by hydrogen bonding according to motif **I** and are further connected by single N-H···N(pyridine) hydrogen bonds to nearly orthogonal adjacent molecules.

Crystals of the monohydrate of pyridyl-substituted diaminotriazine **2a** (**2a** • 1 H_2O) proved to belong to the triclinic space group *P*-1. A view of its structure is shown in Figure 9, and other crystallographic data are presented in Table 2. Molecules of compound **2a** are paired by hydrogen bonding of type **I** (average N-H···N distance = 3.044 Å) to give a layered structure closely similar to that shown in Figure 8, except that hydrogen bonding to pyridyl groups is mediated by intervening molecules of H_2O (Figure 9). This allows the molecular components of each layer to lie approximately in the same plane, giving sheets that pack to create the overall three-dimensional structure.[11]

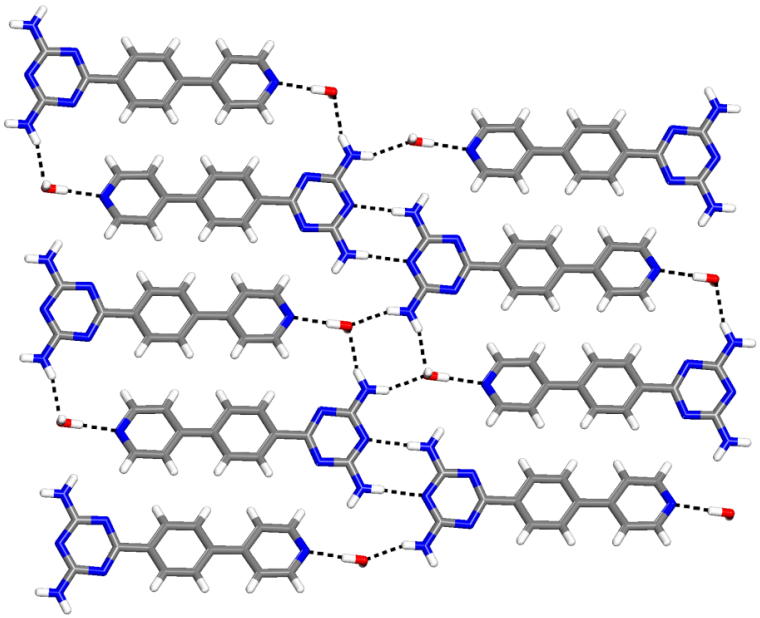

Figure 9. View of the structure of crystals of the monohydrate of 2,4-diamino-6-[4-(4-pyridyl)phenyl-1,3,5-triazine (**2a**) grown from wet DMSO. Hydrogen bonds are represented by broken lines, and carbon atoms are shown in gray, hydrogen atoms in white, nitrogen atoms in blue, and oxygen atoms in red. Molecules of compound **2a** are paired by hydrogen bonds of type **I**, and sheets result from additional hydrogen bonds involving molecules of H_2O.

Crystals of the dihydrate of elongated pyridyl-substituted diaminotriazine **2a** (**2a** • 2 H_2O) were found to belong to the monoclinic space group $P2_1/n$. Figure 10 provides a view of its structure, and Table 2 summarizes other crystallographic data. Molecules of compound **2a** are linked into chains along the *ac* diagonal by hydrogen bonding of type **III** (average N-H···N distance = 3.083 Å). The chains are connected to form sheets by further coplanar hydrogen bonding between pyridyl and triazinyl groups, mediated by intervening molecules of H_2O (Figure 10).

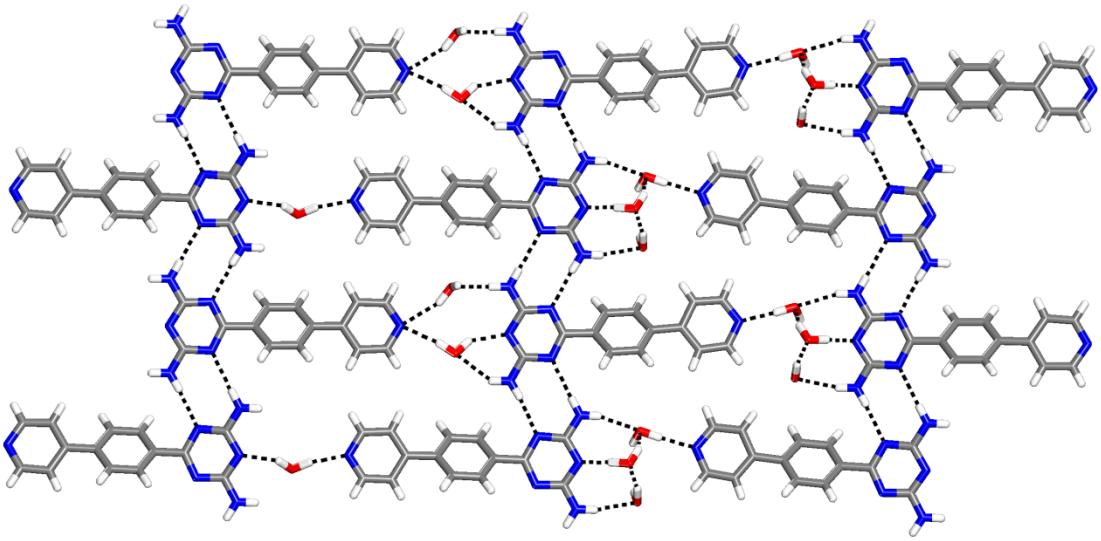

Figure 10. View of the structure of crystals of the dihydrate of 2,4-diamino-6-[4-(4-pyridyl)phenyl-1,3,5-triazine (**2a**) grown from wet DMSO. Hydrogen bonds are represented by broken lines, and carbon atoms are shown in gray, hydrogen atoms in white, nitrogen atoms in blue, and oxygen atoms in red. Molecules of compound **2a** are linked into chains by hydrogen bonds of type **III**, and the chains are connected to form sheets by additional hydrogen bonds involving molecules of H_2O.

The polymorphs and hydrates of elongated pyridyl-substituted diaminotriazine **2a** show certain expected features, including a preference for a flattened molecular structure that forms coplanar hydrogen bonds according to standard motifs. However, the behavior of compound **2a** is not always completely analogous to that of relatives **1a-c** and **3**; in particular, the $P2_1/n$ polymorph of compound **2a** clearly shows the effects of its increased aromatic surface, which favors a structure with more significant π-stacking and edge-to-face interactions.

Structure of Crystals of 2,4-Diamino-6-[4-(3-pyridyl)phenyl]-1,3,5-triazine (2b). To complete our analysis of the effect of altered molecular topology, we studied the behavior of a second isomer, elongated pyridyl-substituted diaminotriazine **2b**. Crystals grown from DMSO/MeCN proved to belong to the orthorhombic space group *Pbca*. A view of its structure is shown in Figure 11, and other crystallographic data are provided in Table 2. The molecular organization is essentially identical to that of the *P*-1 polymorph of isomer **2a** (Figure 7). Again, the molecules adopt flattened conformations and form chains linked by hydrogen bonds of type **II** (average N-H···N distance = 3.002 Å). Adjacent chains are further connected by N-H···N(pyridine) hydrogen bonds (3.019 Å) to give a three-dimensional network.

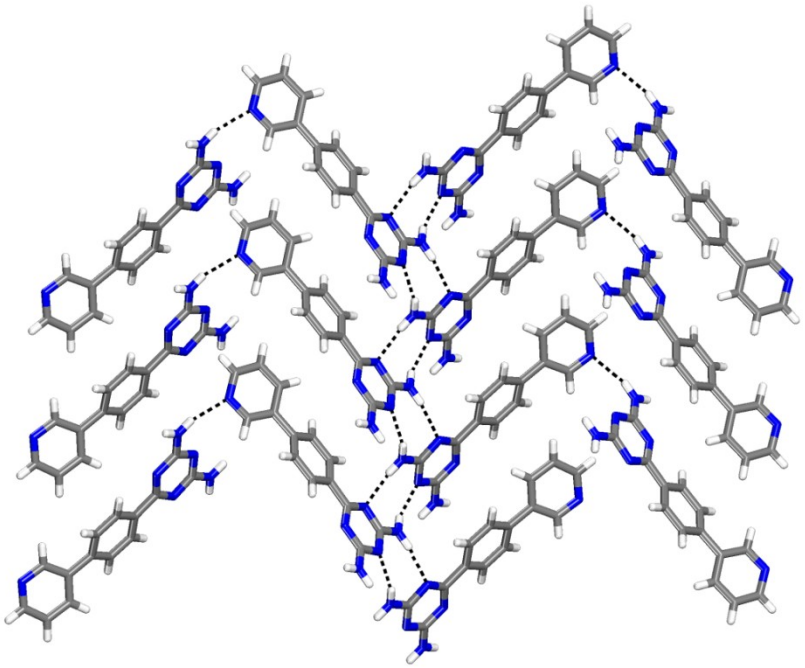

Figure 11. View of the structure of crystals of 2,4-diamino-6-[4-(3-pyridyl)phenyl-1,3,5-triazine (**2b**) grown from DMSO/MeCN. Hydrogen bonds are represented by broken lines, and carbon atoms are shown in gray, hydrogen atoms in white, and nitrogen atoms in blue. Chains aligned with the *a* axis are formed by hydrogen bonding according to motif **II**, and adjacent chains are connected by N-H···N(pyridine) hydrogen bonds to give a three-dimensional network.

Conclusions

We have found that crystals of isomeric pyridyl-substituted diaminotriazines **1a-c**, isomeric elongated analogs **2a**-**b**, and related phenyl-substituted diaminotriazine **3** have three shared features : 1) The compounds favor flattened conformations; 2) they participate in approximately coplanar hydrogen bonding according to motifs characteristic of diaminotriazines (**I-III**); and 3) these interactions play a key role in directing molecular organization. Together, the consistent molecular topologies and the shared presence of a dominant site of association ensure that the compounds crystallize similarly under various conditions to give structures that feature chains, tapes, and layers. In certain cases, in fact, the molecular organization adopted by different pyridyl-substituted diaminotriazines is virtually identical, even when the length of the molecule or the orientation of the pyridyl group has been changed. Together, these observations show how substituents such as the diaminotriazinyl group, which can control association by forming multiple directional intermolecular interactions according to motifs that have a useful degree of reliability, can be incorporated within more complex molecular structures to control how crystallization will occur.

Experimental Section

General Notes. Pyridyl-substituted diaminotriazines **1a**,[4] **1b**,[6] **1c**,[7] and **2a**[8] were prepared by methods reported previously. Elongated compound **2b** was made by the procedure summarized below. Other chemicals were purchased from commercial sources and used without further purification.

3-(4-Cyanophenyl)pyridine.[9] A dried pressure tube was charged with $Pd(OAc)_2$ (0.031 g, 0.14 mmol), 4-bromobenzonitrile (0.50 g, 2.7 mmol), 3-pyridineboronic acid (0.37 g, 3.0 mmol), and SPhos (0.11 g, 0.27 mmol). Toluene (15 mL), water (5 mL), and methanol (5 mL) were added, and the tube was capped with a septum. The mixture was stirred under N_2 for 10 min at 25 ^oC, and then K_3PO_4 (5.8 g, 27 mmol) was added. The septum was replaced with a screw cap, and the mixture was heated at 110 ^oC until 4-bromobenzonitrile was consumed, as judged by thin-layer chromatography. The mixture was cooled to 25 ^oC and extracted with dichloromethane. Solvent was removed from the extracts by evaporation under reduced pressure, and the residue was purified by flash chromatography (silica gel, ethyl acetate/hexane 1:4) to give 3-(4-cyanophenyl)pyridine (0.42 g, 2.3 mmol, 85%) as a colorless solid : mp 96 ^oC; IR (ATR) 3058, 3039, 2224 cm^{-1}; ^1H NMR (400 MHz, $CDCl_3$) δ 8.89 (1H, d, ^4J = 2.1 Hz), 8.70 (1H, dd, ^3J = 4.8 Hz, ^4J = 1.6 Hz), 7.91 (1H, ddd, ^3J = 7.8 Hz, ^4J = 2.1 Hz, ^4J = 1.6 Hz), 7.80 (2H, d, ^3J = 8.6 Hz), 7.72 (2H, d, ^3J = 8.6 Hz), 7.45 (1H, dd, ^3J = 7.8 Hz, ^3J = 4.8 Hz); ^{13}C NMR (100 MHz, $CDCl_3$) δ 150.12, 148.60, 142.69, 135.16, 134.91, 133.27, 128.19, 124.22, 118.96, 112.30; HRMS (ESI) calcd for $C_{12}H_8N_2$ + H *m/e* 181.0760, found 181.0763.

2,4-Diamino-6-[3-(pyridinyl)phenyl]-1,3,5-triazine (2b). A mixture of 3-(4-cyanophenyl)pyridine (0.594 g, 3.30 mmol), dicyandiamide (0.555 g, 6.60 mmol), and KOH (0.203 g, 3.62 mmol) in 2-methoxyethanol (30 mL) was heated at reflux for 12 h. The resulting mixture was cooled to 25 ^oC, the precipitated solid was separated by filtration, and the solid was washed with hot water to give pure 2,4-diamino-6-[3-(pyridinyl)phenyl]-1,3,5-triazine (**2b**; 0.829 g, 3.14 mmol, 95%) as a colorless solid : mp 320 ^oC; IR (ATR) 3472, 3289, 3150, 1671, 1623, 1504, 1446, 1382 cm^{-1}; ^1H NMR (400 MHz, DMSO-d_6) δ 8.97 (1H, dd, ^4J = 2.3 Hz, ^5J = 0.8 Hz), 8.61 (1H, dd, ^3J = 4.7 Hz, ^4J = 1.6 Hz), 8.37 (2H, d, ^3J = 8.5 Hz), 8.15 (1H, ddd, ^3J = 7.9 Hz, ^4J = 2.3 Hz, ^4J = 1.6 Hz), 7.85 (2H, d, ^3J = 8.5 Hz), 7.52 (1H, ddd, ^3J = 7.9 Hz, ^3J = 4.7 Hz, ^5J = 0.8),

6.79 (4H, bs); ^{13}C NMR (100 MHz, DMSO-d_6) δ 170.57, 168.31, 149.75, 148.58, 140.32, 137.70, 135.81, 135.06, 129.29, 127.52, 124.80; HRMS (ESI) calcd for $C_{14}H_{12}N_6$ + H *m/e* 265.1196, found 265.1207. Anal. Calcd for $C_{14}H_{12}N_6$: C, 63.62; H, 4.58; N, 31.80. Found : C, 62.83; H, 4.36; N, 31.20.

Crystallization of Pyridyl-Substituted Diaminotriazines 1a-c and 2a-b. All crystallizations were carried out at 25 ^{o}C. Crystals of compound **1a** were grown by exposing solutions in DMSO (5 mg/mL) to vapors of MeCN or MeOH in closed vessels. Compounds **1b-c**were crystallized by the slow evaporation of solutions in DMSO (5 mg/mL) or in MeCN (saturated). Crystals of compound **2a** were obtained in various forms by exposing solutions in DMSO (5 mg/mL) to vapors of H_2O. Crystals of compound **2b** were grown by exposing solutions in DMSO (5 mg/mL) to vapors of MeCN.

Analysis of the Structures of Pyridyl-Substituted Diaminotriazines 1a-c and 2a-b by X-Ray Crystallography. Crystallographic data were collected at 150 K using a Bruker Microstar diffractometer with Cu Kα radiation. The structures were solved by direct methods using SHELXS-97, and non-hydrogen atoms were refined anisotropically with SHELXL-97.[12] Hydrogen atoms were treated by first locating them from difference Fourier maps, recalculating their positions using standard values for distances and angles, and then refining them as riding atoms. In selected structural studies, calculated powder X-ray diffraction patterns were found to closely match those obtained experimentally by analysis of bulk crystalline samples, thereby establishing that the samples consisted primarily of a single phase.[11]

Acknowledgments

We are grateful to the Natural Sciences and Engineering Research Council of Canada, the Ministère de l'Éducation du Québec, the Canada Foundation for Innovation, the Canada Research Chairs Program, and Université de Montréal for financial support. In addition, we thank Dr. Valérie Métivaud for analyzing bulk crystalline samples by powder X-ray diffraction.

Supporting Information Available. Additional crystallographic details (including thermal atomic displacement ellipsoid plots, powder X-ray diffraction patterns, tables of structural data in CIF format, and supplementary figures). This material is available free of charge via the Internet at http://pubs.acs.org.

Notes and References

1. For recent references, see: Maly, K. E.; Gagnon, E.; Maris, T.; Wuest, J. D. *J. Am. Chem. Soc.* **2007,***129*, 4306-4322.
2. Díaz-Ortiz, Á.; Elguero, J.; Foces-Foces, C.; de la Hoz, A.; Moreno, A.; del Carmen Mateo, M.; Sánchez-Migallón, A.; Valiente, G. *New J. Chem.* **2004**, *28*, 952-958.
3. Ma, D.-L.; Che, C.-M. *Chem. Eur. J.* **2003**, *9*, 6133-6144.
4. Chan, C.-W.; Mingos, D. M. P.; White, A. J. P.; Williams, D. J. *Polyhedron* **1996**, *15*, 1753-1767.
5. Nangia, A.; Desiraju, G. R. *Top. Curr. Chem.* **1998**, *198*, 57-95. Desiraju, G. R. *Angew. Chem., Int. Ed*. **1995**, *34*, 2311-2327.

6. Baibulova, M. S.; Akkulova, Z. G.; Afanas'eva, T. A. *Izv. Akad. Nauk Kazakh. SSR, Ser. Khim.* **1989**, 40-42.
7. Case, F. H.; Koft, E. *J. Am. Chem. Soc.* **1959**, *81*, 905-906.
8. Duong, A.; Dubois, M.-A.; Maris, T.; Métivaud, V.; Yi, J.-H.; Nanci, A.; Rochefort, A.; Wuest, J. D. submitted for publication.
9. Sase, S.; Jaric, M.; Metzger, A.; Malakhov, V.; Knochel, P. *J. Org. Chem.* **2008**, *73*, 7380-7382.
10. Simons, J. K.; Saxton, M. R. *Organic Syntheses*; Wiley : New York, 1963; Collect. Vol. IV, p 78.
11. See the Supporting Information for details.
12. Sheldrick, G. M. *Acta Crystallogr*. **2008**, *A64*, 112-122.

5.4 Conclusions

Nous avons remarqué que les composés réunissant des groupes pyridyle et DAT ont plusieurs caractéristiques communes : 1) Ces composés favorisent une conformation planaire des cycles aromatiques; 2) ils participent aux assemblages par ponts hydrogène avec approximativement une disposition coplanaire de tous les cycles; et 3) les groupes DAT s'associent selon les motifs connus et jouent un rôle clé dans l'organisation moléculaire. Les topologies que nous observons sont similaires dans les différentes structures et favorisent des chaînes, des bandes et des couches. Dans certains cas, on observe une organisation moléculaire presqu'identique, même lorsque la longueur de la molécule ou l'orientation du groupe pyridyle a été modifiée. Ces observations montrent comment des substituants tels que le groupe DAT permettent de contrôler l'association moléculaire en formant de multiples interactions intermoléculaires directionnelles selon des motifs fiables.

Chapitre 6

Synthèses et structures des 2,2'-bipyridines et 1,10-phénantrolines substituées avec des groupements diaminotriazinyles

6.1 Introduction

Nous avons entrepris une étude cristallographique des composés de type pyridyldiaminotriazine pour permettre de mieux comprendre leurs propriétés associatives. Dans cette étude, résumée dans le chapitre 5, nous avons montré que ces composés ont une tendance à adopter des conformations planaires à l'état cristallin et que les groupes DAT participent dans la formation de ponts hydrogène selon des motifs caractéristiques. Ces observations ont démontré que l'association des unités DAT joue un rôle déterminant dans l'organisation moléculaire à l'état solide. Tous les isomères et analogues des pyridyldiaminotriazines que nous avons analysés par diffraction des rayons-X favorisent des structures similaires avec une organisation moléculaire en chaine, en ruban ou en couche. L'étude présentée dans le chapitre 6 s'inspire des résultats du chapitre 5. Intrigués par le comportement des unités DAT, nous voulions les incorporer dans des structures plus complexes afin de voir l'effet sur l'association moléculaire. Deux séries d'isomères de type bipyridinyle et phénantrolinyle substituées avec des unités DAT ont été choisies pour étudier l'organisation moléculaire dirigée par la capacité des groupes DAT à former des ponts hydrogène. Ces composés offrent la possibilité de former des complexes métalliques pouvant s'auto-assembler par ponts hydrogène sous la direction des unités DAT.

6.2 Nos objectifs

Pour concevoir des architectures supramoléculaires utilisant une stratégie qui combine la coordination métallique avec les ponts hydrogène, nous avons pris l'initiative de synthétiser et d'étudier les structures 3D d'une série de ligands bidentate formée à partir d'une bipyridine ou d'une phénantroline substituée à des groupements DAT. Ces ligands ont été élaborés en vue

d'avoir une coordination forte et pour obtenir des complexes de stabilité élevée. La présence des groupements DAT se justifie par les mêmes raisons citées dans les chapitres précédents, notamment la faciliter d'incorporer ces groupements dans des structures complexes et leur participation dans des motifs d'association fiable. Avec l'incorporation de deux groupements DAT sur la bipyridine et la phénantroline, nous avons favorisé la formation des architectures supramoléculaires robustes, retenues par plusieurs ponts hydrogène. Dans le chapitre 6, nous présentons la synthèse de ces ligands ainsi que leurs études cristallographiques par diffraction des rayons-X. Nous montrons qu'il est possible de contrôler la position des groupements DAT par des stratégies de synthèse organique. Nous nous attardons à comprendre l'organisation de ces ligands à l'état cristallin pour son intérêt intrinsèque en chimie supramoléculaire, mais aussi pour collecter les informations nécessaires qui serviront pour mieux comprendre le comportement associatif des complexes métalliques dérivés de ces composés.

6.3 Article 5

Syntheses and Structures of Isomeric Diaminotriazinyl-Substituted 2,2'-Bipyridines and 1,10-Phenanthrolines

Adam Duong, Thierry Maris, Olivier Lebel,[1] and James D. Wuest*

Journal of Organic Chemistry, **2011**, *76(5)*, 1333-1341

Abstract

Isomeric 2,2'-bipyridines **4a**-**6a** and 1,10-phenanthrolines **7a**-**9a** with two diaminotriazinyl (DAT) substituents were synthesized to explore their dual ability to direct association by the chelation of metals and the characteristic hydrogen bonding of DAT groups. Crystals of compounds **4a**-**6a** and **7a**-**9a** were grown under diverse conditions, and their structures were solved by X-ray crystallography. Analysis revealed multiple shared features analogous to those observed in the structures of simpler DAT-substituted pyridines **1**-**3**. For example, the bipyridines and phenanthrolines favor flattened conformations except in the cases of compounds **8a**-**9a**, where the patterns of substitution prevent the DAT groups from lying in the plane of the phenanthroline core. As expected, the DAT groups form approximately coplanar hydrogen bonds according to standard motifs **I**-**III**, which play a key role in directing molecular organization. However, the structures of simple pyridines **1**-**3**, which favor efficiently packed chains and sheets,differ predictably from those of bipyridines **4a**-**6a** and phenanthrolines **7a**-**9a** in two ways : 1) The larger number of DAT groups in compounds **4a**-**9a** typically leads to complex three-dimensional networks held together by a larger number of hydrogen bonds per molecule; and 2) the need to respect multiple directional interactions prevents compounds **4a**-**9a** from forming closely packed structures, and significant quantities of guests are included. Together, these observations confirm the effectiveness of incorporating special groups such as DAT within more complex molecular structures to control association according to reliable patterns. Bipyridines **4a**-**6a** and phenanthrolines **7a**-**9a** promise to be particularly rich sources of new supramolecular chemistry because they have well-defined molecular topologies and a dual ability to direct association by chelating metals and by engaging in multiple hydrogen bonds according to reliable patterns.

Introduction

Isomeric diaminotriazinyl-substituted pyridines **1-3** form a family of compounds with diverse properties of interest. In particular, the dual presence of diaminotriazinyl (DAT) and

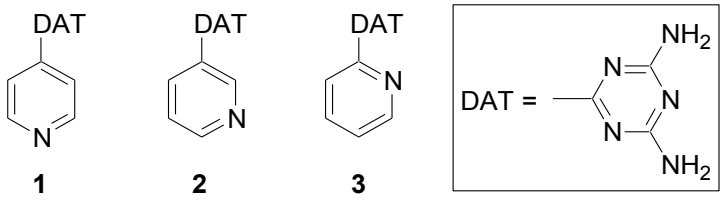

1 **2** **3**

pyridyl groups creates a significant potential for association controlled by hydrogen bonds,[2] aromatic interactions, and coordination to metals.[3-7] As a result, such compounds are well designed to serve as components of ordered molecular structures created by design, such as three-dimensional crystals or two-dimensional networks adsorbed on surfaces. In addition, such compounds and their complexes have potential applications in biological science; for example, they show promise in cancer chemotherapy as cytotoxic DNA-metallointercalators,[4] and they are also effective insect chemosterilants and larvicides.[8]

To provide a deeper understanding of the associative properties of such compounds, we have recently reported the structures of DAT-substituted pyridines **1-3** and various analogs.[9] Comparison of the structures revealed significant underlying similarities. Specifically, the compounds tend to adopt predictably flattened conformations,[2] and they form approximately coplanar hydrogen bonds according to motifs characteristic of DAT groups, as defined by isomeric supramolecular homosynthons **I-III**.[2,10] These interactions play a dominant role in

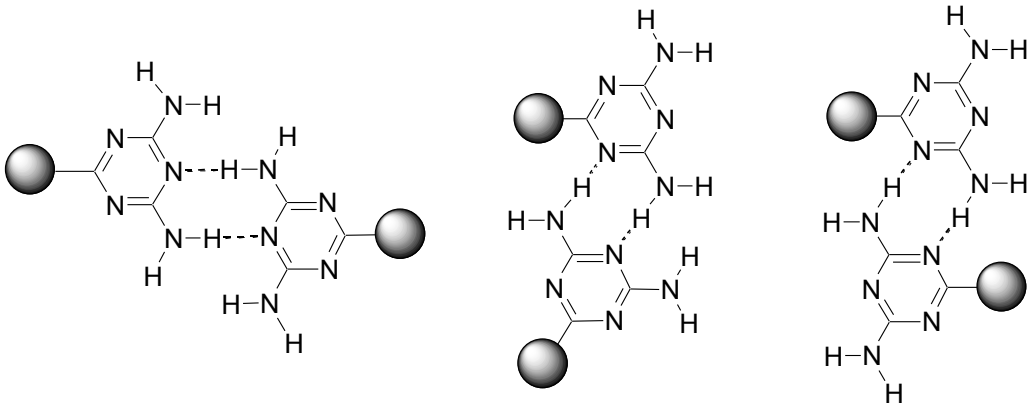

I **II** **III**

directing molecular organization in the crystalline state. Together, the flattened molecular topologies and the shared presence of a dominant site of association ensure that compounds **1**-**3** and simple analogs crystallize in related ways to give structures that feature chains, tapes, and layers. In certain cases, in fact, the molecular organization adopted by different DAT-substituted pyridines was found to be virtually identical, even when the orientation of the pyridyl group was changed. These observations show that the DAT group has a special ability to control aggregation by forming multiple directional intermolecular interactions according to reliable patterns. This suggests that the group can be incorporated within more complex molecular structures to determine how association will occur.

The intriguing behavior of relatively simple DAT-substituted pyridines **1**-**3** encouraged us to study two sets of more complex relatives, isomeric DAT-substituted 2,2'-bipyridines **4a**-**6a** and

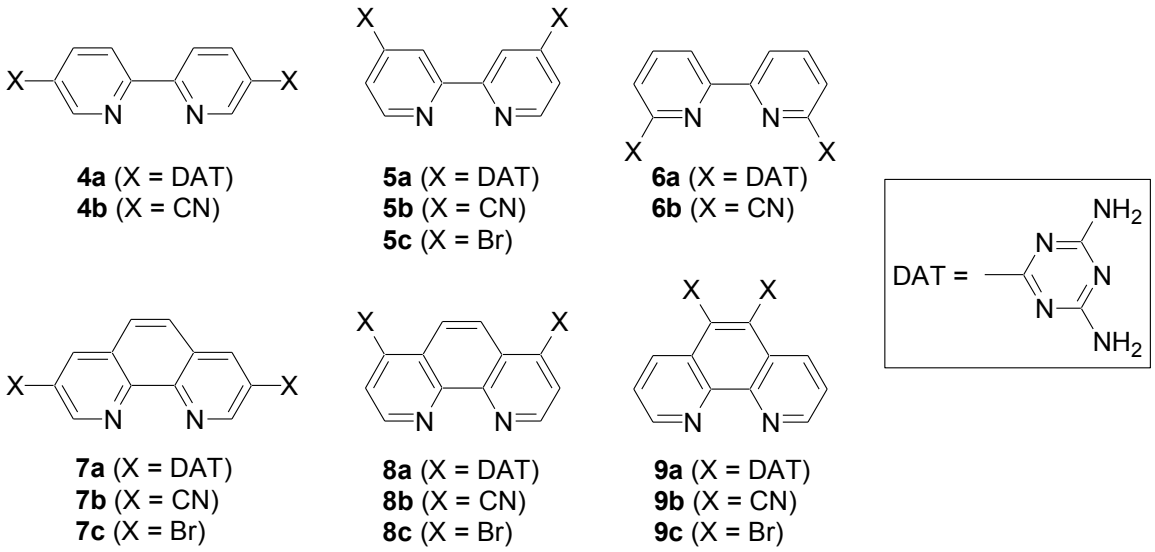

1,10-phenanthrolines **7a-9a**. By offering well-defined molecular structures, combined with the ability of DAT groups to direct association by hydrogen bonding and with the capacity of 2,2'-bipyridines and 1,10-phenanthrolines to chelate metals,[11] compounds **4a-9a** promise to be rich sources of new supramolecular chemistry. Syntheses and structures of these compounds are reported below to provide a foundation for future studies.

Results and Discussion

Syntheses of Isomeric DAT-Substituted 2,2'-Bipyridines 4a-6a and 1,10-Phenanthrolines 7a-9a. Bipyridines **4a**, **5a**, and **6a** were prepared from the corresponding dinitriles **4b**,[12-14] **5b**,[14-16] and **6b**,[16,17] respectively, by heating with dicyandiamide and KOH under standard conditions.[18] Phenanthrolines **7a**, **8a**, and **9a** were synthesized in an analogous way from dinitriles **7b**, **8b**,[19] and **9b**, respectively. Yields of DAT-substituted compounds **4a-8a** were all excellent (85-90%), but *ortho*-disubstituted phenanthroline **9a** was obtained in only 20% yield. Other arenes with adjacent DAT groups have been prepared by the normal method,[20] so we

attribute the poor yield of phenanthroline **9a** to the high degree of substitution of the central ring. Dinitrile precursor **4b** was made from the corresponding dibromide as reported by John et al.,[12] and isomeric dinitrile **6b** was obtained by a modified Reissert-Henze reaction, as described by Stanek et al.[16] Known dinitrile **5b** was prepared by a new route in 63% yield from dibromide **5c**[21] by applying the catalytic methodology of John et al.[12] This procedure was also used to convert 3,8-dibromo-1,10-phenanthroline (**7c**),[22] 4,7-dibromo-1,10-phenanthroline (**8c**),[23] and 5,6-dibromo-1,10-phenanthroline (**9c**)[24] into dinitriles **7b**-**9b**, respectively, in good yields (52-62%).

Structure of Crystals of DAT-Substituted 2,2'-Bipyridine 4a. Compound **4a** proved to have low solubility in most organic solvents, but crystals suitable for X-ray diffraction could be grown from DMSO/MeOH and H_2O/CF_3COOH (TFA). Crystals obtained from DMSO/MeOH were found to belong to the monoclinic space group *P*2/*c* and to have the composition **4a** • 2 MeOH. Views of the structure are provided in Figure 1, and other crystallographic data are presented in Table 1. As expected, the bipyridyl core of compound **4a** adopts an essentially coplanar *anti* conformation (dihedral angle = 0.0°),[25] and the DAT groups lie close to the plane of the core. Molecules associate to form zig-zag chains by hydrogen bonding according to a variant of synthon **I**, with intervening molecules of MeOH (Figure 1a). In the intrachain hydrogen bonds, the O-H···N and N-H···O distances have normal values (2.772 Å and 2.960 Å, respectively). Face-to-face aromatic interactions of the chains direct the formation of layers, which are linked to form the ultimate three-dimensional structure by various interlayer interactions (Figure 1b), including N-H···N(pyridine) hydrogen bonds (2.976 Å) and N-H···O hydrogen bonds (2.960 Å and 2.998 Å).

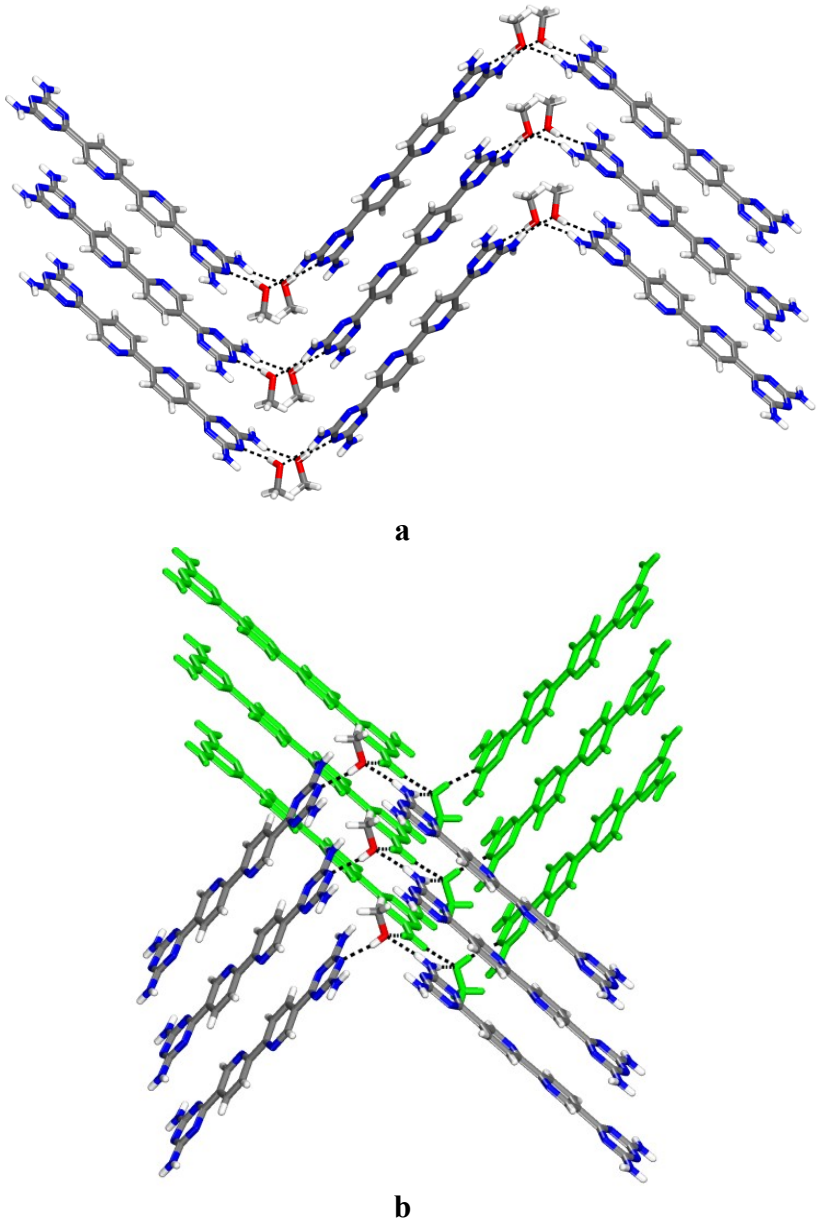

Figure 1. Views of the structure of crystals of the 1:2 solvate of DAT-substituted bipyridine **4a** with MeOH. (a) View showing how hydrogen bonding according to a variant of motif **I** with intervening molecules of MeOH produces chains and how the chains stack to produce layers. Hydrogen bonds are represented by broken lines, and carbon atoms are shown in gray, hydrogen atoms in white, nitrogen atoms in blue, and oxygen atoms in red. (b) View showing hydrogen bonding between two adjacent layers, with one layer highlighted in green.

Table 1. Crystallographic Data for Isomeric DAT-Substituted Bipyridines **4a**-**6a**.

compound	**4a** • 2 MeOH	**4a** • 2 TFA • H_2O	**5a** • 7 TFA	**6a** • 2 DMSO
crystallization medium	DMSO/MeOH	TFA/H_2O	TFA/H_2O	DMSO/CH_2Cl_2
formula	$C_{18}H_{22}N_{12}O_2$	$C_{20}H_{18}F_6N_{12}O_5$	$C_{30}H_{21}F_{21}N_{12}O_{14}$	$C_{20}H_{26}N_{12}O_2S_2$
crystal system	monoclinic	monoclinic	monoclinic	monoclinic
space group	$P2/c$	$P2_1/c$	$P2_1/c$	$P2_1/c$
c (Å)	15.4348(4)	17.4190(17)	18.1219(19)	7.9366(2)
b (Å)	5.1653(2)	7.4383(7)	15.1818(15)	16.990(1)
c (Å)	12.6502(3)	19.102(2)	17.9876(16)	19.563(1)
α (°)	90	90	90	90
β (°)	95.858(1)	107.558(5)	119.092(4)	113.204(9)
γ(°)	90	90	90	90
V (Å^3)	1003.3(1)	2359.7(4)	4325.7(7)	2424.5(5)
Z	2	4	4	4
ρ_{calc} (g cm^{-3})	1.451	1.746	1.801	1.454
T (K)	100	150	100	100
μ (mm^{-1})	0.861	1.423	1.803	2.382
R_1, $I>2\sigma(I)$	0.0446	0.0616	0.0689	0.0541
R_1, all data	0.0456	0.0739	0.0779	0.0544
wR_2, $I>2\sigma(I)$	0.1381	0.1406	0.1633	0.1278
wR_2, all data	0.1396	0.1425	0.1784	0.1279
independent reflections	1791	3061	7988	4402
observed reflections [$I>2\ \sigma(I)$]	1681	1601	5352	4356

Crystals of DAT-substituted bipyridine **4a** grown from TFA/H_2O proved to belong to the monoclinic space group $P2_1/c$ and to have the composition **4a** • 2 TFA • H_2O. Figure 2 provides a view of the proposed structure, and Table 1 presents other crystallographic data. The bipyridyl core adopts a twisted *anti* conformation (dihedral angle = 32.1°), but each pyridyl ring and its DAT substituent are nearly coplanar. The proposed structure (Figure 2) shows that both DAT groups are engaged in hydrogen bonding with TFA according to a variant of standard heterosynthon **IV**, with full proton transfer (**IV'**).[26-29] Each molecule of doubly protonated

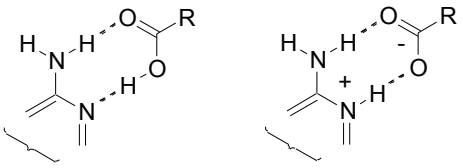

IV **IV'**

compound **4a** is joined to two neighbors to form tapes by a total of four N-H···N(pyridine) hydrogen bonds (average distance = 2.972 Å), reinforced by various C-H···N and C-H···O interactions (Figure 2).[30,31] Additional hydrogen bonds involving H_2O link the tapes to form corrugated sheets (Figure 2), which stack to generate the full three-dimensional structure.[32] Surprisingly, the pyridyl nitrogen atoms of compound **4a** are not protonated by TFA to give a salt, despite the potential exothermicity of this process.[27-29] It is possible that the N-H···N(pyridine) hydrogen-bonding motif of neighboring molecules (Figure 2) is favorable enough to engage the pyridyl nitrogen atoms and prevent their protonation by TFA.

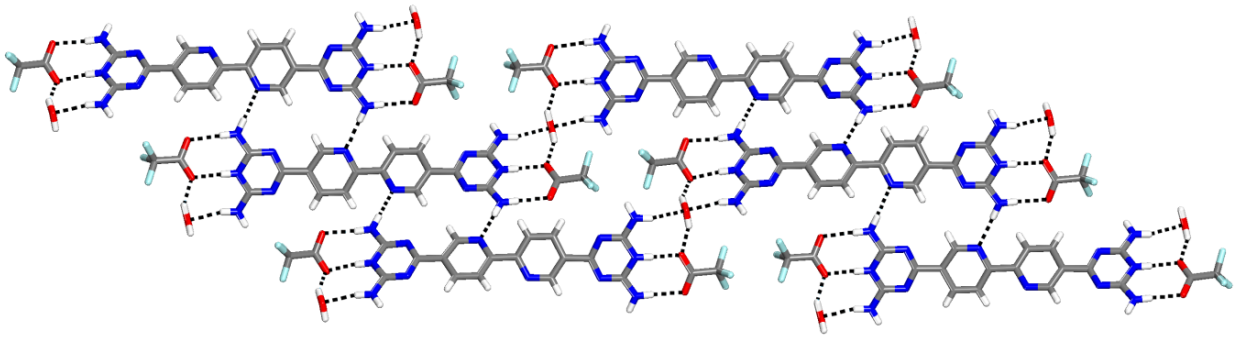

Figure 2. View of the structure of crystals of the 1:2:1 solvate of DAT-substituted bipyridine **4a** with TFA and H_2O. The view shows how doubly protonated compound **4a** forms hydrogen bonds according to standard motif **IV'**, how tapes are produced by additional N-H···N(pyridine) hydrogen bonds, and how the tapes are further linked by molecules of H_2O to give sheets. Hydrogen bonds are represented by broken lines, and carbon atoms are shown in gray, hydrogen atoms in white, fluorine atoms in light blue, nitrogen atoms in dark blue, and oxygen atoms in red.

Structure of Crystals of Isomeric DAT-Substituted 2,2'-Bipyridine 5a. Crystals of isomeric DAT-substituted bipyridine **5a** grown from TFA/H_2O were found to belong to the monoclinic space group $P2_1/c$ and to have the composition **5a** • 7 TFA. A view of the proposed structure appears in Figure 3, and other crystallographic data are provided in Table 1. The bipyridyl core of compound **5a** unexpectedly adopts a nearly coplanar *syn* conformation (dihedral angle = 2.2°), and each DAT substituent lies essentially in the plane of the core (Figure 3). In the structure shown in Figure 3, a DAT group is protonated by TFA according to motif **IV'**, and the preference for a *syn* conformation is rationalized by proposing that a pyridyl nitrogen atom is also protonated by TFA.[27-29] Molecules of the doubly protonated form of compound **5a** are not in direct contact but are instead virtually surrounded by hydrogen-bonded TFA (Figure 3).

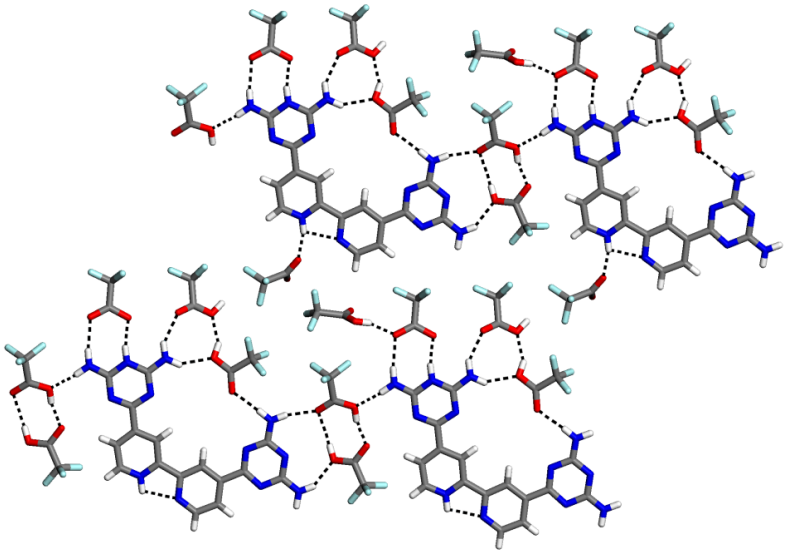

Figure 3. View of the structure of crystals of the 1:7 solvate of DAT-substituted bipyridine **5a** with TFA. The view shows that molecules of the doubly protonated form of compound **5a** are prevented from entering into direct contact by surrounding hydrogen-bonded TFA. Hydrogen bonds are represented by broken lines, and carbon atoms are shown in gray, hydrogen atoms in white, fluorine atoms in light blue, nitrogen atoms in dark blue, and oxygen atoms in red.

Structure of Crystals of Isomeric DAT-Substituted 2,2'-Bipyridine 6a. Crystals of DAT-substituted bipyridine **6a** grown from DMSO/CH_2Cl_2 proved to belong to the monoclinic space group $P2_1/c$ and to have the composition **6a** • 2 DMSO. Figure 4 provides a view of the structure, and Table 1 summarizes other crystallographic data. As usual, the bipyridyl core of compound **6a** favors a nearly coplanar *anti* conformation (dihedral angle = 0.0°), and the DAT substituents lie close to the same plane (Figure 4). Each DAT group participates in four N-H···N(triazine) hydrogen bonds of type **II** (average distance = 3.162 Å), leading to the construction of robust layers in which each molecule of compound **6a** is linked to four neighbors by a total of eight hydrogen bonds (Figure 4). Molecular organization in the resulting layers is closely analogous to that observed in certain structures of simpler analogs **1-3** and their relatives.[9] Adjacent layers are separated by included molecules of DMSO,[32] which form N-H···O hydrogen bonds (average distance = 3.037 Å) with nearby DAT groups.

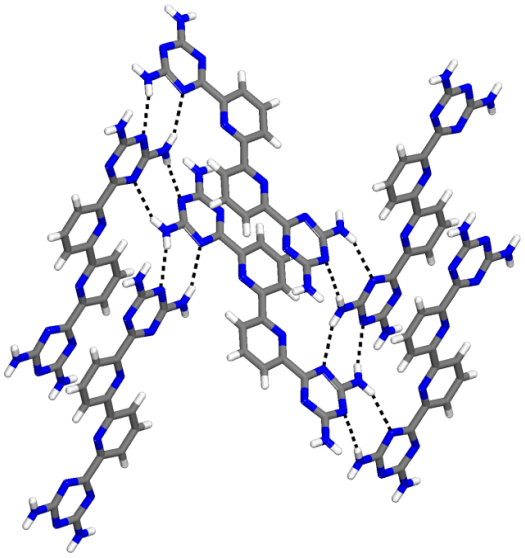

Figure 4. View of robust hydrogen-bonded layer in the structure of crystals of the 1:2 solvate of DAT-substituted bipyridine **6a** with DMSO. Hydrogen bonds are represented by broken lines, and carbon atoms are shown in gray, hydrogen atoms in white, and nitrogen atoms in blue. Molecules of DMSO are omitted for clarity.

Crystallization of simple DAT-substituted pyridines **1-3** and their relatives has been shown to be controlled primarily by their flattened molecular topologies and by the ability of DAT groups to direct the formation of coplanar hydrogen bonds of type **I-III**.[9] As a result, these compounds typically crystallize in similar ways to give structures that incorporate chains, tapes, and layers. More complex DAT-substituted bipyridines **4a**-**6a** have the same key features, including a preference for flattened conformations and multiple DAT groups, so their behavior should be analogous. Indeed, both compounds **4a** and **6a** crystallize under selected conditions to give layered structures built from nearly planar conformers that engage in hydrogen bonding according to motifs **I-III** or similar patterns. In contrast, crystals of compounds **4a** and **5a** grown from TFA/H_2O have largely unrelated structures. This inconsistency can be attributed to the ability of TFA to protonate DAT groups and thereby disrupt their standard patterns of self-association. For this reason, we avoided using TFA in subsequent efforts to crystallize analogous DAT-substituted phenanthrolines **7a**-**9a**.

Structure of Crystals of DAT-Substituted 1,10-Phenanthroline 7a. Crystals of DAT-substituted phenanthroline **7a** grown from DMSO/$CHCl_3$ were found to belong to the triclinic space group *P*-1 and to have the composition **7a** • 2 DMSO • $CHCl_3$. Views of the structure are presented in Figure 5, and other crystallographic data are summarized in Table 2. As expected, molecules of compound **7a** adopt a flattened conformation, with the DAT substituents lying close to the plane of the phenanthroline core (dihedral angles of 5.7° and 32.4°). As illustrated in Figure 5a, molecules of compound **7a** are connected by N-H···N(triazine) hydrogen bonds of type **I** (average distance = 2.970 Å) to form chains, which are then joined to adjacent chains by N-H···N(triazine) hydrogen bonds of type **III** (3.012 Å), as well as by additional N-H···N(pyridine) hydrogen bonds (3.010 Å) and C-H···N(pyridine) interactions involving $CHCl_3$ (C···N distance =

3.109 Å). The result is a robust corrugated layer in which each molecule is linked to four neighbors by a total of eight hydrogen bonds (Figure 5b). Adjacent layers are separated by included molecules of DMSO and $CHCl_3$.[32]

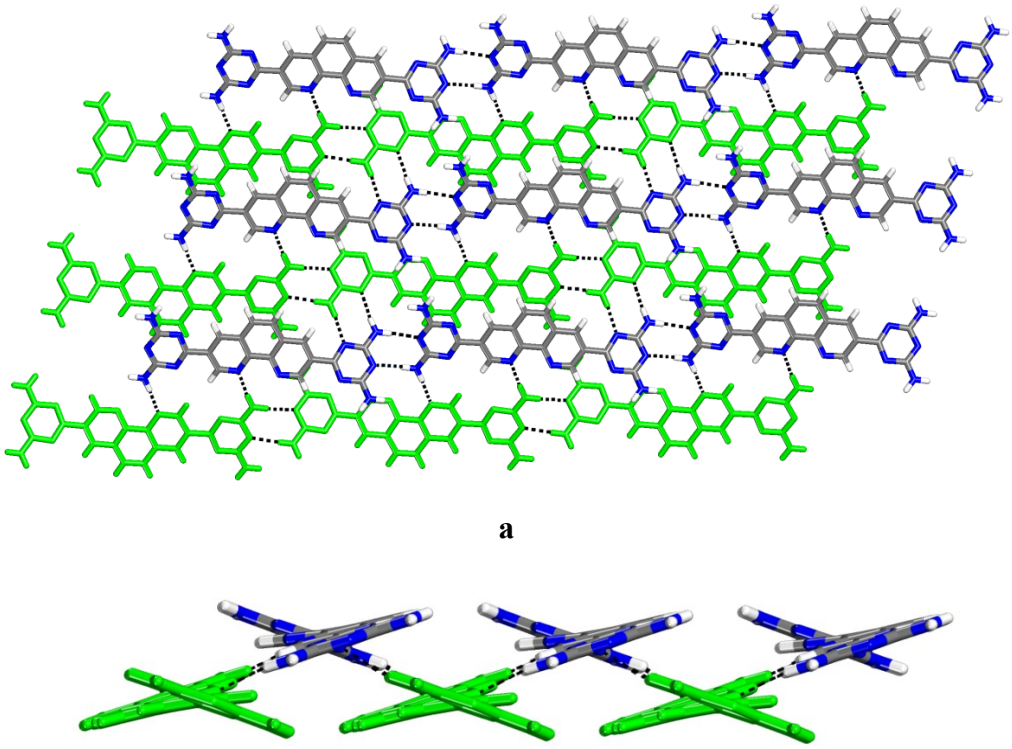

a

b

Figure 5. Views of the structure of crystals of the 1:2:1 solvate of DAT-substituted phenanthroline **7a** with DMSO and $CHCl_3$. Hydrogen bonds are represented by broken lines, and carbon atoms are shown in gray, hydrogen atoms in white, and nitrogen atoms in blue, except when selected molecules are highlighted in green. Molecules of DMSO and $CHCl_3$ are omitted for clarity. (a) View showing how hydrogen bonding of molecules of compound **7a** according to motif **I** generates chains and how the chains are connected to produce layers by hydrogen bonds of type **III** and additional interactions. Chains in the upper level are shown in normal colors and chains in the lower level are highlighted in green. (b) View along the chains showing the relationship between the upper and lower chains in a single layer.

Table 2. Crystallographic Data for Isomeric DAT-Substituted Phenanthrolines **7a**-**9a**.

compound	**7a** • 2 DMSO • $CHCl_3$	3 **8a** • 2 DMSO • CH_2Cl_2	**9a** • 2 DMSO
crystallization medium	DMSO/$CHCl_3$	DMSO/CH_2Cl_2	DMSO/CH_2Cl_2
formula	$C_{23}H_{27}Cl_3N_{12}O_2S_2$	$C_{59}H_{56}Cl_2N_{36}O_2S_2$	$C_{22}H_{26}N_{12}O_2S_2$
crystal system	triclinic	triclinic	triclinic
space group	*P*-1	*P*-1	*P*-1
c (Å)	9.4341(4)	14.5409(13)	11.0524(2)
b (Å)	9.6042(5)	14.7369(12)	11.1745(2)
c (Å)	16.7333(13)	21.9376(17)	11.6989(3)
α (°)	95.152(5)	84.221(4)	88.330(1)
β (°)	98.059(4)	82.535(4)	67.213(1)
γ(°)	111.604(3)	69.260(4)	76.467(1)
V (Å^3)	1379.16(14)	4351.5(6)	1292.10(5)
Z	2	2	2
ρ_{calc} (g cm^{-3})	1.623	1.096[a]	1.426
T (K)	150	150	150
μ (mm^{-1})	4.848	1.590	2.263
R_1, $I>2\sigma(I)$	0.0892	0.0646	0.0537
R_1, all data	0.1994	0.0707	0.0570
wR_2, $I>2\sigma(I)$	0.1831	0.1544	0.1280
wR_2, all data	0.2195	0.1553	0.1288
independent reflections	5004	13545	4559
observed reflections [$I>2\sigma(I)$]	3511	7919	3089

[a]The value of ρ_{calc} does not take into account all molecules of guests included in the structure, but only those that occupy well-located positions.

Structure of Crystals of Isomeric DAT-Substituted 1,10-Phenanthroline 8a. Crystals of isomeric DAT-substituted phenanthroline **8a** grown from DMSO/CH_2Cl_2 were found to belong to the triclinic space group *P*-1 and to have the approximate composition 3 **8a** • 2 DMSO • CH_2Cl_2. Views of the structure are shown in Figure 6, and other crystallographic data are presented in Table 2. The structure is composed of three crystallographically independent molecules **A**, **B**, and **C**, which interact to form a complex three-dimensional hydrogen-bonded network. As expected, the 4,7-pattern of disubstitution prevents the DAT groups from lying in the plane of the phenanthroline core, and the dihedral angles lie in the range 23.9°- 69.3°. The

structure can be considered to be built from a fundamental pair of molecules **A** and **B**, which are joined by a total of four N-H···N(triazine) hydrogen bonds of type **III** with an average distance of 3.068 Å (Figure 6a). The **AB** pairs are linked into columns along the *b* axis by intervening molecules **C**, each of which engages in a total of five intracolumn hydrogen bonds, including four of type **II** with an average distance of 3.011 Å (Figure 6b). Adjacent columns are further connected by the formation of various intercolumn hydrogen bonds of types **II** and **III** involving pairs $\mathbf{A_2}$ and $\mathbf{B_2}$.

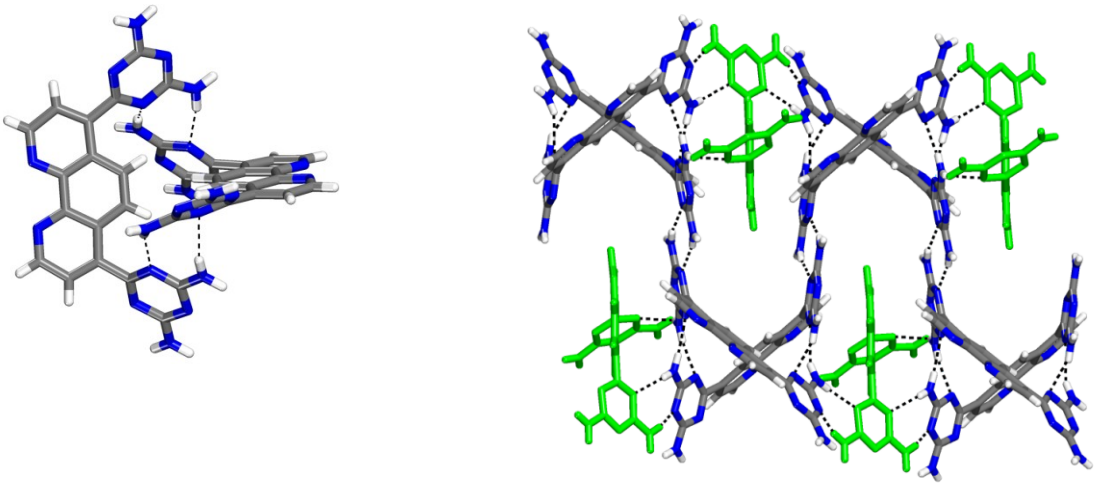

a **b**

Figure 6. Views of the structure of crystals of the 3:2:1 solvate of DAT-substituted phenanthroline **8a** with DMSO and CH_2Cl_2. Hydrogen bonds are represented by broken lines, and carbon atoms are shown in gray, hydrogen atoms in white, and nitrogen atoms in blue. Molecules of DMSO and CH_2Cl_2 are omitted for clarity. (a) View showing how hydrogen bonding of molecules **A** and **B** according to motif **III** generates pairs. (b) View showing how the **AB** pairs are further connected to form columns by hydrogen bonding to molecules **C**, which are shown in green.

Structure of Crystals of Isomeric DAT-Substituted 1,10-Phenanthroline 9a. Crystals of isomeric DAT-substituted phenanthroline **9a** grown from DMSO/CH_2Cl_2 were found to belong to the triclinic space group *P*-1 and to have the composition **9a** • 2 DMSO. Figure 7 provides a view of the structure, and Table 2 summarizes other crystallographic data. In the structure, molecules of compound **9a** interact to generate a complex three-dimensional hydrogen-bonded network. As anticipated, the 5,6-pattern of disubstitution forces the DAT groups to twist significantly out the plane of the phenanthroline core, and the dihedral angles are 54° and 74°. As shown in Figure 7, molecules of compound **9a** are linked into chains aligned with the *c* axis by N-H···N(triazine) hydrogen bonds of type **III** (average distance = 2.956 Å), augmented by single N-H···N(pyridine) hydrogen bonds (3.013 Å). Adjacent chains are further connected by N-H···N(triazine) hydrogen bonds of type **I** (3.039 Å) to form a three-dimensional network. Each molecule of compound **9a** thereby participates in a total of seven N-H···N hydrogen bonds involving four neighbors.

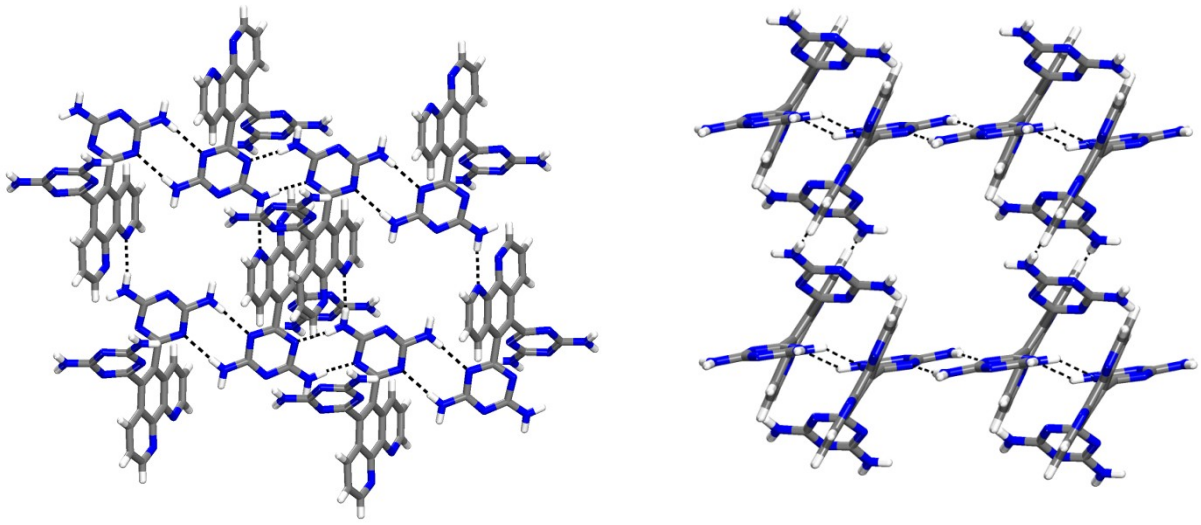

a **b**

Figure 7. View of the structure of crystals of the 1:2 solvate of DAT-substituted phenanthroline **9a** with DMSO. Hydrogen bonds are represented by broken lines, and carbon atoms are shown in gray, hydrogen atoms in white, and nitrogen atoms in blue. Molecules of DMSO are omitted for clarity. The view shows how chains are formed by N-H···N(triazine) hydrogen bonds of type **III**, reinforced by single N-H···N(pyridine) hydrogen bonds. Adjacent chains are further connected by N-H···N(triazine) hydrogen bonds of type **I** to form a three-dimensional network.

Conclusions

Previous work has established that isomeric DAT-substituted pyridines **1-3** and simple relatives tend to crystallize in foreseeable ways.[9] In particular, they prefer to adopt flattened conformations and to engage in approximately coplanar intermolecular hydrogen bonds of types **I-III**, which are characteristic of DAT groups.[2] Together, these properties ensure that molecular association is dominated by the presence of the DAT groups and favors the formation of networks that incorporate linear or planar elements such as chains, tapes, or layers.

Our present results confirm that the crystallization of more complex analogs such as DAT-substituted bipyridines **4a**-**6a** and phenanthrolines **7a**-**9a** normally follows similar patterns, as expected. Again, flattened conformations are adopted in all cases except those of compounds **8a** and **9a**, which have patterns of substitution that prevent the DAT groups from lying in the plane of the phenanthroline core. Nevertheless, DAT groups in all compounds **4a**-**9a** continue to play a dominant role in directing molecular association according to standard motifs **I**-**III** or related patterns. Notable exceptions to this generalization arise when crystallization is carried out in media with components such as TFA, which can protonate the DAT groups and thereby prevent them from engaging in normal self-association.

Detailed comparison of the hydrogen-bonded networks generated by simple DAT-substituted pyridines **1**-**3** with those of more complex analogs **4a**-**9a** reveals a series of predictable differences in connectivity and architecture. In particular, compounds **1**-**3** contain a single DAT group per molecule, whereas analogs **4a**-**9a** incorporate two DAT groups per molecule and can thereby form structures in which each molecule is connected to more neighbors by a larger number of hydrogen bonds. As a result, compounds **4a**-**9a** are able in many cases to generate potentially robust architectures maintained by three-dimensional networks of hydrogen bonds, whereas simpler analogs **1**-**3** are typically limited to connectivity in one or two dimensions.[9]

In addition, the structures of simple compounds **1**-**3** differ predictably from those of more complex analogs **4a**-**9a** in the efficiency of molecular packing. Compounds with multiple substituents that engage in strong directional intermolecular interactions cannot normally form periodic structures in which the interactions and packing are optimized simultaneously.[2] As a result, such compounds tend to form open networks with significant volumes occupied by

molecules of solvent or other guests. This pattern of behavior is nicely illustrated by the structures of compounds **1-3**, **4a-6a**, and **7a-9a**. Simple compounds **1-3**, in which directional interactions are derived primarily from a single DAT group, can crystallize without excessive constraints, and they form compact, guest-free structures in four out of six cases studied, with no structure showing a molar guest : host ratio larger than 1. In contrast, more complex analogs **4a-9a**, in which directional interactions are approximately doubled, fail to generate guest-free structures in any of the seven cases examined, and the molar guest : host ratios range up to 7.

Our work identifies DAT-substituted bipyridines **4a-6a** and phenanthrolines **7a-9a** as potentially rich sources of new supramolecular chemistry and describes how they can be made. The compounds feature well-defined molecular topologies and an ability to engage extensively in strong intermolecular interactions, directed both by hydrogen bonding and chelation of metals. Our initial structural studies have confirmed that the DAT groups of compounds **4a-9a** can play a dominant role in directing crystallization by self-associating according to standard hydrogen-bonding motifs **I-III**. This observation suggests that the sites of hydrogen bonding and chelation in compounds **4a-9a** can accomplish their tasks independently and can thereby control association without mutual interference. Future studies will examine how metal complexes of compounds **4a-9a** can be formed and used to construct complex three-dimensional hydrogen-bonded networks. As a result, the present work is a promising starting point for a wide range of projects in organic and inorganic chemistry that target the design and synthesis of related ligands for the self-assembly of metal-organic materials with predetermined structures.

Experimental Section

General Notes. 2,2'-Bipyridine-5,5'-dicarbonitrile (**4b**),[12] 4,4'-dibromo-2,2'-bipyridine (**5c**),[21] 2,2'-bipyridine-6,6'-dicarbonitrile (**6b**),[16] 3,8-dibromo-1,10-phenanthroline (**7c**),[22] 4,7-dibromo-1,10-phenanthroline (**8c**),[23] and 5,6-dibromo-1,10-phenanthroline (**9c**)[24] were prepared by methods reported previously. The syntheses of dinitriles **5b** and **7b-9b** are described below, followed by the preparation of DAT-substituted derivatives **4a-9a**. Other chemicals were purchased from commercial sources and used without further purification.

Syntheses of Dinitriles 5b and 7b-9b

2,2'-Bipyridine-4,4'-dicarbonitrile (5b).[14-16] A stirred mixture of 4,4'-dibromo-2,2'-bipyridine (**5c**; 0.873 g, 2.78 mmol),[21] NaCN (0.274 g, 5.59 mmol), $Pd(OAc)_2$ (0.031 g, 0.14 mmol), 1,5-bis(diphenylphosphino)pentane (0.247 g, 0.561 mmol), TMEDA (0.488 g, 4.20 mmol), and mesitylene (15 mL) was sparged with N_2 for 10 min and then was heated at reflux under N_2 for 12 h. The mixture was allowed to cool, degassed water was added, and the resulting slurry was stirred for 10 min. The slurry was filtered, and the solid was rinsed with pentane and then purified by flash chromatography (silica gel, hexane/ethyl acetate 7/3) to give 2,2'-bipyridine-4,4'-dicarbonitrile (**5b**; 0.363 g, 1.76 mmol, 63%) as a colorless solid : mp 220 ^{o}C; IR (ATR) 2238 cm^{-1}; ^{1}H NMR (400 MHz, $CDCl_3$) δ 8.90 (dd, 2H, ^{5}J = 0.87 Hz, ^{3}J = 4.9 Hz), 8.74 (dd, 2H, ^{4}J = 1.5 Hz, ^{5}J = 0.93 Hz), 7.62 (dd, 2H, ^{3}J = 4.9 Hz, ^{4}J = 1.5 Hz); ^{13}C NMR (100 MHz, $CDCl_3$) δ 155.9, 150.7, 126.3, 123.5, 122.2, 116.8; HRMS (ESI) calcd for $C_{12}H_6N_4$ + H *m/e* 207.06652, found 207.06687.

1,10-Phenanthroline-3,8-dicarbonitrile (7b). A stirred mixture of 3,8-dibromo-1,10-phenanthroline (**7c**; 1.10 g, 3.25 mmol),[22] NaCN (0.322 g, 6.57 mmol), $Pd(OAc)_2$ (0.036 g, 0.16 mmol), 1,5-bis(diphenylphosphino)pentane (0.291 g, 0.661 mmol), TMEDA (0.572 g, 4.92 mmol), and mesitylene (15 mL) was sparged with N_2 for 10 min and then was heated at reflux under N_2 for 12 h. The mixture was allowed to cool, degassed water was added, and the resulting slurry was stirred for 10 min. The slurry was filtered, and the solid was rinsed with pentane and then purified by flash chromatography (silica gel, hexane/ethyl acetate 1/1) to give 1,10-phenanthroline-3,8-dicarbonitrile (**7b**; 0.460 g, 2.00 mmol, 62%) as a yellow-orange solid : mp > 250 ^oC (dec); IR (ATR) 2230 cm^{-1}; ^1H NMR (400 MHz, $CDCl_3$) δ 9.44 (d, 2H, ^4J = 2.0 Hz), 8.71 (d, 2H, ^4J = 2.0 Hz), 8.03 (s, 2H); ^{13}C NMR (100 MHz, $CDCl_3$) δ 151.3, 146.6, 140.9, 128.5, 127.9, 116.3, 110.1; HRMS (ESI) calcd for $C_{14}H_6N_4$ + H *m/e* 231.0665, found 231.0662.

1,10-Phenanthroline-4,7-dicarbonitrile (8b).[19] Compound **8b** was prepared in 60% yield by the method described above for making isomer **7b**. Crystallization from $CHCl_3$/MeCN provided yellow blocks : mp > 250 ^oC (dec); IR (ATR) 2105 cm^{-1}; ^1H NMR (400 MHz, $CDCl_3$) δ 9.43 (d, 2H, ^3J = 4.4 Hz), 8.46 (s, 2H), 8.08 (d, 2H, ^3J = 4.4 Hz); ^{13}C NMR (100 MHz, $CDCl_3$) δ 151.2, 146.4, 127.8, 127.4, 126.3, 119.8, 115.4; HRMS (ESI) calcd for $C_{14}H_6N_4$ + H *m/e* 231.0665, found 231.0677.

1,10-Phenanthroline-5,6-dicarbonitrile (9b). Compound **9b** was prepared in 52% yield by the method described above for making isomer **7b**.Crystallization from CH_2Cl_2/MeCN provided red blocks : mp > 250 ^oC (dec); IR (ATR) 2231 cm^{-1}; ^1H NMR (400 MHz, $CDCl_3$) δ 9.46 (dd, 2H, ^3J = 4.3 Hz, ^4J = 1.7 Hz), 8.77 (dd, 2H, ^3J = 8.3 Hz, ^4J = 1.7 Hz), 7.97 (dd, 2H, ^3J =

8.3 Hz, ^{3}J = 4.3 Hz); ^{13}C NMR (100 MHz, $CDCl_3$) δ 154.8, 147.0, 135.3, 126.0, 125.7, 117.1, 114.0; HRMS (ESI) calcd for $C_{14}H_6N_4$ + H *m/e* 231.0665, found 231.0658.

Syntheses of DAT-Substituted Bipyridines 4a-6a and Phenanthrolines 7a-9a

6,6'-(2,2'-Bipyridine-5,5'-diyl)bis(1,3,5-triazine-2,4-diamine) (4a). A mixture of 2,2'-bipyridine-4,4'-dicarbonitrile (**4b**; 0.673 g, 3.26 mmol),[12] dicyandiamide (0.688 g, 8.18 mmol), and KOH (0.202 g, 3.60 mmol) in 2-methoxyethanol (25 mL) was heated at reflux for 12 h. The mixture was allowed to cool, and precipitated solids were then separated by filtration, washed with hot water, rinsed with MeOH, and dried under vacuum to provide DAT-substituted bipyridine **4a** (1.10 g, 2.94 mmol, 90%) as a nearly colorless solid : mp > 350 ^{o}C; IR (ATR) 3459, 3327, 3153, 1662, 1633, 1525, 1442, 1394, 1359, 857 cm^{-1}; ^{1}H NMR (400 MHz, DMSO-d_6) δ 9.47 (d, 2H, ^{4}J = 2.0 Hz), 8.69 (dd, 2H, ^{3}J = 8.3 Hz, ^{4}J = 2.0 Hz), 8.58 (d, 2H, ^{3}J = 8.3 Hz), 6.929 (br s, 8H); ^{13}C NMR (100 MHz, DMSO-d_6) δ 169.4, 168.2, 157.4, 149.8, 137.2, 133.8, 121.5; HRMS (ESI) calcd for $C_{16}H_{14}N_{12}$ + H *m/e* 375.1537, found 375.1547.

6,6'-(2,2'-Bipyridine-4,4'-diyl)bis(1,3,5-triazine-2,4-diamine) (5a). Compound **5a** was prepared from 2,2'-bipyridine-4,4'-dicarbonitrile (**5b**) in 85% yield by the method described above for making analog **4a** : mp > 350 ^{o}C; IR (ATR) 3463, 3317, 3119, 1643, 1531, 1396, 809 cm^{-1}; ^{1}H NMR (400 MHz, DMSO-d_6) δ 9.27 (s, 2H), 8.86 (d, 2H, ^{3}J = 4.9 Hz), 8.17 (dd, 2H, ^{3}J = 4.9 Hz), 7.02 (br d, 8H); ^{13}C NMR (100 MHz, DMSO-d_6) δ 169.5, 168.4, 156.6, 150.8, 146.7, 122.9, 119.5; HRMS (ESI) calcd for $C_{16}H_{14}N_{12}$ + H *m/e* 375.1537, found 375.1538.

6,6'-(2,2'-Bipyridine-6,6'-diyl)bis(1,3,5-triazine-2,4-diamine) (6a). Compound **6a** was prepared from 2,2'-bipyridine-6,6'-dicarbonitrile (**6b**)[16] in 90% yield by the method described above for making analog **4a** : mp > 350°C; IR (ATR) 3479, 3357, 3146, 1617, 1538, 1403, 805 cm^{-1}; ^{1}H NMR (400 MHz, DMSO-d_6) δ 8.55 (d, 2H, ^{3}J = 7.8 Hz), 8.23 (d, 2H, ^{3}J = 7.6 Hz), 8.11 (t, 2H, ^{3}J = 7.8 Hz), 6.92 (br d, 8H). ^{13}C NMR (100 MHz, DMSO-d_6) δ 171.3, 168.5, 155.8, 155.7, 138.6, 124.6, 123.1; HRMS (ESI) calcd for $C_{16}H_{14}N_{12}$ + H *m/e* 375.1537, found 375.1537.

6,6'-(1,10-Phenanthroline-3,8-diyl)bis(1,3,5-triazine-2,4-diamine) (7a). Compound **7a** was prepared from 1,10-phenanthroline-3,8-dicarbonitrile (**7b**) in 89% yield by the method described above for making analog **4a** : mp > 350 °C; IR (ATR) 3325, 3165, 1634, 1531, 1391 cm^{-1}; ^{1}H NMR (400 MHz, DMSO-d_6) δ 9.88 (s, 2H), 9.20 (s, 2H), 8.18 (s, 2H), 7.01 (br s, 8H); ^{13}C NMR (100 MHz, DMSO-d_6) δ 169.1, 167.8, 149.7, 147.0, 135.9, 132.3, 128.9, 128.2; HRMS (ESI) calcd for $C_{18}H_{14}N_{12}$ + H *m/e* 399.1537, found 399.1537.

6,6'-(1,10-Phenanthroline-4,7-diyl)bis(1,3,5-triazine-2,4-diamine) (8a). Compound **8a** was prepared from 1,10-phenanthroline-4,7-dicarbonitrile (**8b**) in 85% yield by the method described above for making analog **4a** : mp > 350 °C; IR (ATR) 3330, 3150, 1532 cm^{-1}; ^{1}H NMR (400 MHz, DMSO-d_6) δ 9.20 (d, 2H, ^{3}J = 4.4 Hz), 8.66 (s, 2H), 8.03 (d, 2H, ^{3}J = 4.4 Hz), 7.03 (br s, 8H); ^{13}C NMR (400 MHz, DMSO-d_6) δ 172.4, 167.9, 150.4, 147.0, 144.3, 126.0, 125.5, 123.8; HRMS (ESI) calcd for $C_{18}H_{14}N_{12}$ + H *m/e* 399.1537, found 399.1543.

6,6'-(1,10-Phenanthroline-5,6-diyl)bis(1,3,5-triazine-2,4-diamine) (9a). Compound **9a** was prepared from 1,10-phenanthroline-5,6-dicarbonitrile (**9b**) in 20% yield by the method described above for making analog **4a** : mp > 350 °C; IR (ATR) 3120, 1629, 1540 cm^{-1}; ^{1}H NMR

(400 MHz, DMSO-d_6) δ 9.12 (d, 2H, ^3J = 3.0 Hz), 8.36 (d, 2H, ^3J = 8.3 Hz), 7.75 (dd, 2H, ^3J = 3.0 Hz, ^3J = 8.0 Hz), 6.66 (br s, 8H); ^{13}C NMR (100 MHz, DMSO-d_6) δ 172.7, 167.5, 150.9, 146.0, 136.0, 134.0, 127.1, 124.1; HRMS (ESI) calcd for $C_{18}H_{14}N_{12}$ + H *m/e* 399.1537, found 399.1535.

Crystallization of DAT-Substituted Bipyridines 4a-6a and Phenanthrolines 7a-9a. Crystals used for structural studies by X-ray diffraction were grown at 25 ^oC in the following ways. DAT-substituted bipyridine **4a** was crystallized by allowing vapors of MeOH to diffuse into a saturated solution in DMSO. In addition, crystal**s** of compound **4a** and isomer **5a** were obtained by allowing vapors of water to diffuse into solutions in TFA (~5 mg/mL). Crystals of DAT-substituted bipyridine **6a** were grown by allowing vapors of CH_2Cl_2 to diffuse into a saturated solution in DMSO. Similarly, DAT-substituted phenanthrolines **7a**, **8a**, and **9a** were crystallized by allowing vapors of $CHCl_3$ (compound **7a**) or CH_2Cl_2 (compounds **8a** and **9a**) to diffuse into saturated solutions in DMSO.

Analysis of the Structures of DAT-Substituted Bipyridines 4a-6a and Phenanthrolines 7a-9a by X-Ray Crystallography. Crystallographic data were collected using a Bruker Microstar diffractometer with Cu Kα radiation. The structures were solved by direct methods using SHELXS-97, and non-hydrogen atoms were refined anisotropically with SHELXL-97.[33] Hydrogen atoms were first located from difference Fourier maps, and then their positions were recalculated, using standard values of distances and angles, before refining them as riding atoms. In the structures of compounds **4a** and **6a** crystallized from TFA, the positions of hydrogen-bonded atoms of hydrogen derived from TFA could not be determined reliably. These atoms were assigned to the nitrogen atom of the hydrogen-bond acceptor, and a full proton transfer was assumed to occur. In the case of crystals of compound **8a** grown from

DMSO/CH_2Cl_2, only part of the included molecules of solvent could be resolved. The SQUEEZE option of the program PLATON[34] was used to eliminate the contribution of included molecules that were highly disordered, thereby giving a final model for the most ordered part of the structure.

Acknowledgments

We are grateful to the Natural Sciences and Engineering Research Council of Canada, the Ministère de l'Éducation du Québec, the Canada Foundation for Innovation, the Canada Research Chairs Program, and Université de Montréal for financial support.

Supporting Information Available. Additional crystallographic details (including thermal atomic displacement ellipsoid plots, tables of structural data in CIF format, and supplementary figures), as well as ^{1}H and ^{13}C NMR spectra for all new compounds. This material is available free of charge via the Internet at http://pubs.acs.org.

Notes and References

1. Fellow of the Ministère de l'Éducation du Québec, 2002-2004.
2. For recent references, see: Maly, K. E.; Gagnon, E.; Maris, T.; Wuest, J. D. *J. Am. Chem. Soc.* **2007,** *129*, 4306-4322.
3. Zhao, Q.-H.; Fan, A.-L.; Li, L.-N.; Xie, M.-J. *Acta Crystallogr.* **2009**, *E65*, m622.
4. Ma, D.-L.; Che, C.-M. *Chem. Eur. J.* **2003**, *9*, 6133-6144.
5. Chan, C.-W.; Mingos, D. M. P.; White, A. J. P.; Williams, D. J. *Polyhedron* **1996**, *15*, 1753-1767.

6. Diehl, H.; Buchanan, E. B., Jr.; Smith, G. F. *Anal. Chem.* **1960**, *32*, 1117-1119.

7. Case, F. H.; Koft, E. *J. Am. Chem. Soc.* **1959**, *81*, 905-906.

8. DeMilo, A. B.; Bořkovec, A. B.; Cohen, C. F.; Robbins, W. E. *J. Agric. Food Chem.* **1981**, *29*, 82-84.

9. Duong, A.; Maris, T.; Wuest, J. D. *Cryst. Growth Des.* **2011**, *1(1)*, 287-294.

10. Nangia, A.; Desiraju, G. R. *Top. Curr. Chem.* **1998**, *198*, 57-95. Desiraju, G. R. *Angew. Chem., Int. Ed*. **1995**, *34*, 2311-2327.

11. For a recent review, see: Ye, B.-H.; Tong, M.-L.; Chen, X.-M. *Coord. Chem. Rev.* **2005**, *249*, 545-565.

12. Veauthier, J. M.; Carlson, C. N.; Collis, G. E.; Kiplinger, J. L; John, K. D. *Synthesis* **2005**, 2683-2686.

13. Wu, H.-P.; Janiak, C.; Rheinwald, G.; Lang, H. *J. Chem. Soc., Dalton Trans.* **1999**, 183-190. Janiak, C.; Deblon, S.; Wu, H.-P. *Synth. Commun.* **1999**, *29*, 3341-3352. Pichot, F.; Beck, J. H.; Elliott, C. M. *J. Phys. Chem. A* **1999**, *103*, 6263-6267. Whittle, C. P. *J. Heterocycl. Chem.* **1977**, *14*, 191-194.

14. Baxter, P. N. W.; Connor, J. A. *J. Organomet. Chem.* **1988**, *355*, 193-196.

15. Losse, S.; Görls, H.; Groarke, R.; Vos, J. G.; Rau, S. *Eur. J. Inorg. Chem.* **2008**, 4448-4452.

16. Stanek, J.; Caravatti, G.; Capraro, H.-G.; Furet, P.; Mett, H.; Schneider, P.; Regenass, U. *J. Med. Chem.* **1993**, *36*, 46-54.

17. Mukkala, V.-M.; Kwiatkowski, M.; Kankare, J.; Takalo, H. *Helv. Chim. Acta***1993**, *76*, 893-899. Baxter, P. N. W.; Connor, J. A.; Schweizer, W. B.; Wallis, J. D. *J. Chem. Soc., Dalton Trans.* **1992**, 3015-3019. Burstall, F. H. *J. Chem. Soc.* **1938**, 1662-1672.

18. Simons, J. K.; Saxton, M. R. *Organic Syntheses*; Wiley : New York, 1963; Collect. Vol. IV, p 78.

19. Gooßen, L. J.; Rodríguez, N.; Linder, C.; Lange, P. P.; Fromm, A. *ChemCatChem* **2010**, *2*, 430-442.

20. Díaz-Ortiz, Á.; Elguero, J.; Foces-Foces, C.; de la Hoz, A.; Moreno, A.; del Carmen Mateo, M.; Sánchez-Migallón, A.; Valiente, G. *New J. Chem.* **2004**, *28*, 952-958. Mackenzie, S. M.; Stevens, M. F. G. *J. Chem. Soc. C* **1970**, 2298-2308. Iwakura, Y.; Uno, K.; Shiraishi, S. *Bull. Chem. Soc. Jpn.* **1965**, *38*, 1820-1824.

21. Carlson, B.; Phelan, G. D.; Kaminsky, W.; Dalton, L.; Jiang, X.; Liu, S.; Jen, A. K.-Y. *J. Am. Chem. Soc.* **2002**, *124*, 14162-14172.

22. Saitoh, Y.; Koizumi, T.-a.; Osakada, K.; Yamamoto, T. *Can. J. Chem.* **1997**, *75*, 1336-1339.

23. Graf, G. I.; Hastreiter, D.; Everson da Silva, L.; Andrade Rebelo, R.; Garrido Montalban, A.; McKillop, A. *Tetrahedron* **2002**, *58*, 9095-9100.

24. Feng, M.; Chan, K. S. *Organometallics* **2002**, *21*, 2743-2750.

25. For recent references, see: Chein, R.-J.; Corey, E. J. *Org. Lett.* **2010**, *12*, 132-135. Zahn, S.; Reckien, W.; Kirchner, B.; Staats, H.; Matthey, J.; Lützen, A. *Chem. Eur. J.* **2009**, *15*, 2572-2580. Amarante, T. R.; Figueiredo, S.; Lopes, A. D.; Gonçalves, I. S.; Almeida Paz, F. A. *Acta Crystallogr.* **2009**, *E65*, o2047.

26. For recent references, see: Singh, D.; Bhattacharyya, P. K.; Baruah, J. B. *Cryst. Growth Des.* **2010**, *10*, 348-356. Shattock, T. R.; Arora, K. K.; Vishweshwar, P.; Zaworotko, M. J. *Cryst. Growth Des.* **2008**, *8*, 4533-4545. Babu, N. J.; Nangia, A. *Cryst. Growth Des.* **2006**, *6*, 1995-1999. Aakeröy, C. B.; Desper, J.; Urbina, J. F. *CrystEngComm* **2005**, 7, 193-201. Dale, S. H.; Elsegood, M. R. J.; Hemmings, M.; Wilkinson, A. L. *CrystEngComm* **2004**, 6, 207-214.

27. The large difference between the pK_a value of TFA (pK_a 0.5) and those of the conjugate acids of pyridine (pK_a 5.2) or aminotriazines such as melamine (pK_a 5)[28] provides a substantial driving force for proton transfer.[29]

28. Jang, Y. H.; Hwang, S.; Chang, S. B.; Ku, J.; Chung, D. S. *J. Phys. Chem. A* **2009**, *113*, 13036-13040.

29. For discussion, see: He, G.; Chow, P. S.; Tan, R. B. H. *Cryst. Growth. Des.* **2009**, *9*, 4529-4532. Mohamed, S.; Tocher, D. A.; Vickers, M.; Karamertzanis, P. G.; Price, S. L. *Cryst. Growth. Des.* **2009**, *9*, 2881-2889. Childs, S. L.; Stahly, G. P.; Park, A. *Mol. Pharmaceutics* **2007**, *4*, 323-338. Bhogala, B. R.; Basavoju, S.; Nangia, A. *CrystEngComm* **2005**, 7, 551-562.

30. Desiraju, G. R.; Steiner, T., *The Weak Hydrogen Bond in Structural Chemistry and Biology*; Oxford University Press: Oxford, U. K., 1999.

31. For a review of C-H···O interactions, see: Desiraju, G. R. *Chem. Commun.* **2005**, 2995-3001.

32. See the Supporting Information for details.

33. Sheldrick, G. M. *Acta Crystallogr*. **2008**, *A64*, 112-122.

34. Spek, A. L. *PLATON, A Multipurpose Crystallographic Tool*; Utrecht University : Utrecht, The Netherlands, 2001. van der Sluis, P.; Spek, A. L. *Acta Crystallogr.* **1990**, *A46*, 194-201.

6.4 Conclusions

Lors de ce travail, nous avons systématiquement utilisé une stratégie commune pour former les ligands cibles. Cette stratégie implique la préparation des intermédiaires cyano puis la transformation des groupements cyano en DAT selon une procédure traditionnelle. Deux séries de ligands bidentates, dérivés de la famille des bipyridines et des phénantrolines, ont été synthétisées. Dans notre étude, nous avons fait varier la position des groupements DAT sur les unités coordinantes. Cette approche, typique de l'ingénierie cristalline, permet de faire varier l'architecture supramoléculaire de manière systématique. Tel que nous l'avons prévu, à l'état non coordonné les atomes d'azote de la bipyridine et de la phénantroline participent dans la formation de ponts hydrogène pour consolider l'édifice supramoléculaire. Les structures que nous avons révélées par diffraction des rayons-X ont montré des modes de reconnaissance prévisibles des groupements DAT. Cependant, certaines structures sont encore difficiles à prédire du fait de l'inclusion du solvant dans le réseau. Les ligands bidentates obtenus sont prometteurs pour la chimie de coordination du fait de leur fort caractère coordinant et devraient donner des résultats pouvant aboutir à des applications dans la chimie des matériaux hybrides qui sont structurés par une combinaison des liaisons de coordination et des ponts hydrogène.

Chapitre 7

Combinaison de la coordination métallique et des ponts hydrogène

7.1 Introduction

La plupart des tectons ont été jusqu'à là des composés retenus par des liens covalents. Ces composés sont robustes et utiles mais sont typiquement obtenus par des synthèses multi-étapes laborieuses. Une alternative intéressante est de construire des tectons à partir de ligands qui peuvent se coordonner aux métaux pour former des complexes fonctionnalisés appelés *métallotectons*. Cette stratégie de synthèse est avantageuse, car elle permet de modifier facilement la topologie du métallotecton en faisant varier le centre métallique.

Dans cette thèse, nous avons identifié une série de ligands pouvant être utilisés pour synthétiser des métallotectons. Il s'agit de ligands fonctionnalisés avec des groupements qui ont la capacité de participer dans la formation des interactions inter-complexes fiables telles des liaisons hydrogène. Nous avons préalablement identifié le substituant diaminotriazinyle (DAT) comme étant peu coordonnant comparativement à la pyridine, la 2,2'-bipyridine et la phénantroline (voir chapitres 4-6). La modification de ces ligands hétérocycliques classiques par l'ajout des groupements DAT offre la possibilité de contrôler la coordination métallique et la formation de ponts hydrogène inter-complexes de manière orthogonale. Cette stratégie, qui combine la chimie de coordination et les liaisons hydrogène, peut donner lieu à la formation de nouveaux matériaux.

7.2 Nos objectifs

Afin d'évaluer le potentiel de cette stratégie, nous avons choisi d'examiner le comportement d'une série de complexes de Pd(II). Nous avons sélectionné le Pd(II) car sa géométrie de coordination est connue et prévisible. Nos objectifs sont donc de construire des métallotectons de Pd(II) par la voie simple de coordination spontanée, de confirmer que la géométrie de coordination respecte les généralisations établies et d'examiner comment les substituants DAT régissent l'organisation inter-complexe des métallotectons.

7.3 Article 6

Using Pyridinyl-Substituted Diaminotriazines to Bind Pd(II) and Create Metallotectons for Engineering Hydrogen-Bonded Crystals

Adam Duong, Thierry Maris, and James D. Wuest*

Inorganic Chemistry, **2011***, 50(12),* 5605-5618

Abstract

The pyridinyl groups of pyridinyl-substituted diaminotriazines **3a**-**b** and **4a**-**b** can bind metals, and the diaminotriazinyl (DAT) groups serve independently to ensure that the resulting complexes can participate in intercomplex hydrogen bonding according to characteristic motifs. As planned, ligands **3a**-**b** and **4a**-**b** form *trans* square-planar 2:1 complexes with $PdCl_2$, and further association of the complexes is directed in part by hydrogen bonding of the DAT groups. Similarly, ligands **3a**-**b** and **4a**-**b** form cationicsquare-planar 4:1 complexes with $Pd(BF_4)_2$, $Pd(PF_6)_2$, and $Pd(NO_3)_2$, and the complexes again typically associate by hydrogen bonding of the peripheral DAT groups. The observed complexes have predictable constitutions and shared structural features that result logically from their characteristic topologies and the ability of DAT groups to engage in hydrogen bonding. These results illustrate the potential of a hybrid inorganic/organic strategy for constructing materials in which coordinative bonds to metals are used in conjunction with other interactions, both to build the molecular components and to control their organization.

Introduction

For nearly a century, X-ray diffraction has been used to reveal the atomic structure of crystals.[1] During that time, more than 500,000 structures of molecular crystals have been resolved and catalogued.[2] Despite the imposing mass of collected data, however, full understanding of the factors underlying structural preferences remains elusive.[3] Each added structure is unique, and its crystallographic parameters cannot be predicted reliably. Designing new molecular crystals and other ordered materials is a profoundly difficult enterprise, yet it is essential for progress in many areas of science and technology. Under these circumstances,

qualitative guidelines for controlling molecular organization are indispensable and must be improved.

A widely-used approach is based on the concept of building ordered materials by the spontaneous association of tectons, which are molecules with suitable topologies and an ability to engage in multiple predictable interactions with neighbors.[4] When properly exploited, this approach can yield materials with predetermined organization and with collective properties that depend on those of the individual molecular components, modified in a programmable way by the effect of their neighbors. Even though structural parameters cannot be predicted reliably in detail, this strategy allows gross features to be introduced with confidence, and it will continue to be an important source of new molecular materials.

This strategy must be further tested and refined by using it to build materials from the widest possible range of molecular components, held together by a full spectrum of interactions that meet basic criteria of strength and reliability. Most tectons that have been studied so far are typified by structure **1**, which consists of a covalently bonded molecular core, functionalized by

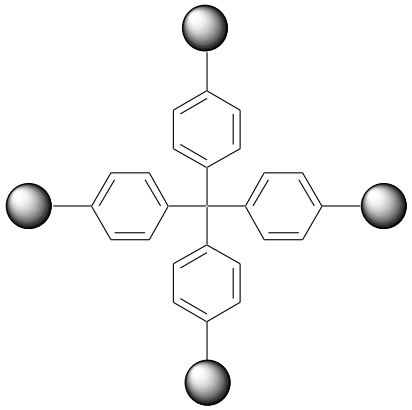

1

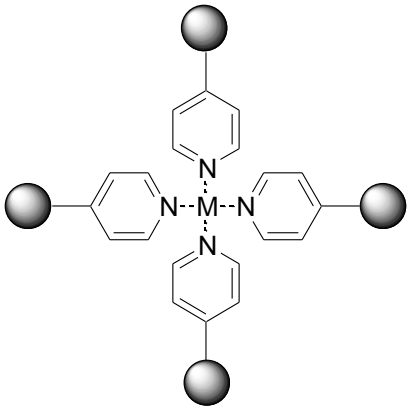

2

multiple peripheral groups (●) that engage in interactions according to established patterns. Covalently bonded cores are attractive because they are robust, but they must often be made laboriously by multistep syntheses. An appealing alternative is the self-assembly of topologically related structures represented by metallotecton **2**, which is held together by coordinative bonds to a metal.[5-7] Moreover, this alternative approach allows the geometry of coordination to be altered systematically by varying the metal. Despite the conspicuous advantages of this strategy, metallotectons remain underexploited in the effort to engineer new materials, possibly because their use requires a dual understanding of both organic and inorganic chemistry.

To further explore the potential of this approach, we elected to study the behavior of metallic complexes of substituted pyridine **3a**[8] and its elongated derivative **3b**,[9] as well as isomeric pair **4a**[10] and **4b**.[11] The design of this set of ligands is based on the well-established

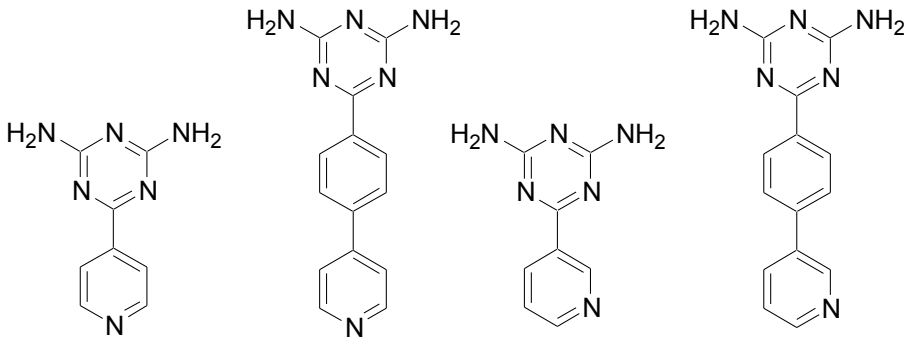

ability of pyridines to bind metals, combined with the tendency of diaminotriazinyl (DAT) groups to engage in multiple hydrogen bonds according to motifs **I**-**III**.[12] Pyridines are typically stronger ligands than triazines, so we expected the two distinct parts of compounds **3a**-**b** and **4a**-**b**

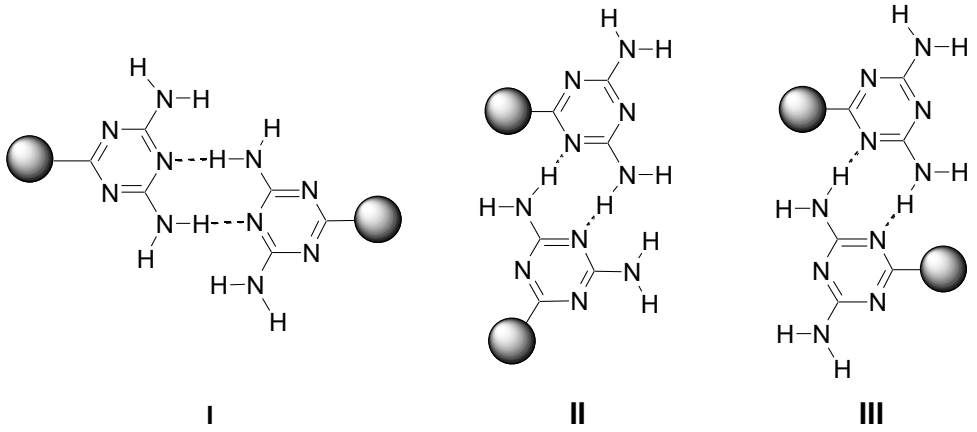

I **II** **III**

to operate orthogonally, one to ensure formation of a metallotecton by coordination, and the other to direct intermolecular association by hydrogen bonding. In initial work, we decided to examine the ability of ligands **3a-b** and **4a-b** to bind Pd(II), which is known to favor related complexes with a square-planar geometry.[13-14] By focusing on a single metal with a predictable geometry of coordination, bound by a family of ligands that vary systematically, we designed our study to produce a set of closely related structures that can be compared to reveal basic principles of metallotectonic assembly.

Results and Discussion

Syntheses of Ligands 3a-b and 4a-b. 6-(Pyridin-4-yl)-1,3,5-triazine-2,4-diamine (**3a**),[8] 6-[4-(pyridin-4-yl)phenyl]-1,3,5-triazine-2,4-diamine (**3b**),[9] 6-(pyridin-3-yl)-1,3,5-triazine-2,4-diamine (**4a**),[10] and 6-[4-(pyridin-3-yl)phenyl]-1,3,5-triazine-2,4-diamine (**4b**)[11] were prepared by reported methods.

Structures of Unbound Ligands 3a-b and 4a-b. To provide a basis for understanding the association of metallotectons derived from compounds **3a-b** and **4a-b**, we examined the

structures of crystals of the unbound ligands themselves in a preliminary study.[11] Comparison of the structures identified three shared features: (1) The compounds adopt flattened conformations typical of aryl-substituted triazines;[12] (2) they form approximately coplanar hydrogen bonds according to characteristic motifs **I-III**; and (3) these interactions play a major role in directing molecular organization. Because compounds **3a-b** and **4a-b** have similar flattened molecular shapes and incorporate DAT groups, they crystallize similarly to give hydrogen-bonded structures built from chains, tapes, and layers. The same factors can be expected to help direct the association of metallotectons derived from compounds **3a-b** and **4a-b** when they are used as ligands.

Syntheses and Structures of Complexes of Ligands 3a-b and 4a-b with $PdCl_2$. Complexes were prepared by mixing the ligands (2 equiv) with $PdCl_2$ (1 equiv) in MeCN. The precipitated solids were then crystallized, and the structures were determined by X-ray crystallography.

(a) Structures of the 2:1 Complex of 6-(Pyridin-4-yl)-1,3,5-triazine-2,4-diamine (3a) with $PdCl_2$. Pyridine itself is known to react with $PdCl_2$ to give square-planar complex **5** with *trans*-oriented pyridinyl ligands,[13] so we expected ligand **3a** to yield an analogous 2:1 complex.

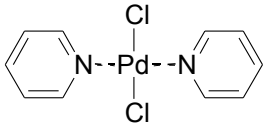

5

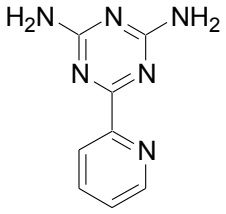

6

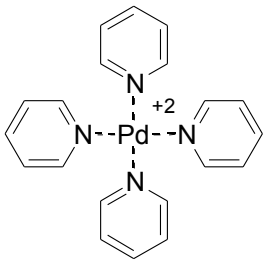

7

Crystals grown from DMSO/H_2O were found to have the composition $PdCl_2$(**3**)$_2$ • 2 DMSO and to belong to the orthorhombic space group *I*222. Views of the structure are provided in Figure 1, and other crystallographic data are presented in Table 1. As anticipated, the pyridinyl groups of compound **3a** are bound in a *trans* orientation to give a square-planar Pd(II) complex (Figure 1a), with normal Pd-N distances (2.012(18) Å) and Pd-Cl distances (2.309(3) Å).[13] The pyridinyl and triazinyl rings in each ligand are nearly coplanar, as expected,[12] and the torsional angle between the average planes is only 4.8°. The average planes of the two *trans*-oriented ligands form an angle of 57.9° with respect to each other, and they lie at angles of 4.9° and 52.9° with respect to the essentially planar PdN_2Cl_2 core of the metallotecton.

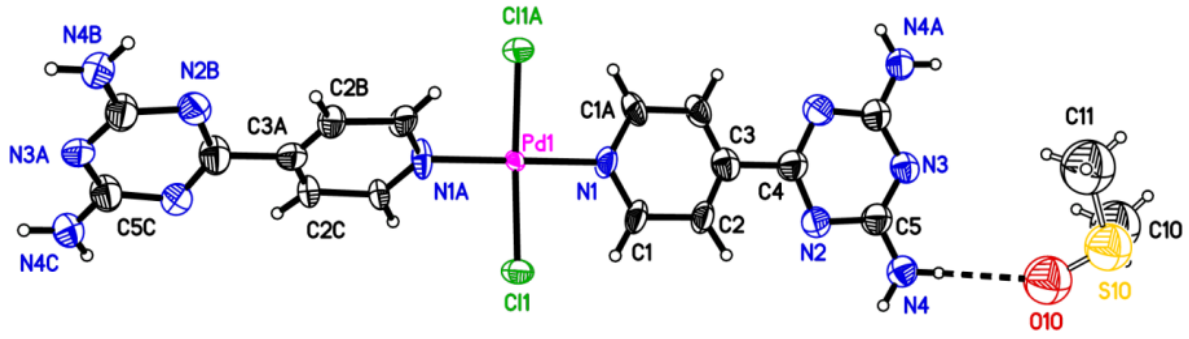

a

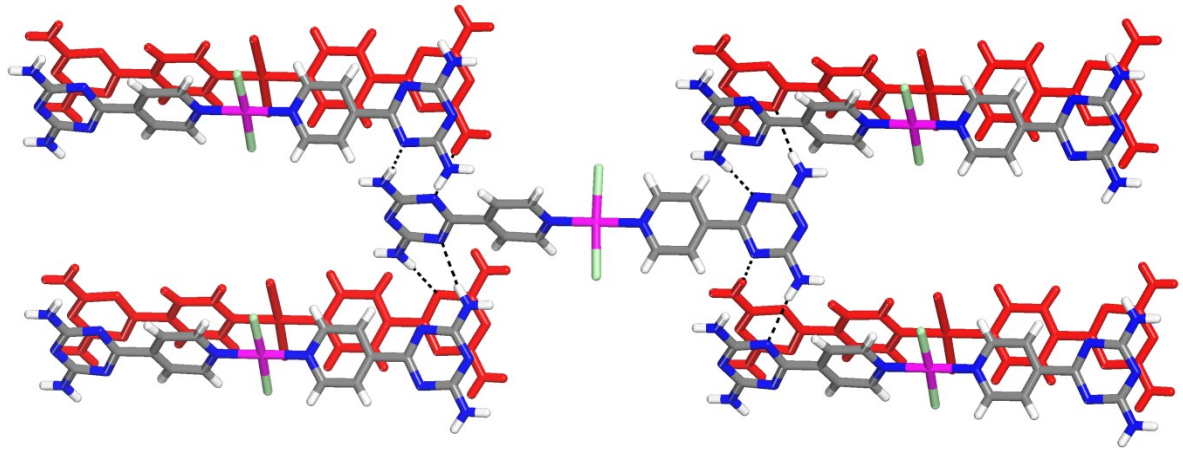

b

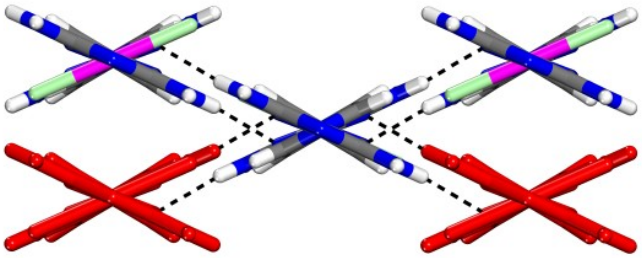

c

Figure 1. Structure of complex $PdCl_2$(**3a**)$_2$ • 2 DMSO in crystals grown from DMSO/H_2O. Hydrogen bonds are represented by broken lines. Except where noted otherwise, carbon atoms are shown in gray, hydrogen atoms in white, nitrogen atoms in blue, oxygen atoms in red, sulfur atoms in yellow, chlorine atoms in green, and palladium atoms in rose. (a) Thermal atomic displacement ellipsoid plot, with ellipsoids of non-hydrogen atoms drawn at the 50% probability level and hydrogen atoms represented by a sphere of arbitrary size. Key bond lengths include Pd1-N1 = 2.012(18) Å and Pd1-Cl1 = 2.309(3) Å. Key bond angles include Cl1-Pd1-Cl1A = 177.0(6)°, N1-Pd1-N1A = 180°, and N1-Pd1-Cl1 = 91.5(3)°. (b) View along the *a* axis showing eight N-H···N hydrogen bonds of modified type **III** (3.103(12) Å) formed by the central metallotecton and eight neighbors, four in an upper plane (normal colors) and four in a lower plane (red). Guest molecules of DMSO are omitted for clarity. (c) Alternative view along the *c* axis showing the relationship between the central metallotecton and its neighbors.

Table 1. Crystallographic Data for 1:2 and 1:1 Complexes of $PdCl_2$ with Pyridinyl-Substituted Diaminotriazines **3a-b**, **4a-b**, and **6**.

complex	$PdCl_2$(**3a**)$_2$ • 2 DMSO	$PdCl_2$(**3a**)$_2$ • 2 DMSO • dioxane	$PdCl_2$(**3b**)$_2$	$PdCl_2$(**4a**)$_2$ • 3 DMSO	$PdCl_2$(**6**)
crystallization medium	DMSO/H_2O	DMSO/dioxane	DMSO/EtOAc	DMSO	DMSO/H_2O
formula	$C_{20}H_{28}Cl_2N_{12}O_2PdS_2$	$C_{24}H_{36}Cl_2N_{12}O_4PdS_2$	$C_{28}H_{24}Cl_2N_{12}Pd$	$C_{22}H_{34}Cl_2N_{12}O_3PdS_3$	$C_8H_8Cl_2N_5Pd$
crystal system	orthorhombic	triclinic	monoclinic	monoclinic	monoclinic
space group	*I*222	*P*-1	$P2_1$/n	*C*2/c	$P2_1$/n
a (Å)	3.7721(10)	6.1250(8)	13.6163(10)	37.2003(9)	7.9908(3)
b (Å)	11.346(3)	9.7568(13)	10.9178(9)	8.0105(2)	9.1500(4)
c (Å)	28.990(7)	15.6448(18)	18.8566(15)	11.0946(3)	15.4450(16)
α (°)	90	105.458(6)	90	90	90
β (°)	90	96.393(6)	93.775(3)	93.530(1)	98.586(2)
γ(°)	90	97.755(7)	90	90	90
V (Å^3)	1240.7(6)	882.19(19)	2797.1(4)	3299.84(15)	1116.62(8)
Z	2	1	4	4	4
ρ_{calc} (g cm^{-3})	1.900	1.502	1.676	1.586	2.174
T (K)	100	150	150	100	150
μ (mm^{-1})	10.014	7.152	7.477	8.192	17.711
R_1, $I>2\sigma(I)$	0.0734	0.0491	0.0583	0.0235	0.0263
R_1, all data	0.0740	0.0533	0.0623	0.0248	0.0290
wR_2, $I>2\sigma(I)$	0.1754	0.1340	0.1350	0.0659	0.0709
wR_2, all data	0.1758	0.1377	0.1355	0.0669	0.0721
measured reflections	2699	12588	30310	25455	14799
independent reflections	1091	3156	5280	2910	2213
observed reflections [$I>2\sigma(I)$]	1023	2882	3201	2761	2027

The resulting metallotecton predictably defines a linear structure with DAT groups at its two extremities. Each DAT group participates in four N-H···N hydrogen bonds according to a modified version of motif **III**, and each metallotecton thereby forms a total of eight hydrogen bonds with eight neighbors to give a three-dimensional network (Figures 1b-c). Channels aligned with the *a* axis contain disordered molecules of DMSO, which form hydrogen bonds with the DAT groups (Figure 1a) and thereby prevent the metallotectons from associating end-to-end by forming hydrogen bonds of type **I**. As planned, the observed structure is organized by a combination of coordinative interactions and hydrogen bonds. Key features of the structure are a logical result of (1) the tendency of $PdCl_2$ to form trans square-planar 1:2 complexes with

pyridines and (2) the creation of a metallotecton with DAT groups at the ends of an elongated linear structure, which favors a parallel alignment held together by hydrogen bonds.

To probe the effect of solvent on the formation and association of metallotectons derived from $PdCl_2$ and ligand **3a**, we also grew crystals from DMSO/dioxane. They proved to have the composition $PdCl_2$(**3a**)$_2$ • 2 DMSO • dioxane and to belong to the triclinic space group *P*-1. Views of the structure are shown in Figure 2, and other crystallographic data are summarized in Table 1. Again, a square-planar complex with trans-oriented pyridinyl groups is formed (Figure 2a), with normal Pd-N and Pd-Cl distances.[13] The pyridinyl and triazinyl rings in each ligand are essentially coplanar, and both ligands lie in the same plane, which forms an angle of 62.7(1)° with the PdN_2Cl_2 core of the metallotecton.

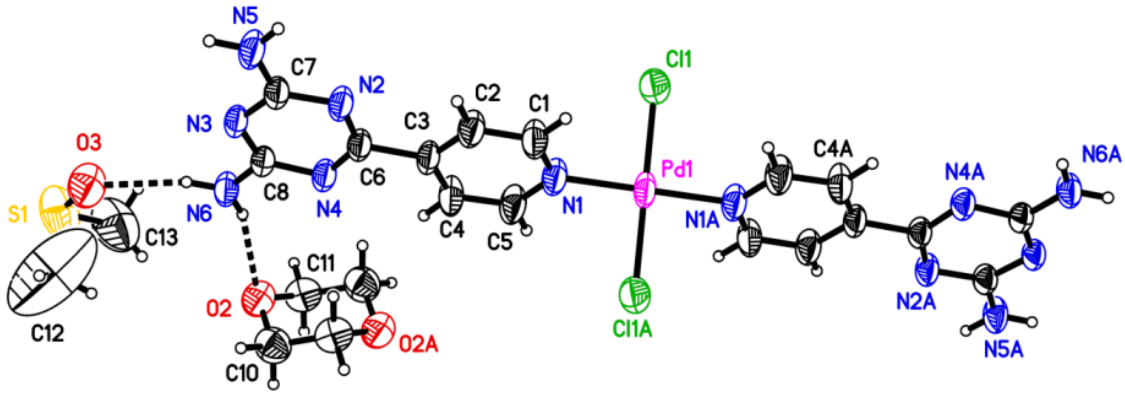

a

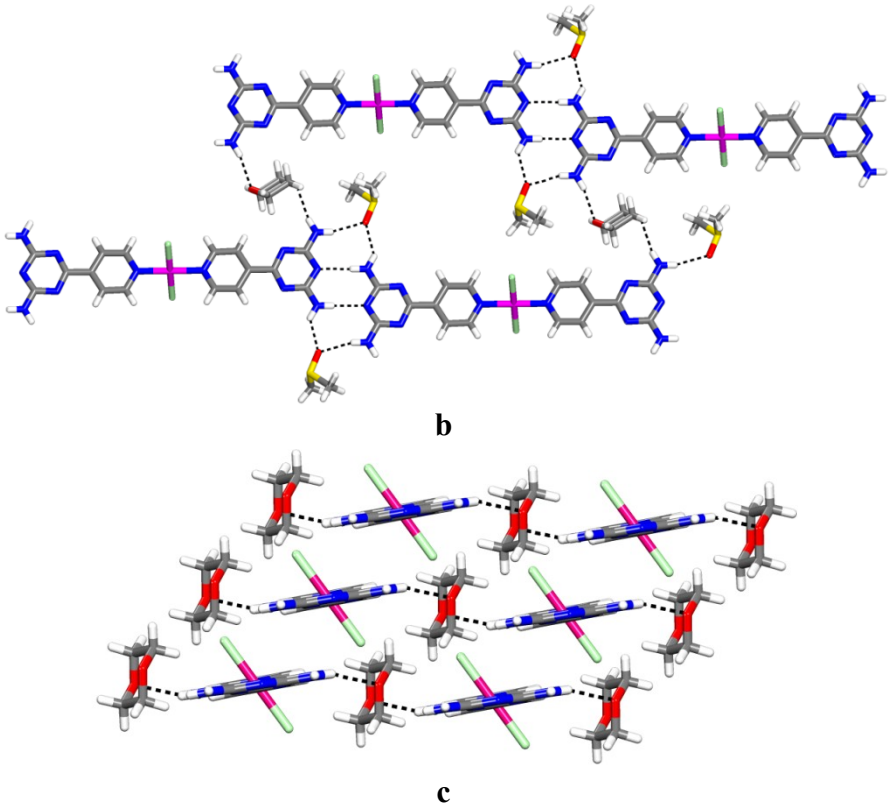

Figure 2. Structure of complex $PdCl_2$(**3a**)$_2$ • 2 DMSO • dioxane in crystals grown from DMSO/dioxane. Hydrogen bonds are represented by broken lines. Carbon atoms are shown in gray, hydrogen atoms in white, nitrogen atoms in blue, oxygen atoms in red, sulfur atoms in yellow, chlorine atoms in green, and palladium atoms in rose. (a) Thermal atomic displacement ellipsoid plot, with ellipsoids of non-hydrogen atoms drawn at the 50% probability level and hydrogen atoms represented by a sphere of arbitrary size. Key bond lengths include Pd1-N1 = 2.018(3) Å and Pd1-Cl1 = 2.3207(13) Å. Representative bond angles include Cl1-Pd1-Cl1A = 180°, N1-Pd1-N1A = 180°, and N1-Pd1-Cl1 = 90.20(12)°. (b) View showing how N-H···N hydrogen bonds of type **I** (2.980(5) Å), reinforced by N-H···O hydrogen bonds involving bridging molecules of DMSO (average distance = 2.959(5) Å), link the metallotectons into chains, which are further connected into sheets by N-H···O hydrogen bonds (3.049(5) Å) involving intervening molecules of dioxane. (c) View showing alternating layers of metallotectons and guests, with molecules of DMSO omitted for clarity.

As shown in Figure 2b, the metallotectons are linked into chains by hydrogen bonding of DAT groups according to motif **I**, reinforced by N-H···O hydrogen bonds involving bridging molecules of DMSO. The chains are further joined to form sheets by N-H···O hydrogen bonds with connecting molecules of dioxane (Figure 2b), and the sheets stack to give a structure that consists of layers of metallotectons separated by intervening layers of DMSO and dioxane (Figure 2c). Together, these results confirm that the product of the reaction of $PdCl_2$ with ligand **3a** can be crystallized under different conditions to give structures built predictably from a metallotecton with a single well-defined constitution. However, the conformation of the metallotecton can vary, thereby allowing somewhat different structures to be formed. Nevertheless, both observed structures predictably share two key features: (1) The elongated linear metallotectons are arranged in a parallel orientation; and (2) they are positioned by multiple coplanar hydrogen bonds involving DAT groups.

(b) Structure of the 2:1 Complex of 6-[4-(Pyridin-4-yl)phenyl]-1,3,5-triazine-2,4-diamine (3b) with $PdCl_2$. Based on the observed behavior of 6-(pyridin-4-yl)-1,3,5-triazine-2,4-diamine (**3a**), we expected elongated analogue **3b** to behave in a similar way. Crystals of the complex of $PdCl_2$ with ligand **3b** were grown from DMSO/EtOAc. They were found to have the composition $PdCl_2$(**3b**)$_2$ and to belong to the monoclinic space group $P2_1/n$. Figure 3 provides views of the structure, and Table 1 contains other crystallographic data. As planned, a square-planar complex with trans-oriented pyridinyl groups is produced (Figure 3a), with normal Pd-N and Pd-Cl distances.[13] The bound ligands adopt nearly planar conformations, and their average planes form similar angles (44.4(1)° and 71.6(1)°) with the PdN_2Cl_2 core of the metallotecton.

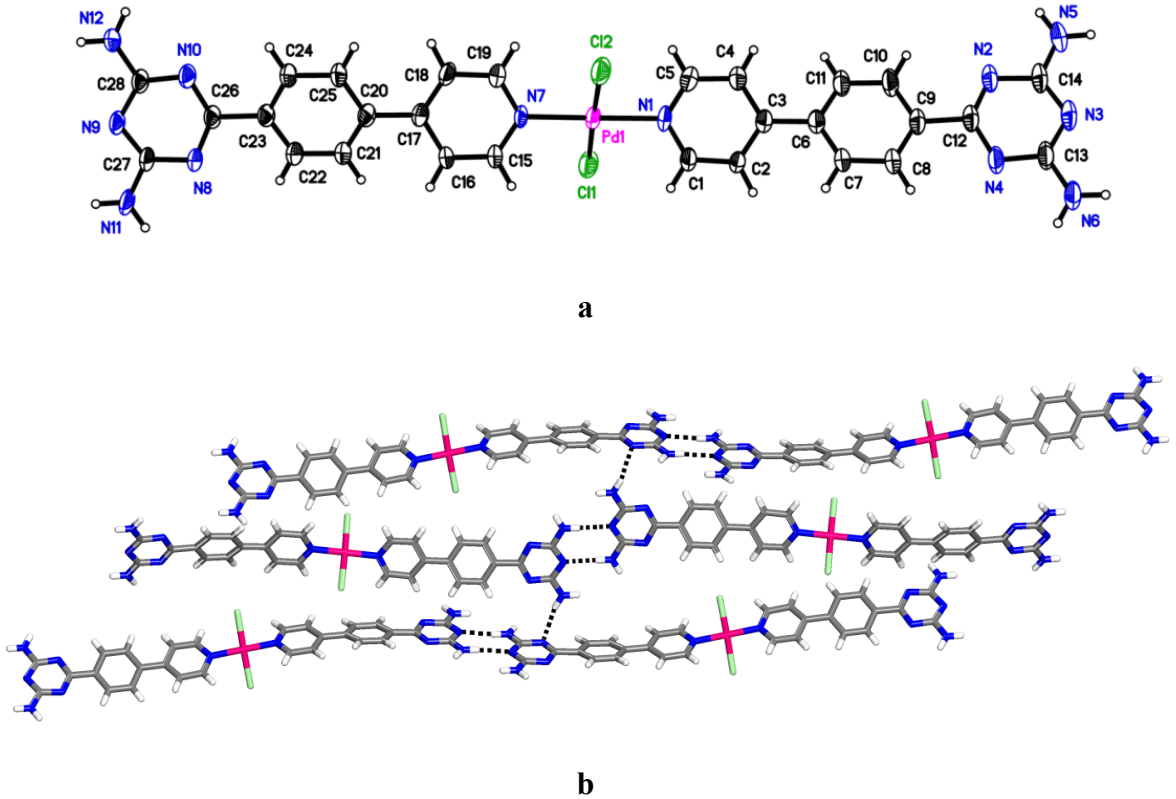

a

b

Figure 3. Structure of complex $PdCl_2$(**3b**)$_2$ in crystals grown from DMSO/EtOAc. Hydrogen bonds are represented by broken lines. Carbon atoms are shown in gray, hydrogen atoms in white, nitrogen atoms in blue, chlorine atoms in green, and palladium atoms in rose. (a) Thermal atomic displacement ellipsoid plot, with ellipsoids of non-hydrogen atoms drawn at the 50% probability level and hydrogen atoms represented by a sphere of arbitrary size. Key bond lengths include Pd1-N1 = 2.026(4) Å, Pd1-N7 = 2.033(4) Å, Pd1-Cl1 = 2.3079(15) Å, and Pd1-Cl2 = 2.2968(15) Å. Representative bond angles include Cl1-Pd1-Cl2 = 177.21(5)°, N1-Pd1-N7 = 179.4(2)°, and N1-Pd1-Cl1 = 88.33(15)°. (b) View showing how N-H···N hydrogen bonds of type **I** (2.961(6) Å) link the metallotectons into chains, which are further connected into sheets by edge-to-face N-H···N hydrogen bonds (3.081(6) Å).

As shown in Figure 3b, the metallotectons are joined to form chains by N-H···N hydrogen bonds of type **I** involving DAT groups, and the chains are further connected to form sheets by edge-to-face N-H···N hydrogen bonds. Again, $PdCl_2$ reacts predictably with ligand **3b** to form a metallotecton that crystallizes to generate a structure with expected features, dictated in part by hydrogen bonding of the DAT groups and by the elongated topology of the molecular constituents, which favors a parallel arrangement.

(c) Structure of the 2:1 Complex of 6-(Pyridin-3-yl)-1,3,5-triazine-2,4-diamine (4a) with $PdCl_2$. To probe the effect of distorting the linear geometry of metallotectons derived from ligand **3a** and its extended analogue **3b**, we grew crystals of the complex of $PdCl_2$ with ligand **4a** from DMSO. They proved to have the composition $PdCl_2$(**4a**)$_2$ • 3 DMSO and to belong to the monoclinic space group *C*2/*c*. Views of the structure are shown in Figure 4, and other crystallographic data are presented in Table 1. As expected, complexation yields a square-planar complex with *trans*-oriented pyridinyl groups (Figure 4a), and the Pd-N and Pd-Cl distances are normal.[13] Each bound ligand adopts a flattened conformation, and the two ligands lie in essentially the same plane, which forms an angle of 66.8(1)° with the PdN_2Cl_2 core of the metallotecton. The two DAT groups are oriented on opposite sides of the PdN_2Cl_2 core.

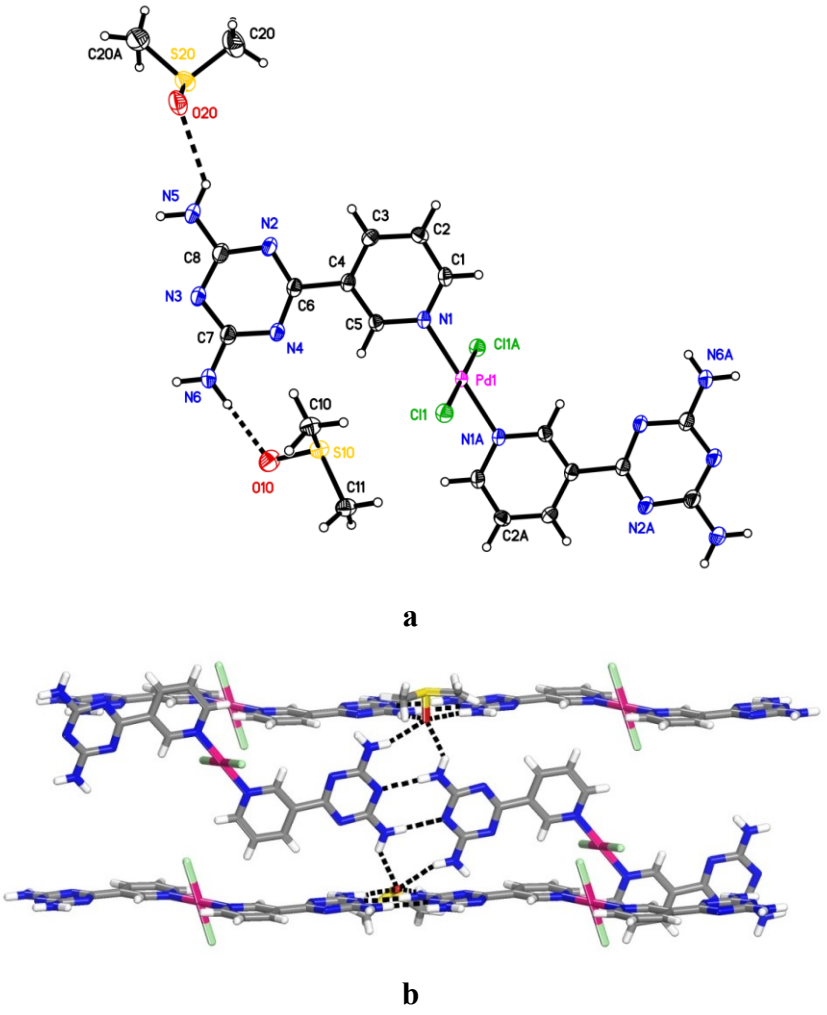

Figure 4. Structure of complex $PdCl_2$(**4a**)$_2$ • 3 DMSO in crystals grown from DMSO. Hydrogen bonds are represented by broken lines. Carbon atoms are shown in gray, hydrogen atoms in white, nitrogen atoms in blue, oxygen atoms in red, sulfur atoms in yellow, chlorine atoms in green, and palladium atoms in rose. (a) Thermal atomic displacement ellipsoid plot, with ellipsoids of non-hydrogen atoms drawn at the 50% probability level and hydrogen atoms represented by a sphere of arbitrary size. Key bond lengths include Pd1-N1 = 2.0150(16) Å and Pd1-Cl1 = 2.2981(5) Å. Representative bond angles include Cl1-Pd1-Cl1A = 180°, N1-Pd1-N1A = 180°, and N1-Pd1-Cl1 = 90.97(5)°. (b) View showing how N-H···N hydrogen bonds of type **I** (2.961(3) Å) link the metallotectons into chains, which interact with adjacent chains by N-H···O hydrogen bonds involving bridging molecules of DMSO.

Although the DAT groups of each metallotecton no longer have a collinear orientation, as maintained in analogous complexes of ligands **3a** and **3b**, association occurs in essentially the same way. Specifically, N-H···N hydrogen bonding of type **I** (2.961(3) Å) leads to the formation of zig-zag chains, which engage in additional intra- and interchain N-H···O hydrogen bonds involving bridging molecules of DMSO (Figure 4b). Again, complexation of $PdCl_2$ produces a metallotecton with a predictable constitution; furthermore, its elongated geometry and the incorporated DAT groups ensure the formation of a structure in which the components have an approximately parallel orientation and engage in multiple intermolecular hydrogen bonds according to reliable patterns.

Synthesis and Structure of the 1:1 Complex of 6-(Pyridin-2-yl)-1,3,5-triazine-2,4-diamine (6) with $PdCl_2$. Ligands **3a**, **3b**, and **4a** all behave as expected by producing square-planar trans 2:1 complexes with $PdCl_2$ analogous to structure **5**. In these complexes, the pyridinyl and DAT groups operate orthogonally to ensure coordination and intermolecular hydrogen bonding, respectively, without mutual interference. In contrast, ligand **6**[15] promises to allow the two groups to cooperate by chelating Pd(II). To test this possibility, ligand **6** and $PdCl_2$ were mixed in a 1:1 ratio in MeCN, the precipitated solid was then crystallized from DMSO/H_2O, and the structure was determined by X-ray crystallography.

The crystals were found to have the composition $PdCl_2$(**6**) and to belong to the monoclinic space group $P2_1/n$. Views of the structure are presented in Figure 5, and other crystallographic data are provided in Table 1. As expected, complexation yields a square-planar chelate (Figure 5a) with normal Pd-N and Pd-Cl distances.[13] The Pd-$N_{triazine}$ bond is longer than the Pd-$N_{pyridine}$ bond, reflecting the weaker coordination of triazines. The bound ligand is essentially planar and lies close to the average plane of the PdN_2Cl_2 core of the complex.

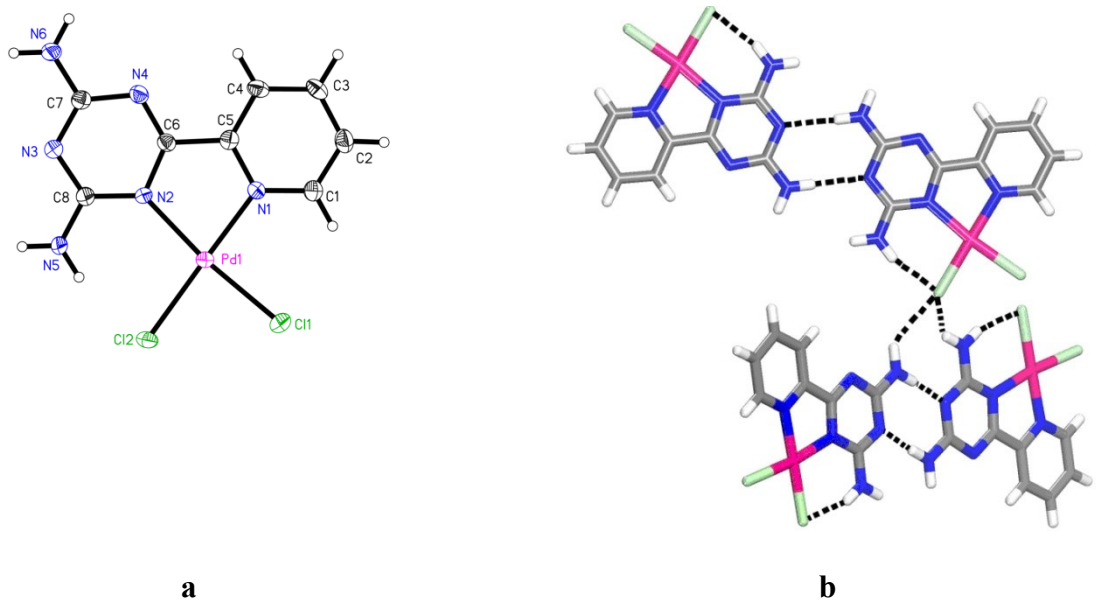

Figure 5. Structure of complex $PdCl_2$(**6**) in crystals grown from DMSO/H_2O. Hydrogen bonds are represented by broken lines. Carbon atoms are shown in gray, hydrogen atoms in white, nitrogen atoms in blue, chlorine atoms in green, and palladium atoms in rose. (a) Thermal atomic displacement ellipsoid plot, with ellipsoids of non-hydrogen atoms drawn at the 50% probability level and hydrogen atoms represented by a sphere of arbitrary size. Key bond lengths include Pd1-N1 = 2.029(2) Å, Pd1-N2 = 2.087(2) Å, Pd1-Cl1 = 2.2897(8) Å, and Pd1-Cl2 = 2.3041(7) Å. Representative bond angles include Cl1-Pd1-Cl2 = 86.12(3)°, N1-Pd1-N2 = 80.54(10)°, N1-Pd1-Cl1 = 93.06(8)°, and N2-Pd1-Cl2 = 173.35(7)°. (b) View showing how N-H···N hydrogen bonds of type **I** (3.023(4) Å) link the chelates into dimers, which associate with adjacent dimers in various ways, such as by forming N-H···Cl interactions.

The chelates are paired by N-H···N hydrogen bonds of type **I** to form dimers, which associate with adjacent dimers in various ways, such as by forming N-H···Cl interactions (Figure 5b). The structure of the complex is noteworthy because it establishes that compound **6** can serve as a bidentate ligand analogous to 2,2'-bipyridine. This suggests a potentially general strategy in

which heteroaromatic groups in other well-known multidentate ligands are replaced with DAT groups to create surrogates with two characteristic properties: (1) They can chelate metals in analogous ways, and (2) the resulting complexes have similar topologies, but they are endowed with the additional ability to engage in extensive hydrogen bonding according to reliable patterns. However, metallotectons derived from $PdCl_2$ and bidentate ligand **6** have only one DAT group per complex, so they are less able to engage in intermolecular hydrogen bonding than complexes derived from monodentate ligands **3a**-**b** and **4a**-**b**, which have two DAT groups. For this reason, we elected to reserve further study of ligand **6** and bidentate analogues for future work and to focus in the present study on the behavior of monodentate ligands **3a**-**b** and **4a**-**b**.

Syntheses and Structures of 4:1 Complexes of Ligands 3a-b and 4a-b with $Pd(BF_4)_2$, $Pd(PF_6)_2$, and $Pd(NO_3)_2$. Complexes were prepared by mixing the ligands (4 equiv) with salts of Pd(II) (1 equiv) in MeCN. The precipitated solids were then crystallized, after exchange of anions if needed, and the structures were determined by X-ray crystallography.

(a) Structure of the 4:1 Complex of 6-(Pyridin-4-yl)-1,3,5-triazine-2,4-diamine (3a) with $Pd(BF_4)_2$. Pyridine reacts with $Pd(BF_4)_2$ to give square-planar dication **7**,[14] so we expected ligand **3a** to yield an analogous 4:1 complex. Crystals grown from DMSO/H_2O/MeCN proved to have the composition $[Pd(\mathbf{3a})_4](BF_4)_2 \bullet 9\ H_2O$ and to belong to the monoclinic space group $P2_1/n$. Figure 6 shows views of the structure, and Table 2 summarizes other crystallographic data. As anticipated, the pyridinyl groups of ligand **3a** bind Pd(II) to give a square-planar complex (Figure 6a), with normal Pd-N distances.[14] The pyridinyl and triazinyl rings in each ligand are nearly coplanar, and the pyridinyl groups lie essentially perpendicular to the PdN_4 core of the metallotecton, as observed in related structures.[14]

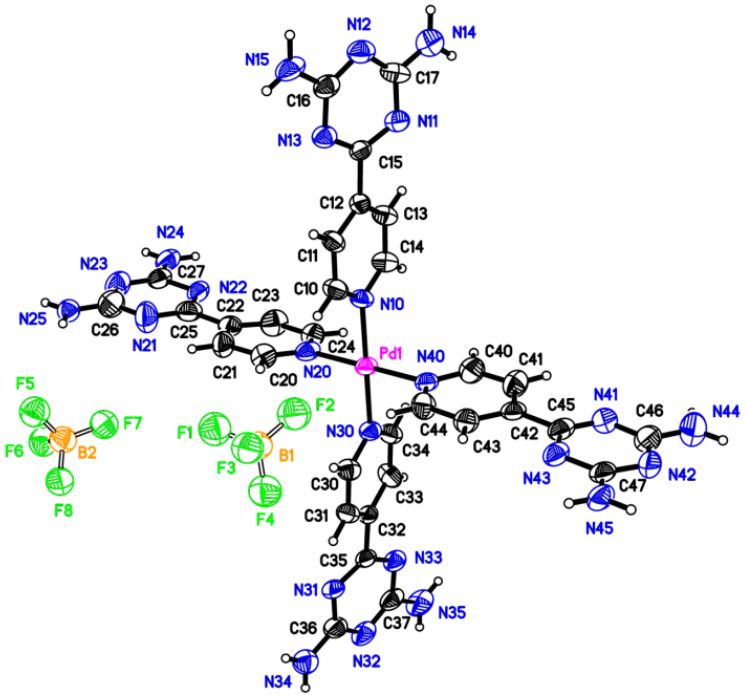
N12
N14
N15
C17
C16
N11
N13
C15
C12
C13
N24
C11
C14
N23
C27
C10
N10
N22
C23
C22
N25
C26
C25
N21
C24
Pd1
N40
C40
C41
C21
N20
C20
F5
F2
N41
C45
C46
N44
F7
F1
N30
C44
C43
C42
F6
B2
B1
C34
N43
N42
F3
C30
C33
C47
F8
F4
C31
C32
N45
C35
N33
N31
N35
C37
C36
N32
N34

a

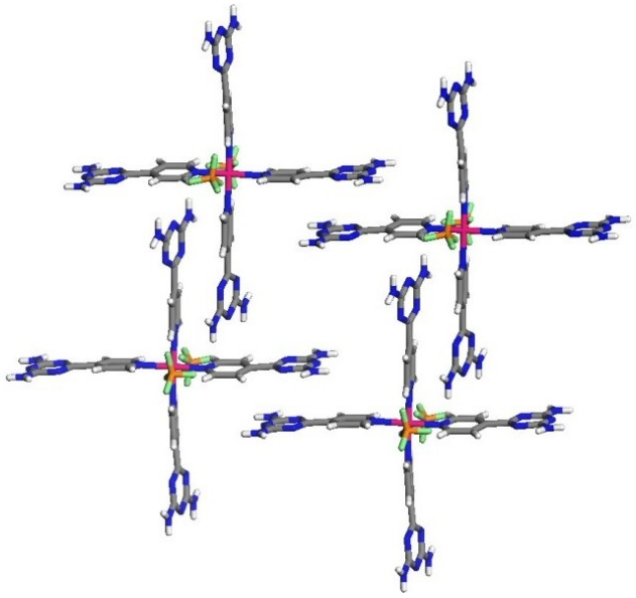

b

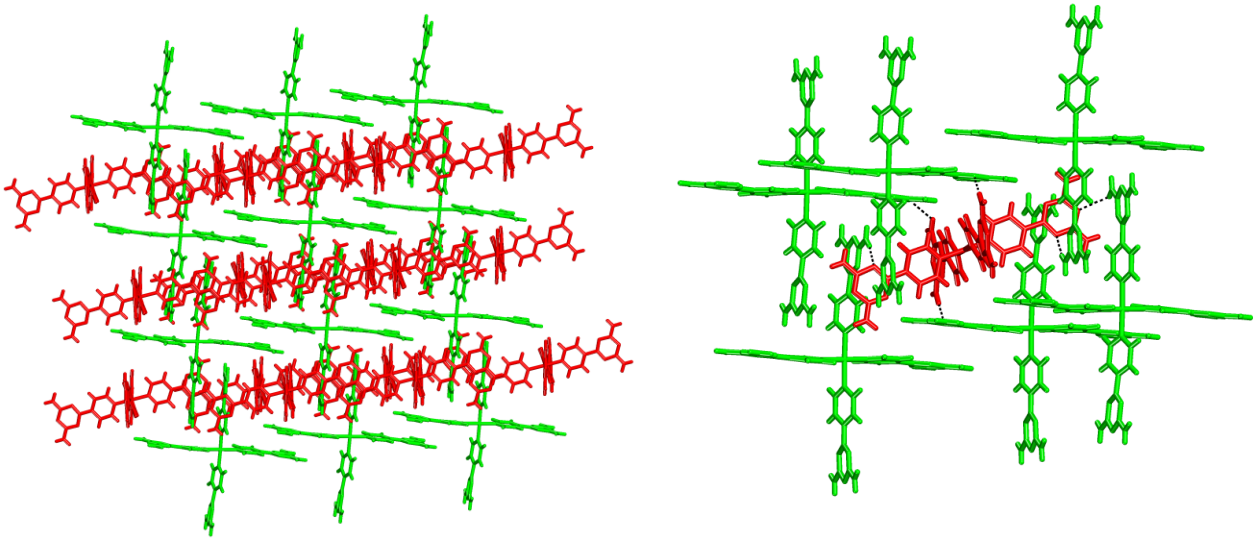

c **d**

Figure 6. Structure of complex $[Pd(\mathbf{3a})_4](BF_4)_2 \bullet 9\ H_2O$ in crystals grown from DMSO/H_2O/MeCN. Except where noted otherwise, carbon atoms are shown in gray, hydrogen atoms in white, boron atoms in orange, nitrogen atoms in blue, fluorine atoms in green, and palladium atoms in rose. (a) Thermal atomic displacement ellipsoid plot, with ellipsoids of non-hydrogen atoms drawn at the 50% probability level and hydrogen atoms represented by a sphere of arbitrary size. Key bond lengths include Pd1-N10 = 2.031(3) Å, Pd1-N20 = 2.024(4) Å, Pd1-N30 = 2.027(3) Å, and Pd1-N40 = 2.029(3) Å. Representative bond angles include N10-Pd1-N20 = 89.42(13)°. (b) View showing the construction of cationic grids built from tetrameric aggregates. Guest molecules of H_2O and BF_4^- are omitted for clarity. (c) View illustrating the interpenetration of grids, with one drawn in green and three independent grids in red. (d) View showing N-H···N hydrogen bonds between molecules in the green and red grids.

Table 2. Crystallographic Data for 1:4 Complexes of Pd(II) with Pyridinyl-Substituted Diaminotriazines **3a-b** and **4a-b**.

complex	Pd(**3a**)$_4^{+2}$ • 2 BF_4^- • 9 H_2O	Pd(**3b**)$_4^{+2}$ • 2 NO_3^- • 5 DMSO • 2 H_2O • MeOH	Pd(**4a**)$_4^{+2}$ • PF_6^- • OH^- • 4 H_2O • 2 EtOH	Pd(**4b**)$_4^{+2}$ • 2 NO_3^- • 6 DMSO • 4 H_2O
crystallization medium	DMSO/H_2O/MeCN	DMSO/H_2O/MeOH	DMSO/H_2O/EtOH	DMSO/H_2O
formula	$C_{32}H_{50}B_2F_8N_{24}O_9Pd$	$C_{67}H_{86}N_{26}O_{14}PdS_5$	$C_{36}H_{53}F_6N_{24}O_7PPd$	$C_{68}H_{92}N_{26}O_{16}PdS_6$
crystal system	monoclinic	triclinic	monoclinic	monoclinic
space group	$P2_1/n$	P-1	$C2/m$	$C2/m$
a (Å)	15.2752(3)	11.4019(17)	12.914(3)	20.6228(6)
b (Å)	18.5707(4)	16.516(2)	20.449(3)	21.2334(6)
c (Å)	17.5545(4)	24.136(3)	11.744(4)	15.2728(5)
α (°)	90	95.452(7)	90	90
β (°)	98.680(1)	91.174(6)	101.709(6)	126.999(1)
γ(°)	90	108.713(6)	90	90
V (Å^3)	4922.67(18)	4279.2(11)	3036.9(12)	5341.2(3)
Z	4	2	2	2
ρ_{calc} (g cm^{-3})	1.612	1.355	1.296	1.132
T (K)	200	150	150	150
μ (mm^{-1})	3.987	3.500	3.400	3.016
R_1, $I>2\sigma(I)$	0.0769	0.0709	0.0528	0.0620
R_1, all data	0.0791	0.0901	0.0529	0.0623
wR_2, $I>2\sigma(I)$	0.1869	0.1536	0.1736	0.1579
wR_2, all data	0.1884	0.1560	0.1739	0.1585
measured reflections	67694	60316	24003	41486
independent reflections	8948	15194	2709	4841
observed reflections [$I>2\sigma(I)$]	7082	6471	2703	4337

The resulting metallotecton has a molecular structure that adheres closely to expectations; moreover, it appears to be properly designed to create a robust open rectangular grid held together by hydrogen bonding of four tetragonally directed DAT groups. In fact, however, the observed structure is relatively compact and can be considered to be built from the tetrameric units shown in Figure 6b, in which face-to-face and edge-to-face aromatic interactions of DAT groups are present but normal hydrogen bonds are absent. Interpenetration of the resulting cationic grids (Figure 6c) leads to a three-dimensional structure in which each molecule in a grid forms a total of six N-H···N hydrogen bonds with six adjacent molecules in an interpenetrating grid (Figure 6d). In addition, H_2O and BF_4^- included within the structure engage in extensive hydrogen bonding.

(b) Structure of the 4:1 Complex of 6-[4-(Pyridin-4-yl)phenyl]-1,3,5-triazine-2,4-diamine (3b) with $Pd(NO_3)_2$. To further assess the potential of pyridinyl-substituted diaminotriazines to form metallotectons related to complex **7**, we examined the product of the reaction of extended ligand **3b** with $Pd(NO_3)_2$. Crystals grown from DMSO/H_2O/MeOH were found to have the composition $[Pd(\mathbf{3b})_4](NO_3)_2 \bullet 5$ DMSO $\bullet$ 2 H_2O $\bullet$ MeOH and to belong to the triclinic space group *P*-1. Views of the structure are presented in Figure 7, and other crystallographic data are provided in Table 2. Again, the pyridinyl groups of the ligand bind Pd(II) to give a square-planar complex (Figure 7a), with normal Pd-N distances.[14] The ligands adopt a variety of nonplanar conformations, and their average planes lie an average angle of 36.0(3)° with respect to the PdN_4 core of the metallotecton.

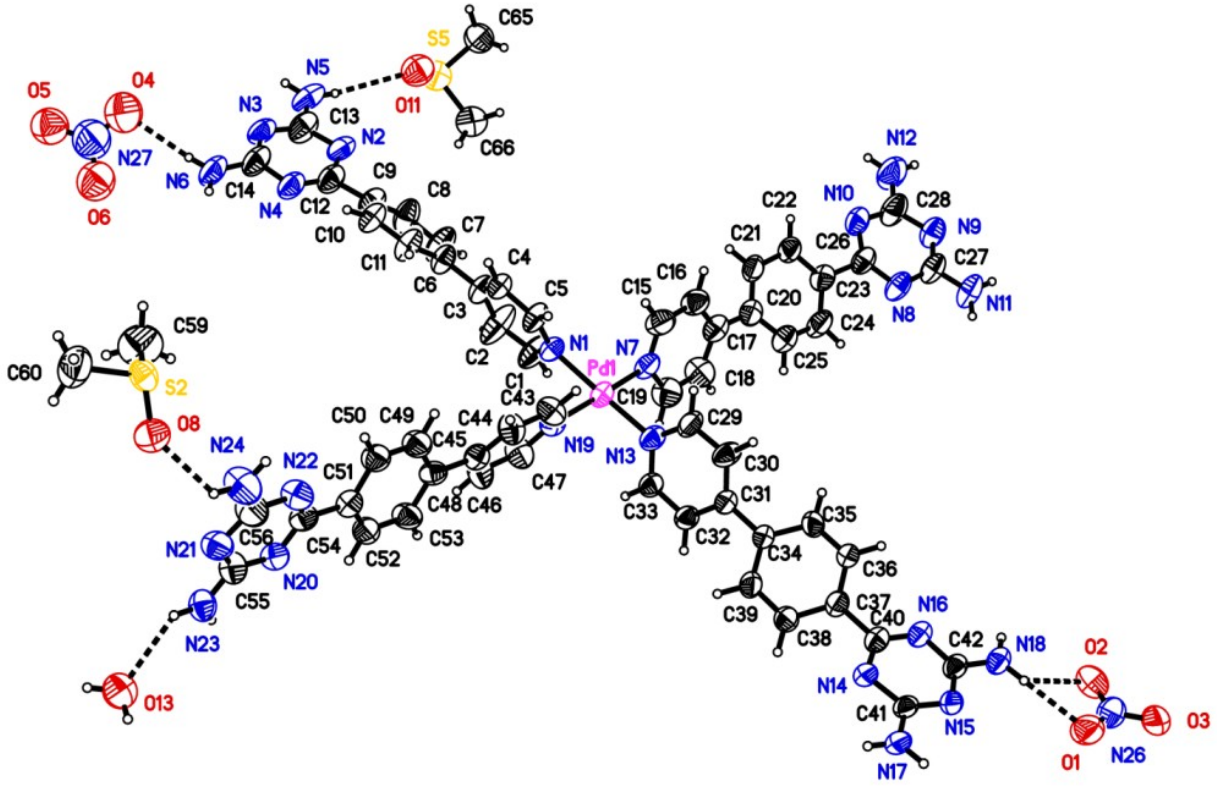

a

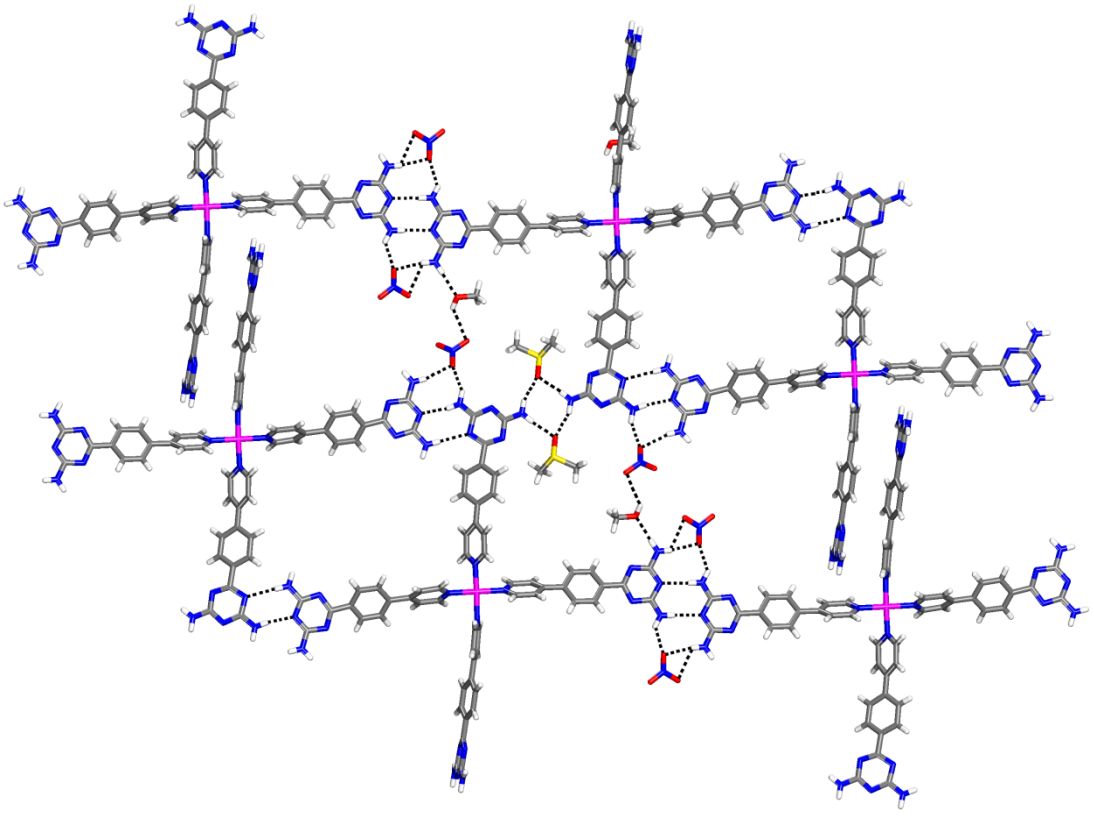

b

Figure 7. Structure of complex $[Pd(\mathbf{3b})_4](NO_3)_2 \bullet 5$ DMSO $\bullet$ 2 $H_2O \bullet$ MeOH in crystals grown from DMSO/H_2O/MeOH. Hydrogen bonds are represented by broken lines. Carbon atoms are shown in gray, hydrogen atoms in white, nitrogen atoms in blue, oxygen atoms in red, sulfur atoms in yellow, and palladium atoms in rose. (a) Thermal atomic displacement ellipsoid plot, with ellipsoids of non-hydrogen atoms drawn at the 50% probability level and hydrogen atoms represented by a sphere of arbitrary size. Key bond lengths include Pd1-N1 = 2.032(5) Å, Pd1-N7 = 1.983(5) Å, Pd1-N13 = 1.997(5) Å, and Pd1-N19 = 2.023(5) Å. Representative bond angles include N1-Pd1-N7 = 90.07(19)°. (b) View showing how N-H···N hydrogen bonds of type **II** (average distance = 3.084(9) Å) join the metallotectons to form dimers, which interact with adjacent dimers by additional N-H···N hydrogen bonds of type **I** (3.054(7) Å), N-H···O hydrogen bonds involving bridging molecules of DMSO (average distance = 2.936(8) Å), and aromatic interactions.

Two arms of each metallotecton participate in the formation of a total of four N-H···N hydrogen bonds of type **II** to form characteristic dimers (Figure 7b), which associate with adjacent dimers to form sheets held together by additional N-H···N hydrogen bonds of type **I**, N-H···O hydrogen bonds involving bridging molecules of DMSO, and aromatic interactions. All hydrogen bonding between DAT groups is reinforced by bridging nitrate anions.

As planned, both ligand **3a** and extended version **3b** form square-planar dicationic Pd(II) complexes analogous to structure **7**. The resulting metallotectons have similar topologies and a shared ability to engage in hydrogen bonding directed by peripheral DAT groups, yet their patterns of association are distinctly different. The observed differences may arise in part because the counterions are not the same and because the crystallizations are necessarily conducted in solvents that can compete with DAT groups as participants in hydrogen bonding.

(c) Structure of the 4:1 Complex of 6-(Pyridin-3-yl)-1,3,5-triazine-2,4-diamine (4a) with $Pd(PF_6)_2$. The solid formed by the reaction of $Pd(BF_4)_2$ with isomeric ligand **4a** proved to have low solubility, so it was subjected to metathesis by the addition of excess $NaPF_6$ in H_2O/MeCN, and crystals of the ion-exchanged product were grown from DMSO/H_2O/EtOH. They were found to have the composition $[Pd(\mathbf{4a})_4](PF_6)(OH) \cdot 4\ H_2O \cdot 2$ EtOH and to belong to the monoclinic space group *C*2/*m*. Views of the structure are shown in Figure 8, and other crystallographic data are presented in Table 2. As expected, a square-planar complex is formed (Figure 8a), with a normal Pd-N distance.[14] The ligands adopt flattened conformations, and their average planes lie at an average angle of 63.9(1)° with respect to the PdN_4 core of the metallotecton. The DAT groups of trans-disposed ligands have an opposed orientation, with one DAT group above the PdN_4 plane and the other below it.

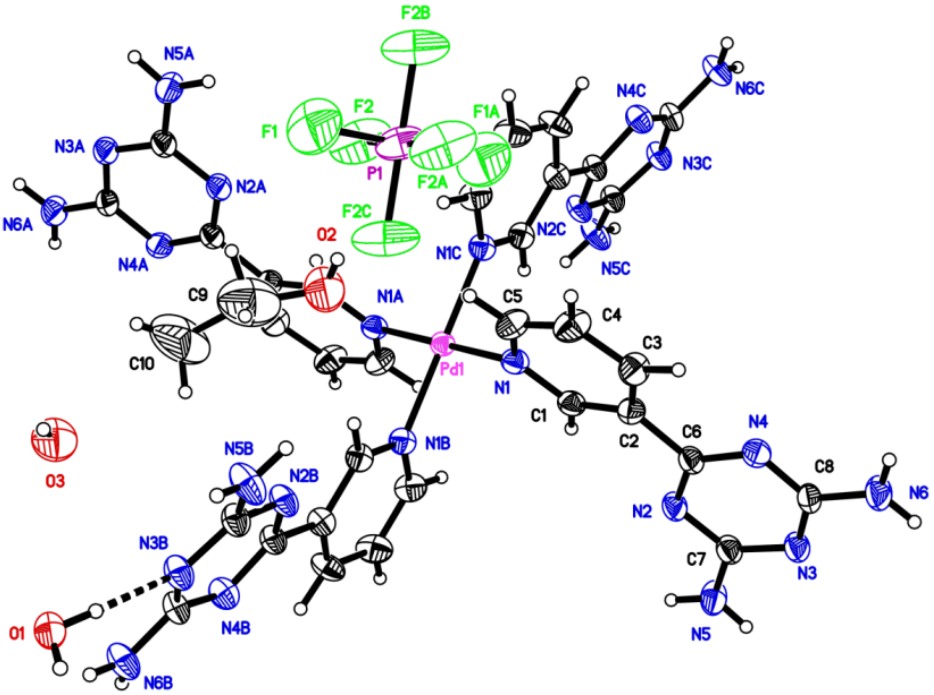
F2B
N5A
F2
F1
F1A
N4C
N6C
N3A
P1
N3C
F2A
N2A
N6A
F2C
O2
N2C
N1C
N5C
N4A
C9
N1A
C5
C4
C10
C3
Pd1
N1
C1
C2
C6
N4
O3
N5B
N1B
C8
N2B
N2
N6
N3B
C7
N3
N4B
O1
N5
N6B

a

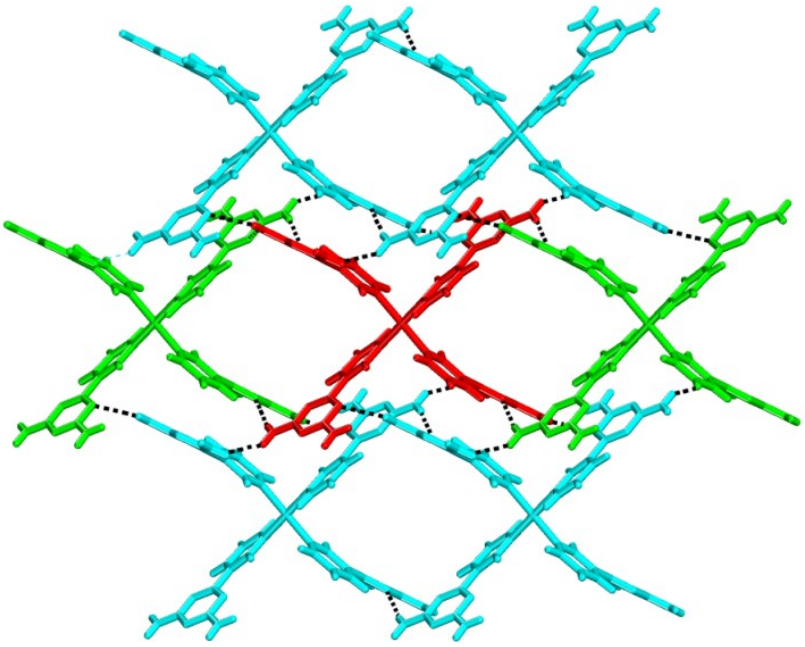

b

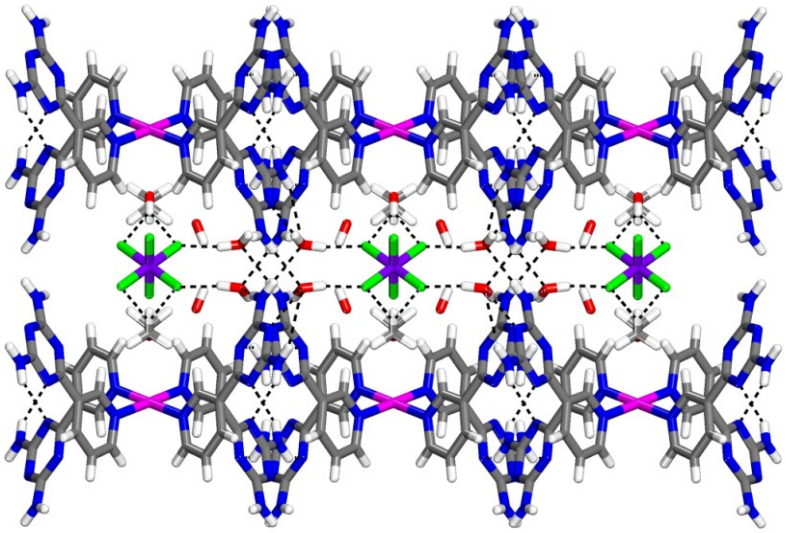

c

Figure 8. Structure of complex $[Pd(\mathbf{4a})_4](PF_6)(OH) \bullet 4\ H_2O \bullet 2$ EtOH in crystals grown from DMSO/H_2O/EtOH. Except where noted otherwise, carbon atoms are shown in gray, hydrogen atoms in white, nitrogen atoms in blue, fluorine atoms in green, phosphorus atoms in purple, and palladium atoms in rose. (a) Thermal atomic displacement ellipsoid plot, with ellipsoids of non-hydrogen atoms drawn at the 50% probability level and hydrogen atoms represented by a sphere of arbitrary size. Key bond lengths include Pd1-N1 = 2.023(4) Å. Representative bond angles include N1-Pd1-N1B = 90.95(19)°. (b) View showing the formation of cationic sheets in the *ab* plane, in which the four DAT groups of a central metallotecton (red) engage in a total of sixteen N-H···N hydrogen bonds with six neighbors (blue and green). Each DAT group forms two N-H···N hydrogen bonds of type **III** (3.091(6) Å) involving the two neighbors shown in green, as well as two additional single N-H···N hydrogen bonds (3.069(6) Å) with neighbors in red. In addition, the structure is reinforced by aromatic interactions. Neutral guests and counterions are omitted for clarity. (c) View along the *a* axis showing how cationic sheets of the metallotecton are separated by intervening anionic layers containing hydrogen-bonded PF_6^-, disordered OH^-, H_2O, and EtOH.

The structure can be considered to consist of cationic sheets in the *ab* plane, in which the four DAT groups of each metallotecton participate in a total of sixteen N-H···N hydrogen bonds (Figure 8b). Each DAT group engages in two N-H···N hydrogen bonds of type **III**, as well as two additional single N-H···N hydrogen bonds. The extensively hydrogen-bonded structure is also reinforced by aromatic interactions. The cationic sheets are separated by intervening anionic layers containing hydrogen-bonded PF_6^-, disordered OH^-, H_2O, and EtOH (Figure 8c). Again, the complexation of ligand **4a** with Pd(II) occurs predictably to give a square planar metallotecton analogous to structure **7**, and the peripheral DAT groups play a key role in directing molecular association by engaging in hydrogen bonds according to established patterns.

(d) Structure of the 4:1 Complex of 6-[4-(Pyridin-3-yl)phenyl]-1,3,5-triazine-2,4-diamine (4b) with $Pd(NO_3)_2$. To complete our assessment of the ability of pyridinyl-substituted diaminotriazines to form metallotectons related to complex **7**, we examined the product of the reaction of extended ligand **4b** with $Pd(NO_3)_2$. Crystals grown from DMSO/H_2O proved to have the approximate composition $[Pd(\mathbf{4b})_4](NO_3)_2$ • 6 DMSO • 4 H_2O and to belong to the monoclinic space group *C*2/*m*. Figure 9 provides views of the structure, and Table 2 summarizes other crystallographic data. As planned, coordination yields a square-planar complex (Figure 9a), with a normal Pd-N distance.[14] The ligands adopt flattened conformations, and their average planes form an average angle of 76.3(1)° with respect to the PdN_4 core of the metallotecton. The DAT groups of trans-disposed ligands have an opposed orientation, with one DAT group above the PdN_4 plane and the other below it, giving the metallotecton an elongated topology. As shown in Figure 9b, the metallotectons associate to form sheets maintained by N-H···N hydrogen bonds of type **I**. Other interactions help control the overall molecular organization, including N-H···O hydrogen bonds involving two types of bridging DMSO, one that reinforces motif **I** (average N-

H···O distance = 2.888(6) Å) and the other that helps orient adjacent arms of each metallotecton (N-H···O distance = 3.038(3) Å).

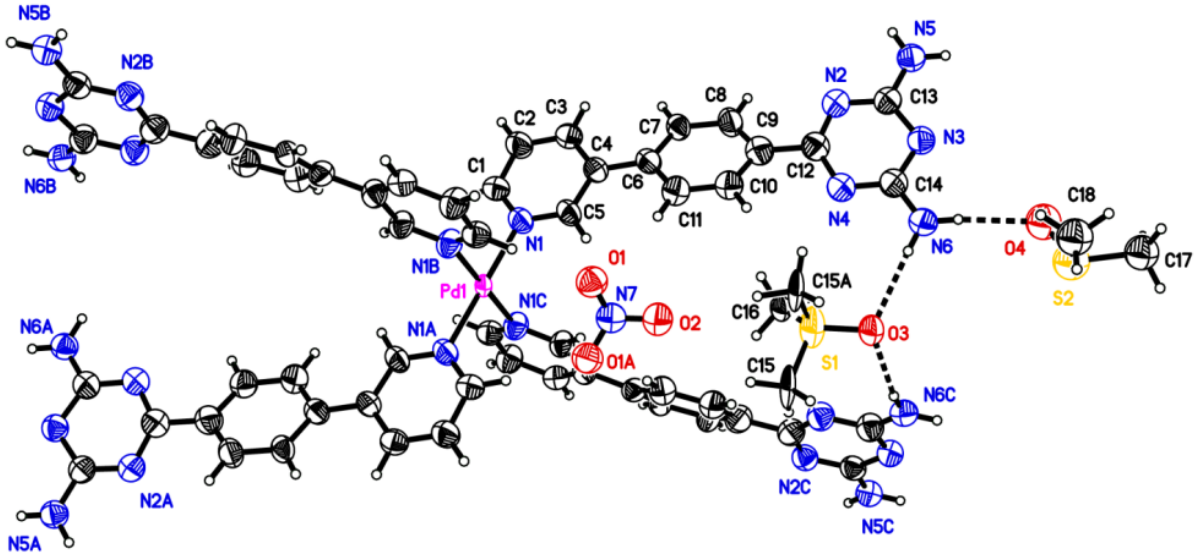

a

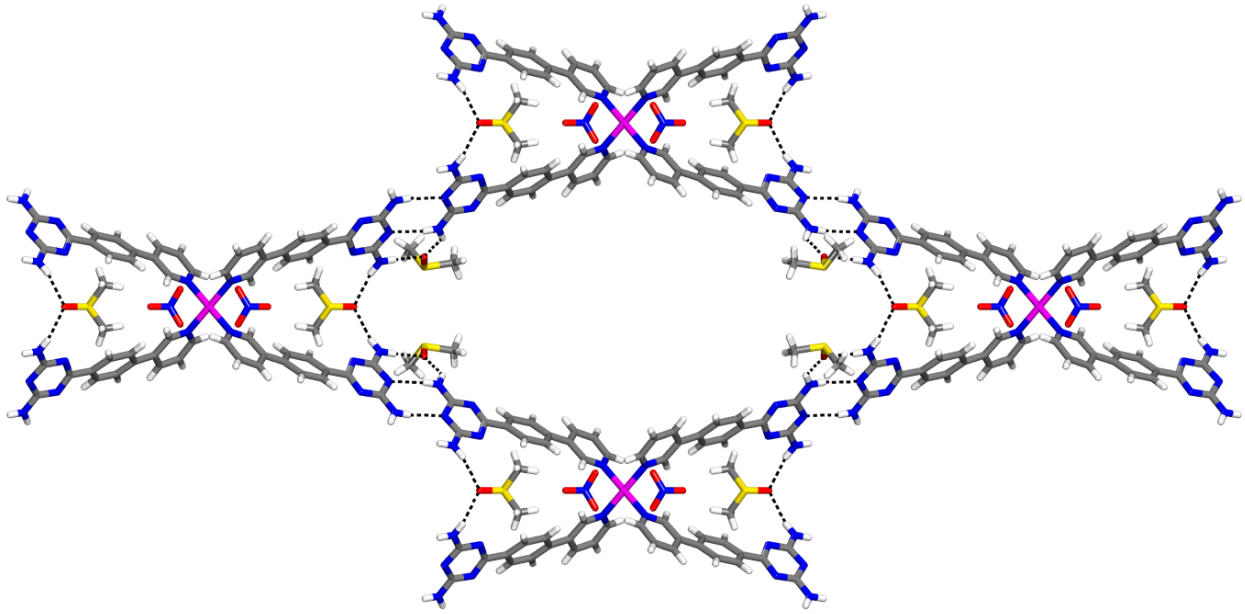

b

Figure 9. Structure of complex $[Pd(\mathbf{4b})_4](NO_3)_2$ • 6 DMSO • 4 H_2O in crystals grown from DMSO/H_2O. Hydrogen bonds are represented by broken lines. Carbon atoms are shown in gray, hydrogen atoms in white, nitrogen atoms in blue, oxygen atoms in red, sulfur atoms in yellow, and palladium atoms in rose. (a) Thermal atomic displacement ellipsoid plot, with ellipsoids of non-hydrogen atoms drawn at the 50% probability level and hydrogen atoms represented by a sphere of arbitrary size. Key bond lengths include Pd1-N1 = 2.046(2) Å. Representative bond angles include N1-Pd1-N1B = 90.81(11)°. (b) View showing the formation of sheets held together by N-H···N hydrogen bonds of type **I** (2.955(5) Å), reinforced by N-H···O hydrogen bonds involving bridging molecules of DMSO.

Conclusions

Our results provide a deeper understanding of how coordinative bonds to metals can be used in conjunction with other interactions to direct molecular assembly. In particular, our work illustrates how materials with predictable structural features can be built from metallotectons, which are well-defined complexes incorporating ligands that can bind metals and can simultaneously engage in multiple intercomplex interactions according to reliable motifs. To further gauge the potential of this approach, we have examined the behavior of Pd(II) complexes of ligands **3a-b**, **4a-b**, and **6**, which incorporate pyridinyl groups to bind metals and DAT groups to help ensure participation in reliable intermolecular hydrogen bonds.

As planned, based on established patterns of coordination involving pyridine and simple derivatives, ligands **3a-b**, **4a-b**, and **6** all bind Pd(II) to gave square-planar complexes with predicted constitutions. Although the precise geometry of the resulting metallotectons could not be foreseen with confidence, in all cases the ligands adopted normal flattened conformations and maintained expected orientations with respect to the PdL_4 core. As anticipated, subsequent association of the resulting metallotectons was found to be directed in part by their logical topologies and by the ability of the peripheral DAT groups to engage in intermolecular hydrogen bonding according to established motifs **I-III**. In only one case were such interactions not present.

Complexes of ligands **3a-b**, **4a-b**, and **6** have shared structural features that can be considered to be introduced reliably by design. However, comparisons of molecular organization reveal few striking analogies and structural details vary widely, particularly in the ionic PdL_4^{+2} complexes. These differences presumably reflect diverse factors, such as the contributions of

ionic interactions, the role of the specific anions, and competitive hydrogen bonding involving molecules of solvent.

Despite the present lack of perfect control, our work nevertheless affirms the promise of designing new ordered materials based on the hybrid inorganic/organic strategy of using metallotectons. A conspicuous advantage of this strategy is that the molecular core can be constructed spontaneously by coordination, and peripheral functionality can independently control how the complexes are positioned with respect to their neighbors.

Experimental Section

General Notes. 6-(Pyridin-4-yl)-1,3,5-triazine-2,4-diamine (**3a**),[8] 6-[4-(pyridin-4-yl)phenyl]-1,3,5-triazine-2,4-diamine (**3b**),[9] 6-(pyridin-3-yl)-1,3,5-triazine-2,4-diamine (**4a**),[10] 6-[4-(pyridin-3-yl)phenyl]-1,3,5-triazine-2,4-diamine (**4b**)[11], and 6-(pyridin-2-yl)-1,3,5-triazine-2,4-diamine (**6**)[15] were prepared by reported methods. Their complexes with Pd(II) were made by the procedures summarized below. Other chemicals were purchased from commercial sources and used without further purification.

General Procedure for Preparing $PdCl_2$ Complexes of Ligands 3a-b, 4a-b, and 6. A stirred suspension of $PdCl_2$ (1.0 equiv) and the ligand (2.0 equiv in the cases of compounds **3a-b** and **4a-b**; 1.0 equiv in the case of compound **6**) was heated at reflux in MeCN (20 mL) for 12 h. The resulting mixture was cooled, and precipitated solids were separated by filtration, washed thoroughly with H_2O, MeCN, and acetone, and then finally dried under vacuum before being purified by crystallization.

2:1 Complex of 6-(Pyridin-4-yl)-1,3,5-triazine-2,4-diamine (3a) with $PdCl_2$ (Orthorhombic Form). The reaction of ligand **3a** (51 mg, 0.27 mmol) with $PdCl_2$ (24 mg, 0.14 mmol) according to the general procedure yielded the crude 2:1 complex (62 mg, 0.11 mmol, 81%). Pale yellow crystals of composition $PdCl_2$(**3a**)$_2$ • 2 DMSO were grown by allowing H_2O to diffuse slowly into a solution in DMSO: IR (ATR) 3429, 3330, 3202, 1651, 1614, 1529, 1445, 1421, 1398, 1061, 811 cm^{-1}; HRMS (ESI) calcd for $[C_{16}H_{16}ClN_{12}Pd]^+$ *m/e* 517.03388, found 517.03406.

2:1 Complex of 6-(Pyridin-4-yl)-1,3,5-triazine-2,4-diamine (3a) with $PdCl_2$ (Triclinic Form). The crude 2:1 complex was prepared as described above, and pale yellow crystals of composition $PdCl_2$(**3a**)$_2$ • 2 DMSO • dioxane were grown by slow evaporation of a solution in DMSO/dioxane: IR (ATR) 3429, 3330, 3202, 1651, 1614, 1529, 1445, 1421, 1398, 1061, 811 cm^{-1}; HRMS (ESI) calcd for $[C_{16}H_{16}ClN_{12}Pd]^+$ *m/e* 517.03388, found 517.03406.

2:1 Complex of 6-[4-(Pyridin-4-yl)phenyl]-1,3,5-triazine-2,4-diamine (3b) with $PdCl_2$. The reaction of ligand **3b** (80 mg, 0.30 mmol) with $PdCl_2$ (27 mg, 0.15 mmol) according to the general procedure yielded the crude 2:1 complex (88 mg, 0.12 mmol, 80%). Pale yellow crystals of composition $PdCl_2$(**3b**)$_2$ were grown by slow evaporation of a solution in DMSO/EtOAc: IR (ATR) 3481, 3435, 3395, 3303, 3129, 1613, 1586, 1520, 1436, 1396, 808 cm^{-1}; HRMS (ESI) calcd for $[C_{28}H_{24}ClN_{12}Pd]^+$ *m/e* 669.09648, found 669.09845. Anal. Calcd for $C_{28}H_{24}Cl_2N_{12}Pd$: C, 47.64; H, 3.43; N, 23.81. Found: C, 47.49; H, 3.27; N, 23.32.

2:1 Complex of 6-(Pyridin-3-yl)-1,3,5-triazine-2,4-diamine (4a) with $PdCl_2$. The reaction of ligand **4a** (74 mg, 0.39 mmol) with $PdCl_2$ (35 mg, 0.20 mmol) according to the general procedure yielded the crude 2:1 complex (79 mg, 0.14 mmol, 72%). Pale yellow crystals of composition $PdCl_2$(**4a**)$_2$ • 3 DMSO were grown by slow evaporation of a solution in DMSO:

IR (ATR) 3465, 3382, 3323, 3196, 3140, 1626, 1614, 1546, 1397, 805 cm^{-1}; HRMS (ESI) calcd for $[C_{16}H_{16}ClN_{12}Pd]^+$ *m/e* 517.03388, found 517.03405. Anal. Calcd for $C_{16}H_{16}Cl_2N_{12}Pd \bullet H_2O$: C, 33.61; H, 3.17; N, 29.40. Found: C, 33.37; H, 3.06; N, 28.68.

1:1 Complex of 6-(Pyridin-2-yl)-1,3,5-triazine-2,4-diamine (6) with $PdCl_2$. The reaction of ligand **6** (67 mg, 0.36 mmol) with $PdCl_2$ (63 mg, 0.36 mmol) according to the general procedure yielded the crude 1:1 complex (116 mg, 0.32 mmol, 89%). Yellow crystals of composition $PdCl_2$(**6**) were grown by slow evaporation of a solution in DMSO/H_2O: IR (ATR) 3448, 3400, 3188, 3119, 1659, 1634, 1581, 1518, 1489, 1397, 1262, 1058, 1031, 779 cm^{-1}; HRMS (ESI) calcd for $[C_8H_8ClN_6Pd]^+$ *m/e* 328.95283, found 328.95347. Anal. Calcd for $C_8H_8Cl_2N_6Pd$: C, 26.29; H, 2.21; N, 22.91. Found: C, 26.28; H, 2.26; N, 22.35.

General Procedures for Preparing Other Pd(II) Complexes of Ligands 3a-b and 4a-b. A stirred suspension of $Pd(BF_4)_2$ or $Pd(NO_3)_2$ (1.0 equiv) and the ligand (4.0 equiv) was heated at reflux in MeCN (20 mL) for 12 h. The resulting mixture was cooled, and precipitated solids were separated by filtration, washed thoroughly with H_2O, MeCN, and acetone, and then finally dried under vacuum before being purified by crystallization. In the case of the complex of ligand **4a** with $Pd(BF_4)_2$, the crude product was subjected to ion exchange before crystallization by treatment with excess $NaPF_6$ in H_2O/MeCN.

4:1 Complex of 6-(Pyridin-4-yl)-1,3,5-triazine-2,4-diamine (3a) with $Pd(BF_4)_2$. The reaction of ligand **3a** (80 mg, 0.43 mmol) with $Pd(BF_4)_2 \bullet 4$ MeCN (47 mg, 0.11 mmol) according to the general procedure yielded the crude 4:1 complex (87 mg, 0.084 mmol, 78%). Colorless crystals of composition $[Pd(\mathbf{3a})_4](BF_4)_2 \bullet 9\ H_2O$ were grown by allowing H_2O and MeCN to diffuse slowly into a solution in DMSO: IR (ATR) 3500-3000 (b), 1615, 1425, 1392, 1301, 1217, 957, 821 cm^{-1}; HRMS (ESI) calcd for $[C_{32}H_{32}N_{24}Pd]^{+2}$ *m/e* 429.11383, found

429.11505. Anal. Calcd for $C_{32}H_{32}B_2F_8N_{24}Pd \bullet 2\ H_2O$: C, 35.96; H, 3.40; N, 31.45. Found: C, 35.91; H, 3.10; N, 30.86.

4:1 Complex of 6-[4-(Pyridin-4-yl)phenyl]-1,3,5-triazine-2,4-diamine (3b) with $Pd(NO_3)_2$. The reaction of ligand **3b** (55 mg, 0.21 mmol) with $Pd(NO_3)_2$ (12 mg, 0.052 mmol) according to the general procedure yielded the crude 4:1 complex (57 mg, 0.044 mmol, 85%). Yellow crystals of composition $[Pd(\mathbf{3b})_4](NO_3)_2 \bullet 5$ DMSO $\bullet 2\ H_2O \bullet$ MeOH were grown by allowing H_2O and MeOH to diffuse slowly into a solution in DMSO: IR (ATR) 3319, 3100 (b), 1612, 1526, 1438, 1394, 1324, 811 cm^{-1}; HRMS (ESI) calcd for $[C_{56}H_{48}N_{24}Pd]^{+2}$ *m/e* 581.17588, found 581.17864. Anal. Calcd for $C_{56}H_{48}N_{26}O_6Pd$: C, 52.24; H, 3.76; N, 28.28. Found: C, 52.30; H, 3.71; N, 27.74.

4:1 Complex of 6-(Pyridin-3-yl)-1,3,5-triazine-2,4-diamine (4a) with $Pd(PF_6)_2$. The reaction of ligand **4a** (76 mg, 0.40 mmol) with $Pd(BF_4)_2 \bullet 4$ MeCN (45 mg, 0.10 mmol) according to the general procedure yielded a solid, which was then treated with $NaPF_6$ (67 mg, 0.40 mmol) in a mixture of H_2O (10 mL) and MeCN (10 mL) to give the crude 4:1 complex (82 mg, 0.071 mmol, 71%). Colorless crystals of composition $[Pd(\mathbf{4a})_4](PF_6)(OH) \bullet 4\ H_2O \bullet 2$ EtOH were grown by allowing H_2O and EtOH to diffuse slowly into a solution in DMSO: IR (ATR) 3469, 3349, 3100 (b), 1625, 1536, 1450, 1382, 1023, 807 cm^{-1}; HRMS (ESI) calcd for $[C_{32}H_{32}N_{24}Pd]^{+2}$ *m/e* 429.11383, found 429.11355.

4:1 Complex of 6-[4-(Pyridin-3-yl)phenyl]-1,3,5-triazine-2,4-diamine (4b) with $Pd(NO_3)_2$. The reaction of ligand **4b** (60 mg, 0.23 mmol) with $Pd(NO_3)_2$ (14 mg, 0.061 mmol) according to the general procedure yielded the crude 4:1 complex (65 mg, 0.050 mmol, 87%). Yellow crystals of composition $[Pd(\mathbf{4b})_4](NO_3)_2 \bullet 6$ DMSO $\bullet 4\ H_2O$ were grown by allowing H_2O to diffuse slowly into a solution in DMSO: IR (ATR) 3475, 3307, 3166, 1623, 1527, 1447,

1390, 789 cm^{-1}; HRMS (ESI) calcd for $[C_{56}H_{48}N_{24}Pd]^{+2}$ *m/e* 581.17588, found 581.17864. Anal. Calcd for $C_{56}H_{48}N_{26}O_6Pd$: C, 52.24; H, 3.76; N, 28.28. Found: C, 52.21; H, 3.72; N, 27.35.

X-Ray Crystallographic Studies. Crystallographic data were collected with Cu Kα radiation at the temperatures indicated in Tables 1 and 2 using a Bruker Microstar diffractometer equipped with a rotating anode. Intensity data were integrated using the *SAINT* program,[16] and semi-empirical absorption corrections were applied using the *SADABS* program.[17] The structures were solved by direct methods, and non-hydrogen atoms were refined anisotropically on F^2 with full least squares using the SHELXL-97 software package.[18] In most cases, hydrogen atoms of ligands and guest molecules were treated by first locating them from difference Fourier maps, recalculating their positions using standard values for distances and angles, and then refining them as riding atoms. Hydrogen atoms from water molecules were located directly and refined using restraints.

In complex $PdCl_2$(**3a**)$_2$ • 2 DMSO, the complex and the included molecules of DMSO lie on a two-fold axis, which results in statistical disorder over two positions with a half-occupancy factor for each atom of chlorine and DMSO. Certain molecules of DMSO are also disordered in the crystals $PdCl_2$(**3a**)$_2$ • 2 DMSO • dioxane, $PdCl_2$(**4a**)$_2$ • 3 DMSO, and [Pd(**3b**)$_4$]$(NO_3)_2$ • 5 DMSO • 2 H_2O • MeOH. In crystals [Pd(**4b**)$_4$]$(NO_3)_2$ • 6 DMSO • 4 H_2O, DMSO lies on a mirror plane, giving two alternative positions for one of the methyl groups with a half-occupancy factor. In certain cases, guest molecules proved to be significantly disordered and could not be modeled properly; therefore, the SQUEEZE option in the *PLATON* software package[19] was used to calculate the region of solvent disorder and to remove its contribution from the overall intensity data.

In the case of crystals $[Pd(\mathbf{4a})_4](PF_6)(OH) \bullet 4\ H_2O \bullet 2$ EtOH, the structural solution led to the position of the Pd center with one attached ligand **4a**, half a PF_6^- counterion, three atoms from a guest molecule of EtOH, and two isolated atoms of oxygen. After subsequent cycles of least-squares refinement, the positions of two atoms of hydrogen linked to one of the isolated atoms of oxygen were clearly visible in the Fourier difference map, revealing a molecule of H_2O that is doubly hydrogen bonded. The second isolated atom of oxygen was found to be disordered over four symmetry-related positions. The closest peak of high electron density found in the difference Fourier map was attributed to an atom of hydrogen, thereby defining an OH^- and assuring charge balance in the crystal lattice.

Acknowledgments

We are grateful to the Natural Sciences and Engineering Research Council of Canada, the Ministère de l'Éducation du Québec, the Canada Foundation for Innovation, the Canada Research Chairs Program, and Université de Montréal for financial support.

Supporting Information Available. Tables of structural data in CIF format. This material is available free of charge via the Internet at http://pubs.acs.org.

Notes and References

1. Bragg, W. L. *Proc. Roy. Soc. London* **1913**, *89*, 248-277.
2. Allen, F. H. *Acta Crystallogr.* **2002**, *B58*, 380-388.
3. Dunitz, J. D.; Gavezzotti, A. *Chem. Soc. Rev.* **2009**, *38*, 2622-2633. Dunitz, J. D. *Chem. Commun.* **2003**, 545-548. Desiraju, G. R. *Nature Materials* **2002**, *1*, 77-79. Gavezzotti, A. *Acc. Chem. Res.* **1994**, *27*, 309-314. Maddox, J. *Nature* **1988**, *335*, 201.

4. For references, see: Ward, M. D. *Struct. Bond.* **2009**, *132*, 1-23. Robson, R. *Dalton Trans.* **2008**, 5113-5131. Wuest, J. D. *Chem. Commun.* **2005**, 5830-5837. Hosseini, M. W. *Acc. Chem. Res.* **2005**, *38*, 313-323. Nangia, A.; Desiraju, G. R. *Top. Curr. Chem.* **1998**, *198*, 57-95. Desiraju, G. R. *Angew. Chem., Int. Ed*. **1995**, *34*, 2311-2327. Etter, M. C. *Acc. Chem. Res.* **1990**, *23*, 120-126.

5. Telfer, S. G.; Wuest, J. D. *Cryst. Growth. Des.* **2009**, *9*, 1923-1931. Wan, C.-Q.; Li, G.-S.; Chen, X.-D.; Mak, T. C. W. *Cryst. Growth Des.* **2008**, *8*, 3897-3901. Constable, E. C.; Housecroft, C. E.; Neuberger, M.; Schaffner, S.; Schaper, F. *Inorg. Chem. Commun.* **2006**, *9*, 433-436.

6. For reviews, see: Braga, D.; Brammer, L.; Champness, N. R. *CrystEngComm* **2005,** *7*, 1-19. Brammer, L. *Chem. Soc. Rev.* **2004**, *33*, 476-489. Aakeröy, C. B.; Beatty, A. M. In *Comprehensive Coordination Chemistry II*; McCleverty, J. A., Meyer, T. J., Lever, A. B. P., Eds.; Elsevier : Oxford, 2004; Vol. 1, pp 679-688. Beatty, A. M. *Coord. Chem. Rev.* **2003**, *246*, 131-143.

7. Ouerfelli, I.; Gatri, R.; Efrit, M. L.; Dua, N.; Perruchon, J.; Golhen, S.; Toupet, L.; Fillaut, J.-L. *J. Organomet. Chem.* **2011**, *696*, 670-675. Santillan, G. A.; Carrano, C. J. *Dalton Trans.* **2009**, 6599-6605. McMorran, D. A. *Inorg. Chem.* **2008**, *47*, 592-601. Salazar-Mendoza, D.; Baudron, S. A.; Hosseini, M. W. *Chem. Commun.* **2007**, 2252-2254. Braga, D.; Giaffreda, S. L.; Grepioni, F.; Maini, L.; Polito, M. *Coord. Chem. Rev.* **2006**, *250*, 1267-1285. Goldberg, I. *Chem. Commun.* **2005**, 1243-1254.Katsuki, I.; Motoda, Y.; Sunatsuki, Y.; Matsumoto, N.; Nakashima, T.; Kojima, M. *J. Am. Chem. Soc.* **2002**, *124*, 629-640.

8. Chan, C.-W.; Mingos, D. M. P.; White, A. J. P.; Williams, D. J. *Polyhedron* **1996**, *15*, 1753-1767.

9. Duong, A.; Dubois, M.-A.; Maris, T.; Métivaud, V.; Yi, J.-H.; Nanci, A.; Rochefort, A.; Wuest, J. D. *J. Phys. Chem. C*, submitted for publication.

10. Baibulova, M. S.; Akkulova, Z. G.; Afanas'eva, T. A. *Izv. Akad. Nauk Kazakh. SSR, Ser. Khim.* **1989**, 40-42.
11. Duong, A.; Maris, T.; Wuest, J. D. *Cryst. Growth Des.* **2011**, *11*, 287-294.
12. For recent references, see: Maly, K. E.; Gagnon, E.; Maris, T.; Wuest, J. D. *J. Am. Chem. Soc.* **2007,** *129*, 4306-4322.
13. Lee, H. M.; Liao, C.-Y. *Acta Crystallogr.* **2008**, *E64*, m1447. Liao, C.-Y.; Lee, H. M. *Acta Crystallogr.* **2006**, *E62*, m680-m681. Viossat, B.; Dung, N.-H.; Robert, F. *Acta Crystallogr.* **1993**, *C49*, 84-85.
14. De León, A.; Pons, J.; Solans, X.; Font-Bardia, M. *Acta Crystallogr*. **2007**, *E63*, m2164. Ma, L.; Smith, R. C.; Protasiewicz, J. D. *Inorg. Chim. Acta* **2005**, *358*, 3478-3482. Holzbock, J.; Sawodny, W.; Thewalt, U. *Z. Anorg. Allg. Chem.* **2000**, *626*, 2563-2568.
15. Case, F. H.; Koft, E. *J. Am. Chem. Soc.* **1959**, *81*, 905-906.
16. *SAINT*, *Version 7.68A*; Bruker AXS Inc.: Madison, WI 53719-1173, 2009.
17. Sheldrick, G. M., *SADABS*, *Version 2008/1*; Bruker AXS Inc., Madison, WI 53719-1173, 2008.
18. Sheldrick, G. M. *Acta Crystallogr*. **2008**, *A64*, 112-122.
19. Spek, A. L. *PLATON, A Multipurpose Crystallographic Tool*; Utrecht University : Utrecht, The Netherlands, 2001. van der Sluis, P.; Spek, A. L. *Acta Crystallogr.* **1990**, *A46*, 194-201.

7.4 Conclusions

Nos résultats ont apporté une meilleure compréhension de la façon dont la coordination métallique peut être utilisée en coopération avec d'autres interactions pour diriger l'assemblage moléculaire. En particulier, notre travail illustre comment les matériaux avec des caractéristiques structurelles prévisibles peuvent être construits à partir de métallotectons, qui sont des complexes bien définis obtenus par coordination d'un métal avec des ligands spéciaux qui ont la capacité de s'engager dans des interactions inter-complexes supplémentaires. Les métallotectons sont programmés pour adopter une géométrie prévisible et pour également s'engager dans des interactions inter-complexes multiples selon des motifs fiables. Afin de mieux évaluer le potentiel de cette approche, nous avons examiné le comportement des complexes de Pd(II) avec des ligands **3a-b**, **4a-b** et **6**, qui intègrent les groupes pyridinyles pour lier les métaux et les groupes DAT pour assurer une association dirigée par des liaisons hydrogène.

Comme prévu, sur la base des modèles établis de coordination impliquant la pyridine et ses dérivés simples, les ligands **3a-b**, **4a-b** et **6** ont permis d'obtenir des complexes de Pd(II) de géométrie plan carré avec des constitutions prédictibles. Bien que la géométrie exacte du métallotecton résultant ne puisse être prévue avec certitude, dans tous les cas les ligands adoptent des conformations aplaties et orientées de manière attendue par rapport à la base du complexe. Comme prévu, l'association des métallotectons résultants génère dans la grande majorité des cas des réseaux d'architecture logique via la formation des liaisons hydrogène intermoléculaires selon des motifs établis **I-III** des unités DAT.

Les complexes des ligands **3a-b**, **4a-b** et **6** ont montré des caractéristiques structurelles communes qui peuvent être considérées comme introduites de manière fiable par la conception.

Les comparaisons de l'organisation moléculaire révèlent quelques analogies frappantes, mais quand même certains détails sont très variables, en particulier dans les complexes de stœchiométrie PdL_4. Ces différences reflètent sans doute divers facteurs, tels que les contributions des interactions ioniques, le rôle des anions spécifiques et la formation de liaisons hydrogène concurrentielles impliquant des molécules de solvant.

Malgré l'absence de contrôle parfait, notre travail affirme néanmoins la promesse de la conception de nouveaux matériaux hybrides inorganiques/organiques par la stratégie des métallotectons. Un avantage remarquable de cette stratégie est que le noyau moléculaire peut être construit spontanément par la coordination et la fonctionnalité périphérique des complexes peut contrôler l'association et l'organisation de métallotectons de façon indépendante.

Chapitre 8

Création de métallotectons de topologies similaires à celle du complexe Ag(2,2'-bipy)$_2^+$

8.1 Introduction

Au cours des chapitres 2-6, nous avons examiné l'organisation 3D et 2D d'une série de ligands respectivement par diffraction des rayons-X (XRD) et par microscopie de balayage à effet tunnel (STM). Les résultats obtenus dans les chapitres 2 à 4 ont illustré de façon convaincante le potentiel d'une approche comparative 2D et 3D pour confirmer les interprétations d'organisations observées par STM. Dans l'ensemble, les observations structurelles ont montré l'efficacité du groupe diaminotriazinyle (DAT) pour contrôler l'association moléculaire en formant de multiples interactions intermoléculaires directionnelles avec des motifs fiables. Précédemment, nous avons illustré l'intérêt de ces ligands pour la construction rapide et efficace de réseaux supramoléculaires par la stratégie combinant la chimie de coordination et la reconnaissance moléculaire par la formation de ponts hydrogène (voir chapitre 7). Le succès et les promesses de ce travail nous encouragent à poursuive dans cette direction.

Pour compléter cette thèse, nous proposons une étude qui réitère la stratégie adoptée dans le chapitre 7 mais qui présente cette fois-ci une approche interprétative de l'ingénierie cristalline. En se basant sur le complexe d'Ag(I) coordonné avec le 2,2'-bipyridine (2,2'-bipy), qui est un motif d'association classique, nous avons conçu une série de ligands qui permettent de créer des complexes métalliques de topologies similaires avec en plus la capacité de former des interactions inter-complexe par ponts hydrogène.

8.2 Nos objectifs

Dans ce chapitre, nous proposons de réitérer la stratégie qui combine la chimie de coordination et l'association dirigée par la formation des ponts hydrogène pour construire les architectures supramoléculaires à l'état cristallin. Nous avons synthétisé une série de métallotectons d'Ag(I) qui présentent une topologie similaire à celle du complexe Ag(2,2'-bipy)$_2^+$ mais qui sont capables de s'associer par liaisons hydrogène avec des motifs fiables. Plus précisément, nous avons crée une série de tectoligands contenant un cycle pyridinyle, pyrazinyle ou pyrimidinyle substitué avec une unité diaminotriazinyle (DAT), qui coopèrent ensemble pour donner un caractère de coordination bidentate aux ligands. Nous avons tenté de montrer l'intérêt et l'efficacité des groupements DAT pour contrôler la coordination métallique et l'architecture globale du réseau cristallin. Notre travail a démontré la puissance d'une approche basée sur une compréhension double de la chimie inorganique et organique.

7.3 Article 7

Surrogates of 2,2'-Bipyridine Designed to Chelate Ag(I) and Create Metallotectons for Engineering Hydrogen-Bonded Crystals

Adam Duong, Thierry Maris, and James D. Wuest*

Crystal Growth and Design, **2011**, *11(5)*, 2026-2034

Abstract

6-(Pyridin-2-yl)-1,3,5-triazine-2,4-diamine (**1**), 6-(pyrazin-2-yl)-1,3,5-triazine-2,4-diamine (**2**), and 6-(pyrimidin-2-yl)-1,3,5-triazine-2,4-diamine (**3**) incorporate two key structural features : (1) They resemble 2,2'-bipyridine and can therefore be expected to chelate suitable metals; and (2) they simultaneous incorporate diaminotriazinyl (DAT) groups, which engage in hydrogen bonding according to reliable patterns. As a result, ligands **1**-**3** are designed to react with metals to generate predictable structures held together by multiple coordinative interactions and hydrogen bonds. In particular, they react with salts of Ag(I) to yield cationic chelates analogous to those formed by 2,2'-bipyridine itself. As planned, DAT groups play a primary role in determining the observed structures, as demonstrated by their ability to engage in particularly favorable patterns of hydrogen bonding that require substantial deformation of the geometry of metallic coordination. An elegant hydrogen-bonded zipper, created spontaneously by combining simple ligand **3** with Ag(I), illustrates the power of qualitative approaches to crystal engineering based on a dual understanding of inorganic and organic chemistry.

Introduction

Nearly 100 years have elapsed since the epochal discovery by W. H. Bragg and W. L. Bragg that X-ray diffraction can be used to reveal the atomic structures of crystals.[1] Subsequent improvements in technology have made X-ray crystallography increasingly routine and powerful, and now more than 500,000 resolved molecular structures are included in the Cambridge Structural Database.[2] The collected structural details are of immense value, but deep understanding of the data has been slow to emerge. Sustained effort has not yet produced reliable theoretical methods for predicting structures,[3] and current computational approaches do not readily yield useful general guidelines that advance chemical understanding. Even if reliable methods for computing structures are eventually developed, they will not necessarily explain why the calculated results are favored, nor will they give crystal engineers the type of broad understanding needed to know where promising opportunities may lie hidden among an infinite number of molecular possibilities. As a result, better qualitative guidelines for engineering crystals are urgently needed and are likely to have enduring utility, even if successful computational methods emerge in the future.

Developing such generalizations is partly an interpretive (hermeneutic) exercise, in which the mass of existing structural data can be examined fruitfully from diverse perspectives. For example, a topological approach to engineering crystals focuses on the complementarity of molecular shapes as a key determinant of packing, as set out by Kitaigorodsky.[4] A valuable counterpoint, introduced by Desiraju, Etter, Robson, Wuest, and others,[5] emphasizes the structuring effect of dominant intermolecular interactions, such as hydrogen bonds or coordinative bonds involving metals. Each perspective adds insight but is necessarily incomplete.

Structural preferences have subtle origins, and no crystal engineer can afford to neglect the hermeneutic aspects of the field and be limited by a single fixed perspective.

In crystal engineering, the perspective of inorganic chemistry creates a bias for structures in which molecular components are linked by coordination to metals, whereas the perspective of organic chemistry favors the exploitation of other intermolecular interactions. However, many opportunities await hybrid researchers who can pursue both approaches at the same time, using molecular components programmed to form predictable structures maintained by the joint effect of coordinative interactions and other directional forces. Such structures, which can be considered to be built from subunits called *metallotectons*,[6-8] are known but remain unfamiliar, and they deserve to be more fully exploited by crystal engineers.

Of special interest to crystal engineers who wish to combine inorganic and organic approaches are families of ligands that can bind metals according to reliable patterns and can simultaneously engage in predictable intermolecular interactions such as hydrogen bonds. Compounds of this type, which can be called *tectoligands*, are exemplified by relatives **1**,[9] **2**,[10] and **3**[10] of 2,2'-bipyridine (**4** = 2,2'-bipy). Compounds **1-3** retain the characteristic chelating ability of 2,2'-bipy[11] but also incorporate a diamino-1,3,5-triazinyl group (DAT), which is known to engage in hydrogen bonding according to established motifs **I-III**.[12] Compounds **1-3** illustrate a potentially general strategy in which aryl or heteroaryl units are replaced with DAT groups to create new molecules with similar topologies and capacities for coordination, but with significant added abilities to engage in strong directional intermolecular interactions. To test this strategy, we have used tectoligands **1-3** to bind Ag(I), and we have found that the resulting adducts have unusual structural features that result from combining chelation with inter-complex hydrogen bonding.

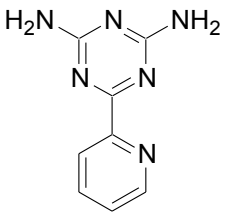

1

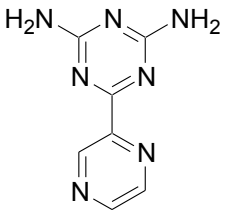

2

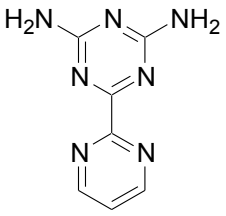

3

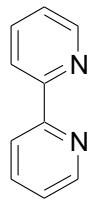

4 (2,2'-bipy)

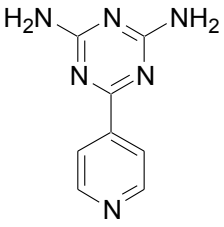

5

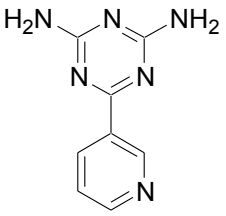

6

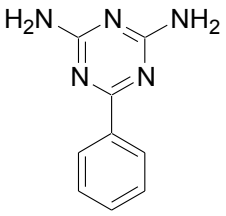

7

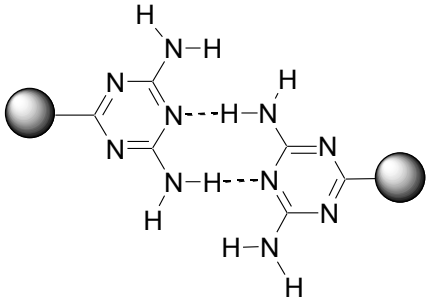

I

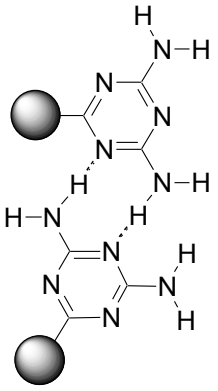

II

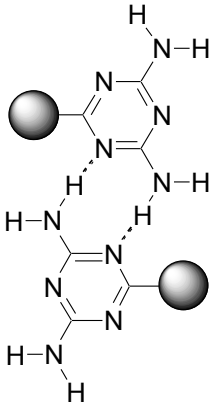

III

Results and Discussion

Syntheses and Structures of Tectoligands 1-3. 6-(Pyridin-2-yl)-1,3,5-triazine-2,4-diamine (**1**),[9] 6-(pyrazin-2-yl)-1,3,5-triazine-2,4-diamine (**2**),[10] and 6-(pyrimidin-2-yl)-1,3,5-triazine-2,4-diamine (**3**)[10] were prepared by reported methods. To provide a foundation for understanding the association of their metal complexes, we began by examining the structures of the unbound ligands themselves.

(a) Structure of 6-(Pyridin-2-yl)-1,3,5-triazine-2,4-diamine (1).[9] As reported previously,[13] pyridinyl-substituted diaminotriazine **1** crystallizes from MeCN to give a structure closely analogous to those formed by isomeric pyridinyl-substituted diaminotriazines **5**-**6** and 6-phenyl-1,3,5-triazine-2,4-diamine (**7**). In particular, crystallographically independent molecules **A** and **B** in the structure of compound **1** adopt flattened conformations with small torsional angles between the pyridinyl and triazinyl rings (15° and 32°, respectively). In addition, molecules **A** are paired by characteristic hydrogen bonding according to motif **I**, with N-H···N distances of 3.050 Å (Figure 1), and pairs $\mathbf{A}_2$ are linked into tapes by additional hydrogen bonding of type **III** with intervening molecules **B**. In all cases, crystallization of aryl-substituted diaminotriazines **1** and **5**-**7** appears to be controlled primarily by their similar flattened topologies and by their shared ability to form approximately coplanar hydrogen bonds directed by DAT groups.

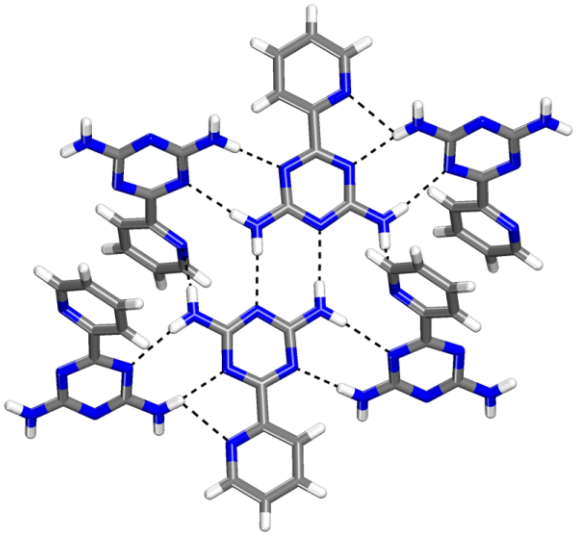

Figure 1. View of the structure of crystals of 6-(pyridin-2-yl)-1,3,5-triazine-2,4-diamine (**1**) grown from MeCN,[13] showing crystallographically independent molecules **A** and **B**. Pairs $\mathbf{A}_2$ are held together by hydrogen bonds of type **I**, and the pairs are linked into tapes by additional hydrogen bonds of type **III** involving intervening molecules **B**. Hydrogen bonds are represented by broken lines, and carbon atoms are shown in gray, hydrogen atoms in white, and nitrogen atoms in blue.

(b) Structure of 6-(Pyrazin-2-yl)-1,3,5-triazine-2,4-diamine (2). The similar molecular organization observed in crystals of phenyl-substituted diaminotriazine **7** and isomeric pyridinyl-substituted analogues **1**, **5**, and **6** suggested that the introduction of an additional atom of nitrogen to create pyrazinyl-substituted derivative **2** would not have major structural consequences. Crystals of compound **2** grown from DMSO/MeCN were found to belong to the monoclinic space group $P2_1/n$. A view of the structure is provided in Figure 2, and other crystallographic data are presented in Table 1. The average planes of the pyrazinyl and triazinyl rings form a small angle (4.9°), as expected, and molecules are paired by characteristic hydrogen bonding of type **I**,

with N-H···N distances of 3.041 Å (Figure 2). The pairs are linked to form a three-dimensional structure by additional hydrogen bonds involving the pyrazinyl nitrogen atoms as acceptors.

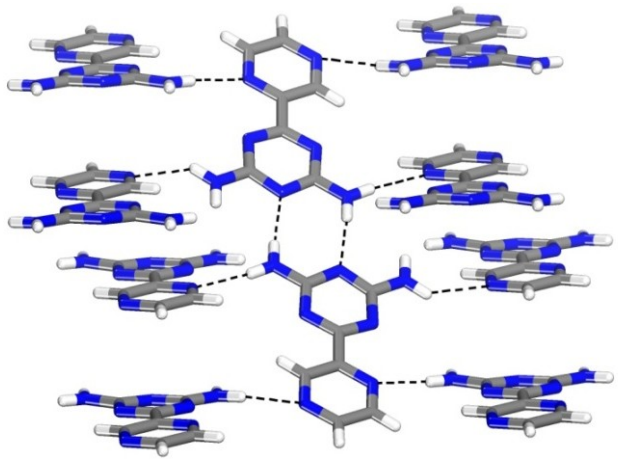

Figure 2. View of the structure of crystals of 6-(pyrazin-2-yl)-1,3,5-triazine-2,4-diamine (**2**) grown from DMSO/MeCN. Hydrogen bonds are represented by broken lines, and carbon atoms are shown in gray, hydrogen atoms in white, and nitrogen atoms in blue.

Table 1. Crystallographic Data for Pyrazinyl-Substituted Diaminotriazine **2** and Pyrimidinyl-Substituted Diaminotriazine **3**.

compound	**2**	**3**
formula	$C_7H_7N_7$	$C_7H_7N_7$
crystal system	monoclinic	tetragonal
space group	$P2_1/n$	$P4_32_12$
a (Å)	9.0902(6)	7.8000(2)
b (Å)	6.8526(4)	7.8000(2)
c (Å)	12.9990(8)	13.6369(3)
α (°)	90	90
β (°)	103.304(3)	90
γ (°)	90	90
V (Å^3)	788.00(9)	829.67(4)
Z	4	4
ρ_{calcd} (g cm^{-3})	1.595	1.515
T (K)	150	150
μ (mm^{-1})	0.936	0.889
R_1, $I>2\sigma$	0.0359	0.0274
R_1, all data	0.0423	0.0274
ωR_2, $I>2\sigma$	0.1021	0.0735
ωR_2, all data	0.1178	0.0735
measured reflections	16462	17296
independent reflections	1481	789
observed reflections, $I>2\sigma(I)$	1283	787

(c) Structure of 6-(Pyrimidin-2-yl)-1,3,5-triazine-2,4-diamine (3). Crystals of pyrimidyl-substituted diaminotriazine **3** were grown from DMSO/CH_2Cl_2, and they proved to belong to the chiral tetragonal space group $P4_32_12$. A view of the structure is shown in Figure 3, and other crystallographic data are summarized in Table 1. Attractive intramolecular C-H···N interactions that help stabilize flattened conformations of aryl-substituted triazines **1**-**2** and **5**-**7** are replaced by repulsive N···N interactions in pyrimidinyl-substituted derivative **3**, leading to a torsional angle of 26° between the pyrimidinyl and triazinyl rings. By forming hydrogen bonds of type **II** with two neighbors (average N-H···N distance = 3.222 Å), reinforced by additional N-

H···N interactions involving pyrimidinyl nitrogen atoms (3.046 Å), molecules of compound **3** are linked into helices aligned with the *c* axis (Figure 3). Adjacent helices of the same configuration are linked by additional hydrogen bonds of type **II** (average N-H···N distance = 3.222 Å), again strengthened by N-H···N interactions involving pyrimidinyl nitrogen atoms (3.046 Å). The overall structure defines a robust three-dimensional network in which each molecule forms a total of twelve N-H···N hydrogen bonds with four neighbors.

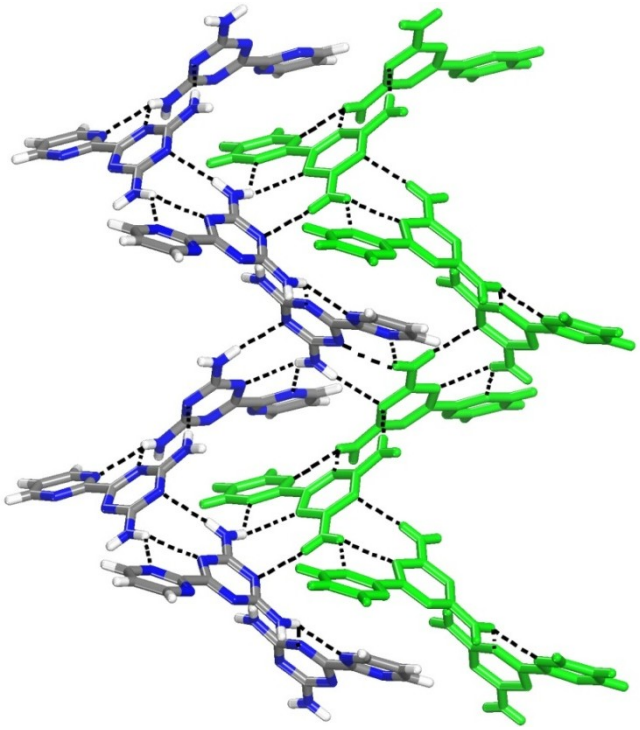

Figure 3. View of the structure of crystals of 6-(pyrimidin-2-yl)-1,3,5-triazine-2,4-diamine (**3**) grown from DMSO/CH_2Cl_2, showing two adjacent hydrogen-bonded helices. Hydrogen bonds are represented by broken lines. In one helix, carbon atoms are shown in gray, hydrogen atoms in white, and nitrogen atoms in blue. The adjacent helix is shown in contrasting green.

Syntheses and Structures of Ag(I) Complexes of Tectoligands 1-3. To evaluate the potential of diaminotriazines **1-3** to serve as tectoligands and to produce structures in which coordination to metals and hydrogen bonding both play critical roles, we elected to study the binding of Ag(I).[14-15] Ag(I) is a d^{10} ion and therefore has no electronically imposed preference for a particular geometry of coordination. As a result, observed structures are likely to reflect intra- and inter-complex interactions of the ligands, and multiple strong hydrogen bonds such as those characteristic of DAT groups should have a particularly important structure-directing effect. To prepare a series of complexes for comparison, $AgClO_4$ or $AgBF_4$ were mixed in MeCN with 6-(pyridin-2-yl)-1,3,5-triazine-2,4-diamine (**1**), 6-(pyrazin-2-yl)-1,3,5-triazine-2,4-diamine (**2**), and 6-(pyrimidin-2-yl)-1,3,5-triazine-2,4-diamine (**3**), and the precipitated solids were crystallized.

(a) Structures of 2:1 Complexes of 6-(Pyridin-2-yl)-1,3,5-triazine-2,4-diamine (1) with $AgClO_4$. 2,2'-Bipy (**4**) and related bidentate ligands are known to react with suitable salts of Ag(I) to give derivatives of 2:1 cationic complex **8** with geometries of coordination ranging from distorted tetrahedral to nearly square planar.[16-18] Based on these precedents, we expected pyridinyl-substituted diaminotriazine **1** to yield chiral complex **9**, which can undergo further association directed by the characteristic hydrogen bonding of DAT groups.

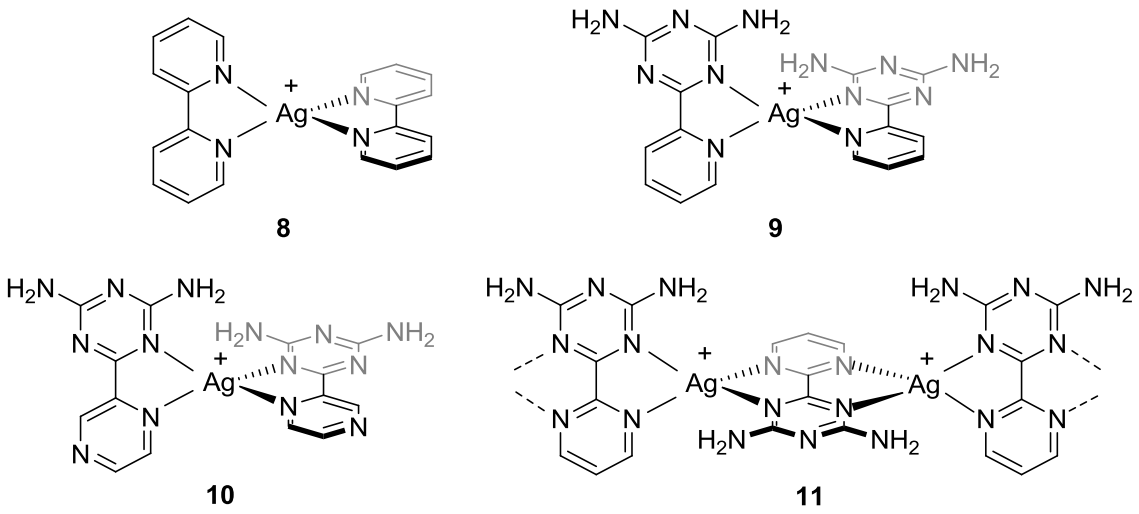

Crystals of complexes of ligand **1** with $AgClO_4$ were grown from DMSO/MeCN. Two crystalline forms were obtained under similar conditions, one a solvate including MeCN and the other solvent-free. Crystals of the solvate were found to belong to the monoclinic space group *P*2/c and to have the composition 2 **1** • $AgClO_4$ • 2 MeCN. Figure 4 provides views of the structure, and other crystallographic data are presented in Table 2. The observed structure incorporates expected cationic complex **9** and its enantiomer, which are linked alternately into chains held together by hydrogen bonding of DAT groups according to standard motif **I**, reinforced by additional N-H···O hydrogen bonds involving bridging perchlorate (Figure 4a). The average Ag-N distances within complex **9** (2.317 Å for both Ag-N_{DAT} and Ag-N_{py}), N-H···N distances in hydrogen-bonded pairs of DAT groups (3.048 Å), and average N-H···O distances in hydrogen bonds involving perchlorate (3.228 Å) have normal values.[13,16]

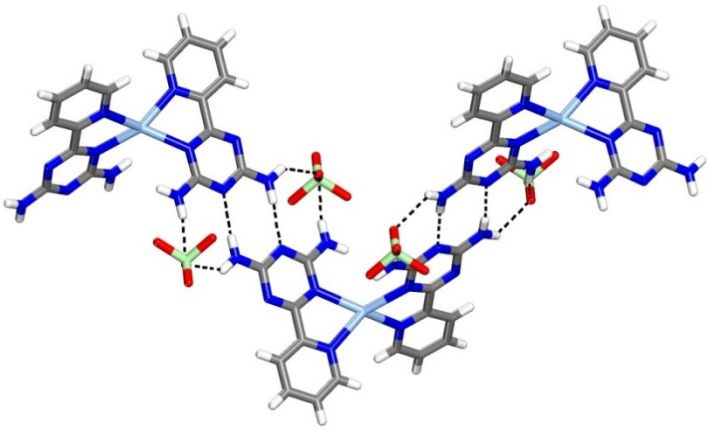

a

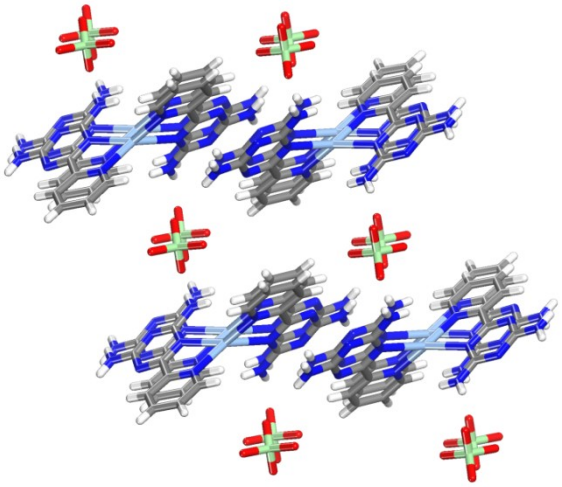

b

Figure 4. Views of the structure of crystals of the solvated form of the 2:1 complex of 6-(pyridin-2-yl)-1,3,5-triazine-2,4-diamine (**1**) with $AgClO_4$ grown from DMSO/MeCN. (a) Alternating chains of cationic complex **9** and its enantiomer, which are held together by hydrogen bonding of DAT groups according to motif **I**, reinforced by hydrogen bonding involving bridging perchlorate. (b) Alternating cationic layers and anionic layers containing guest molecules of MeCN. In both views, hydrogen bonds are represented by broken lines, and guest molecules are omitted for clarity. Carbon atoms are shown in gray, hydrogen atoms in white, chlorine atoms in pale green, nitrogen atoms in dark blue, oxygen atoms in red, and silver atoms in medium blue.

Table 2. Crystallographic Data for Complexes of Pyridinyl-Substituted Diaminotriazine **1**, Pyrazinyl-Substituted Diaminotriazine **2**, and Pyrimidinyl-Substituted Diaminotriazine **3** with Ag(I).

cocrystal	2 **1** • $AgClO_4$ • 2 MeCN	2 **1** • $AgClO_4$	2 **2** • $AgClO_4$	2 **2** • $AgBF_4$	**3** • $AgClO_4$
formula	$C_{20}H_{22}AgClN_{14}O_4$	$C_{16}H_{16}AgClN_{12}O_4$	$C_{14}H_{14}AgClN_{14}O_4$	$C_{14}H_{14}AgBF_4N_{14}$	$C_7H_7AgClN_7O_4$
crystal system	monoclinic	monoclinic	monoclinic	monoclinic	monoclinic
space group	*P*2/c	*P*2$_1$/n	*P*2$_1$/c	*P*2$_1$	*P*2$_1$/c
a (Å)	10.5537(8)	11.6531(3)	7.7000(4)	7.3464(3)	8.5605(5)
b (Å)	7.5440(6)	14.1616(3)	16.4473(9)	15.6714(5)	11.7582(6)
c (Å)	18.6318(14)	12.6255(3)	15.7512(8)	16.9610(6)	11.9111(7)
α (°)	90	90	90	90	90
β (°)	115.300(4)	93.576(1)	93.649(3)	91.854(2)	103.195(2)
γ (°)	90	90	90	90	90
V (Å^3)	1341.12(18)	2079.49(9)	1990.75(18)	1951.67(12)	1167.27(11)
Z	2	4	4	4	4
ρ_{calcd} (g cm^{-3})	1.649	1.865	1.954	1.950	2.256
T (K)	150	150	150	150	150
μ (mm^{-1})	7.440	9.46	9.915	9.002	16.278
R_1, $I > 2\sigma$	0.0652	0.0402	0.0293	0.0250	0.0357
R_1, all data	0.0658	0.0459	0.0324	0.0253	0.0358
ωR_2, $I > 2\sigma$	0.1555	0.1071	0.0808	0.0635	0.0978
ωR_2, all data	0.1558	0.1122	0.0846	0.0641	0.0979
measured reflections	18209	43524	40966	22953	21808
independent reflections	2398	3921	3757	7054	2193
observed reflections, $I > 2\sigma(I)$	2068	3452	3474	6981	2182

The geometry of coordination of Ag(I) in complex **9** is far from tetrahedral, as measured by the angle formed by the average planes of the two bound ligands **1** (56°). The distortion occurs in a way that produces a flattened structure in which the DAT groups point approximately in the same direction. Within each ligand, the pyridinyl and triazinyl rings are nearly coplanar, and the average planes form an angle of 9.6°. The hydrogen-bonded chains of complex **9** pack closely to form cationic sheets, which are separated from other cationic sheets by intervening anionic layers containing hydrogen-bonded perchlorate and guest molecules of MeCN (Figure 4b). No significant Ag···Ag interactions are observed in the structure.

Solvent-free crystals of composition 2 **1** • $AgClO_4$ were found to belong to the monoclinic space group $P2_1/n$ and to have a structure similar to that of the solvated form. Various crystallographic data are presented in Table 2. Again, the structure consists of cationic complex **9** and its enantiomer, linked alternately into chains joined by characteristic hydrogen bonding of type **I** between DAT groups (average N-H···N distance = 3.126 Å), strengthened by additional N-H···O hydrogen bonds involving bridging perchlorate.[19] As in the solvate, cationic complex **9** is flattened, and the average planes of bound ligands **1** form an angle of 45°. Again, the distortion orients the DAT groups in the same direction. With the assistance of hydrogen bonds involving perchlorate, the cationic chains pack to form sheets, and the sheets stack to produce the observed three-dimensional structure. Sheets in the unsolvated form integrate cations and anions, whereas sheets in the solvated form are largely cationic and are separated from adjacent sheets by intervening anionic layers; nevertheless, the molecular structure and interactions of cation **9** remain similar in both crystalline forms.

Together, these observations confirm that pyridinyl-substituted diaminotriazine **1** is properly designed to serve as a surrogate for 2,2'-bipy (**4**), and it can produce metal chelates with analogous structures, endowed with the further ability to engage predictably in inter-complex association directed by hydrogen bonding of DAT groups. It is noteworthy that hydrogen bonding is strong enough to overcome the coulombic repulsion of cationic metallotectons **9** and ensure their association. Moreover, inter-complex hydrogen bonding and packing forces also appear to be able to help flatten the geometry of coordination, despite the potential for increased inter-ligand repulsion.

(b) Structure of the 2:1 Complex of 6-(Pyrazin-2-yl)-1,3,5-triazine-2,4-diamine (2) with $AgClO_4$. Like pyridinyl-substituted diaminotriazine **1**, pyrazinyl analogue **2** is designed to imitate 2,2'-bipy (**4**) by chelating Ag(I) and forming a cationic 2:1 complex.[20-21] Moreover, crystallization of uncomplexed tectoligands **1** and **2** favors similar molecular organization (Figures 1-2), which is dictated in part by hydrogen bonding of DAT groups according to standard motifs. For these reasons, we expected pyrazinyl-substituted diaminotriazine **2** to react with Ag(I) to form chiral complex **10**, which can then engage in inter-complex hydrogen bonding directed by the DAT groups.

Crystals of the complex of tectoligand **2** with $AgClO_4$ were grown from DMSO/MeCN and proved to belong to the monoclinic space group $P2_1/c$. Views of the structure are shown in Figure 5, and other crystallographic data are provided in Table 2. The flattening observed in complexes **9** of pyridinyl-substituted ligand **1** is even more extreme in complex **10** of pyrazinyl analog **2**, and the angle formed by the average planes of the two bound ligands decreases to only 28°. As a result, the coordination of Ag(I) can be better described as distorted square planar instead of tetrahedral, and the DAT groups are held in a *cis* orientation.

This distortion has a dramatic effect on the ability of complex **10** to engage in intermolecular hydrogen bonding. As shown in Figure 5a, severe flattening allows the formation of racemic pairs held together by four N-H···N hydrogen bonds of type **I** (average distance = 3.084 Å), augmented by additional N-H···O hydrogen bonds involving bridging perchlorate (average distance = 3.139 Å). The pairs are then linked into tapes by N-H···N hydrogen bonds (3.013 Å) between DAT groups and N4 of the pyrazinyl rings, and the tapes are further connected to form corrugated sheets by C-H···N interactions involving C3 and N4 of pyrazinyl rings (Figure 5a).[22-23] Additional N-H···O hydrogen bonds involving bridging perchlorate, as well

as π-stacking of DAT groups and pyrazinyl rings, then help direct packing of the sheets to produce the ultimate three-dimensional structure (Figure 5b). As in the case of the complexes of pyridinyl-substituted analog **1** with Ag(I), no significant Ag···Ag interactions are observed.

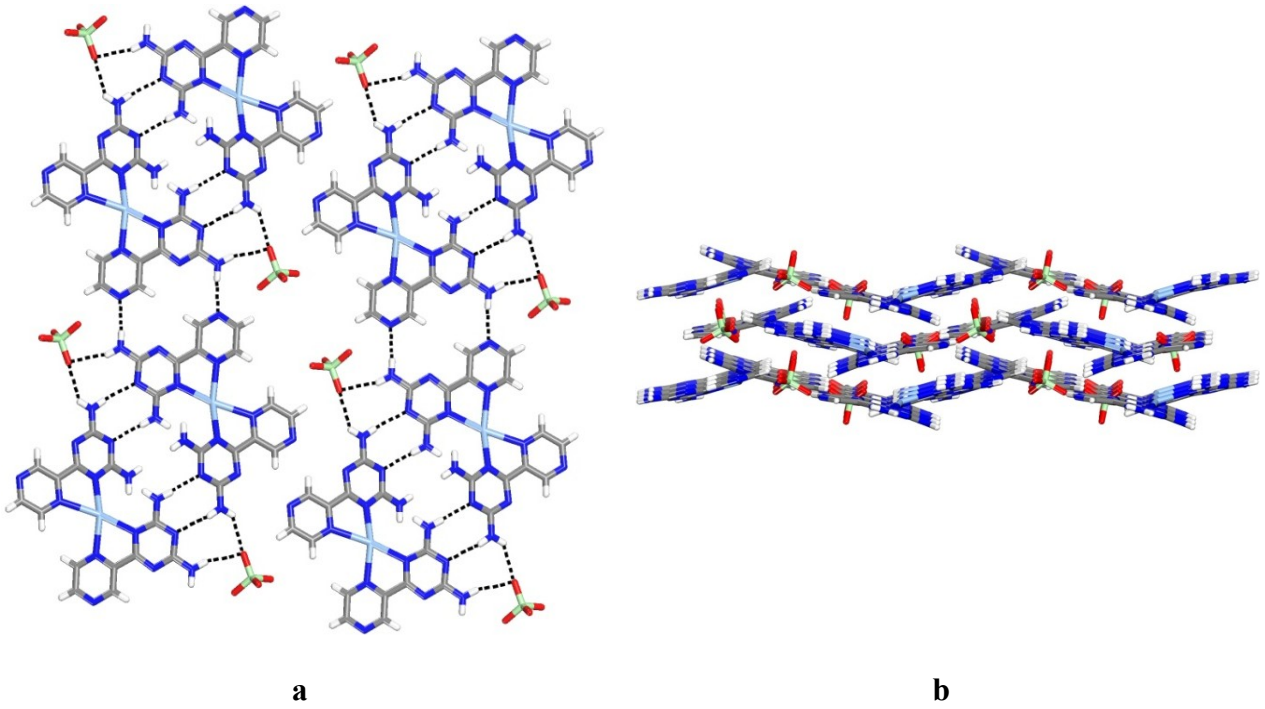

a **b**

Figure 5. Views of the structure of crystals of the 2:1 complex of 6-(pyrazin-2-yl)-1,3,5-triazine-2,4-diamine (**2**) with $AgClO_4$ grown from DMSO/MeCN. (a) Racemic pairs of flattened cationic complex **10** are held together by four N-H···N hydrogen bonds of type **I**, augmented by hydrogen bonds involving bridging perchlorate. The pairs are linked into tapes by N-H···N hydrogen bonds involving pyrazinyl rings, and the tapes are further joined to form corrugated sheets by C-H···N interactions of paired pyrazinyl rings. (b) View of adjacent sheets, which are held together in part by N-H···O hydrogen bonds involving bridging perchlorate, as well as by π-stacking of DAT groups and pyrazinyl rings. In both views, hydrogen bonds are represented by broken lines. Carbon atoms are shown in gray, hydrogen atoms in white, chlorine atoms in pale green, nitrogen atoms in dark blue, oxygen atoms in red, and silver atoms in medium blue.

(c) Structure of the 2:1 Complex of 6-(Pyrazin-2-yl)-1,3,5-triazine-2,4-diamine (2) with $AgBF_4$. In the structures of the 2:1 complexes of pyridinyl-substituted diaminotriazine **1** and its pyrazinyl analogue **2** with $AgClO_4$, perchlorate plays a structuring role by serving as a counterion, by reinforcing hydrogen bonding according to standard motif **I**, and by forming additional hydrogen bonds that help to maintain the cohesion of adjacent sheets. To probe the importance of these effects, we prepared the 2:1 complex of tectoligand **2** with $AgBF_4$. Crystals grown from DMSO/MeCN were found to belong to the monoclinic space group $P2_1$. Figure 6 shows a view of the structure, and other crystallographic data are presented in Table 2. The observed structure is closely analogous to that of the complex of tectoligand **2** with $AgClO_4$, suggesting that the molecular organization is programmed largely by compound **2** and does not depend uniquely on particular features of perchlorate.

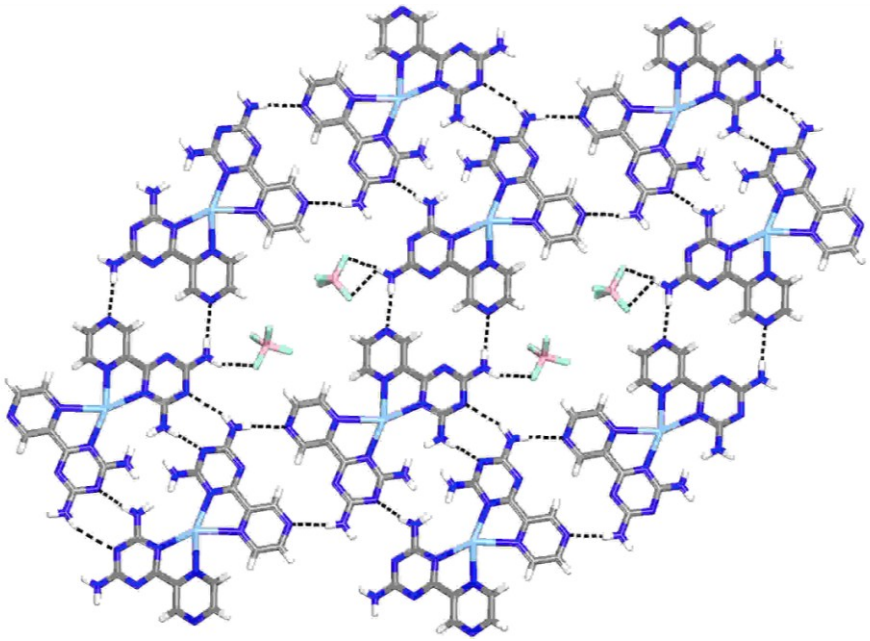

Figure 6. View of the structure of crystals of the 2:1 complex of 6-(pyrazin-2-yl)-1,3,5-triazine-2,4-diamine (**2**) with $AgBF_4$ grown from DMSO/MeCN. Flattened cations **10** are paired by N-H···N hydrogen bonds of type **I**, reinforced by hydrogen bonds involving bridging tetrafluoroborate, and the pairs are further connected into sheets by N-H···N hydrogen bonds involving pyrazinyl rings. Hydrogen bonds are represented by broken lines. Carbon atoms are shown in gray, hydrogen atoms in white, boron atoms in rose, fluorine atoms in light blue, nitrogen atoms in dark blue, and silver atoms in medium blue.

Again, cation **10** in the structure of the complex of tectoligand **2** with $AgBF_4$ is highly flattened, with an average angle of only 30° between the planes of the two bound ligands. A *cis* orientation of the DAT groups allows pairing of cation **10** by the formation of four intermolecular hydrogen bonds of type **I** (average distance = 3.418 Å), augmented by additional N-H···F hydrogen bonds involving bridging tetrafluoroborate (Figure 6). In this case, the pairs are not strictly racemic; instead, they are formed by crystallographically independent molecules that differ primarily in configuration, but also slightly in geometry as well. The pairs are then linked

into sheets by a total of eight N-H···N hydrogen bonds per pair (average distance = 3.124 Å) involving DAT groups and N4 of the pyrazinyl rings. It is interesting to note that the sheets can be considered to be constructed from hydrogen-bonded hexameric rosettes of cation **10**.[19] As in the structure of the corresponding complex with $AgClO_4$, additional hydrogen bonds involving bridging anions, as well as π-stacking of DAT groups and pyrazinyl rings, then help control packing of the sheets to produce the final three-dimensional structure.[19]

Together, these observations show that pyrazinyl-substituted diaminotriazine **2**, like pyridinyl-substituted analogue **1**, can effectively mimic 2,2'-bipy (**4**) and chelate Ag(I) to give similar 2:1 cationic complexes, which then associate by hydrogen bonding of DAT groups according to reliable motifs. In the complex of tectoligand **2** with $AgBF_4$, each metallotecton **10** is held together by four Ag···N coordinative bonds and forms a total of eight N-H···N hydrogen bonds with neighboring complexes. Ag···N interactions are considered to be similar to hydrogen bonds in strength,[15] so the directing effects of hydrogen bonding are not merely secondary to the role of metal coordination, as in previously studied metallotectons, but instead are key determinants of the overall structure. A likely manifestation of this hierarchy is the conspicuous flattening of metallotecton **10**, which has the effect of orienting the DAT groups to create a well-aligned self-complementary DADA pattern of hydrogen-bond donors (D) and acceptors (A). Flattening favors pairing of metallotectons **10** and also allows the pairs to further associate by hydrogen bonding to form easily packed sheets. These favorable topological features do not arise automatically from complexation, but appear instead to reflect the malleable geometry of coordination of Ag(I), which is distorted by the concerted effect of multiple hydrogen bonds.

(d) Structure of the 1:1 Complex of 6-(Pyrimidin-2-yl)-1,3,5-triazine-2,4-diamine (3) with $AgClO_4$. Under various conditions, both pyridinyl-substituted tectoligand **1** and its

pyrazinyl analogue **2** chelate Ag(I) as planned to form flattened cationic complexes, which associate further to produce unusual three-dimensional structures maintained by a combination of metallic coordination and hydrogen bonding. Based on these observations, we reasoned that symmetric pyrimidyl analogue **3** would react with Ag(I) to form cationic chains **11** of 1:1 stoichiometry.[24] These chains have a remarkable feature : Whatever geometry of coordination is adopted by the metal, the DAT groups are necessarily arranged in rows, thereby allowing the chains to be zipped together by extensive hydrogen bonding according to motif **I**. This illustrates the powerful synergy that can arise when metallic coordination and other strong intermolecular interactions are used in proper combination to direct molecular assembly.

Crystals of the complex of pyrimidinyl-substituted diaminotriazine **3** with $AgClO_4$ were grown from DMSO/MeOH, and they proved to belong to the monoclinic space group $P2_1/c$. Views of the structure are provided in Figure 7, and other crystallographic data are summarized in Table 2. As anticipated, complexation produces cationic chains **11** (Figure 7a), and the geometry of coordination of Ag(I) is flattened, as measured by the angle between the average planes of the two bound ligands **3** (55°). Flattening occurs in a way that places the DAT groups in each chain in a *cis* orientation, and alternate DAT groups along the chain lie approximately in one of two planes, which intersect along the axis of the chain at an angle of 73°. N-H···N hydrogen bonds of type **I** between the two sets of DAT groups (3.177 Å), reinforced by N-H···O hydrogen bonds involving bridging perchlorate (average N-H···O distance = 3.033 Å), join the chains into highly corrugated sheets, and the sheets pack efficiently to produce the observed structure (Figure 7b). Again, significant Ag···Ag interactions are absent.

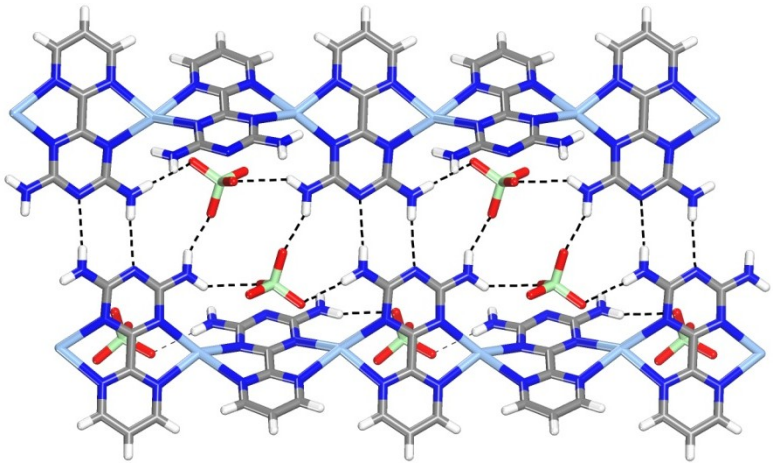

a

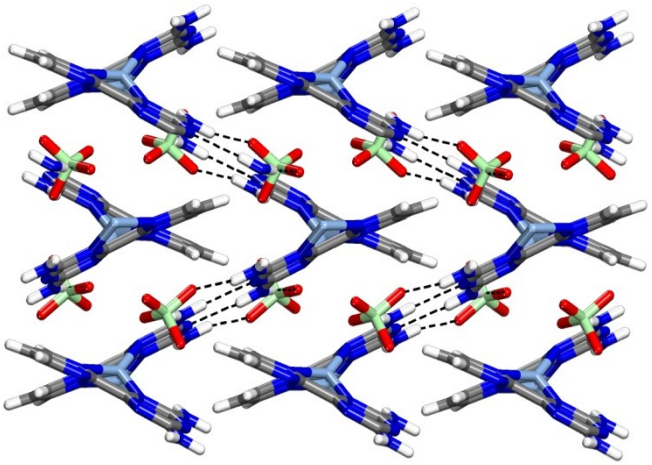

b

Figure 7. Views of the structure of crystals of the 1:1 complex of 6-(pyrimidin-2-yl)-1,3,5-triazine-2,4-diamine (**3**) with $AgClO_4$ grown from DMSO/MeOH. (a) Cationic chains **11** are zipped together by N-H···N hydrogen bonds of type **I**, strengthened by hydrogen bonds involving bridging perchlorate. (b) View showing how the zipped chains form corrugated sheets and how the sheets stack to form the three-dimensional structure. In both views, hydrogen bonds are represented by broken lines. Carbon atoms are shown in gray, hydrogen atoms in white, chlorine atoms in pale green, nitrogen atoms in dark blue, oxygen atoms in red, and silver atoms in medium blue.

Conclusions

Our results affirm the value of a hermeneutic approach to crystal engineering, in which broadly useful qualitative understanding is acquired by interpreting structural data according to diverse perspectives. General guidelines will always be an invaluable tool in the field, because they will help direct crystal engineers to particular areas of opportunity in a wilderness of possibilities. Our present work blends the perspective of inorganic crystal engineering, which focuses on the use of coordinative bonds to metals as a primary directing force, with an organic approach, which exploits other strong intermolecular interactions such as hydrogen bonds.

Previous attempts to unite these two perspectives have led to the concept of metallotectons, which are discrete metallic complexes that can engage in reliable inter-complex interactions. A conspicuous advantage of building crystals from metallotectons is that they can normally be made by the spontaneous ligation of metals, rather than by complex multistep syntheses. In addition, the characteristic geometries of metallic coordination yield molecular topologies not otherwise readily available. In the past, metallotectons have typically been derived from standard complexes, altered substantially by adding multiple substituents that are designed to direct inter-complex interactions. Our present work introduces a promising alternative strategy in which heteroaromatic ligands in conventional complexes are replaced by surrogates of very similar size and shape, but with a greatly enhanced ability to engage in strong directional inter-complex interactions.

We have tested this strategy by replacing heteroaromatic groups in 2,2'-bipy (**4**) and related bidentate ligands with DAT groups to create structures **1**-**3**, which are designed to chelate metals and to engage simultaneously in hydrogen bonding according to reliable motifs. The

behavior of tectoligands **1-3** persuasively illustrates the potential of this approach. As planned, they react with suitable salts of Ag(I) to yield cationic chelates analogous to those formed by 2,2'-bipy (**4**) itself. In addition, the chelating core and the incorporated DAT group of ligands **1-3** operate orthogonally without mutual interference, leaving the DAT group free to direct inter-complex association by forming multiple hydrogen bonds.

Our work reveals the unique advantages of controlling molecular organization by using hydrogen bonds in conjunction with coordinative interactions involving malleable d^{10} metals. In the observed structures, hydrogen bonds play a primary role, as demonstrated by their repeated ability to achieve particularly favorable patterns of association that require substantial deformations of the geometry of metallic coordination. In a conventional tectonic approach to constructing ordered molecular materials, the geometry of the individual components and the directional preferences of their intermolecular interactions must be properly matched to attain a mutually satisfactory architecture. Placing a malleable d^{10} metal at the core of the components ensures strong coordination, yet introduces an element of controlled flexibility that brings inter-complex interactions to the fore, as illustrated by the elegant hydrogen-bonded zipper shown in Figure 7a. This structure and analogues, created spontaneously by combining simple tectoligands **1-3** with Ag(I), demonstrate the power of qualitative approaches to crystal engineering based on a dual understanding of inorganic and organic chemistry.

Experimental Section

General Notes. 6-(Pyridin-2-yl)-1,3,5-triazine-2,4-diamine (**1**),[9] 6-(pyrazin-2-yl)-1,3,5-triazine-2,4-diamine (**2**),[10] and 6-(pyrimidin-2-yl)-1,3,5-triazine-2,4-diamine (**3**)[10] were prepared by reported methods. Their complexes with Ag(I) were made by the procedures summarized below. Other chemicals were purchased from commercial sources and used without further purification.

General Procedure for Preparing Ag(I) Complexes of Tectoligands 1-3. Solid tectoligands **1** (2.0 equiv), **2** (2.0 equiv), or **3** (1.0 equiv) were added in small portions at 25 °C to stirred solutions of $AgClO_4$ or $AgBF_4$ (1.0 equiv) in MeCN (20 mL). The resulting mixtures were stirred for 12 h, and precipitated solids were then separated by filtration, washed thoroughly with MeCN, and dried under vacuum before being purified by crystallization.

Crystallization of Tectoligands 2-3 and the Ag(I) Complexes of Tectoligands 1-3. All crystallizations were carried out at 25 °C. Crystals of uncomplexed tectoligands **2** and **3** were obtained by allowing MeCN and CH_2Cl_2, respectively, to diffuse slowly into solutions of the compounds in DMSO (5 mg/mL). Crude samples of the Ag(I) complexes of tectoligands **1-3** could be crystallized by allowing MeCN (compounds **1-2**) or MeOH (compound **3**) to diffuse slowly into saturated solutions in DMSO. Crystals of the unsolvated form of the complex of tectoligand **1** with $AgClO_4$ were grown in vials containing a solution of the crude complex (5 mg) in DMSO (1 mL) by carefully placing an overlayer of 1:1 MeCN/DMSO (2 mL) on top, then adding a third layer of pure MeCN (2 mL), and allowing diffusion of the layers to take place.

2:1 Complex of 6-(Pyridin-2-yl)-1,3,5-triazine-2,4-diamine (1) with $AgClO_4$ (Solvated Form). Yield 89%. Crystallized as colorless blocks : IR (ATR) 3081, 3057, 3021, 2230, 1488, 1445, 1017, 751 cm^{-1}; ^{1}H NMR (500 MHz, DMSO-d_6) δ 8.57 (d, 2H, ^3J = 4.5 Hz), 8.51 (d, 2H, ^3J = 7.9 Hz), 8.13 (dd, 2H, ^3J = 9.1 Hz, ^3J = 7.9 Hz^3), 7.70 (dd, 2H, ^3J = 9.1 Hz, ^3J = 4.5 Hz), 7.21 (bs, 8H); HRMS (ESI) calcd for $[C_{16}H_{16}AgN_{12}]^+$ *m/e* 483.06663, found 483.06888.

2:1 Complex of 6-(Pyridin-2-yl)-1,3,5-triazine-2,4-diamine (1) with $AgClO_4$ (Unsolvated Form). Yield 71%. Crystallized as colorless blocks. Anal. Calcd for $C_{16}H_{16}AgClN_{12}O_4$: C, 32.92; H, 2.76; N, 28.80. Found : C, 32.78; H, 2.62; N, 28.31.

2:1 Complex of 6-(Pyrazin-2-yl)-1,3,5-triazine-2,4-diamine (2) with $AgClO_4$. Yield 77%. Crystallized as pale yellow blocks : IR (ATR) 3450, 3350, 3187, 1613, 1520, 1449, 1374, 1081, 1024, 810, 622 cm^{-1}; ^{1}H NMR (500 MHz, DMSO-d_6) δ 9.56 (d, 2H, ^4J = 1.4 Hz), 8.93 (d, 2H, ^3J = 2.5 Hz), 8.68 (dd, 2H, ^3J = 2.5 Hz, ^4J = 1.4 Hz), 7.31 (bs, 8H); HRMS (ESI) calcd for $[C_{14}H_{14}AgN_{14}]^+$ *m/e* 485.05713, found 485.05489. Anal. Calcd for $C_{14}H_{14}AgClN_{14}O_4$: C, 28.71; H, 2.41; N, 33.48. Found : C, 28.69; H, 1.86; N, 33.01.

2:1 Complex of 6-(Pyrazin-2-yl)-1,3,5-triazine-2,4-diamine (2) with $AgBF_4$. Yield 83%. Crystallized as pale yellow blocks : IR (ATR) 3455, 3367, 3311, 1615, 1593, 1563, 1520, 1451, 1374, 1159, 1056, 1009, 811, 570 cm^{-1}; ^{1}H NMR (500 MHz, DMSO-d_6) δ 9.61 (d, 2H, ^4J = 1.4 Hz), 8.98 (d, 2H, ^3J = 2.5 Hz), 8.71 (dd, 2H, ^3J = 2.5 Hz, ^4J = 1.4 Hz), 7.40 (bs, 8H); HRMS (ESI) calcd for $[C_{14}H_{14}AgN_{14}]^+$ *m/e* 485.05713, found 485.05844.

1:1 Complex of 6-(Pyrimidin-2-yl)-1,3,5-triazine-2,4-diamine (3) with $AgClO_4$. Yield 71%. Crystallized as pale yellow blocks : IR (ATR) 3454, 3352, 3214, 1660, 1624, 1556, 1522,

1465, 1445, 1392, 1057, 1004, 799 cm^{-1}; ^{1}H NMR (500 MHz, DMSO-d_6) δ 9.00 (d, 4H, ^3J = 4.9 Hz), 7.80 (t, 2H, ^3J = 4.9 Hz), 7.35 (bs, 8H); HRMS (ESI) calcd for $[C_{14}H_{14}AgN_{14}]^+$ *m/e* 485.05713, found 485.05905.

X-Ray Crystallographic Studies. Crystallographic data were collected at 150 K using a Bruker Microstar diffractometer with Cu Kα radiation. The structures were solved by direct methods using SHELXS-97, and non-hydrogen atoms were refined anisotropically with SHELXL-97.[25] Hydrogen atoms were treated by first locating them from difference Fourier maps, recalculating their positions using standard values for distances and angles, and then refining them as riding atoms. In all structural studies except that of solvated crystals of the Ag(I) complex of tectoligand **1**, which decomposed when removed from the mother liquors, calculated powder X-ray diffraction patterns closely matched those obtained experimentally by analysis of bulk crystalline samples, thereby establishing that the samples consisted primarily of a single phase.[19]

Acknowledgments

We are grateful to the Natural Sciences and Engineering Research Council of Canada, the Ministère de l'Éducation du Québec, the Canada Foundation for Innovation, the Canada Research Chairs Program, and Université de Montréal for financial support.

Supporting Information Available. Additional crystallographic details (including thermal atomic displacement ellipsoid plots, powder X-ray diffraction patterns, supplementary figures, and tables of structural data in CIF format). This material is available free of charge via the Internet at http://pubs.acs.org.

Notes and References

1. Bragg, W. L. *Proc. Roy. Soc. London* **1913**, *89*, 248-277.
2. Allen, F. H. *Acta Crystallogr.* **2002**, *B58*, 380-388.
3. Dunitz, J. D.; Gavezzotti, A. *Chem. Soc. Rev.* **2009**, *38*, 2622-2633. Dunitz, J. D. *Chem. Commun.* **2003**, 545-548. Desiraju, G. R. *Nature Materials* **2002**, *1*, 77-79. Gavezzotti, A. *Acc. Chem. Res.* **1994**, *27*, 309-314. Maddox, J. *Nature* **1988**, *335*, 201.
4. Kitaigorodskii, A. I. *Organic Chemical Crystallography*; Consultants Bureau : New York, 1961.
5. For references, see: Ward, M. D. *Struct. Bond.* **2009**, *132*, 1-23. Robson, R. *Dalton Trans.* **2008**, 5113-5131. Wuest, J. D. *Chem. Commun.* **2005**, 5830-5837. Hosseini, M. W. *Acc. Chem. Res.* **2005**, *38*, 313-323. Nangia, A.; Desiraju, G. R. *Top. Curr. Chem.* **1998**, *198*, 57-95. Desiraju, G. R. *Angew. Chem., Int. Ed*. **1995**, *34*, 2311-2327. Etter, M. C. *Acc. Chem. Res.* **1990**, *23*, 120-126.
6. Telfer, S. G.; Wuest, J. D. *Cryst. Growth. Des.* **2009**, *9*, 1923-1931. Wan, C.-Q.; Li, G.-S.; Chen, X.-D.; Mak, T. C. W. *Cryst. Growth Des.* **2008**, *8*, 3897-3901. Constable, E. C.; Housecroft, C. E.; Neuberger, M.; Schaffner, S.; Schaper, F. *Inorg. Chem. Commun.* **2006**, *9*, 433-436.
7. For reviews, see: Braga, D.; Brammer, L.; Champness, N. R. *CrystEngComm* **2005,** *7*, 1-19. Brammer, L. *Chem. Soc. Rev.* **2004**, *33*, 476-489. Aakeröy, C. B.; Beatty, A. M. In *Comprehensive Coordination Chemistry II*; McCleverty, J. A., Meyer, T. J., Lever, A. B. P., Eds.; Elsevier : Oxford, 2004; Vol. 1, pp 679-688. Beatty, A. M. *Coord. Chem. Rev.* **2003**, *246*, 131-143.
8. Santillan, G. A.; Carrano, C. J. *Dalton Trans.* **2009**, 6599-6605. McMorran, D. A. *Inorg. Chem.* **2008**, *47*, 592-601. Salazar-Mendoza, D.; Baudron, S. A.; Hosseini, M. W. *Chem.*

Commun. **2007**, 2252-2254. Braga, D.; Giaffreda, S. L.; Grepioni, F.; Maini, L.; Polito, M. *Coord. Chem. Rev.* **2006**, *250*, 1267-1285. Goldberg, I. *Chem. Commun.* **2005**, 1243-1254. Katsuki, I.; Motoda, Y.; Sunatsuki, Y.; Matsumoto, N.; Nakashima, T.; Kojima, M. *J. Am. Chem. Soc.* **2002**, *124*, 629-640.

9. Case, F. H.; Koft, E. *J. Am. Chem. Soc.* **1959**, *81*, 905-906.
10. Case, F. H. *J. Heterocycl. Chem.* **1968**, *5*, 223-226.
11. For a recent review, see: Ye, B.-H.; Tong, M.-L.; Chen, X.-M. *Coord. Chem. Rev.* **2005**, *249*, 545-565.
12. For recent references, see: Maly, K. E.; Gagnon, E.; Maris, T.; Wuest, J. D. *J. Am. Chem. Soc.* **2007,** *129*, 4306-4322.
13. Duong, A.; Maris, T.; Wuest, J. D. *Cryst. Growth Des.* **2011**, *11*, 287-294.
14. For a recent review of the metallosupramolecular chemistry of Ag(I), see : Chen, C.-L.; Kang, B.-S.; Su, C.-Y. *Aust. J. Chem.* **2006**, *59*, 3-18.
15. Khlobystov, A. N.; Blake, A. J.; Champness, N. R.; Lemenovskii, D. A.; Majouga, A. G.; Zyk, N. V.; Schröder, M. *Coord. Chem. Rev.* **2001**, *222*, 155-192. Blake, A. J.; Champness, N. R.; Hubberstey, P.; Li, W.-S.; Withersby, M. A.; Schröder, M. *Coord. Chem. Rev.* **1999**, *183*, 117-138.
16. For references to previous structural studies of Ag(2,2'-bipy)$_2^+$ and related complexes, see : Chen, J.; Sha, J.-q.; Peng, J.; Shi, Z.-y.; Tian, A.-x.; Zhang, P.p. *J. Mol. Struct.* **2009**, *917*, 10-14. Constable, E. C.; Housecroft, C. E.; Kariuki, B. M.; Smith, C. B. *Aust. J. Chem.* **2006**, *59*, 30-33. Bowmaker, G. A.; Effendy; Marfuah, S.; Skelton, B. W.; White, A. H. *Inorg. Chim. Acta* **2005**, *358*, 4371-4388. Corongiu, G.; Nava, P. *Int. J. Quant. Chem.* **2003**, *93*, 395-404. Goodwin, K. V.; McMillin, D. R.; Robinson, W. R. *Inorg. Chem.* **1986**, *25*, 2033-2036.

17. For references to related studies of complexes of Ag(I) with 2-(pyridin-2-yl)-1,3,5-triazines, see: Najafpour, M. M.; Hołyńska, M.; Amini, M.; Kazemi, S. H.; Lis, T.; Bagherzadeh, M. *Polyhedron* **2010**, *29*, 2837-2843. Yan, C.; Chen, L.; Feng, R.; Jiang, F.; Hong, M. *CrystEngComm* **2009**, *11*, 2529-2535. Lin, J.-D.; Lin, M.-Z.; Jia, C.-C.; Li, Z.-H.; Du, S.-W. *Inorg. Chem. Commun.* **2009**, *12*, 487-489. Zhou, X.-P.; Zhang, X.; Lin, S.-H.; Li, D. *Cryst. Growth Des.* **2007**, *7*, 485-487.
18. For a recent review of square-planar complexes of Ag(I), see : Young, A. G.; Hanton, L. R. *Coord. Chem. Rev.* **2008**, *252*, 1346-1386.
19. See the Supporting Information for details.
20. For a recent review of complexes of Ag(I) with pyrazine and related ligands, see : Steel, P. J.; Fitchett, C. M. *Coord. Chem. Rev.* **2008**, *252*, 990-1006.
21. Ligand **2** has recently been used to form the perchlorate salt of the complex [Ru(2,2'-bipy)$_2$(**2**)]$^{2+}$, but the DAT groups form hydrogen bonds only with perchlorate. Chen, Y.; Xu, W.-C.; Kou, J.-F.; Yu, B.-L.; Wei, X.-H.; Chao, H.; Ji, L.-N. *Inorg. Chem. Commun.* **2010**, *13*, 1140-1143.
22. Desiraju, G. R.; Steiner, T. *The Weak Hydrogen Bond in Structural Chemistry and Biology*; Oxford University Press: Oxford, U. K., 1999.
23. For a review of C-H···O interactions, see: Desiraju, G. R. *Chem. Commun.* **2005**, 2995-3001.
24. For related reports of oligomeric chains produced by the chelation of Ag(I) by 2,2'-bipyrimidine, see : Pointillart, F.; Herson, P.; Boubekeur, K.; Train, C. *Inorg. Chim. Acta* **2008**, *361*, 373-379. Marinescu, G.; Lescouëzec, R.; Armentano, D.; De Munno, G.; Andruh, M.; Uriel, S.; Llusar, R.; Lloret, F.; Julve, M. *Inorg. Chim. Acta* **2002**, *336*, 46-54.
25. Sheldrick, G. M. *Acta Crystallogr*. **2008**, *A64*, 112-122.

8.4 Conclusions

Nos résultats soulignent l'intérêt de l'approche herméneutique en ingénierie cristalline, dans laquelle la compréhension qualitative est acquise par l'interprétation des données de structures selon divers points de vue. Notre travail incorpore la perspective de l'ingénierie cristalline inorganique, qui met l'accent sur l'utilisation des liaisons de coordination à des métaux comme une force directrice principale, avec une approche organique, qui exploite d'autres fortes interactions intermoléculaires comme les liaisons hydrogène.

Les précédentes tentatives de concilier ces deux perspectives ont conduit au concept de métallotectons, qui sont des complexes métalliques discrets pouvant s'engager dans des interactions inter-complexes fiables. Un avantage remarquable de la construction de métallotectons est qu'ils peuvent normalement être obtenus par la coordination spontanée des ligands aux métaux, plutôt que par des synthèses multi-étapes sophistiquées. En outre, les géométries caractéristiques de coordination métallique permettent d'avoir des topologies moléculaires qui ne sont pas disponibles par des voies de synthèse purement organique. Dans une première approche, les ingénieurs de l'état cristallin ont créé des métallotectons en modifiant des complexes classiques par l'ajout de multiples substituants qui peuvent diriger les interactions entre les complexes. Notre travail actuel introduit une nouvelle stratégie prometteuse dans laquelle les ligands hétéroaromatiques conventionnels dans les complexes classiques sont remplacés par des substituts de taille et de forme très similaires, mais avec une capacité grandement améliorée de se livrer à une forte interaction inter-complexe directionnelle. Nous avons testé cette stratégie en remplacement un cycle pyridinyle du 2,2'-bipy (**4**) par un groupement DAT pour créer les structures **1-3**, qui sont conçues pour chélater les métaux et pour

s'engager simultanément dans des interactions inter-complexes par liaison hydrogène avec des motifs fiables.

Le comportement des tectoligands **1-3** illustre de façon convaincante le potentiel de cette approche herméneutique. Comme prévu, ils réagissent avec des sels d'Ag(I) pour former des complexes analogues à ceux générés avec le 2,2'-bipy (**4**) lui-même. En outre, le centre chélatant et le groupement DAT intégré dans les ligands **1-3** fonctionnent orthogonalement sans interférence mutuelle, laissant ainsi le groupement DAT libre pour former des associations inter-complexes directionnelles en créant de multiples liaisons hydrogène. Tel qu'on peut le voir, les structures obtenues montrent que les liaisons hydrogène jouent un rôle primordial dans l'organisation moléculaire des métallotectons, imposant ainsi des déformations importantes de la géométrie de coordination métallique. En particulier, l'élégante structure en fermeture éclair obtenue par liaisons hydrogène (Figure 7a), créée spontanément par simple combinaison du tectoligand **3** avec l'Ag(I), démontre la puissance de l'approche basée sur une compréhension double de la chimie inorganique et organique.

Chapitre 9

Conclusions et perspectives

9.1 Conclusions

9.1.1 Vue d'ensemble de la thèse

Pour répondre aux défis technologiques, de nouvelles stratégies de synthèse continuent à être développées. Traditionnellement, un accent important a été placé sur la découverte de nouvelles méthodes pour la construction de molécules individuelles. Cependant, les propriétés des matériaux dépendent non seulement de l'identité des composantes moléculaires, mais aussi de leurs interactions et de l'organisation collective de l'ensemble. La conception et la préparation de nouveaux matériaux moléculaires demandent donc une approche qui intègre la synthèse moléculaire et supramoléculaire.

Les voies de synthèse organique traditionnelle peuvent générer une énorme diversité de structures différentes, mais quand même elles ne sont pas adéquates pour résoudre tous les problèmes rencontrés en science des matériaux. Par exemple, les molécules purement organiques sont typiquement construites par la formation consécutive de nouvelles liaisons covalentes, dans un processus linéaire qui est souvent laborieux. De plus, certaines géométries moléculaires sont difficiles d'accès. Pour contourner ces contraintes, nous avons exploré une stratégie hybride qui réunit les approches classiques organique et inorganique. Plus précisément, cette approche repose sur l'utilisation de la chimie de coordination pour rapidement générer de nouvelles entités moléculaires, appelées métallotectons, par la complexation spontanée des ligands avec un centre métallique bien choisi, suivi de l'association des métallotectons dirigée par la formation de ponts hydrogène ou d'autres liaisons non-covalentes fiables.

Pour explorer cette nouvelle approche hybride, nous avons construit une série de tectoligands ditopiques comportant soit une pyridine, une bipyridine ou une phénantroline pour

favoriser la coordination métallique, substitués avec des groupements diaminotriazinyles (DAT) pour permettre aux métallotectons de s'associer par la formation de ponts hydrogène. En plus d'offrir la possibilité de créer des métallotectons par coordination, nos tectoligands ont un intérêt intrinsèque en chimie supramoléculaire en tant qu'entités pouvant s'associer elles-mêmes en 3D et en 2D. Nous avons donc examiné l'association des tectoligands par la diffraction des rayons-X (XRD) et par la microscopie de balayage à effet tunnel (STM). Un élément important de la thèse, résumé dans les chapitres 2 à 4, est la comparaison systématique des structures observées en 2D et en 3D. Cette comparaison aide à identifier des modèles plausibles d'organisation 2D et contribue directement à la compréhension de l'origine des préférences structurales observées en 2D et en 3D. Les paragraphes suivants résument plus en détail les résultats que nous avons obtenus au cours de nos études.

9.1.2 Ingénierie cristalline en 2D et en 3D

Les chapitres 2 à 4 ont permis de démontrer qu'il est possible de programmer une longue série de molécules aptes à s'organiser de manière prévisible avec une forte homologie en 2D et en 3D. Dans cette série d'études, l'organisation moléculaire est contrôlée principalement par la formation de ponts hydrogène. Afin de favoriser une homologie 2D et 3D, nos résultats ont confirmé l'importance de choisir des composantes moléculaires ayant les deux propriétés suivantes : 1) une forte affinité pour la surface utilisée (le graphite dans nos études) et 2) la capacité à s'engager dans de fortes interactions intermoléculaires directionnelles (ponts hydrogène dans nos études). Les structures observées par STM et par diffraction des rayons-X révèlent une organisation préférentielle en rubans qui se regroupent pour former des feuillets. L'ensemble des résultats résumés dans les chapitres 2 à 4 illustre de façon convaincante le potentiel de notre approche comparative 2D et 3D pour confirmer les modèles d'organisation 2D.

Le succès de cette méthode comparative souligne l'ampleur croissante de l'ingénierie cristalline moléculaire et son potentiel comme outil fondamental dans la science des matériaux.

9.1.3 Le groupement diaminotriazinyle (DAT)

Lors des travaux des chapitres 5 et 6, nous avons remarqué que les groupements diaminotriazinyles (DAT) s'associent selon les motifs connus et jouent un rôle clé dans l'organisation moléculaire. Liés aux cycles aromatiques, les groupements DAT favorisent une orientation coplanaire, créant ainsi une topologie moléculaire qui favorise une organisation supramoléculaire en chaînes, en bandes et en couches. Dans le cas des tectoligands du chapitre 5, qui réunissent des groupements DAT avec des cycles hétéroaromatiques pouvant agir comme ligands, nous avons observé une organisation moléculaire quasi identique, même lorsque la longueur de la molécule ou l'orientation du groupement DAT a été variée autour des sites coordinants. Pour les ligands du chapitre 6, nous avons noté une plus grande différence d'un isomère à un autre, probablement à cause de l'inclusion de solvant dans les réseaux, ce qui rend plus difficile la prédiction des structures. Cependant, l'organisation principale est toujours dirigée par l'assemblage des unités DAT. Dans l'ensemble des deux chapitres, nos observations ont confirmé que le groupement DAT permet de contrôler l'association moléculaire en formant de multiples interactions intermoléculaires directionnelles selon des motifs fiables. Les ligands que nous avons synthétisés sont prometteurs pour la chimie de coordination du fait de leur fort caractère coordinant. Ils ont été utilisés pour construire des matériaux hybrides inorganiques et organiques dont les propriétés sont résumées dans le paragraphe suivant.

9.1.4 Stratégie de construction supramoléculaire inorganique/organique

Les tectoligands présentés dans cette thèse ont permis de construire un grand nombre de métallotectons par coordination avec les métaux de la première série de transition. Des métallotectons de topologies linéaire, coudée, carrée, rectangulaire et tétraédrique déformée ont été synthétisés puis caractérisés par diffraction des rayons-X. Des architectures supramoléculaires en ruban, en grille, en torsade et en fermeture éclaire ont été observées. Nos résultats ont apporté une meilleure compréhension de la façon dont les coordinations métalliques peuvent être utilisées en coopération avec d'autres interactions pour diriger l'assemblage moléculaire. Notre travail illustre comment des métallotectons peuvent être aisément synthétisés avec des caractéristiques structurelles prévisibles en combinant la coordination et la formation des ponts hydrogène. Nos résultats montrent également comment différents groupes fonctionnels introduits au sein du métallotecton peuvent coopérer pour diriger l'assemblage supramoléculaire.

Dans cette thèse, nous avons démontré que la stratégie combinant la chimie de coordination et la formation des ponts hydrogène est efficace pour l'édification des structures supramoléculaires. Elle permet d'obtenir un grand nombre de métallotectons en peu d'étapes de synthèse. La géométrie du métallotecton, et par conséquent l'architecture du réseau supramoléculaire, peuvent être contrôlées par les caractéristiques du tectoligand ainsi que par la topologie de la sphère de coordination du métal. La structure des métallotectons individuels est relativement facile à prédire parce que la géométrie de coordination du métal est souvent fiable. Les réseaux supramoléculaires qui résultent de l'association des métallotectons sont plus difficiles à prédire, mais on y retrouve néanmoins des motifs caractéristiques d'association des groupements DAT.

9.2 Perspectives

Nos études ont démontré le potentiel des principes modernes de l'ingénierie cristalline pour ordonner les molécules en 2D et en 3D. Le succès que nous avons eu dans ces études comparatives 2D et 3D confirme le choix des composantes utilisées pour la création de structures analogues en 2D et 3D. Nous nous attendons à ce que notre approche comparative 2D et 3D devienne une méthode fiable pour concevoir de nouveaux matériaux moléculaires qui doivent posséder une organisation semblable dans différents états, ce qui permet leur utilisation dans les applications exigeant un comportement prévisible en 2D et 3D.

Les composés ainsi que les architectures que nous avons créées au cours de cette thèse ne sont qu'une petite minorité de ce qui peut être imaginé. De nombreuses autres structures peuvent être obtenues par la stratégie combinant la chimie de coordination et les ponts hydrogène ou d'autres interactions intermoléculaires. Il existe autant de possibilités que de combinaisons métal/tectoligand. Notre prochain défi est d'examiner si l'affinité pour les surfaces montrée par les tectoligands que nous avons étudiés est partagée également par les métallotectons dérivés des tectoligands. Si oui, les métallotectons eux-mêmes pourraient être organisés de manière prédictible en 2D. C'est en partie pour cette raison que nous avons synthétisé une série de métallotectons pouvant adopter des conformations aplaties. L'organisation en 2D des métallotectons permettrait donc obtenir des surfaces modifiées par la présence d'un réseau de sites métalliques avec une topologie difficile ou même impossible à obtenir avec des composés purement organiques. Nous pensons qu'il est possible de concevoir une famille de métallotectons qui pourraient s'organiser de manière prédictible en 2D et en 3D avec une forte homologie. Nous croyons que les stratégies que nous avons utilisées dans cette thèse peuvent servir de modèle pour comprendre le comportement des métallotectons dans des études en science des surfaces.

Pour développer davantage les thèmes explorés dans cette thèse, nous envisageons la possibilité d'entreprendre plusieurs études futures. Une priorité est d'étudier l'organisation moléculaire de nos tectoligands déposés sur d'autres surfaces que le graphite. Par exemple, l'adsorption des tectoligands sur des surfaces métalliques telles que l'argent, le cuivre, l'or ou le palladium pourrait induire une coordination avec les métaux de la surface pour former des structures organométalliques en 2D. Nous comptons également étudier la déposition sur le graphite et sur d'autres surfaces des métallotectons synthétisés. Une telle étude nous permettra d'explorer les phénomènes d'absorption des métallotectons et leurs interactions sur des surfaces métalliques. Un autre objectif important est d'étendre nos études de construction supramoléculaire inorganique/organique, basées initialement sur les complexes d'argent et du palladium, en utilisant d'autres métaux de transition. Le nickel et le cuivre, qui sont des métaux dont la chimie de coordination est bien connue, sont des choix particulièrement intéressants pour des études futures. Nous proposons dans une étude ultérieure de remplacer les unités diaminotriazinyles (DAT) de nos tectoligands, qui sont responsables de l'association des métallotectons par ponts hydrogène, par des groupements participant dans d'autres interactions intermoléculaires telles que les interactions π-π, l'embrassement des groupements triphényles et encore bien d'autres. Finalement, la mise en application de nos découvertes est un objectif prioritaire. Par exemple, les études que nous avons menées dans cette thèse et celles que nous proposons de réaliser présentent toutes des intérêts pour la création de dispositifs optoélectroniques et, de manière générale, pour la création de nanomatériaux. Nous sommes optimistes que nos résultats auront un impact visible dans ces domaines prometteurs.

Annexe 1

Partie supplémentaire de l'article 1

Supporting Information

Engineering Homologous Molecular Organization in 2D and 3D. Cocrystallization of Aminoazines and Alkanecarboxylic Acids

Adam Duong, Thierry Maris, and James D. Wuest*

Département de Chimie, Université de Montréal

Montréal, Québec, H3C 3J7 Canada

Contents **Page**

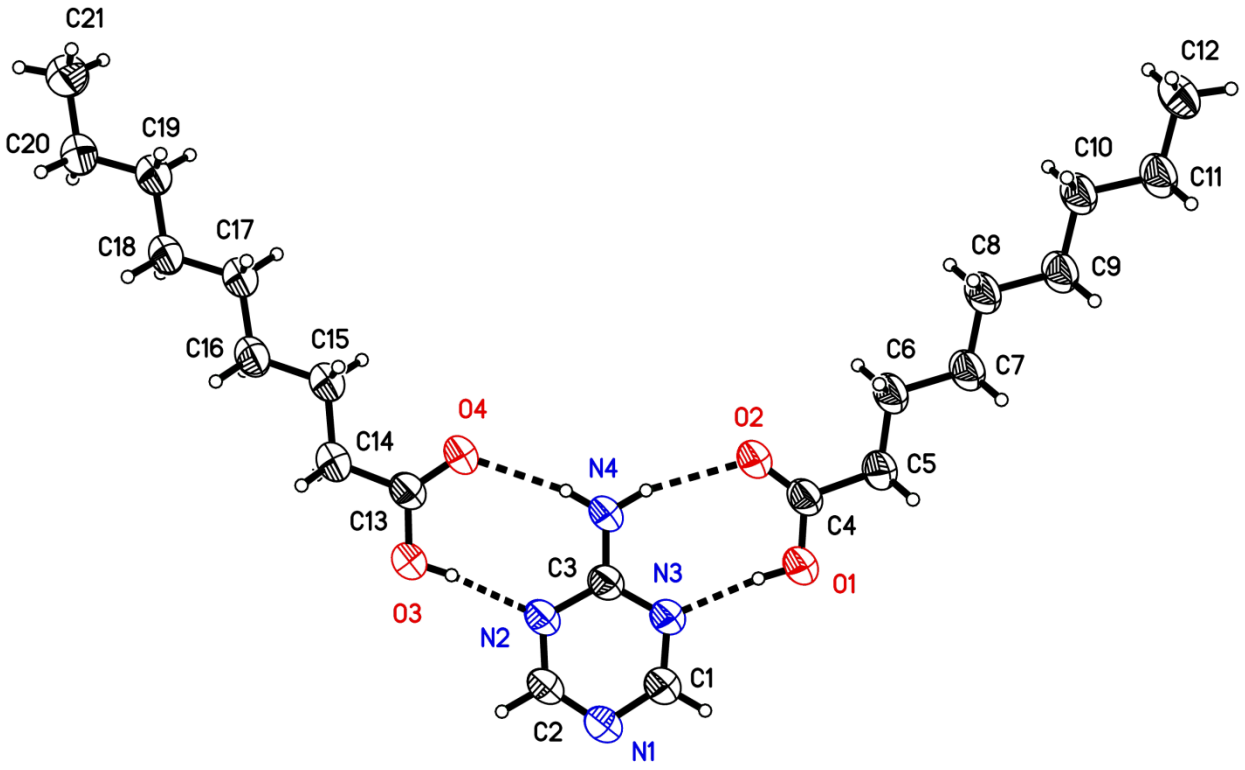

Figure S1. Thermal atomic displacement ellipsoid plot of the structure of the 1:2 cocrystals of 2-amino-1,3,5-triazine (**1**) with nonanoic acid. The ellipsoids of non-hydrogen atoms are drawn at the 50% probability level, and hydrogen atoms are represented by a sphere of arbitrary size.

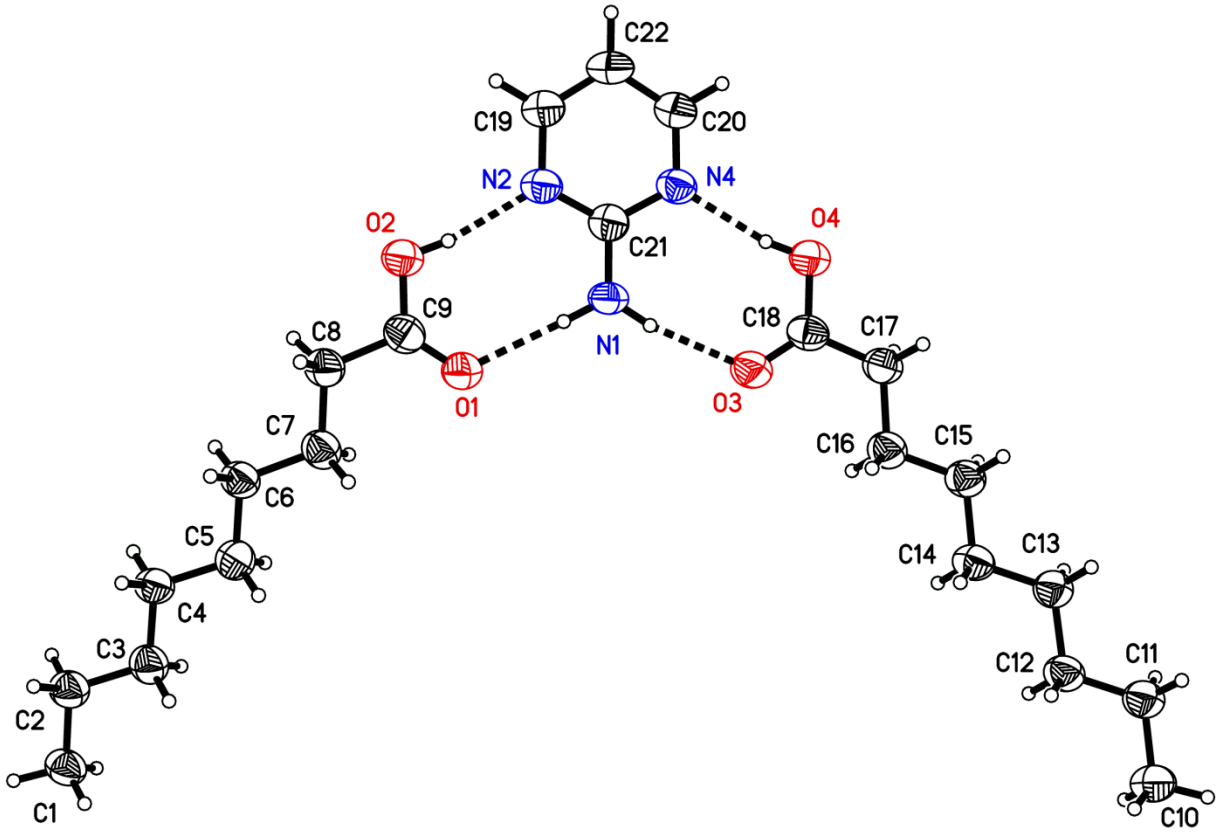

Figure S2. Thermal atomic displacement ellipsoid plot of the structure of the 1:2 cocrystals of 2-aminopyrimidine (**2**) with nonanoic acid. The ellipsoids of non-hydrogen atoms are drawn at the 50% probability level, and hydrogen atoms are represented by a sphere of arbitrary size.

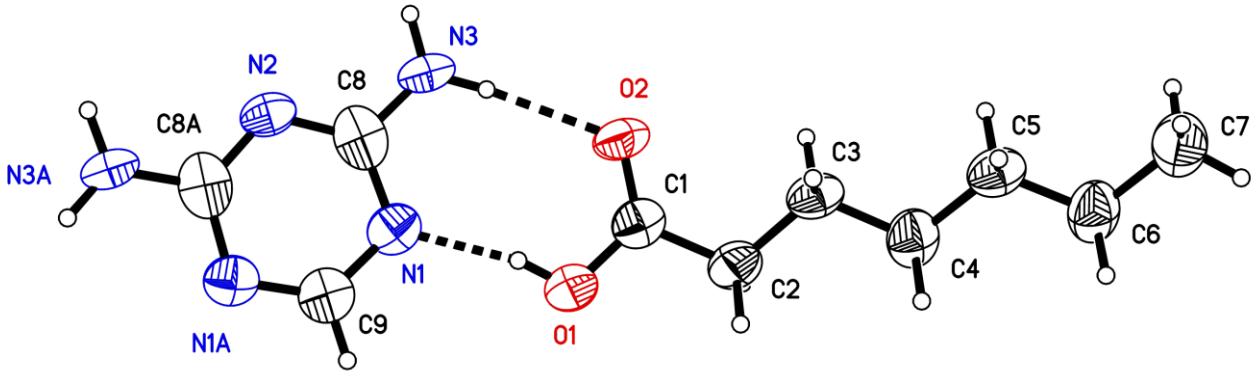

Figure S3. Thermal atomic displacement ellipsoid plot of the structure of the 1:2 cocrystals of 2,4-diamino-1,3,5-triazine (**3**) with heptanoic acid. The ellipsoids of non-hydrogen atoms are drawn at the 50% probability level, and hydrogen atoms are represented by a sphere of arbitrary size.

Homogeneity of Bulk Crystalline Samples

In all structural studies, experimental powder X-ray diffraction patterns were recorded for each bulk crystalline sample and then compared with those calculated from single-crystal X-ray diffraction data. In all cases, these comparisons confirmed that the single-crystal specimens selected for structural analysis were representative of the bulk crystalline samples from which they were chosen. Experimental powder X-ray diffraction patterns were recorded using one of the following two instruments :

1) Bruker D8 Discover diffractometer with GADDS HTS, using graphite monochromatized Cu Kα radiation generated at 40 kV and 40 mA, working in reflection mode. The 2D general area detector was positioned at a distance of 15 cm from the powder sample, which was placed on a glass plate. This allowed simultaneous collection of data over an

angular domain up to 35° in 2θ. Measurements were carried out 293 K in coupled scan mode (θ-θ geometry). Four separate images (diffraction arcs) were collected (scanning time : 5 min/image), and intensity along each arc was integrated to create the 1D powder pattern of intensity versus 2θ, over the angular range $10° < 2\theta < 105°$.

2) Single-crystal Bruker Microstar diffractometer mounted with an FR591 rotating anode generator, Helios optics, and a 2D Pt135 CCD detector, working in transmission mode. A small amount of ground sample was mounted in a fiber loop, and the diffraction patterns were recorded at 150 K by phi-scan over five different detector positions, merged, and integrated to give the 1D powder diffraction pattern.

Structural data from single-crystal analyses were used to calculate theoretical powder X-ray diffraction patterns with the aid of Mercury software.[1] The diffraction pattern of the 1:2 cocrystals of 2,4-diamino-1,3,5-triazine (**3**) with heptanoic acid was subject to strong preferred orientation affecting *(h00)* reflections, so the calculated pattern was modeled using a March-Dollase function[2] as implemented in the powder diffraction module of Materials Studio.[3] Peak fitting and the refinement of lattice parameters were carried out using TOPAS software,[4] and Pawley fitting was applied to the powder X-ray diffraction patterns.

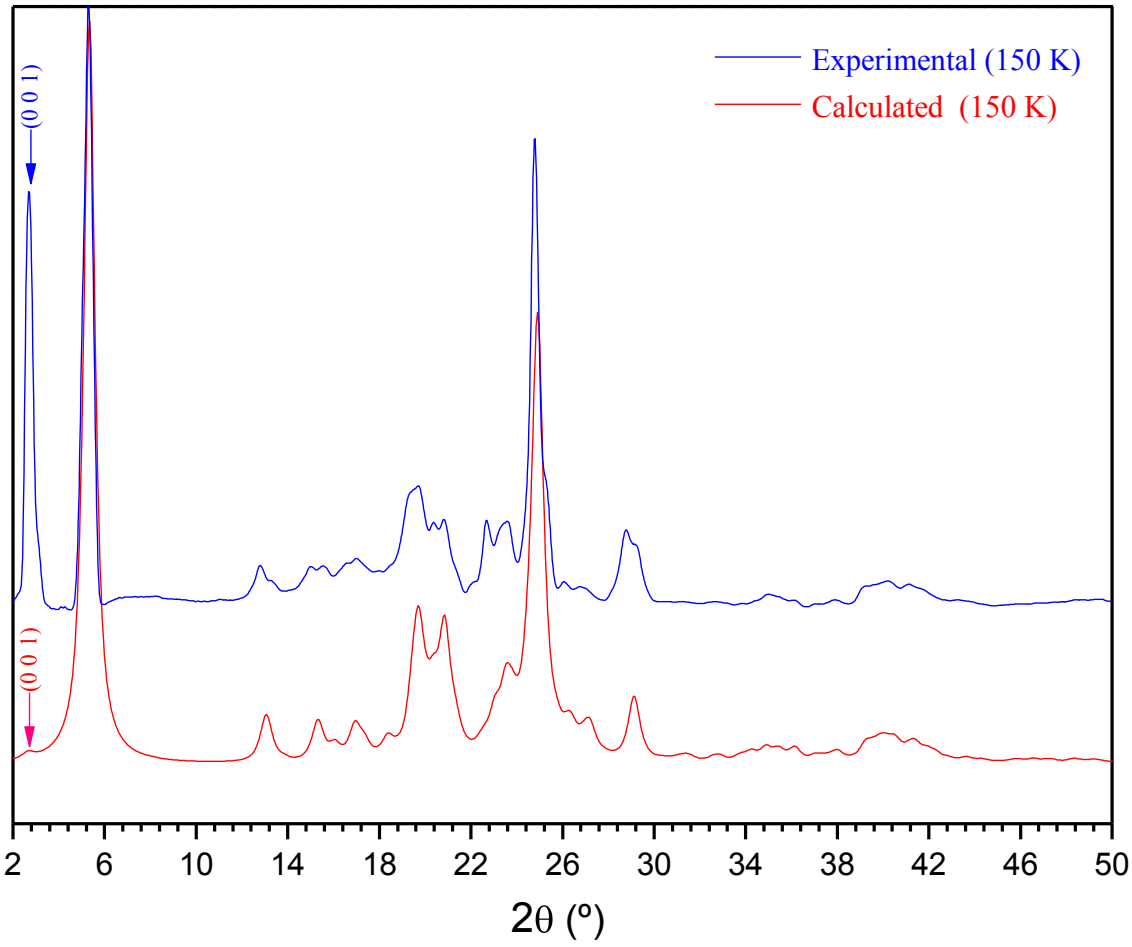

Figure S4. Comparison between experimental (collected using Bruker Microstar) and calculated powder X-ray diffraction patterns for the 1:2 cocrystals of 2-amino-1,3,5-triazine (**1**) with nonanoic acid. The two diffractograms are closely similar, confirming that the bulk crystalline sample consists of a single phase.

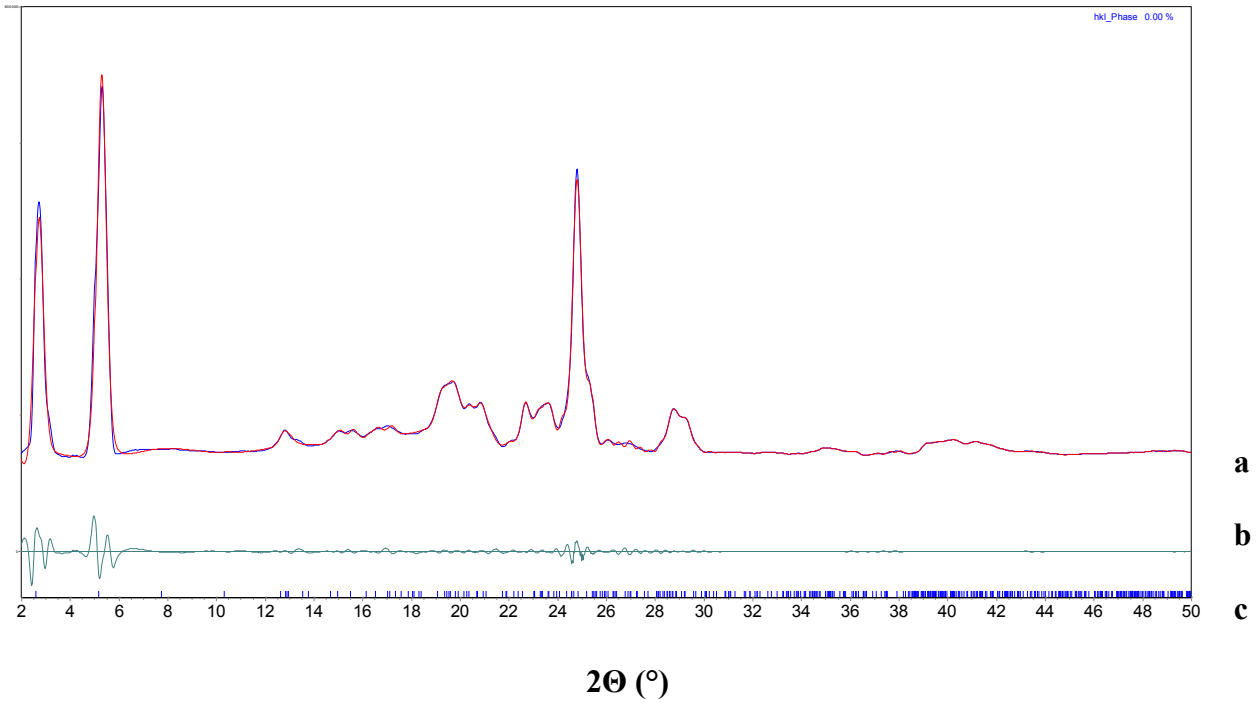

Figure S5. (a) Simulated powder X-ray diffraction pattern of the 1:2 cocrystals of 2-amino-1,3,5-triazine (**1**) with nonanoic acid (red curve), as determined by Pawley fitting of the experimental powder X-ray diffraction pattern (nearly superimposed blue curve). (b) Difference between experimental and calculated intensities. (c) Position of calculated reflections.

Table S1. Crystallographic Data for the 1:2 Cocrystals of 2-Amino-1,3,5-triazine (**1**) with Nonanoic Acid, as Determined by Pawley Fitting of Powder X-Ray Diffraction Data at 150 K.

compound	**1** • 2 nonanoic acid
composition	$C_3H_4N_4 \cdot 2(C_9H_{18}O_2)$
temperature (K)	150
crystal system	triclinic
space group	$P\bar{1}$
a (Å)	5.292(14)
b (Å)	7.120(26)
c (Å)	34.337(30)
α(º)	90.86(25)
β(º)	92.47(25)
γ(º)	100.18(65)
V (Å^3)	1271.8(65)
Z	2

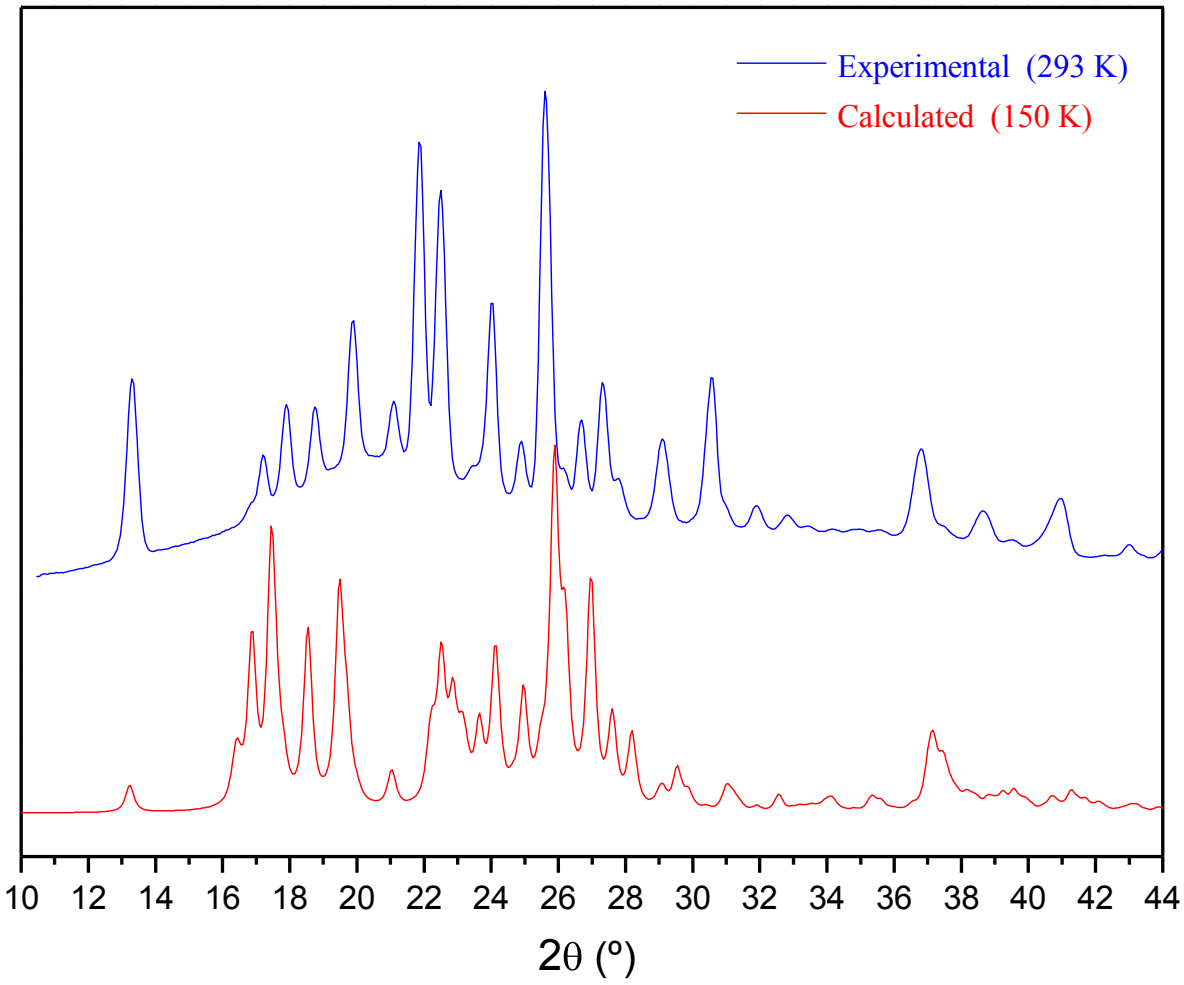

Figure S6. Comparison between experimental (collected using D8 Discover) and calculated powder X-ray diffraction patterns for the 1:2 cocrystals of 2-aminopyrimidine (**2**) with nonanoic acid. The *x*-axis of the experimental pattern was shifted to minimize the slight angular shift due to the effect of temperature. The two diffractograms are closely similar, confirming that the bulk crystalline sample consists of a single phase.

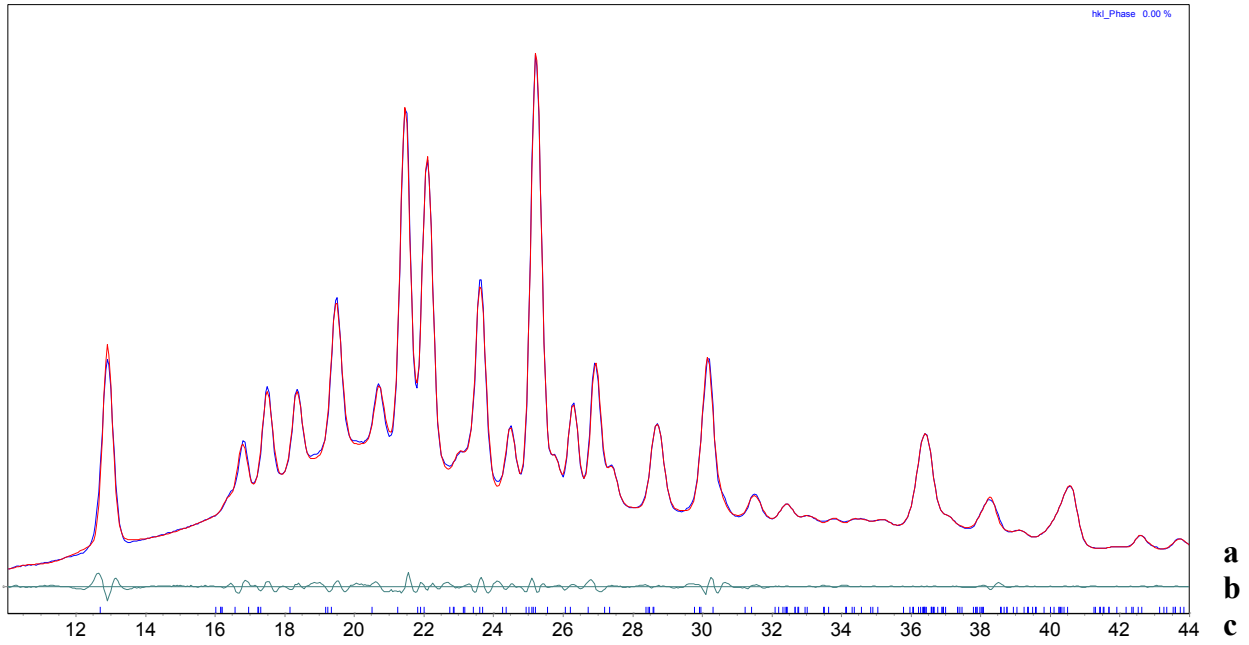

Figure S7. (a) Simulated powder X-ray diffraction pattern of the 1:2 cocrystals of 2-aminopyrimidine (**2**) with nonanoic acid (red curve) as determined by Pawley fitting of the experimental powder X-ray diffraction pattern (nearly superimposed blue curve). (b) Difference between experimental and calculated intensities. (c) Position of calculated reflections.

Table S2. Crystallographic Data for the 1:2 Cocrystals of 2-Aminopyrimidine (**2**) with Nonanoic Acidas Determined by Pawley Fitting of Powder X-Ray Diffraction Data at 293 K.

compound	**2** • 2 nonanoic acid
composition	$C_4H_5N_3 \cdot 2(C_9H_{18}O_2)$
temperature (K)	293
crystal system	monoclinic
space group	*P*c
a (Å)	5.5201(43)
b (Å)	5.5275(10)
c (Å)	42.1094(77)
α (º)	90
β (º)	97.059(50)
γ (º)	90
V (Å^3)	1275.1(10)
Z	2

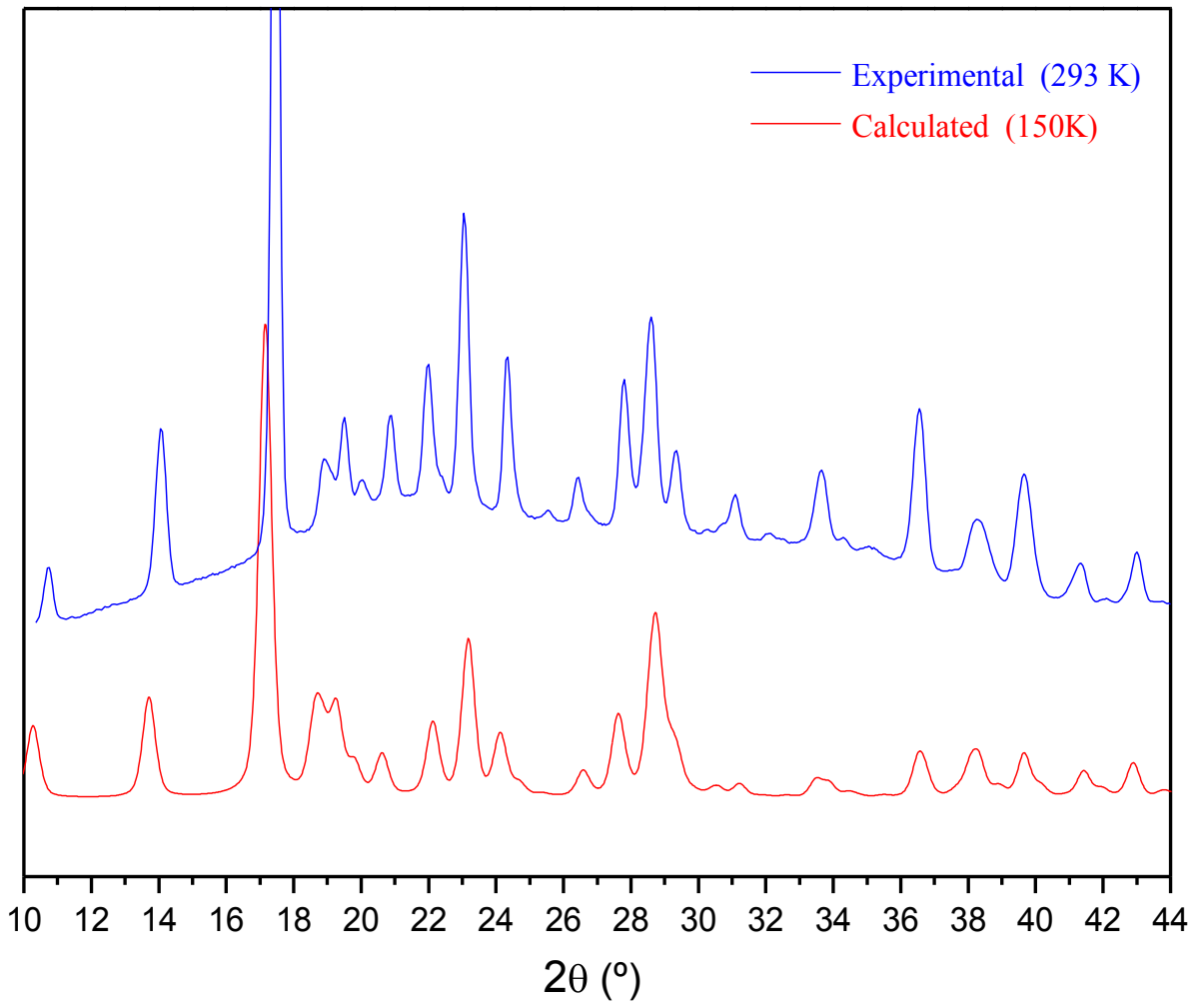

Figure S8. Comparison between experimental (collected using D8 Discover) and calculated powder X-ray diffraction patterns for the 1:2 cocrystals of 2,4-diamino-1,3,5-triazine (**3**) with heptanoic acid. The *x*-axis of the experimental pattern was shifted to minimize the slight angular shift due to the effect of temperature. The two diffractograms are closely similar, confirming that the bulk crystalline sample consists of a single phase.

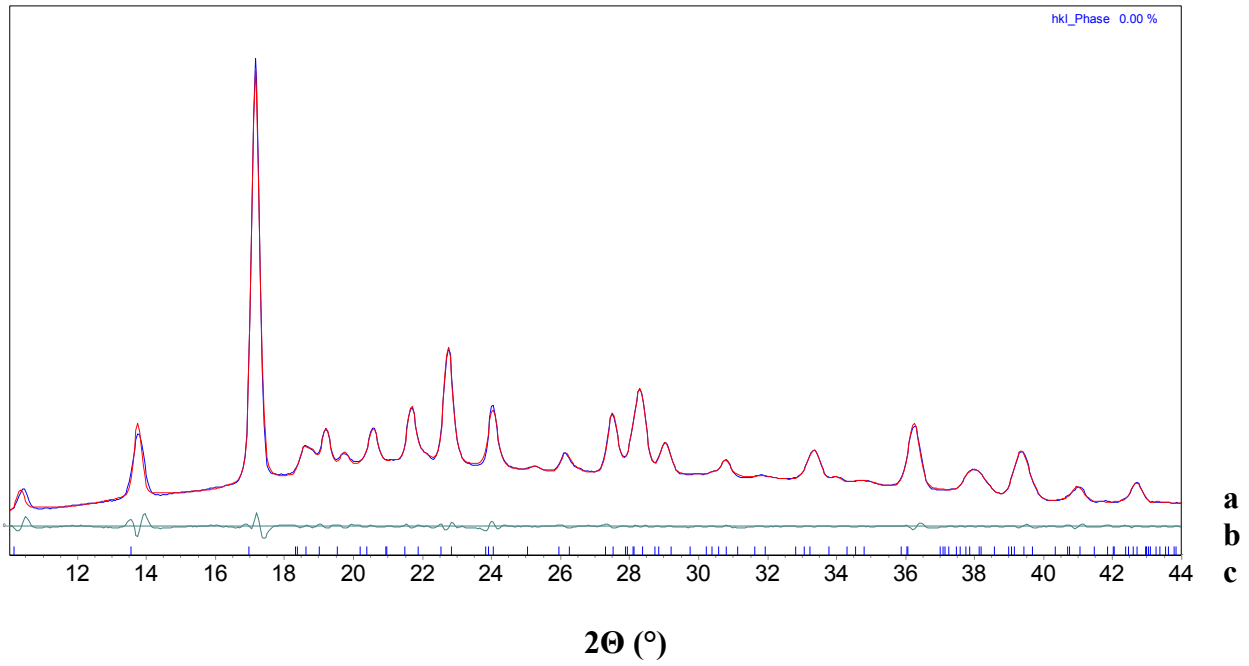

Figure S9. (a) Simulated powder X-ray diffraction pattern of the 1:2 cocrystals of 2,4-diamino-1,3,5-triazine (**3**) with heptanoic acid (red curve) as determined by Pawley fitting of the experimental powder X-ray diffraction pattern (nearly superimposed blue curve). (b) Difference between experimental and calculated intensities. (c) Position of calculated reflections.

Table S3. Crystallographic Data for the 1:2 Cocrystals of 2,4-Diamino-1,3,5-triazine (**3**) with Heptanoic acid as Determined by Pawley Fitting of Powder X-Ray Diffraction Data at 293 K.

compound	**3** • 2 heptanoic acid
composition	$C_3H_5N_5 \cdot 2(C_7H_{14}O_2)$
temperature (K)	293
crystal system	orthorhombic
space group	$Pmn2_1$
a (Å)	52.233(17)
b (Å)	4.8431(20)
c (Å)	4.2549(11)
α (º)	90
β (º)	90
γ (º)	90
V (Å^3)	1076.37(62)
Z	2

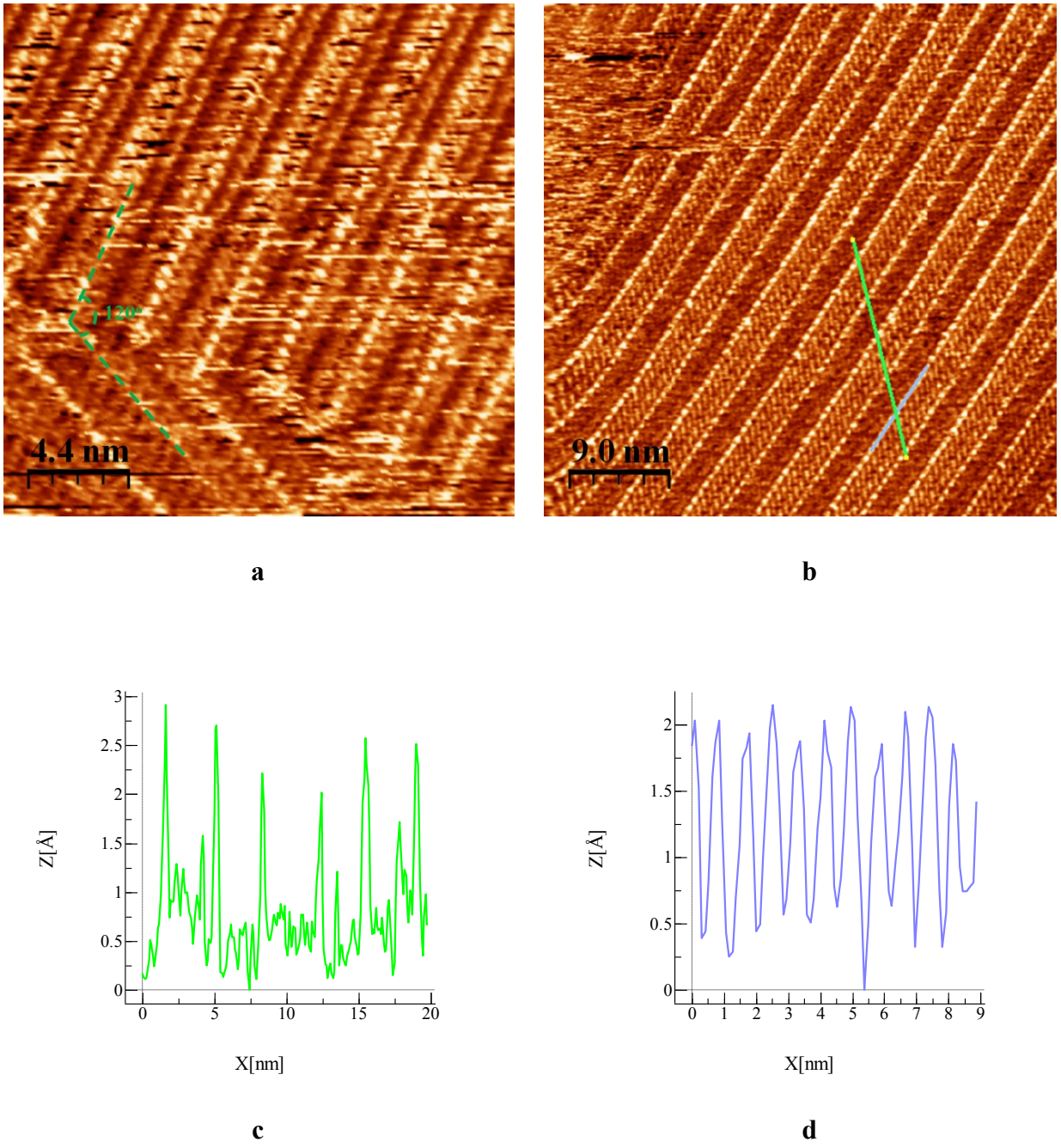

Figure S10. (a) Supplementary STM image of the 2D cocrystallization of 2-amino-1,3,5-triazine (**1**) and nonanoic acid on HOPG, showing the intersection of two domains (deposition from nonanoic acid, with V_{bias} = -1.39 V and I_{set} = 0.22 nA). (b) Large-scale STM image obtained under the same conditions. (c) Profile along the green axis shown in Figure S10b. (d) Profile along the blue axis shown in Figure S10b.

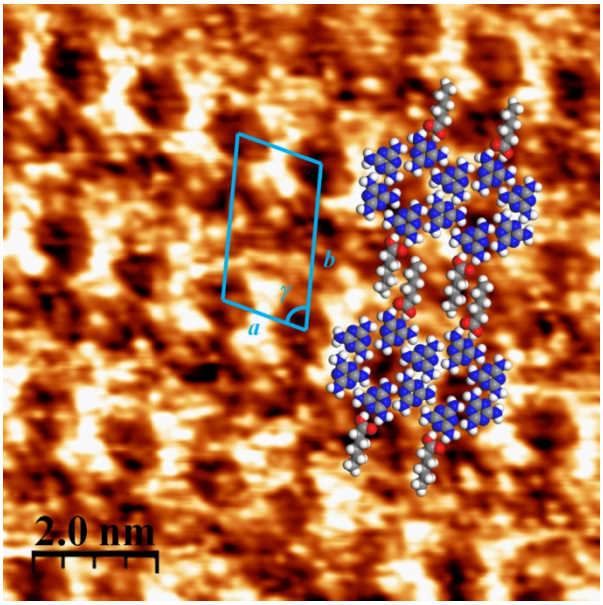

Figure S11. STM image of the 2D cocrystallization of melamine (**4**) and hexanoic acid on HOPG (deposition from hexanoic acid, with V_{bias} = -1.40 V and I_{set} = 0.25 nA). Superimposed on the image are a scale bar, the measured unit cell, and a model of the proposed assembly. The unit cell parameters are a = 10.1 Å, b = 22.8 Å, and γ = 80°.

References

1) Macrae, C. F.; Edgington, P. R.; McCabe, P.; Pidcock, E.; Shields, G. P.; Taylor, R.; Towler, M.; van de Streek, J. *J. Appl. Cryst.* **2006**, *39*, 453-457.
2) Dollase, W. A. *J. Appl. Cryst.* **1986**, *19*, 267-272.
3) Accelrys, Inc., 10188 Telesis Court, Suite 100, San Diego, California 92121 USA.
4) Coelho, A. A. *TOPAS User Manual*, Version 3.1 ed.; Bruker-AXS GmbH : Karlsruhe, Germany, 2003.

Annexe 2

Partie supplémentaire de l'article 2

Supporting Information

2D Molecular Organization of Pyridinecarboxylic Acids Adsorbed on Graphite

Adam Duong, Marc-André Dubois, and James D. Wuest*

Département de Chimie, Université de Montréal

Montréal, Québec, H3C 3J7 Canada

Contents **Page**

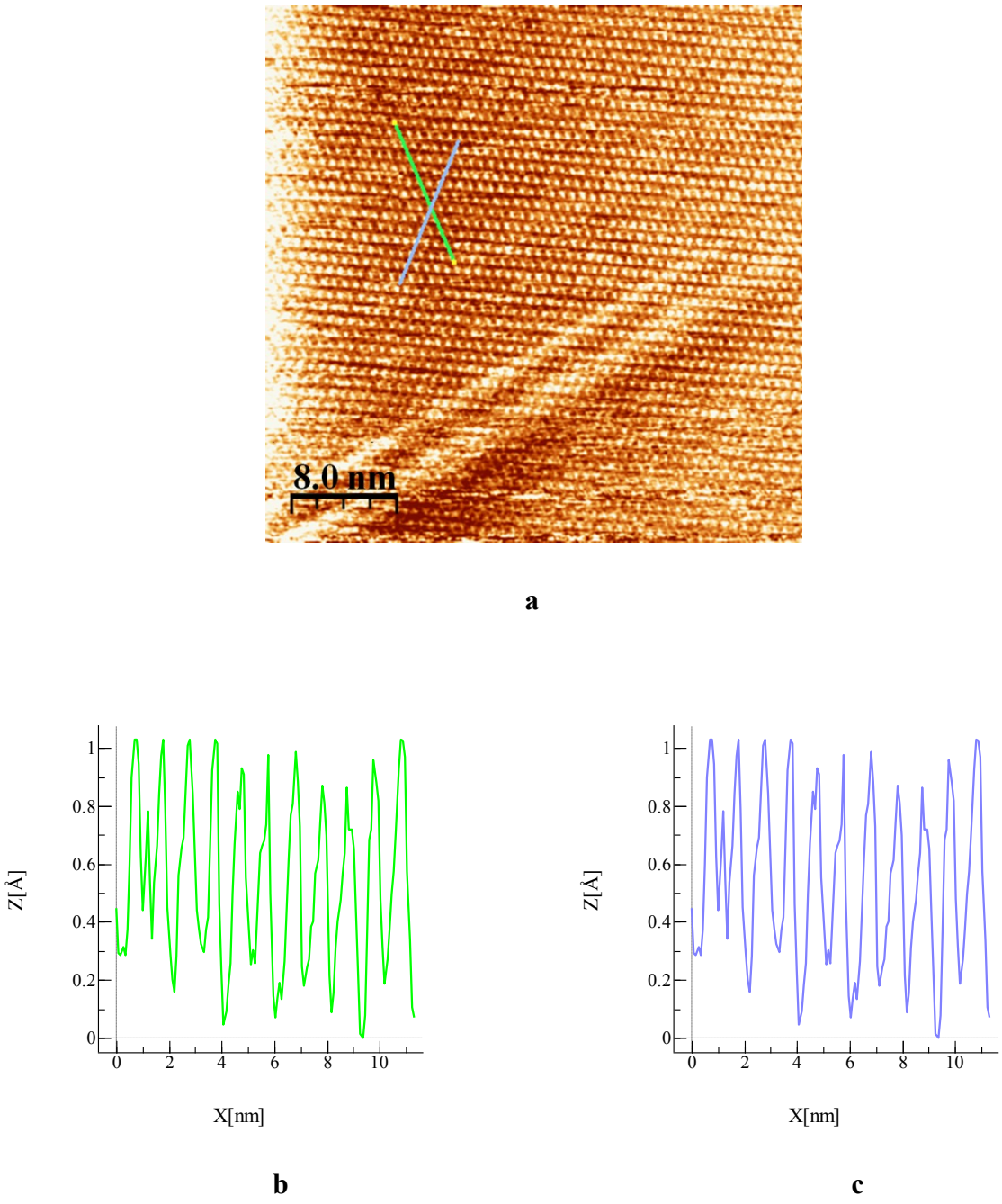

Figure S1. (a) Supplementary large-scale STM image of the adsorption of 4-pyridinecarboxylic acid (**3**) on HOPG (deposition from heptanoic acid, with V_{bias} = -1.39 V and I_{set} = 0.13 nA). (b) Profile along the green axis shown in Figure S1a. (c) Profile along the blue axis shown in Figure S1a.

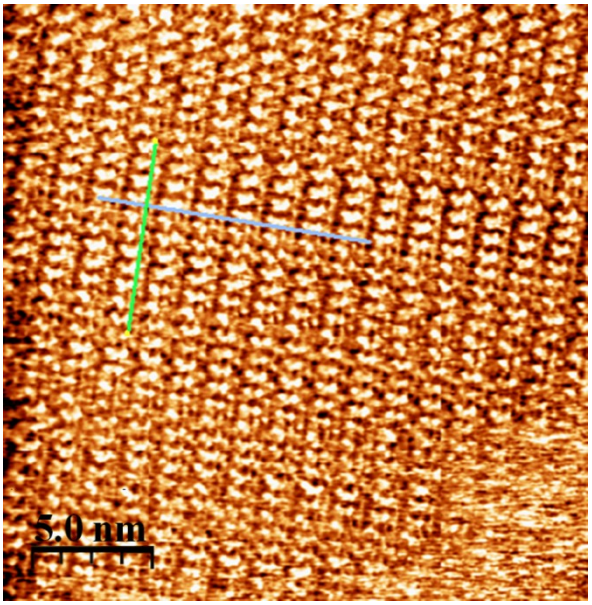

a

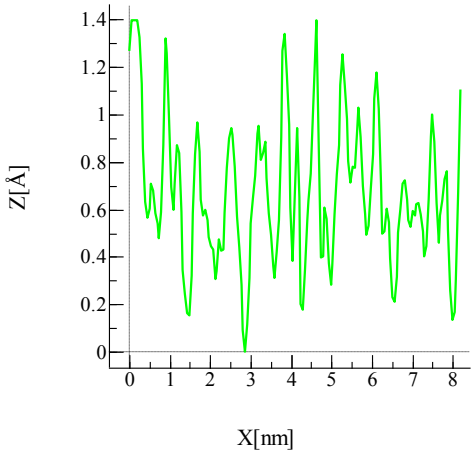

b

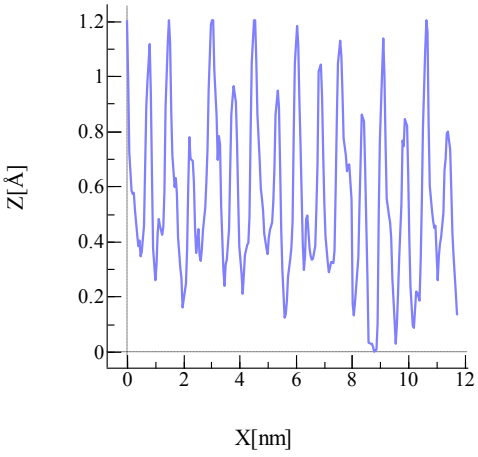

c

Figure S2. (a) STM image of the adsorption of 3-pyridinecarboxylic acid (**4**) on HOPG (deposition from heptanoic acid, with V_{bias} = -1.50 V and I_{set} = 0.08 nA). (b) Profile along the green axis shown in Figure S2a. (c) Profile along the blue axis shown in Figure S2a.

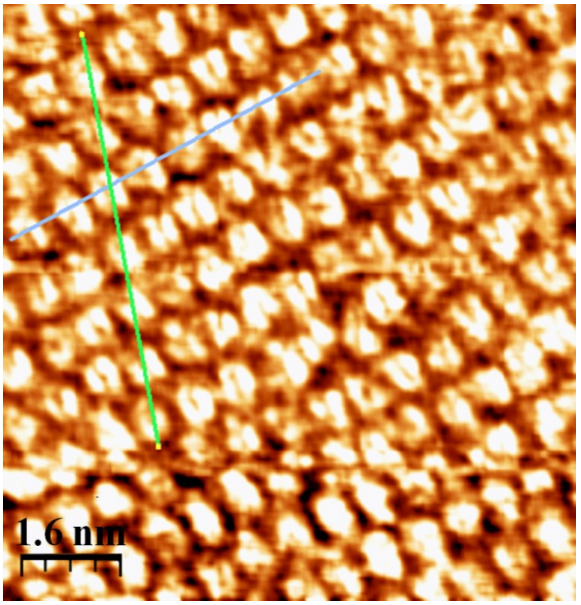

a

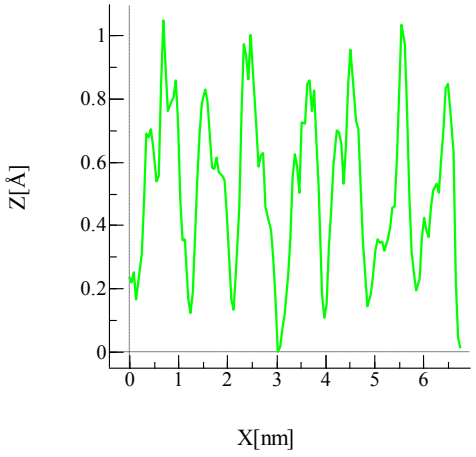

b

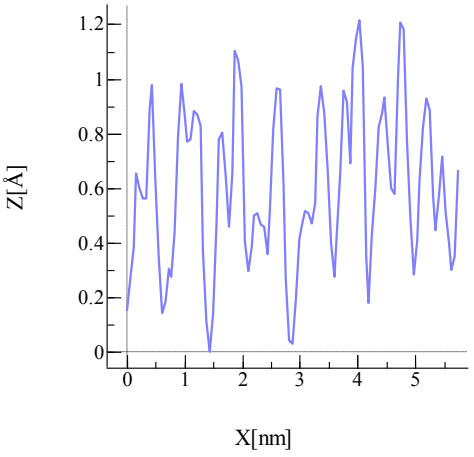

c

Figure S3. (a) STM image of the adsorption of 2-pyridinecarboxylic acid (**5**) on HOPG (deposition from heptanoic acid, with V_{bias} = -1.50 V and I_{set} = 0.09 nA). (b) Profile along the green axis shown in Figure S3a. (c) Profile along the blue axis shown in Figure S3a.

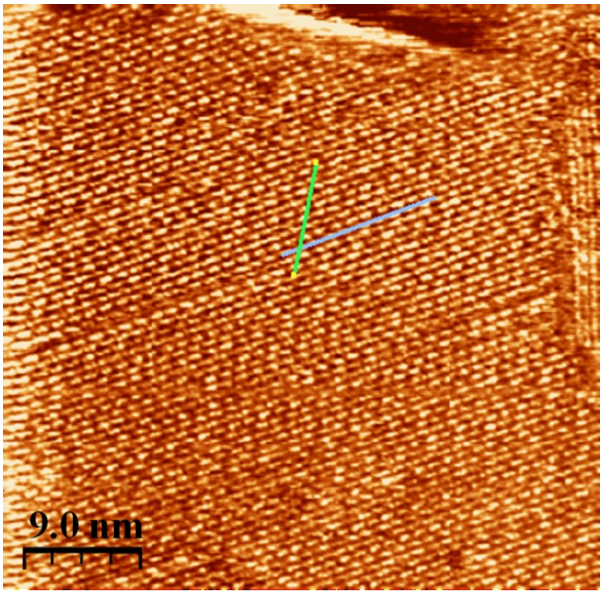

a

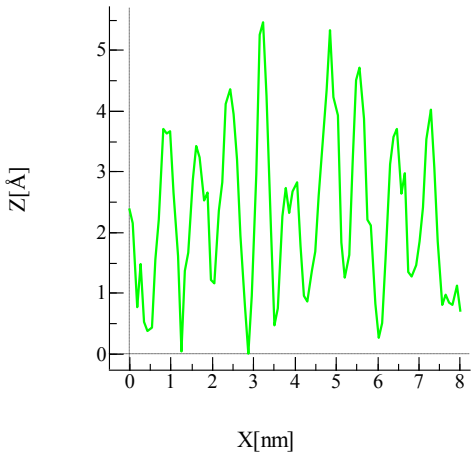

b

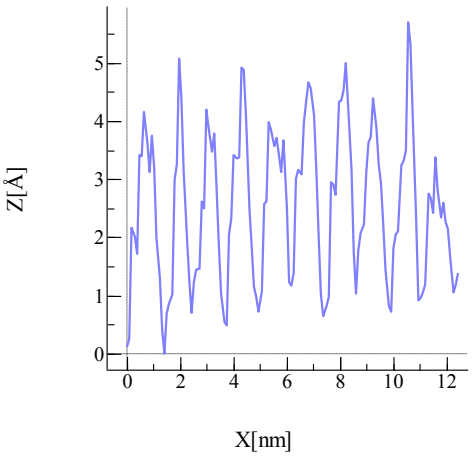

c

Figure S4. (a) Large-scale STM image of the adsorption of 4-(4-carboxyphenyl)pyridine (**6**) on HOPG (deposition from heptanoic acid, with V_{bias} = -1.50 V and I_{set} = 0.27 nA). (b) Profile along the green axis shown in Figure S4a. (c) Profile along the blue axis shown in Figure S4a.

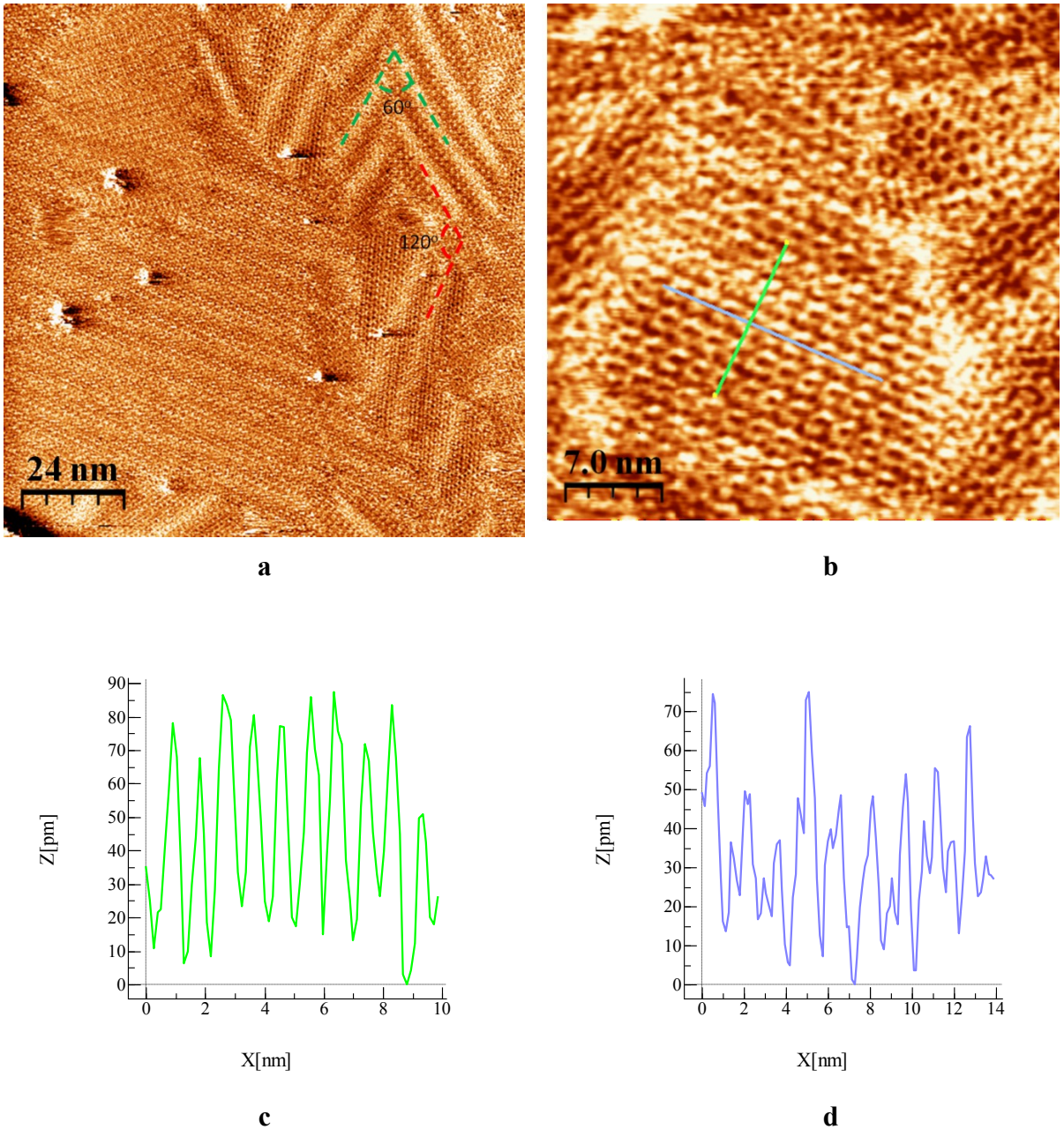

Figure S5. (a) Supplementary large-scale STM image of the adsorption of 3,5-pyridinedicarboxylic acid (**7**) on HOPG (deposition from heptanoic acid, with V_{bias} = -1.49 V and I_{set} = 0.10 nA). (b) An additional STM image obtained under the same conditions. (c) Profile along the green axis shown in Figure S5b. (d) Profile along the blue axis shown in Figure S5b.

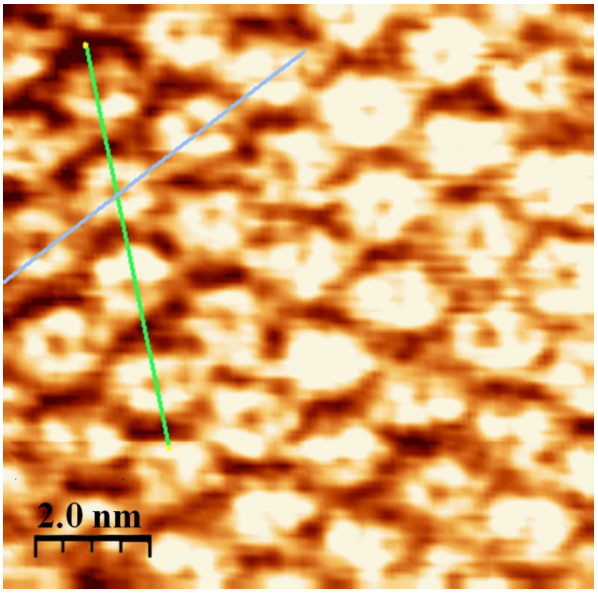

a

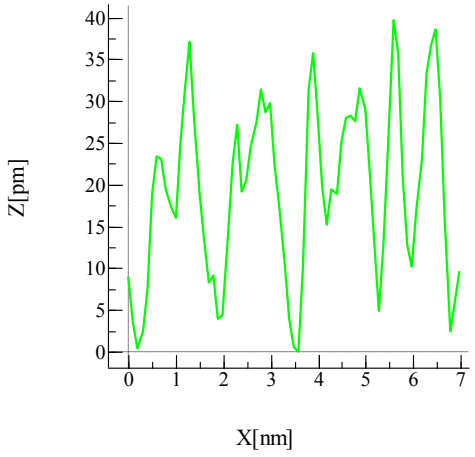

b

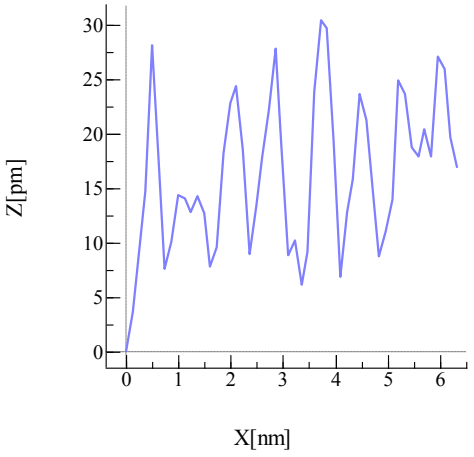

c

Figure S6. (a) STM image of the adsorption of 2,6-pyridinedicarboxylic acid (**8**) on HOPG (deposition from heptanoic acid, with V_{bias} = -0.70 V and I_{set} = 0.23 nA). (b) Profile along the green axis shown in Figure S6a. (c) Profile along the blue axis shown in Figure S6a.

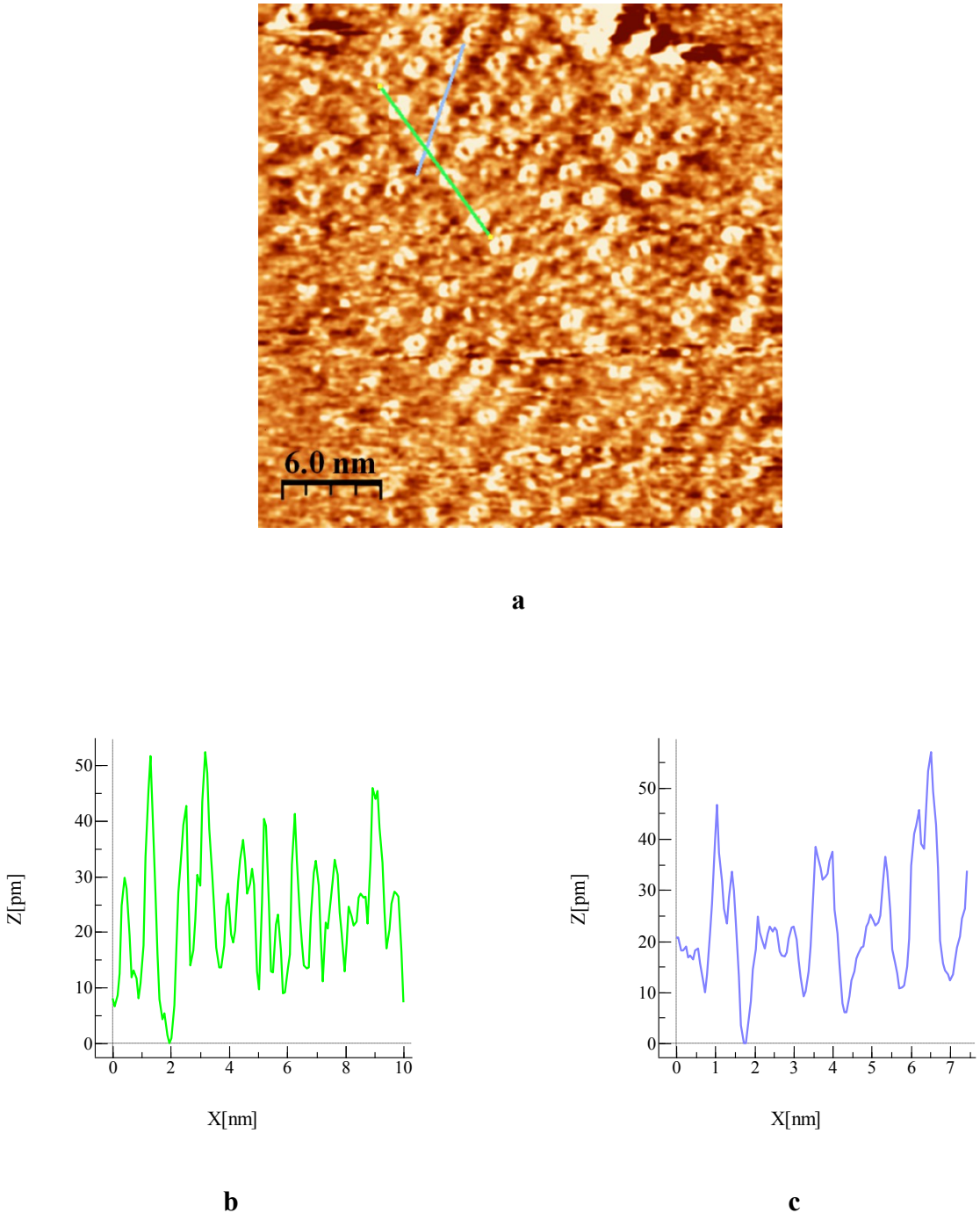

Figure S7. (a) STM image of the adsorption of 2,4,6-pyridinetricarboxylic acid (**9**) on HOPG (deposition from heptanoic acid, with V_{bias} = -1.50 V and I_{set} = 0.10 nA). (b) Profile along the green axis shown in Figure S7a. (c) Profile along the blue axis shown in Figure S7a.

Annexe 3

Partie supplémentaire de l'article 3

Supporting Information

Engineering Homologous Molecular Organization in 2D and 3D. Cocrystallization of Pyridyl-Substituted Diaminotriazines with Alkanecarboxylic Acids

Adam Duong,[†] Marc-André Dubois,[†] Thierry Maris,[†] Valérie Métivaud,[†] Ji-Hyun Yi,[‡] Antonio Nanci,[‡] Alain Rochefort,[§] and James D. Wuest*[,†]

[†]Département de Chimie and [‡]Faculté de Médecine Dentaire, Université de Montréal, Montréal, Québec H3C 3J7, Canada; [§]Département de Génie Physique, École Polytechnique de Montréal, Montréal, Québec H3A 3A7, Canada

Contents **Page**

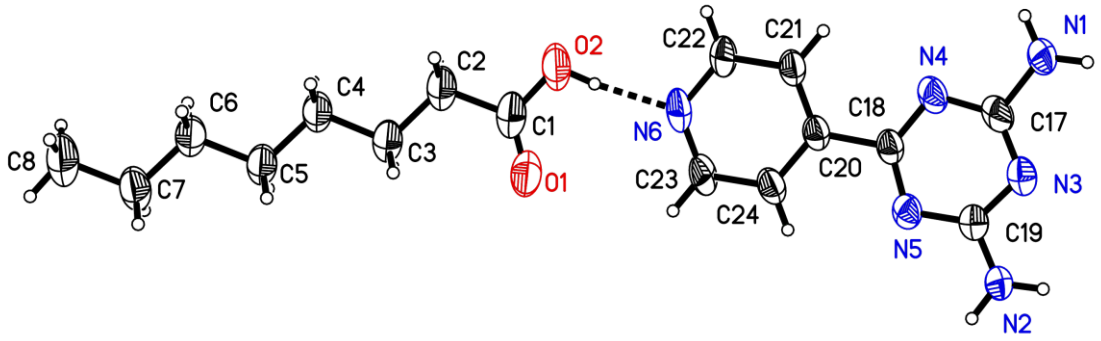

Figure S1. Thermal atomic displacement ellipsoid plot of the structure of 1:2 cocrystals of 2,4-diamino-6-(4-pyridyl)-1,3,5-triazine (**2a**) with octanoic acid. The ellipsoids of non-hydrogen atoms are drawn at the 50% probability level, hydrogen atoms are represented by a sphere of arbitrary size, and hydrogen bonds are represented by broken lines. Only one orientation of the disordered molecules of compound **2a** is shown.

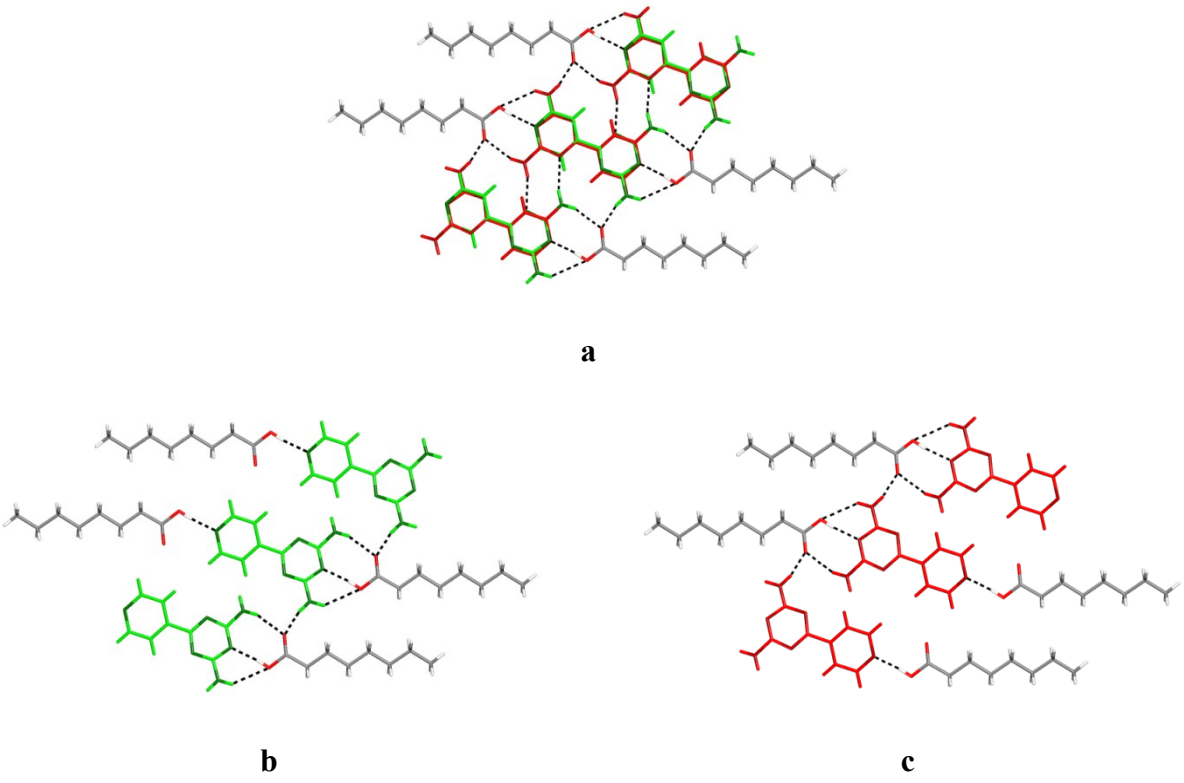

Figure S2. Representations of disorder in the structure of 1:2 cocrystals of 2,4-diamino-6-(4-pyridyl)-1,3,5-triazine (**2a**) with octanoic acid. (a) Partial view of one plane, showing two possible orientations of molecules of compound **2a** around a center of inversion. Molecules in the two orientations are drawn in green and red. (b) View of only the molecules shown in green. (c) View of only the molecules shown in red.

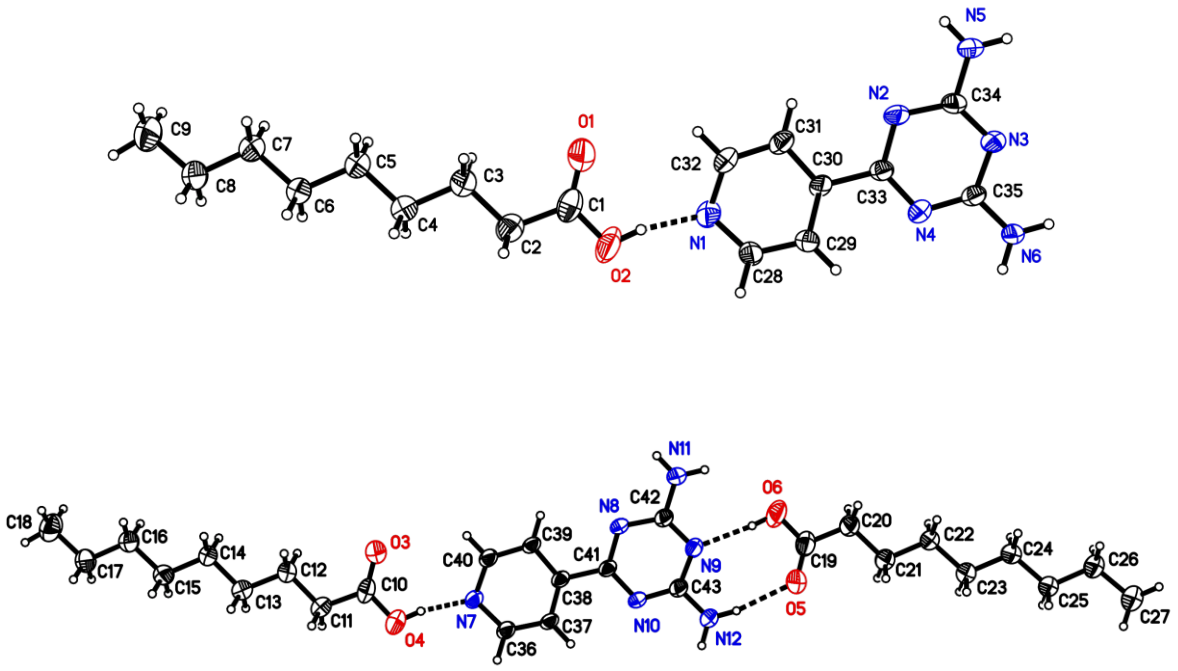

Figure S3. Thermal atomic displacement ellipsoid plots of the structure of 1:2 cocrystals of 2,4-diamino-6-(4-pyridyl)-1,3,5-triazine (**2a**) with nonanoic acid. The ellipsoids of non-hydrogen atoms are drawn at the 50% probability level, hydrogen atoms are represented by a sphere of arbitrary size, and hydrogen bonds are represented by broken lines. Only one orientation of the disordered molecules of compound **2a** is shown.

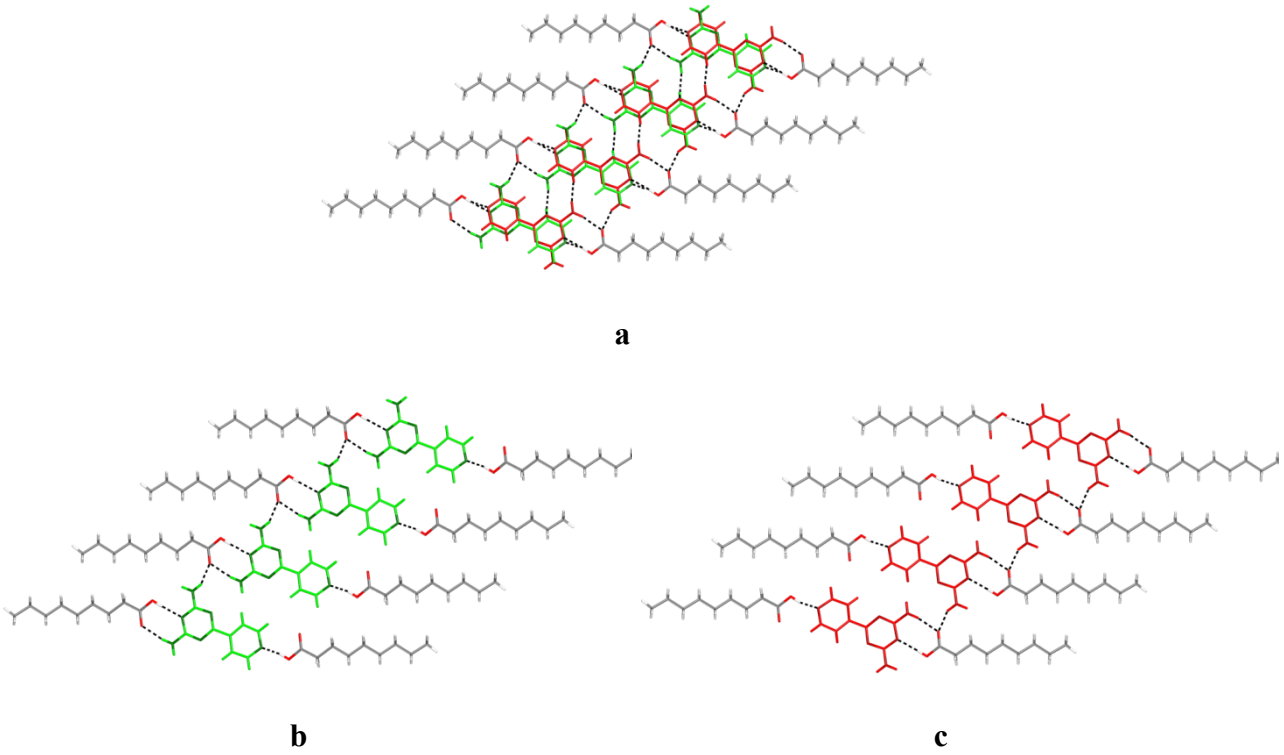

Figure S4. Representations of disorder in the structure of 1:2 cocrystals of 2,4-diamino-6-(4-pyridyl)-1,3,5-triazine (**2a**) with nonanoic acid. (a) Partial view of one plane, showing two possible orientations of molecules of compound **2a** around a center of inversion. Molecules in the two orientations are drawn in green and red. (b) View of only the molecules shown in green. (c) View of only the molecules shown in red.

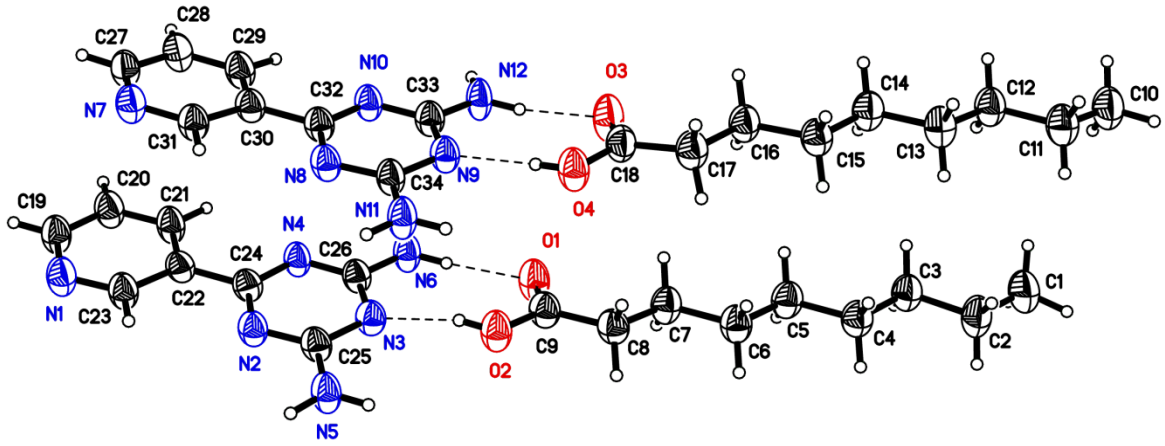

Figure S5. Thermal atomic displacement ellipsoid plot of the structure of 1:1 cocrystals of 2,4-diamino-6-(3-pyridyl)-1,3,5-triazine (**2b**) with nonanoic acid. The ellipsoids of non-hydrogen atoms are drawn at the 50% probability level, hydrogen atoms are represented by a sphere of arbitrary size, and hydrogen bonds are represented by broken lines.

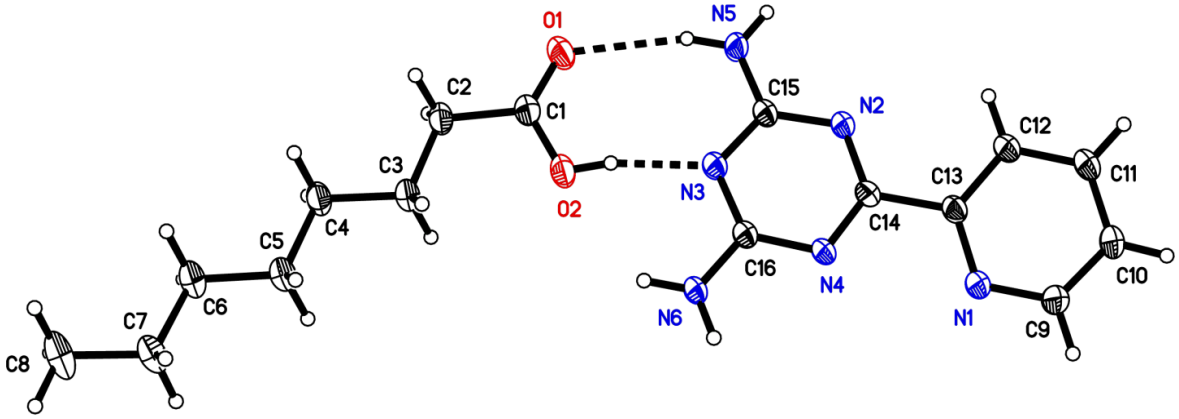

Figure S6. Thermal atomic displacement ellipsoid plot of the structure of 1:1 cocrystals of 2,4-diamino-6-(2-pyridyl)-1,3,5-triazine (**2c**) with octanoic acid. The ellipsoids of non-hydrogen atoms are drawn at the 50% probability level, hydrogen atoms are represented by a sphere of arbitrary size, and hydrogen bonds are represented by broken lines.

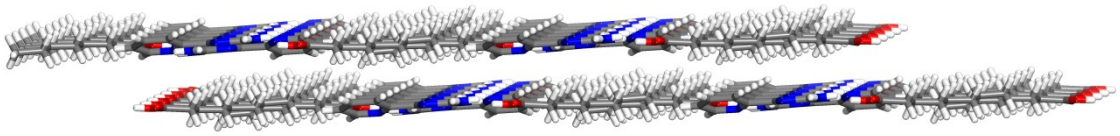

Figure S7. View of two stacked sheets in the structure of 1:1 cocrystals of 6-(2-pyridyl)-2,4-diamino-1,3,5-triazine (**2c**) with octanoic acid. Carbon atoms are shown in gray, hydrogen atoms in white, nitrogen atoms in blue, and oxygen atoms in red.

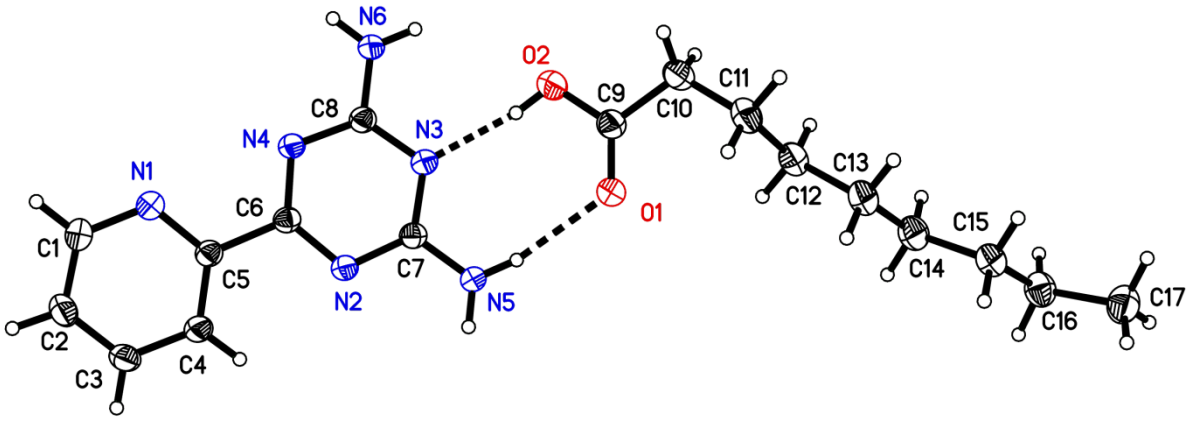

Figure S8. Thermal atomic displacement ellipsoid plot of the structure of 1:1 cocrystals of 2,4-diamino-6-(2-pyridyl)-1,3,5-triazine (**2c**) with nonanoic acid. The ellipsoids of non-hydrogen atoms are drawn at the 50% probability level, hydrogen atoms are represented by a sphere of arbitrary size, and hydrogen bonds are represented by broken lines.

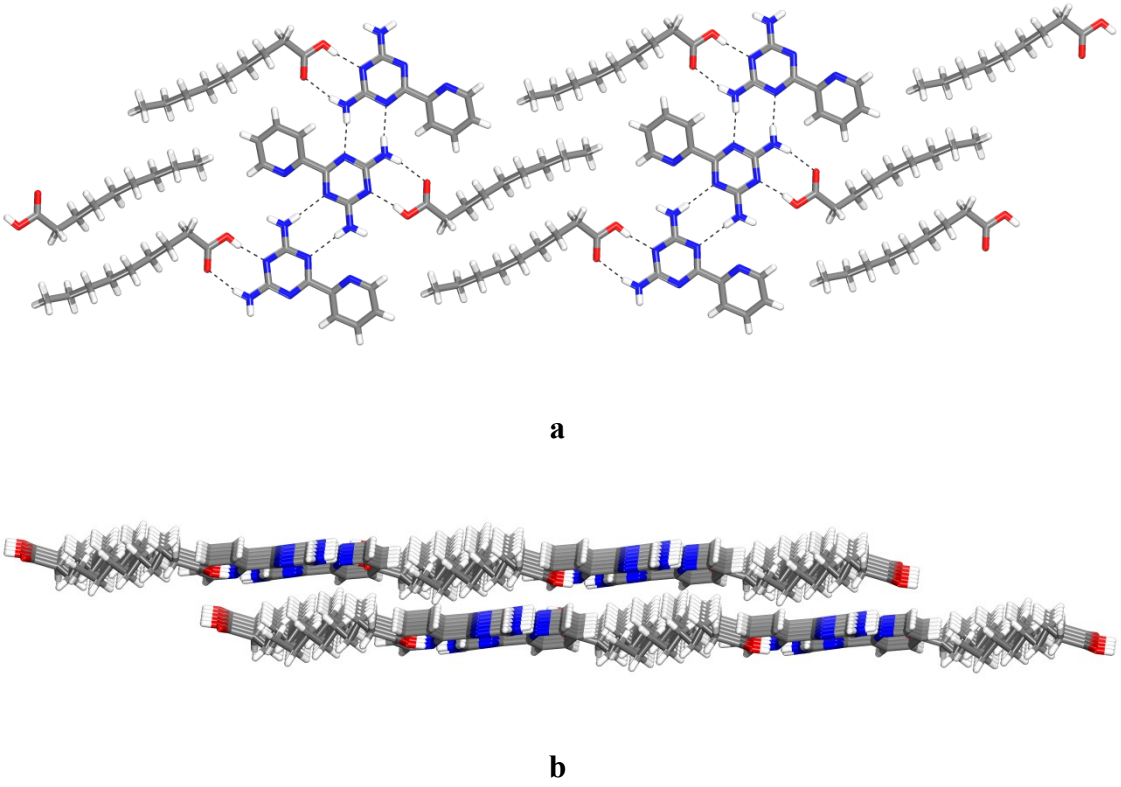

a

b

Figure S9. Views of the structure of 1:1 cocrystals of 2,4-diamino-6-(2-pyridyl)-1,3,5-triazine (**2c**) with nonanoic acid. (a) View of part of a sheet constructed from hydrogen-bonded tapes. Hydrogen bonds are represented by broken lines, and carbon atoms are shown in gray, hydrogen atoms in white, nitrogen atoms in blue, and oxygen atoms in red. (b) View of two stacked sheets.

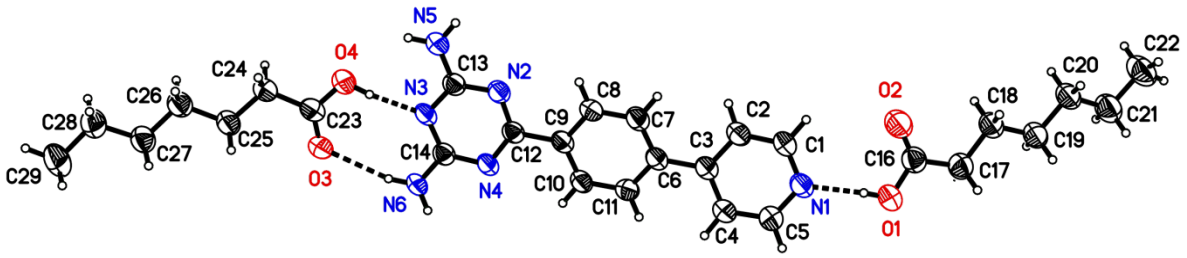

Figure S10. Thermal atomic displacement ellipsoid plots of the structure of 1:2 cocrystals of 2,4-diamino-6-[4-(4-pyridyl)phenyl]-1,3,5-triazine (**3**) with heptanoic acid. The ellipsoids of non-hydrogen atoms are drawn at the 50% probability level, hydrogen atoms are represented by a sphere of arbitrary size, and hydrogen bonds are represented by broken lines.

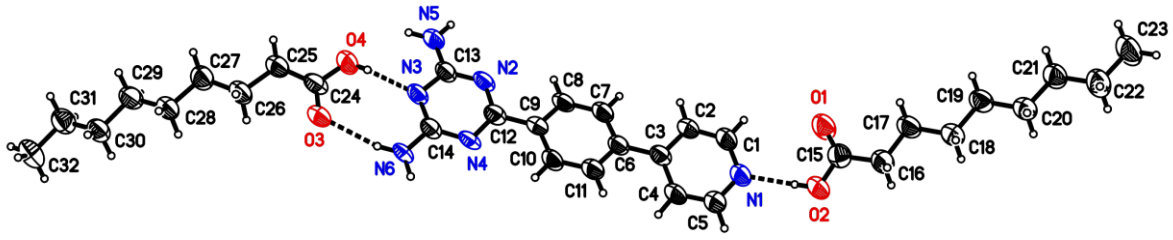

Figure S11. Thermal atomic displacement ellipsoid plots of the structure of 1:2 cocrystals of 2,4-diamino-6-[4-(4-pyridyl)phenyl]-1,3,5-triazine (**3**) with nonanoic acid. The ellipsoids of non-hydrogen atoms are drawn at the 50% probability level, hydrogen atoms are represented by a sphere of arbitrary size, and hydrogen bonds are represented by broken lines.

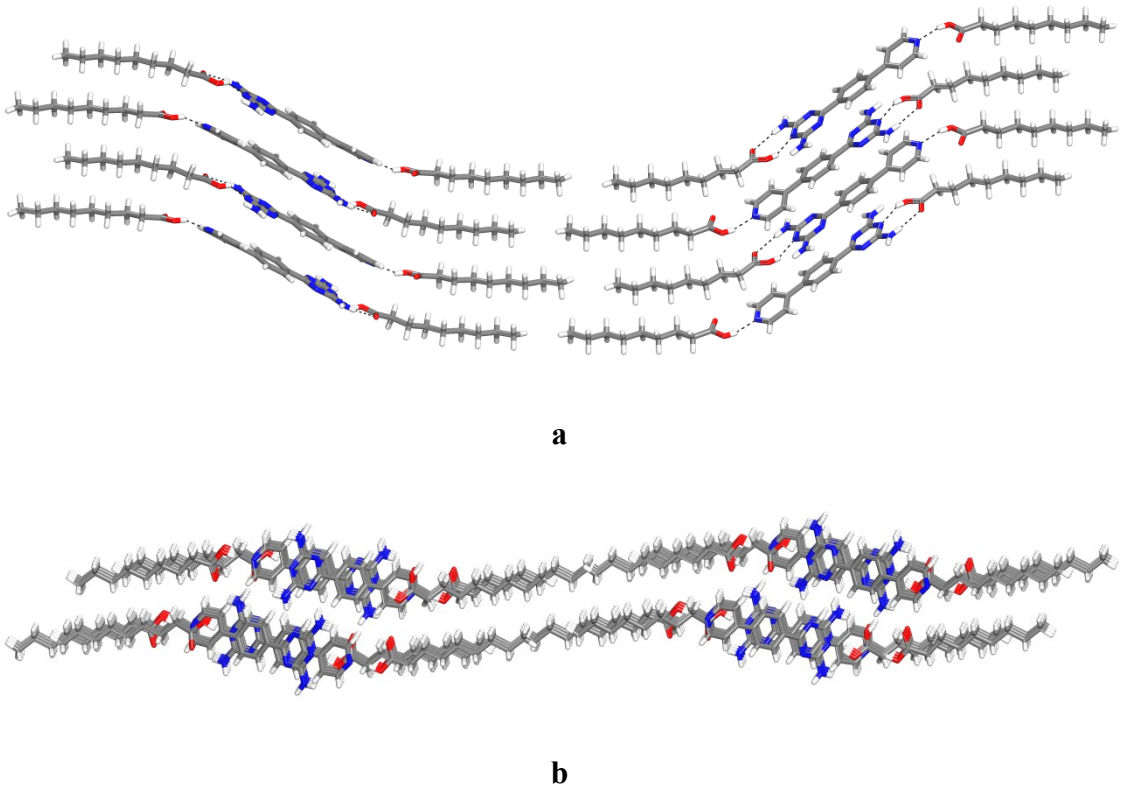

a

b

Figure S12. Views of the structure of 1:2 cocrystals of 2,4-diamino-6-[4-(4-pyridyl)phenyl]-1,3,5-triazine (**3**) with nonanoic acid. (a) View of part of a sheet constructed from hydrogen-bonded tapes. Hydrogen bonds are represented by broken lines, and carbon atoms are shown in gray, hydrogen atoms in white, nitrogen atoms in blue, and oxygen atoms in red. (b) View of two stacked sheets.

Homogeneity of Bulk Crystalline Samples

In all structural studies, experimental powder X-ray diffraction patterns were recorded for each bulk crystalline sample and then compared with those calculated from single-crystal X-ray diffraction data. In all cases, these comparisons confirmed that the single-crystal specimens selected for structural analysis were representative of the bulk crystalline samples from which they were chosen. Experimental powder X-ray diffraction patterns were recorded using one of the following two instruments :

1) Bruker D8 Discover diffractometer with GADDS HTS, working in reflection mode and using graphite monochromatized Cu Kα radiation generated at 40 kV and 40 mA. The 2D general area detector was positioned at a distance of 15 cm from the powder sample, which was placed on a glass plate. This allowed simultaneous collection of data over an angular domain up to 35° in 2θ. Measurements were carried out at 293 K in coupled scan mode (θ-θ geometry). Four separate images (diffraction arcs) were collected (scanning time : 5 min/image), and intensity along each arc was integrated to create the 1D powder pattern of intensity versus 2θ, over the angular range $10° < 2\theta < 105°$.
2) Single-crystal Bruker Microstar diffractometer equipped with a FR591 rotating anode generator, Helios optics, and a 2D Pt135 CCD detector, working in transmission mode. A small amount of powdered sample was mounted in a fiber loop, and the diffraction patterns were recorded at 150 K by phi-scan over five different detector positions, merged, and integrated to give the 1D powder diffraction pattern.

Structural data from single-crystal analyses were used to calculate theoretical powder X-ray diffraction patterns with the aid of Mercury software.[1] Peak fitting and the refinement of lattice parameters were carried out using TOPAS software,[2] and Pawley fitting was applied to the powder X-ray diffraction patterns. The quality of the refinement was checked by evaluating the weighted agreement factor R_{wp}, which was calculated on background subtracted intensity data as

$$R_{wp} = \sqrt{\frac{\sum w(Yo - Yc)^2}{\sum w(Yo - Bkg)^2}}$$

where Yo is the observed intensity, Yc is the calculated intensity, Bkg is the background intensity, and w is the weighting factor defined by $w = 1/\sigma(Yo)^2$, $\sigma(Yo)$ being the error in the measured intensity.[2]

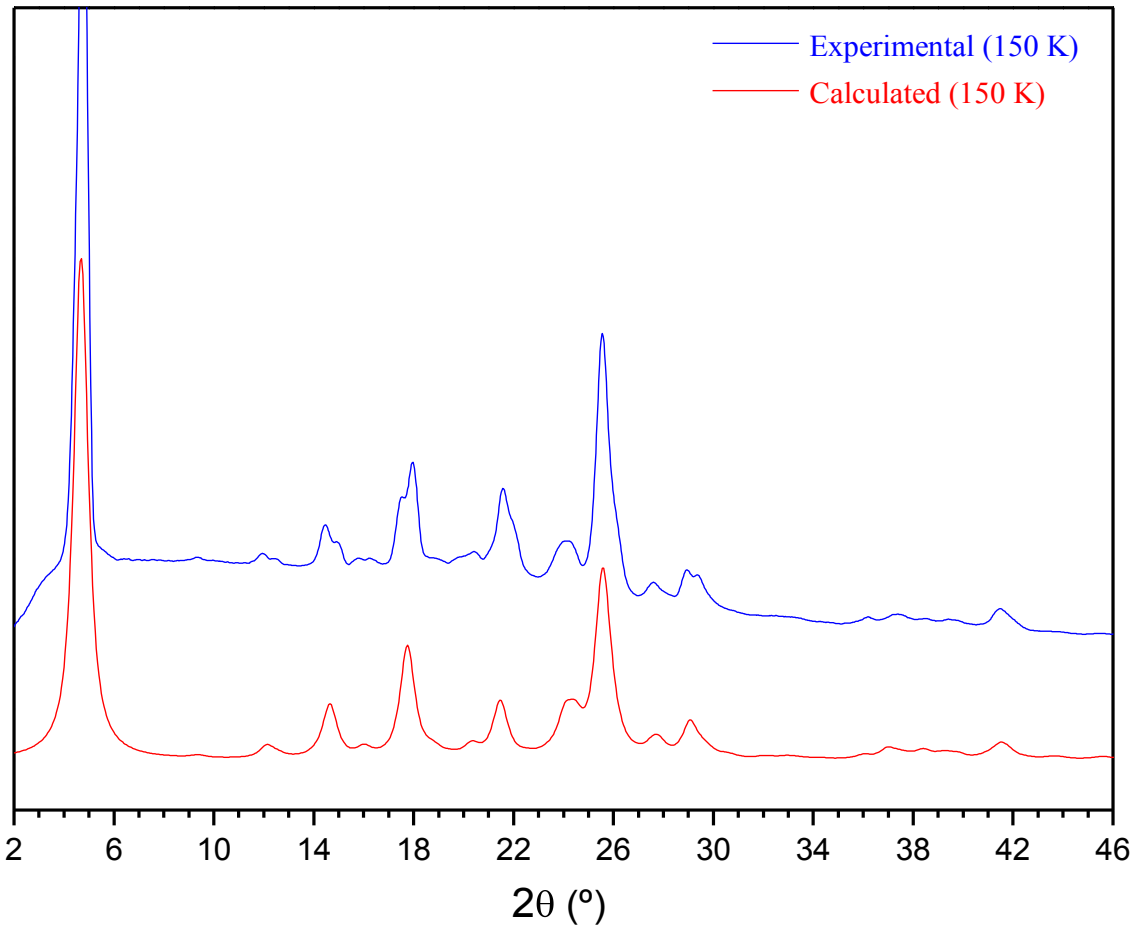

Figure S13. Comparison between experimental (collected using a Bruker Microstar diffractometer) and calculated powder X-ray diffraction patterns for 1:2 cocrystals of 2,4-diamino-6-(4-pyridyl)-1,3,5-triazine (**2a**) with octanoic acid. The two diffractograms are closely similar, confirming that the bulk crystalline sample consists of a single phase.

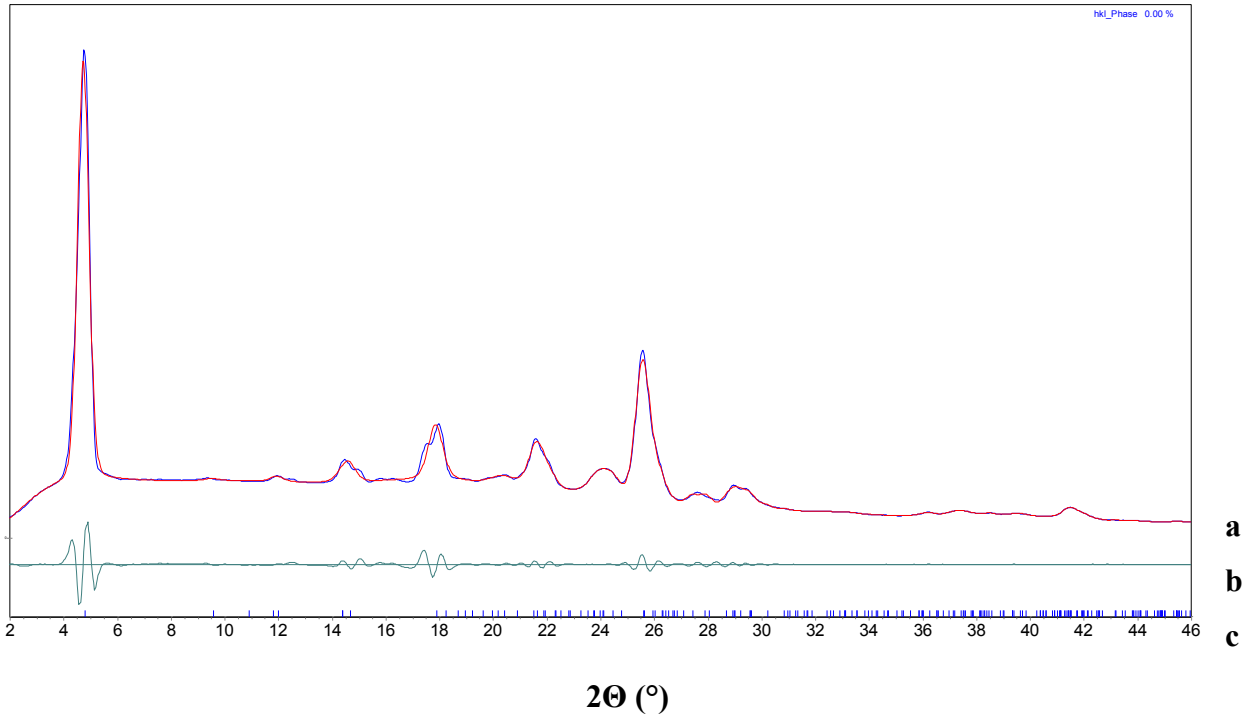

Figure S14. (a) Simulated powder X-ray diffraction pattern of 1:2 cocrystals of 2,4-diamino-6-(4-pyridyl)-1,3,5-triazine (**2a**) with octanoic acid (red curve) as determined by Pawley fitting of the experimental powder X-ray diffraction pattern (nearly superimposed blue curve). (b) Difference between experimental and calculated intensities. (c) Position of calculated reflections.

Table S1. Crystallographic Data for 1:2 Cocrystals of 2,4-Diamino-6-(4-pyridyl)-1,3,5-triazine (**2a**) with Octanoic Acidas Determined by Pawley Fitting of Powder X-Ray Diffraction Data at 150 K.

compound	**2a** • 2 octanoic acid
composition	$C_8H_8N_6 \cdot 2(C_8H_{16}O_2)$
temperature (K)	150
crystal system	triclinic
space group	$P\bar{1}$
a (Å)	4.832(49)
b (Å)	8.245(38)
c (Å)	18.52(13)
α (º)	88.12(36)
β (º)	85.69(35)
γ (º)	80.00(65)
V (Å^3)	724.6(96)
Z	1
R_{wp}	6.68

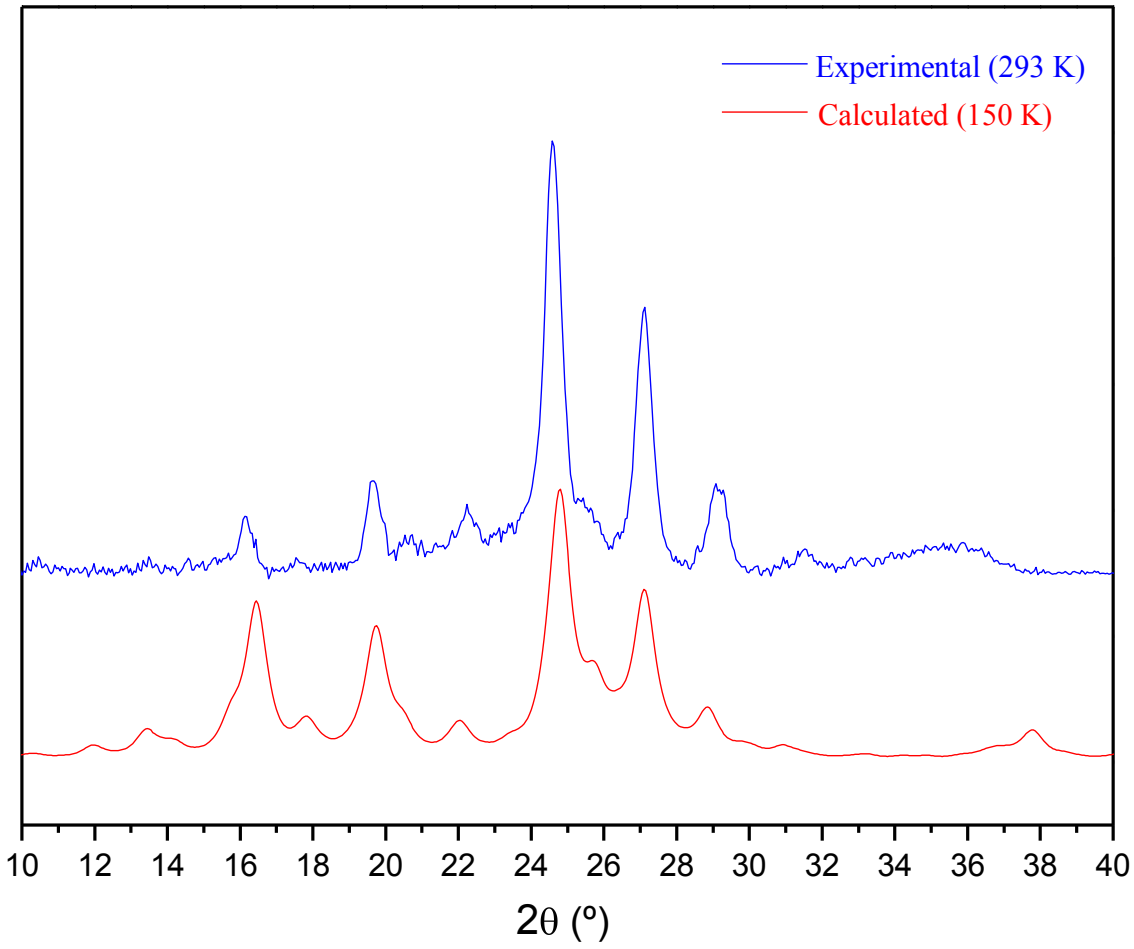

Figure S15. Comparison between experimental (collected using a Bruker Discover diffractometer) and calculated powder X-ray diffraction patterns for 1:2 cocrystals of 2,4-diamino-6-(4-pyridyl)-1,3,5-triazine (**2a**) with nonanoic acid. The *x* axis of the experimental pattern was shifted to minimize the slight angular shift due to the effect of temperature. The two diffractograms are closely similar, confirming that the bulk crystalline sample consists of a single phase.

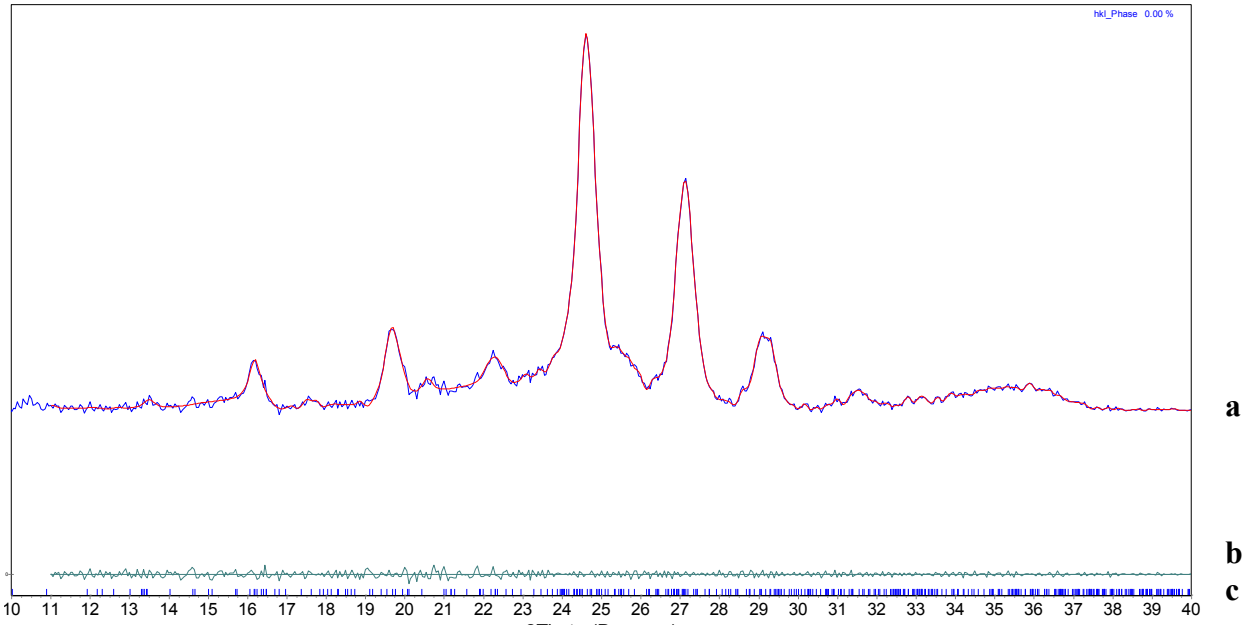

Figure S16. (a) Simulated powder X-ray diffraction pattern of 1:2 cocrystals of 2,4-diamino-6-(4-pyridyl)-1,3,5-triazine (**2a**) with nonanoic acid (red curve) as determined by Pawley fitting of the experimental powder X-ray diffraction pattern (nearly superimposed blue curve). (b) Difference between experimental and calculated intensities. (c) Position of calculated reflections.

Table S2. Crystallographic Data for 1:2 Cocrystals of 2,4-Diamino-6-(4-pyridyl)-1,3,5-triazine (**2a**) with Nonanoic Acid as Determined by Pawley Fitting of Powder X-Ray Diffraction Data at 293 K.

compound	**2a** • 2 nonanoic acid
composition	$C_8\ H_8\ N_6 \bullet 2(C_9\ H_{18}\ O_2)$
temperature (K)	293
crystal system	triclinic
space group	$P\bar{1}$
a (Å)	7.57(95)
b (Å)	11.20(68)
c (Å)	26.7(32)
α (º)	94.3(72)
β (º)	92.7(42)
γ (º)	101.2(63)
V (Å^3)	2210(410)
Z	2
R_{wp}	1.80

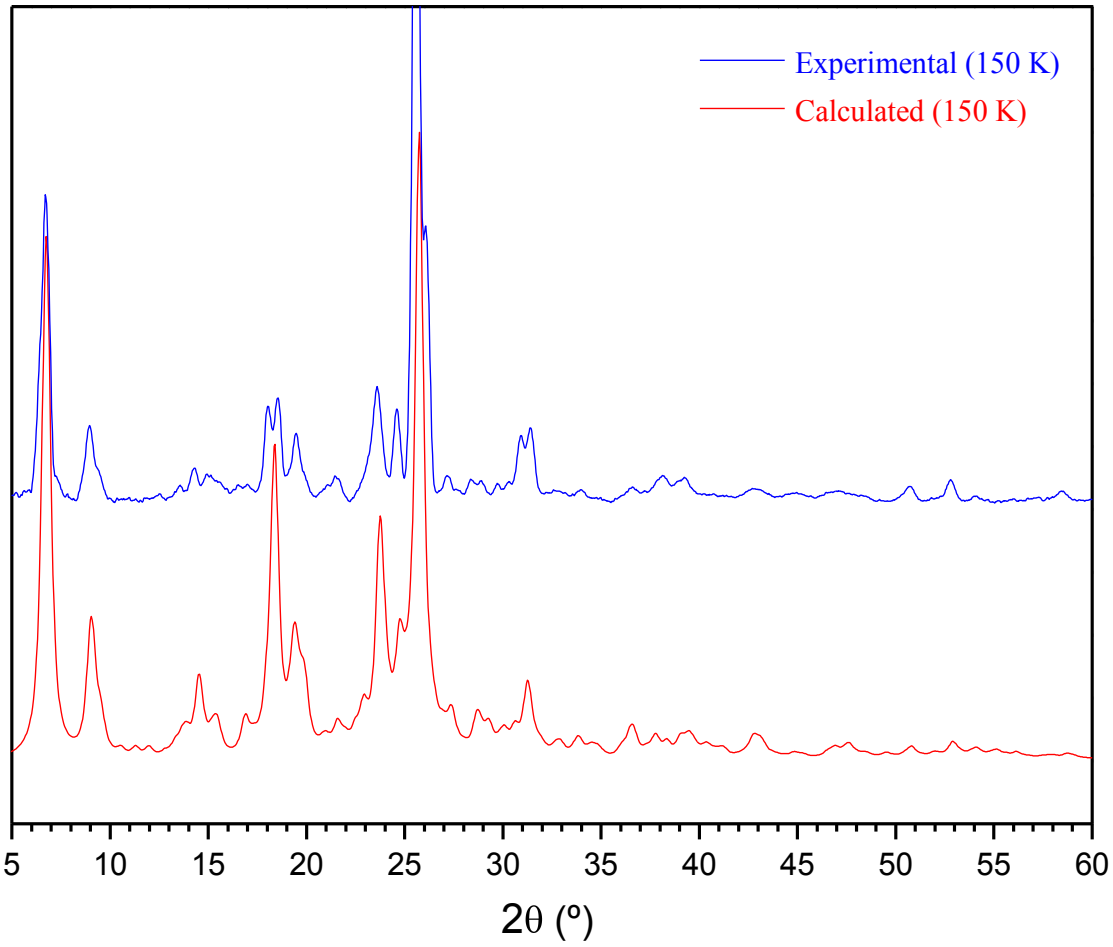

Figure S17. Comparison between experimental (collected using a Bruker Microstar diffractometer) and calculated powder X-ray diffraction patterns for 1:1 cocrystals of 2,4-diamino-6-(3-pyridyl)-1,3,5-triazine (**2b**) with nonanoic acid. The two diffractograms are closely similar, confirming that the bulk crystalline sample consists of a single phase.

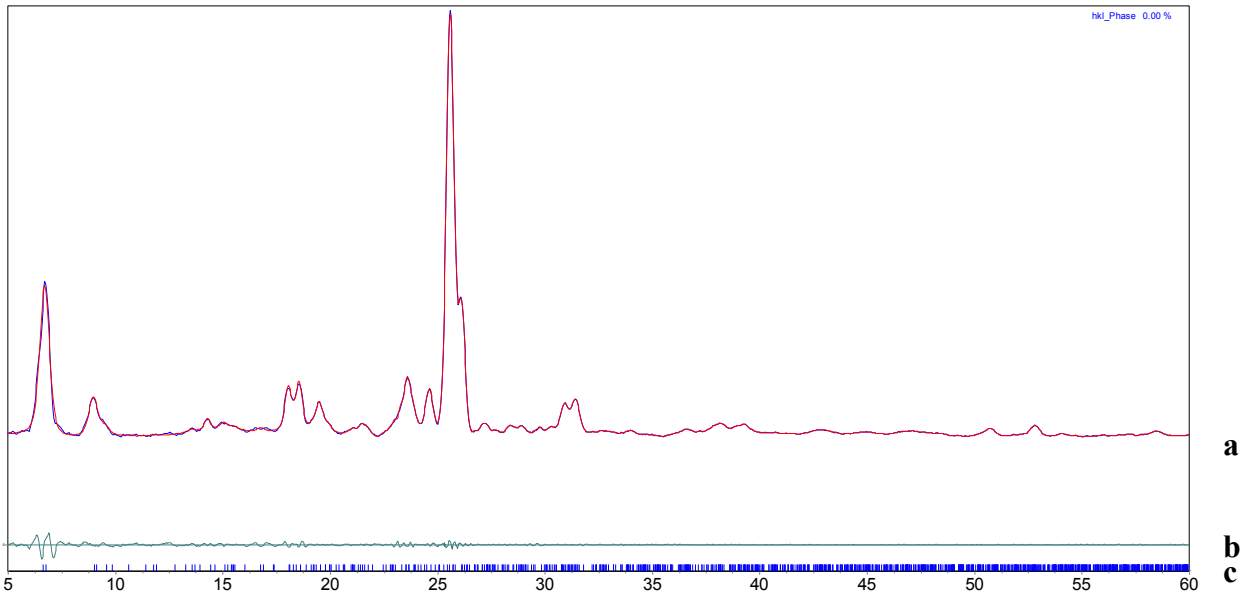

Figure S18. (a) Simulated powder X-ray diffraction pattern of 1:1 cocrystals of 2,4-diamino-6-(3-pyridyl)-1,3,5-triazine (**2b**) with nonanoic acid (red curve) as determined by Pawley fitting of the experimental powder X-ray diffraction pattern (nearly superimposed blue curve). (b) Difference between experimental and calculated intensities. (c) Position of calculated reflections.

Table S3. Crystallographic Data for 1:1 Cocrystals of 2,4-Diamino-6-(3-pyridyl)-1,3,5-triazine (**2b**) with Nonanoic Acid as Determined by Pawley Fitting of Powder X-Ray Diffraction Data at 150 K.

compound	**2b** • 1 nonanoic acid
composition	$C_8\ H_8\ N_6 \bullet C_9\ H_{18}\ O_2$
temperature (K)	150
crystal system	triclinic
space group	$P\bar{1}$
a (Å)	10.281(32)
b (Å)	13.422(27)
c (Å)	13.656(62)
α (º)	92.78(19)
β (º)	106.61(27)
γ (º)	95.15(19)
V (Å^3)	1793(11)
Z	4
R_{wp}	1.47

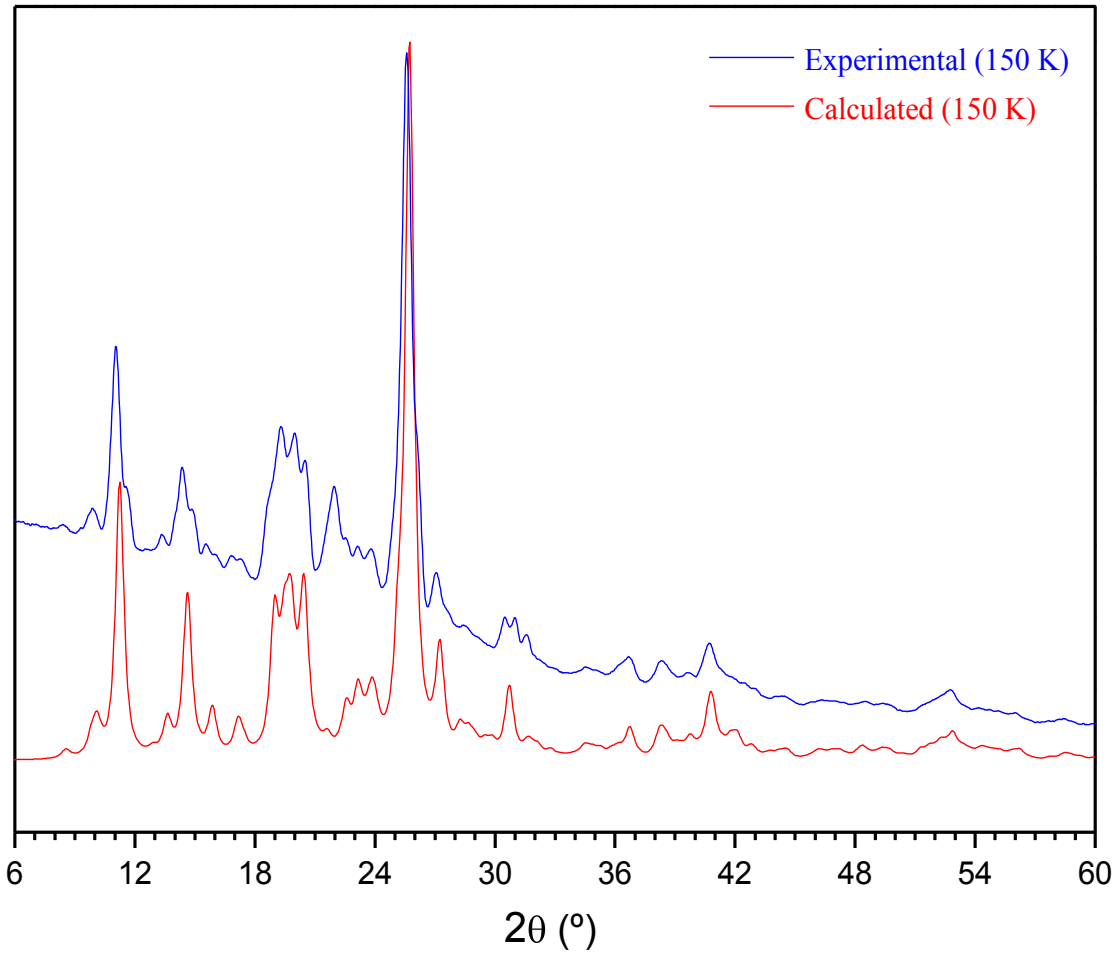

Figure S19. Comparison between experimental (collected using a Bruker Microstar diffractometer) and calculated powder X-ray diffraction patterns for 1:1 cocrystals of 2,4-diamino-6-(2-pyridyl)-1,3,5-triazine (**2c**) with octanoic acid. The two diffractograms are closely similar, confirming that the bulk crystalline sample consists of a single phase.

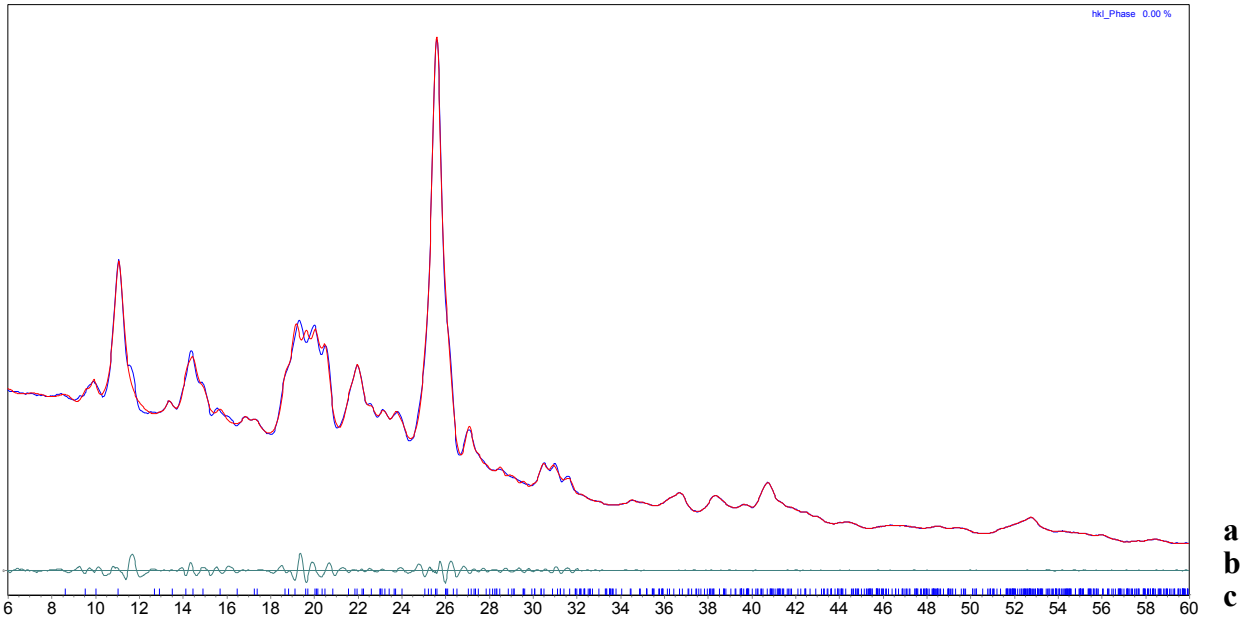

Figure S20. (a) Simulated powder X-ray diffraction pattern of 1:1 cocrystals of 2,4-diamino-6-(2-pyridyl)-1,3,5-triazine (**2c**) with octanoic acid (red curve) as determined by Pawley fitting of the experimental powder X-ray diffraction pattern (nearly superimposed blue curve). (b) Difference between experimental and calculated intensities. (c) Position of calculated reflections.

Table S4. Crystallographic Data for 1:1 Cocrystals of 2,4-Diamino-6-(2-pyridyl)-1,3,5-triazine (**2c**) with Octanoic Acid as Determined by Pawley Fitting of Powder X-Ray Diffraction Data at 150 K.

compound	**2c** • 1 octanoic acid
composition	$C_8\,H_8\,N_6 \bullet C_8\,H_{16}\,O_2$
temperature (K)	150
crystal system	triclinic
space group	$P\bar{1}$
a (Å)	8.942(11)
b (Å)	9.726(17)
c (Å)	10.651(20)
α (º)	105.012(65)
β (º)	90.087(90)
γ (º)	98.84(10)
V (Å^3)	883.2(25)
Z	2
R_{wp}	3.32

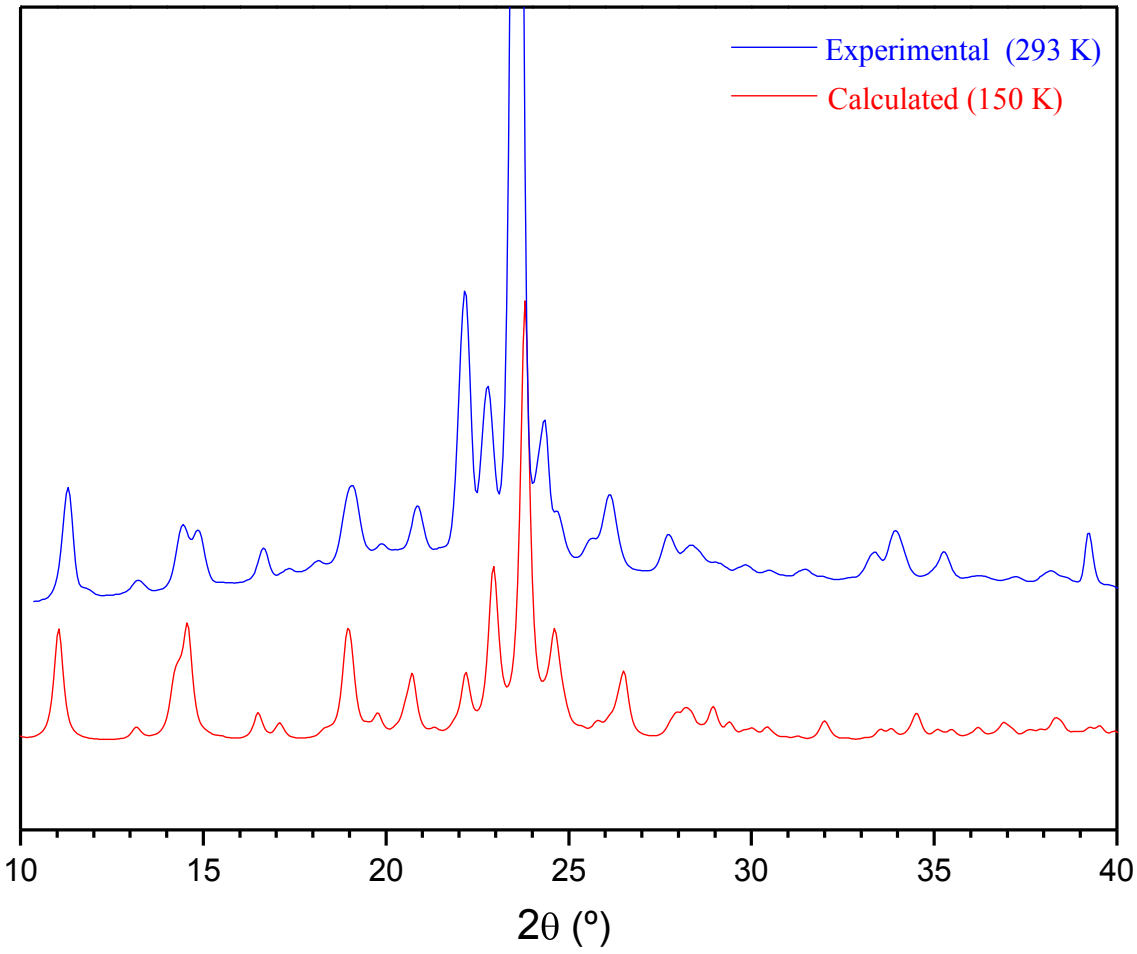

Figure S21. Comparison between experimental (collected using a Bruker Discover diffractometer) and calculated powder X-ray diffraction patterns for 1:1 cocrystals of 2,4-diamino-6-(2-pyridyl)-1,3,5-triazine (**2c**) with nonanoic acid. The *x* axis of the experimental pattern was shifted to minimize the slight angular shift due to the effect of temperature. The two diffractograms are closely similar, confirming that the bulk crystalline sample consists of a single phase.

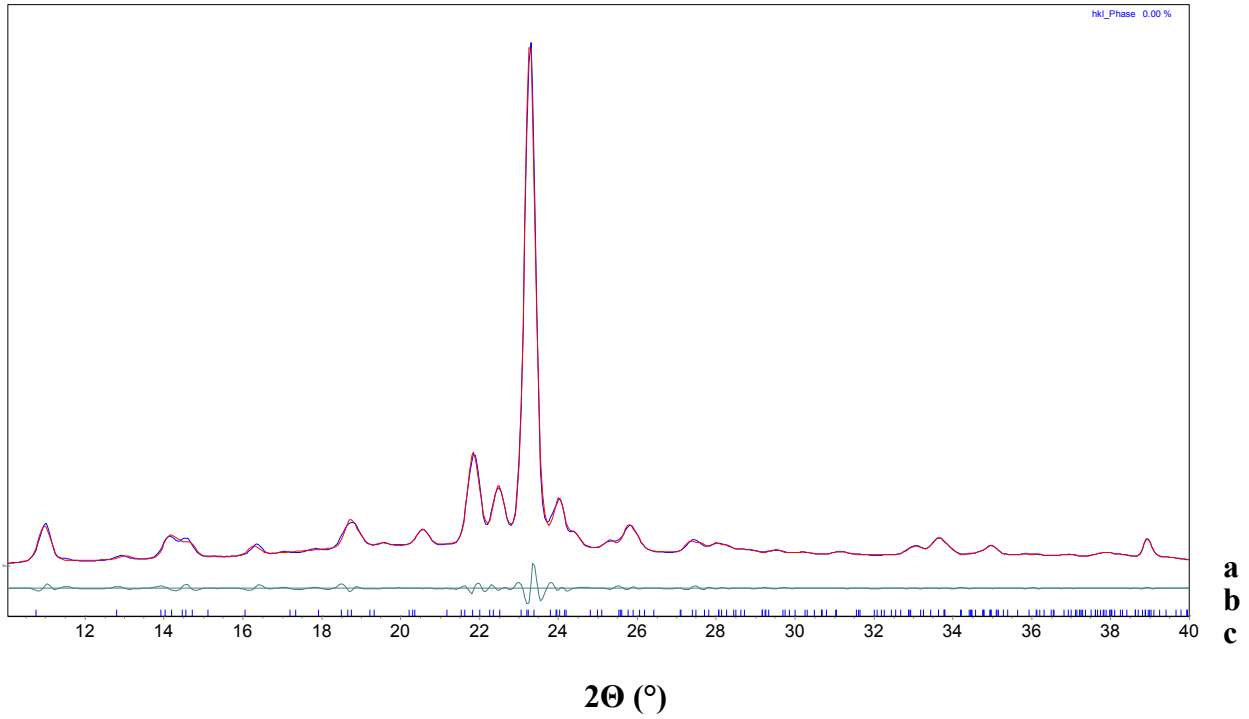

Figure S22. (a) Simulated powder X-ray diffraction pattern of 1:1 cocrystals of 2,4-diamino-6-(2-pyridyl)-1,3,5-triazine (**2c**) with nonanoic acid (red curve) as determined by Pawley fitting of the experimental powder X-ray diffraction pattern (nearly superimposed blue curve). (b) Difference between experimental and calculated intensities. (c) Position of calculated reflections.

Table S5. Crystallographic Data for 1:1 Cocrystals of 2,4-Diamino-6-(2-pyridyl)-1,3,5-triazine (**2c**) with Octanoic Acid as Determined by Pawley Fitting of Powder X-Ray Diffraction Data at 293 K.

compound	**2c** • 1 nonanoic acid
composition	$C_8\ H_8\ N_6 \bullet C_9\ H_{18}\ O_2$
temperature (K)	293
crystal system	triclinic
space group	$P\bar{1}$
a (Å)	8.240(15)
b (Å)	10.316(20)
c (Å)	11.997(15)
α (º)	67.13(13)
β (º)	84.96(15)
γ (º)	90.02(20)
V (Å^3)	938.8(21)
Z	2
R_{wp}	6.85

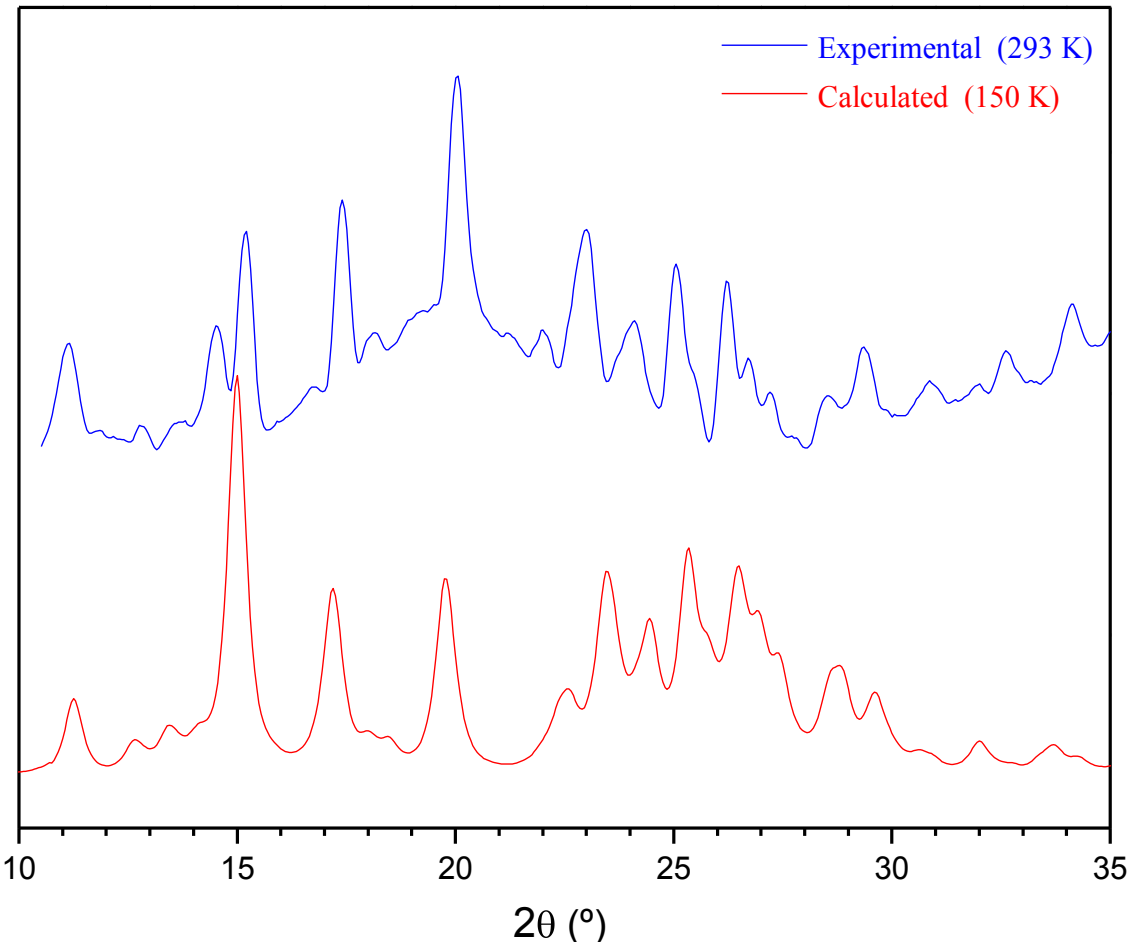

Figure S23. Comparison between experimental (collected using a Bruker Discover diffractometer) and calculated powder X-ray diffraction patterns for 1:2 cocrystals of 2,4-diamino-6-[4-(4-pyridyl)phenyl]-1,3,5-triazine (**3**) with heptanoic acid. The *x* axis of the experimental pattern was shifted to minimize the slight angular shift due to the effect of temperature. The two diffractograms are closely similar, confirming that the bulk crystalline sample consists of a single phase.

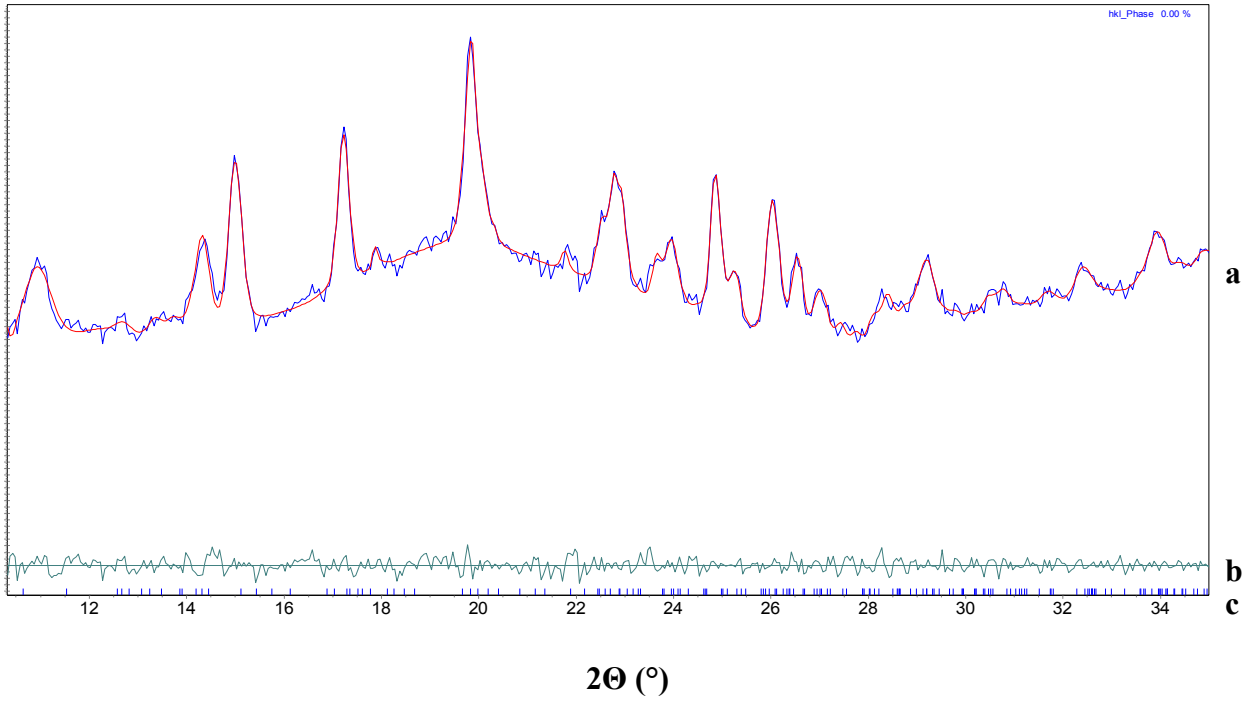

Figure S24. (a) Simulated powder X-ray diffraction pattern of 1:2 cocrystals of 2,4-diamino-6-[4-(4-pyridyl)phenyl]-1,3,5-triazine (**3**) with heptanoic acid (red curve) as determined by Pawley fitting of the experimental powder X-ray diffraction pattern (nearly superimposed blue curve). (b) Difference between experimental and calculated intensities. (c) Position of calculated reflections.

Table S6. Crystallographic Data for 1:2 Cocrystals of 2,4-Diamino-6-[4-(4-pyridyl)phenyl]-1,3,5-triazine (**3**) with Heptanoic Acid as Determined by Pawley Fitting of Powder X-Ray Diffraction Data at 293 K.

compound	**3** • 2 heptanoic acid
composition	$C_{14}H_{12}N_6 \bullet 2(C_7H_{14}O_2)$
temperature (K)	293
crystal system	monoclinic
space group	*C*2/c
a (Å)	49.78(46)
b (Å)	7.880(46)
c (Å)	14.19(15)
α (º)	90
β (º)	93.37(51)
γ (º)	90
V (Å^3)	5556(13)
Z	8
R_{wp}	1.38

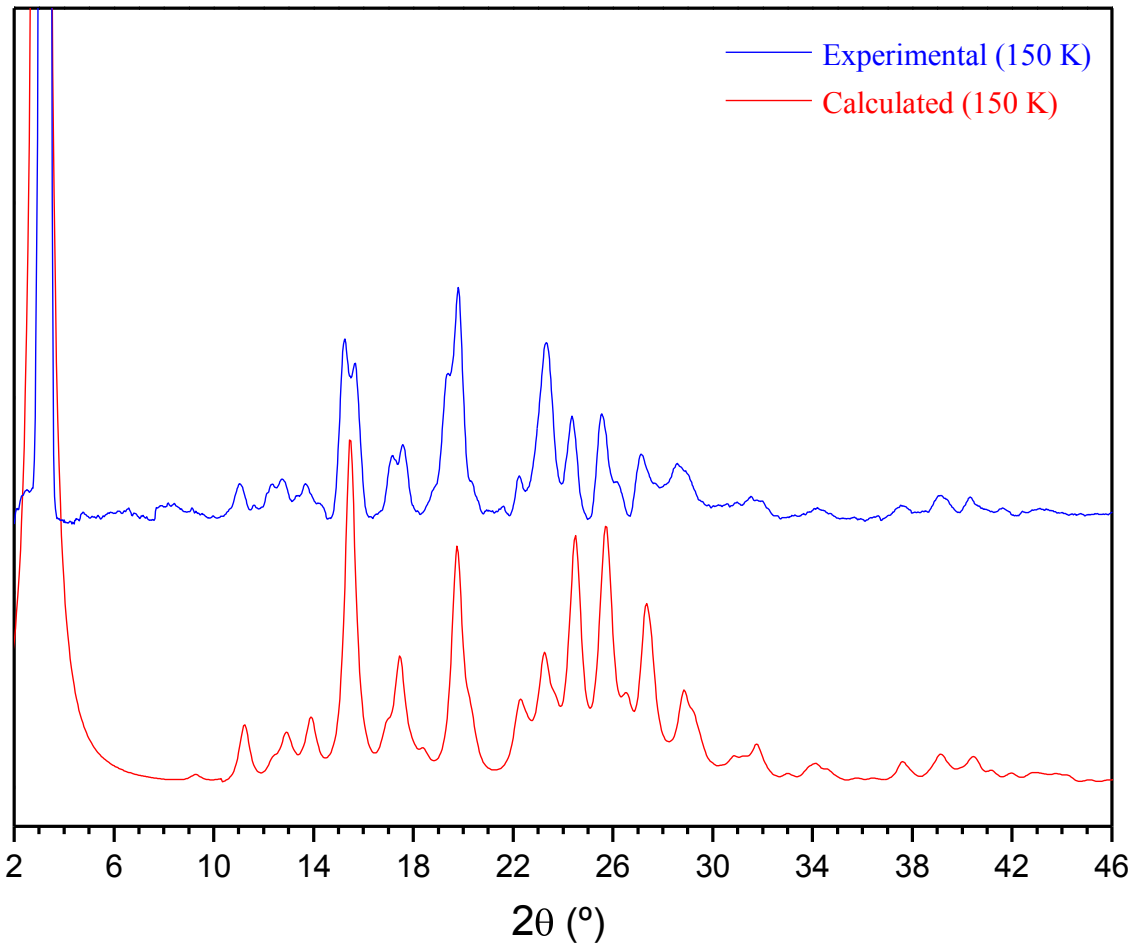

Figure S25. Comparison between experimental (collected using a Bruker Microstar diffractometer) and calculated powder X-ray diffraction patterns for 1:2 cocrystals of 2,4-diamino-6-[4-(4-pyridyl)phenyl]-1,3,5-triazine (**3**) with nonanoic acid. The two diffractograms are closely similar, confirming that the bulk crystalline sample consists of a single phase.

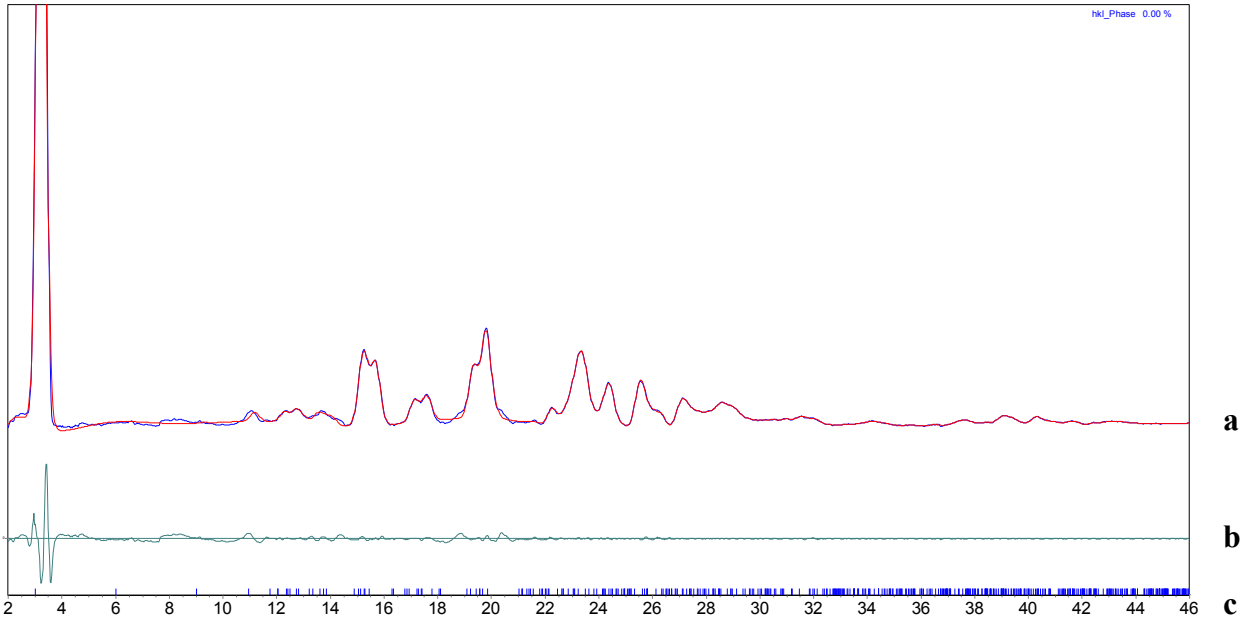

Figure S26. (a) Simulated powder X-ray diffraction pattern of 1:2 cocrystals of 2,4-diamino-6-[4-(4-pyridyl)phenyl]-1,3,5-triazine (**3**) with nonanoic acid (red curve) as determined by Pawley fitting of the experimental powder X-ray diffraction pattern (nearly superimposed blue curve). (b) Difference between experimental and calculated intensities. (c) Position of calculated reflections.

Table S7. Crystallographic Data for 1:2 Cocrystals of 2,4-Diamino-6-[4-(4-pyridyl)phenyl]-1,3,5-triazine (**3**) with Nonanoic Acid as Determined by Pawley Fitting of Powder X-Ray Diffraction Data at 150 K.

compound	**3** • 2 nonanoic acid
composition	$C_{14}H_{12}N_6 \bullet 2(C_9H_{18}O_2)$
temperature (K)	150
crystal system	monoclinic
space group	*C*2/c
a (Å)	60.27(76)
b (Å)	8.153(35)
c (Å)	14.68(28)
α (º)	90
β (º)	102.7(13)
γ (º)	90
V (Å^3)	7040(170)
Z	16
R_{wp}	9.58

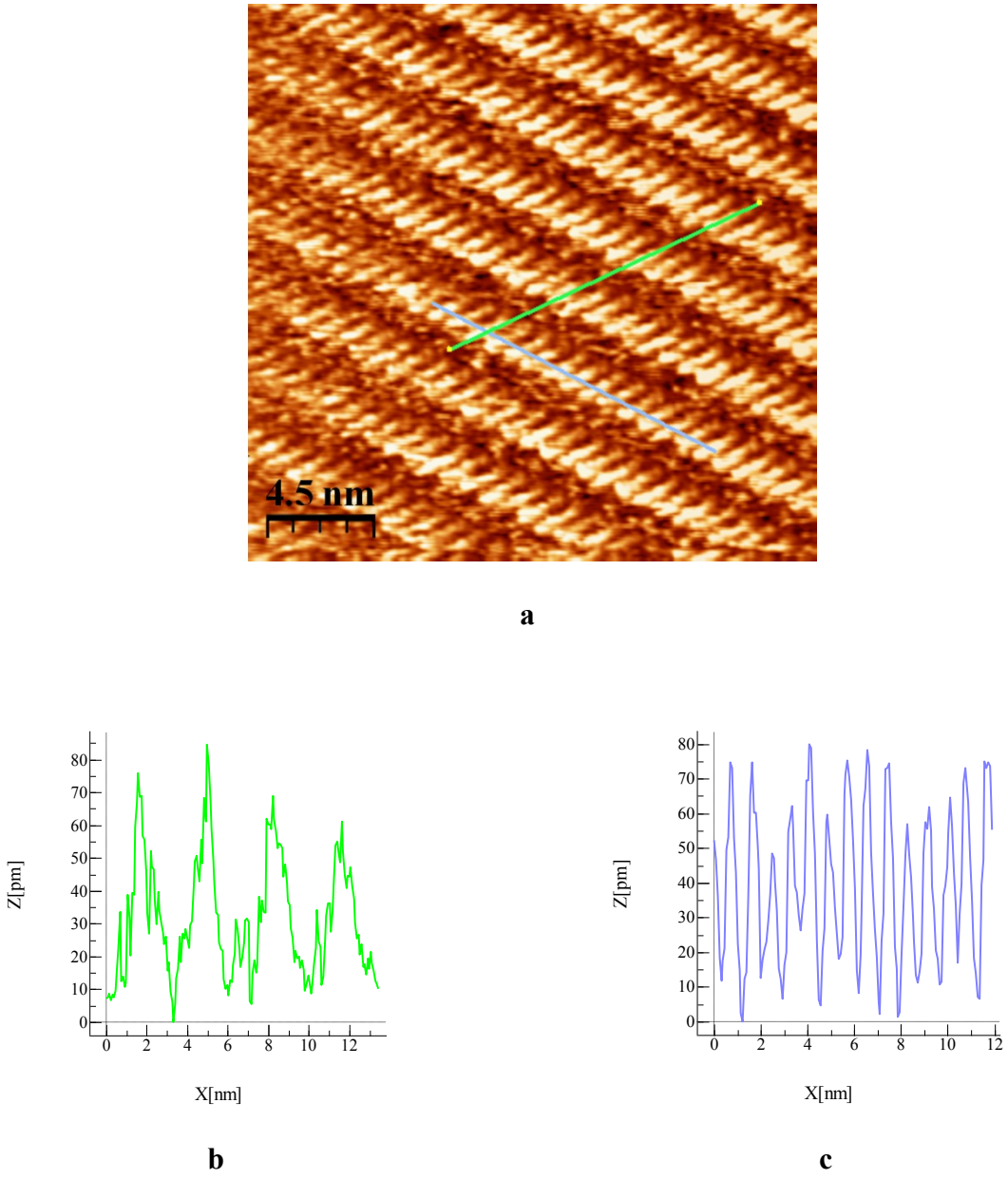

Figure S27. (a) STM image of the 2D cocrystallization of 2,4-diamino-6-(4-pyridyl)-1,3,5-triazine (**2a**) with heptanoic acid on HOPG (deposition from heptanoic acid, with V_{bias} = -1.51 V and I_{set} = 0.09 nA). (b) Profile along the green axis shown in Figure S25a. (c) Profile along the blue axis shown in Figure S25a.

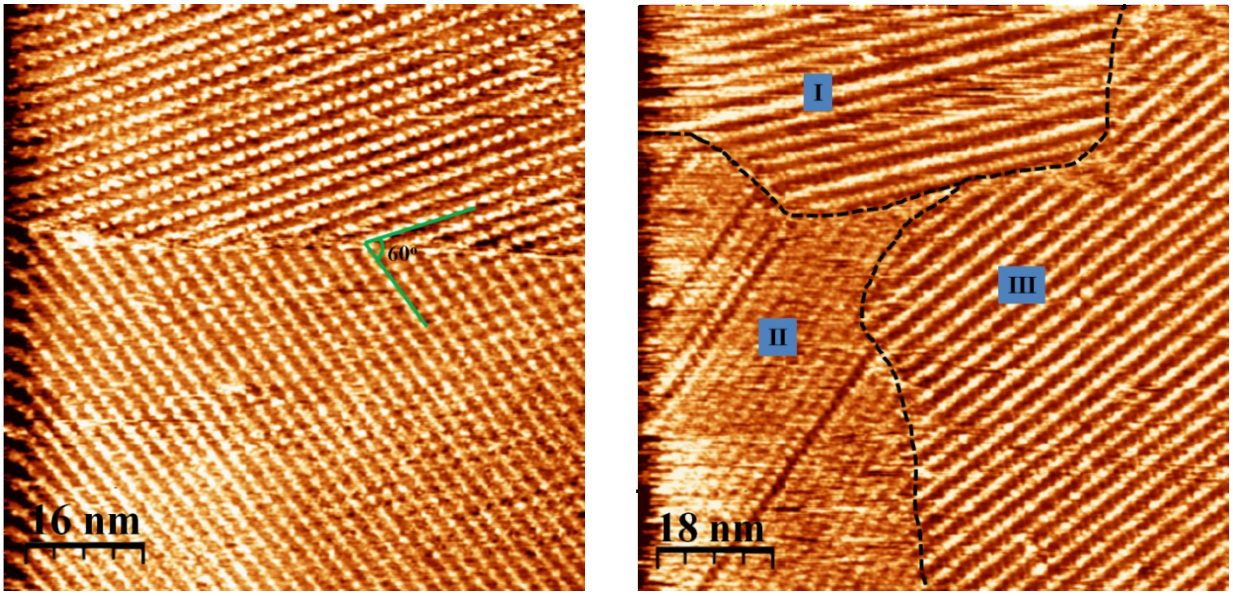

a **b**

Figure S28. (a) STM image of the 2D cocrystallization of 2,4-diamino-6-(4-pyridyl)-1,3,5-triazine (**2a**) with heptanoic acid on HOPG, showing the intersection of two domains (deposition from heptanoic acid, with V_{bias} = -1.50 V and I_{set} = 0.09 nA). (b) STM image of the 2D cocrystallization of 2,4-diamino-6-(3-pyridyl)-1,3,5-triazine (**2b**) with nonanoic acid on HOPG (deposition from nonanoic acid, with V_{bias} = -1.40 V and I_{set} = 0.09 nA).

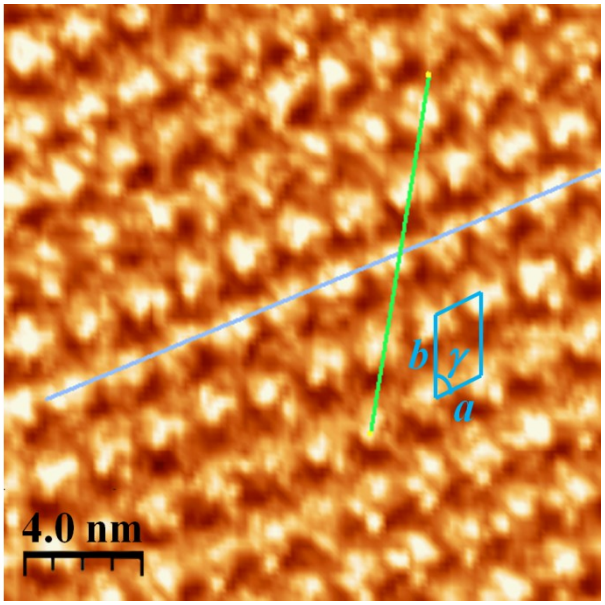

a

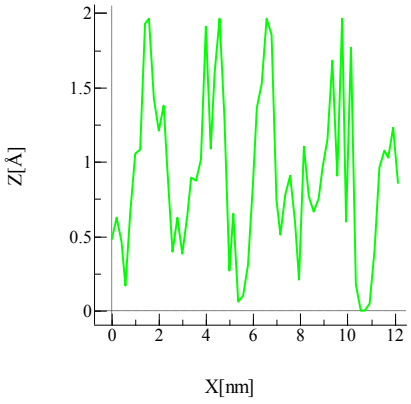

b

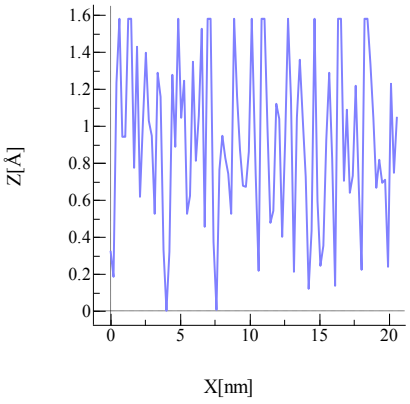

c

Figure S29. (a) STM image of the 2D cocrystallization of 2,4-diamino-6-(3-pyridyl)-1,3,5-triazine (**2b**) with heptanoic acid on HOPG (deposition from heptanoic acid, with V_{bias} = -1.50 V and I_{set} = 0.09 nA). (b) Profile along the green axis shown in Figure S27a. (c) Profile along the blue axis shown in Figure S27a.

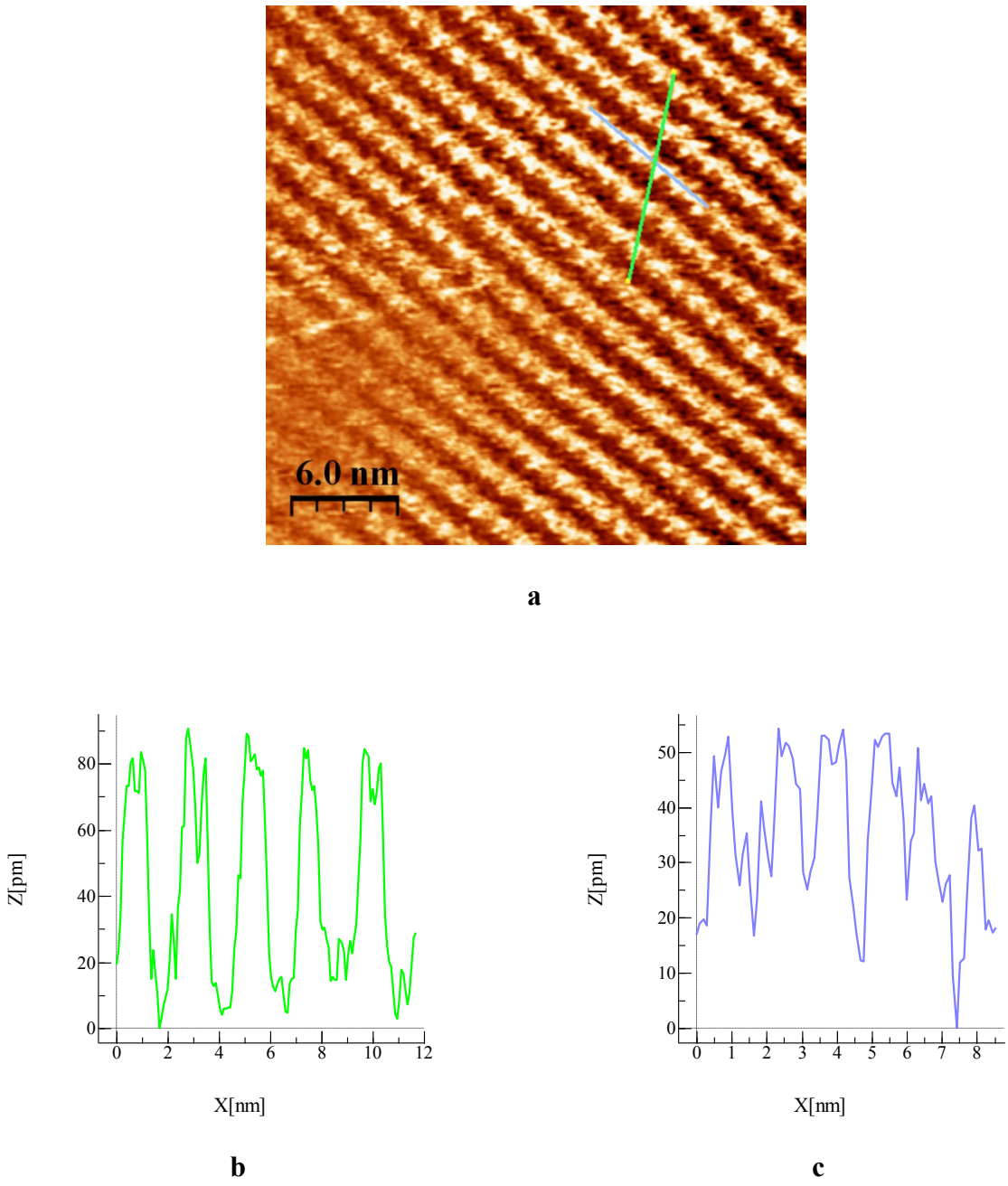

Figure S30. (a) STM image of the 2D cocrystallization of 2,4-diamino-6-(2-pyridyl)-1,3,5-triazine (**2c**) with heptanoic acid on HOPG (deposition from heptanoic acid, with V_{bias} = -1.50 V and I_{set} = 0.06 nA). (b) Profile along the green axis shown in Figure S28a. (c) Profile along the blue axis shown in Figure S28a.

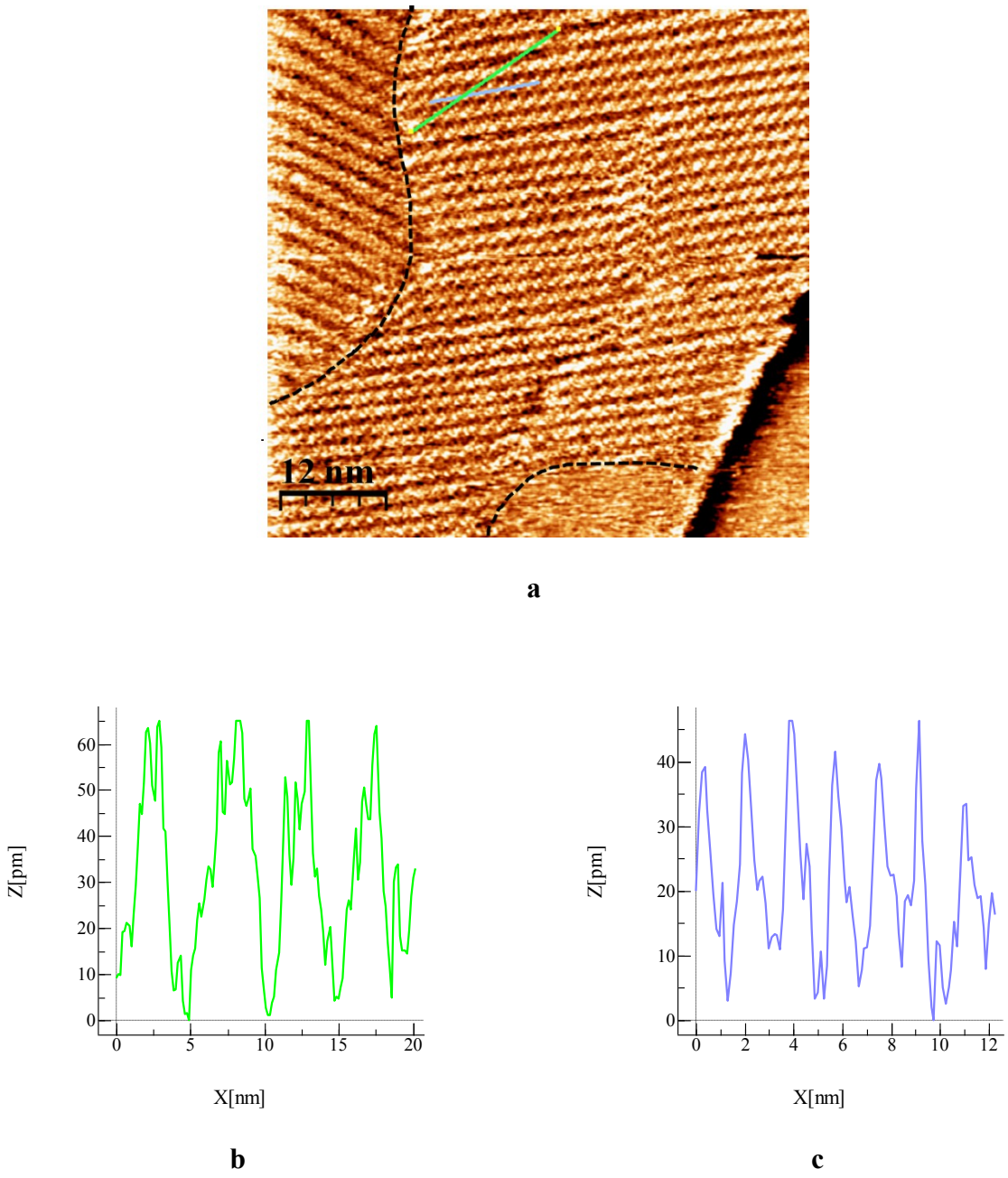

Figure S31. (a) STM image of the 2D cocrystallization of 2,4-diamino-6-[4-(4-pyridyl)phenyl]-1,3,5-triazine (**3**) with heptanoic acid on HOPG (deposition from heptanoic acid, with V_{bias} = -1.16 V and I_{set} = 0.09 nA). (b) Profile along the green axis shown in Figure S29a. (c) Profile along the blue axis shown in Figure S29a.

References

1) Macrae, C. F.; Edgington, P. R.; McCabe, P.; Pidcock, E.; Shields, G. P.; Taylor, R.; Towler, M.; van de Streek, J. *J. Appl. Cryst.* **2006**, *39*, 453-457.
2) Coelho, A. A. *TOPAS User Manual*, Version 3.1 ed.; Bruker-AXS GmbH : Karlsruhe, Germany, 2003.

Annexe 4

Partie supplémentaire de l'article 4

Supporting Information

Structural Similarity of Hydrogen-Bonded Networks in Crystals of Isomeric Pyridyl-Substituted Diaminotriazines

Adam Duong, Thierry Maris, and James D. Wuest*

[†]*Département de Chimie, Université de Montréal, Montréal, Québec H3C 3J7, Canada*

Contents **Page**

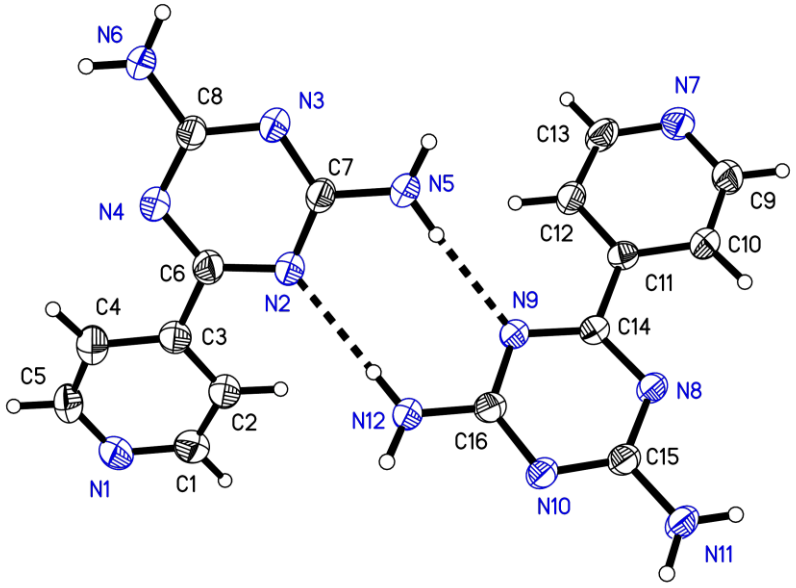

Figure S1. Thermal atomic displacement ellipsoid plot of the structure of crystals of 2,4-diamino-6-(4-pyridyl)-1,3,5-triazine (**1a**) grown from DMSO/MeCN. Ellipsoids of non-hydrogen atoms are drawn at the 50% probability level, hydrogen atoms are represented by a sphere of arbitrary size, and hydrogen bonds are represented by broken lines.

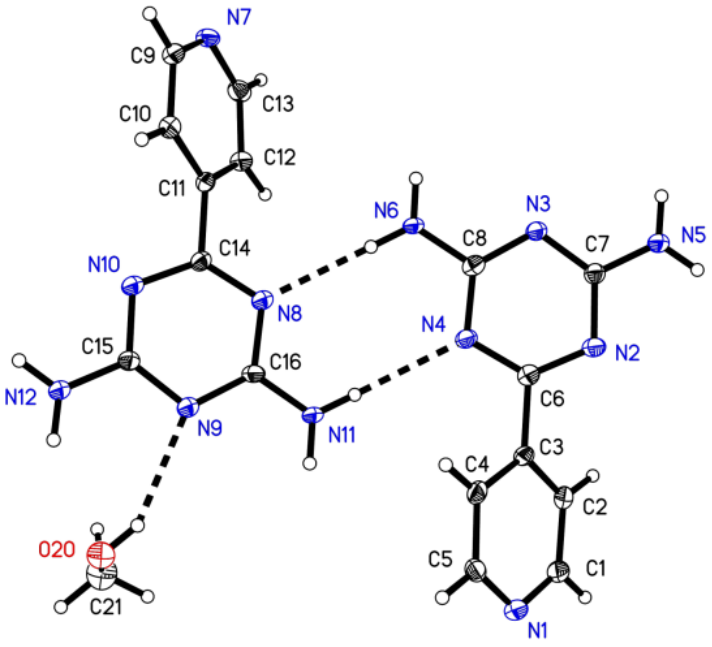

Figure S2. Thermal atomic displacement ellipsoid plot of the structure of the 2:1 solvate of 2,4-diamino-6-(4-pyridyl)-1,3,5-triazine (**1a**) with MeOH grown from DMSO/MeOH. The ellipsoids of non-hydrogen atoms are drawn at the 50% probability level, hydrogen atoms are represented by a sphere of arbitrary size, and hydrogen bonds are represented by broken lines.

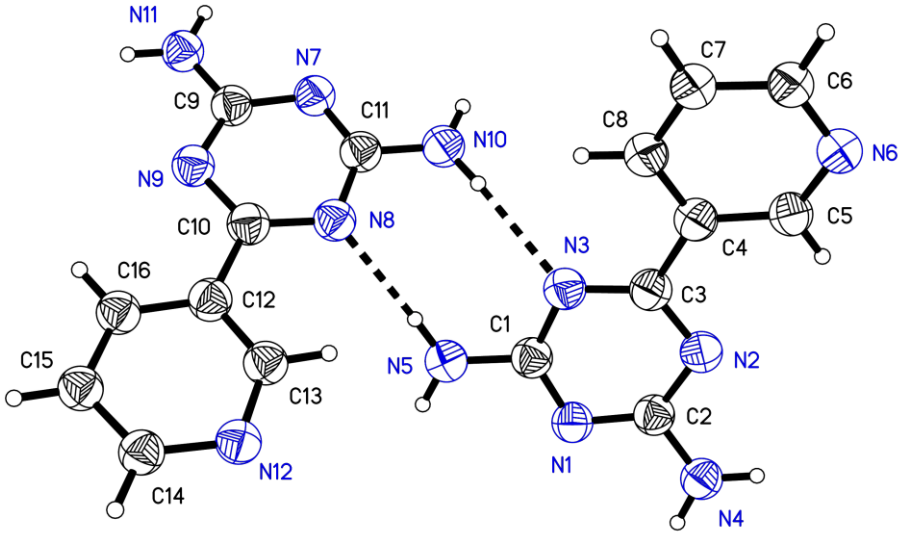

Figure S3. Thermal atomic displacement ellipsoid plot of the structure of crystals of 2,4-diamino-6-(3-pyridyl)-1,3,5-triazine (**1b**) grown from DMSO. The ellipsoids of non-hydrogen atoms are drawn at the 50% probability level, hydrogen atoms are represented by a sphere of arbitrary size, and hydrogen bonds are represented by broken lines.

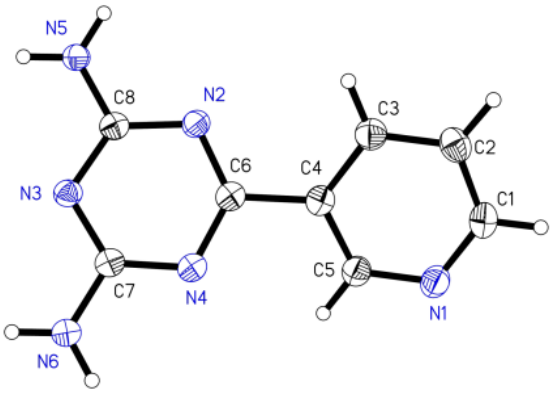

Figure S4. Thermal atomic displacement ellipsoid plot of the structure of crystals of 2,4-diamino-6-(3-pyridyl)-1,3,5-triazine (**1b**) grown from MeCN. The ellipsoids of non-hydrogen atoms are drawn at the 50% probability level, hydrogen atoms are represented by a sphere of arbitrary size, and hydrogen bonds are represented by broken lines.

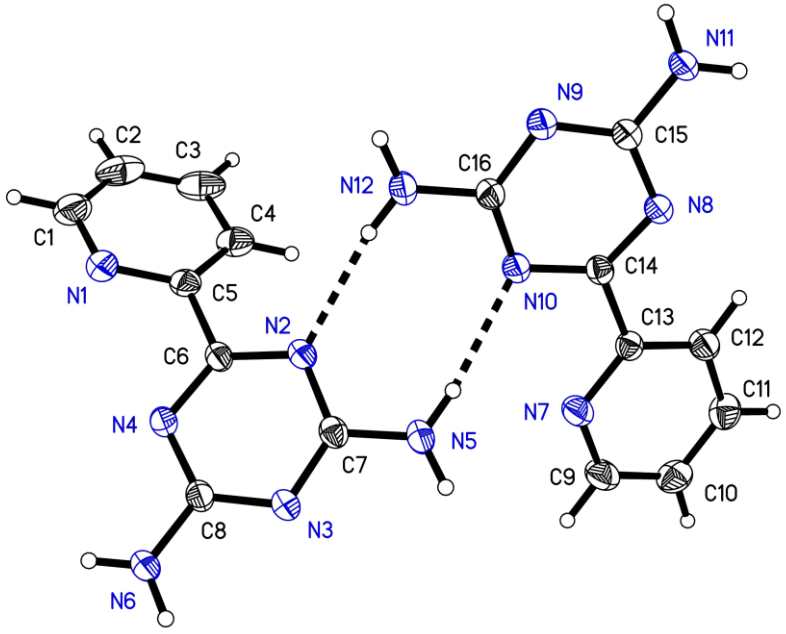

Figure S5. Thermal atomic displacement ellipsoid plot of the structure of crystals of 2,4-diamino-6-(2-pyridyl)-1,3,5-triazine (**1c**) grown from MeCN. The ellipsoids of non-hydrogen atoms are drawn at the 50% probability level, hydrogen atoms are represented by a sphere of arbitrary size, and hydrogen bonds are represented by broken lines.

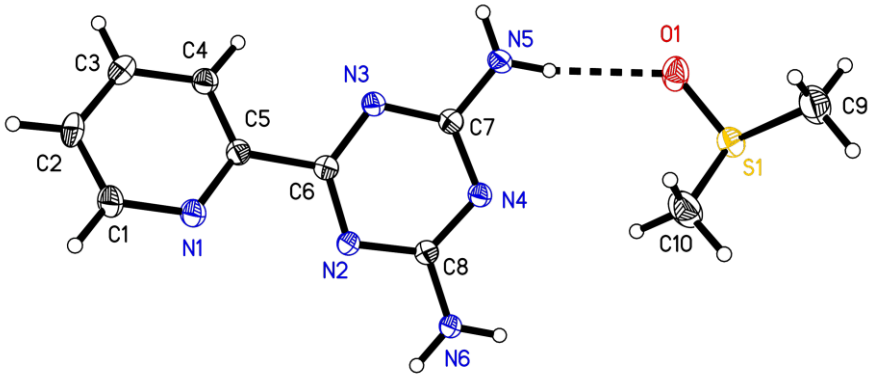

Figure S6. Thermal atomic displacement ellipsoid plot of the structure of the 1:1 solvate of 2,4-diamino-6-(2-pyridyl)-1,3,5-triazine (**1c**) with DMSO. The ellipsoids of non-hydrogen atoms are drawn at the 50% probability level, hydrogen atoms are represented by a sphere of arbitrary size, and hydrogen bonds are represented by broken lines.

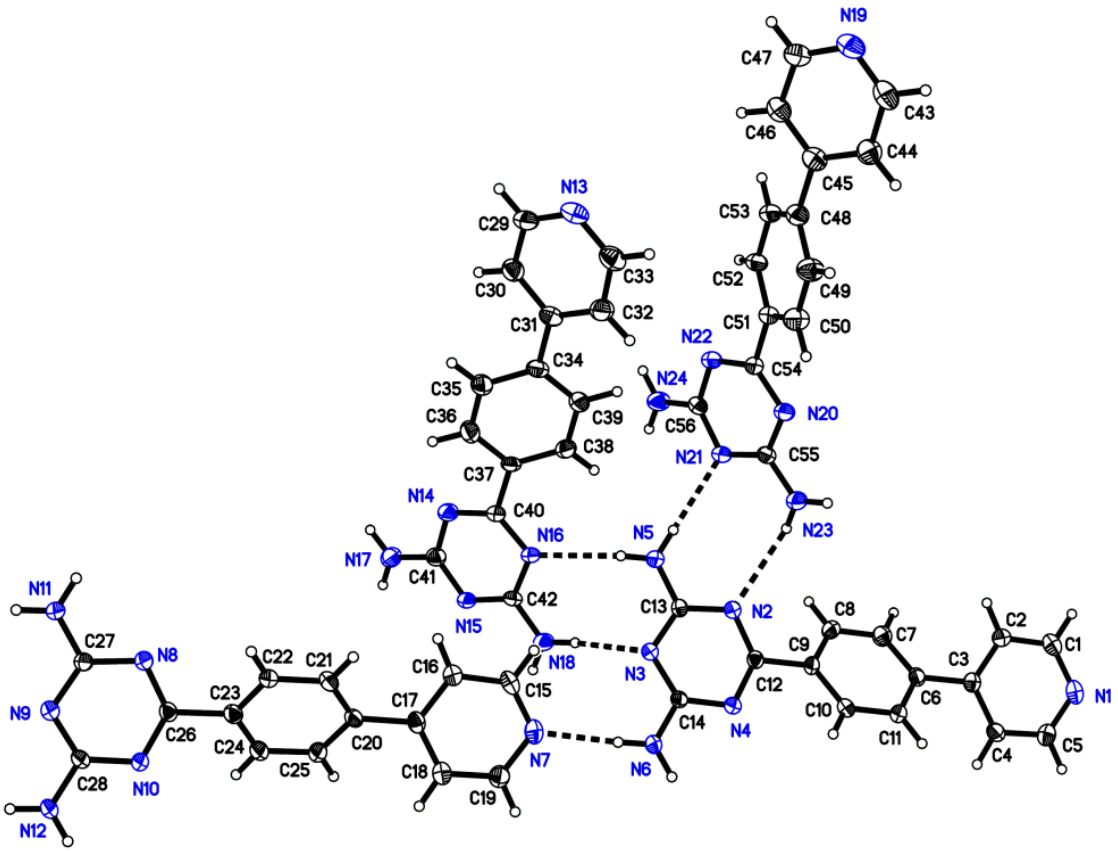

Figure S7. Thermal atomic displacement ellipsoid plot of the structure of crystals of the triclinic *P*-1 polymorph of 2,4-diamino-6-[4-(4-pyridyl)phenyl-1,3,5-triazine (**2a**) grown from wet DMSO. The ellipsoids of non-hydrogen atoms are drawn at the 50% probability level, hydrogen atoms are represented by a sphere of arbitrary size, and hydrogen bonds are represented by broken lines.

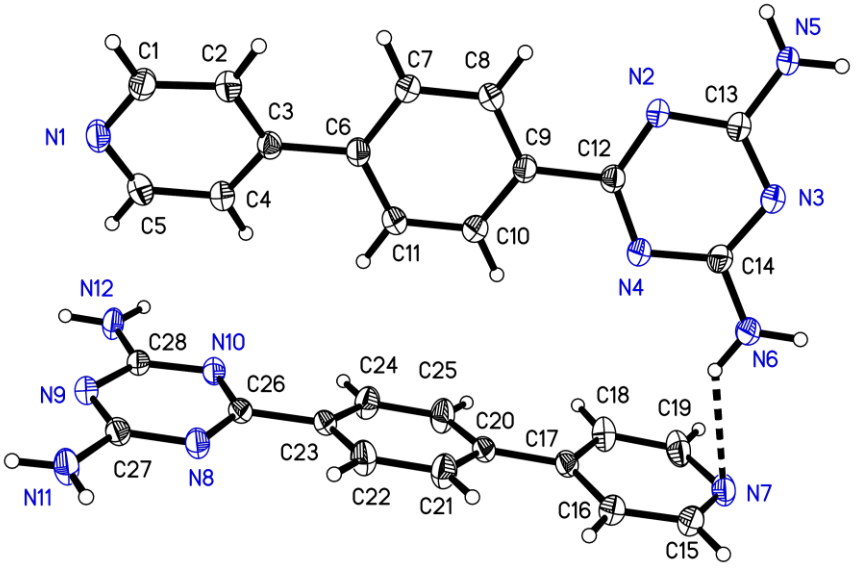

Figure S8. Thermal atomic displacement ellipsoid plot of the structure of crystals of the monoclinic $P2_1/n$ polymorph of 2,4-diamino-6-[4-(4-pyridyl)phenyl-1,3,5-triazine (**2a**) grown from wet DMSO. The ellipsoids of non-hydrogen atoms are drawn at the 50% probability level, hydrogen atoms are represented by a sphere of arbitrary size, and hydrogen bonds are represented by broken lines.

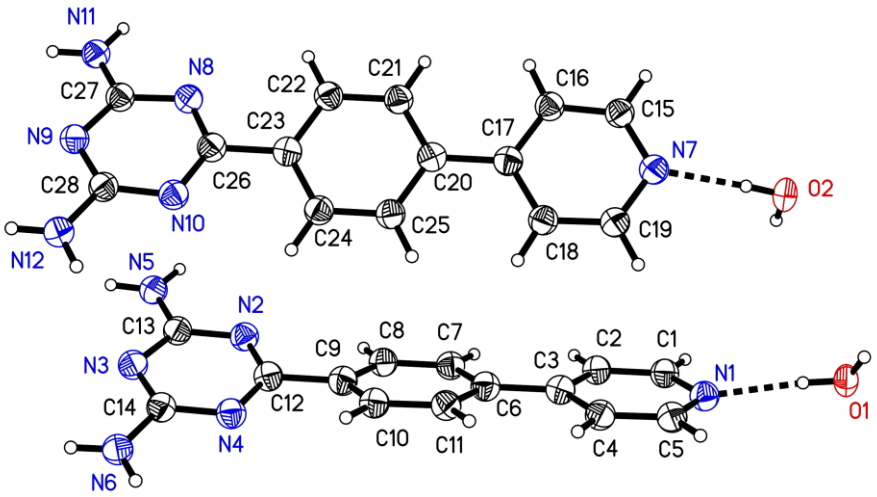

Figure S9. Thermal atomic displacement ellipsoid plots of the structure of crystals of the monohydrate of 2,4-diamino-6-[4-(4-pyridyl)phenyl-1,3,5-triazine (**2a**) grown from wet DMSO. The ellipsoids of non-hydrogen atoms are drawn at the 50% probability level, hydrogen atoms are represented by a sphere of arbitrary size, and hydrogen bonds are represented by broken lines.

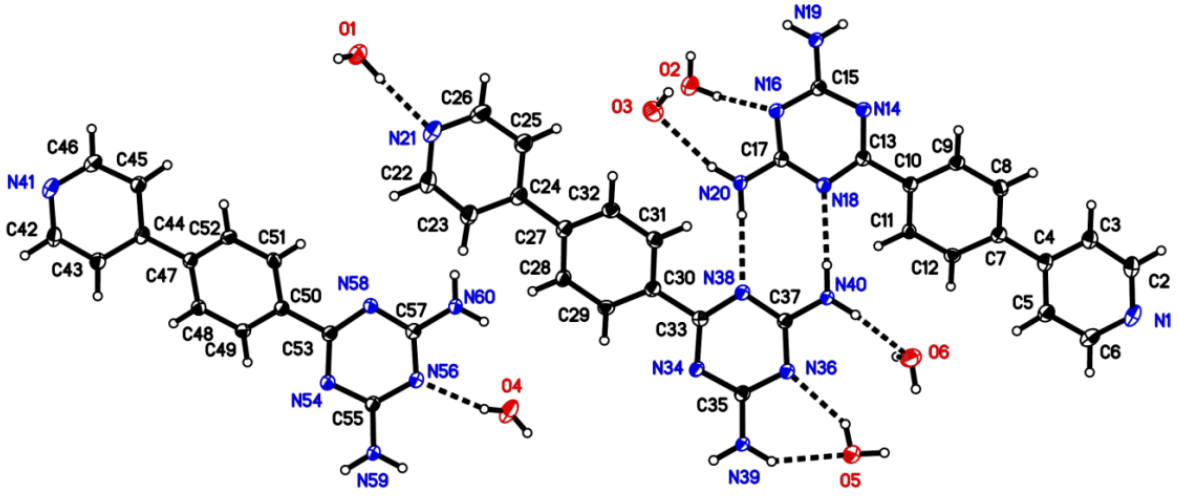

Figure S10. Thermal atomic displacement ellipsoid plot of the structure of crystals of the dihydrate of 2,4-diamino-6-[4-(4-pyridyl)phenyl-1,3,5-triazine (**2a**) grown from wet DMSO. The ellipsoids of non-hydrogen atoms are drawn at the 50% probability level, hydrogen atoms are represented by a sphere of arbitrary size, and hydrogen bonds are represented by broken lines.

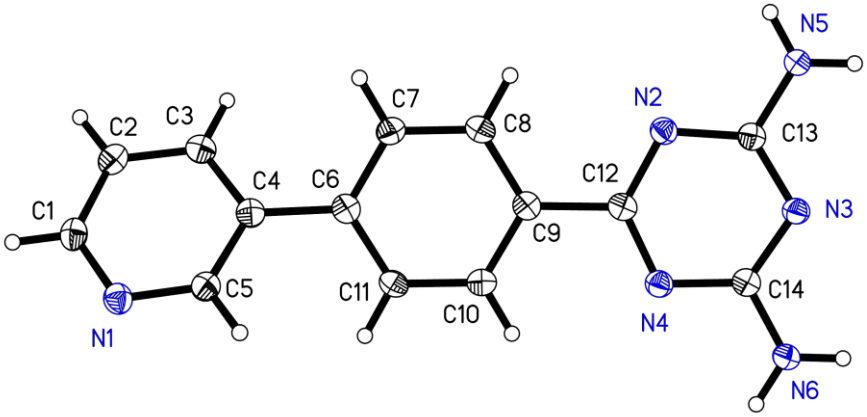

Figure S11. Thermal atomic displacement ellipsoid plot of the structure of crystals of 2,4-diamino-6-[4-(3-pyridyl)phenyl-1,3,5-triazine (**2b**) grown from DMSO/MeCN. The ellipsoids of non-hydrogen atoms are drawn at the 50% probability level, hydrogen atoms are represented by a sphere of arbitrary size, and hydrogen bonds are represented by broken lines.

Homogeneity of Bulk Crystalline Samples

In selected structural studies, experimental powder X-ray diffraction patterns were recorded for bulk crystalline samples and then compared with patterns calculated from single-crystal X-ray diffraction data. These comparisons confirmed that the single-crystal specimens selected for structural analysis were representative of the bulk crystalline samples from which they were chosen. Experimental powder X-ray diffraction patterns were recorded using one of the following two instruments :

1) Bruker D8 Discover diffractometer with GADDS HTS, working in reflection mode and using graphite monochromatized Cu Kα radiation generated at 40 kV and 40 mA.The 2D general area detector was positioned at a distance of 15 cm from the powder sample, which was placed on a glass plate. This allowed simultaneous collection of data over an angular domain up to 35° in 2θ. Measurements were carried out at 293 K in coupled scan mode (θ-θ geometry). Four separate images (diffraction arcs) were collected (scanning time : 5 min/image), and intensity along each arc was integrated to create the 1D powder pattern of intensity versus 2θ, over the angular range $10° < 2\theta < 105°$.
2) Single-crystal Bruker Microstar diffractometer equipped with a FR591 rotating anode generator, Helios optics, and a 2D Pt135 CCD detector, working in transmission mode. A small amount of powdered sample was mounted in a fiber loop, and the diffraction patterns were recorded at 150 K by phi-scan over five different detector positions, merged, and integrated to give the 1D powder diffraction pattern.

Structural data from single-crystal analyses were used to calculate theoretical powder X-ray diffraction patterns with the aid of Mercurysoftware.[1] Peak fitting and the refinement of lattice parameters were carried out using TOPAS software,[2] and Pawley fitting was applied to the powder X-ray diffraction patterns. The quality of the refinement was checked by evaluating the weighted agreement factor R_{wp}, which was calculated on background subtracted intensity data as

$$R_{wp} = \sqrt{\frac{\sum w(Yo - Yc)^2}{\sum w(Yo - Bkg)^2}}$$

where *Y*o is the observed intensity, *Y*c is the calculated intensity, *Bkg* is the background intensity, and *w* is the weighting factor defined by $w = 1/\sigma(Yo)^2$, $\sigma(Yo)$ being the error in the measured intensity.[2]

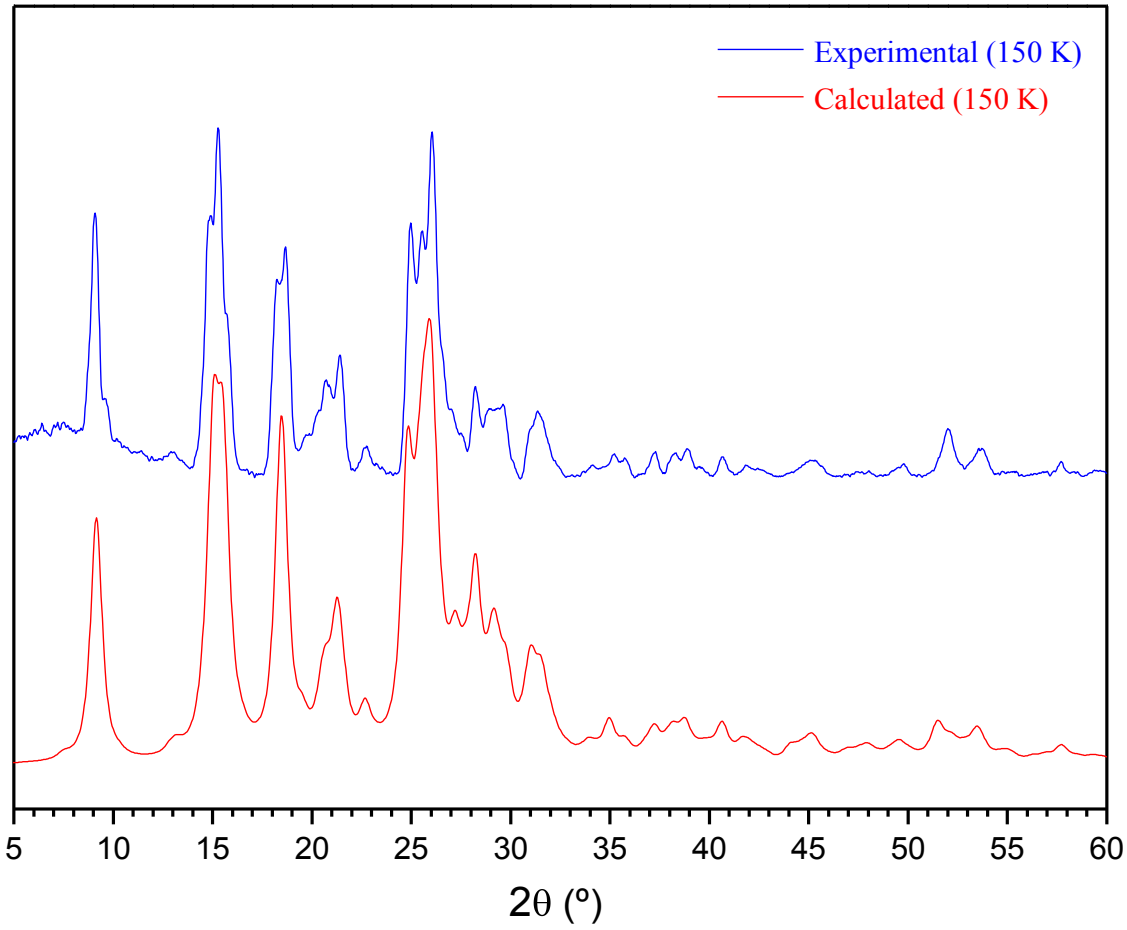

Figure S12. Comparison between experimental (collected using a Bruker Microstar diffractometer) and calculated powder X-ray diffraction patterns for crystals of 2,4-diamino-6-(4-pyridyl)-1,3,5-triazine (**1a**) grown from DMSO/MeCN. The two diffractograms are closely similar, confirming that the bulk crystalline sample consists of a single phase.

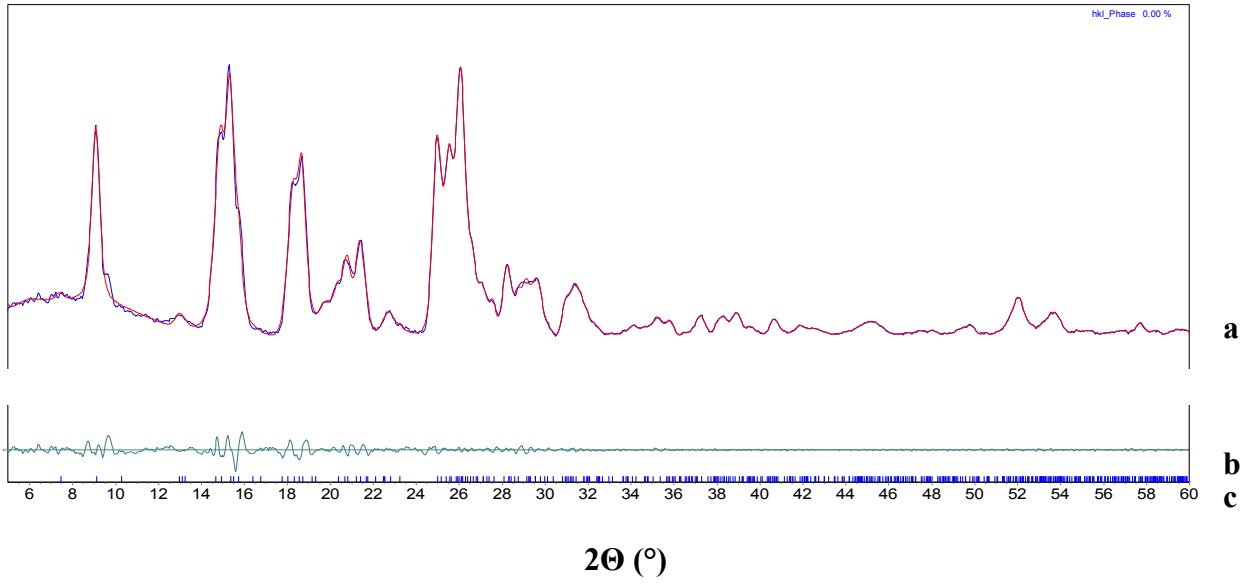

Figure S13. (a) Simulated powder X-ray diffraction pattern of crystals of 2,4-diamino-6-(4-pyridyl)-1,3,5-triazine (**1a**) grown from DMSO/MeCN (red curve) as determined by Pawley fitting of the experimental powder X-ray diffraction pattern (nearly superimposed blue curve). (b) Difference between experimental and calculated intensities. (c) Position of calculated reflections.

Table S1. Crystallographic Data for Crystals of 2,4-Diamino-6-(4-pyridyl)-1,3,5-triazine (**1a**) Grown from DMSO/MeCN as Determined by Pawley Fitting of Powder X-Ray Diffraction Data at 150 K.

compound	**1a**
composition	$C_8H_8N_6$
temperature (K)	150
crystal system	monoclinic
space group	*C*2/*c*
a (Å)	27.651(28)
b (Å)	7.1289(38)
c (Å)	20.051(22)
α (º)	90
β (º)	120.617(76)
γ (º)	90
V (Å^3)	3401.5(60)
Z	16
R_{wp}	0.0277

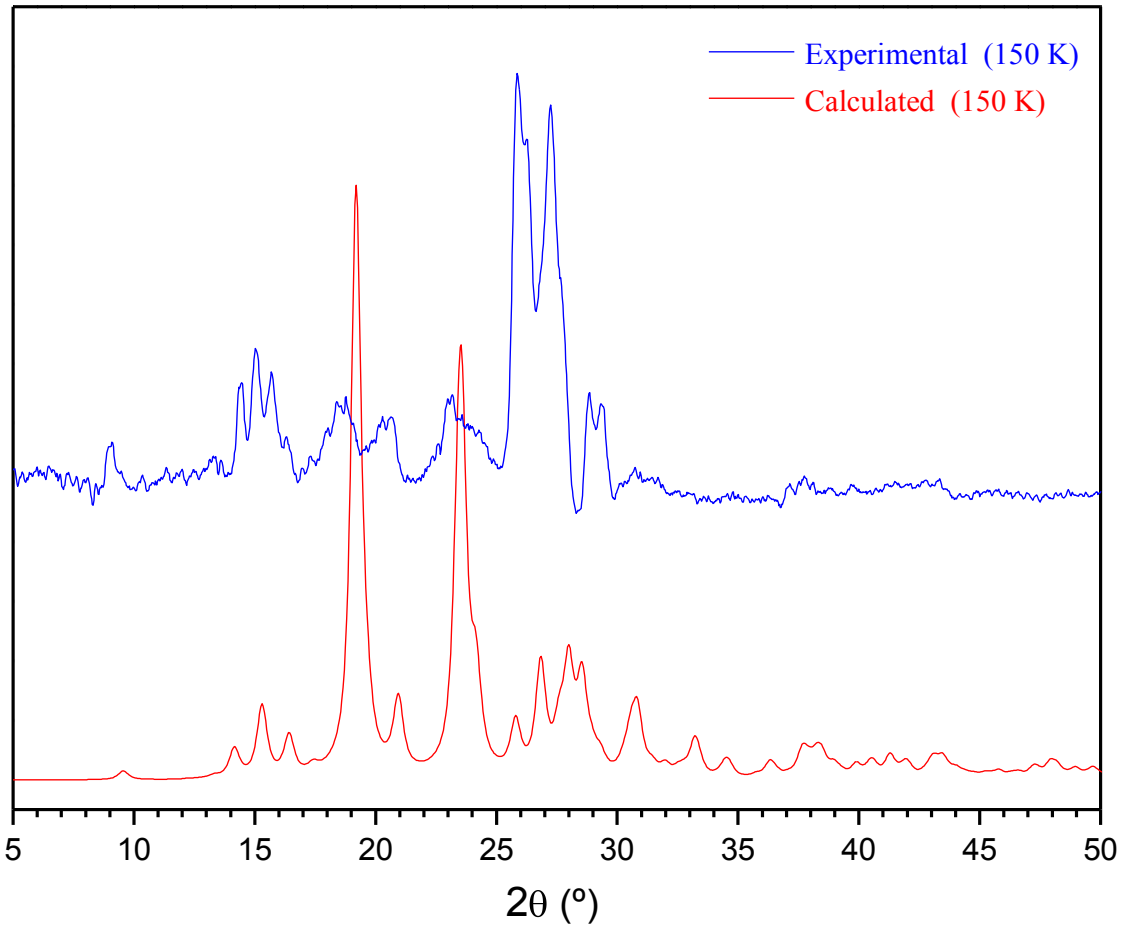

Figure S14. Comparison between experimental (collected using a Bruker Microstar diffractometer) and calculated powder X-ray diffraction patterns for crystals of 2,4-diamino-6-(3-pyridyl)-1,3,5-triazine (**1b**) grown from MeCN. The two diffractograms are closely similar, confirming that the bulk crystalline sample consists of a single phase.

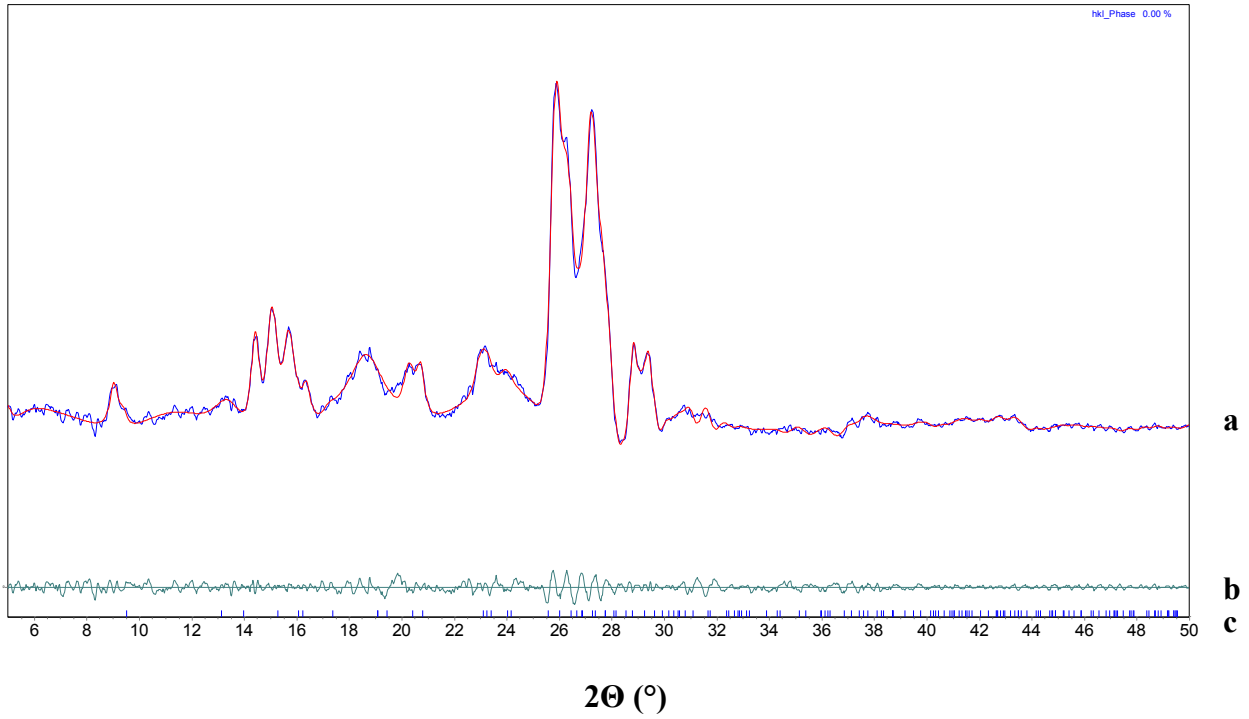

Figure S15. (a) Simulated powder X-ray diffraction pattern of crystals of 2,4-diamino-6-(3-pyridyl)-1,3,5-triazine (**1b**) grown from MeCN (red curve) as determined by Pawley fitting of the experimental powder X-ray diffraction pattern (nearly superimposed blue curve). (b) Difference between experimental and calculated intensities. (c) Position of calculated reflections.

Table S2. Crystallographic Data for Crystals of 2,4-Diamino-6-(3-pyridyl)-1,3,5-triazine (**1b**) Grown from MeCN as Determined by Pawley Fitting of Powder X-Ray Diffraction Data at 150 K.

compound	**1b**
composition	$C_8H_8N_6$
temperature (K)	150
crystal system	orthorhombic
space group	*Pbca*
a (Å)	6.789(12)
b (Å)	13.345(24)
c (Å)	18.275(38)
α (º)	90
β (º)	90
γ (º)	90
V (Å^3)	1655.7(55)
Z	8
R_{wp}	0.0617

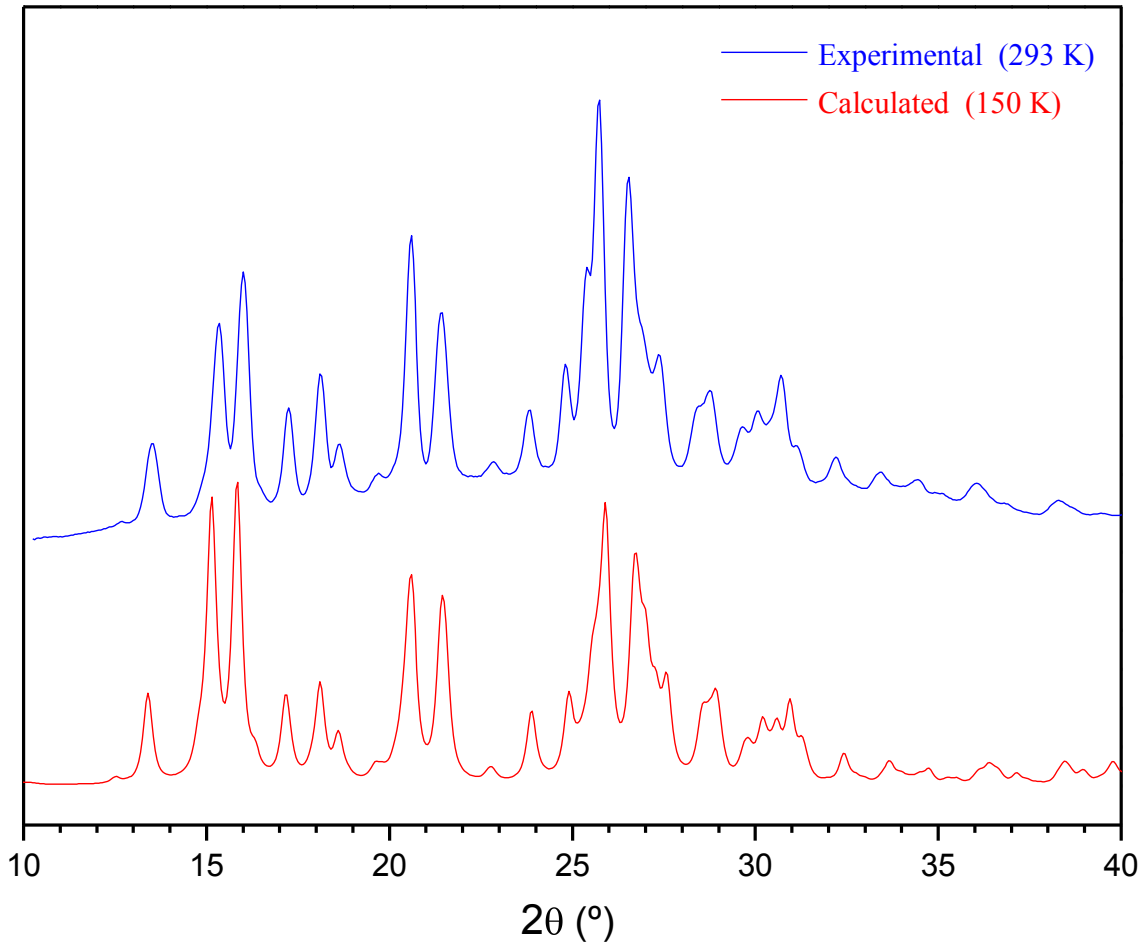

Figure S16. Comparison between experimental (collected using a Bruker Discover diffractometer) and calculated powder X-ray diffraction patterns for crystals of 2,4-diamino-6-(2-pyridyl)-1,3,5-triazine (**1c**) grown from MeCN. The *x* axis of the experimental pattern was shifted to minimize the slight angular shift due to the effect of temperature. The two diffractograms are closely similar, confirming that the bulk crystalline sample consists of a single phase.

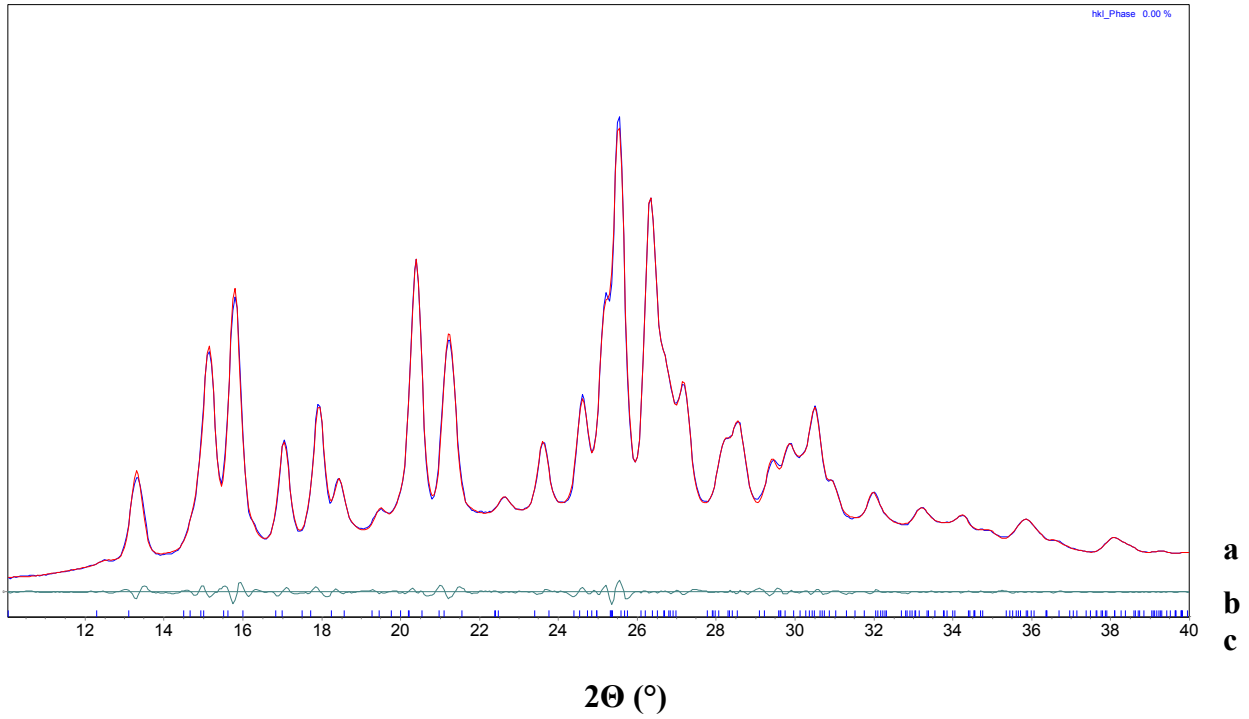

Figure S17. (a) Simulated powder X-ray diffraction pattern of crystals of 2,4-diamino-6-(2-pyridyl)-1,3,5-triazine (**1c**) grown from MeCN (red curve) as determined by Pawley fitting of the experimental powder X-ray diffraction pattern (nearly superimposed blue curve). (b) Difference between experimental and calculated intensities. (c) Position of calculated reflections.

Table S3. Crystallographic Data for Crystals of 2,4-Diamino-6-(2-pyridyl)-1,3,5-triazine (**1c**) Grown from MeCN as Determined by Pawley Fitting of Powder X-Ray Diffraction Data at 293 K.

compound	**1c**
composition	$C_8\ H_8\ N_6$
temperature (K)	293
crystal system	monoclinic
space group	$P2_1/c$
a (Å)	12.0990(43)
b (Å)	7.1241(21)
c (Å)	21.4872(63)
α (º)	90
β (º)	101.505(20)
γ (º)	90
V (Å^3)	1814.96(10)
Z	8
R_{wp}	0.0285

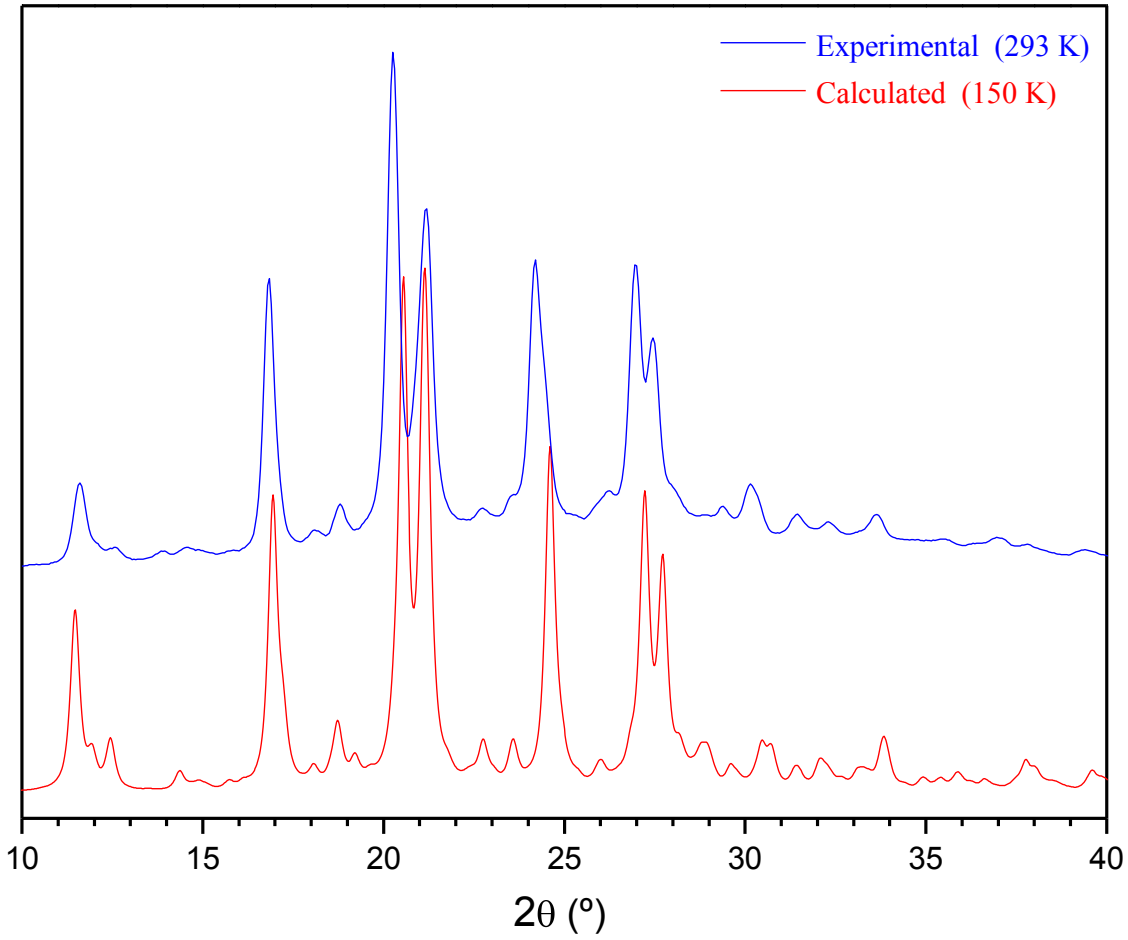

Figure S18. Comparison between experimental (collected using a Bruker Discover diffractometer) and calculated powder X-ray diffraction patterns for crystals of the monoclinic $P2_1/n$ polymorph of 2,4-diamino-6-[4-(4-pyridyl)phenyl-1,3,5-triazine (**2a**) grown from wet DMSO. The *x* axis of the experimental pattern was shifted to minimize the slight angular shift due to the effect of temperature. The two diffractograms are closely similar, confirming that the bulk crystalline sample consists of a single phase.

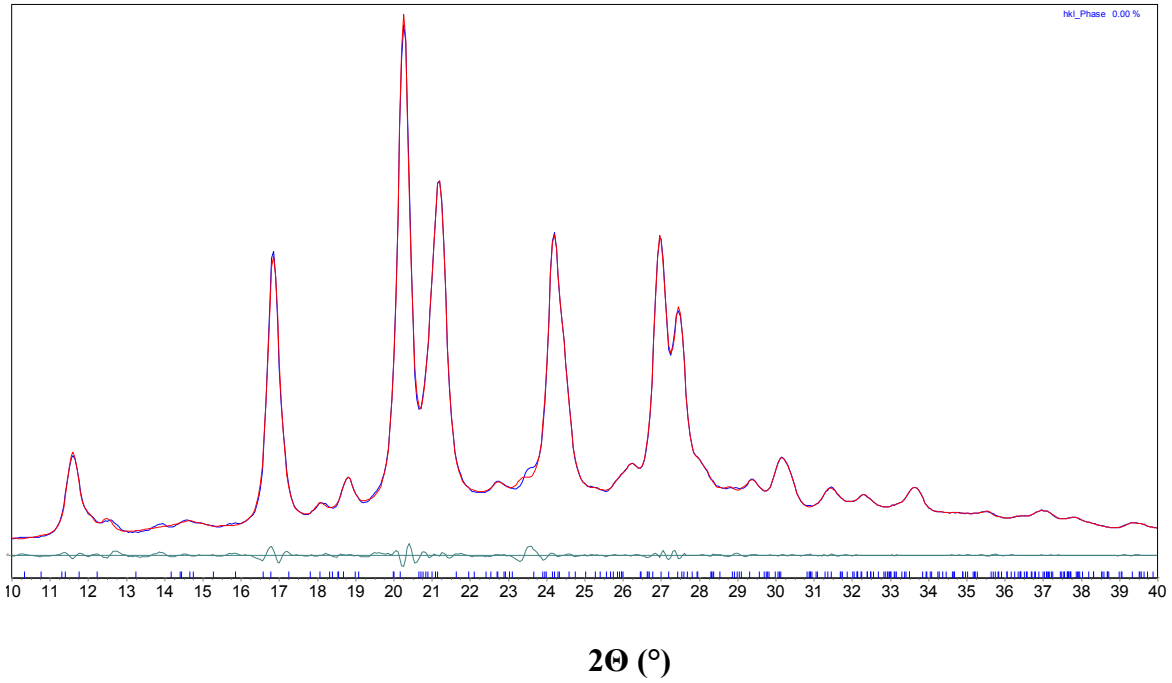

Figure S19. (a) Simulated powder X-ray diffraction pattern of crystals of the monoclinic $P2_1/n$ polymorph of 2,4-diamino-6-[4-(4-pyridyl)phenyl-1,3,5-triazine (**2a**) grown from wet DMSO (red curve) as determined by Pawley fitting of the experimental powder X-ray diffraction pattern (nearly superimposed blue curve). (b) Difference between experimental and calculated intensities. (c) Position of calculated reflections.

Table S4. Crystallographic Data for Crystals of the Monoclinic $P2_1/n$ Polymorph of 2,4-diamino-6-[4-(4-pyridyl)phenyl-1,3,5-triazine (**2a**) Grown from Wet DMSO as Determined by Pawley Fitting of Powder X-Ray Diffraction Data at 293 K.

compound	**2a**
composition	$C_{14}\,H_{12}\,N_6$
temperature (K)	293
crystal system	monoclinic
space group	$P2_1/n$
a (Å)	17.391(60)
b (Å)	8.817(29)
c (Å)	18.091(28)
α (º)	90
β (º)	109.672(97)
γ (º)	90
V (Å^3)	2612(13)
Z	8
R_{wp}	0.0522

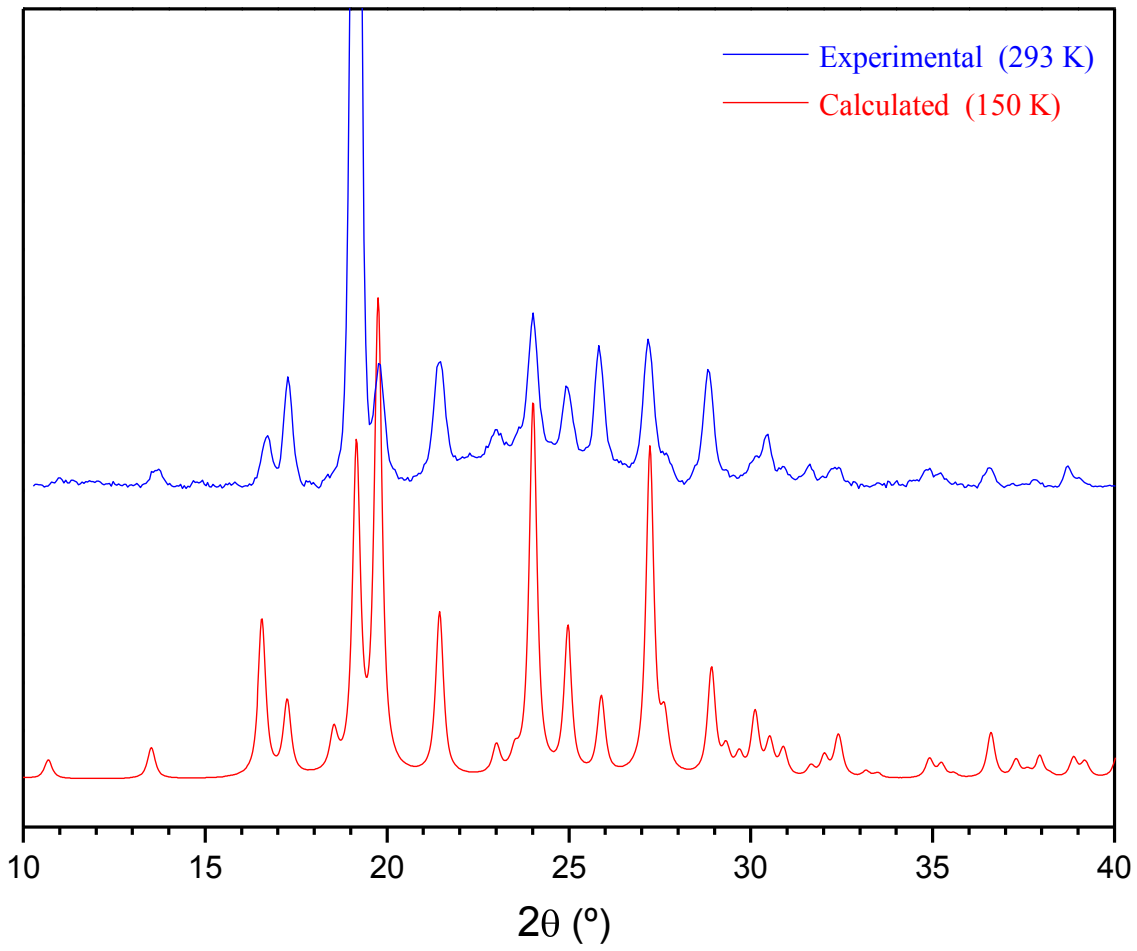

Figure S20. Comparison between experimental (collected using a Bruker Discover diffractometer) and calculated powder X-ray diffraction patterns for crystals of 2,4-diamino-6-[4-(3-pyridyl)phenyl-1,3,5-triazine (**2b**) grown from DMSO/MeCN. The *x* axis of the experimental pattern was shifted to minimize the slight angular shift due to the effect of temperature. The two diffractograms are closely similar, confirming that the bulk crystalline sample consists of a single phase.

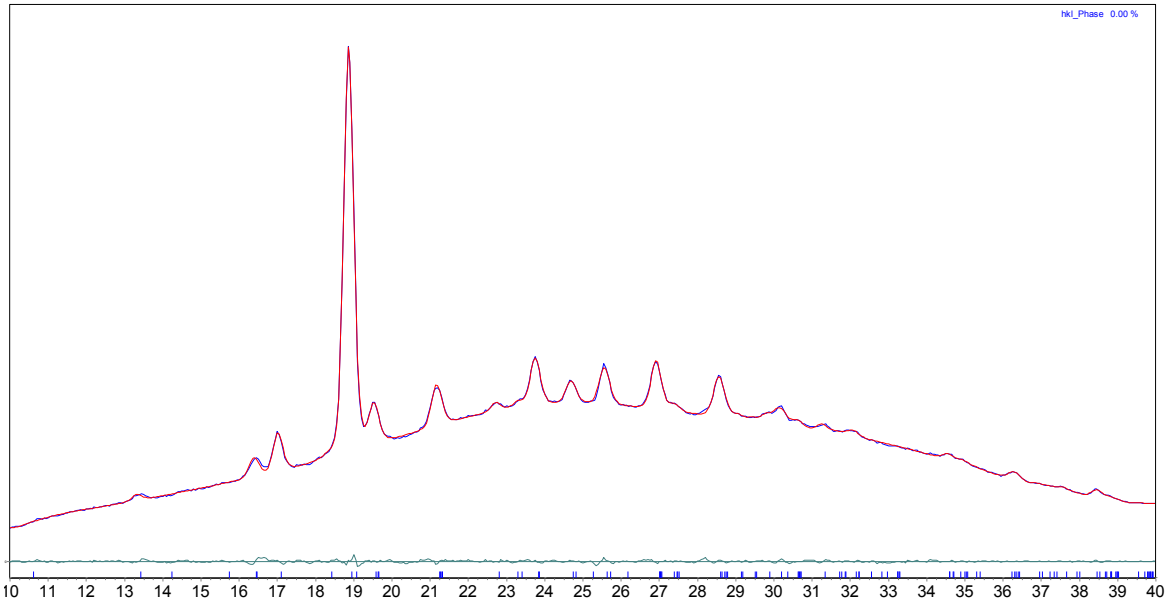

Figure S21. (a) Simulated powder X-ray diffraction pattern of crystals of 2,4-diamino-6-[4-(3-pyridyl)phenyl-1,3,5-triazine (**2b**) grown from DMSO/MeCN (red curve) as determined by Pawley fitting of the experimental powder X-ray diffraction pattern (nearly superimposed blue curve). (b) Difference between experimental and calculated intensities. (c) Position of calculated reflections.

Table S5. Crystallographic Data for Crystals of 2,4-Diamino-6-[4-(3-pyridyl)phenyl-1,3,5-triazine (**2b**) Grown from DMSO/MeCN as Determined by Pawley Fitting of Powder X-Ray Diffraction Data at 293 K.

compound	**2b**
composition	$C_{14}\,H_{12}\,N_6$
temperature (K)	293
crystal system	orthorhombic
space group	*Pbca*
a (Å)	7.0382(70)
b (Å)	18.539(14)
c (Å)	18.6621(62)
α (º)	90
β (º)	90
γ (º)	90
V (Å^3)	2435.1(31)
Z	8
R_{wp}	0.042

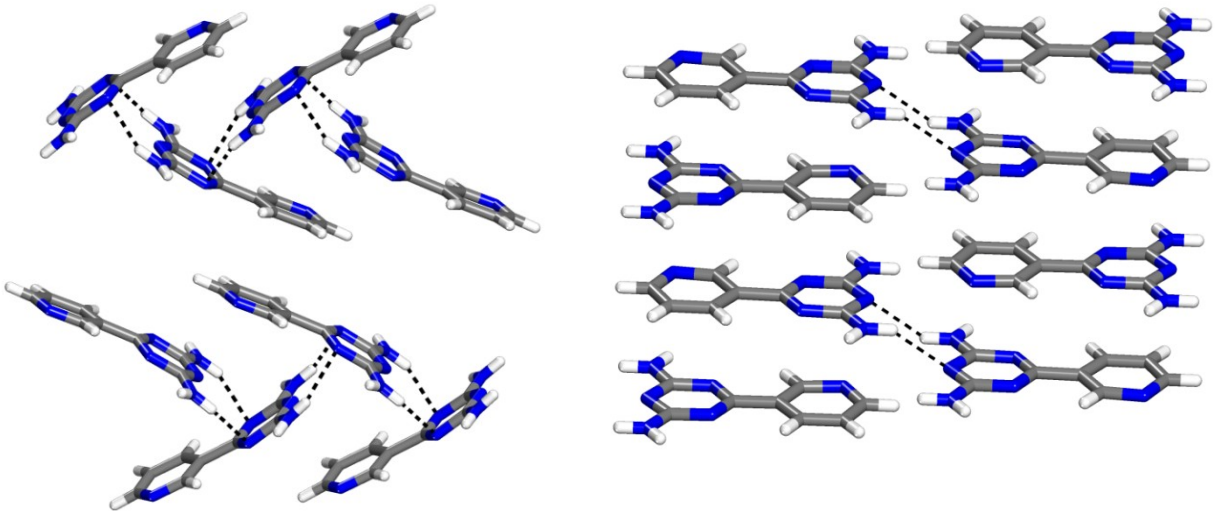

a **b**

Figure S22. Supplementary views showing the association of independent molecules **A** and **B** in the structure of crystals of 2,4-diamino-6-(3-pyridyl)-1,3,5-triazine (**1b**) grown from DMSO. Hydrogen bonds are represented by broken lines, and carbon atoms are shown in gray, hydrogen atoms in white, and nitrogen atoms in blue. a) View of π-stacking and edge-to-face N-H···N interactions within a herringbone arrangement of molecules **B**. b) View showing association of molecules **A** by hydrogen bonding of type **I** and head-to-tail π-stacking.

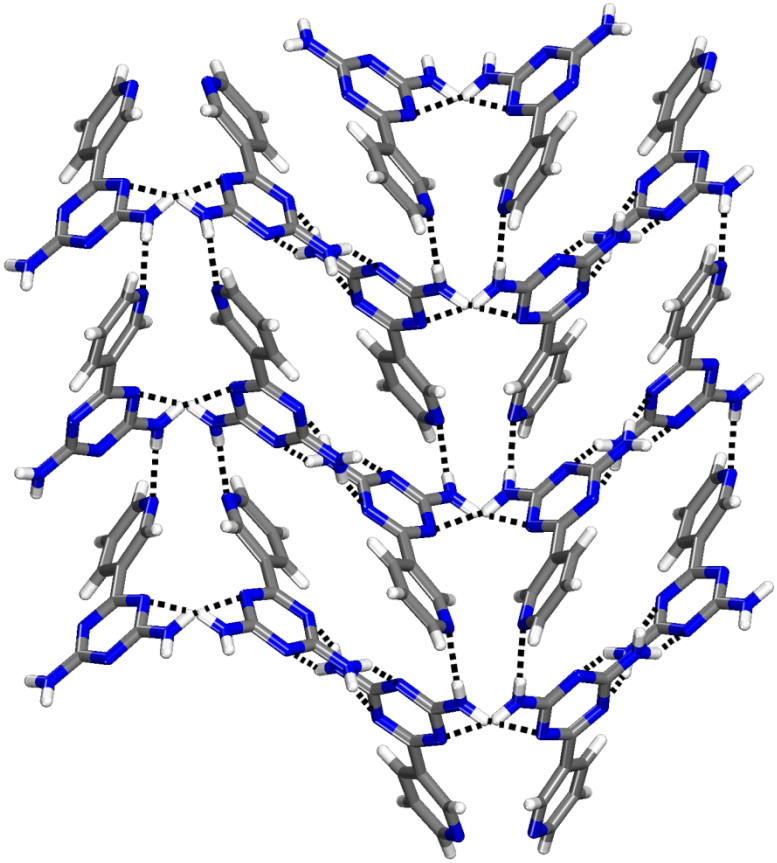

Figure S23. Supplementary view in the direction of the characteristic hydrogen-bonded chains (*a* axis) in the structure of crystals of 2,4-diamino-6-(3-pyridyl)-1,3,5-triazine (**1b**) grown from MeCN. The view shows how the chains are packed and connected by N-H···N(pyridine) hydrogen bonds to define layers parallel to the *ab* plane. Hydrogen bonds are represented by broken lines, and carbon atoms are shown in gray, hydrogen atoms in white, and nitrogen atoms in blue.

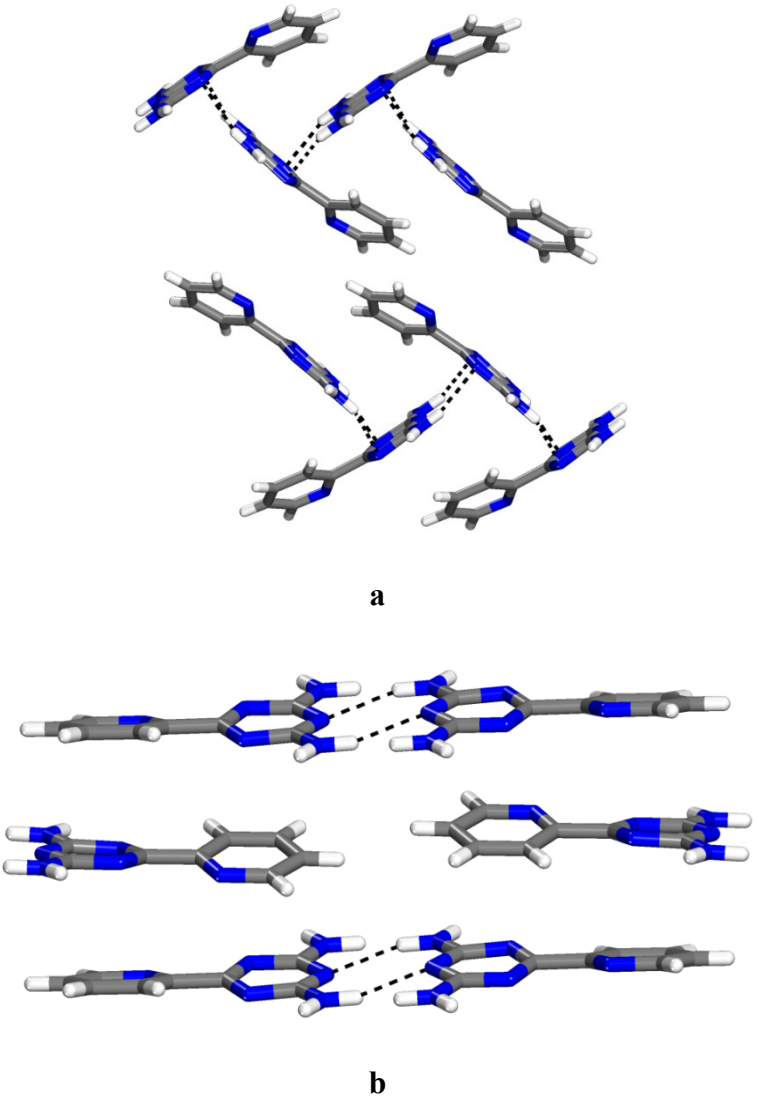

a

b

Figure S24. Supplementary views showing the association of independent molecules **A** and **B** in the structure of crystals of 2,4-diamino-6-(2-pyridyl)-1,3,5-triazine (**1c**) grown from MeCN. Hydrogen bonds are represented by broken lines, and carbon atoms are shown in gray, hydrogen atoms in white, and nitrogen atoms in blue. a) View of π-stacking and edge-to-face N-H···N interactions within a herringbone arrangement of molecules **B**. b) View showing association of molecules **A** by hydrogen bonding of type **I** and head-to-tail π-stacking.

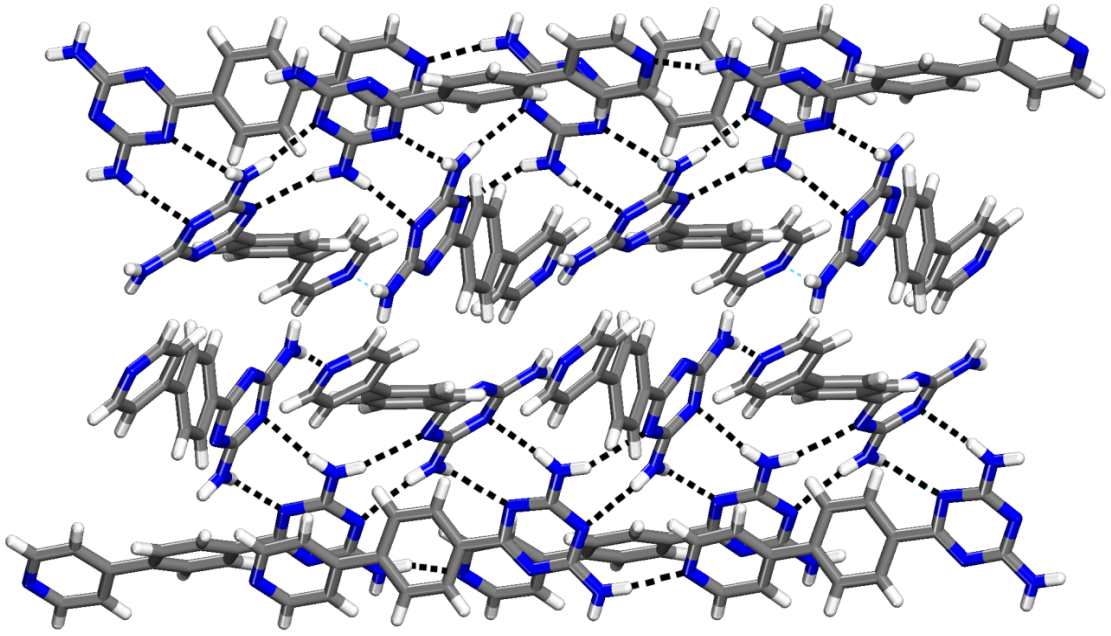

Figure S25. Supplementary view of the structure of crystals of the triclinic *P*-1 polymorph of 2,4-diamino-6-[4-(4-pyridyl)phenyl-1,3,5-triazine (**2a**) grown from wet DMSO. Hydrogen bonds are represented by broken lines, and carbon atoms are shown in gray, hydrogen atoms in white, and nitrogen atoms in blue.

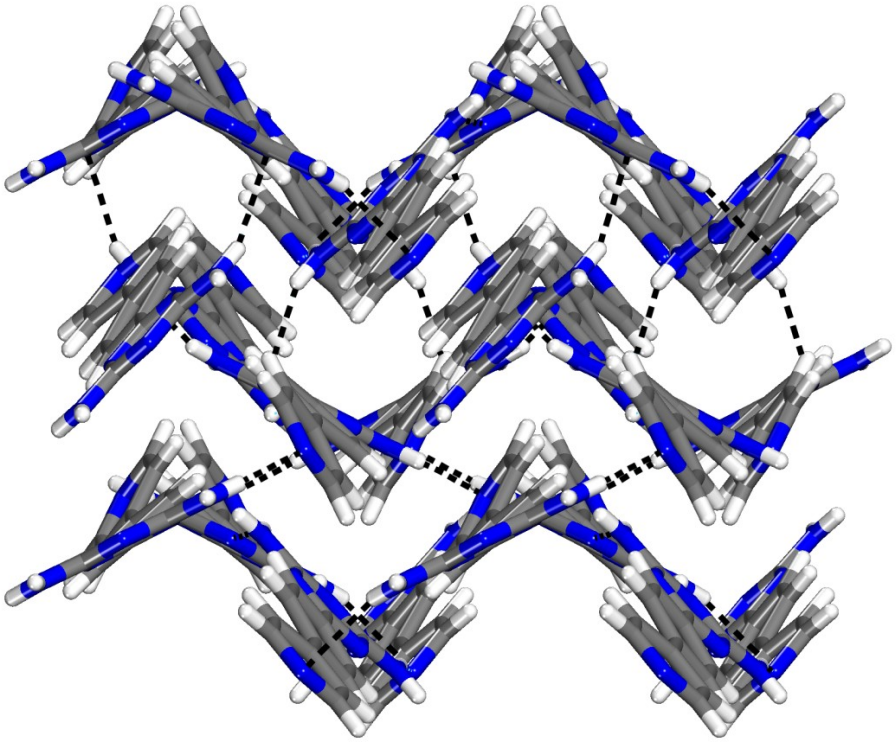

Figure S26. Supplementary view of corrugated hydrogen-bonded sheets in the structure of crystals of the monoclinic $P2_1/n$ polymorph of 2,4-diamino-6-[4-(4-pyridyl)phenyl-1,3,5-triazine (**2a**) grown from wet DMSO. Hydrogen bonds are represented by broken lines, and carbon atoms are shown in gray, hydrogen atoms in white, and nitrogen atoms in blue.

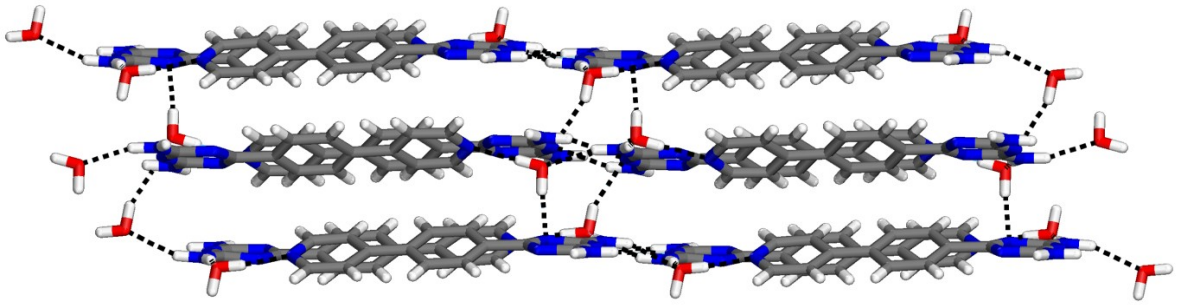

Figure S27. Supplementary view of hydrogen-bonded sheets in the structure of crystals of the monohydrate of 2,4-diamino-6-[4-(4-pyridyl)phenyl-1,3,5-triazine (**2a**) grown from wet DMSO. Hydrogen bonds are represented by broken lines, and carbon atoms are shown in gray, hydrogen atoms in white, nitrogen atoms in blue, and oxygen atoms in red.

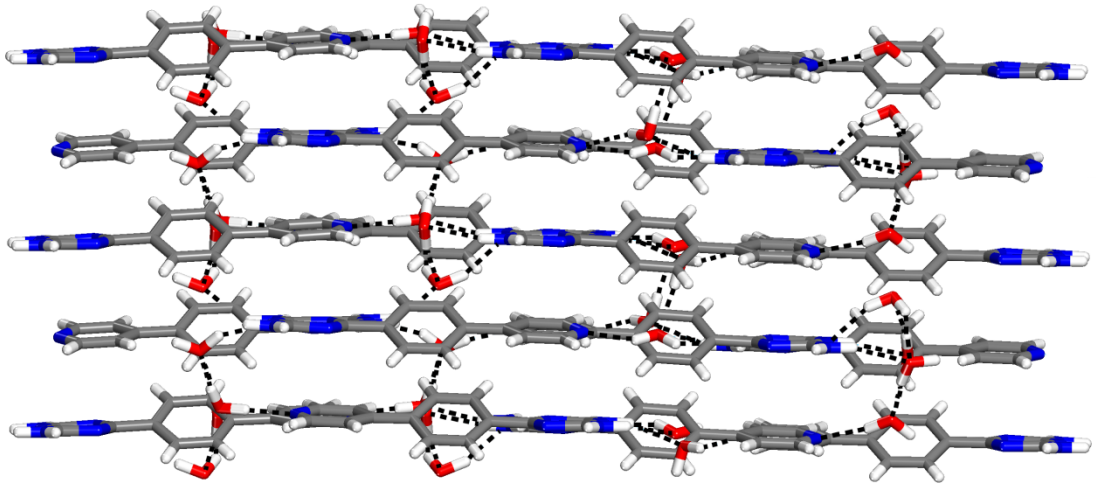

Figure S28. Supplementary view of hydrogen-bonded sheets in the structure of crystals of the dihydrate of 2,4-diamino-6-[4-(4-pyridyl)phenyl-1,3,5-triazine (**2a**) grown from wet DMSO. Hydrogen bonds are represented by broken lines, and carbon atoms are shown in gray, hydrogen atoms in white, nitrogen atoms in blue, and oxygen atoms in red.

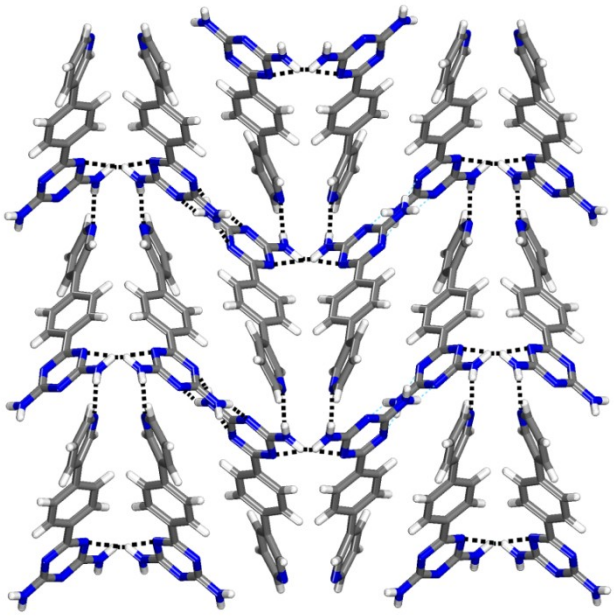

Figure S29. Supplementary view in the direction of the characteristic hydrogen-bonded chains (*a* axis) in the structure of crystals of 2,4-diamino-6-[4-(3-pyridyl)phenyl-1,3,5-triazine (**2b**) grown from DMSO/MeCN. The view shows how the chains are packed and connected by N-H···N(pyridine) hydrogen bonds to define layers parallel to the *ab* plane. Hydrogen bonds are represented by broken lines, and carbon atoms are shown in gray, hydrogen atoms in white, and nitrogen atoms in blue.

References

1) Macrae, C. F.; Edgington, P. R.; McCabe, P.; Pidcock, E.; Shields, G. P.; Taylor, R.; Towler, M.; van de Streek, J. *J. Appl. Cryst.* **2006**, *39*, 453-457.
2) Coelho, A. A. *TOPAS User Manual*, Version 3.1 ed.; Bruker-AXS GmbH : Karlsruhe, Germany, 2003.

Annexe 5

Partie supplémentaire de l'article 5

Supporting Information

Syntheses and Structures of Isomeric Diaminotriazinyl-Substituted 2,2'-Bipyridines and 1,10-Phenanthrolines

Adam Duong, Thierry Maris, Olivier Lebel, and James D. Wuest*

Département de Chimie, Université de Montréal, Montréal, Québec H3C 3J7 Canada

Contents **Page**

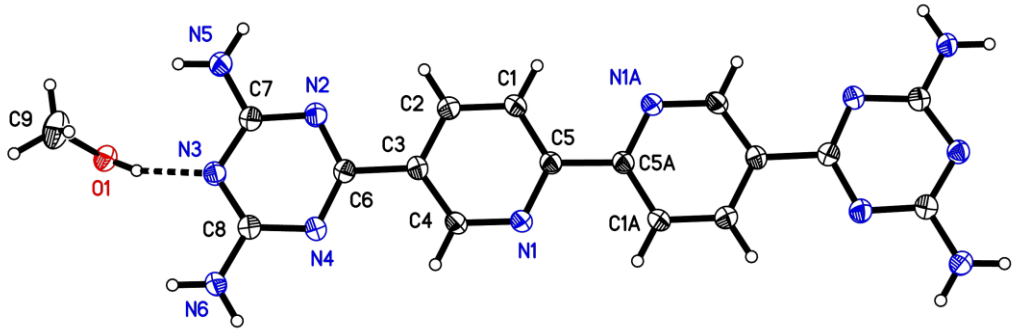

Figure S1. Thermal atomic displacement ellipsoid plot of the structure of crystals of the 1:2 solvate of DAT-substituted bipyridine **4a** with MeOH. The ellipsoids of non-hydrogen atoms are drawn at the 50% probability level, hydrogen atoms are represented by a sphere of arbitrary size, and hydrogen bonds are represented by broken lines.

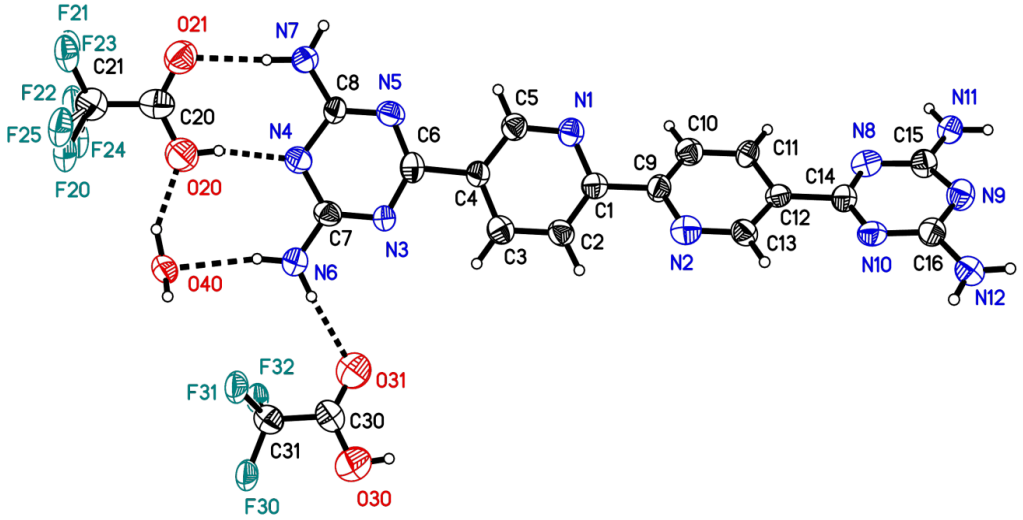

Figure S2. Thermal atomic displacement ellipsoid plot of the structure of crystals of the 1:2:1 solvate of DAT-substituted bipyridine **4a** with TFA and H_2O. The ellipsoids of non-hydrogen atoms are drawn at the 50% probability level, hydrogen atoms are represented by a sphere of arbitrary size, and hydrogen bonds are represented by broken lines.

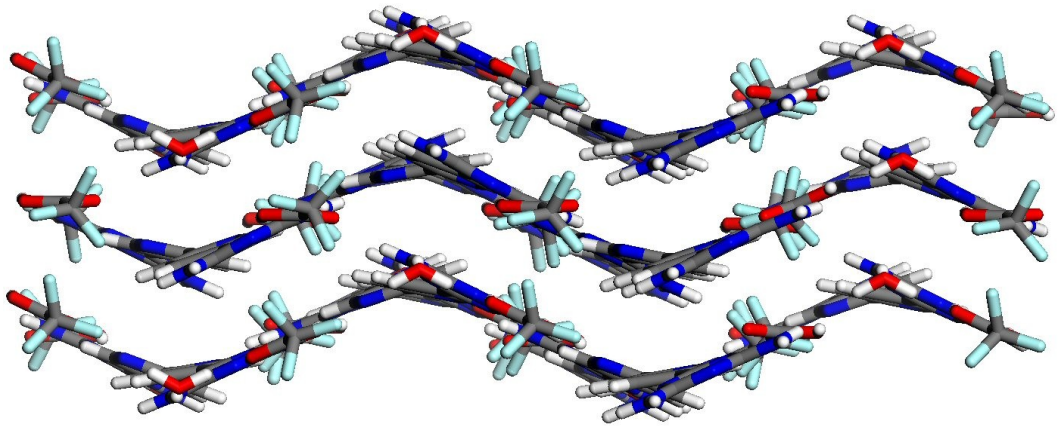

Figure S3. Stacking of corrugated sheets in the structure of crystals of the 1:2:1 solvate of DAT-substituted bipyridine **4a** with TFA and H_2O. Carbon atoms are shown in gray, hydrogen atoms in white, fluorine atoms in light blue, nitrogen atoms in dark blue, and oxygen atoms in red.

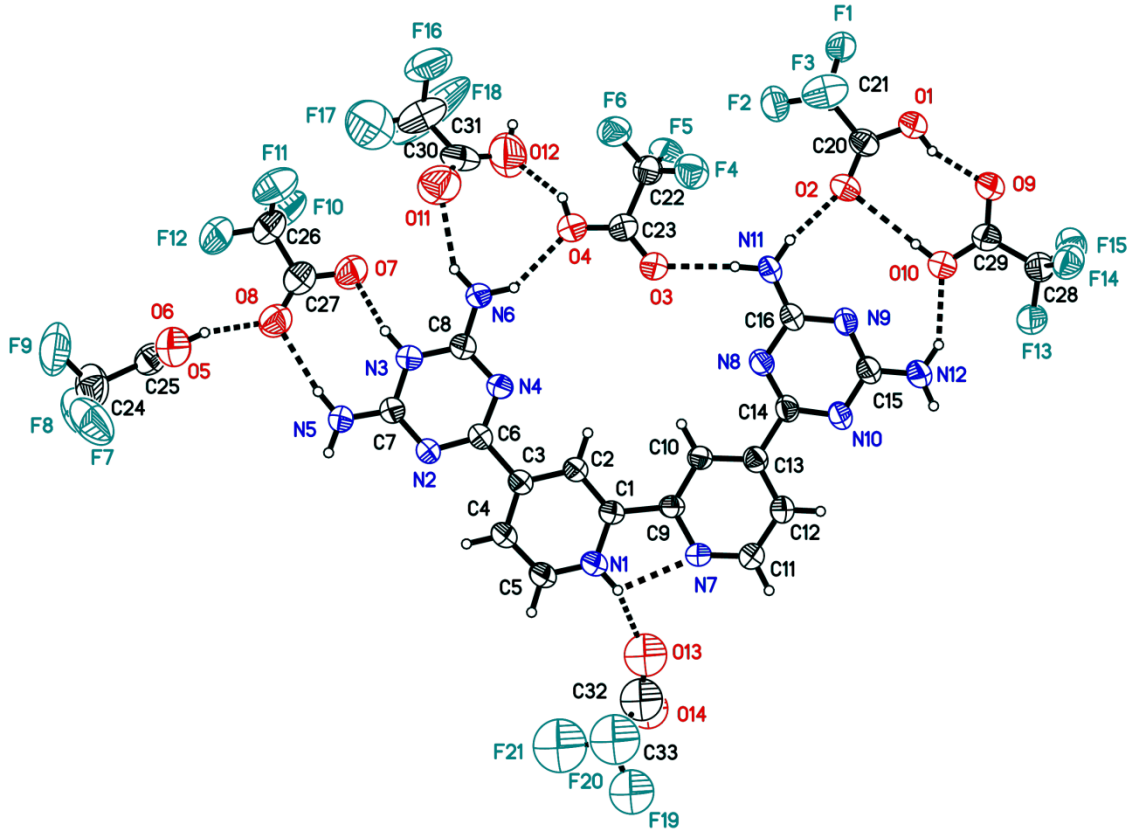

Figure S4. Thermal atomic displacement ellipsoid plot of the structure of crystals of the 1:7 solvate of DAT-substituted bipyridine **5a** with TFA. The ellipsoids of non-hydrogen atoms are drawn at the 50% probability level, hydrogen atoms are represented by a sphere of arbitrary size, and hydrogen bonds are represented by broken lines. Only one part of the disordered TFA is shown.

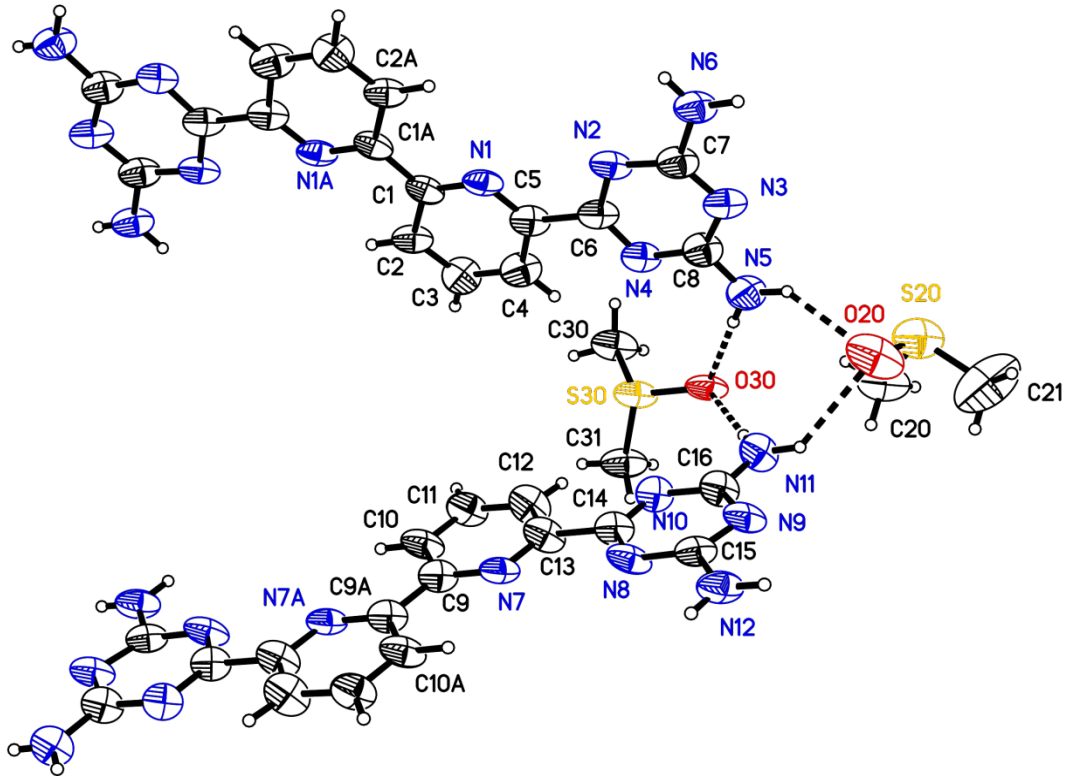

Figure S5. Thermal atomic displacement ellipsoid plot of the structure of crystals of the 1:2 solvate of DAT-substituted bipyridine **6a** with DMSO. The ellipsoids of non-hydrogen atoms are drawn at the 50% probability level, hydrogen atoms are represented by a sphere of arbitrary size, and hydrogen bonds are represented by broken lines.

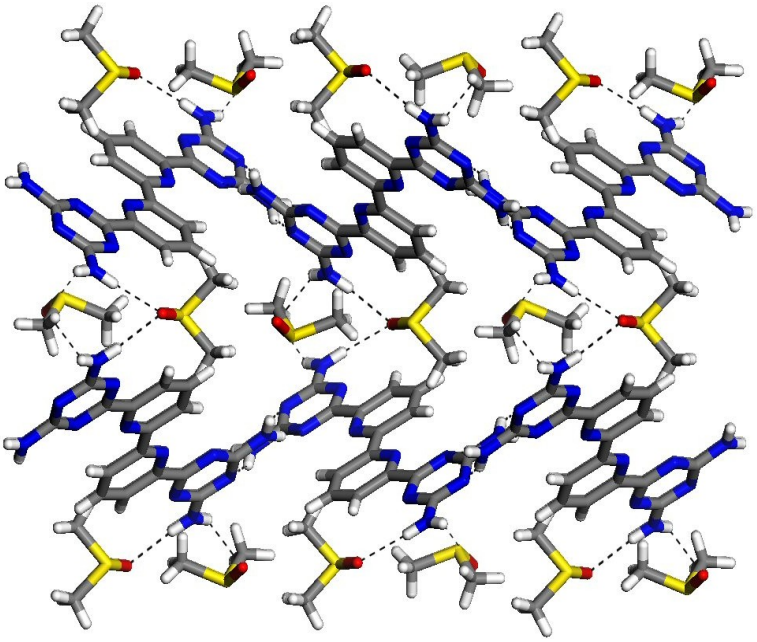

Figure S6. Inclusion of DMSO between layers in the structure of crystals of the 1:2 solvate of DAT-substituted bipyridine **6a** with DMSO. Carbon atoms are shown in gray, hydrogen atoms in white, nitrogen atoms in blue, oxygen atoms in red, and sulfur atoms in yellow. Hydrogen bonds are represented by broken lines.

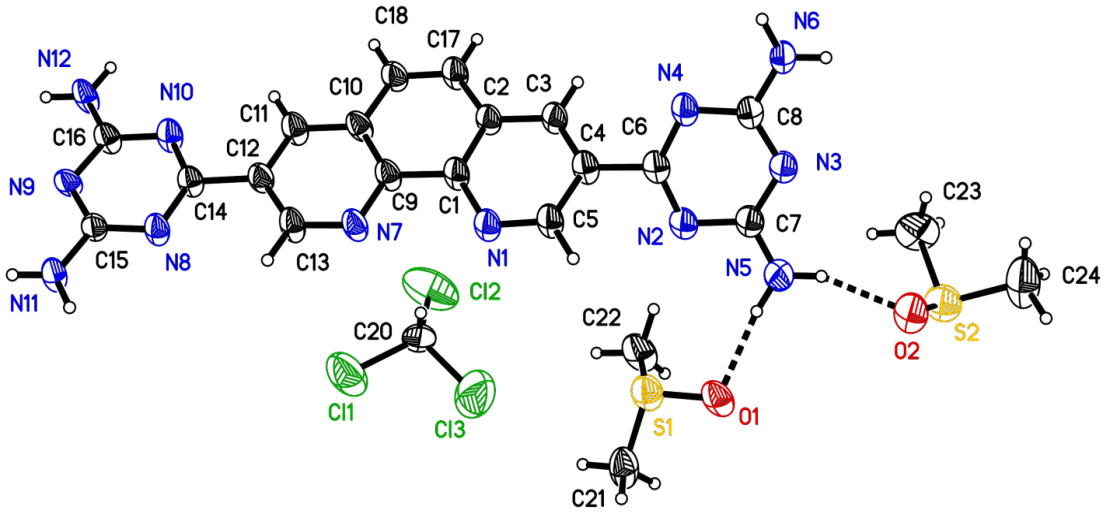

Figure S7. Thermal atomic displacement ellipsoid plot of the structure of crystals of the 1:2:1 solvate of DAT-substituted phenanthroline **7a** with DMSO and $CHCl_3$. The ellipsoids of non-hydrogen atoms are drawn at the 50% probability level, hydrogen atoms are represented by a sphere of arbitrary size, and hydrogen bonds are represented by broken lines.

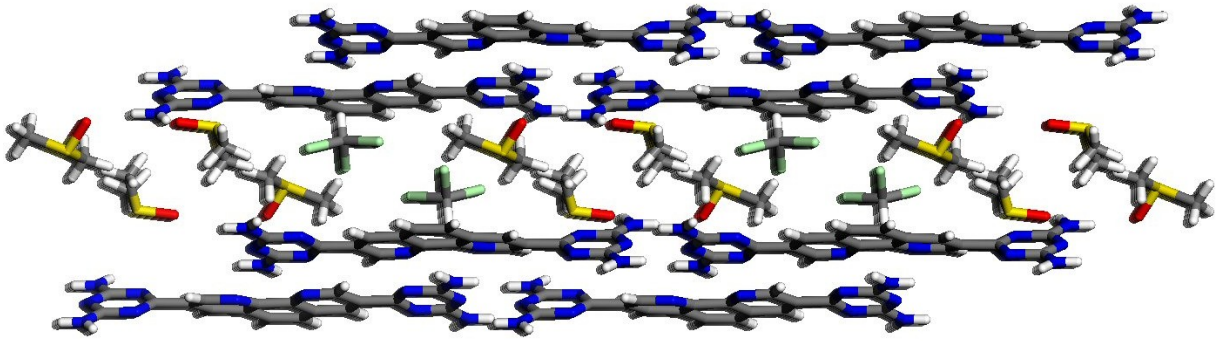

Figure S8. View of layers separated by included molecules of DMSO and $CHCl_3$ in the structure of crystals of the 1:2:1 solvate of DAT-substituted phenanthroline **7a** with DMSO and $CHCl_3$. Carbon atoms are shown in gray, hydrogen atoms in white, nitrogen atoms in blue, oxygen atoms in red, sulfur atoms in yellow, and chlorine atoms in green.

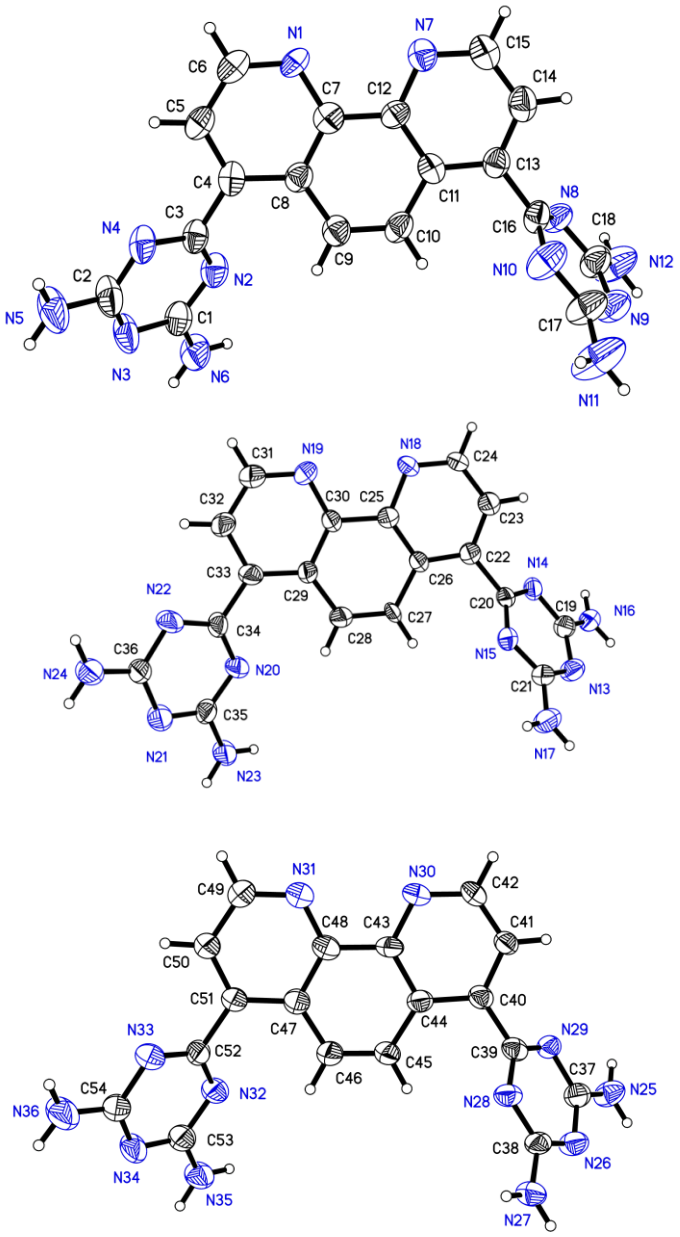

Figure S9. Thermal atomic displacement ellipsoid plots of the structure of crystals of the 3:2:1 solvate of DAT-substituted phenanthroline **8a** with DMSO and CH_2Cl_2, showing the three independent molecules of compound **8a** in the asymmetric unit. The ellipsoids of non-hydrogen atoms are drawn at the 50% probability level, hydrogen atoms are represented by a sphere of arbitrary size, and guest molecules of DMSO and CH_2Cl_2 are omitted.

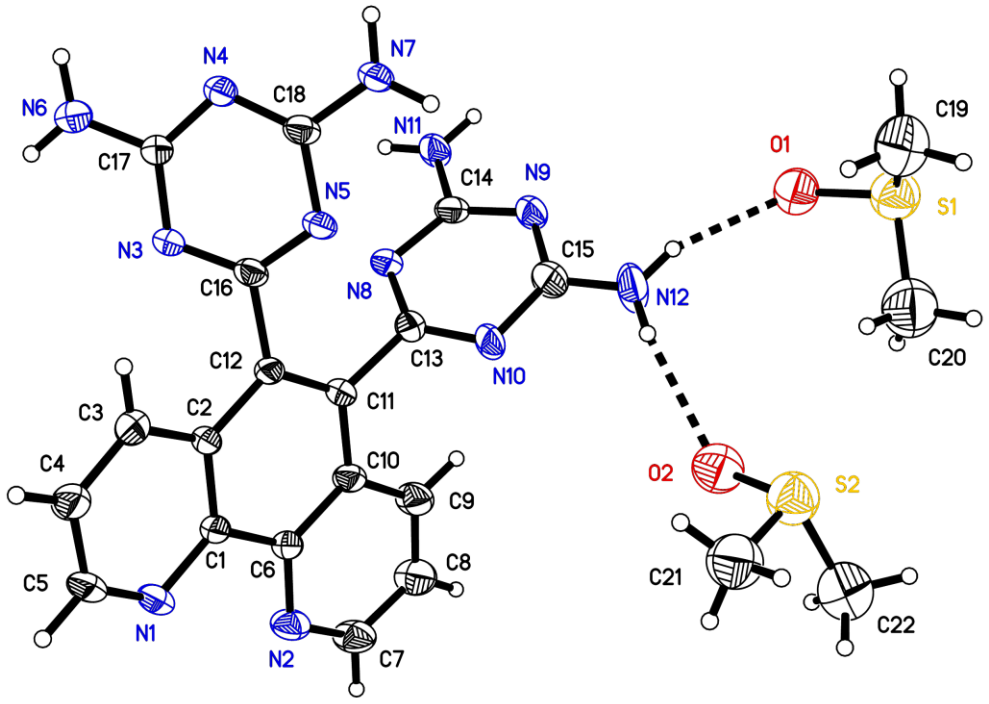

Figure S10. Thermal atomic displacement ellipsoid plot of the structure of crystals of the 1:2 solvate of DAT-substituted phenanthroline **9a** with DMSO. The ellipsoids of non-hydrogen atoms are drawn at the 50% probability level, hydrogen atoms are represented by a sphere of arbitrary size, and hydrogen bonds are represented by broken lines.

Annexe 6

Partie supplémentaire de l'article 7

Supporting Information

Surrogates of 2,2'-Bipyridine Designed to Chelate Ag(I) and Create Metallotectons for Engineering Hydrogen-Bonded Crystals

Adam Duong, Valérie Métivaud, Thierry Maris, and James D. Wuest*

Département de Chimie, Université de Montréal

Montréal, Québec H3C 3J7, Canada

Contents **Page**

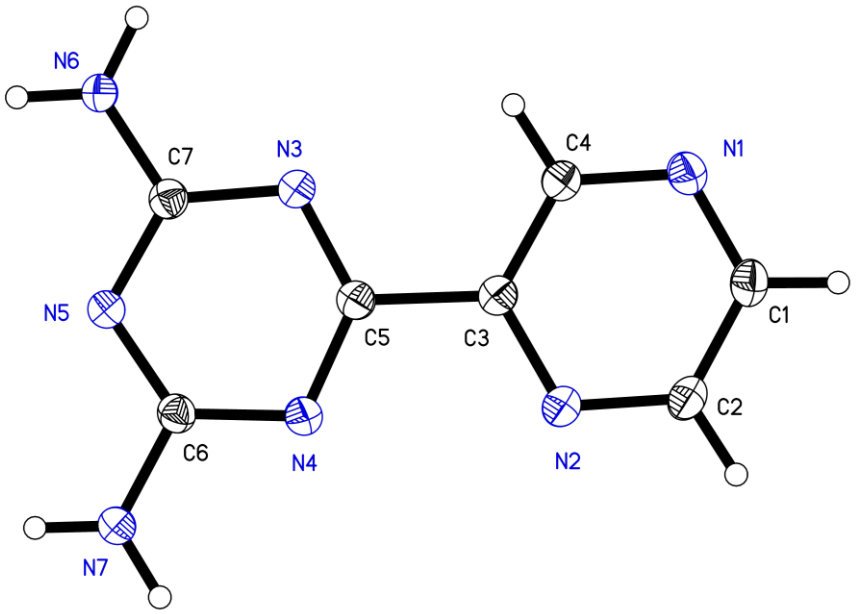

Figure S1. Thermal atomic displacement ellipsoid plot of the structure of crystals of 6-(pyrazin-2-yl)-1,3,5-triazine-2,4-diamine (**2**) grown from DMSO/MeCN. Ellipsoids of non-hydrogen atoms are drawn at the 50% probability level, and hydrogen atoms are represented by a sphere of arbitrary size.

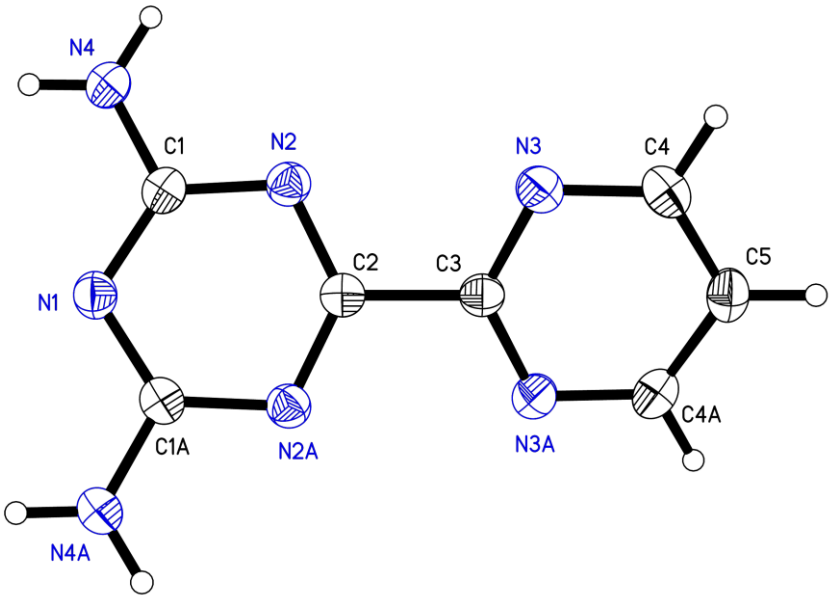

Figure S2. Thermal atomic displacement ellipsoid plot of the structure of crystals of 6-(pyrimidin-2-yl)-1,3,5-triazine-2,4-diamine (**3**) grown from DMSO/CH_2Cl_2. The ellipsoids of non-hydrogen atoms are drawn at the 50% probability level, and hydrogen atoms are represented by a sphere of arbitrary size.

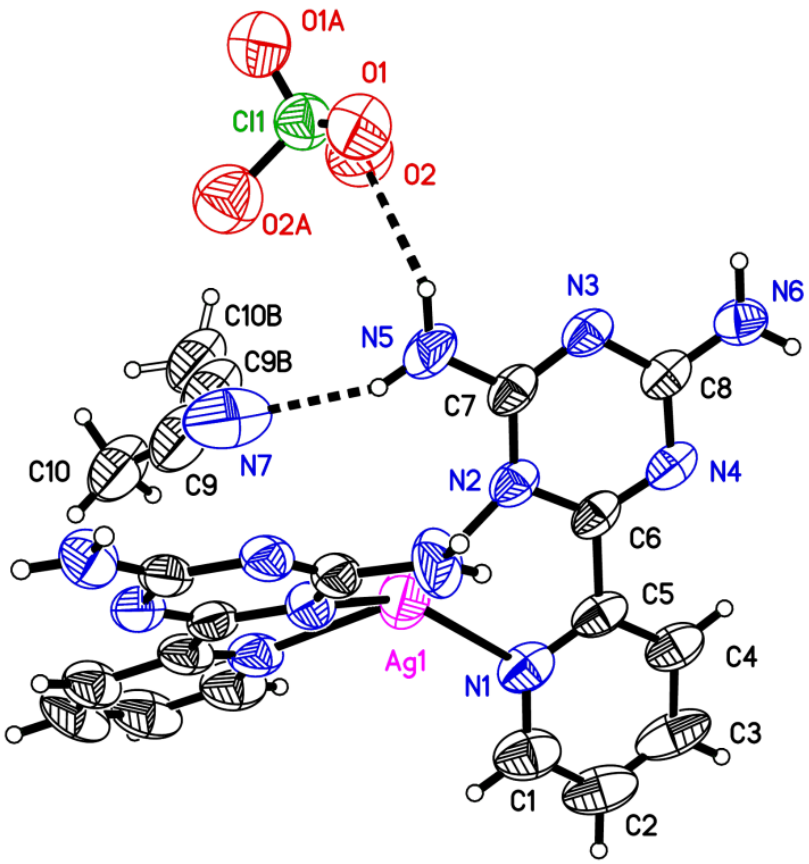

Figure S3. Thermal atomic displacement ellipsoid plot of the structure of crystals of the solvated form of the 2:1 complex of 6-(pyridin-2-yl)-1,3,5-triazine-2,4-diamine (**1**) with $AgClO_4$ grown from DMSO/MeCN. The ellipsoids of non-hydrogen atoms are drawn at the 50% probability level, hydrogen atoms are represented by a sphere of arbitrary size, and hydrogen bonds are represented by broken lines.

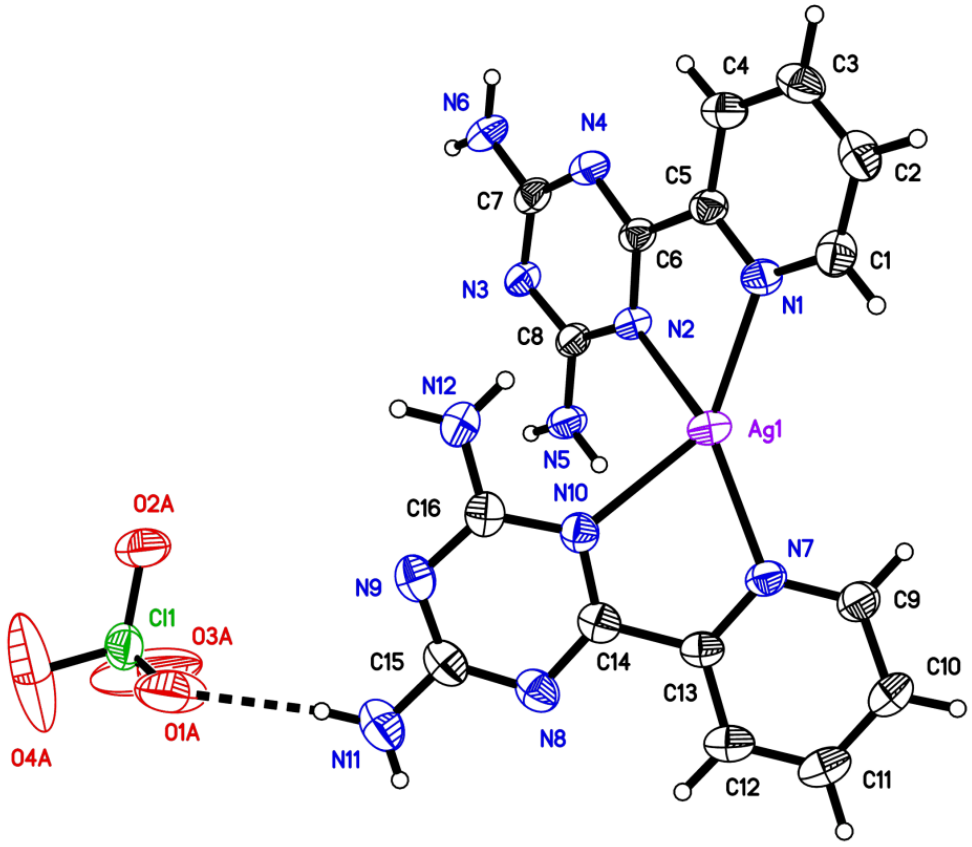

Figure S4. Thermal atomic displacement ellipsoid plot of the structure of crystals of the unsolvated form of the 2:1 complex of 6-(pyridin-2-yl)-1,3,5-triazine-2,4-diamine (**1**) with $AgClO_4$ grown from DMSO/MeCN. The ellipsoids of non-hydrogen atoms are drawn at the 50% probability level, hydrogen atoms are represented by a sphere of arbitrary size, and hydrogen bonds are represented by broken lines.

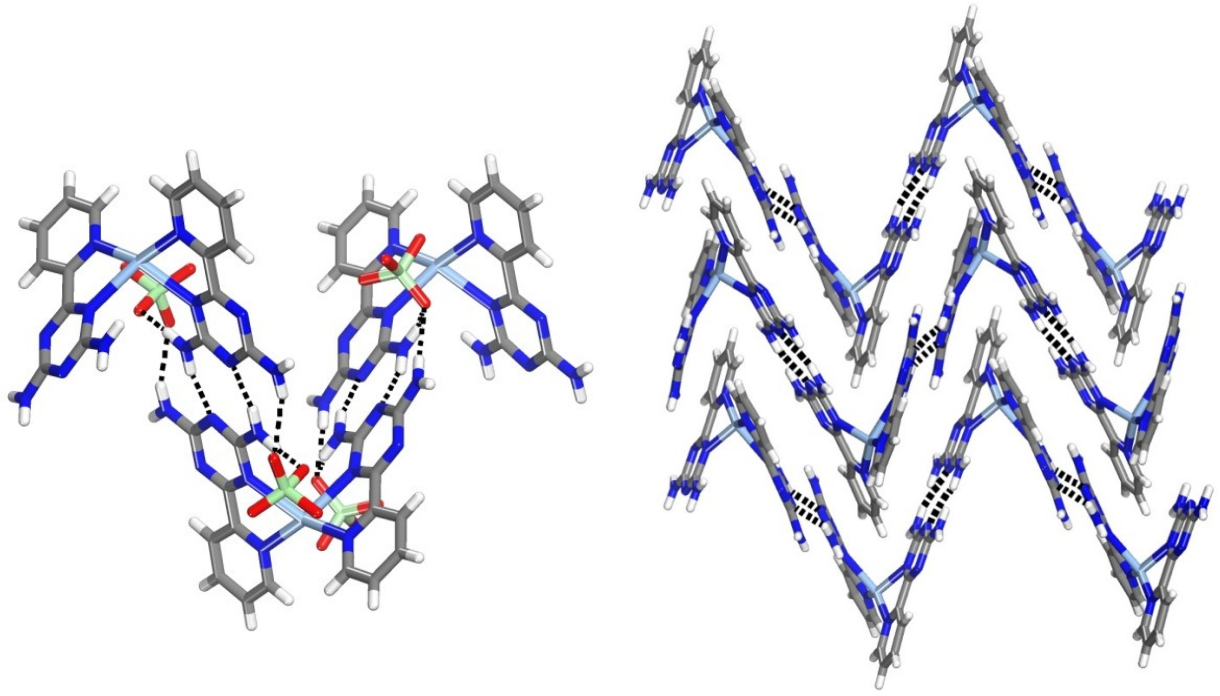

a **b**

Figure S5. Supplementary views of the structure of crystals of the unsolvated form of 2:1 complex of 6-(pyridin-2-yl)-1,3,5-triazine-2,4-diamine (**1**) with $AgClO_4$ grown from DMSO/MeCN. (a) Alternating chains of cationic complex **9** and its enantiomer, which are held together by hydrogen bonding of DAT groups according to motif **I**, reinforced by hydrogen bonding involving bridging perchlorate. (b) Stacking of corrugated sheets. In both views, hydrogen bonds are represented by broken lines. Carbon atoms are shown in gray, hydrogen atoms in white, chlorine atoms in pale green, nitrogen atoms in dark blue, oxygen atoms in red, and silver atoms in medium blue.

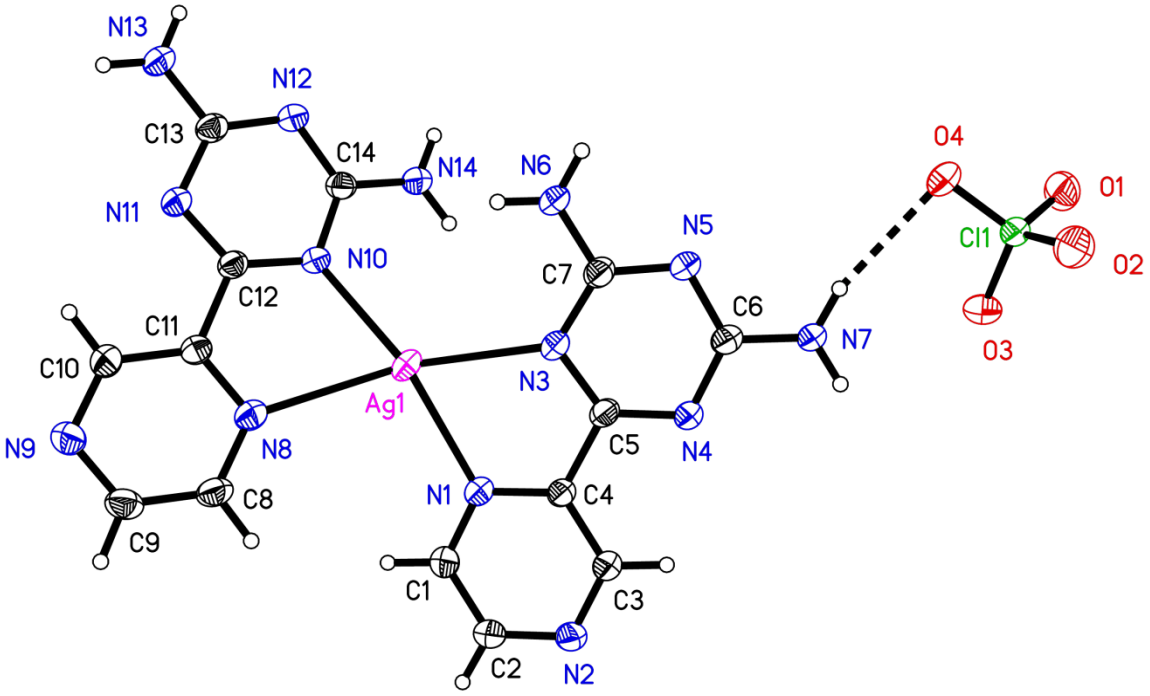

Figure S6. Thermal atomic displacement ellipsoid plot of the structure of crystals of the 2:1 complex of 6-(pyrazin-2-yl)-1,3,5-triazine-2,4-diamine (**2**) with $AgClO_4$ grown from DMSO/MeCN. The ellipsoids of non-hydrogen atoms are drawn at the 50% probability level, hydrogen atoms are represented by a sphere of arbitrary size, and hydrogen bonds are represented by broken lines.

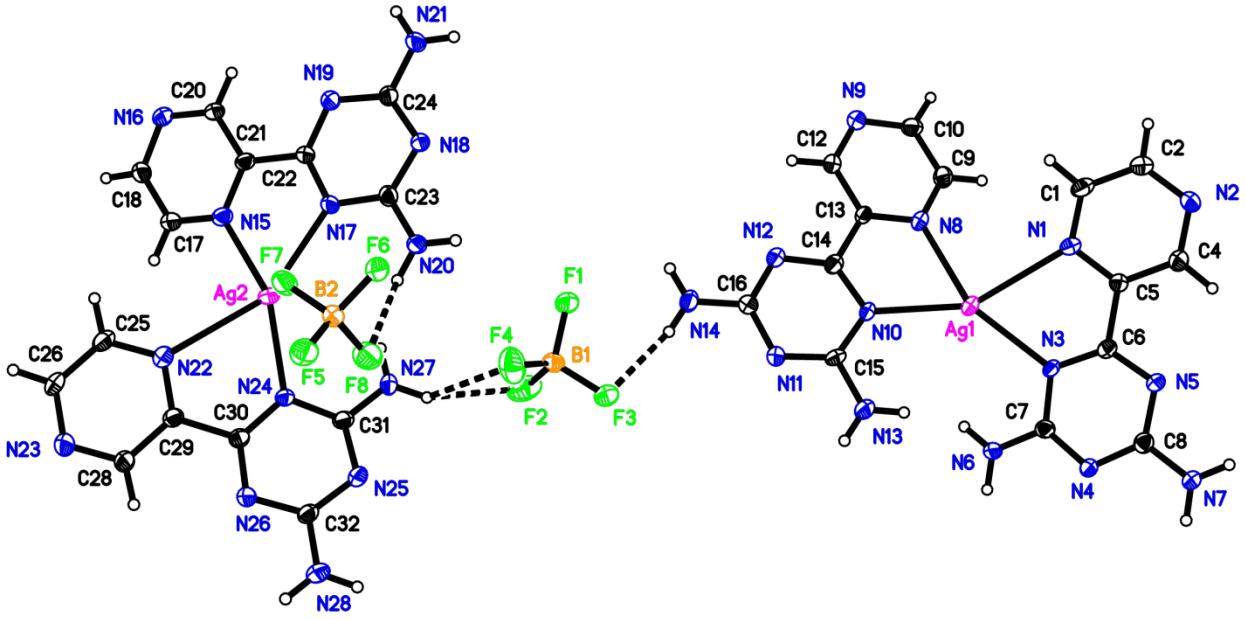

Figure S7. Thermal atomic displacement ellipsoid plot of the structure of crystals of the 2:1 complex of 6-(pyrazin-2-yl)-1,3,5-triazine-2,4-diamine (**2**) with $AgBF_4$ grown from DMSO/MeCN. The ellipsoids of non-hydrogen atoms are drawn at the 50% probability level, hydrogen atoms are represented by a sphere of arbitrary size, and hydrogen bonds are represented by broken lines.

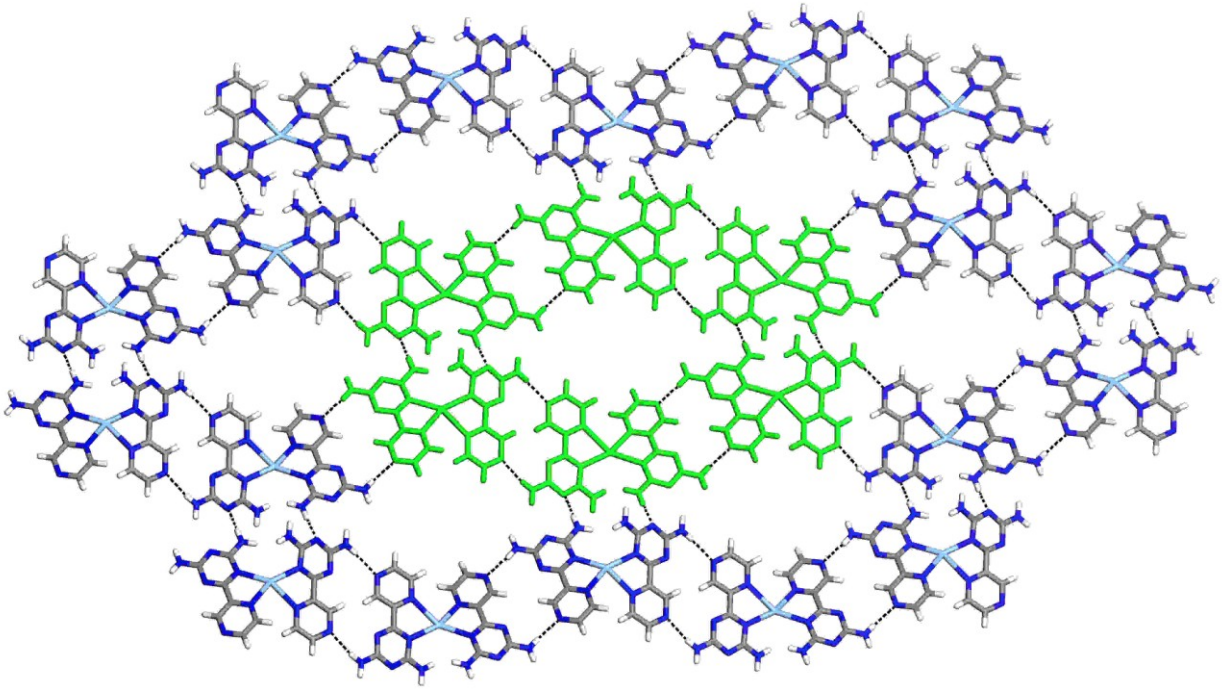

a

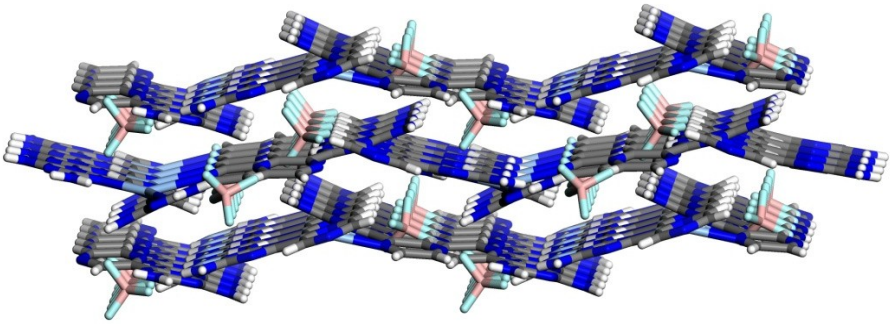

b

Figure S8. Supplementary views of the structure of crystals of the 2:1 complex of 6-(pyrazin-2-yl)-1,3,5-triazine-2,4-diamine (**2**) with $AgBF_4$ grown from DMSO/MeCN. (a) View of a hydrogen-bonded sheet, with a hexameric rosette highlighted in green. (b) View showing the stacking of three adjacent sheets. Unless noted otherwise, carbon atoms are shown in gray, hydrogen atoms in white, boron atoms in rose, fluorine atoms in light blue, nitrogen atoms in dark blue, and silver atoms in medium blue.

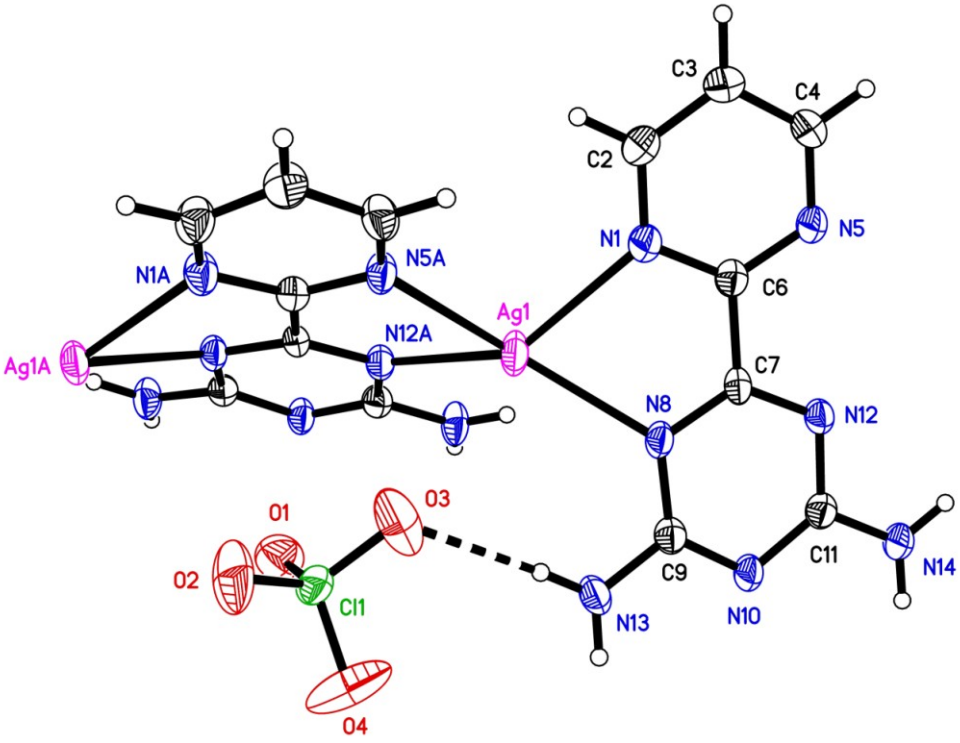

Figure S9. Thermal atomic displacement ellipsoid plot of the structure of crystals of the 1:1 complex of 6-(pyrimidin-2-yl)-1,3,5-triazine-2,4-diamine (**3**) with $AgClO_4$ grown from DMSO/MeOH. The ellipsoids of non-hydrogen atoms are drawn at the 50% probability level, hydrogen atoms are represented by a sphere of arbitrary size, and hydrogen bonds are represented by broken lines.

Homogeneity of Bulk Crystalline Samples

In all structural studies, experimental powder X-ray diffraction patterns were recorded for each bulk crystalline sample and then compared with those calculated from single-crystal X-ray diffraction data. In the case of the solvated form of the 2:1 complex of 6-(pyridin-2-yl)-1,3,5-triazine-2,4-diamine (**1**) with $AgClO_4$, the crystals proved to be unstable, and the experimental and calculated powder diffraction patterns were different. In all other cases, the patterns were similar, and detailed comparisons confirmed that the single-crystal specimens selected for structural analysis were representative of the bulk crystalline samples from which they were chosen. Experimental powder X-ray diffraction patterns were recorded using one of the following two instruments :

1) Bruker D8 Discover diffractometer with GADDS HTS, using graphite monochromatized Cu Kα radiation generated at 40 kV and 40 mA, working in reflection mode. The 2D general area detector was positioned at a distance of 15 cm from the powder sample, which was placed on a glass plate. This allowed simultaneous collection of data over an angular domain up to 35° in 2θ. Measurements were carried out at 293 K in coupled scan mode (θ-θ geometry). Four separate images (diffraction arcs) were collected (scanning time : 5 min/image), and intensity along each arc was integrated to create the 1D powder pattern of intensity versus 2θ, over the angular range $10° < 2\theta < 105°$.
2) Single-crystal Bruker Microstar diffractometer mounted with an FR591 rotating anode generator, Helios optics and a 2D Pt135 CCD detector, working in transmission mode. A small amount of ground sample was mounted in a fiber loop, and the diffraction patterns

were recorded at 150 K by phi-scan over five different detector positions, merged, and integrated to give the 1D powder diffraction pattern.

Structural data from single-crystal analyses were used to calculate theoretical powder X-ray diffraction patterns with the aid of Mercurysoftware.[1] Peak fitting and the refinement of lattice parameters were carried out using TOPAS software,[2] and Pawley fitting was applied to the powder X-ray diffraction patterns. The quality of the refinement was checked by evaluating the weighted agreement factor R_{wp}, which was calculated using background-subtracted intensity data as

$$R_{wp} = \sqrt{\frac{\sum w(Yo - Yc)^2}{\sum w(Yo - Bkg)^2}}$$

where *Y*o is the observed intensity, *Y*c is the calculated intensity, *Bkg* is the background intensity, and *w* is the weighting factor defined by $w = 1/\sigma(Yo)^2$, $\sigma(Yo)$ being the error in the measured intensity.[2]

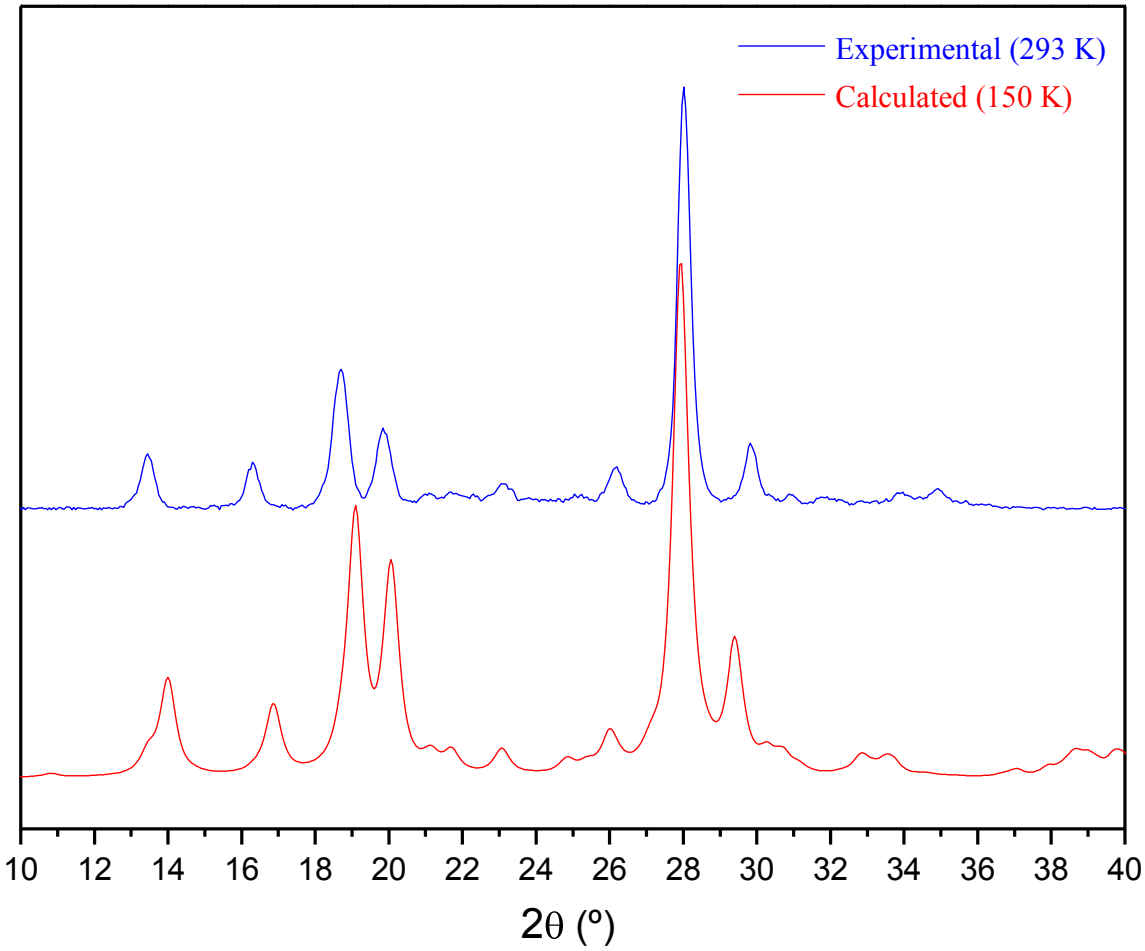

Figure S10. Comparison between experimental (collected using D8 Discover) and calculated powder X-ray diffraction patterns for crystals of 6-(pyrazin-2-yl)-1,3,5-triazine-2,4-diamine (**2**) grown from DMSO/MeCN. The *x* axis of the experimental pattern was shifted to minimize the slight angular shift due to the effect of temperature. The two diffractograms are closely similar, confirming that the bulk crystalline sample consists of a single phase.

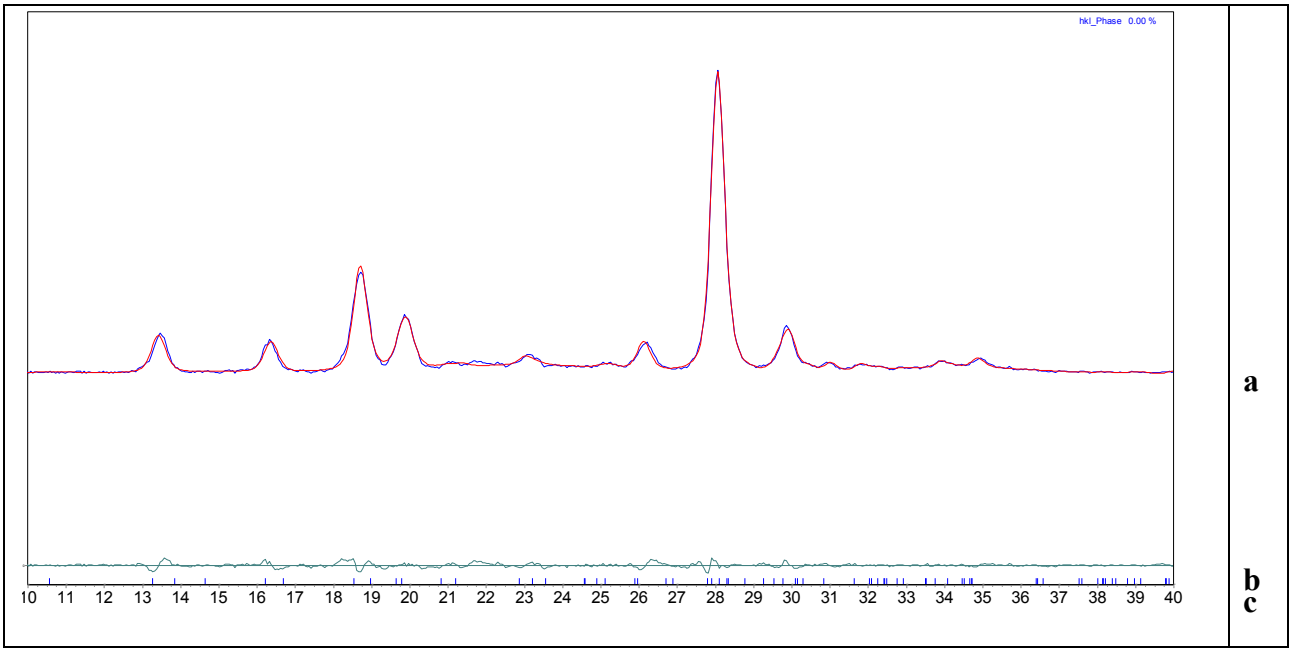

Figure S11. (a) Simulated powder X-ray diffraction pattern of crystals of 6-(pyrazin-2-yl)-1,3,5-triazine-2,4-diamine (**2**) grown from DMSO/MeCN (red curve), as determined by Pawley fitting of the experimental powder X-ray diffraction pattern (nearly superimposed blue curve). (b) Difference between experimental and calculated intensities. (c) Position of calculated reflections.

Table S1. Crystallographic Data for Crystals of 6-(Pyrazin-2-yl)-1,3,5-triazine-2,4-diamine (**2**) Grown from DMSO/MeCN, as Determined by Pawley Fitting of Powder X-Ray Diffraction Data at 293 K.

compound	**2**
composition	$C_7H_7N_7$
temperature (K)	293
crystal system	monoclinic
space group	$P2_1/n$
a (Å)	9.303(11)
b (Å)	6.859(55)
c (Å)	13.159(88)
α (º)	90
β (º)	103.73(72)
γ (º)	90
V (Å^3)	815.8(13)
Z	4
R_{wp}	5.35

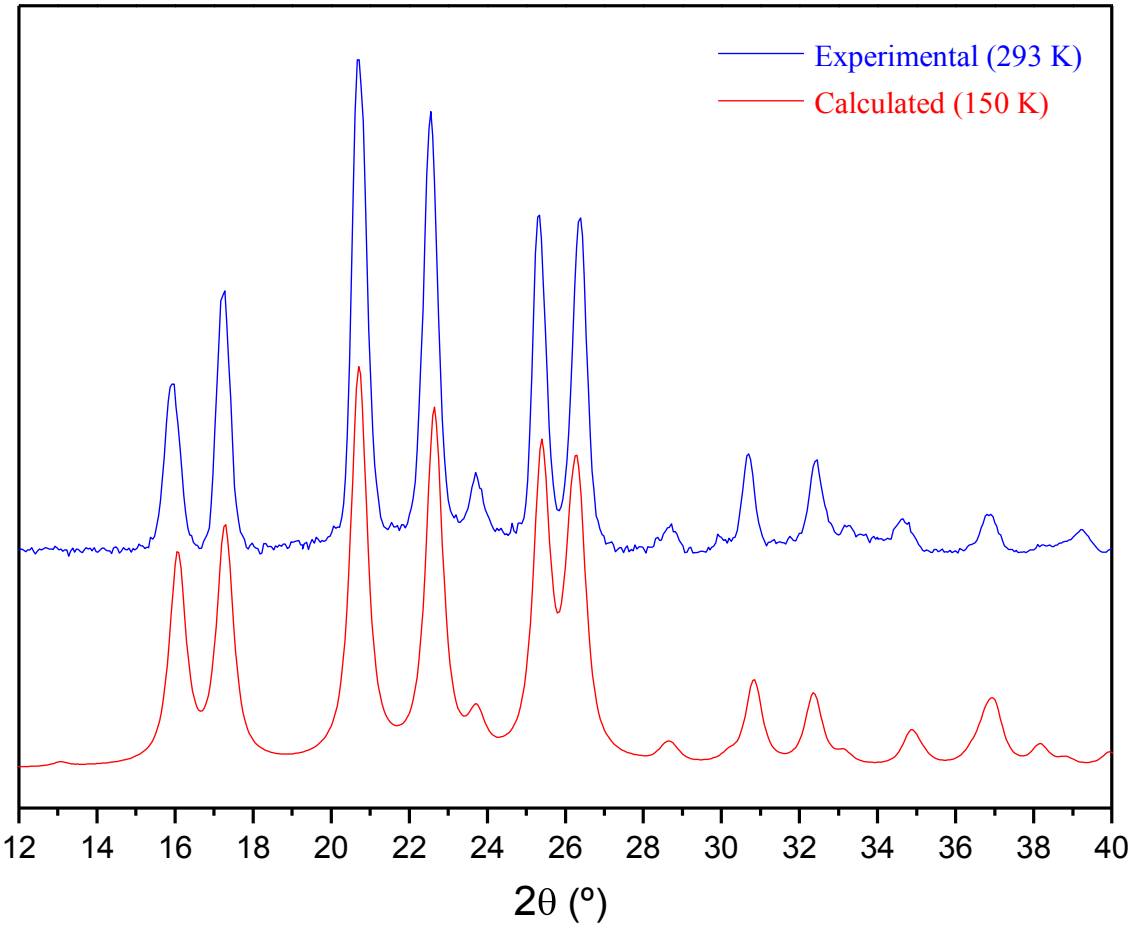

Figure S12. Comparison between experimental (collected using D8 Discover) and calculated powder X-ray diffraction patterns for crystals of 6-(pyrimidin-2-yl)-1,3,5-triazine-2,4-diamine (**3**) grown from DMSO/CH_2Cl_2. The *x* axis of the experimental pattern was shifted to minimize the slight angular shift due to the effect of temperature. The two diffractograms are closely similar, confirming that the bulk crystalline sample consists of a single phase.

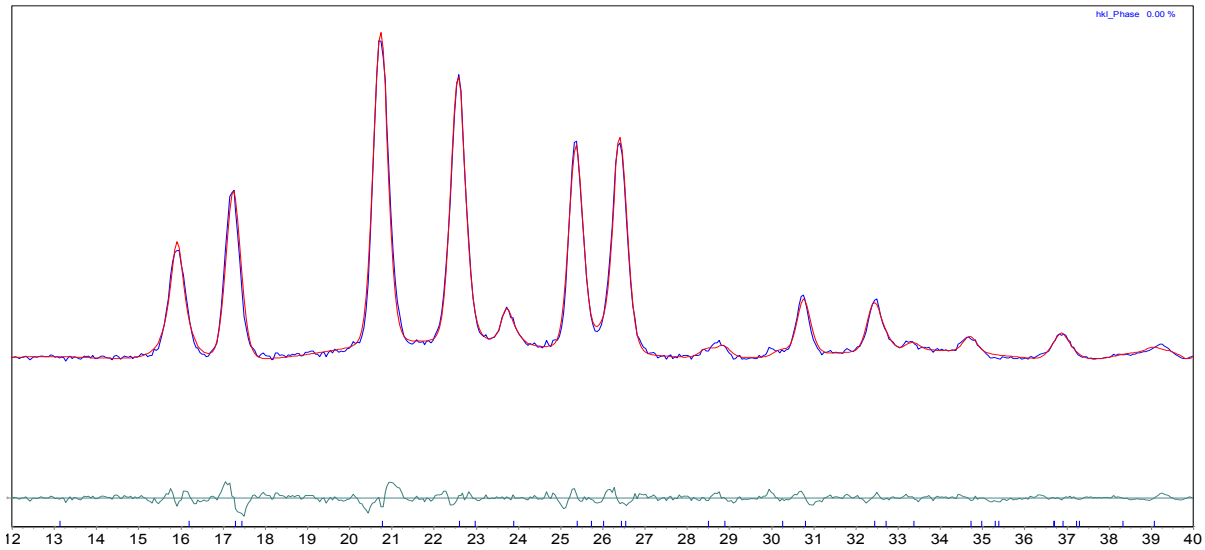

Figure S13. (a) Simulated powder X-ray diffraction pattern of crystals of 6-(pyrimidin-2-yl)-1,3,5-triazine-2,4-diamine (**3**) grown from DMSO/CH_2Cl_2(red curve), as determined by Pawley fitting of the experimental powder X-ray diffraction pattern (nearly superimposed blue curve). (b) Difference between experimental and calculated intensities. (c) Position of calculated reflections.

Table S2. Crystallographic Data for Crystals of 6-(Pyrimidin-2-yl)-1,3,5-triazine-2,4-diamine (**3**) Grown from DMSO/CH_2Cl_2, as Determined by Pawley Fitting of Powder X-Ray Diffraction Data at 293 K.

compound	**3**
composition	$C_7H_7N_7$
temperature (K)	293
crystal system	tetragonal
space group	$P4_32_12$
a (Å)	7.738(51)
b (Å)	7.738(51)
c (Å)	13.689(66)
α (º)	90
β (º)	90
γ (º)	90
V (Å^3)	819.8(11)
Z	4
R_{wp}	3.78

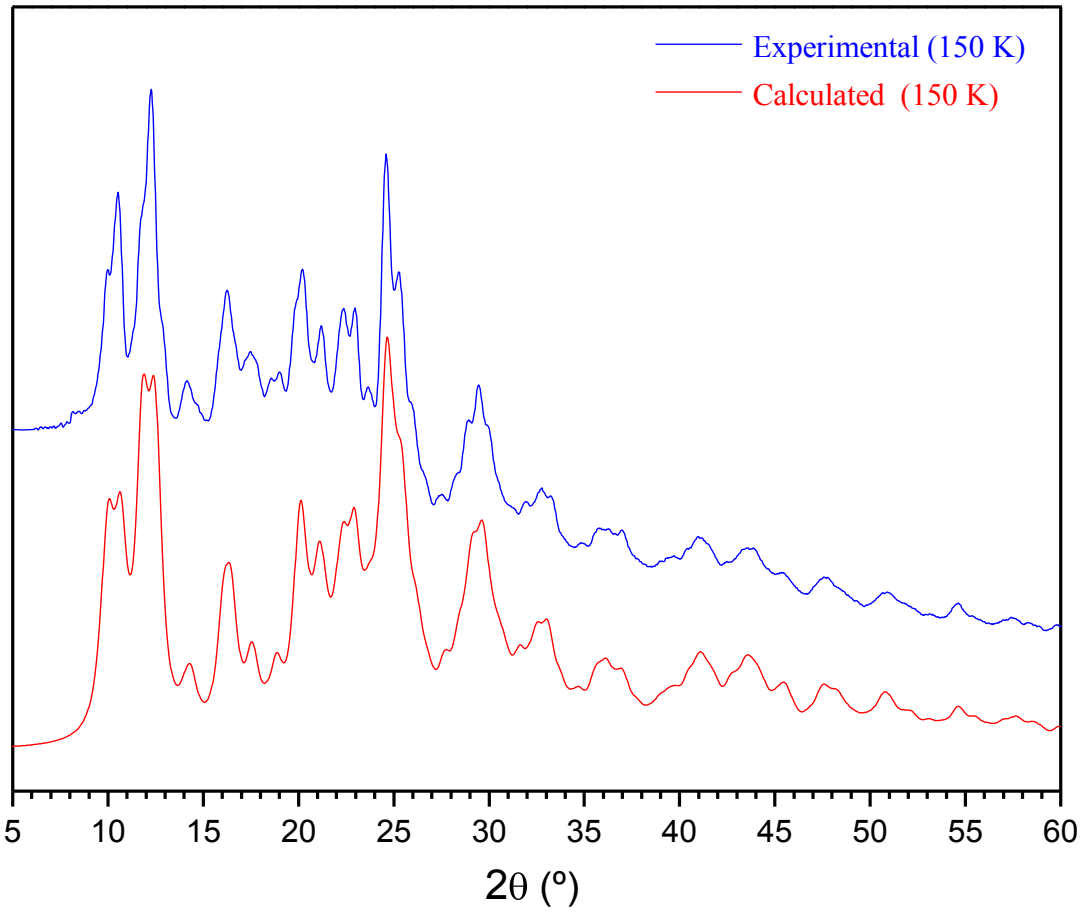

Figure S14. Comparison between experimental (collected using a Bruker Microstar diffractometer) and calculated powder X-ray diffraction patterns for crystals of the unsolvated form of the 2:1 complex of 6-(pyridin-2-yl)-1,3,5-triazine-2,4-diamine (**1**) with $AgClO_4$ grown from DMSO/MeCN. The two diffractograms are closely similar, confirming that the bulk crystalline sample consists of a single phase.

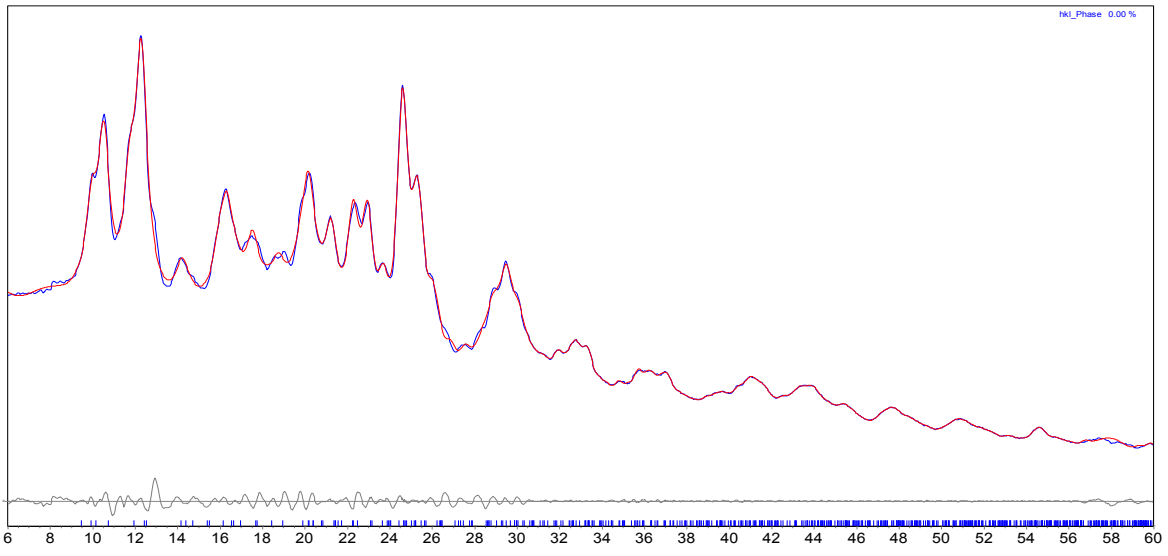

Figure S15. (a) Simulated powder X-ray diffraction pattern of crystals of the unsolvated form of the 2:1 complex of 6-(pyridin-2-yl)-1,3,5-triazine-2,4-diamine (**1**) with $AgClO_4$ grown from DMSO/MeCN (red curve), as determined by Pawley fitting of the experimental powder X-ray diffraction pattern (nearly superimposed blue curve). (b) Difference between experimental and calculated intensities. (c) Position of calculated reflections.

Table S3. Crystallographic Data for Crystals of the Unsolvated Form of the 2:1 Complex of 6-(Pyridin-2-yl)-1,3,5-triazine-2,4-diamine (**1**) with $AgClO_4$ Grown from DMSO/MeCN, as Determined by Pawley Fitting of Powder X-Ray Diffraction Data at 150 K.

compound	2 **1** • $AgClO_4$
composition	$C_{16}H_{16}AgClN_{12}O_4$
temperature (K)	150
crystal system	monoclinic
space group	$P2_1/n$
a (Å)	11.516(59)
b (Å)	14.125(42)
c (Å)	12.517(43)
α (º)	90
β (º)	93.171(59)
γ (º)	90
V (Å^3)	2033(14)
Z	4
R_{wp}	2.26

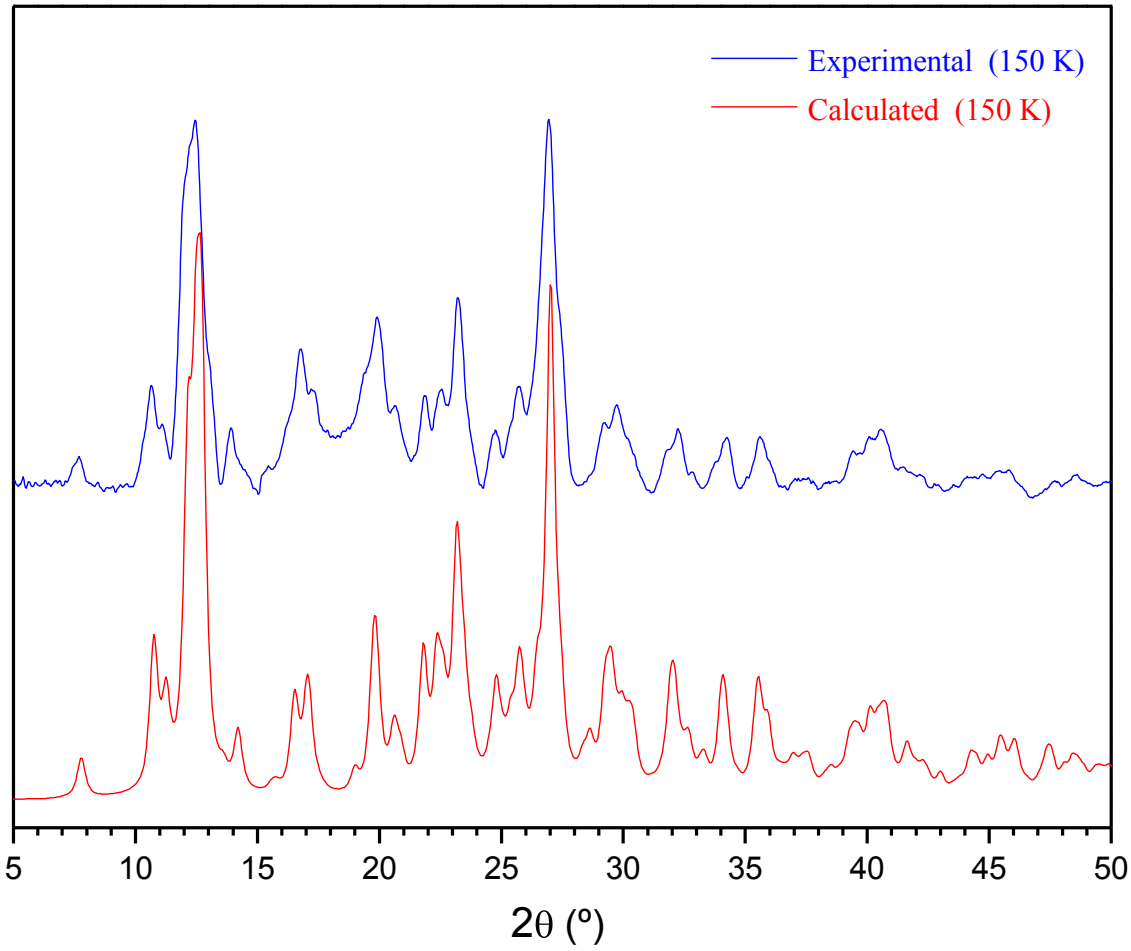

Figure S16. Comparison between experimental (collected using a Bruker Microstar diffractometer) and calculated powder X-ray diffraction patterns for crystals of the 2:1 complex of 6-(pyrazin-2-yl)-1,3,5-triazine-2,4-diamine (**2**) with $AgClO_4$ grown from DMSO/MeCN. The two diffractograms are closely similar, confirming that the bulk crystalline sample consists of a single phase.

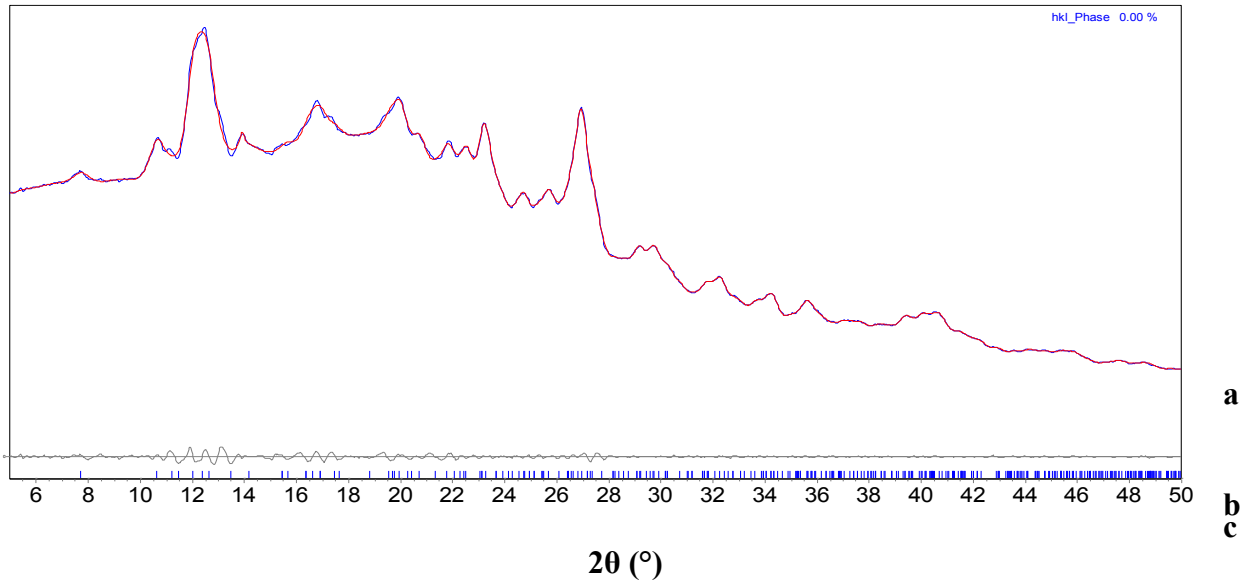

Figure S17. (a) Simulated powder X-ray diffraction pattern of crystals of the 2:1 complex of 6-(pyrazin-2-yl)-1,3,5-triazine-2,4-diamine (**2**) with $AgClO_4$ grown from DMSO/MeCN (red curve), as determined by Pawley fitting of the experimental powder X-ray diffraction pattern (nearly superimposed blue curve). (b) Difference between experimental and calculated intensities. (c) Position of calculated reflections.

Table S4. Crystallographic Data for Crystals of the 2:1 Complex of 6-(Pyrazin-2-yl)-1,3,5-triazine-2,4-diamine (**2**) with $AgClO_4$ Grown from DMSO/MeCN, as Determined by Pawley Fitting of Powder X-Ray Diffraction Data at 150 K.

compound	2 **2** • $AgClO_4$
composition	$C_{14}H_{14}AgClN_{14}O_4$
temperature (K)	150
crystal system	monoclinic
space group	$P2_1/c$
a (Å)	7.743(23)
b (Å)	16.613(64)
c (Å)	15.790(62)
α (º)	90
β (º)	93.85(28)
γ (º)	90
V (Å^3)	2027(13)
Z	4
R_{wp}	2.64

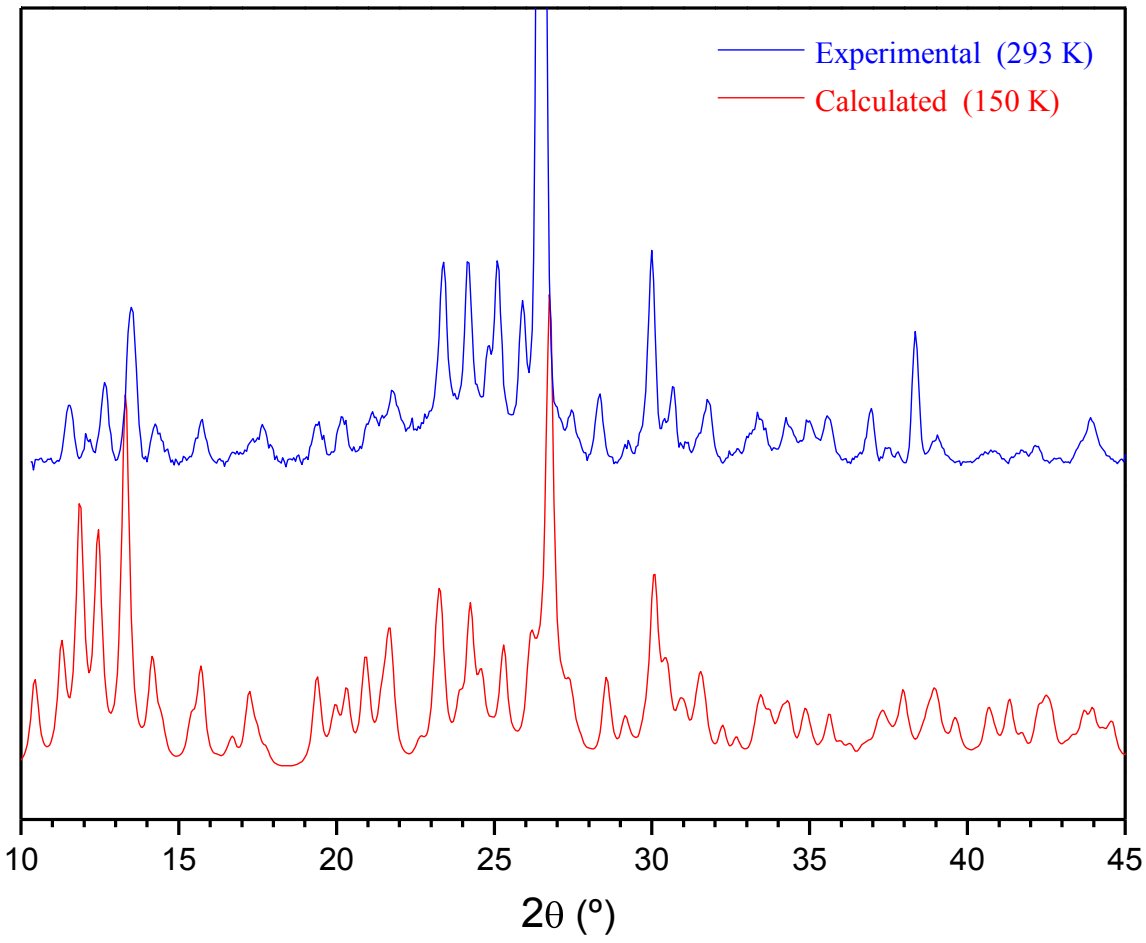

Figure S18. Comparison between experimental (collected using D8 Discover) and calculated powder X-ray diffraction patterns for crystals of the 2:1 complex of 6-(pyrazin-2-yl)-1,3,5-triazine-2,4-diamine (**2**) with $AgBF_4$ grown from DMSO/MeCN. The *x* axis of the experimental pattern was shifted to minimize the slight angular shift due to the effect of temperature. The two diffractograms are closely similar, confirming that the bulk crystalline sample consists of a single phase.

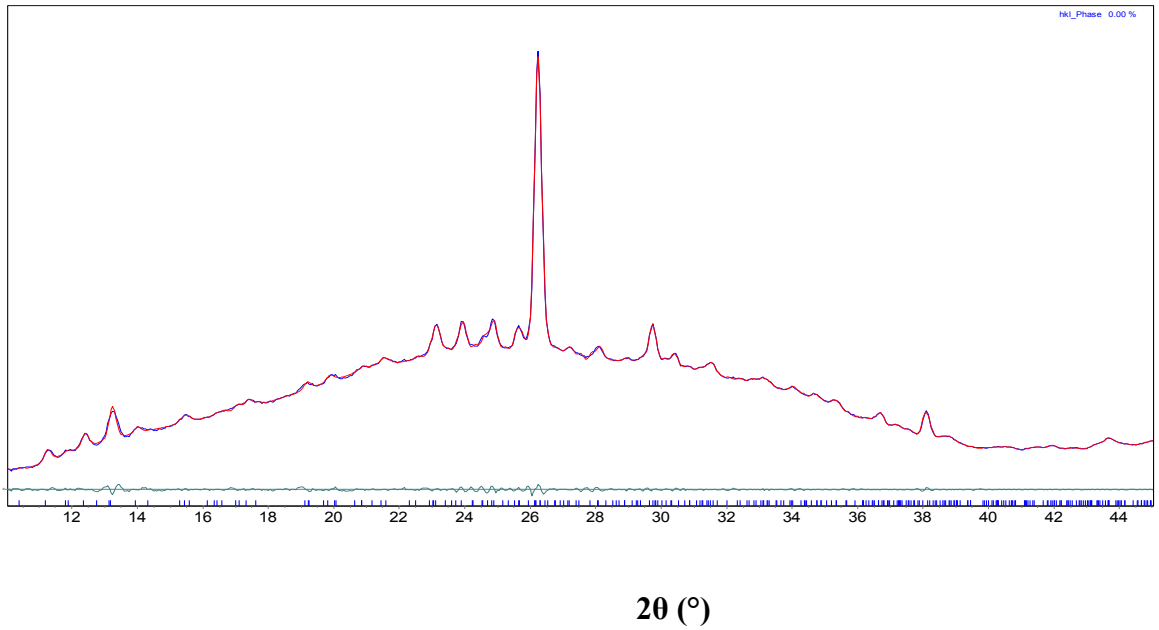

Figure S19. (a) Simulated powder X-ray diffraction pattern of crystals of the 2:1 complex of 6-(pyrazin-2-yl)-1,3,5-triazine-2,4-diamine (**2**) with $AgBF_4$ grown from DMSO/MeCN (red curve), as determined by Pawley fitting of the experimental powder X-ray diffraction pattern (nearly superimposed blue curve). (b) Difference between experimental and calculated intensities. (c) Position of calculated reflections.

Table S5. Crystallographic Data for Crystals of the 2:1 Complex of 6-(Pyrazin-2-yl)-1,3,5-triazine-2,4-diamine (**2**) with $AgBF_4$ Grown from DMSO/MeCN, as determined by Pawley Fitting of Powder X-Ray Diffraction Data at 293 K.

compound	2 **2** • $AgBF_4$
composition	$C_{14}H_{14}AgBF_4N_{14}$
temperature (K)	293
crystal system	monoclinic
space group	$P2_1$
a (Å)	7.4499(40)
b (Å)	15.796(12)
c (Å)	17.048(12)
α (º)	90
β (º)	92.535(84)
γ (º)	90
V (Å^3)	2004.1(24)
Z	4
R_{wp}	4.35

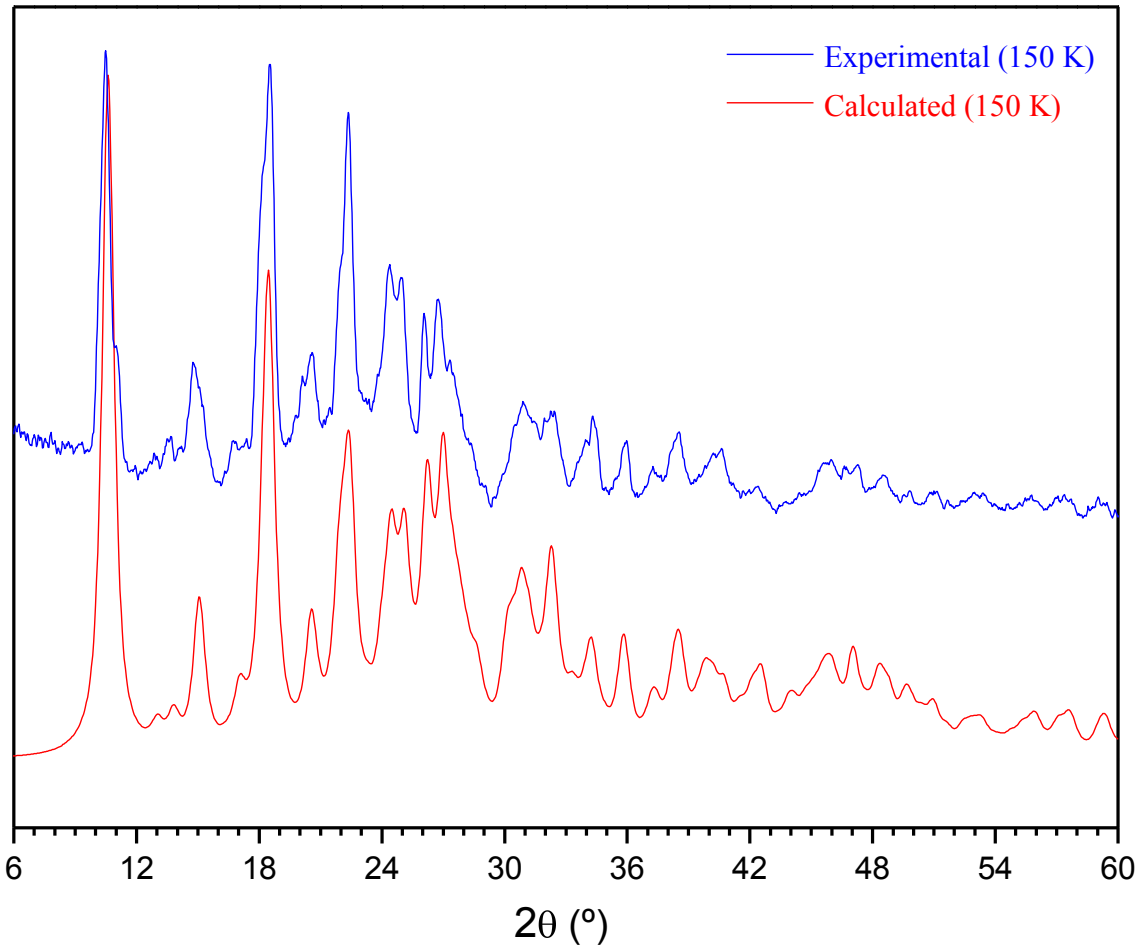

Figure S20. Comparison between experimental (collected using a Bruker Microstar diffractometer) and calculated powder X-ray diffraction patterns for crystals of the 1:1 complex of 6-(pyrimidin-2-yl)-1,3,5-triazine-2,4-diamine (**3**) with $AgClO_4$ grown from DMSO/MeOH. The two diffractograms are closely similar, confirming that the bulk crystalline sample consists of a single phase.

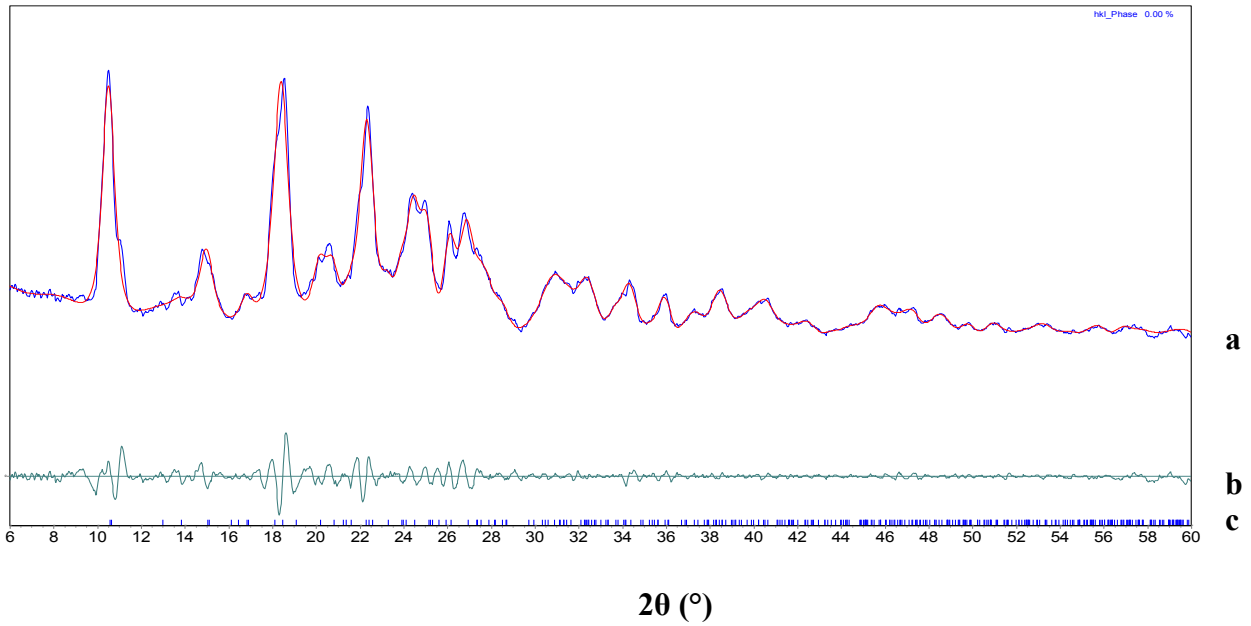

Figure S21. (a) Simulated powder X-ray diffraction pattern of crystals of the 1:1 complex of 6-(pyrimidin-2-yl)-1,3,5-triazine-2,4-diamine (**3**) with $AgClO_4$ grown from DMSO/MeOH (red curve), as determined by Pawley fitting of the experimental powder X-ray diffraction pattern (nearly superimposed blue curve). (b) Difference between experimental and calculated intensities. (c) Position of calculated reflections.

Table S6. Crystallographic Data for Crystals of the 1:1 Complex of 6-(Pyrimidin-2-yl)-1,3,5-triazine-2,4-diamine (**3**) with $AgClO_4$ Grown from DMSO/MeOH, as Determined by Pawley Fitting of Powder X-Ray Diffraction Data at 150 K.

compound	**3** • $AgClO_4$
composition	$C_7H_7AgClN_7O_4$
temperature (K)	150
crystal system	monoclinic
space group	$P2_1/c$
a (Å)	8.564(62)
b (Å)	11.725(64)
c (Å)	12.054(96)
α (º)	90
β (º)	102.36(27)
γ (º)	90
V (Å^3)	1182(14)
Z	4
R_{wp}	5.89

References

1) Macrae, C. F.; Edgington, P. R.; McCabe, P.; Pidcock, E.; Shields, G. P.; Taylor, R.; Towler, M.; van de Streek, J. *J. Appl. Cryst.* **2006**, *39*, 453-457.
2) Coelho, A. A. *TOPAS User Manual*, Version 3.1 ed.; Bruker-AXS GmbH : Karlsruhe, Germany, 2003.